GRI-80/0048

GEOLOGIC STUDIES OF GEOPRESSURED AND HYDROPRESSURED ZONES IN TEXAS: TEST-WELL SITE SELECTION

FINAL REPORT

(January 1979 - May 1980)

Gas Research Institute
8600 West Bryn Mawr Avenue
Chicago, Illinois 60631

GEOLOGIC STUDIES OF GEOPRESSURED AND HYDROPRESSURED ZONES IN TEXAS: TEST-WELL SITE SELECTION

FINAL REPORT

(January 1979 - May 1980)

Prepared By

B. R. Weise, M. B. Edwards, A. R. Gregory,
H. S. Hamlin, L. A. Jirik, and R. A. Morton

Bureau of Economic Geology
W. L. Fisher, Director
The University of Texas at Austin
University Station, Box X
Austin, Texas 78712

For

GAS RESEARCH INSTITUTE
Contract No. 5011-321-0125

GRI Project Manager
John Sharer
Unconventional Natural Gas

September 1981

GRI DISCLAIMER

LEGAL NOTICE. This report was prepared by the Bureau of Economic Geology, The University of Texas at Austin, as an account of work sponsored by the Gas Research Institute (GRI). Neither GRI, members of GRI, nor any person acting on behalf of either:

a. Makes any warranty or representation, express or implied, with respect to the accuracy, completeness, or usefulness of the information contained in this report, or that the use of any information, apparatus, method, or process disclosed in this report may not infringe privately owned rights; or

b. Assumes any liability with respect to the use of, or for damages resulting from the use of, any information, apparatus, method, or process disclosed in this report.

50272-101

REPORT DOCUMENTATION PAGE	1. REPORT NO. GRI-80/0048	2.	3. Recipient's Accession No.

4. Title and Subtitle
Geologic Studies of Geopressured and Hydropressured Zones in Texas: Test-Well Site Selection

5. Report Date
September, 1981

6.

7. Author(s)
B.R. Weise, M.B. Edwards, A.R. Gregory, H.S. Hamlin, L.A. Jirik, and R.A. Morton

8. Performing Organization Rept. No.

9. Performing Organization Name and Address
Bureau of Economic Geology
The University of Texas at Austin
University Station, P.O. Box X
Austin, Texas 78712

10. Project/Task/Work Unit No.

11. Contract(C) or Grant(G) No.
(C) 5011-321-0125
(G)

12. Sponsoring Organization Name and Address
Gas Research Institute
8600 West Bryn Mawr Avenue
Chicago, Illinois 60631

13. Type of Report & Period Covered
Final Report

14.
Jan. 1979-May 1980

15. Supplementary Notes

16. Abstract (Limit: 200 words)

The primary objective achieved in this project was to identify sites for test wells that will be capable of long-term production of methane-bearing water from the shallow geopressured and deep hydropressured zones. The process of test-well site selection involved several steps, each contributing to the basic knowledge of shallow geopressured and deep hydropressured aquifers. First, zones within the geopressured and deep hydropressured section of the Texas Gulf Coast Tertiary were defined on the basis of pressure gradients and temperatures.

Next, high-sandstone corridors, corresponding to the trends of the Wilcox Group and Frio Formation, were identified for each of these zones. Five fairways, or areas of greatest net-sandstone thickness, were located within the corridors. Areas most prospective for testing entrained methane resources in the shallow geopressured and deep hydropressured zones were identified in each fairway. Finally, test sites were selected in four of the prospect areas, the Blessing Prospect in Matagorda County, the Nueces Bay and Corpus Channel Prospects in San Patricio and Nueces Counties, and the Sarita Prospect in Kleberg County.

Knowledge gained from these geologic studies and from subsequent testing will be significant in (1) the evaluation of the technical and economic feasibility of producing solution gas from the shallow geopressured and deep hydropressured zones and (2) comparison of these zones with deeper, hotter geopressured zones (studied previously in DOE-funded projects) as sources of entrained methane.

17. Document Analysis a. Descriptors
Geologic Studies

b. Identifiers/Open-Ended Terms

c. COSATI Field/Group

18. Availability Statement	19. Security Class (This Report)	21. No. of Pages 308
	20. Security Class (This Page)	22. Price

(See ANSI-Z39.18) *See Instructions on Reverse*

OPTIONAL FORM 272 (4-77)
(Formerly NTIS-35)
Department of Commerce

RESEARCH SUMMARY

Title	Geologic Studies of Geopressured and Hydropressured Zones in Texas: Test-Well Site Selection
Contractor	Bureau of Economic Geology The University of Texas at Austin GRI Contract Number 5011-321-0125 Accession Code: GRI-80/0048
Principal Investigator	R. A. Morton
Time Span	January 1979 - May 1980 Final Report
Major Achievements	The primary objective achieved in this project was to identify sites for test wells that will be capable of long-term production of methane-bearing water from the shallow geopressured and deep hydropressured zones. The process of test-well site selection involved several steps, each contributing to the basic knowledge of shallow geopressured and deep hydropressured aquifers. First, zones within the geopressured and deep hydropressured section of the Texas Gulf Coast Tertiary were defined on the basis of pressure gradients and temperatures. These zones are as follows: (1) the A Zone, or deep hydropressured zone below depths of 4,500 ft, in which the fluid pressure gradient is 0.465 psi/ft; (2) the B Zone, in which pressure gradients are greater than 0.465 psi/ft but less than 0.7 psi/ft; (3) the C Zone, in which pressure gradients are greater than 0.7 psi/ft and fluid temperatures are less than 300° F; and (4) the D Zone, in which pressure gradients equal or surpass 0.7 psi/ft and temperatures equal or surpass 300° F. Next, sandstone corridors, corresponding to the trends of the Wilcox Group and Frio Formation, were identified for each of these zones. Five fairways, or areas of greatest net-sandstone thickness, were located within the corridors. Areas most prospective for testing entrained methane resources in the shallow geopressured and deep hydropressured zones were identified in each fairway. Finally, test sites were selected in four of the prospect areas, the Blessing Prospect in Matagorda County, the Nueces Bay and Corpus Channel Prospects in San Patricio and Nueces Counties, and the Sarita Prospect in Kleberg County.

Knowledge gained from these geologic studies and from subsequent testing will be significant in (1) the evaluation of the technical and economic feasibility of producing solution gas from the shallow geopressured and deep hydropressured zones and (2) comparison of these zones with deeper, hotter geopressured zones (studied previously in projects funded by the Department of Energy) as sources of entrained methane.

Recommendations

The Blessing Prospect in the Matagorda Fairway is recommended for testing entrained methane resources in the shallow geopressured C Zone at a depth of approximately 11,000 ft. The Nueces Bay and Corpus Channel Prospects in the Corpus Christi Fairway and the Sarita Shallow Prospect in the Kenedy Fairway are recommended for testing the shallowest geopressured zone (B Zone) and the deep hydropressured zone (A Zone). Depths of testing would be approximately 8,000 to 9,000 ft in the Nueces Bay Prospect, 7,000 to 8,500 ft in the Corpus Channel Prospect, and 8,500 to 9,500 ft in the Sarita Shallow Prospect.

Description of Work Completed

Boundaries of zones within the geopressured and deep hydropressured Tertiary section were defined using a combination of shale resistivity-versus-depth plots, bottom-hole shut-in pressure plots, and mud-weight data from well log headers. These zones were then plotted on a series of regional cross sections of the Texas Gulf Coast. Sandstone distribution was surveyed and Wilcox and Frio sandstone corridors mapped for each zone. Regional net-sandstone maps were constructed to outline fairways. Five fairways were selected for detailed study on the basis of net sandstone, area of sandstone distribution, average bed thickness, permeability, and coincidence with fairways of other zones. Correlation of major sandstone units on preliminary fairway cross sections and other cross sections constructed for previous studies allowed selection of prospect areas within each fairway. Each prospect area was studied in detail by performing well log correlations, constructing structural and stratigraphic cross sections, net-sandstone and structure maps, and temperature, pressure, and salinity profiles, and examining porosity and permeability relationships of sandstones. The suitability of each prospect area for location of a test-well site was judged on the basis of the cross sections, maps, and reservoir data. Test sites were selected in four of the prospects.

GRI Comment

The research completed by the Bureau of Economic Geology was designed to identify favorable test-well sites for the production of geopressured methane along the United States Gulf Coast. In identifying four potential test-well sites, this project complements efforts by the U.S. Department of Energy (DOE) aimed specifically at identifying deep (brine temperatures greater than 300° F) geopressured test-well prospects. GRI has provided DOE with the results and data from this project for future test-well efforts. The prospects that do not meet DOE's test-site criteria will remain under consideration for future GRI well-test programs.

GEOLOGIC STUDIES OF GEOPRESSURED
AND HYDROPRESSURED ZONES IN TEXAS:
TEST-WELL SITE SELECTION

Contents

ILLUSTRATIONS

FIGURES

TABLES

INTRODUCTION

Background and Objectives of the Project

In previous studies conducted by the Bureau of Economic Geology for the U.S. Department of Energy (DOE), well sites were selected to test the geopressured-geothermal energy resources of the Frio Formation (Bebout, 1977) and Wilcox Group (Bebout and others, 1979) of the Texas Gulf Coast (fig. 1). These DOE studies concentrated on deep sandstones where fluid temperatures are at least 300° F. These studies initially focused on the thermal energy, but because of increases in prices of natural gas, the emphasis has now shifted to methane entrained in the water.

The great volume of the geopressured zone of the Gulf Coast suggests a potentially large resource of methane entrained in geopressured waters. The limits of our knowledge of this resource, however, are illustrated by the wide range of estimates of entrained methane in place in Gulf Coast reservoirs. Published estimates range from 5,700 quads (Dorfman, 1977) to 100,000 quads (Brown, 1976). A DOE-sponsored study was conducted by the Bureau of Economic Geology to investigate geopressured water reservoirs without the temperature constraints of 300° F and assess the total entrained methane resource in place in the Texas Gulf Coast (Gregory and others, 1980). From this investigation, the volume of methane entrained in sandstone reservoirs deeper than -8,000 ft was estimated to be 690 quads (Gregory and others, 1980). Even though this estimate is lower than any previous estimate, it still represents a significant resource.

The present study, funded by the Gas Research Institute, was designed to identify favorable sites for test wells that will be capable of long-term production of methane-bearing water from the shallow geopressured

CENOZOIC — TEXAS GULF COAST

SYSTEM	SERIES	GROUP / FORMATION
Quaternary	Recent	Undifferentiated
	Pleistocene	Houston
Tertiary	Pliocene	Goliad
	Miocene	Fleming
	—?—?—	Anahuac
	Oligocene	Frio
		Vicksburg
	Eocene	Jackson / Yegua
		Claiborne
		Wilcox
		Midway

Figure 1. Cenozoic stratigraphic section, Texas Gulf Coast.

zone. Sites were selected to provide a range of test results from reservoirs of markedly different pressure, temperature, salinity, and sandstone characteristics. In addition, some of these sites will provide an opportunity to test a reservoir in the deep hydropressured zone. Technical terms used in this report are defined in the glossary. Appendix A provides metric conversions, and appendix B explains symbols.

The Geological Model

The search for and evaluation of geopressured reservoirs is facilitated by an understanding of the general depositional and structural styles of the Gulf Coast Tertiary basin and the relation of those styles to the development of geopressure. During the Tertiary Period, large quantities of sand and mud were transported across a broad fluvial plain and deposited along the margins of the Gulf of Mexico as a number of wedges which thicken and dip gulfward (fig. 2). The overall trend of the Tertiary was one of gulfward progradation, so that the depocenter of each wedge was shifted basinward of the previous wedge. Large growth-fault systems formed along

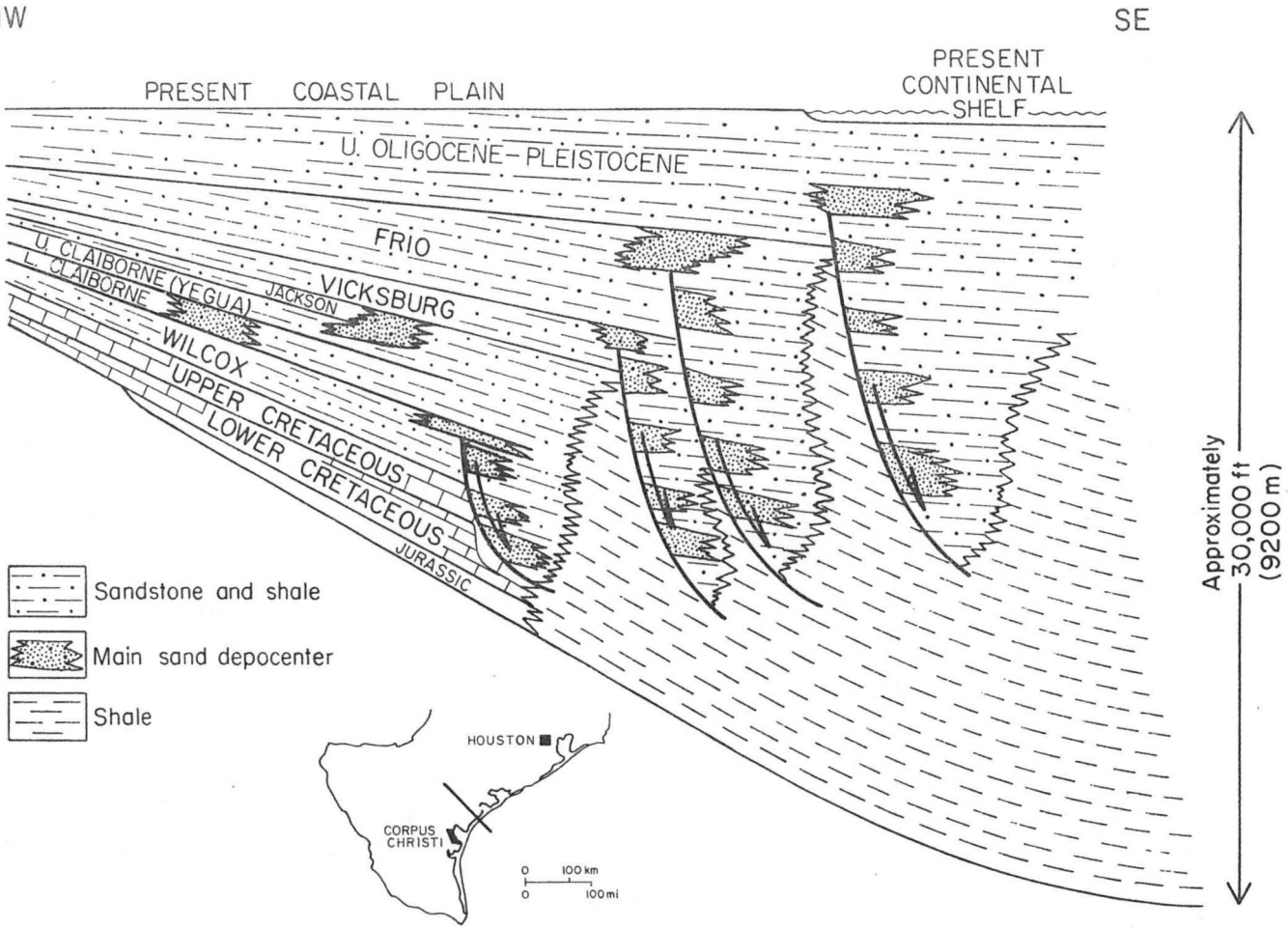

Figure 2. Depositional and structural styles of Tertiary formations, Texas Gulf Coast.

the downdip part of each wedge within the area of maximum deposition. These faults resulted from loading of large quantities of sand and mud on thick, low-density shale along the shelf margin of the previous wedge. Movement of growth faults allowed the accumulation of abnormally thick sections of sand and mud on the downthrown sides of the faults and also caused isolation of porous sandstones downdip. Because of this isolation, fluids within the sandstone reservoirs were trapped and became overpressured (geopressured) with further loading and burial (Bruce, 1973).

At least eight sandstone-shale wedges are recognized along the Texas Gulf Coast (Hardin, 1961), but they vary considerably in sandstone content

and distribution, and in the degree to which they were affected by growth faulting. Wedges identified as the Wilcox Group and the Vicksburg and Frio Formations contain the greatest number of sandstone units that are potential geopressured reservoirs for the Texas Gulf Coast region.

Project Description and Results

The process of selecting shallow geopressured and deep hydropressured test sites within the study area was carried out in four general steps. First, geopressured and deep hydropressured sandstone corridors were identified. A corridor is a linear belt roughly parallel to the Texas Gulf coastline in which Tertiary sandstones occur with the specified pressure and/or temperature conditions of a given geopressured or deep hydropressured zone. Recognized corridors correspond to the Wilcox and Frio/Vicksburg sandstone trends. Secondly, five areas of greatest net-sandstone thickness were outlined as geopressured fairways within the corridors. The average size of these fairways is roughly equal to one or two Texas counties. Thirdly, prospect areas, encompassing either single fault blocks or several adjacent fault blocks, were selected within each fairway for detailed geologic and engineering studies. Finally, four test-well sites were selected on the basis of net sandstone, structure, sandstone continuity, reservoir sandstone size, temperature, pressure, salinity, porosity, and permeability trends within the prospect areas. Three of the four sites were also found to be favorable for tests of the deep hydropressured zone. In addition, three other areas were studied, but no test sites were selected because certain data critical in prospect evaluation and site selection were not available (see Conclusions and Recommendations).

The site selection task involved standard methods of assessing the geologic and engineering parameters of prospective areas. Principal

geologic methods included (1) correlating electric logs (primarily resistivity and spontaneous potential [SP] logs) for tracing marker beds, determining lithologic changes and sandstone continuity, and locating faults; (2) measuring and mapping net sandstone for intervals of interest; (3) mapping structure at significant subsurface horizons; and (4) relating reservoir parameters to geologic units and establishing trends within intervals of interest in the prospect areas. Engineering methods included calculation or application of data in determining temperature, pressure, salinity, porosity, permeability, and for a few selected wells, methane solubility in prospective areas.

Rationale for Study and Projected Benefits to Ratepayers

As conventional natural gas resources are depleted and the price of gas and other hydrocarbons continues to climb, the methane entrained in subsurface waters becomes more attractive as an unconventional energy resource. Although parameters governing the amount of methane in solution and the entrained methane resources in place in a given area have often been estimated, too few actual tests (most of which were in the deep geopressured zone) have been made, and too few data have been gathered for a reasonable study of the feasibility of producing this resource. Many of the questions concerning the resource, its magnitude, and producibility can be answered only by drilling wells and testing the resource.

During the geopressured-geothermal studies funded by DOE, researchers became concerned that there was not adequate permeability in geopressured reservoirs to sustain high flow rates. Permeability and porosity increase significantly in zones shallower than that believed prospective for geothermal development (with fluid temperatures greater than 300° F). In addition to having better reservoir quality, shallower geopressured zones

will be less expensive to drill than deeper zones. On the other hand, pressures and temperatures are lower in the shallow geopressured zone, and therefore, methane solubility generally is less than at greater depths. The magnitudes of these advantages and disadvantages of producing methane-bearing water from the shallow geopressured zone are some of the important unknowns that need to be determined.

Although this study did not investigate the economic questions nor the technical problems of completing wells and producing the entrained methane, it accomplished the essential first step of locating sites favorable for tests. For natural gas producers and transporters, such as the GRI rate-payers, benefits of testing the potentially large resource should be obvious. Well-planned testing should show either that the resource is economically and technically feasible to produce now or in the near future, or that development of the resource is premature.

METHODOLOGY

Work Plan

Tasks involved in reaching the objectives of this project are broadly outlined in the work schedule (fig. 3). Task 1, performed throughout the study, was to keep GRI informed about the progress of the project, as well as related DOE-funded studies, in order to facilitate interaction between DOE and GRI research efforts.

Task 2 consisted of analyses of the organic content and character of cutting samples from the General Crude Oil (GCO) and DOE No. 1 Pleasant Bayou well, Brazoria County, Texas. This work, funded through the initial contract with GRI, was subcontracted to GeoChem Laboratories, Incorporated, and Geo-Strat, Incorporated, and will not be discussed in this report. Results of the organic analyses are reported in "Hydrocarbon Source Facies

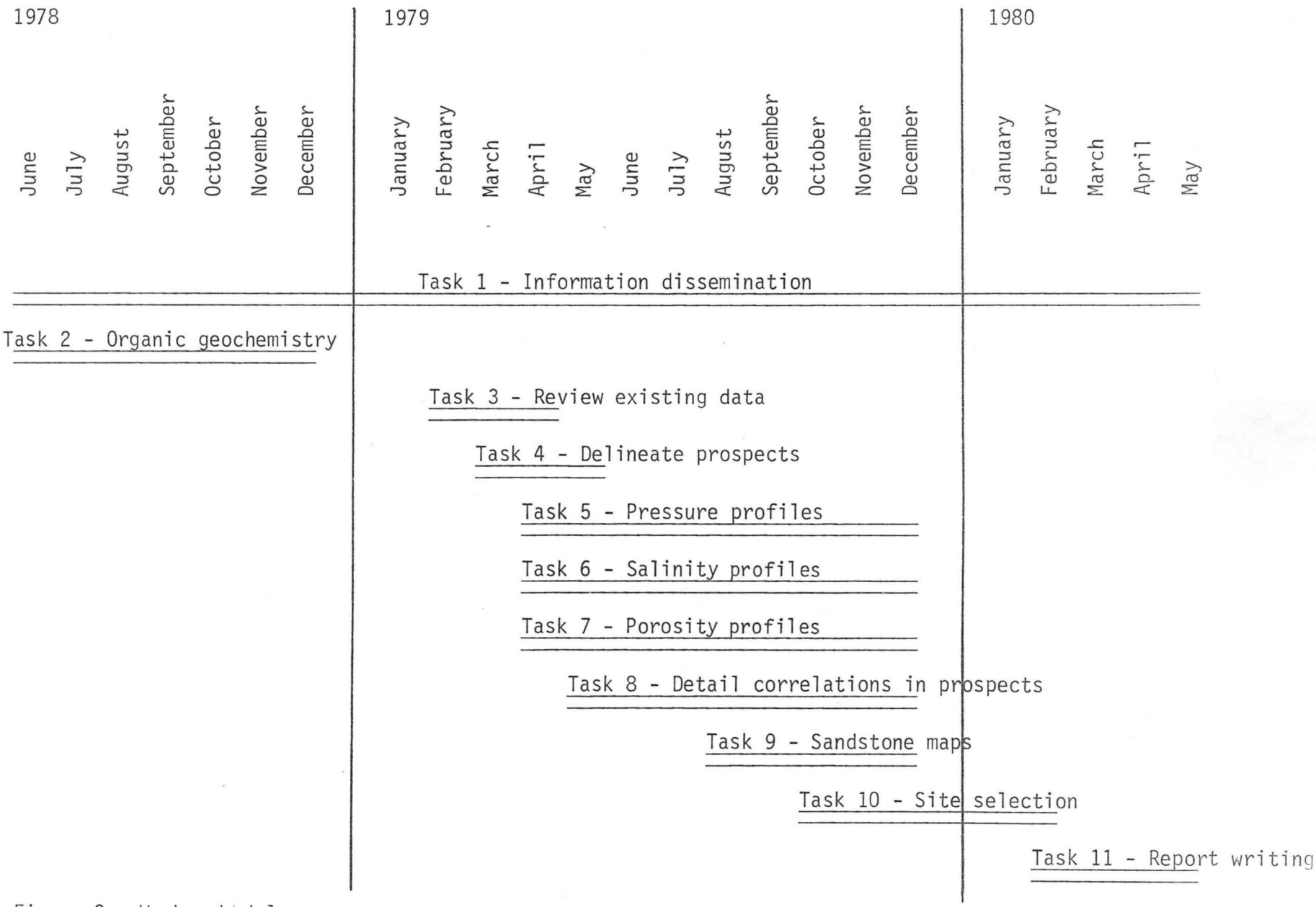

Figure 3. Work schedule.

Analysis, Department of Energy and General Crude Oil Company Pleasant Bayou Nos. 1 and 2 Wells, Brazoria County, Texas" by GeoChem Laboratories, Incorporated (1979), and "Visual Kerogen and Vitrinite Reflectance Analyses of the Pleasant Bayou No. 1 Well, Brazoria County, Texas" by Geo-Strat, Incorporated (1979). Information concerning these reports may be obtained from GRI.

Task 3 was the review of data collected for previous Texas Gulf Coast studies, particularly the geopressured-geothermal studies funded by DOE.

Task 4, the identification of prospects, involved several steps. First, boundaries of zones within the geopressured and deep hydropressured Tertiary section were defined. Broad sandstone corridors corresponding to the Frio/Vicksburg and Wilcox trends were outlined for each of the zones. Fairways, which are areas of maximum net sandstone, were identified within each corridor on the basis of regional net-sandstone maps. Finally, prospect areas composed of single fault blocks or several adjacent fault blocks were selected for detailed study within the fairways.

Tasks 5, 6, and 7 were engineering studies determining pressure, salinity, and porosity profiles of wells in the prospect areas. Also, permeability data were gathered, although whole-core analyses were scarce within most of the prospect areas. Thus, the additional task of investigating porosity/permeability relationships was undertaken.

Task 8 consisted of detailed geologic studies of the prospect areas, including correlations of well logs and construction of structural and stratigraphic cross sections. Task 9, construction of net-sandstone maps, was performed for intervals of interest in the prime prospect areas. Task 10, test-well site selection, involved the assemblage and analysis of all the geologic cross sections, structure maps, sandstone maps, and temperature, pressure, salinity, porosity, and permeability data to recognize

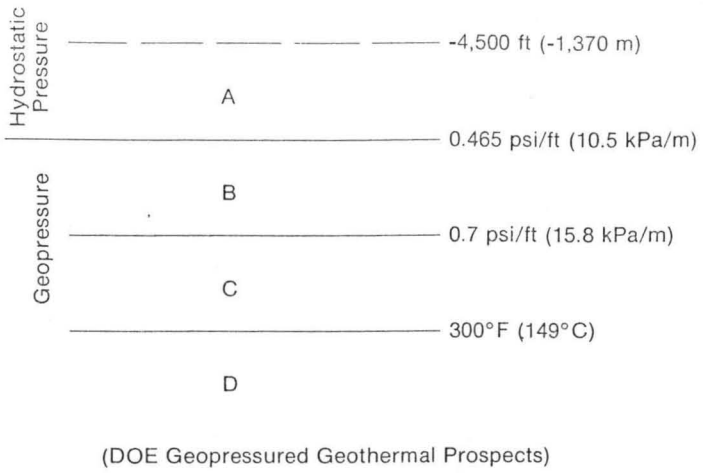

Figure 4. Definition of geopressured and deep hydropressured zones.

trends of the various parameters within the prime prospect areas and choose sites favorable for producing and testing methane-bearing waters from the shallow geopressured zone.

Definition of Pressure Zones

To provide an operational base for this study, four zones were defined within the Gulf Coast Tertiary section according to pressure gradients and temperatures (fig. 4). The A Zone is the deep hydropressured zone below a depth of 4,500 ft in which the pressure gradient is hydrostatic (0.465 psi/ft). The B Zone is a relatively thin zone of transition from hydrostatic pressure gradients (0.465 psi/ft) to abnormally high pressure gradients of about 0.7 psi/ft. The C Zone has fluid pressure gradients greater than 0.7 psi/ft and fluid temperatures less than 300° F. In the D Zone, fluid pressure gradients are greater than 0.7 psi/ft and fluid temperatures are greater than 300° F. This study concentrates on the A, B, and C Zones; the D Zone has been the subject of previous studies funded by DOE.

Total thickness of each zone varies considerably over the Gulf Coast area. For example, in some areas, 300° F temperatures occur several

thousand feet deeper than the shallowest occurrences of the 0.7 psi/ft pressure gradient, resulting in a thick C Zone. In other areas, 300° F temperatures occur at approximately the same depths as 0.7 psi/ft pressure gradients; thus, the C Zone in these areas is either very thin or absent.

Depths to the tops of the zones also vary. The top of the B Zone, for example, occurs at depths ranging from approximately 5,000 to 12,000 ft in the study area. For this reason, the upper boundary of the A Zone was set at a depth of 4,500 ft to ensure that all of the B Zone would be included in the study. Consequently, the A Zone is thin in the area where the top of the B Zone is shallowest.

Parameters Used in Prospect Evaluation

Net Sandstone

Marker beds, most commonly low-resistivity shales that are laterally very continuous, were selected for correlation within each prospect area. Few of these correlation markers can be traced beyond the specific prospect area in which they were selected. Thus, most of the prospects have unique sets of correlation markers.

The correlation markers permitted division of thick sandy sections in the shallow geopressured and deep hydropressured zones into smaller intervals for detailed study. For intervals of prime interest, net sandstone was measured from electric logs and mapped. In some areas, intervals consist of a series of genetically related sandstones and shales. In other areas, however, many intervals are composed of sandstones and shales of more than one depositional system. Therefore, the net-sandstone maps of those intervals should not be used for genetic interpretation. The maps are useful to show sandstone distribution and areas of maximum sandstone thickness where test-well sites may be located.

Continuity of Sandstones

Vertical continuity of sandstones can be observed on individual electric logs. Lateral continuity, on which reservoir capacity of individual sandstone bodies partially depends, can be adequately determined only with dense well control. Sandstone boundaries resulting from faults, depositional pinch-outs, or erosional truncations must be identified in order to determine the areal extent of reservoir sandstones. Because the density of wells varied from area to area, the degree of certainty of reservoir sandstone continuity varied considerably. In general, however, gross characteristics of sandstones, including lateral continuity, could be judged well enough for comparison of sandstones to help select prospective intervals and test-well sites.

It should be emphasized that sandstone continuity is not equivalent to reservoir continuity. One important factor controlling reservoir continuity but not sandstone continuity is diagenesis. Well-cemented sandstones serving as effective reservoir boundaries cannot be detected in an electric log study alone. Detailed study of cores, unavailable for this project, is essential for identifying the cemented zones.

Volume of Reservoir Sandstones

Size of individual reservoirs cannot be determined with the data available in this study nor can the size of individual sandstone bodies be precisely calculated. However, net volume of reservoir sandstones in a given interval can be estimated by multiplying the area of the prospective fault block by the average net sandstone calculated for the interval within the block.

Heat Flow and Formation Temperature

Heat from deep within the earth moves outward to the surface where it is lost as radiant energy into the atmosphere or ocean. The flow of heat, Q, varies in different areas but is essentially constant for a specific locality in a basin (Hunt, 1979). The equation for the flow of heat is

$$Q = k_h A\left(\frac{\Delta T}{Z}\right) \qquad (1)$$

where k_h is the coefficient of thermal conductivity of the material, A is the cross-sectional area of the material measured perpendicular to the flow of heat, and ΔT is the temperature change across the material of thickness Z. When the flow of heat encounters an insulating material with an abnormally low value of k_h, the temperature rises at the face of the material until ΔT is large enough to restore Q to a constant equilibrium value. Hence, to achieve equal flow rates through heat insulators (low values of k_h) and heat conductors (higher values of k_h) occurring in series, a higher temperature gradient is required across the insulator.

Lewis and Rose (1970) developed the concept that geopressured zones are heat insulators with low values of k_h; hence, abnormally high geothermal gradients are expected to exist across them. The low values of k_h in geopressured zones are caused by the higher water content of sediments in these zones. For example, the k_h value for water is 0.363 Btu/hr ft °F which is about one-third of the k_h values for the rock matrices of shale and sandstone. This means that an increase in porosity will reduce the thermal conductivity and increase the geothermal gradient of most sediments. In sandstone/shale sequences, shales have lower thermal conductivity than sandstones. The value of k_h for slate is about 1.138 Btu/hr ft °F; presumably dry shale has about the same value of k_h as

slate. Sandstone has a k_h value of 1.330 Btu/hr ft °F. Therefore, an increase in the sandstone/shale ratio increases the thermal conductivity and decreases the geothermal gradient. The criteria discussed above help explain the "doglegs" observed in geothermal gradients of many geopressured sediments in the Gulf Coast area. The presence of high porosity and low sandstone/shale ratios in geopressured zones causes the geothermal gradient to be higher than in more normally pressured zones located above or below the geopressured zone (Hunt, 1979).

In most areas of the Gulf Coast, the average geothermal gradient is relatively low in the hydropressured zone (a heat conductor), increases substantially through the geopressured zone (a heat insulator), then declines in the underlying zone (a heat conductor), which presumably has more normal pressures as predicted by the model of Lewis and Rose (1970). It is not always easy to document the existence of normally pressured formations in this deep underlying zone that forms the third portion of the geothermal gradient dogleg. An example with incomplete documentation exists in Lavaca County (fig. 5), where the gradient is 1.44° F/100 ft in the hydropressured zone, increases to 3.5° F/100 ft in the geopressured interval at depths from 10,000 to 13,000 ft, then declines to 1.28° F/100 ft below the depth of 13,000 ft. Bottom-hole shut-in pressures plotted for depths below 13,000 ft in Lavaca County (fig. 6) indicate that 70 percent of the formations that were tested had low or subnormal pressure gradients. The remaining 30 percent of the formations had pressure gradients of 0.75 psi/ft or more. Three sandstones located at average depths of 11,781, 12,892, and 13,279 ft were tested in the Magnolia No. 1 Simpson Heirs well. The two shallower sandstones had normal and subnormal pressure gradients (fig. 6), whereas the third and deepest sandstone had a pressure gradient of

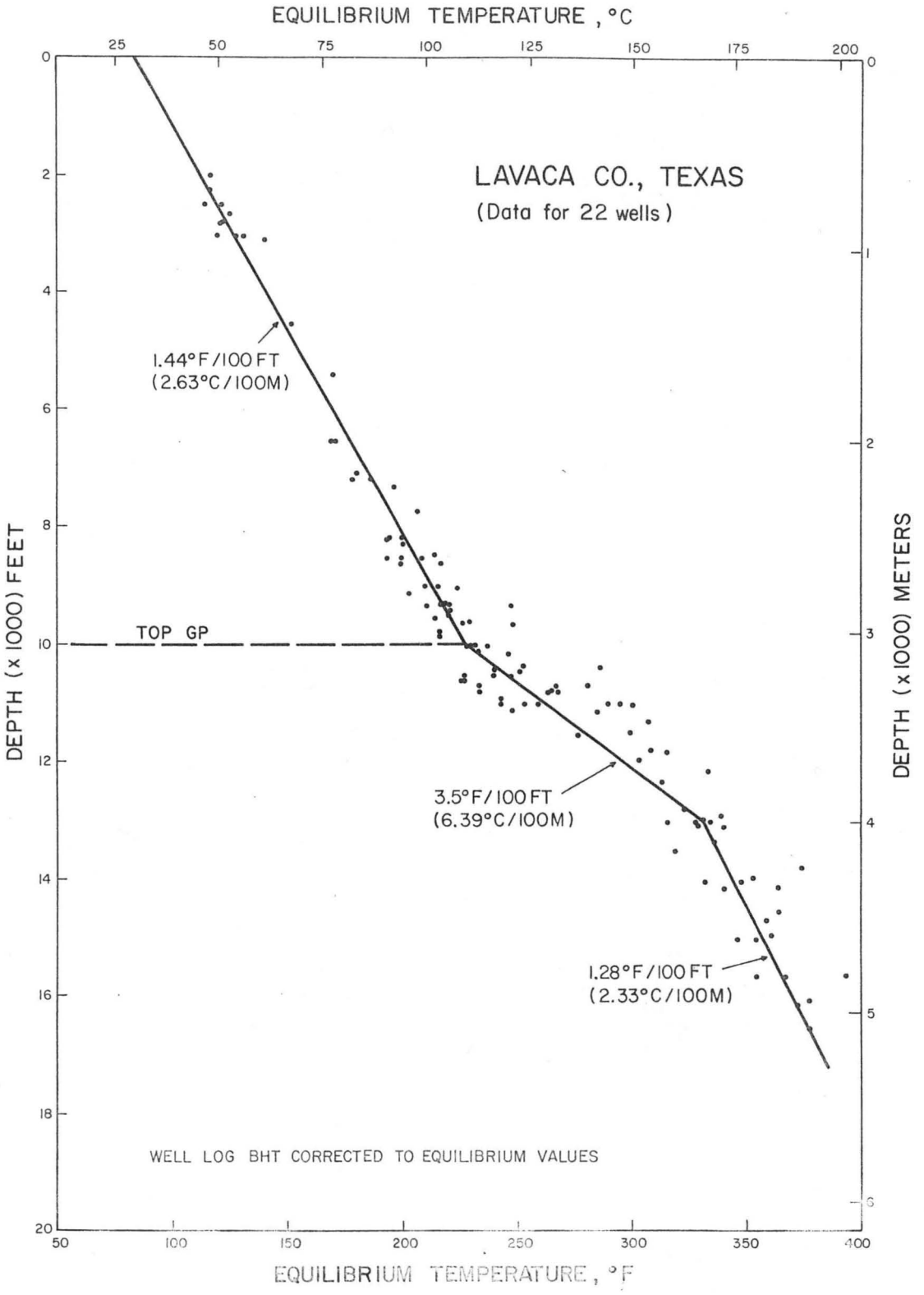

Figure 5. Dogleg geothermal gradients based on well log temperatures corrected to equilibrium values for 22 wells, Lavaca County, Texas.

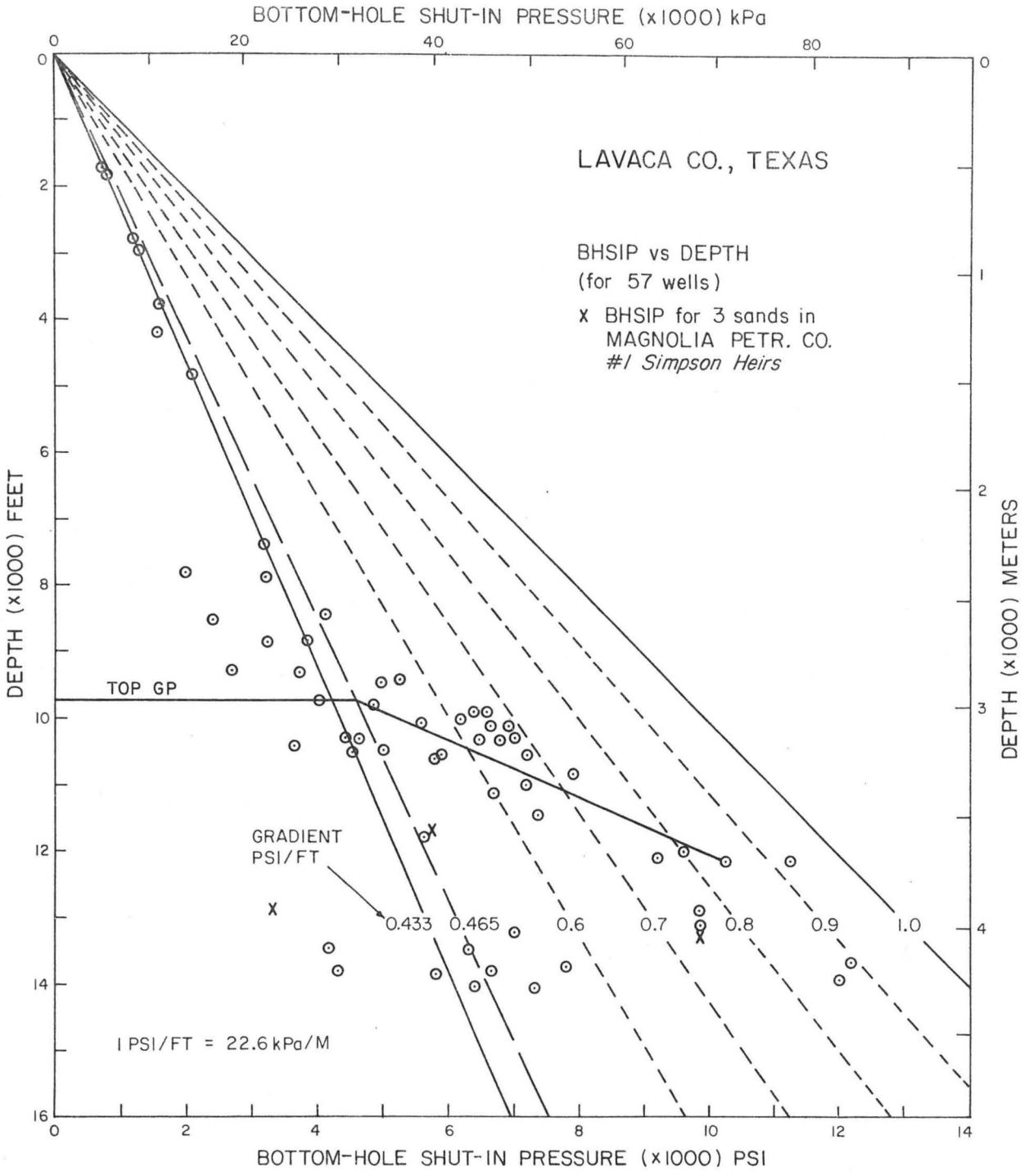

Figure 6. Bottom-hole shut-in pressures versus depth for 57 wells, Lavaca County, Texas.

0.74 psi/ft. All of these sandstones are relatively deep and illustrate the variability of formation pressures in a depth zone where consistently high pressures might be predicted from the general trend of data in the area. Deep zones containing some sandstone units with low pressures (fig. 6) may act as heat conductors and cause the reduced geothermal gradient observed below the depth of 13,000 ft in Lavaca County (fig. 5).

Dogleg geothermal gradients are also observed in Matagorda County (fig. 7), where the Old Ocean and Blessing Prospect Areas are located. The first bend in the dogleg provides an estimate of the top of geopressure. In this case, the reduced geothermal gradient in the third and deepest part of the dogleg occurs in the D Zone at depths below 14,000 ft. In most areas of the Gulf Coast, the deep part of the dogleg occurs below the 300° F isotherm and, therefore, is outside the primary range of interest in this study.

The preceding discussion shows that the geothermal gradient is useful for locating the top of geopressure in an area with adequate well control. The top of geopressure in Lavaca County, for example, can be located from the temperature versus depth plot (fig. 5) with equal or greater confidence than from the bottom-hole shut-in pressure versus depth plot (fig. 6). However, this relationship is not always true in other areas.

Formation temperature has an important influence on diagenetic processes in shales and sandstones. Montmorillonite converts to illite at an increased rate in the approximate critical range of subsurface temperatures from 200° to 220° F (Burst, 1969). Freed (1980) found that the increased rate of conversion of montmorillonite to illite also seems to be associated with the top of geopressure in the No. 1 Pleasant Bayou well, Brazoria County, Texas (fig. 8).

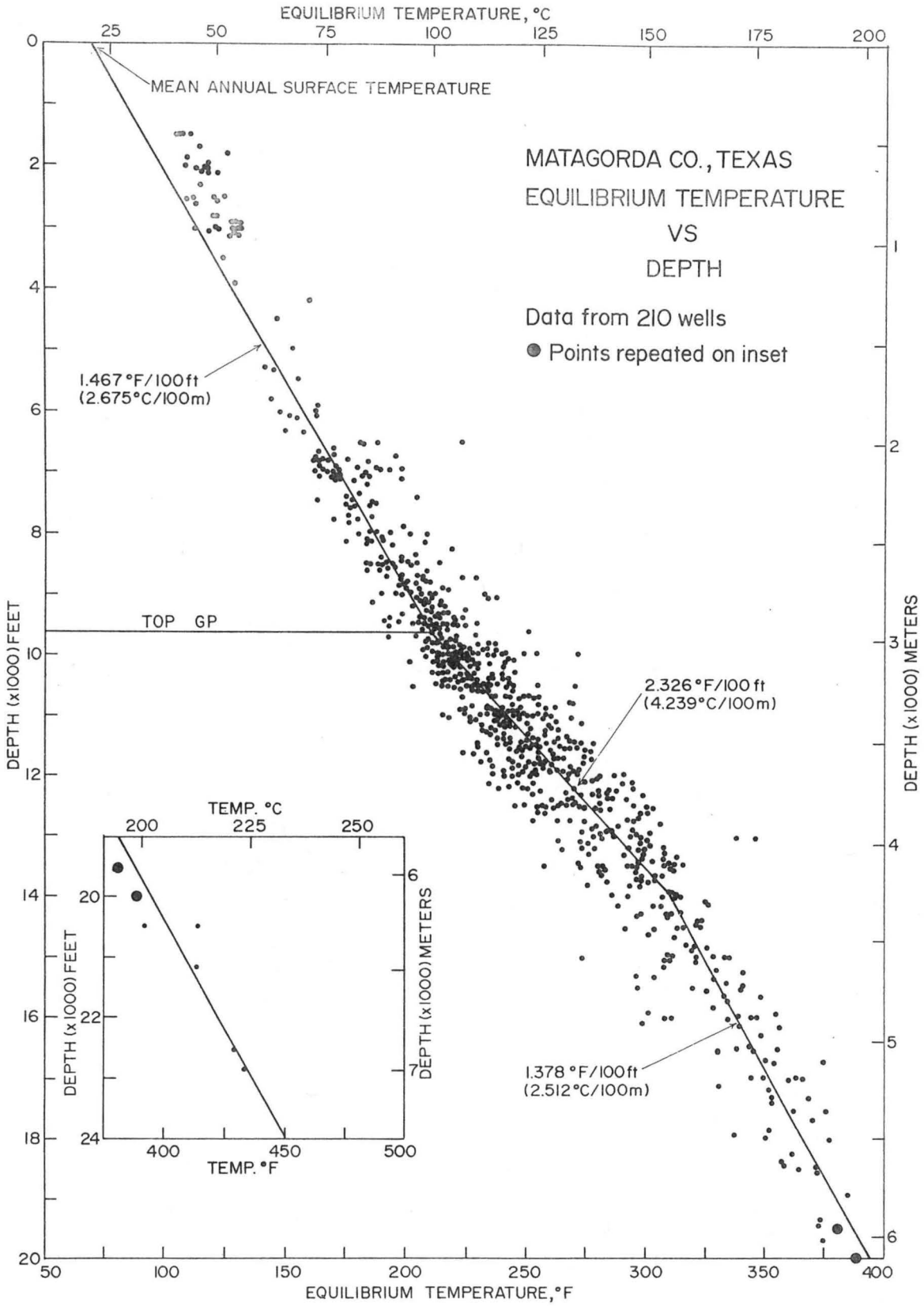

Figure 7. Dogleg geothermal gradients based on well log temperatures corrected to equilibrium values for 210 wells, Matagorda County, Texas.

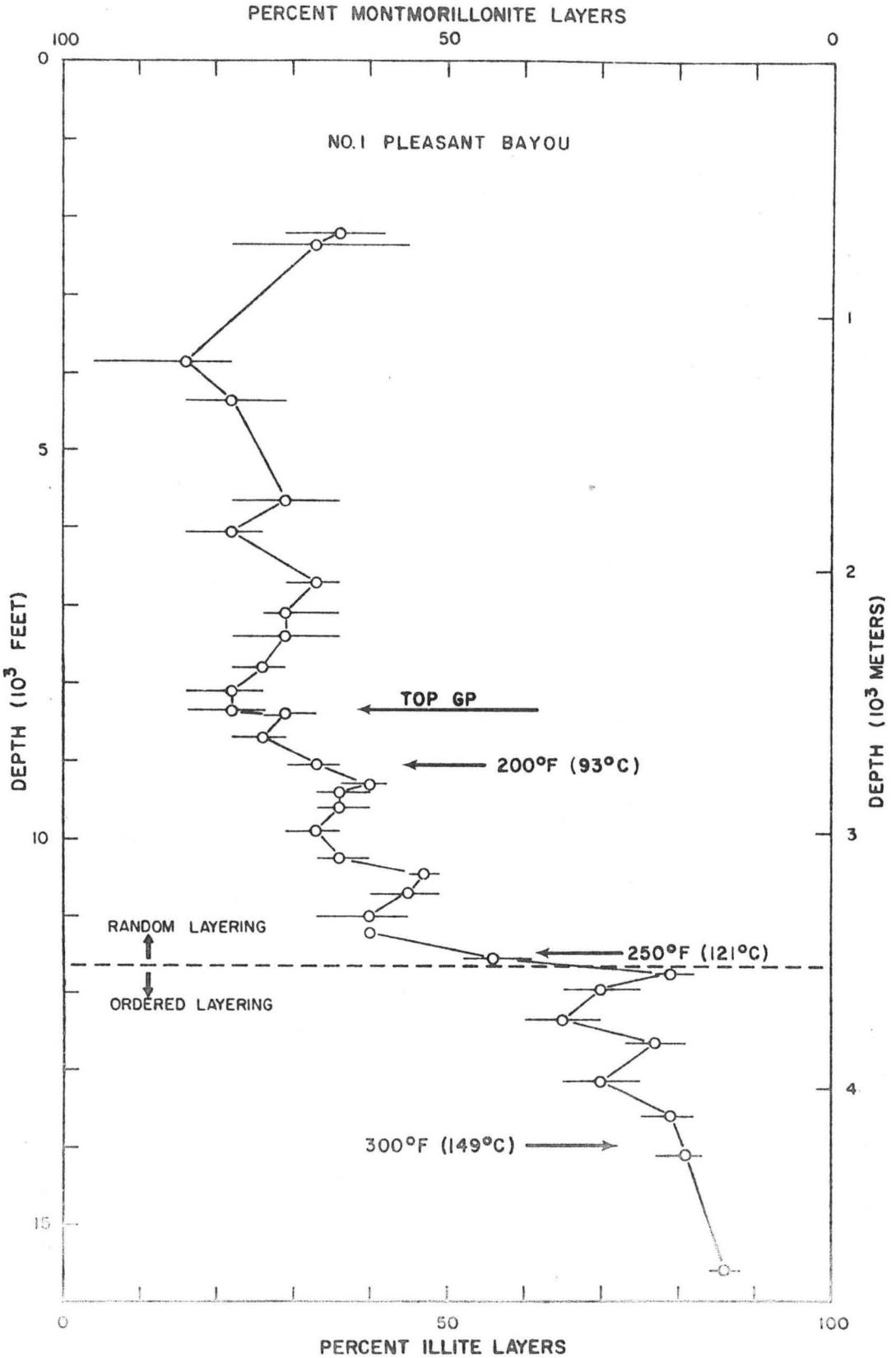

Figure 8. Change in montmorillonite and illite content of shales as a function of depth, General Crude - Department of Energy No. 1 Pleasant Bayou, Brazoria County, Texas (after Freed, 1980).

Formation temperatures in this report are corrected to equilibrium values by the following equation of Kehle (1971):

$$T_E = T_L - 8.819 \times 10^{-12}D^3 - 2.143 \times 10^{-8}D^2 + 4.375 \times 10^{-3}D - 1.018 \qquad (2)$$

where T_E = equilibrium temperature (°F)

T_L = temperature recorded on well log header (°F)

D = depth (ft).

Temperature gradient is the slope of the least squares linear fit of equilibrium temperature data as a function of depth. The gradients are expressed in °F/100 ft and °C/100 m.

Formation Pressure

Formation fluid pressures can be derived from shale resistivity or acoustic travel time data using the method of Hottmann and Johnson (1965). Data from induction logs and from drill-stem tests (DST) for 31 selected wells in Matagorda County (table 1) are used to illustrate the shale resistivity method. Shale resistivity values (R_{sh}) from amplified short normal resistivity curves of induction logs are plotted as a function of depth for both hydropressured and geopressured zones (fig. 9). The normal compaction curve was drawn by a least-squares-regression method. All R_{sh} data fall near this curve when shales are normally pressured or slightly geopressured; R_{sh} data falling to the left of this curve are lower than normal, indicating that pressure gradients are significantly greater than normal and may approach 1 psi/ft in highly geopressured zones.

Wells with bottom-hole shut-in pressure (BHSIP) from DST (table 1) were plotted on a shale resistivity versus depth plot (fig. 10), using the R_{sh} value of shales nearest the sandstone formations that were perforated for DST. Measured values of bottom-hole shut-in pressure and pressure

Table 1. Wells in Matagorda County, Texas, for which bottom-hole shut-in pressure data were available from drill-stem tests.

Well No.	Tobin Grid	Operator	Well Name	Depth (ft)	FPG (psi/ft)	BHSIP (psi)
1	9S-31E-8	Coastal States	No. 2 Cornelius	9,096	0.47	4,317
3	9S-32E-9	Monsanto	No. 1 Mehrens	10,754	0.74	8,075
3	10S-30E-6	C&K Petroleum	No. 1 Potthast	10,509	0.56	5,849
6	10S-30E-6	Tenneco	No. 1-A Gresham	10,538	0.71	7,499
9	10S-30E-6	Tenneco	No. 4 Trull	10,678	0.48	5,136
15	10S-30E-8	Texkan	No. 1 Neuszer	9,821	0.48	4,670
13	10S-30E-8	Tenneco	No. 1 Davis	12,105	0.70	8,477
24a	10S-30E-7	Texkan	No. 1 Slone	10,919	0.69	7,563
24b				10,668	0.71	7,609
26	10S-31E-1	Texkan	No. 1 Cunningham	9,756	0.60	5,879
27a	10S-31E-5	Superior	No. 1 Nelson	9,117	0.46	4,625
27b				9,379	0.49	4,220
27c				9,512	0.42	3,995
28	10S-31E-1	Texkan	No. 1 McKissick	11,505	0.72	8,249
29a	10S-32E-2	Humble	No. 1 Pierce Estate	11,330	0.76	8,720
29b				11,434	0.76	8,654
30	10S-32E-2	Humble	No. 1-C Lewis	10,248	0.69	7,022
33	10S-31E-1	Texkan	No. 1 Peterson	10,663	0.74	7,848
34a	10S-31E-1	Apache	No. 1 Murphy	10,089	0.58	5,892
34b				10,044	0.63	6,365
35	9S-32E-9	Monsanto	No. 1 Moers	9,981	0.50	5,032
18	9S-31E-7	Monsanto	No. 1 Fay	10,125	0.50	5,107
1	9S-32E-1	Cosden Petroleum	No. 1 Cornelius Unit 2	12,340	0.81	9,996
2	11S-34E-3	Ethyl Corporation	No. 1 Baer Ranch	15,700	0.82	12,923
4	10S-34E-9	Falcon Seaboard	No. A-3 Baer Ranch	14,460	0.89	12,850
5	10S-34E-9	Falcon Seaboard	No. A-4 Ber Ranch	13,440	0.84	11,225
14	10S-31E-6	Belco Pet. Corp.	No. 1 Johnson	10,010	0.71	7,115
3	11S-34E-3	Falcon Seaboard	No. A-5 Baer Ranch	14,710	0.78	11,414
5	10S-31E-9	Gardner-Lowe	No. 1 HNG, et al.	14,000	0.76	10,656
7	10S-32E-9	Halbouty	No. 1 Kubela	9,635	0.78	7,517
10	10S-32E-5	Royal Resources	No. 1-A Pierce Estate	11,330	0.78	8,786

Table 1 (cont.)

Well No.	Tobin Grid	Operator	Well Name	Depth (ft)	FPG (psi/ft)	BHSIP (psi)
13	10S-32E-4	Royal Resources	No. 1 Steele	11,130	0.75	8,355
	11S-30E-2	Sinclair	No. 1 Salsbury	10,055	0.78	7,883
35 a	10S-30E-7	Socony Mobil	No. 1 G. Harrison	10,800	0.75	8,104
35 b				10,550	0.76	8,029
11	10S-33E-1	Magnolia	No. 6 Cornelius	11,120	0.67	7,401

gradients from DST are also shown at the average depth of the perforated sandstone intervals. These wells have pressure gradients ranging from 0.42 to 0.89 psi/ft. Many of the perforated sandstones are considered to be geopressured by the conventional definition (pressure gradients exceed 0.465 psi/ft) applicable in the Gulf Coast area. Shale resistivities are lower than normal and fall to the left of the normal compaction curve. Figure 10 shows how the resistivity ratio between the normal values ($R_{sh(n)}$) on the normal compaction curve and the observed values ($R_{sh(ob)}$) from resistivity logs for the 31 wells are used to establish the best relationship for converting resistivity ratio to pressure gradient (fig. 11). The shale resistivities of these 31 wells are believed to be representative of shales in the depth interval 2,000 to 16,000 ft in Matagorda County. Hence, for most wells in Matagorda County, the shale resistivity ratio curve (fig. 11) can be used to calculate pressure profile data; an example of a computed geopressure profile (fig. 12) is shown at four depths below 9,900 ft in the Texaco No. 16 Thomas.

Ideally, the top (0.465 psi/ft) and bottom (about 0.7 psi/ft) of the B Zone should be determined for each well from pressure data that are available for that well. Normally, the bottom of the B Zone (about 0.7 psi/ft)

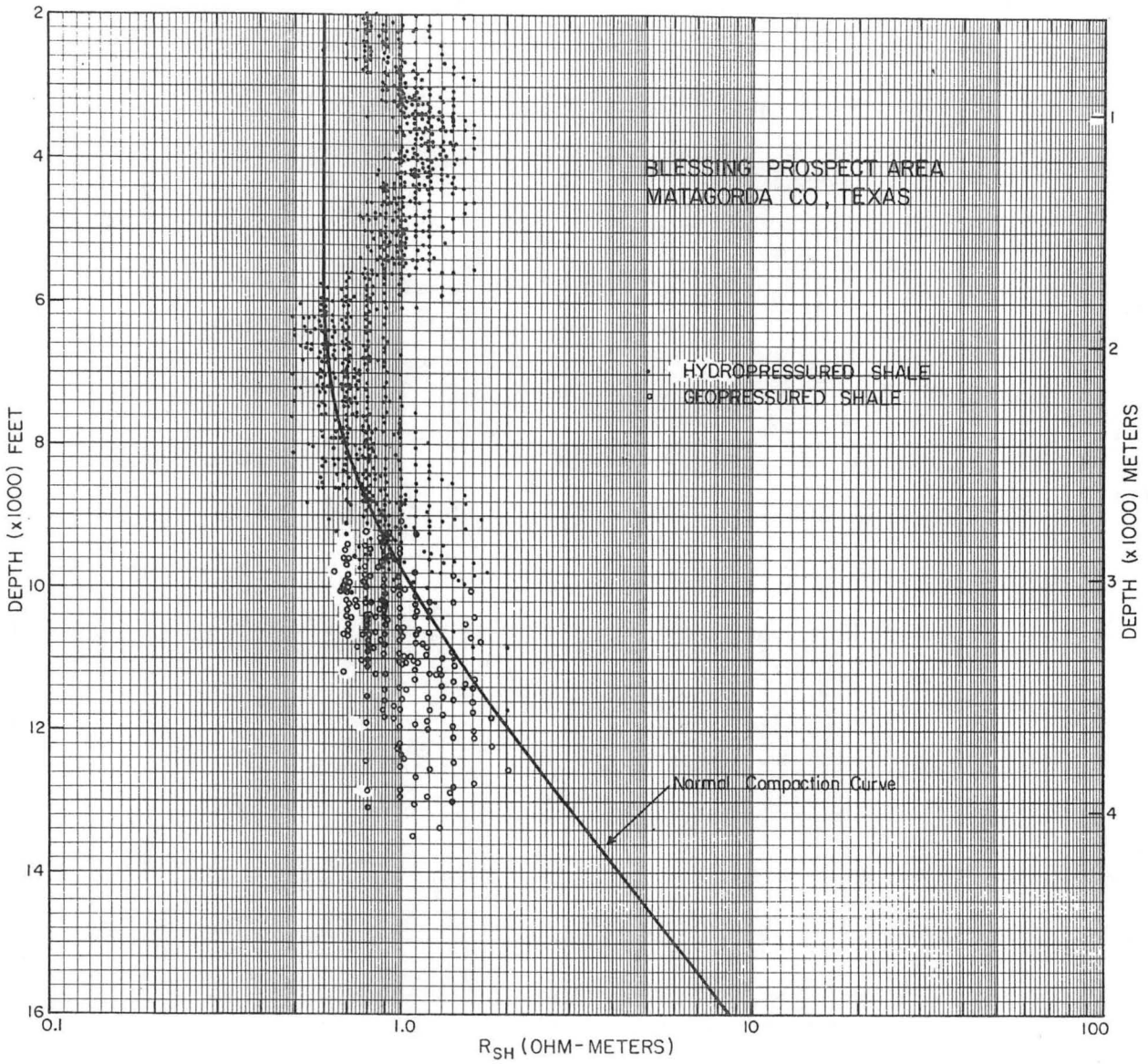

Figure 9. Resistivity versus depth for hydropressured and geopressured shales, Blessing Prospect Area, Matagorda County, Texas.

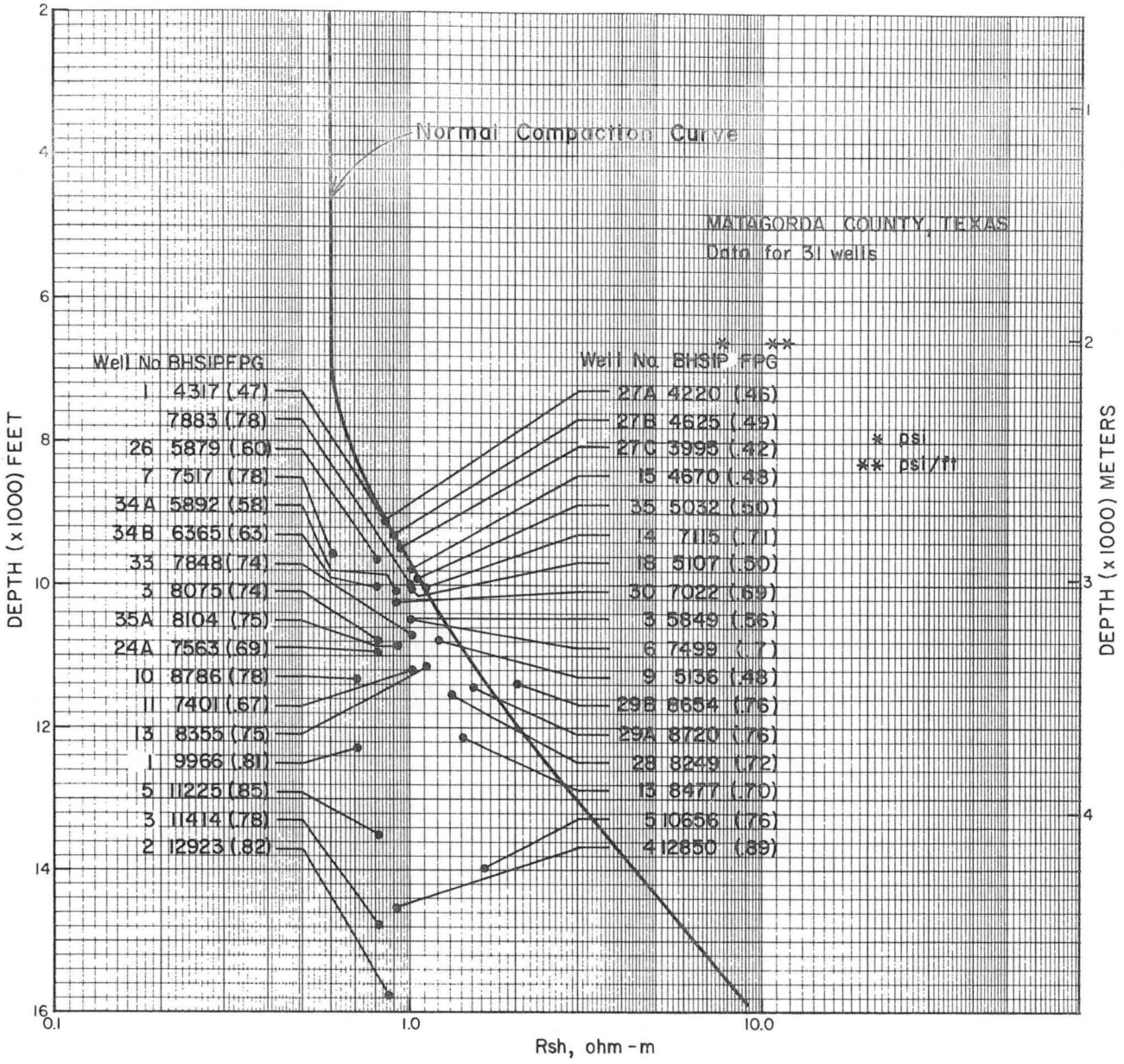

Figure 10. Shale resistivity versus depth, bottom-hole shut-in pressures, and pressure gradients for perforated sandstones in 31 wells, Matagorda County, Texas.

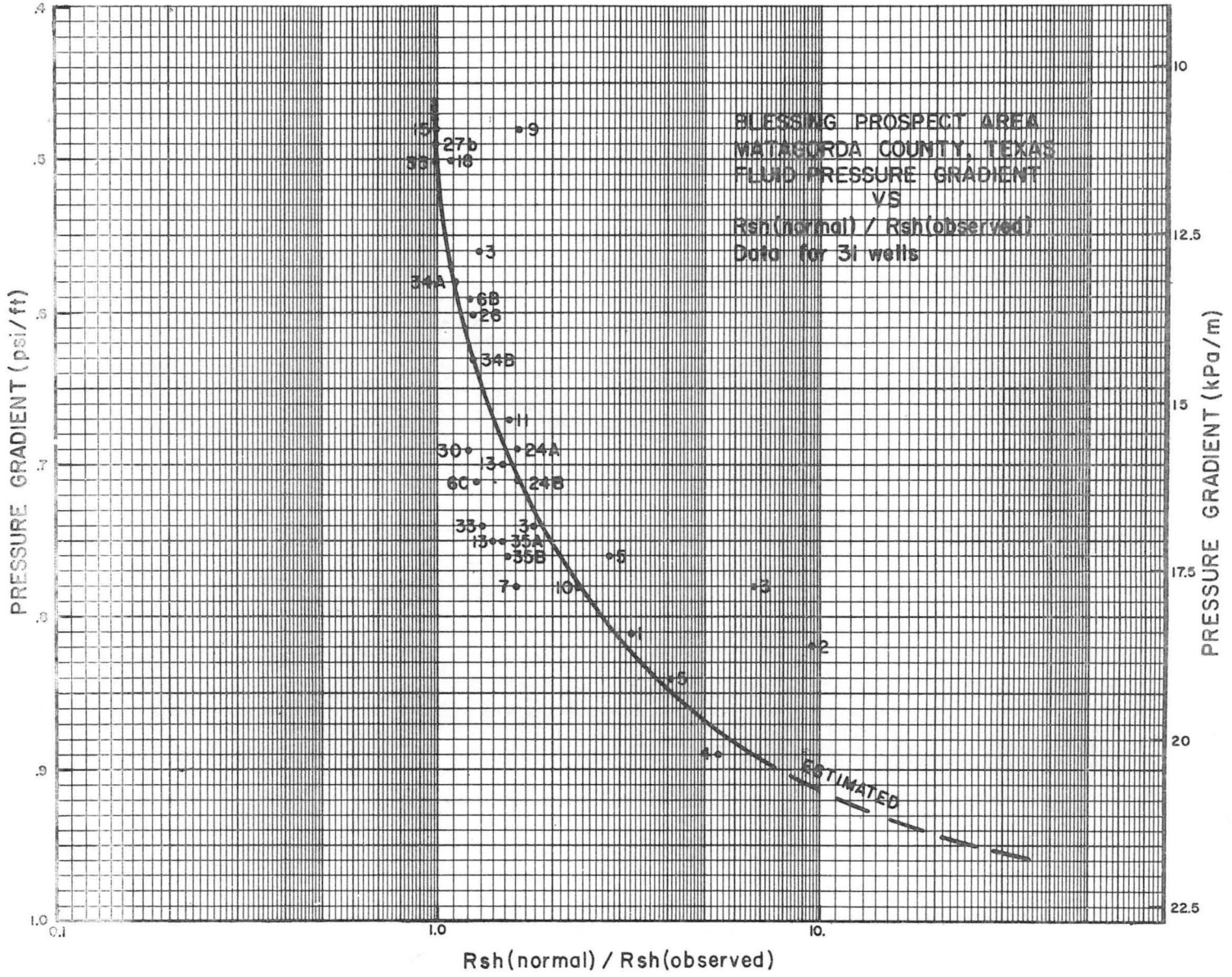

Figure 11. Curve for converting ratio of normal and observed values of shale resistivity to pressure gradient, Blessing Prospect Area, Matagorda County, Texas.

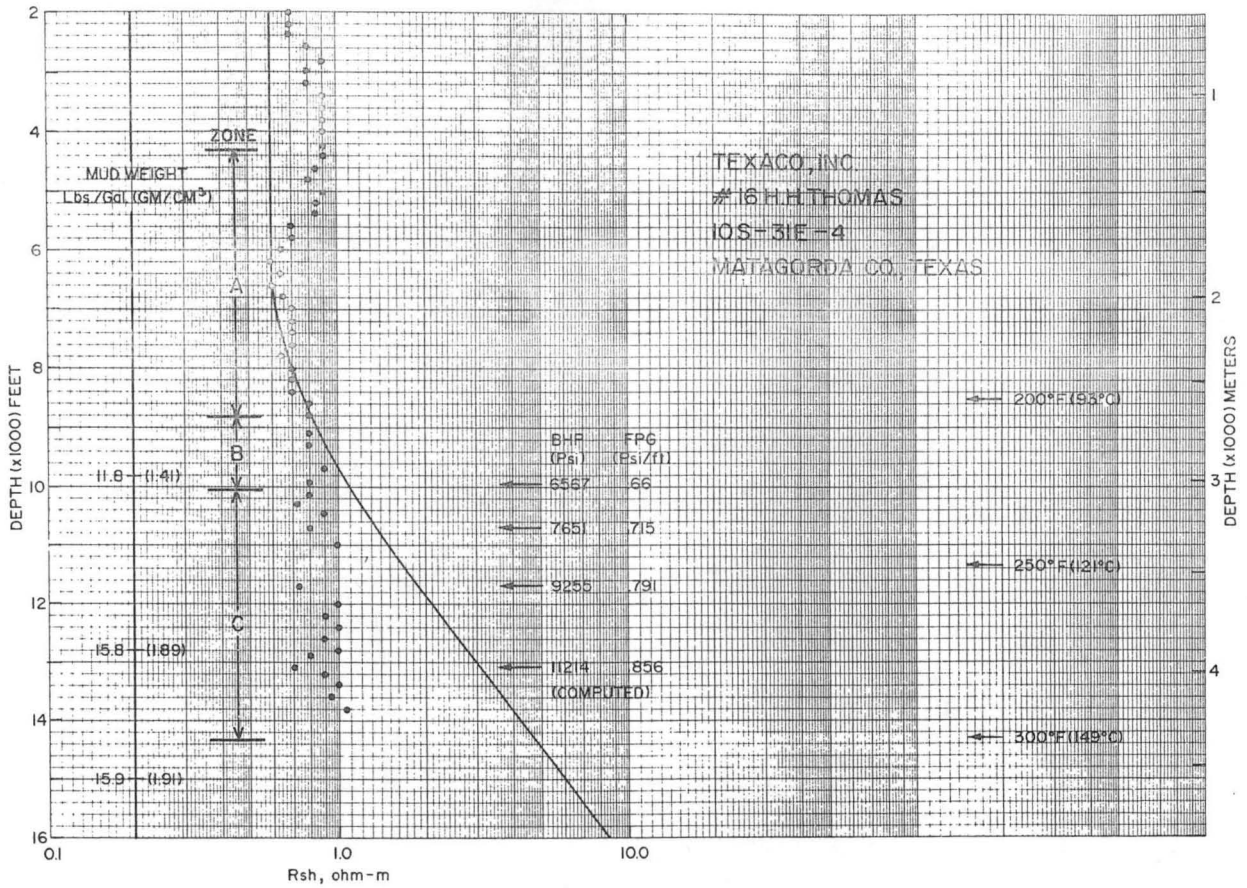

Figure 12. Shale resistivity, mud weight, isotherms, pressure zones, and computed bottom-hole pressures versus depth, Texaco No. 16 Thomas, Blessing Prospect Area, Matagorda County, Texas.

can be determined by an interpretive process after considering some or all of the following types of information: (1) depth at which shale resistivity (fig. 12) or shale transit time departs from the normal compaction trend for the area, (2) pressures and pressure gradients determined from a shale resistivity ratio plot (fig. 11) or from shale transit time difference plots (Gregory and Backus, 1980), (3) mud weights from well log header information, and (4) pressures from drill-stem tests of perforated sandstone intervals.

The top of the B Zone is less easily determined from commonly available information than is its base. For many wells, some logs either were

not run or were not available from the operator for proprietary reasons. Shale resistivity data in many areas of the Gulf Coast are not easily interpreted to locate a pressure gradient of 0.465 psi/ft. Mud weights from well log headers are also unreliable for this purpose. Hence, it was necessary in this study to determine the top of the B Zone from average curves determined for county or prospect area plots of BHSIP and temperature. In Matagorda County, plots of BHSIP versus depth (fig. 13) and equilibrium temperature versus depth (fig. 7) are about equally effective for locating the depth where pressure gradients begin to exceed 0.465 psi/ft. Average thickness of the B Zone indicated by the BHSIP versus depth plot is 1,250 ft. The upper boundary of the B Zone on geologic cross sections and formation parameter plots for wells in Matagorda County is located by subtracting 1,250 ft from the depth of the base of the B Zone (about 0.7 psi/ft gradient) as determined by some or all of the four types of information listed above. Hence, for any given county or prospect area, the B Zone defined by the above methods has a constant thickness but variable depth. For example, the bottom of the B Zone in the Texaco No. 16 Thomas well (fig. 12) is located at a depth of 10,050 ft and the top of the B Zone is located 1,250 ft higher in the section at a depth of 8,800 ft. The disadvantage of using an average curve to determine the top of the B Zone is that it tends to mask local variations in the top of geopressure shown by individual wells. For example, tops of geopressure in many wells in Matagorda County (fig. 7), as well as in other areas, actually lie 1,000 ft or more above or below the average, as indicated by the BHSIP data (fig. 13). However, a better method for determining the top of geopressure from available data was not found.

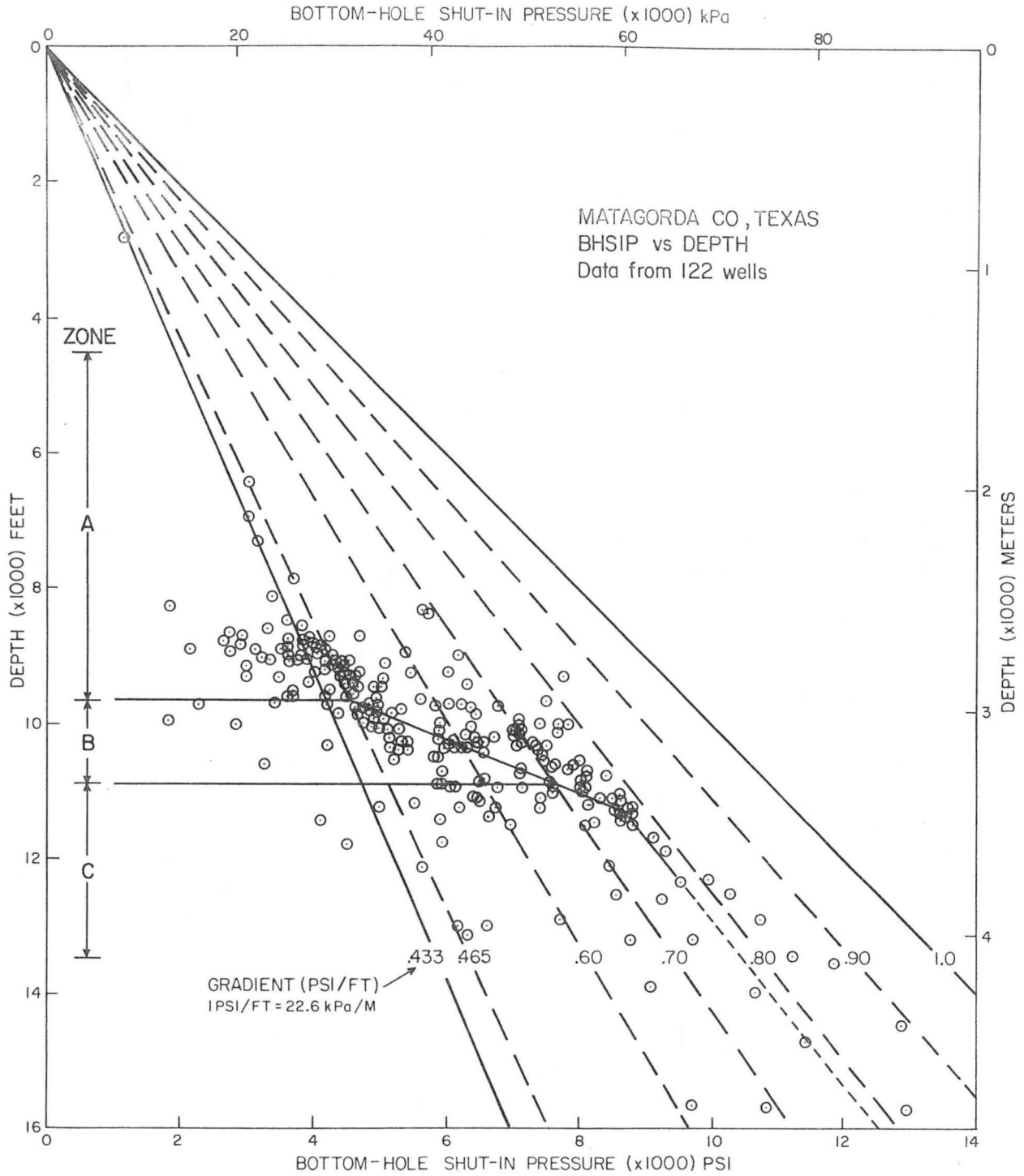

Figure 13. Plot of bottom-hole shut-in pressure versus depth, showing average thickness of the B Zone in Matagorda County, Texas.

The paucity of sonic logs for wells in Matagorda County precluded use of the shale transit time method for determining subsurface pressures. This method, however, has been useful in certain areas of the Gulf Coast, such as Brazoria County (Gregory and Backus, 1980), where numerous sonic logs were available.

Salinity

Salinity of formation waters is controlled by complex interrelations among local and regional geology, presence of faults, salt domes, unconformities, compaction, geopressured zones, clay diagenesis, temperature, fluid migration, rock stress, and pressure depletion history (Fertl and Timko, 1970; Burst, 1969; Fowler, 1970; Hedberg, 1967; Overton and Timko, 1969; Runnells, 1969; Von Engelhardt and Gaida, 1964; and Magara, 1968). Although much has been written about salinity, the subject remains poorly understood. This is unfortunate because geothermal exploration methods are clearly dependent on a knowledge and understanding of salinity.

Salinities vary widely as a function of depth for different areas of the Gulf Coast. Although there are variations, four general salinity trends (fig. 14) are recognized in many areas, as exemplified by the distribution of data for the Blessing Prospect Area in Matagorda County (fig. 15). Salinity increases with depth in shallow sandstones to a zone of reasonably constant average values. The zone of relatively constant salinity extends down to about the top of geopressure. In the geopressured zone, there is a trend of decreasing salinity down to a zone in which salinity becomes erratic and essentially unpredictable. Most of these trends can be recognized in the salinity profile of the Coastal States No. 1 Wylie well, Matagorda County, Texas (fig. 16). In this study, the salinity of formation water was derived from water resistivity (R_W) obtained from the spontaneous potential (SP) log, using mud filtrate resistivity

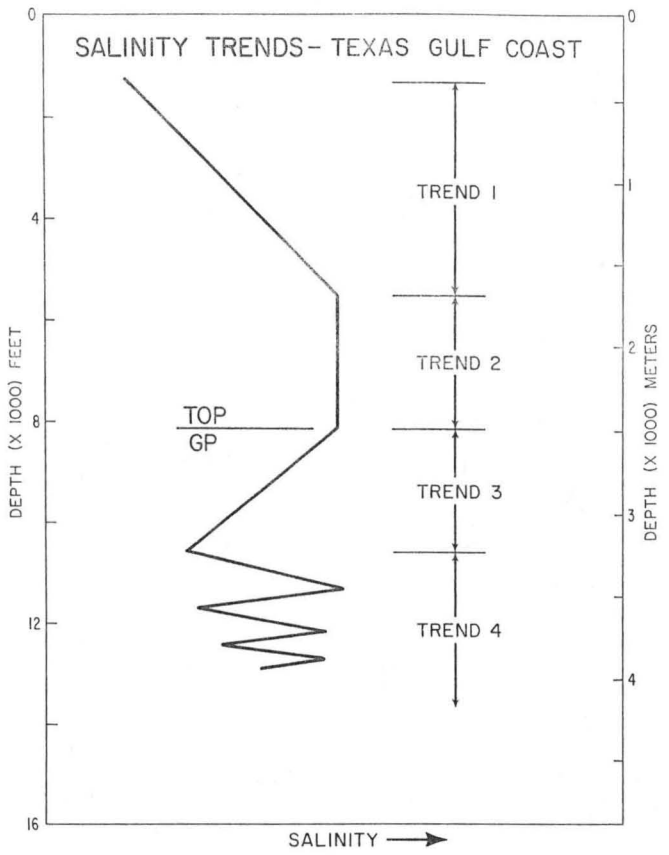

Figure 14. Generalized salinity trends, Texas Gulf Coast.

(R_{mf}) values from well log headers and following the algorithm of Bateman and Konen (1977).

Recent comparisons between salinities determined from the SP log and those measured on samples of reservoir water show large discrepancies in deep geopressured zones where mud weights exceed 14 lb/gal. Typically, calculated salinities are too low (R_w is too high), often by a factor of 2 or more. An example is the primary production interval (depths of 14,644 to 14,704 ft) in the GCO-DOE geothermal test well, No. 2 Pleasant Bayou, Brazoria County, Texas. In that well, the salinity of a water sample measured by Kharaka and others (1980) was 132,000 ppm NaCl compared with 36,000 ppm NaCl calculated from the SP log using the R_{mf} value listed in the well log header. The measured and calculated salinities differ by a factor of 3.7, which is an extreme discrepancy.

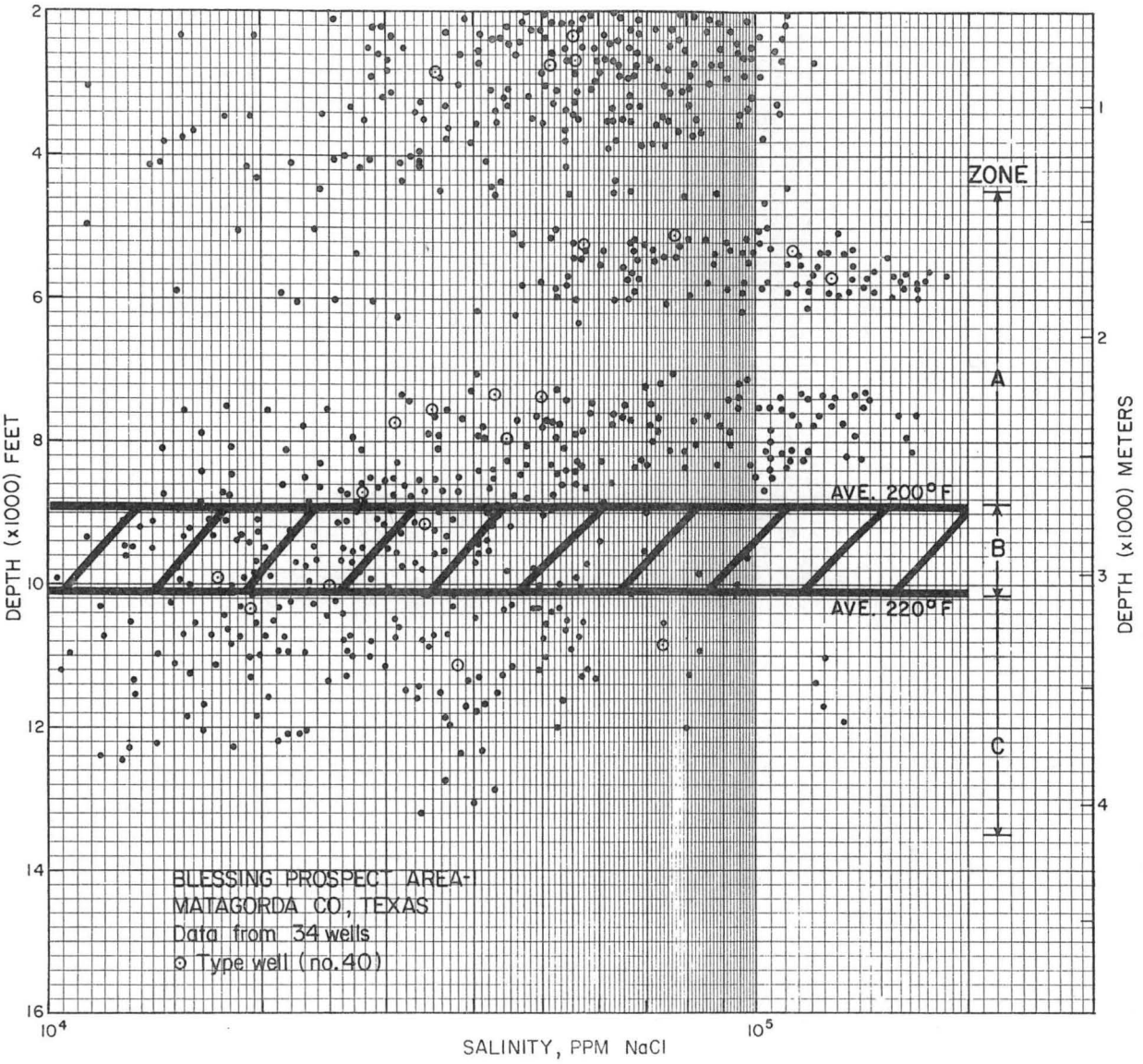

Figure 15. Salinity (computed from SP logs) versus depth for 34 wells, Blessing Prospect Area, Matagorda County, Texas.

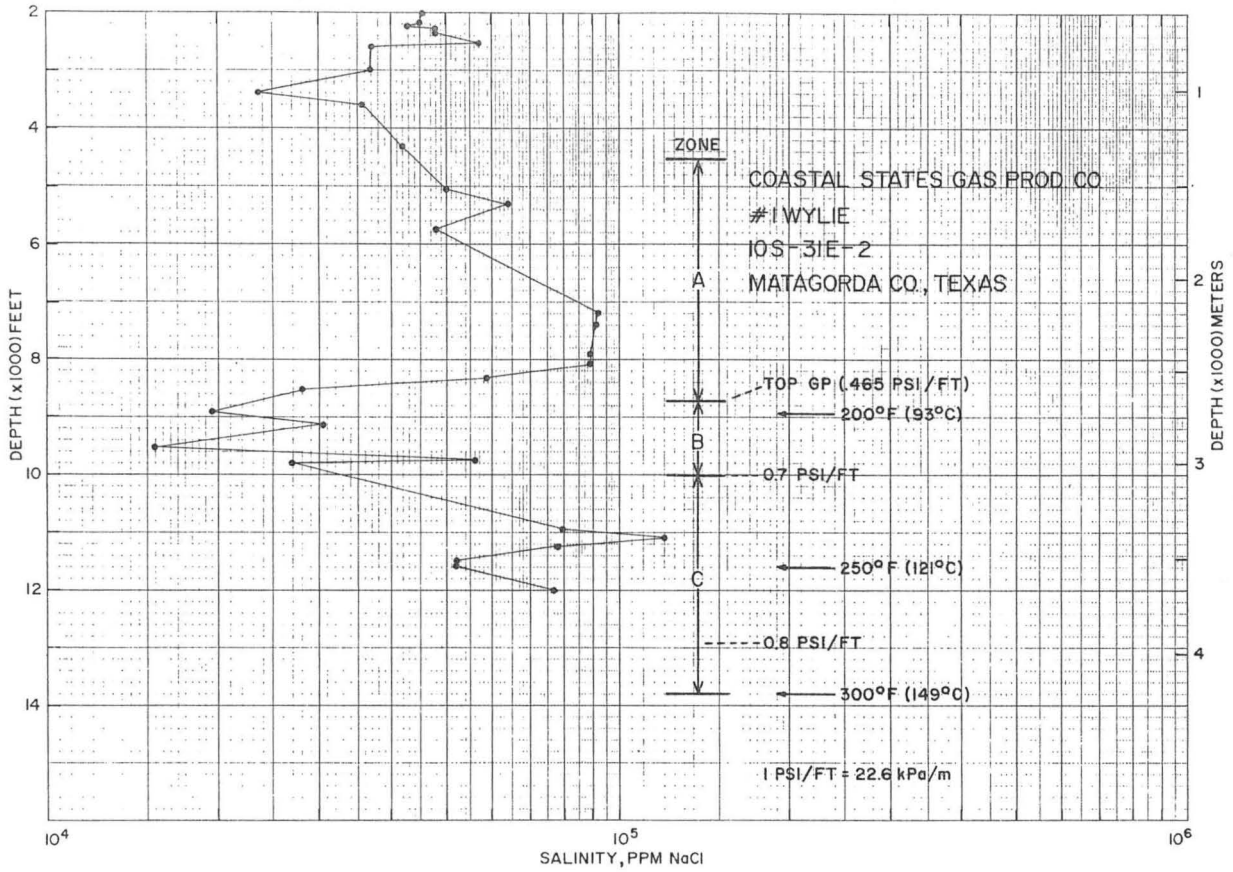

Figure 16. Salinity profile, Coastal States No. 1 Wylie, Matagorda County, Texas.

Several potential sources of error exist for salinities determined from the SP log. Recent work by Dunlap and Dorfman (in press) suggests that a major source of error lies in the use of an incorrect value of R_{mf} when high-density lignosulfonate muds are used (R_{mf} is too large). Lignosulfonate muds have been in use for over 15 years; thus, the scope of the problem is large. Also, the method of determining R_{mf} from mud resistivity using Schlumberger (1978) chart, Gen 7, should not be applied to lignosulfonate muds, as clearly stated on the chart. The chart was based on the work of Overton (1958), which took place before the widespread use of lignosulfonate muds began. The present method of correcting R_{mf} from surface to downhole temperature, using resistivity versus temperature variations for NaCl solutions, may not be applicable to modern muds and mud filtrates, thus introducing further errors into salinity determinations. An improved technique developed by Dunlap and Dorfman (in press) reduces the standard deviation between log-derived salinities and measured salinities from 69,000 ppm (conventional method) to 21,000 ppm. The effect, if any, that these problems may have on generalized salinity trends determined for the Gulf Coast area (fig. 14) cannot be predicted at this time.

Methane Solubility

Methane solubility in formation water is a function of pressure, temperature, and salinity. An increase in pressure or temperature causes an increase in solubility. An increase in salinity reduces solubility. Pressure and temperature are more predictable than salinity, which varies greatly throughout the Gulf Coast area. Because of this variability and the difficulty of determining salinities accurately by indirect methods such as the well log analyses discussed earlier, salinity values generally are the least reliable of the three parameters that control methane solubility.

For this report, methane solubilities were computed by the following empirical equation of Blount and others (1979):

$$\log_e(CH_4) = 3.6003 = 1.1176\times10^{-3}T\log_eP \quad (3)$$
$$+ 0.10002Y - 0.01634T$$
$$- 1.6574\times10^{-5}T^2 - 0.2828\times10^{-3}TY$$
$$- 0.01124Y\log_eP + 2.1262\times10^{-5}YT\log_eP,$$

where (CH_4) = methane solubility, SCF/B

T = temperature, K

P = pressure, psi

and Y = NaCl concentration, weight percent.

Methane solubilities computed from equation (3) are considerably higher than those determined from the algorithm of Haas (1978). An example of this is the solubility profile for the GCO-DOE No. 2 Pleasant Bayou, Brazoria County, Texas, comparing solubility data derived from the Haas and Blount methods (fig. 17). Formation pressures, temperatures, and average salinities are also shown for the well. The average difference between the Haas and Blount solubility profiles in this well is about 6.7 SCF/B. The Blount solubility values are higher than the Haas values by 20 to 60 percent, depending indirectly on depth, because solubility values decrease as depth decreases. A new equation proposed by Price and others (in press) gives lower values of methane solubility, but was not available in time to be used in this work.

Porosity and Permeability

Porosity and permeability values from whole-core analyses are preferred in this work, but whole-core data are rarely available; therefore

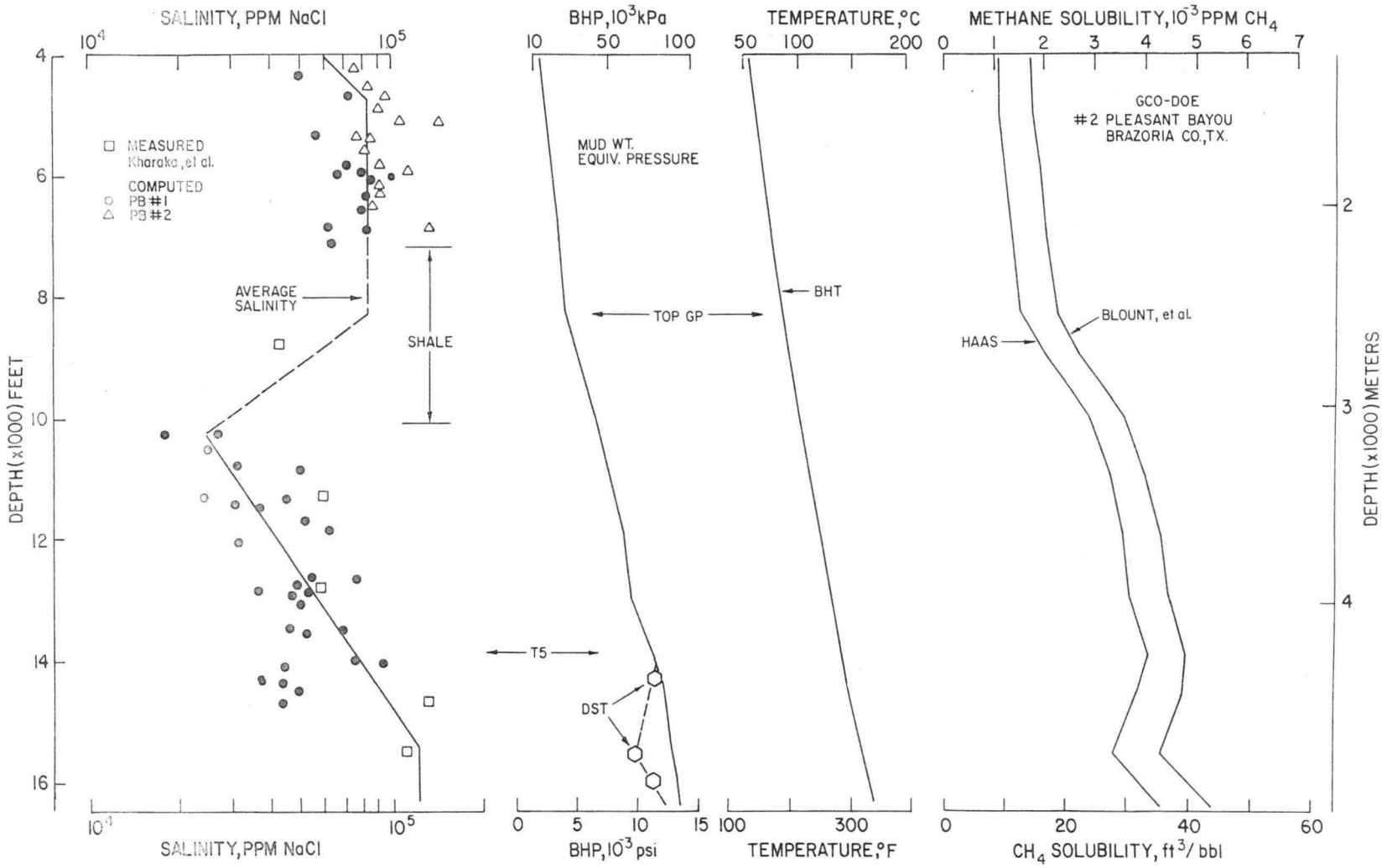

Figure 17. Salinity, pressure, temperature, and methane solubility profiles, General Crude - Department of Energy No. 2 Pleasant Bayou, Brazoria County, Texas (modified from Gregory and Backus, 1980).

porosity (ϕ) is determined by other methods, such as calculation from sonic log parameters using the time average equation (Wyllie and others, 1956). The equation is

$$\phi = \frac{\Delta t_{log} - \Delta t_m}{\Delta t_f - \Delta t_m} \qquad (4)$$

where Δt_{log} = transit time from log (μsec/ft),

Δt_m = transit time of matrix material (μsec/ft), and

Δt_f = transit time of fluid (μsec/ft).

The matrix transit time (Δt_m) in sandstones varies from 55.5 to 51.3 μsec/ft. Fluid transit time (Δt_f) varies from 203.6 to 179.3 μsec/ft for fresh water and brine (200,000 ppm NaCl), respectively. Equation (4) is satisfactory for predicting porosities of sandstones that are well consolidated but overestimates porosities of undercompacted and poorly consolidated sandstones. An empirical correction factor (C_p) is used to obtain a corrected porosity (ϕ_c) in these undercompacted sandstones.

$$\phi_c = \frac{\Delta t_{log} - \Delta t_m}{\Delta t_f - \Delta t_m} \cdot \frac{1}{C_p} \qquad (5)$$

The value of C_p can be obtained by measuring the deviation from the relationship between true porosity and porosity computed from equation (4). The true porosity can be obtained from core analysis data or from cross plots of a suite of porosity logs (Schlumberger, 1974).

Few wells in the areas of interest have been cored or have porosity logs. Normally, induction and SP logs are available and porosity can be

computed from the formation factor (F) and cementation factor (m) using one of several empirical expressions. Values for parameter m depend on rock type and vary from 2.2 for highly cemented quartzite to 1.3 for unconsolidated sand. The general relationship (Archie, 1942) is expressed as

$$F = \phi^{-m} \tag{6}$$

where m = 1.8 for sandstone

ϕ = fractional porosity.

Formation factor is defined as a ratio of resistivities that can be obtained from induction and SP well logs. It is assumed that R_o equals R_t, and

$$F = R_o/R_w \tag{7}$$

where $R_o = R_t$ = resistivity of rock that is 100 percent saturated with formation water of resistivity (R_w), determined from the deep induction log (ohm-meters)

R_w = resistivity of formation water at given temperature and salinity, determined from the SP log (ohm-meters).

Other well log methods can be used for determining porosity, although the Archie relationship was found to be the most useful in this study because only induction and SP logs were available for the majority of wells.

Parameter Plots

Parameter plots consist of a series of selected formation parameters plotted as a function of depth for wells along dip and strike cross sections in the prospect areas (see later sections on specific prospect

areas). The plotted parameters in this report are formation temperature, formation water salinity, shale resistivity, and reservoir porosity. Temperature and salinity were plotted because they directly affect the amount of in-place methane dissolved in formation water. Shale resistivity was plotted because it is empirically related to formation fluid pressure, which also directly affects the solubility of methane in water. Porosity was plotted because it determines the volume of water contained in a reservoir.

Isothermal lines were drawn for 200°, 250°, and 300° F where wells were deep enough to encounter these temperatures. Isopiestic gradient lines, determined from pressures derived by methods discussed earlier in this report, are shown for pressure gradients of 0.465 (top of geopressure) and 0.7 psi/ft, which define the top and base of the B Zone. The depth intervals occupied by the deep hydropressured zone, A, and the two shallow geopressured zones, B and C, are indicated on all plots. Also, the top of the Frio Formation or the top of the Wilcox Group is shown on the shale resistivity and porosity profiles of each parameter plot.

Technical Problems Encountered

One major problem encountered during the study was the lack of sufficient permeability data to determine trends within the prospect areas. Requests for the necessary whole-core analyses were sent to all companies that cored the sandstones of interest in the prospect areas. However, analyses were obtained for only a few wells in some of the prospects; none were received for other areas.

Porosity/permeability relationships were established from whole-core data in a few limited areas such as the Sarita Field in the Sarita Prospect Area, Kenedy County. Some whole-core data were also available for several wells in the Corpus Christi Fairway. Porosity/permeability relationships

in the type well for the Blessing Prospect Area, Matagorda County, were established from sidewall-core data, which normally tend to show values greater than whole-core permeability values.

To offset the lack of core analyses, other methods of establishing porosity/permeability relationships were investigated. Porosities were derived from sonic logs and converted to permeabilities using the relation established from core data. This method works well where sonic logs are available in areas near wells that have core data. Unfortunately, there are large areas where coverage by sonic logs is inadequate. In these areas, a method for transforming resistivity to pseudo-velocity was investigated. The pseudo-velocity was then converted to porosity and hence to permeability using core data to establish the porosity/permeability relation in the area. However, it was again necessary to have some core data. Clearly, the lack of core analyses was a serious limitation in permeability determination.

Another technical problem encountered in the study involved the determination of salinity. Methods of deriving salinities from the SP log were in a development and re-evaluation stage during the period of this investigation. As stated earlier, salinity of formation waters was derived from water resistivity obtained from the SP log, using the value of mud filtrate resistivity listed in the well log heading. Recent research (Dunlap and Dorfman, in press) shows that these log-derived salinities are likely to be too low for deep, hot wells in the Texas and Louisiana Gulf Coast in which lignosulfonate muds were used. Dunlap and Dorfman have developed an improved technique which reduces the standard deviation from 69,000 ppm to 21,000 ppm when comparing log-derived salinities with measured salinities. Results of this new work were not received in time to be used in this

report. Dunlap and Dorfman's technique has been applied only to the Texaco No. 16 Thomas well (for further discussion, see section on Blessing test-well site). In the remainder of this report, the underestimation of salinity will cause an overestimation of methane dissolved in formation waters in wells where lignosulfonate muds were used.

REGIONAL DISTRIBUTION OF SANDSTONES

The first step toward selection of test sites was to determine the regional distribution of sandstone within the geopressured and hydropressured zones in the Texas Gulf Coast region. This step involved mapping the Wilcox and Frio/Vicksburg sandstone corridors within the A, B, C, and D Zones. The corridors were determined by a survey of the regional cross sections (fig. 18) constructed by Gregory and others (1980) for an assessment of entrained methane in the Texas Gulf Coast. For this initial estimation of sandstone distribution, depths to the B-C boundary (0.7 psi/ft pressure gradient) were derived from a composite map (fig. 19) of several geopressure maps produced for earlier studies. On the basis of a few plots of bottom-hole shut-in pressure versus depth, average thickness of the B Zone was estimated to be approximately 1,000 ft. This value was subtracted from the depth determined for the B-C boundary to determine the depth of the A-B boundary in the wells of the cross-sectional grid. However, subsequent study and construction of numerous plots of bottom-hole shut-in pressure from completion card data for the Texas Gulf Coast showed that B Zone thickness was generally several hundred feet greater than that originally estimated. Nevertheless, similar map trends in the B Zone corridors would emerge for either estimate of the zone thickness. For corridor delineation and subsequent phases of this study, the depths at which 300° F

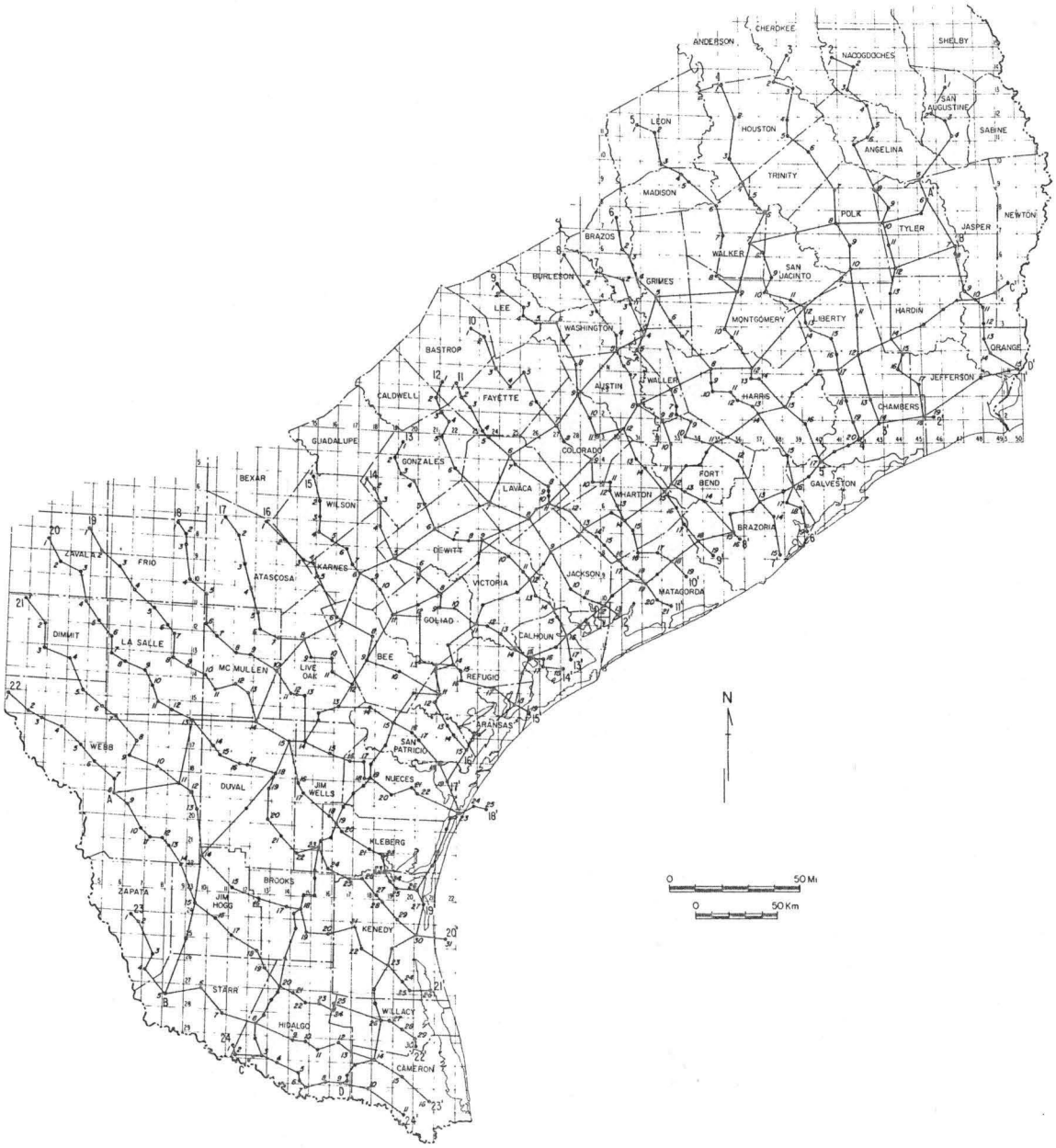

Figure 18. Lines of regional cross sections constructed for the DOE entrained methane assessment (Gregory and others, 1980) and used for regional sandstone mapping in this project.

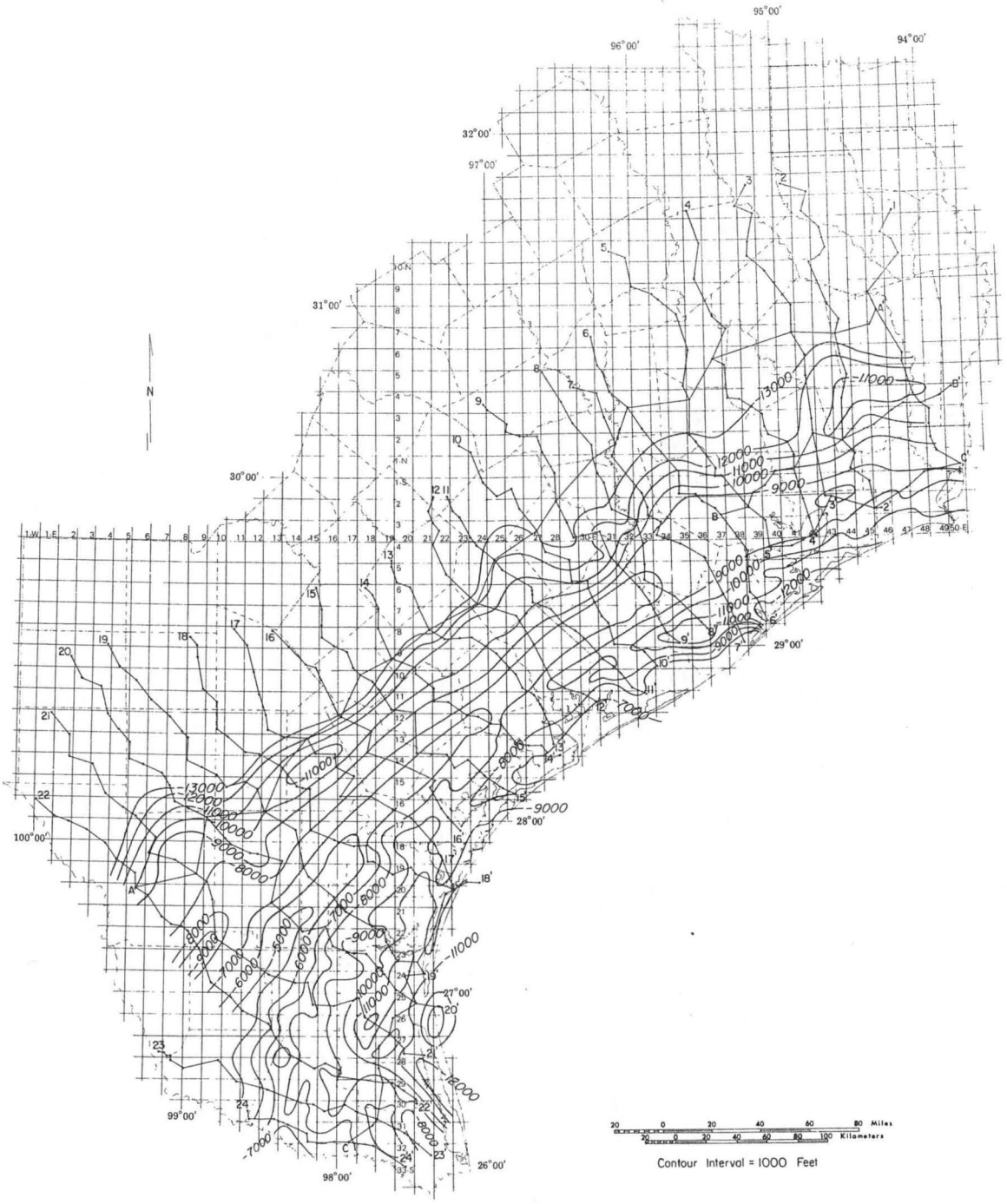

Figure 19. Depth to the B-C Zone boundary (fluid pressure gradients equal about 0.7 psi/ft). This map is a composite of maps from Bebout and others (1975a and b, 1976, and 1978a).

temperatures occur, or the C-D boundary, were interpolated or extrapolated from temperatures derived from well log headers and corrected to equilibrium values (Kehle, 1971).

The corridor maps indicate the general trends of the primary sandstone units within the various pressure zones. The maps for all four zones (figs. 20 through 23) show two main trends--the Wilcox Group and the Frio and Vicksburg Formations.

SHALLOW GEOPRESSURED AND DEEP HYDROPRESSURED FAIRWAYS, PROSPECT AREAS, AND TEST-WELL SITES

To define fairways within the broad corridors, the pressure zones were located on the well logs used on the regional cross sections such as 20-20' (fig. 24), and net sandstone was determined for each zone over the Texas Gulf Coast region. Compared to the methods used for corridor delineations, determination of A-B and B-C Zone boundaries was much more refined with the use of numerous pressure, resistivity, and temperature data, as described in the section on methodology.

After the four zones were defined on the regional cross sections, net sandstone was determined for the zones on each well log and net-sandstone maps were constructed (figs. 25 through 28). The areas of greatest net sandstone were designated as potential fairways. Thirteen potential fairways were outlined in both the B and C Zones, the zones of primary interest. On the basis of the net sandstone, areal distribution, average bed thickness, permeability, and coincidence with fairways of other zones, these fairways were ranked according to favorability for potential test sites. The five prospective fairways are Montgomery, Matagorda, Corpus Christi, Kenedy, and Cameron (fig. 29). The Frio Formation is the primary

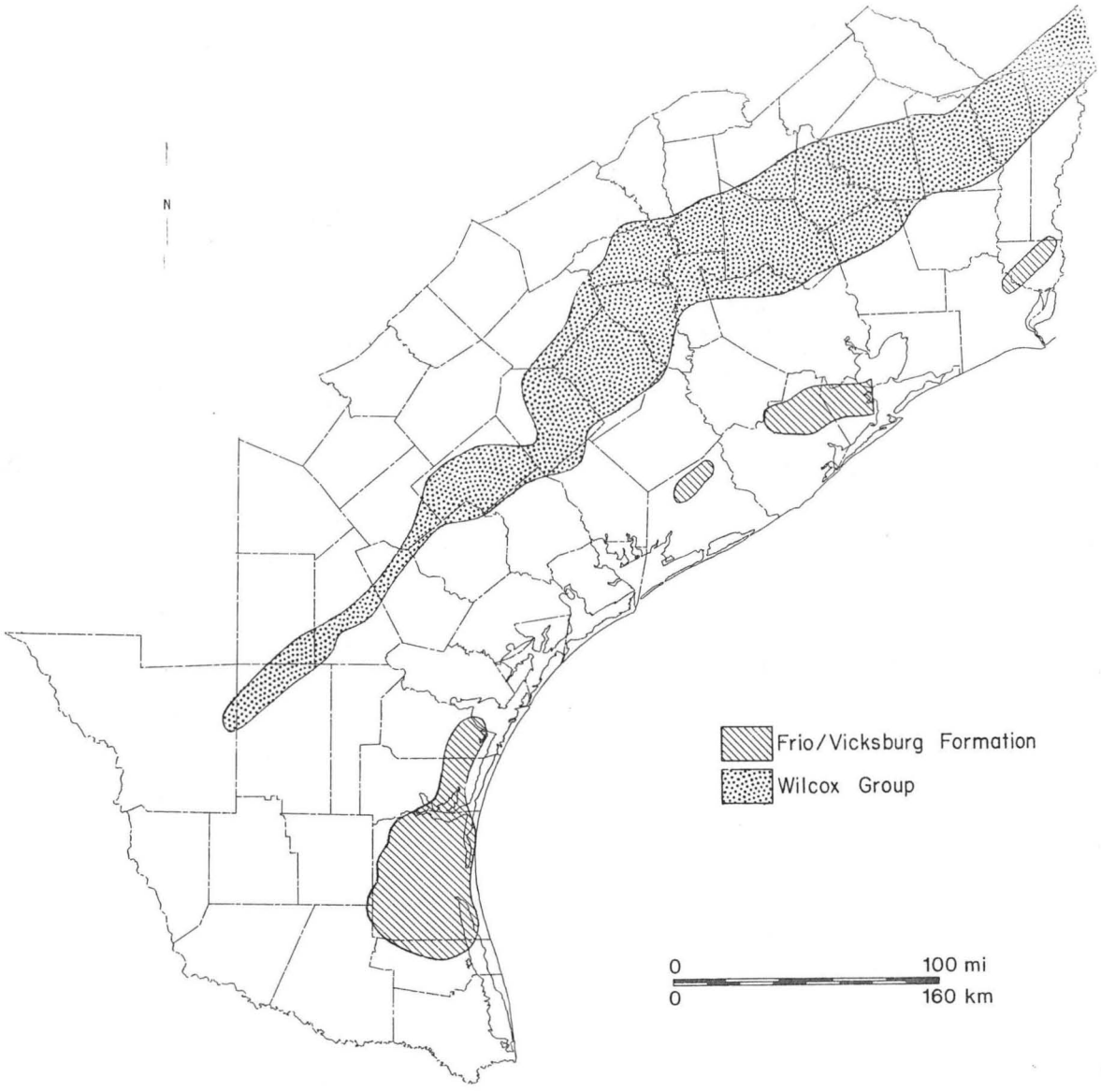

Figure 20. Sandstone corridors of the A Zone.

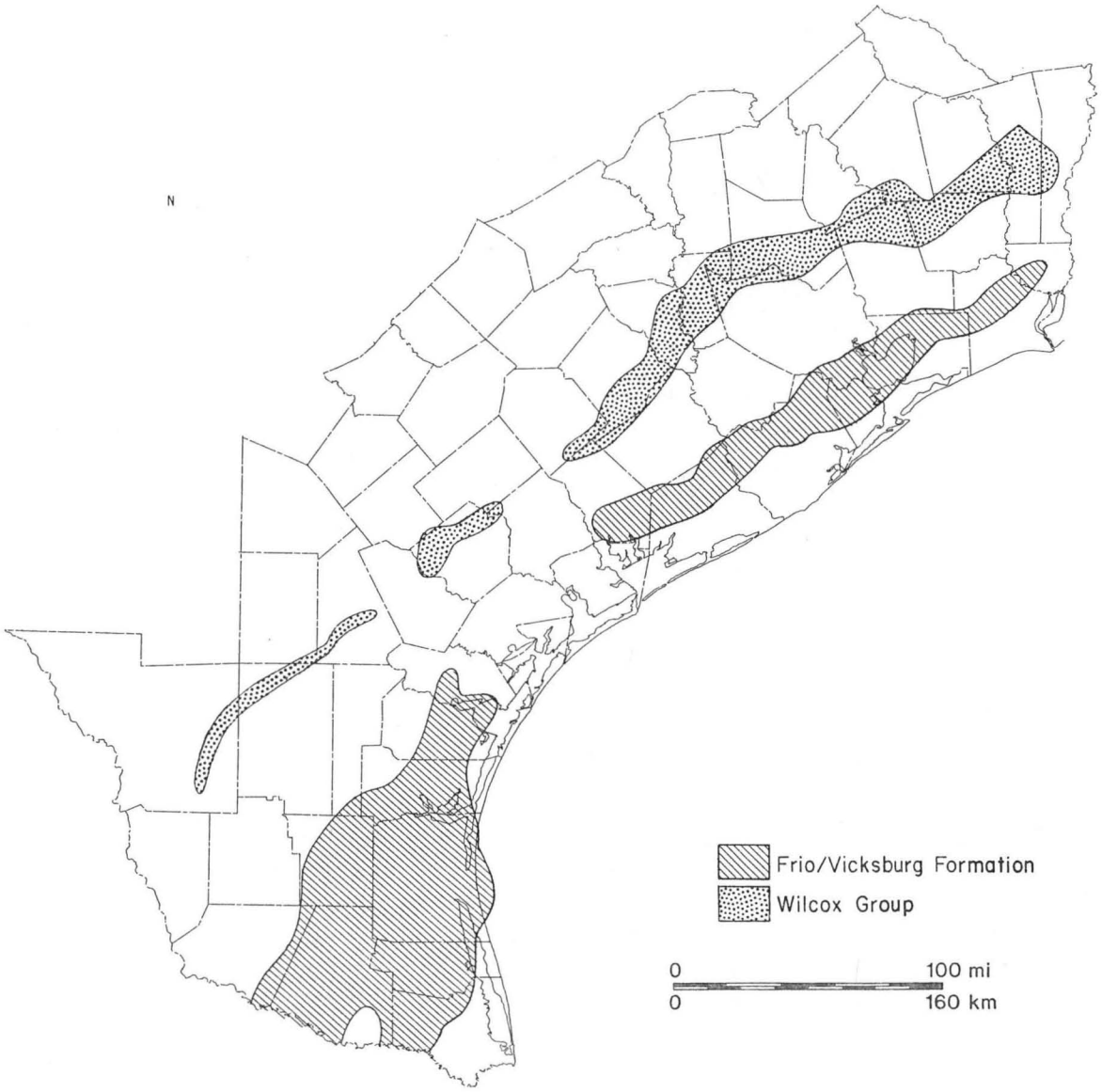

Figure 21. Sandstone corridors of the B Zone.

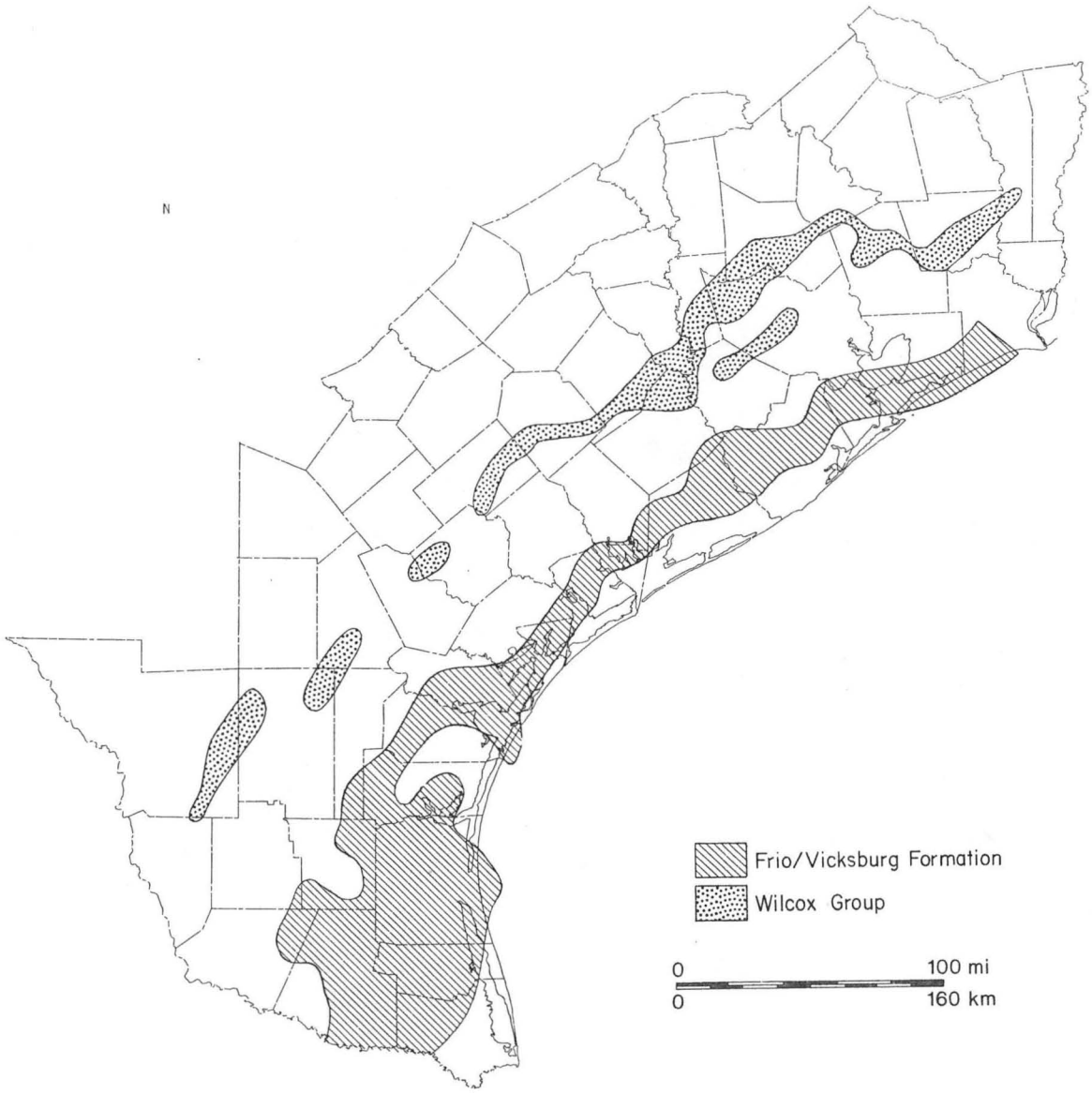

Figure 22. Sandstone corridors of the C Zone.

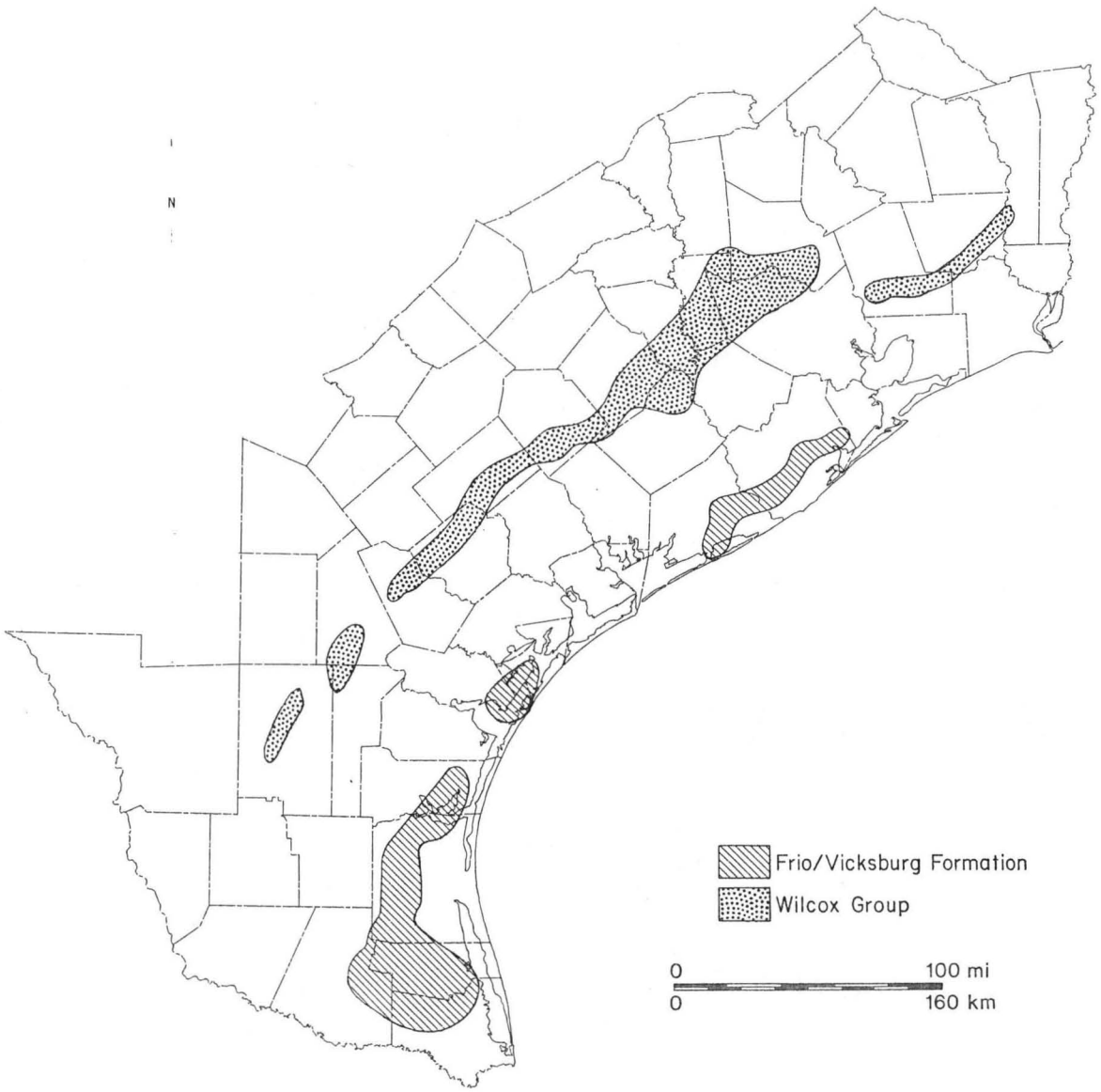

Figure 23. Sandstone corridors of the D Zone.

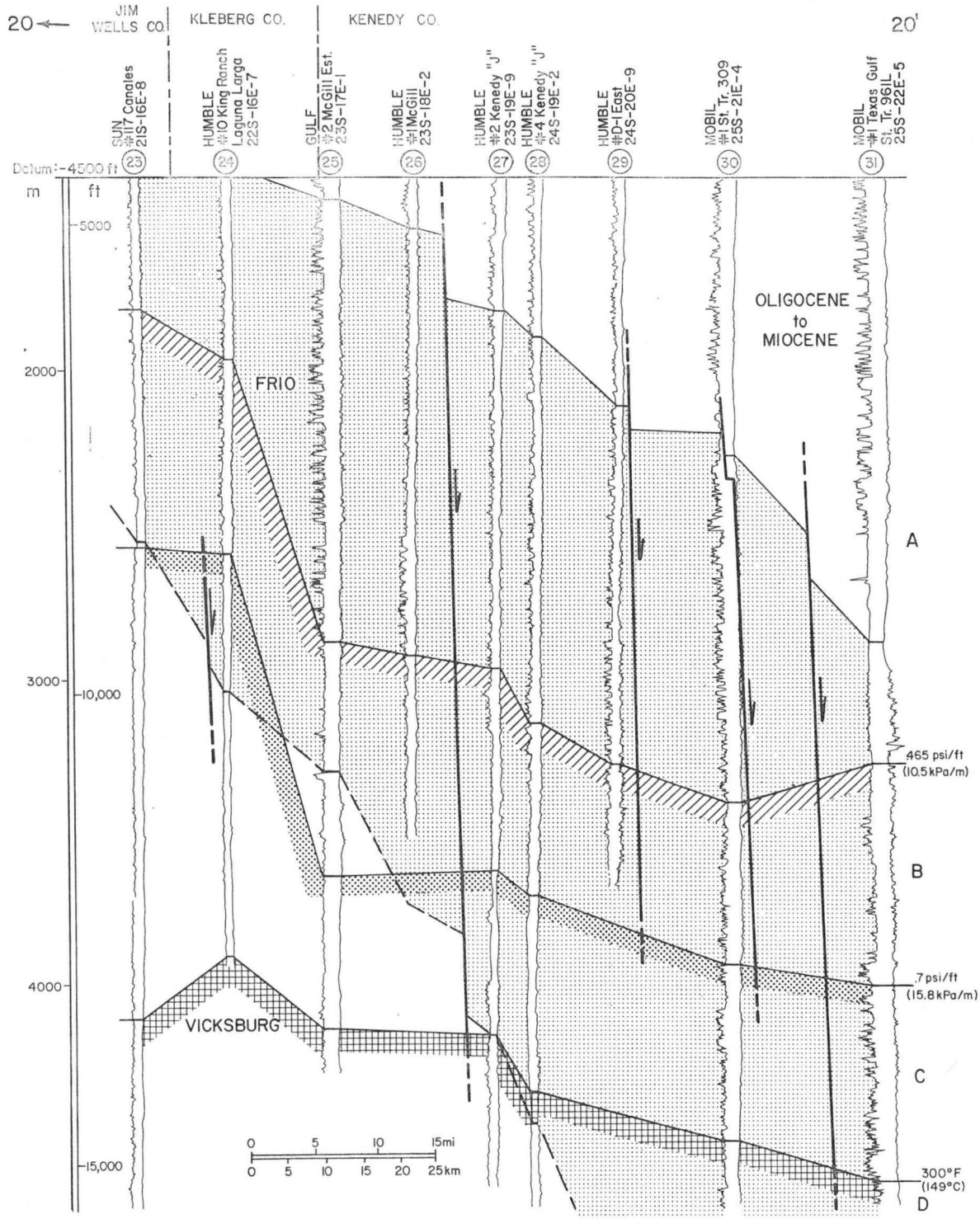

Figure 24. Downdip part of regional cross section 20-20'. Line of section is shown on figure 18. Modified from Gregory and others (1980).

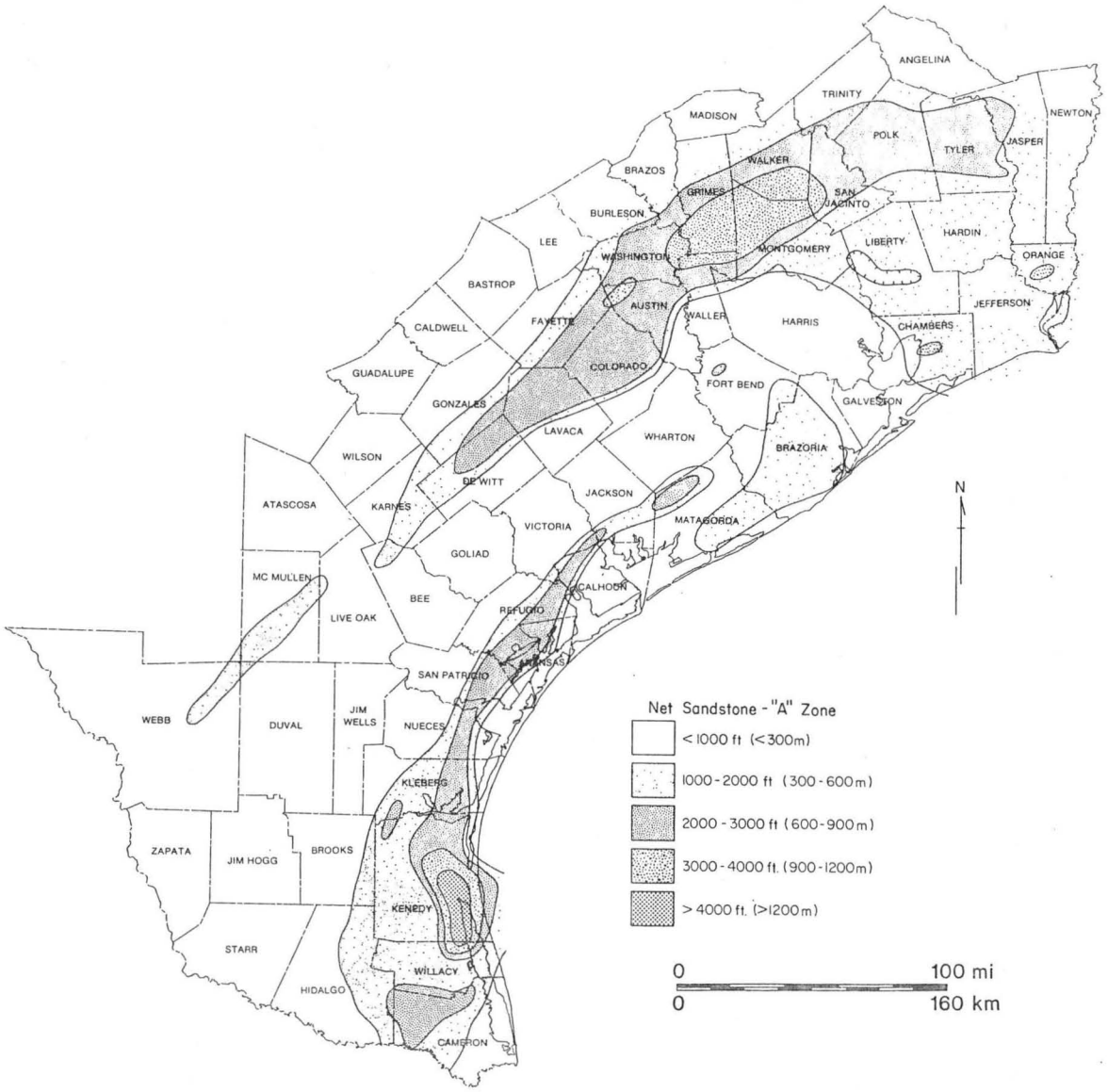

Figure 25. Net sandstone of the A Zone.

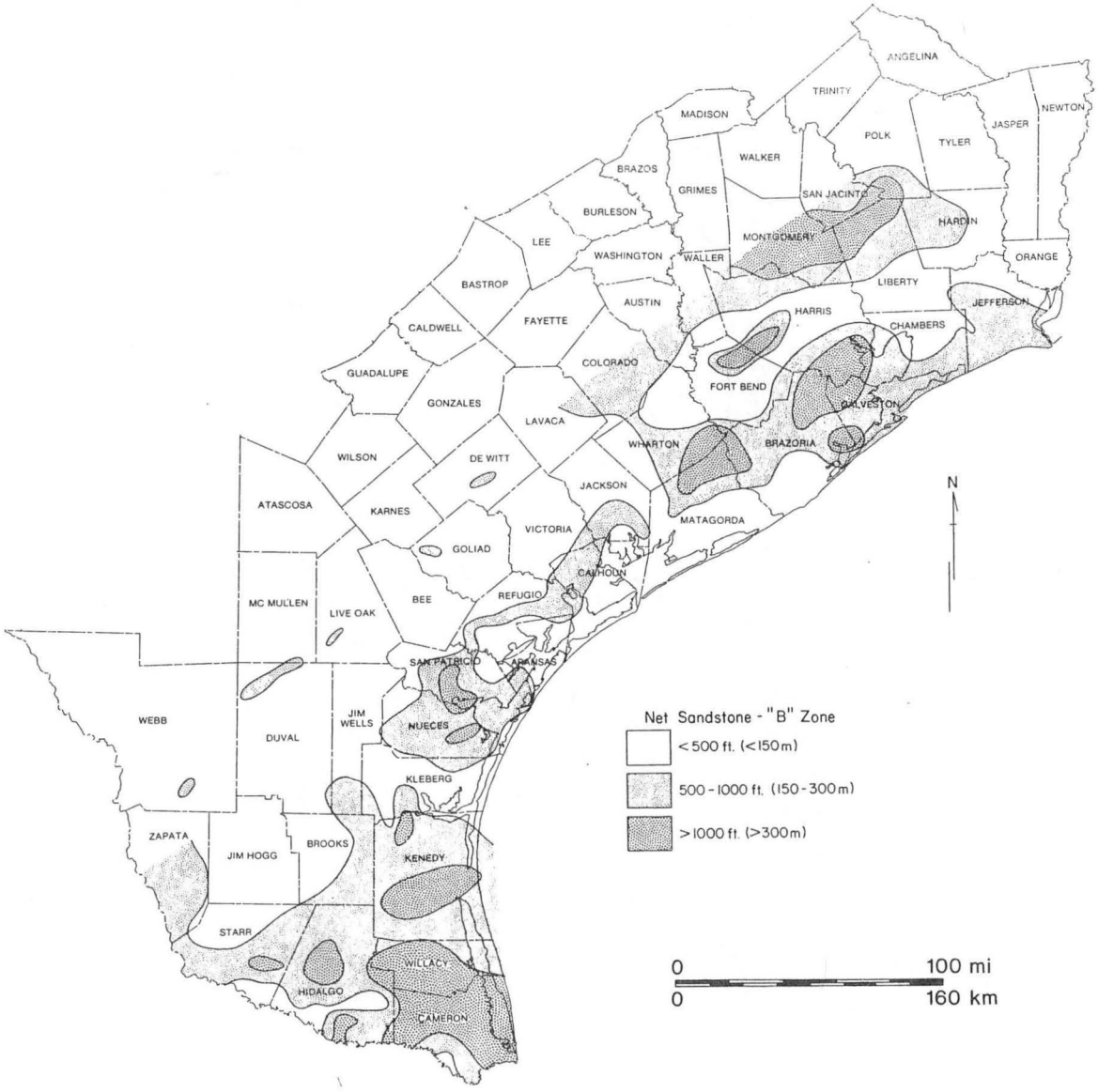

Figure 26. Net sandstone of the B Zone.

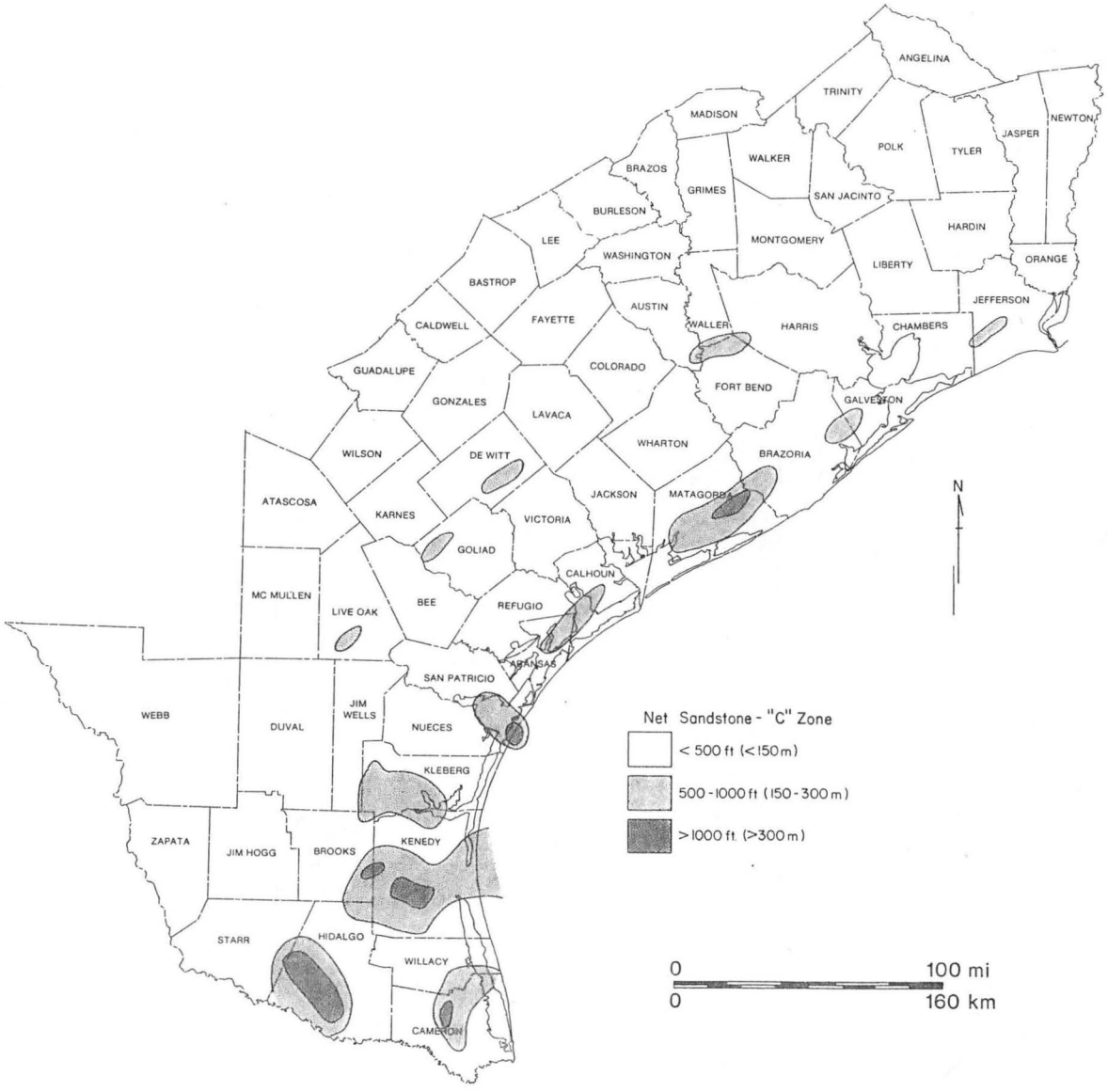

Figure 27. Net sandstone of the C Zone.

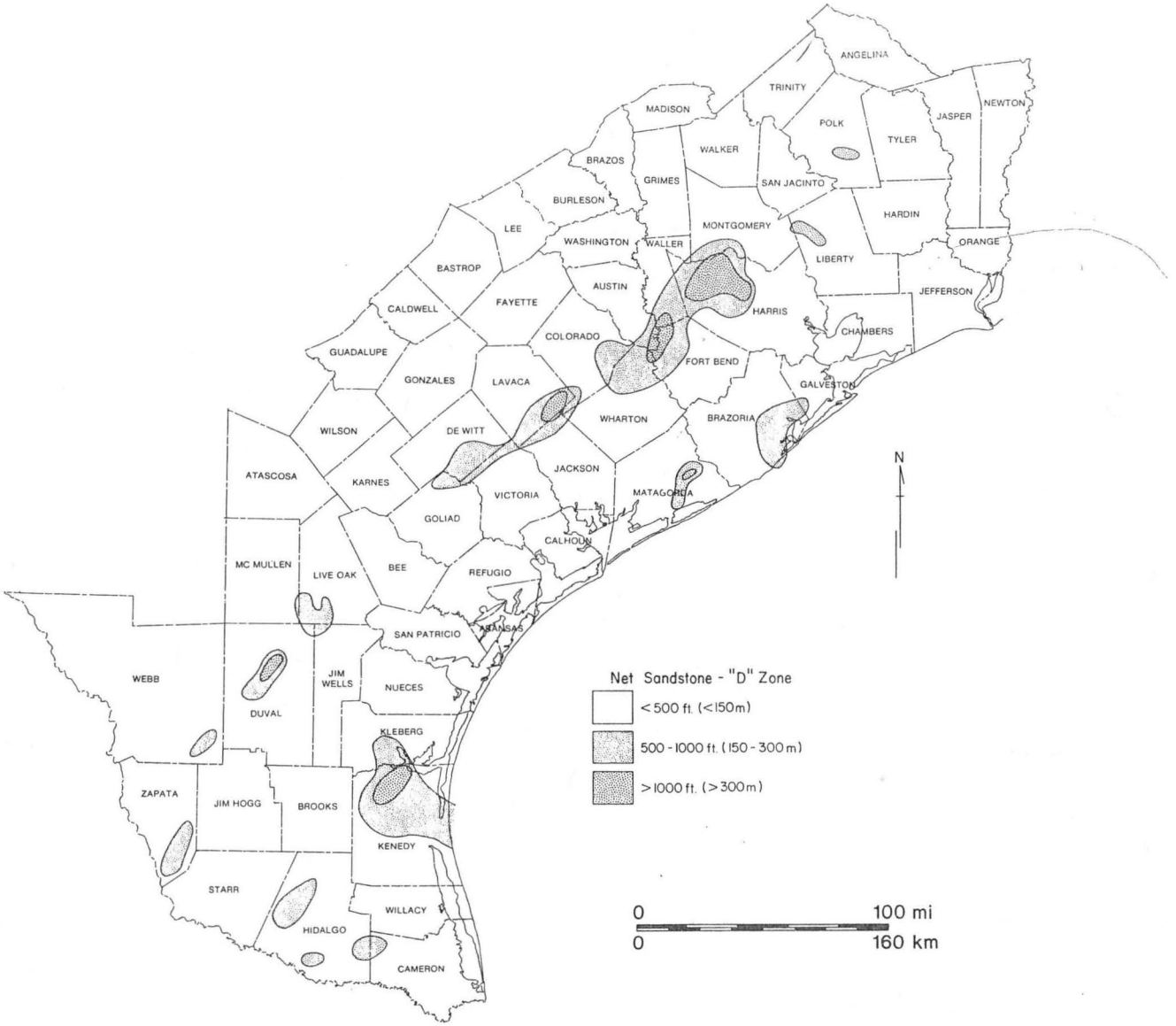

Figure 28. Net sandstone of the D Zone.

Figure 29. Five fairways prospective for testing shallow geopressured and deep hydropressured zones.

stratigraphic unit of interest in all these fairways except Montgomery, where the Wilcox Group contains most of the prospective sandstones.

Correlation of major sandstone units within the fairways and examination of (1) the regional cross sections, (2) detailed cross sections constructed for previous studies, and (3) preliminary cross sections through the fairways aided in defining prospective areas. One or two prospect areas in each fairway were selected for detailed study on the basis of net sandstone and average bed thickness in the zones of primary interest.

Matagorda Fairway

The Matagorda Fairway covers approximately 2,000 mi^2, including all of Matagorda County north of Matagorda Bay and parts of southwestern Brazoria, southeastern Wharton, and southern Fort Bend Counties (figs. 29 and 30). Electric logs from 320 wells fairly evenly distributed throughout this fairway were used to identify the most prospective areas (fig. 31; appendix C). On the basis of the lateral and vertical dimensions of B and C Zone sandstones, the Blessing and Old Ocean areas were selected as most prospective for the production of large quantities of methane-bearing water. An additional 130 electric logs from wells within these areas were obtained for detailed study (figs. 32 and 33).

In the Matagorda Fairway the subsurface Tertiary section occurring between 4,500 ft below sea level and the lower limits of well control (about -15,000 ft) consists of several sandstone/shale formations. The interval from -4,500 ft to the top of the Frio Formation sandstones at -5,000 to -8,500 ft includes the Miocene Fleming and Anahuac Formations (fig. 34). These formations occur within the A Zone throughout the fairway. The Frio Formation of Oligocene age includes all prospective sandstones in the Matagorda Fairway. Within the fairway, the Frio was divided into three

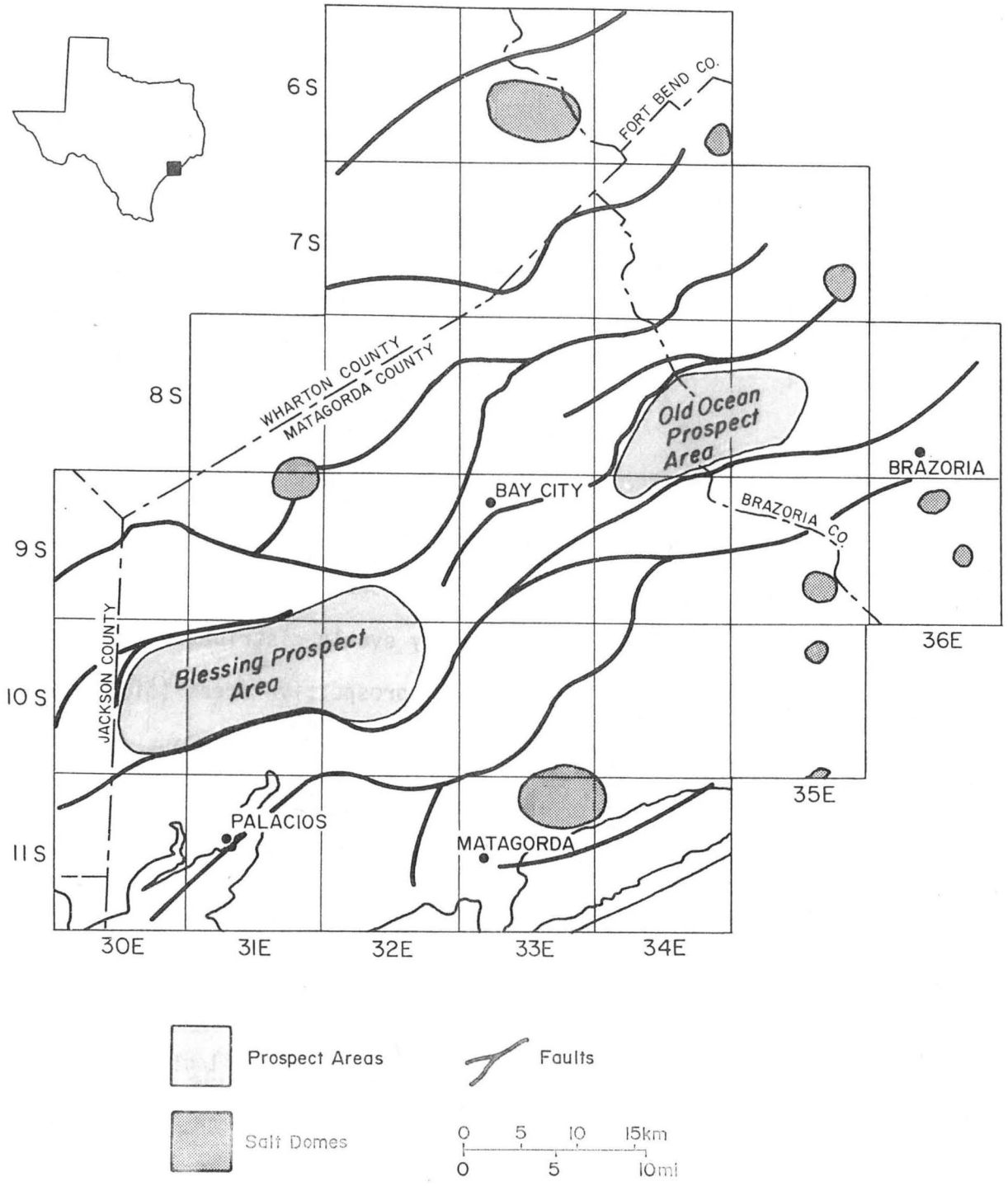

Figure 30. Locations of the prospect areas, major growth faults, and salt domes at the top of the Frio Formation, Matagorda Fairway.

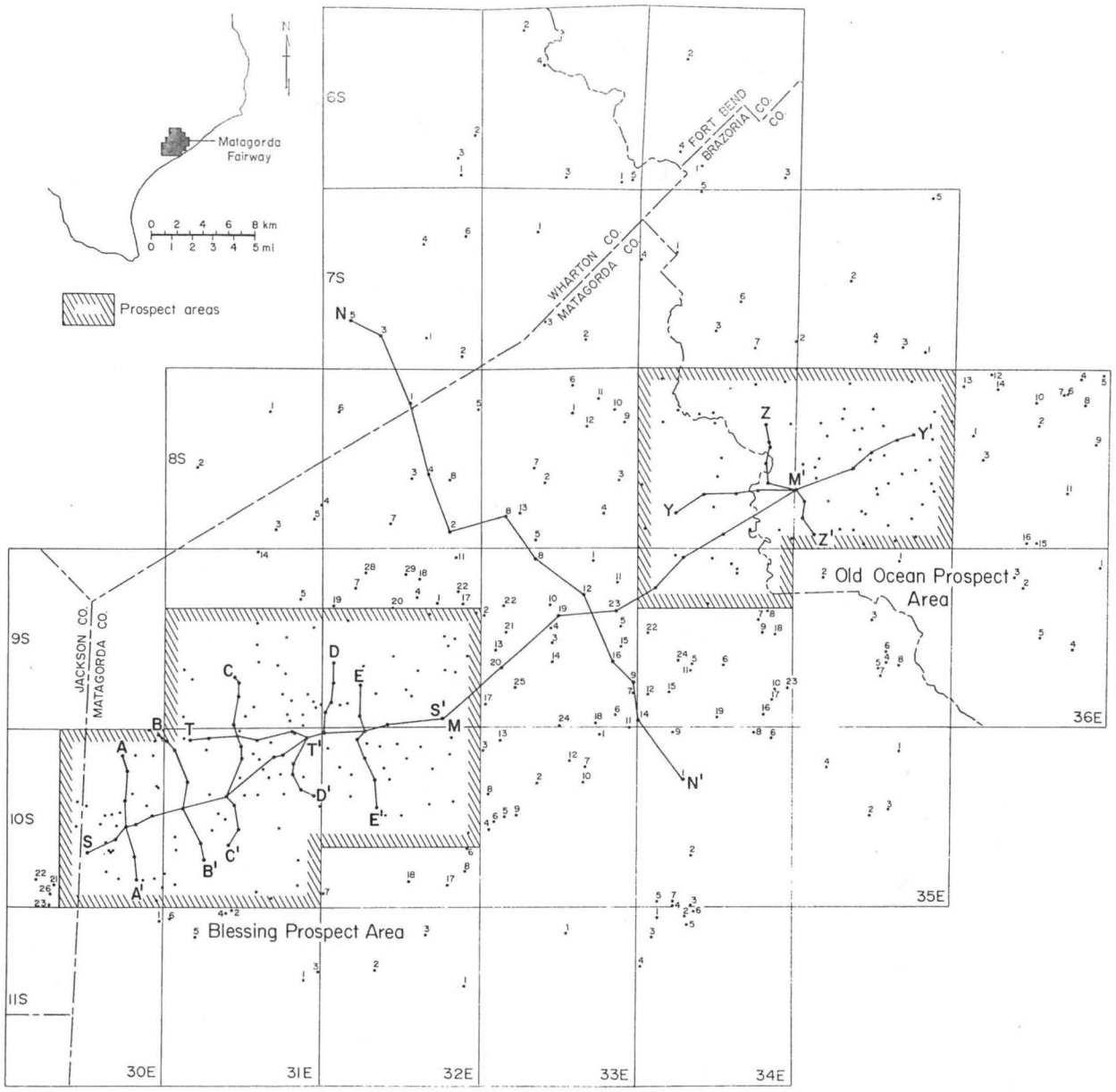

Figure 31. Well locations, lines of section, and prospect areas, Matagorda Fairway.

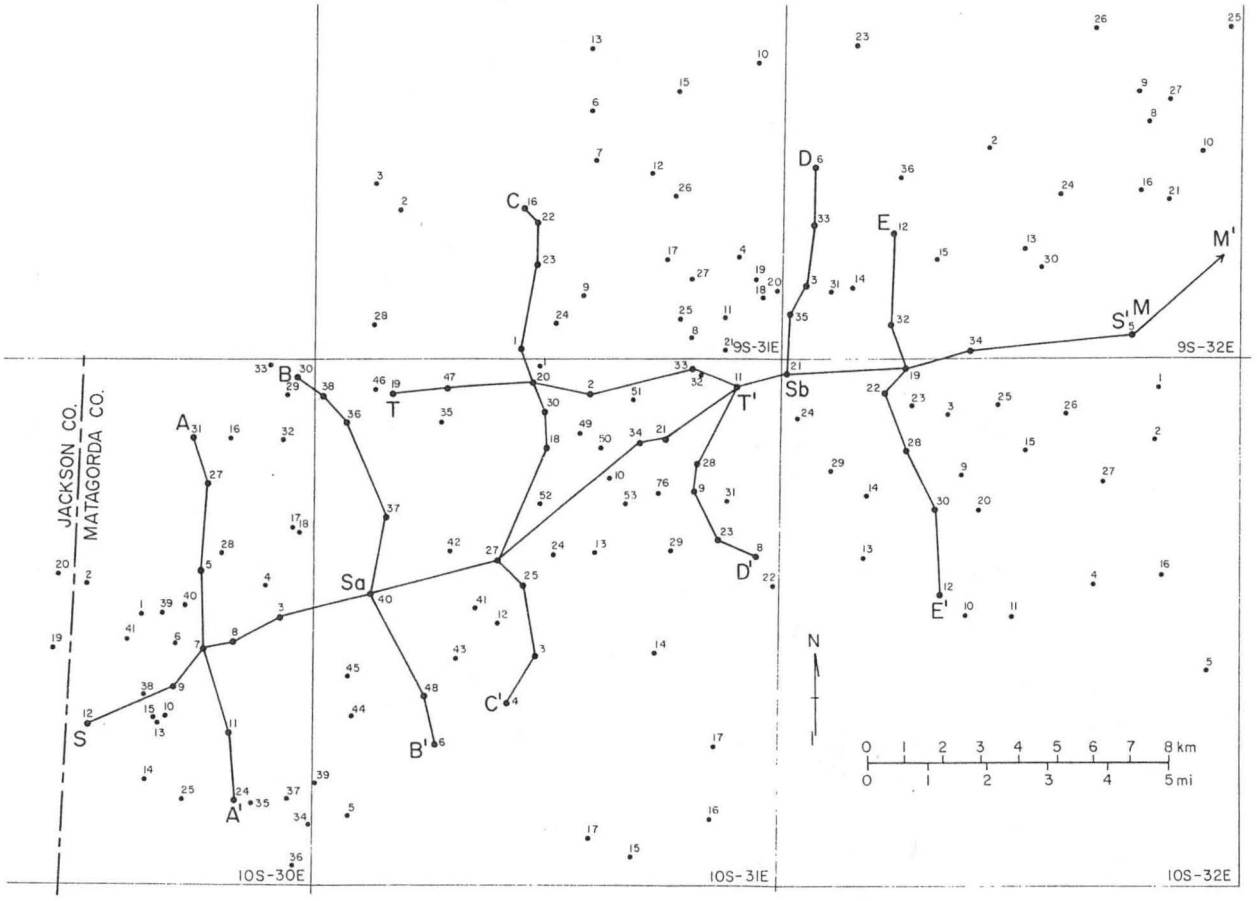

Figure 32. Well locations and lines of section, Blessing Prospect Area.

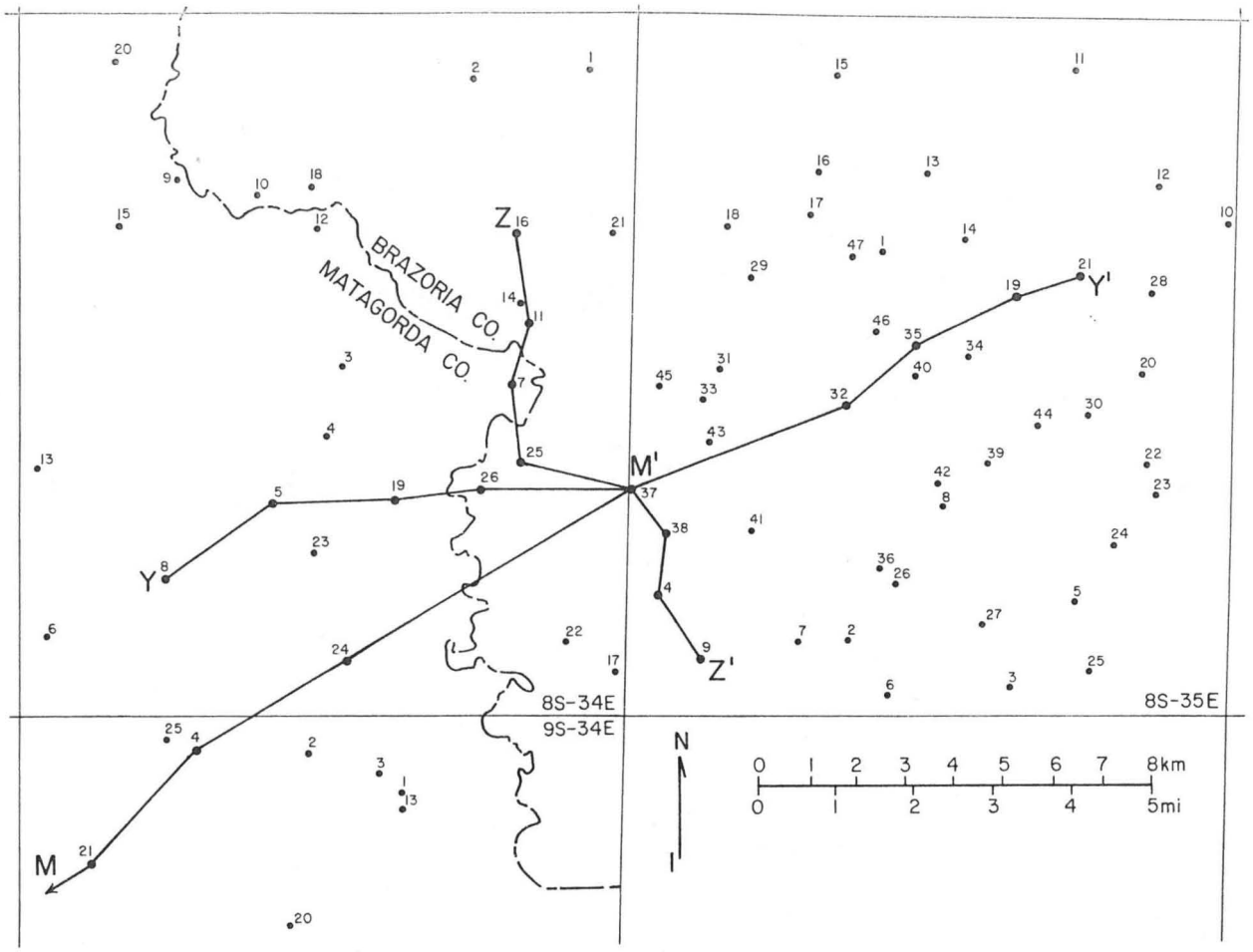

Figure 33. Well locations and lines of section, Old Ocean Prospect Area.

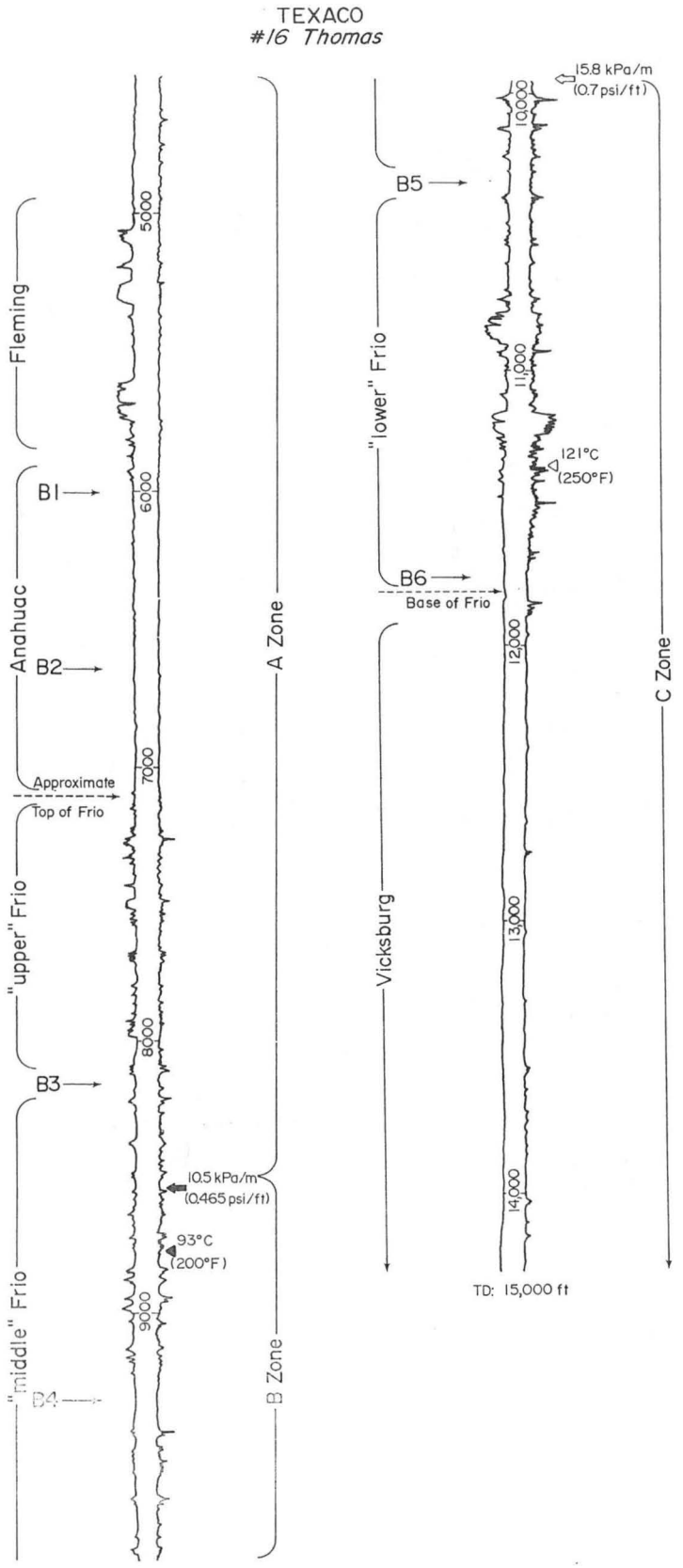

Figure 34. Type well log, Blessing Prospect Area and Matagorda Fairway.

SERIES	GROUP/FORMATION	FORAMINIFERAL ZONE
Miocene	Anahuac	*Discorbis nomada* *Heterostegina texana*
Oligocene	Frio	*Marginulina vaginata* *Cibicides hazzardi* *Nonion struma* *Nodosaria blanpiedi* *Textularia mississippiensis* *Anomalina bilateralis*
	Vicksburg	*Textularia warreni*

Figure 35. Foraminiferal zones, Miocene and Oligocene of the Texas Gulf Coast (from Bebout and others, 1975a).

parts by the correlation of distinctive shale resistivity patterns (fig. 34).

The uppermost third of the Frio consists of 1,000 to 2,000 ft of sandstone and shale occurring within the A Zone. This interval includes many of the well-known gas- and oil-producing sandstones of the Frio trend. However, the total volume of A Zone sandstones in the Matagorda Fairway is far less than in other fairways described in this report. This part of the Frio was named "Upper Frio" by the Houston Geological Society study group (1959) and is defined as the interval between the Heterostegina-Marginulina and Nodosaria blanpiedi foraminiferal zones (fig. 35). However, index fossils were not used for stratigraphic correlations in this study. Detailed electric log correlations were used exclusively.

The middle third of the Frio Formation is 500 to 3,000 ft thick and includes B and C Zone sandstones that are locally prospective for methane-bearing water. This interval is not precisely correlative to any previously defined stratigraphic subdivision of the Frio. It includes parts of the Textularia mississippiensis and Anomalina bilateralis foraminiferal zones (fig. 35).

The lowest third of the Frio in the Matagorda Fairway is 500 to 3,000 ft thick. In this interval, C Zone sandstones are variable in thickness and lateral continuity, and are best developed in the Blessing and Old Ocean Prospect Areas.

D Zone sandstones occur below -14,000 ft along the southern (gulfward) edge of the fairway. These were studied by Bebout and others (1978b) as part of the DOE-funded assessment of the deep geopressured zones of the Texas Gulf Coast. These deep D Zone sandstones were rejected as geothermal test reservoirs because of their limited lateral and vertical extent.

The Frio is underlain by the Vicksburg Formation (Oligocene) which is a thick (greater than 4,000 ft) marine shale in this area. The base of the Frio descends from around -7,500 ft in the northern part of Matagorda Fairway to below the limits of well control (deeper than -15,000 ft) in the southern part. Regional dip, down-to-the-basin faulting, and downdip thickening all contribute to this significant depth increase.

Faulting contemporaneous with sedimentation has affected the distribution and characteristics of geopressured Frio sandstones in the Matagorda Fairway. A series of major growth faults trend northeast-southwest across the fairway (fig. 30). These large faults, with down-to-the-basin, vertical displacements of up to several thousands of feet, typically cut the entire Frio section. Sandstone/shale sections on the downthrown sides of growth faults generally thicken updip toward the faults. As faulting and

sedimentation continued, older sediments were progressively displaced downward. This vertical displacement is greatest immediately adjacent to the growth faults, decreasing rapidly away from them downdip. The result is the characteristic "rollover", or reversal of the regional gulfward dip. Downdip from large growth faults, Frio sandstones and shales typically show this dip reversal to the north in the Matagorda area.

In the Matagorda area large growth faults affected the deposition of progressively younger, shallower intervals gulfward. This phenomenon is related to the sequence of deposition as the ancient shoreline prograded seaward. The geopressured Frio sandstones tend to be most affected (expanded and trapped) in a relatively narrow band (about 15 mi) of growth fault blocks that parallel both the ancient and present shorelines. It is in this elongate trend where the Blessing and Old Ocean Prospect Areas are located (fig. 30). Numerous small, randomly oriented faults (not shown on fig. 30) segment the area and reduce sandstone continuity. Salt domes in the Matagorda area have caused local arching and thinning of sediments and were avoided in the search for geopressured prospects (fig. 30).

Blessing Prospect Area

The Blessing Prospect Area, located in western Matagorda County (fig. 30), is 19 mi long (east-west), 9 mi wide (north-south), and covers approximately 170 mi^2. Detailed electric log correlations were used to establish six markers (B1 to B6) that divide the section of interest (below -4,500 ft) into seven intervals for individual study and mapping (fig. 34). Structural and stratigraphic cross sections were constructed along the lines shown in figure 32.

Structure

Faulting in the Blessing Prospect Area is complex. Figure 36 is a structure map of the area contoured on the B5 correlation marker. The

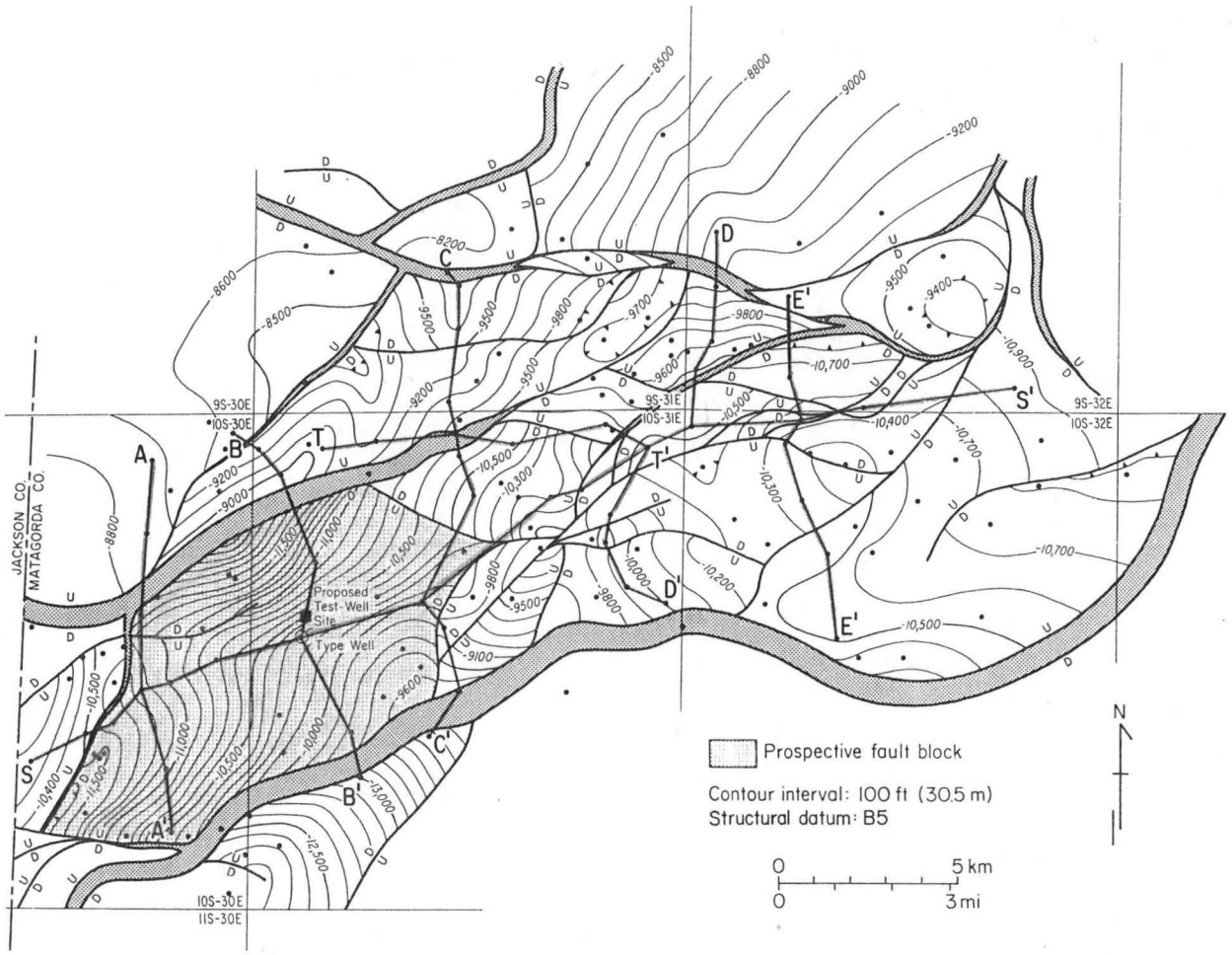

Figure 36. Structure on the B5 correlation marker, Blessing Prospect Area.

0.7 psi/ft geopressure gradient (top of C Zone) occurs near this marker throughout the Blessing area. The map shows several large growth faults trending approximately northeast-southwest. Vertical displacements across these down-to-the-basin faults range from 1,000 ft to more than 3,000 ft. Substantial thickening of section and dip reversal occur on the downthrown sides of these growth faults. This is well displayed on structural cross sections A-A' and B-B' (figs. 37 and 38). A large number of smaller faults with displacements ranging from several tens to a few hundreds of feet segment the geopressured interval and greatly reduce potential reservoir volumes. These smaller faults tend to die out upward so that in the hydropressured interval (A Zone) the density of faulting is lower. Structural cross sections C-C' and D-D' show good examples of the vertical extent of faults (figs. 39 and 40). The smaller faults may have up- or down-to-the-basin displacements. Some appear to have formed to relieve stresses produced by the major growth faulting. Others may have been generated by deep-seated movements of salt or shale.

In the eastern and central parts of the Blessing Prospect Area, high-density faulting resulted in a series of small fault blocks. Structural cross section D-D' shows these blocks and the thick sandstones that occur in some of them (fig. 40). Unfortunately, these sandstones do not have adequate lateral continuities to be considered as prospective. In the western part of the Blessing area, density of faulting is lower, and sandstone continuities are greater.

Sandstone distribution and characteristics

The shallowest interval studied, between -4,500 ft and the B1 correlation marker at about -6,000 ft, contains the Fleming (Miocene) sandstones. In this hydropressured interval, only the largest growth faults interrupt sandstone continuity. Several of these sandstones are over 50 ft

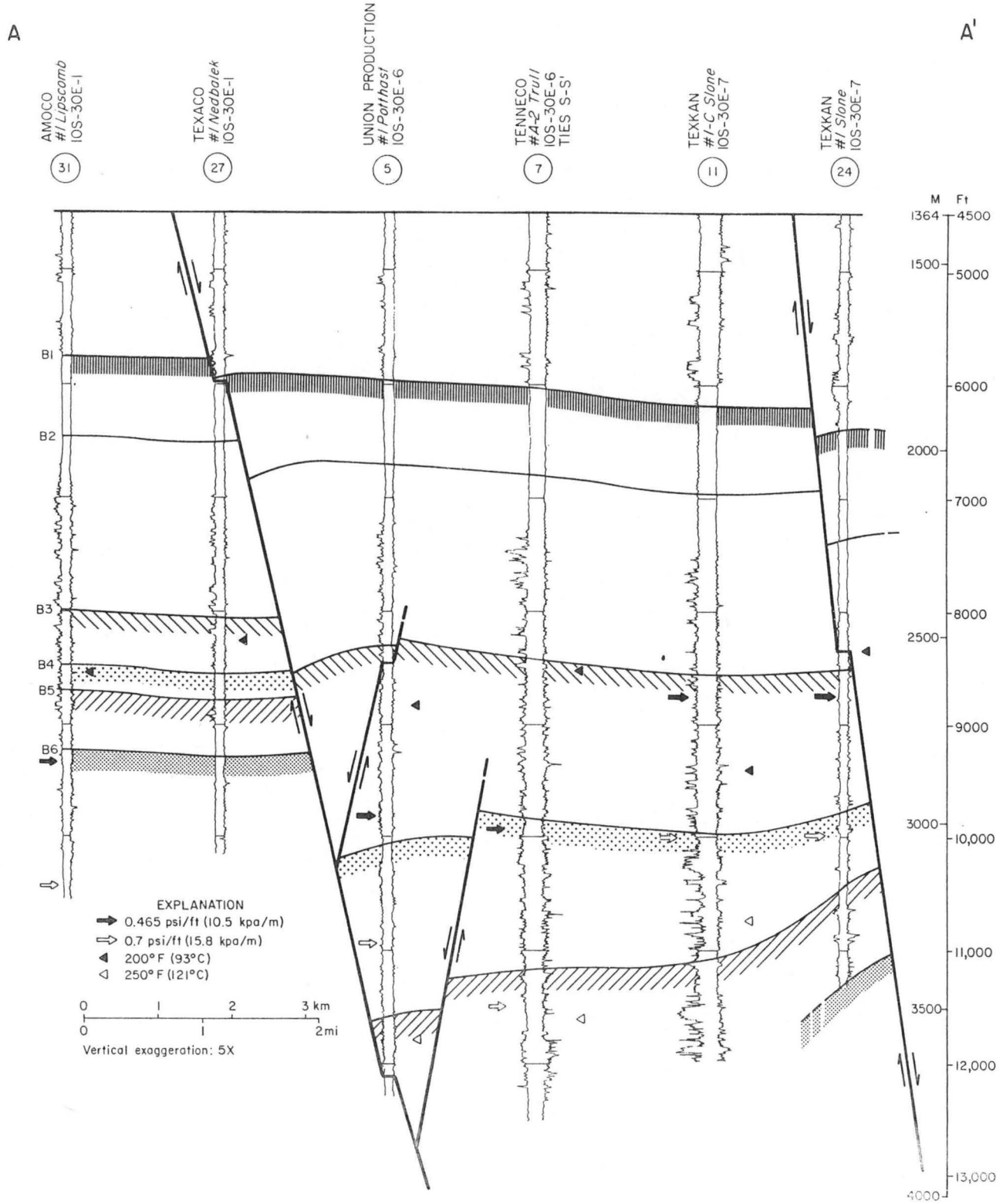

Figure 37. Structural dip section A-A', Blessing Prospect Area.

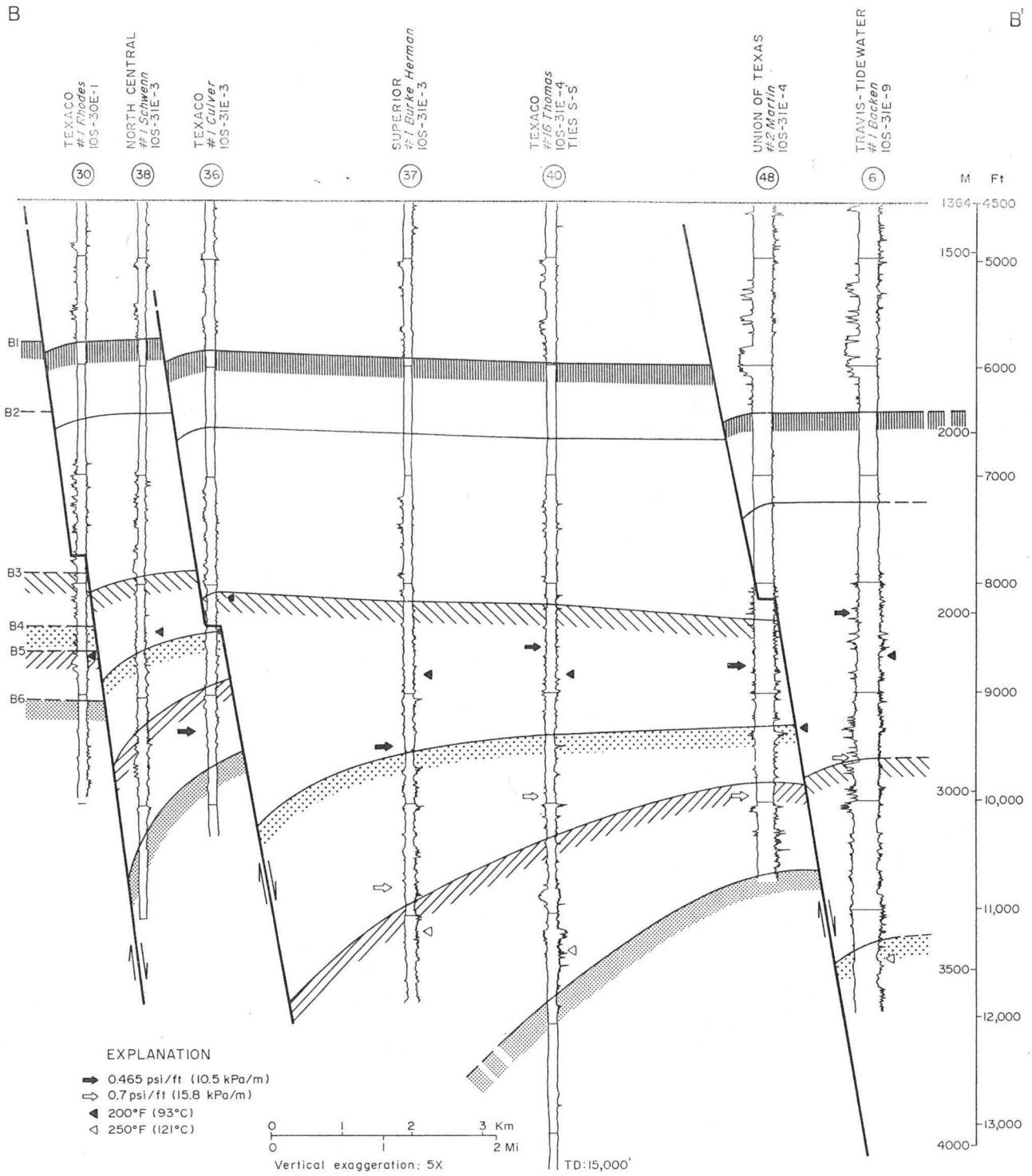

Figure 38. Structural dip section B-B', Blessing Prospect Area.

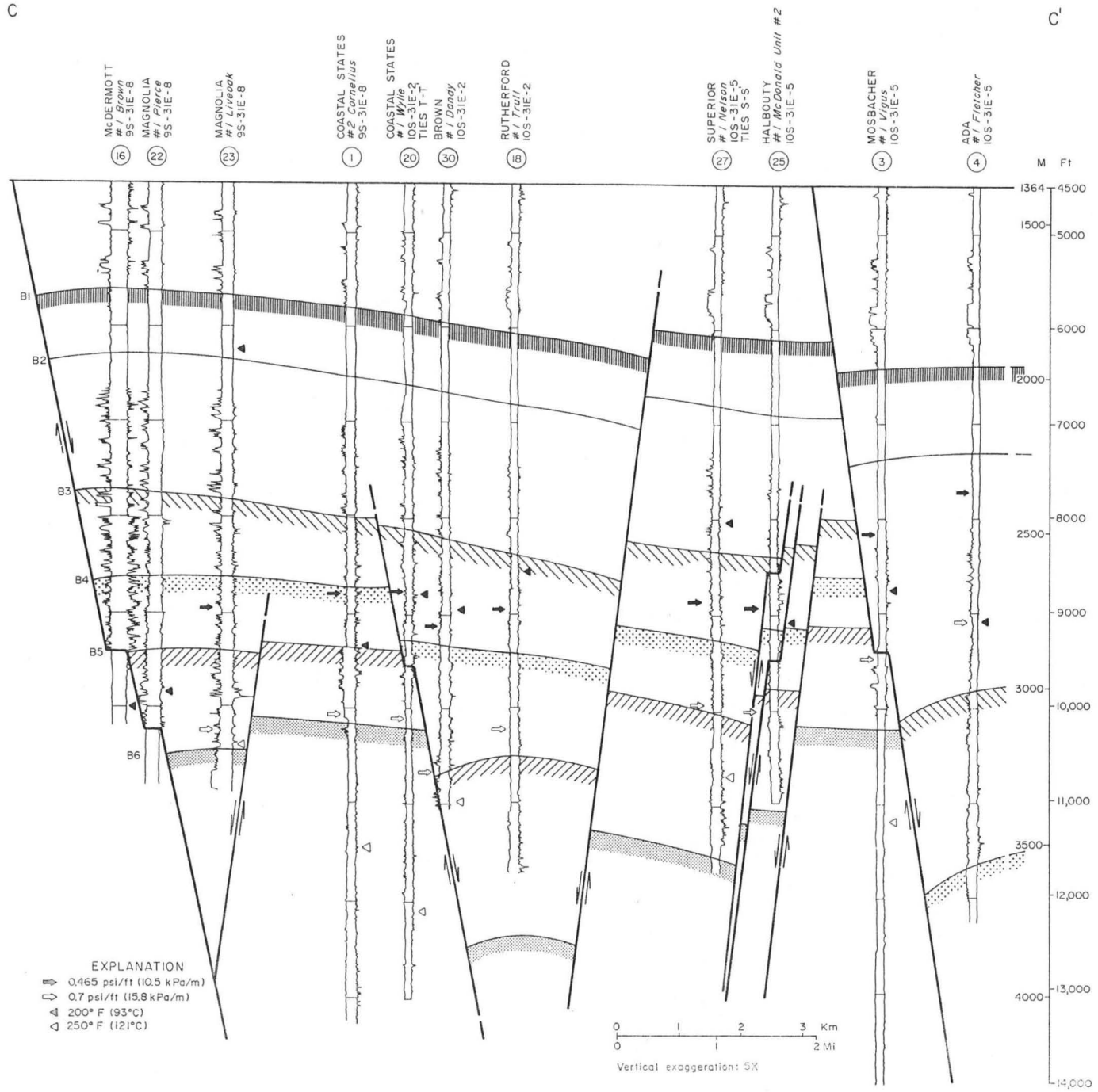

Figure 39. Structural dip section C-C', Blessing Prospect Area.

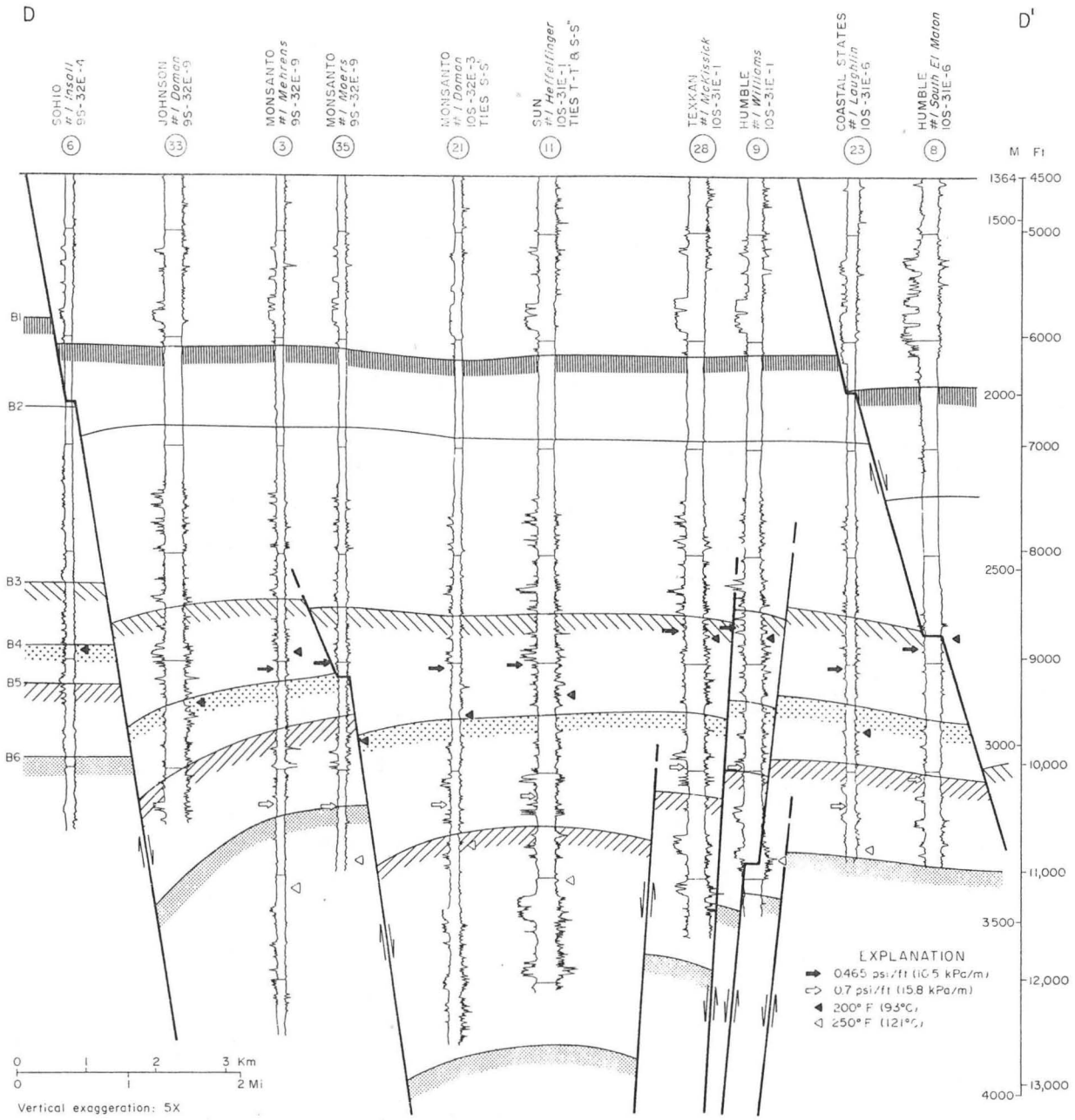

Figure 40. Structural dip section D-D', Blessing Prospect Area.

thick and are continuous throughout fairly large areas (40 mi^2) within the Blessing Prospect Area. However, their pressures and temperatures are too low for them to be prospective for solution gas.

The B1 to B2 correlation interval includes most of the Anahuac Formation; the interval is entirely shale in the Blessing area. The B2 marker is indicated by a distinctive shale resistivity pattern in the lower part of the Anahuac Formation that is easily correlated across most of Matagorda Fairway. This marker was used as the datum for the stratigraphic cross sections (figs. 41 and 42).

The B2 to B3 correlation interval includes the upper third of the Frio Formation and covers the interval from approximately -7,000 ft down to -8,000 or -9,000 ft. This section is also hydropressured (A Zone), but its lower part is near the geopressured zone. Net-sandstone values for this interval generally decrease downdip from more than 500 ft to less than 100 ft. This decrease is irregular along strike, as shown by the net-sandstone contours (fig. 43). Individual sandstones are typically less than 50 ft thick and average less than 20 ft thick. There is little or no structural control over the location of areas of thickest net sandstone in the B2 to B3 interval.

The B3 to B4 interval averages 1,000 ft thick and occurs in the 8,000- to 10,000-ft depth range. The top of the B Zone typically occurs within this interval and temperatures generally exceed 200° F. Net-sandstone values for the B3 to B4 interval exceed 800 ft in one place near the western boundary of the area but decrease rapidly away from this location (fig. 44). Net-sandstone values of 400 ft or greater occur in other isolated areas. Locations of net-sandstone maxima in this interval appear to be influenced by structure. Generally higher values occur along the downthrown sides of large growth faults than occur along the upthrown sides.

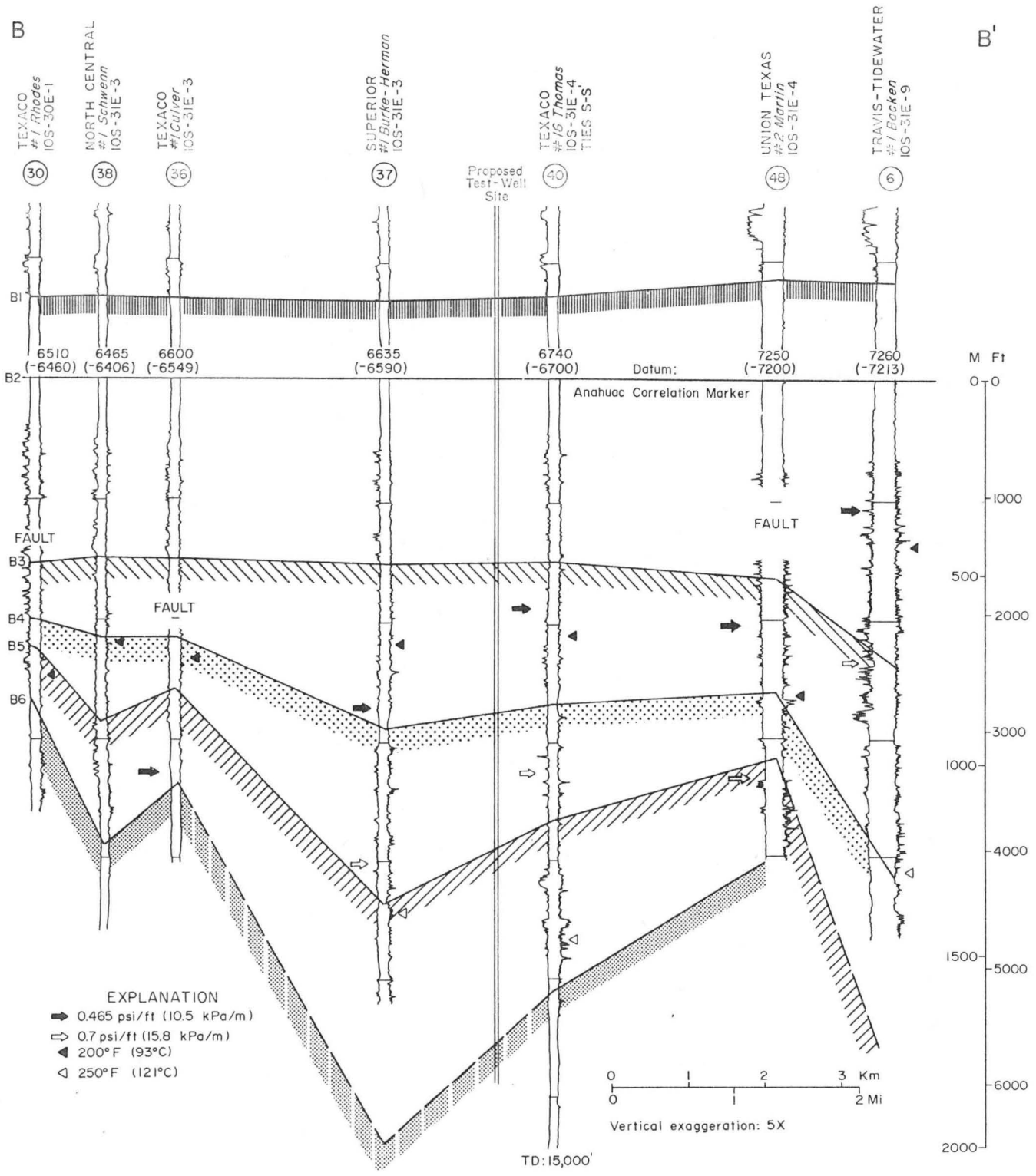

Figure 41. Stratigraphic dip section B-B', Blessing Prospect Area.

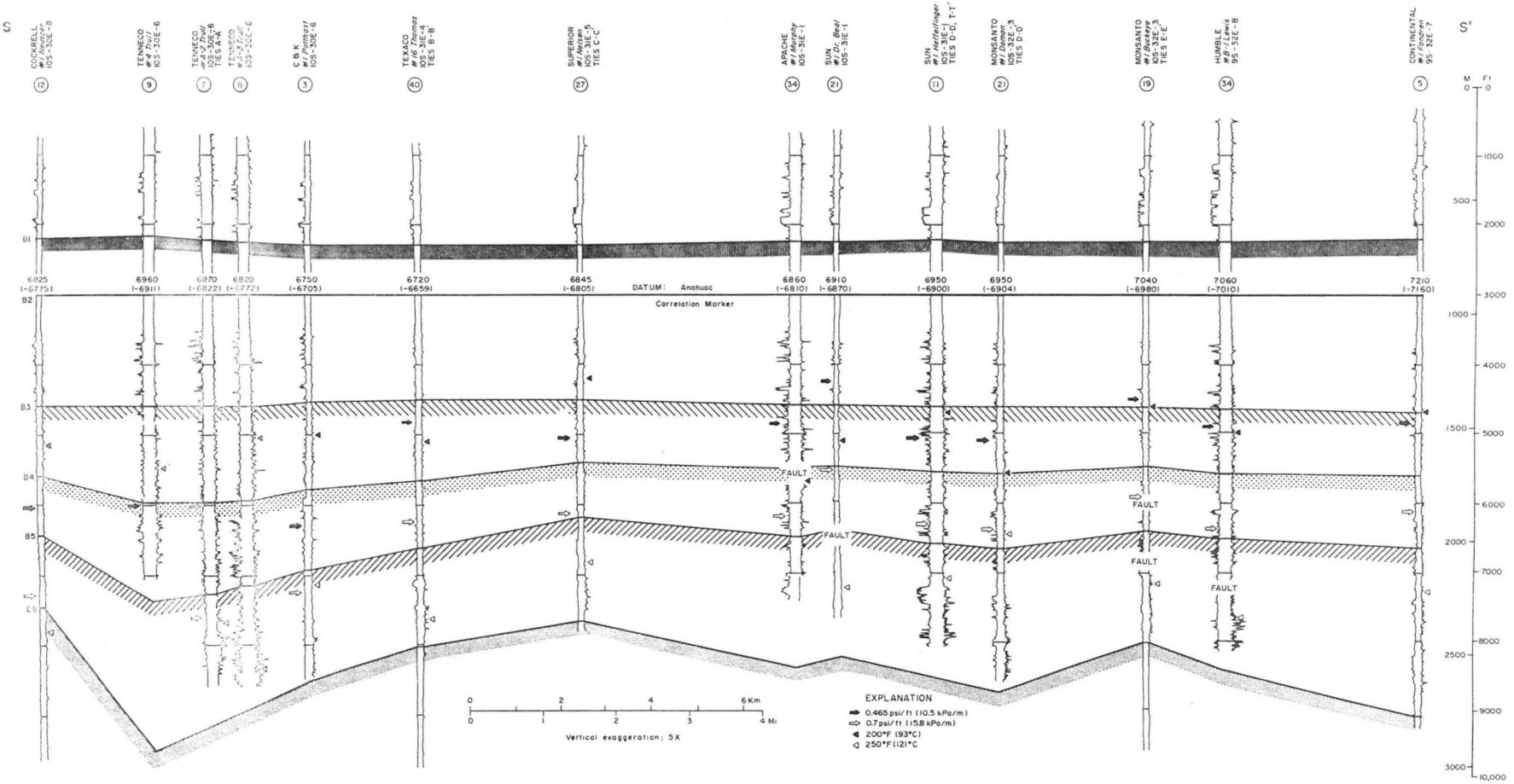

Figure 42. Stratigraphic strike section S-S', Blessing Prospect Area.

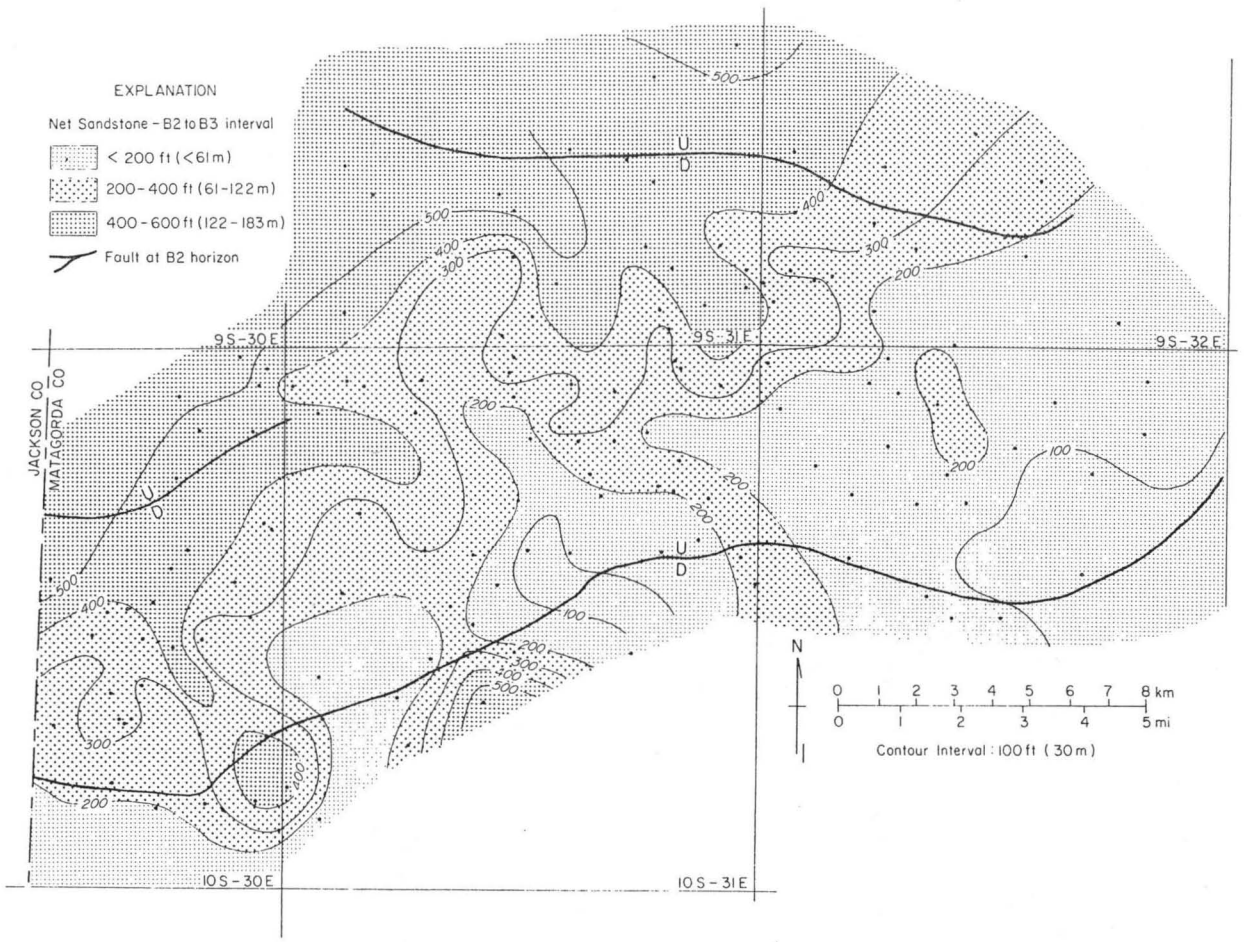

Figure 43. Net sandstone, B2 to B3 interval, Blessing Prospect Area.

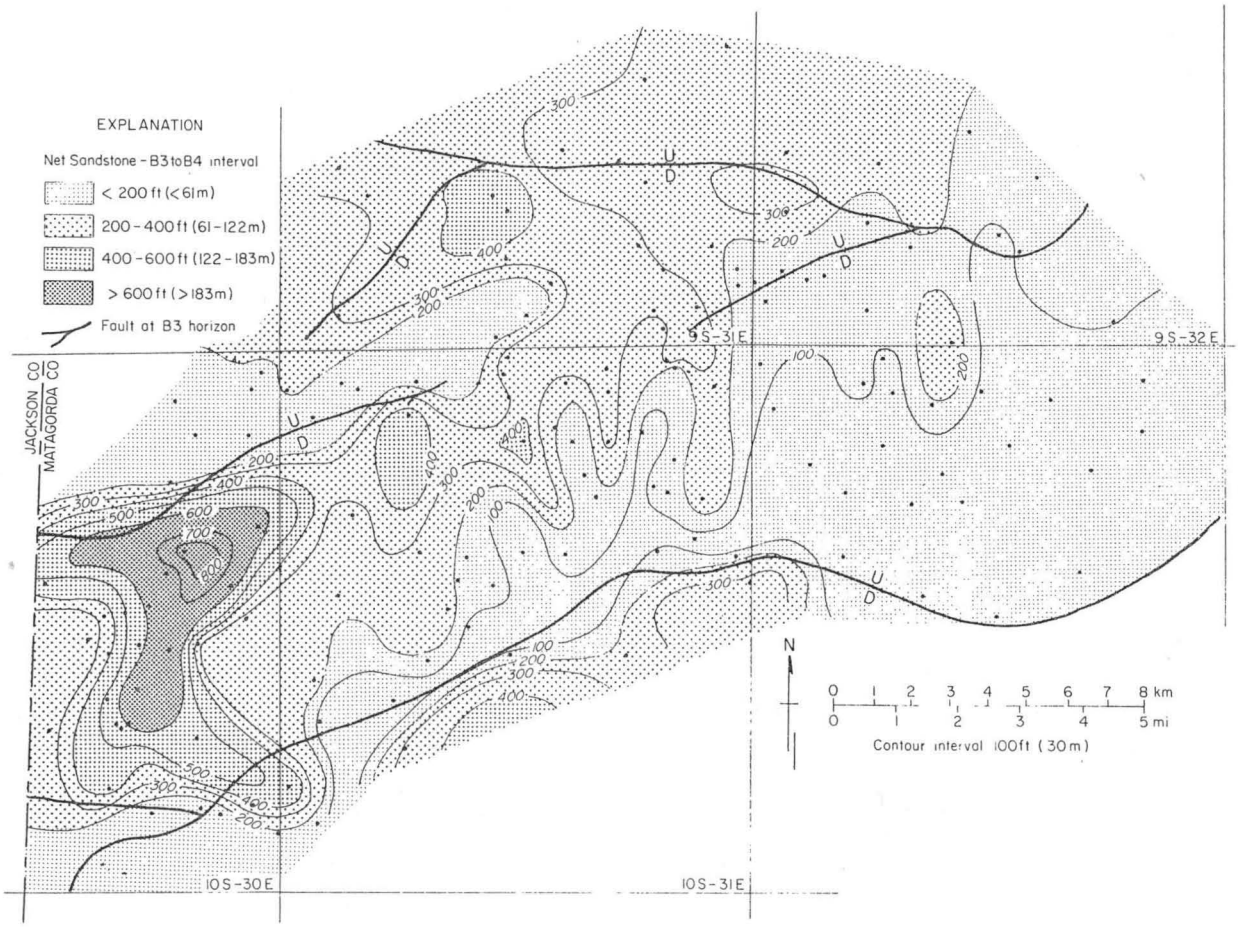

Figure 44. Net sandstone, B3 to B4 interval, Blessing Prospect Area.

Individual B3 to B4 sandstones are similar in size and character to those in the overlying interval. Most are 50 ft thick or less but tend to thicken (up to 100 ft) updip against the growth faults. Structural cross section C-C' (fig. 39) shows thickening of B3 to B4 sandstones against the northernmost fault. Structural cross section B-B' (fig. 38) shows progressive downdip expansion of the B3 to B4 interval across two growth faults (compare wells No. 30, 38 and 37).

The B4 to B5 interval averages 1,000 ft thick, ranging from 200 to 1,500 ft thick. This large range in thickness is due to the greater fault-related expansions occurring in the lower intervals (B4 to B6). The B5 correlation marker is the structural datum for the Blessing Prospect Area structure map (fig. 36). This horizon dips significantly into the downthrown sides of large growth faults. Individual sandstones in the B4 to B5 interval are similar in thickness to those in the overlying B3 to B4 interval, but thickening on the downthrown sides of growth faults is even more pronounced. Sandstone thickening and interval expansion influenced the B4 to B5 net-sandstone patterns (fig. 45). Net-sandstone maxima occur in strike-aligned trends parallel to and downdip from the growth faults.

The B5 to B6 interval includes the deepest Frio sandstones. The B6 correlation marker is probably at or near the base of the Frio Formation. No significant sandstones occur below B6 in this area. The B5 to B6 interval varies greatly in thickness, ranging from 500 ft to 2,500 ft thick in wells penetrating the B6 horizon. Depths to the top of this interval are shown on the structure map (fig. 36). The B5 to B6 net-sandstone map (fig. 46) shows continued structural influence on localization of net-sandstone maxima. Areas with greater than 400 ft of sandstone parallel the large growth faults on their downthrown sides. Net-sandstone contour patterns are similar to those of the B4 to B5 interval.

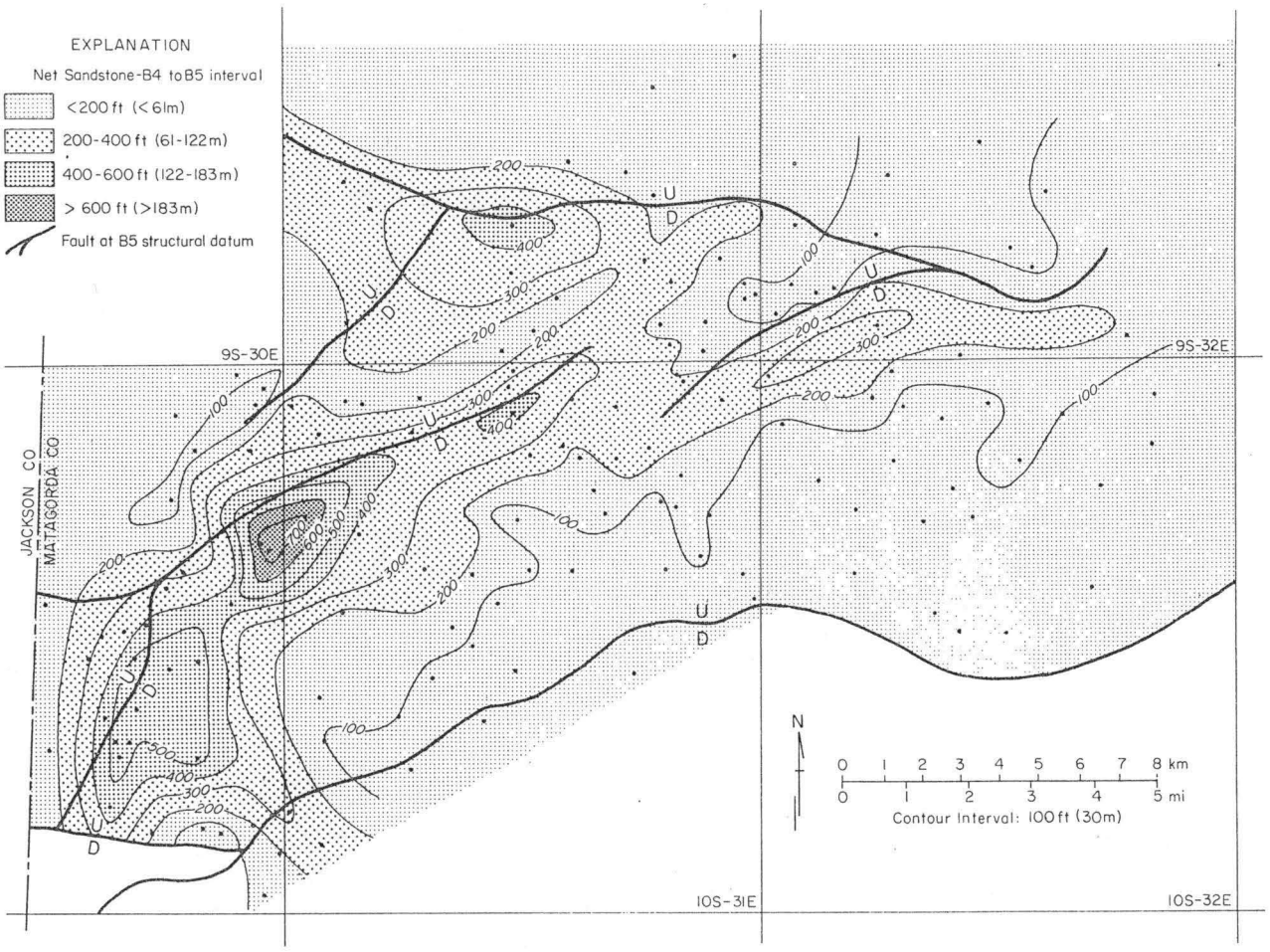

Figure 45. Net sandstone, B4 to B5 interval, Blessing Prospect Area.

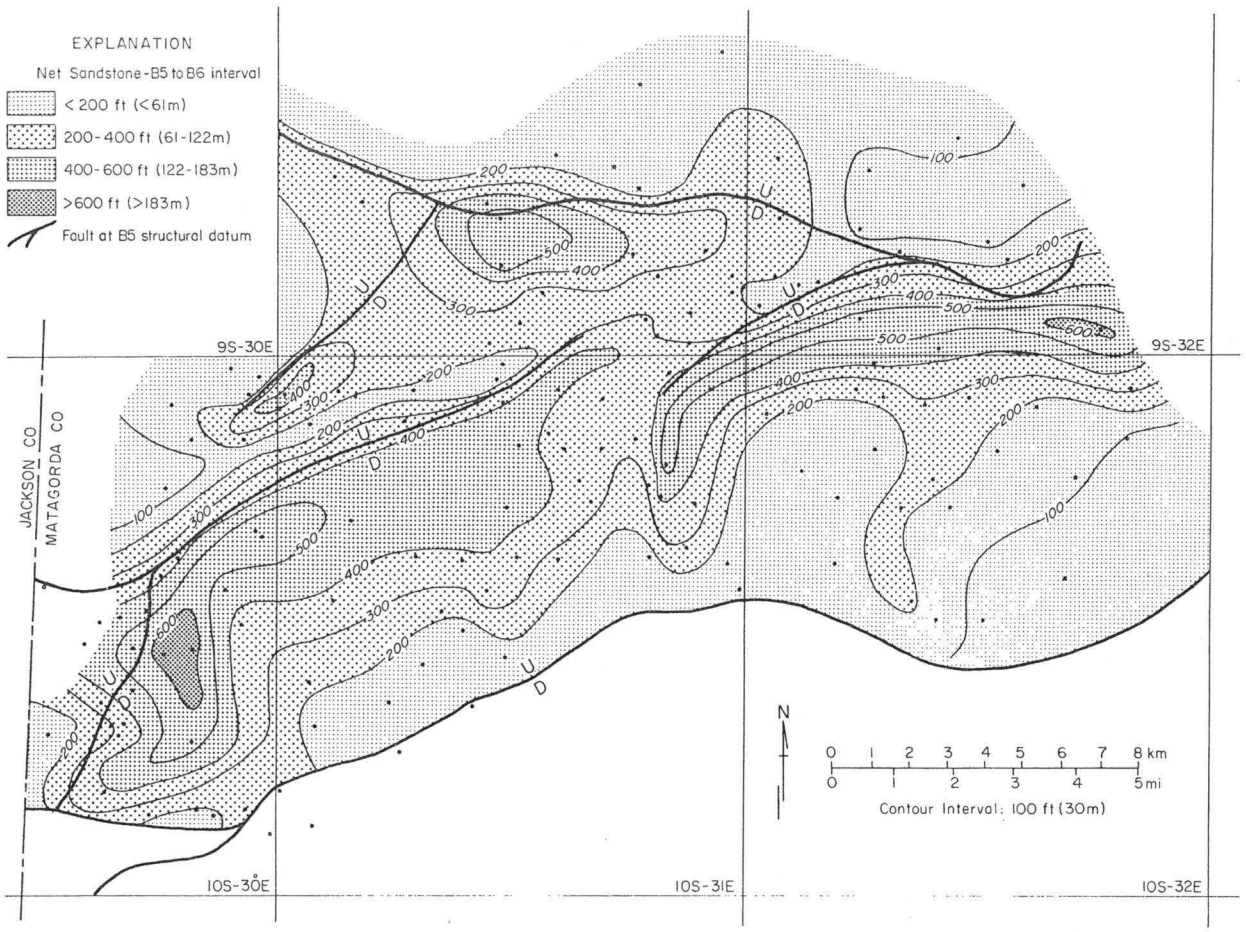

Figure 46. Net sandstone, B5 to B6 interval, Blessing Prospect Area.

Individual sandstones in the B5 to B6 interval are generally the thickest of any in the Blessing area, as shown by electric log patterns. Several of these C Zone sandstones cause pronounced SP deflections to be sustained for 100 to 200 ft vertically. These prospective sandstones occur at depths ranging from 10,500 to 12,500 ft and have temperatures of 250° F or greater. However, their lateral continuity is interrupted by the numerous large and small faults that segment this interval. Because these few thick sandstones constitute most of the total sandstone in the B5 to B6 interval, their lateral thickness changes are expressed by the net-sandstone map for this interval (fig. 46). Electric log patterns for B5 to B6 sandstones are best developed on cross section D-D' (fig. 40, wells 21 and 11), and their lateral changes are shown by strike section S-S' (fig. 42).

Formation fluid pressures and temperatures

Bottom-hole shut-in pressures (BHSIP) measured by drill-stem tests (DST) of reservoirs producing oil and gas in Matagorda County (fig. 13) show that the top of geopressure (0.465 psi/ft) occurs at an average depth of 9,650 ft. A change in geothermal gradient at the same depth (fig. 7) tends to confirm the average top of geopressure determined from BHSIP data as discussed earlier in the section on methodology. Parameter plots for strike and dip sections (fig. 36) show that the B Zone becomes shallower northeastward along strike sections S-Sa and Sa-Sb (figs. 47 and 48) and downdip along section B-B' (fig. 49). The top of the B Zone is deepest (10,800 ft) at well No. 8 on section S-Sa (fig. 47) and reaches its shallowest point (8,800 ft) at well No. 21 (10S-31E-1) on section Sa-Sb (fig. 48) and at well No. 48 (10S-31E-4) on dip section B-B' (fig. 49).

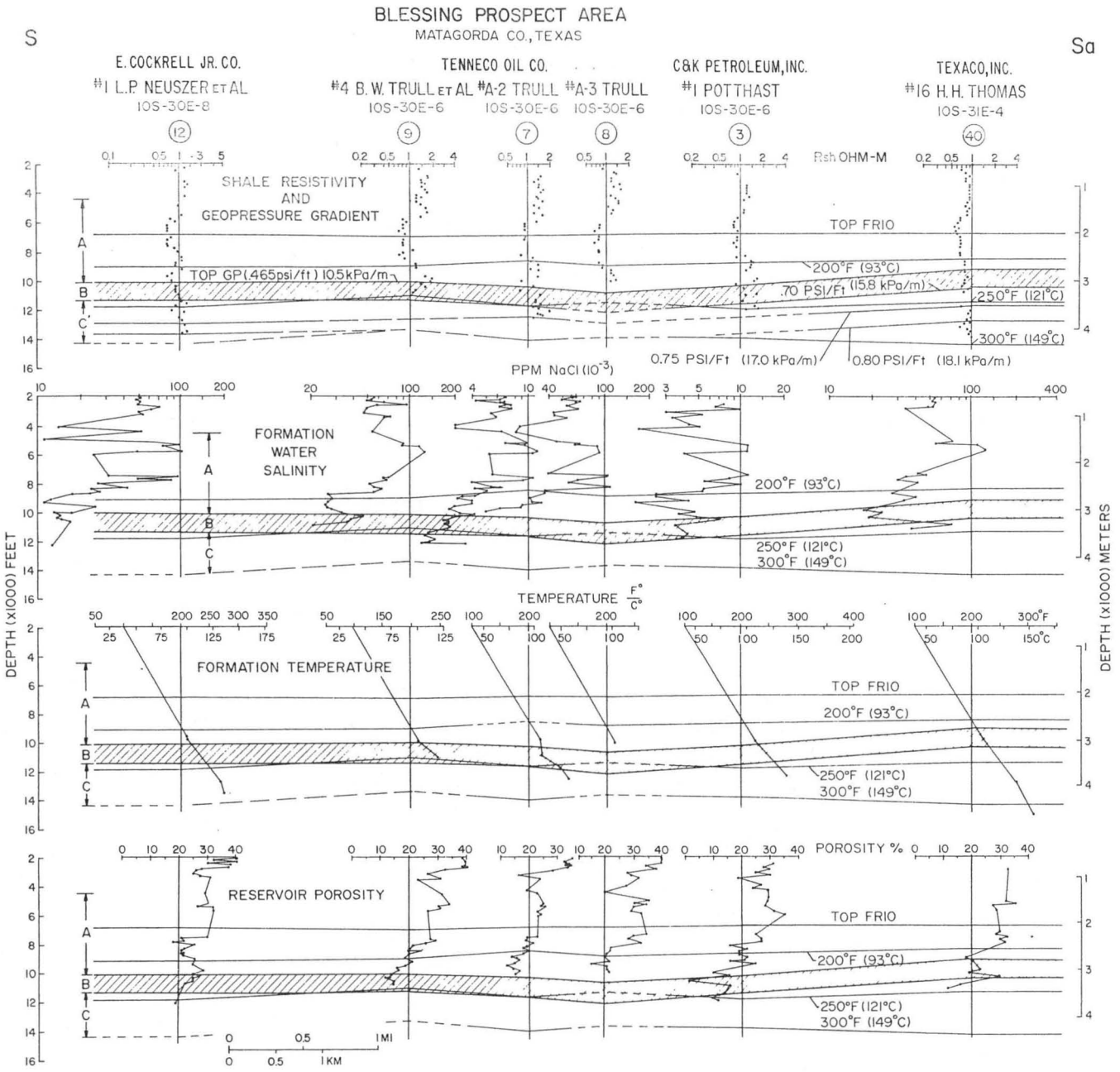

Figure 47. Parameter plots for wells along strike section S-Sa, Blessing Prospect Area, Matagorda County, Texas. Salinity units are given as ppm NaCl (10^{-3}). The factor (10^{-3}) shows that the real units have been multiplied by 10^{-3} to give the numbers indicated on the scale. For example, 100 ppm NaCl on the scale means that the real salinity is 100,000 ppm NaCl.

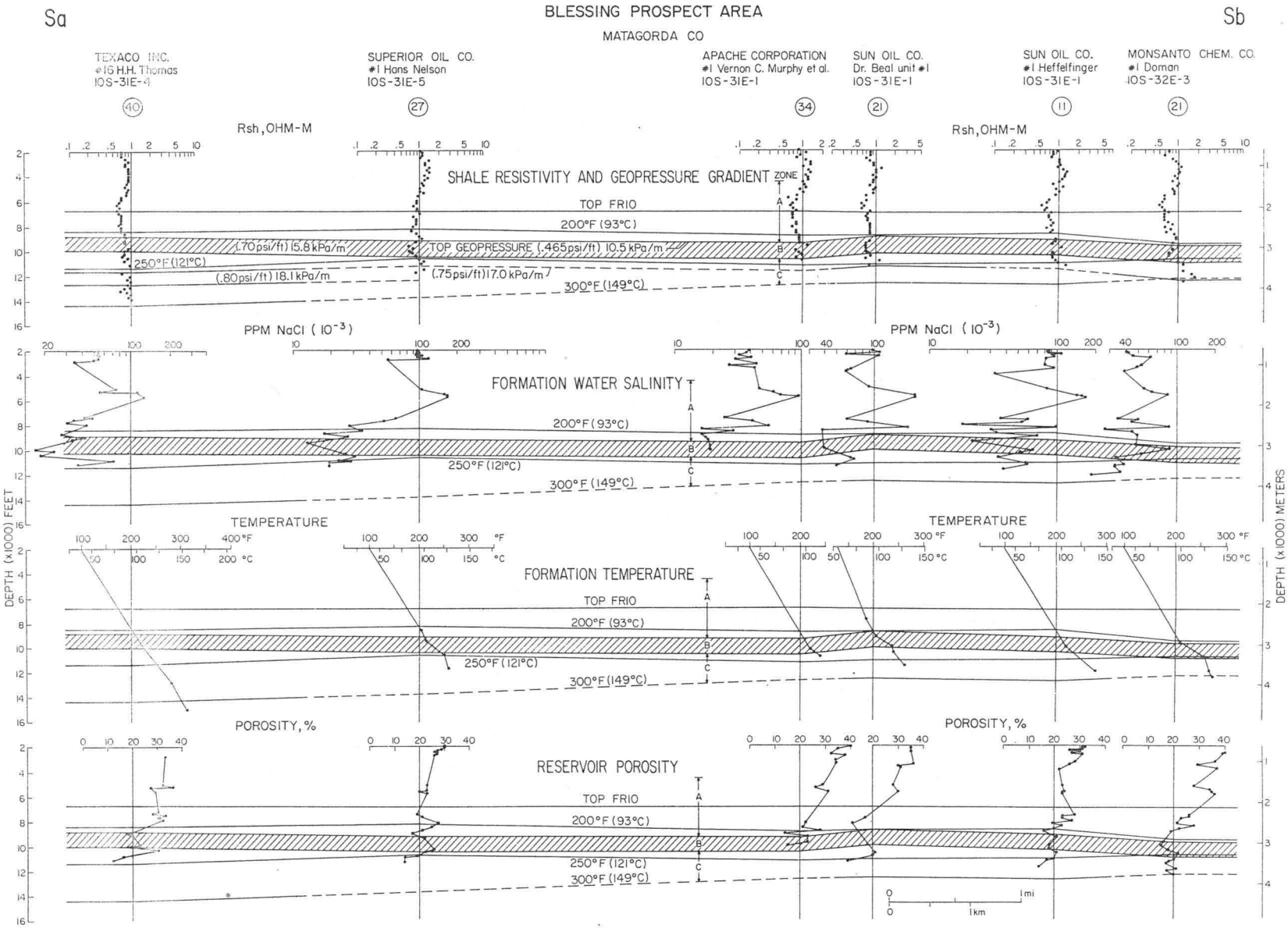

Figure 48. Parameter plots for wells along strike section Sa-Sb, Blessing Prospect Area, Matagorda County, Texas.

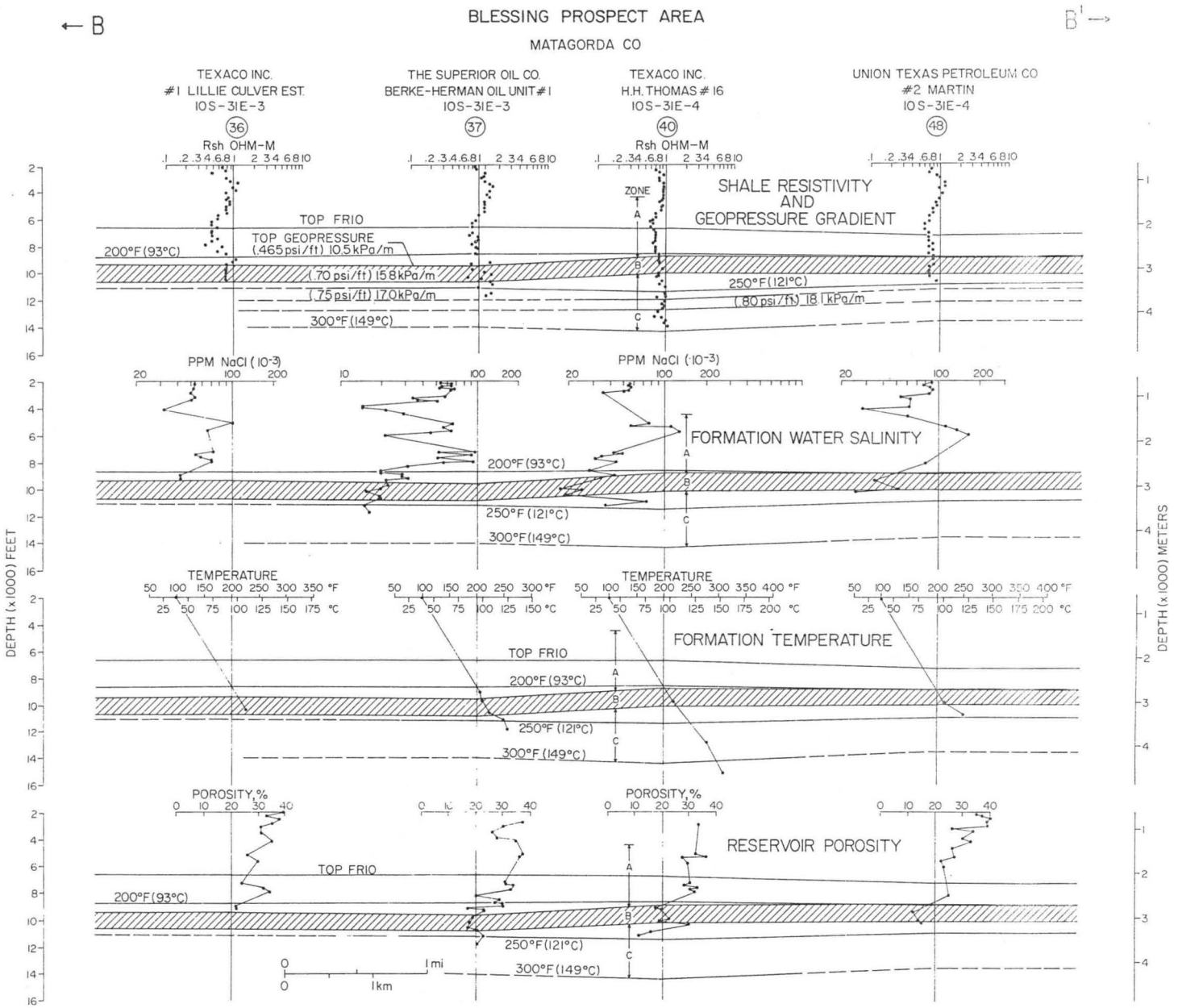

Figure 49. Parameter plots for wells along dip section B-B', Blessing Prospect Area, Matagorda County, Texas.

The top of the B Zone on dip section C-C' (fig. 50) is deepest (-9,600 ft) at updip wells No. 1 and No. 20, and is shallowest (-9,200 ft) at downdip wells No. 27 and No. 25. The thickness of the B Zone in each well is 1,250 ft.

Equilibrium temperatures at the top and base of the B Zone along strike section S-Sa-Sb (figs. 47 and 48) range from 200° to 232° F and 230° to 265° F, respectively. The average temperature difference across the B Zone is 31° F. Tenneco No. 4 Trull, well No. 9 on section S-Sa (fig. 47), shows the highest temperature (265° F) at the base of the B Zone; the temperature difference across the zone is 43° F.

On dip section B-B' (fig. 49) equilibrium temperatures range from 202° to 212° F (average 210° F) at the top of the B Zone and from 215° to 233° F (average 231° F) at the base. Average temperatures show a fairly even distribution across the section in the B Zone.

Section C-C' (fig. 50) shows that temperatures range from 190° to 213° F (average 207° F) at the top and from 212° to 243° F (average 231° F) at the base. The average difference in temperature across the B Zone is 24° F. Superior No. 1 Nelson (well No. 27) shows the highest temperatures, from 210° to 242° F across the B Zone, on section C-C'.

Formation water salinity

Salinity profiles for wells in the Blessing Prospect Area vary considerably in detail but generally follow recognized trends for the Gulf Coast area (fig. 14). Highest salinities occur in the A Zone. These commonly exceed 100,000 ppm NaCl and generally reach peak values at depths between 5,000 and 6,000 ft. The B Zone along strike sections S-Sa and Sa-Sb (figs. 47 and 48) has an average salinity of 29,000 ppm NaCl at both

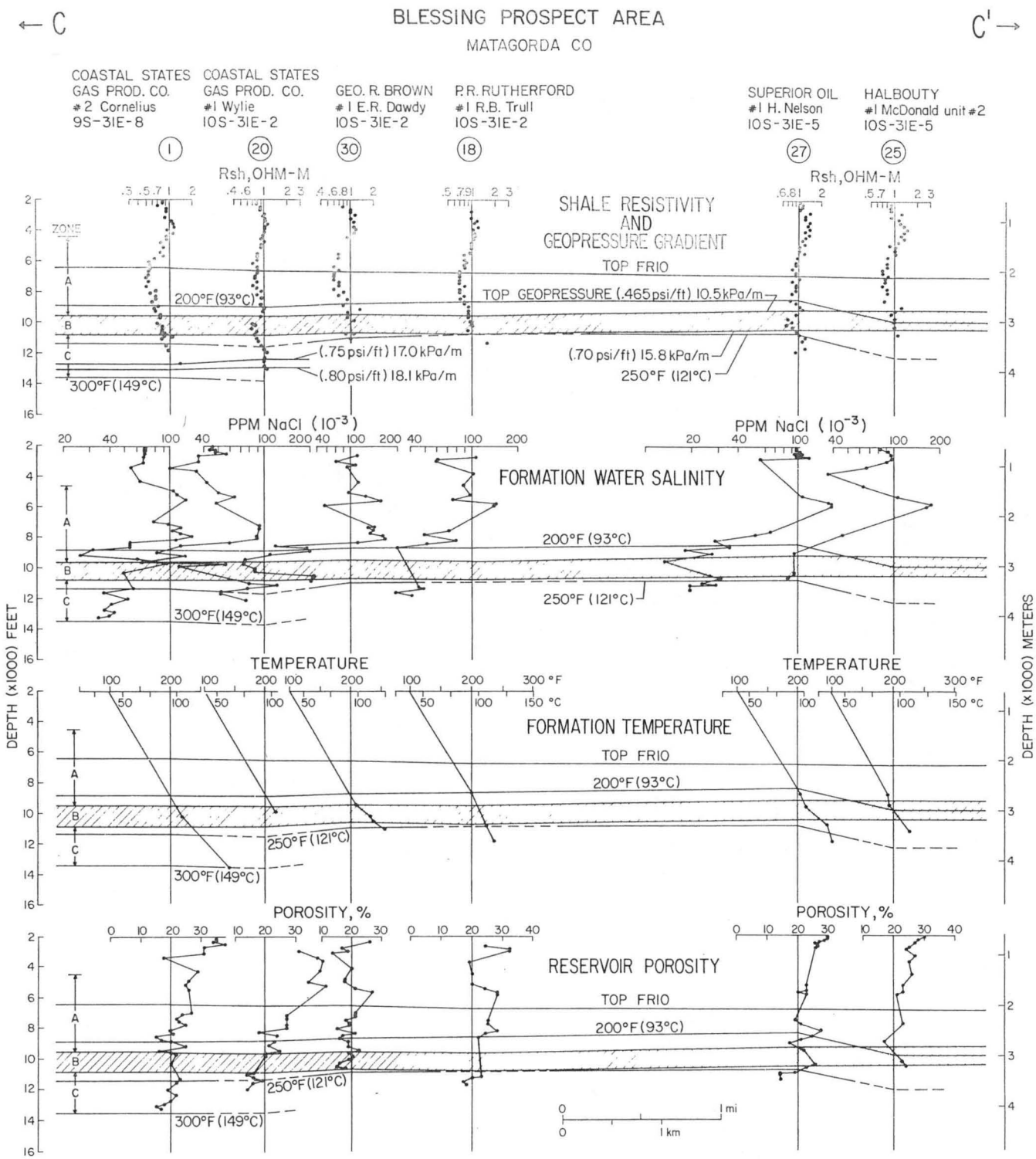

Figure 50. Parameter plots for wells along dip section C-C', Blessing Prospect Area, Matagorda County, Texas.

the top and base, indicating little or no change in salinity with depth in a given well. Across the prospect area, however, large changes in salinity do occur laterally within the B Zone, as indicated by values that vary from 10,000 to 49,000 ppm NaCl at the top and from 14,000 to 46,000 ppm NaCl at the base. Low to moderate salinities are observed in the C Zone. Salinities determined for dip sections B-B' and C-C' (figs. 49 and 50) do not differ markedly from those found on the strike sections.

Porosity

Porosity profiles for wells in the Blessing Prospect Area show local variations within an overall trend of porosity decreasing with depth. These variations are associated with compaction and diagenetic processes that reduce primary porosity and increase secondary porosity of reservoir sandstones. On strike sections S-Sa and Sa-Sb (figs. 47 and 48), porosity ranges from 6 to 25 percent (average 17 percent) along the top of the B Zone and from 12 to 27 percent (average 19 percent) along the base of the B Zone. Through the B Zone, the average decrease in porosity with depth is 2 percent.

On dip section B-B' (fig. 49) porosity along the top of the B Zone ranges from 18 to 20 percent and averages 19 percent. The range along the base is 15 to 27 percent and the average is 21 percent.

Porosity on dip section C-C' (fig. 50) ranges from 18 to 23 percent and averages 20 percent along the top of the B Zone. Along the base of the B Zone porosity ranges from 16 to 26 percent and averages 21 percent.

Blessing test-well site

Geology. -- In the Blessing Prospect Area, the largest unsegmented fault block contains the thickest accumulation of B and C Zone sandstones. Delineated as the prospective fault block, this area has been selected as

suitable for a test-well site (fig. 36). Located in the southwestern part of the Blessing area, the prospective fault block covers at least 25 mi^2 at the B5 horizon. It is bounded to the north and south by large growth faults (1,500 ft of vertical displacement at the B5 horizon); to the west by a smaller growth fault (1,000 ft of vertical displacement); and to the east by several intersecting antithetic faults (vertical displacements less than 300 ft). A proposed test-well site is located 0.5 mi north of the type well, Texaco No. 16 Thomas, along the line of cross section B-B' (fig. 36). On the stratigraphic version of section B-B', this proposed site is shown between wells 37 and 40 (fig. 41).

The prospective fault block includes all or parts of Blessing, Potthast, Trull, Slone, and Pheasant oil and gas fields. In the northern half of the block, gas and oil are produced from A and B Zone sandstones at depths ranging from 8,000 to 9,500 ft. In the southern half of the block, gas production is concentrated in C Zone sandstones at depths of 11,000 ft or greater.

Structural control of sandstone characteristics influenced selection of the Blessing test-well site. Long-term activation of the northern bounding growth fault resulted in expanded intervals and thickened sandstones between the B3 and B6 correlation markers along the downthrown side of this fault. All Frio B and C Zone sandstones in this area are within the B3 to B6 interval. Almost immediately updip from the southern bounding growth fault, expansion of the interval begins and increases northward until it reaches a maximum at the northern fault. Structural and stratigraphic sections B-B' clearly show this expansion (figs. 38 and 41). Net-sandstone maps for the intervals B3 to B4, B4 to B5, and B5 to B6 show an average of 1,000 ft of sandstone in the B and C Zones in the northern half

of the prospective fault block, compared with an average of 500 ft of sandstone in these zones in the southern half of the block (figs. 44, 45, and 46).

Reversal of the regional southward dip to a northward dip is shown on structural cross section B-B' (fig. 38). The northward expansion of each successively lower interval results in progressively steeper northward dips on horizons B4, B5, and B6. Another important aspect of this structural configuration is the progressive deepening of the intervals as one moves northward from the southern bounding growth fault. The contours on the B5 structural datum show almost 2,000 ft of descent from south to north in the prospective fault block (fig. 36).

The net effect of this structural configuration is a southward shift of the structural high at progressively deeper correlation markers. At the B2 and B3 horizons, the shallowest point in the prospective fault block is along the northern margin. Structural section B-B' shows the southward shift of the high until, at the B6 horizon, it is immediately updip from the southern bounding growth fault (fig. 38).

The Blessing test-well site is located in the northern part of the prospective fault block, off the structural high of the B6 horizon. Few wells penetrate the entire Frio Formation in this area. The type log from the Texaco No. 16 Thomas well exhibits characteristic log patterns for the prospective sandstones in this part of the block (fig. 34). In the two intervals, between the B3 and B5 markers (mostly B Zone), individual sandstones range from 10 to 40 ft thick in the Texaco No. 16 Thomas well and from 40 to 100 ft thick in several wells about 1 mi to the north. These sandstones are separated from each other by 30- to 100-ft-thick shales. In the B5 to B6 interval (C Zone), one sandstone consistently exceeds 100 ft thick and typically shows pronounced SP deflection. Several other

sandstones in this interval average 40 to 60 ft thick. A number of sandstones less than 20 ft thick are also present. Shales in the B5 to B6 interval range from less than 10 ft to more than 100 ft thick. At least 1,000 ft of net sandstone occurs between the B3 and B6 markers across the northern part of the prospective fault block.

Formation parameters. -- Pressure gradients derived from shale resistivity relations (fig. 12) exceed 0.85 psi/ft at depths below 13,000 ft in the type well, Texaco No. 16 Thomas. The B Zone is located in the depth interval from 8,800 to 10,050 ft and the base of the C Zone is at a depth of 14,300 ft. Equilibrium temperatures across the B Zone range from 212° to 232° F; salinities within the B Zone range from 18,000 to 69,200 ppm NaCl, and methane solubility ranges from 26 to 29 standard cubic feet per barrel (SCF/B) when Dunlap and Dorfman "curve" values of R_{mf} are used in the calculations (fig. 51). The deepest sandstones show poor SP development, and, thus, salinities were estimated from trends in the area (fig. 51).

Porosity data for the Texaco No. 16 Thomas well were derived from (1) sidewall-core measurements, (2) the resistivity (induction) log, and (3) the sonic log (fig. 52). All of these methods give data that cluster in the depth range from 7,000 to 11,300 ft and that provide a reasonable average relationship between porosity and depth. Porosity determined from transit times from the sonic log requires no compaction correction. Average calculated porosities at the top and base of the B Zone are 19 and 23 percent, respectively.

Most of the permeabilities from sidewall-core measurements range from 8 to 195 md in the depth interval of 7,000 to 10,000 ft (fig. 53). From depths of 10,000 to 12,000 ft, most permeability data cluster in the range from 5 to 60 md. The limited amount of permeability data at an average depth of 14,500 ft shows that permeabilities are less than 11 md.

The least-squares-regression curve for the plot of sidewall-core permeability versus porosity (fig. 54) shows a relation of the form

$$K = ae^{b\phi} \tag{8}$$

where K = permeability, md

ϕ = porosity, fractional

$a = 0.21$

$b = 0.22$

e = base of the system of natural logarithms.

The correlation coefficient for the relation is 0.78. Permeability values are greater than 100 md when the porosity exceeds 25 percent and are less than 10 md when the average porosity is less than 18 percent.

Reservoirs with good strike and dip continuity occur in the depth intervals of 10,790 to 10,890 ft and of 11,160 to 11,230 ft (table 2). These sandstones, which are recommended for testing, occur in the C Zone and pressure gradients average 0.765 psi/ft. In the upper reservoir, fluid temperature is 241° F, salinity is calculated to be 97,000 ppm NaCl, and methane solubility is 23.0 SCF/B. In the lower reservoir, temperature is 248° F, calculated salinity is 85,000 ppm NaCl, and methane solubility is 25.6 SCF/B. Sidewall-core measurements indicate that porosities average 18 percent in the upper sandstone and 21 percent in the lower one and that permeabilities average 23 md in the upper sandstone and 26 md in the lower unit. However, the in situ reservoir permeability may be considerably less than 25 md. The area of the fault block in which these sandstone units occur is about 25 mi^2.

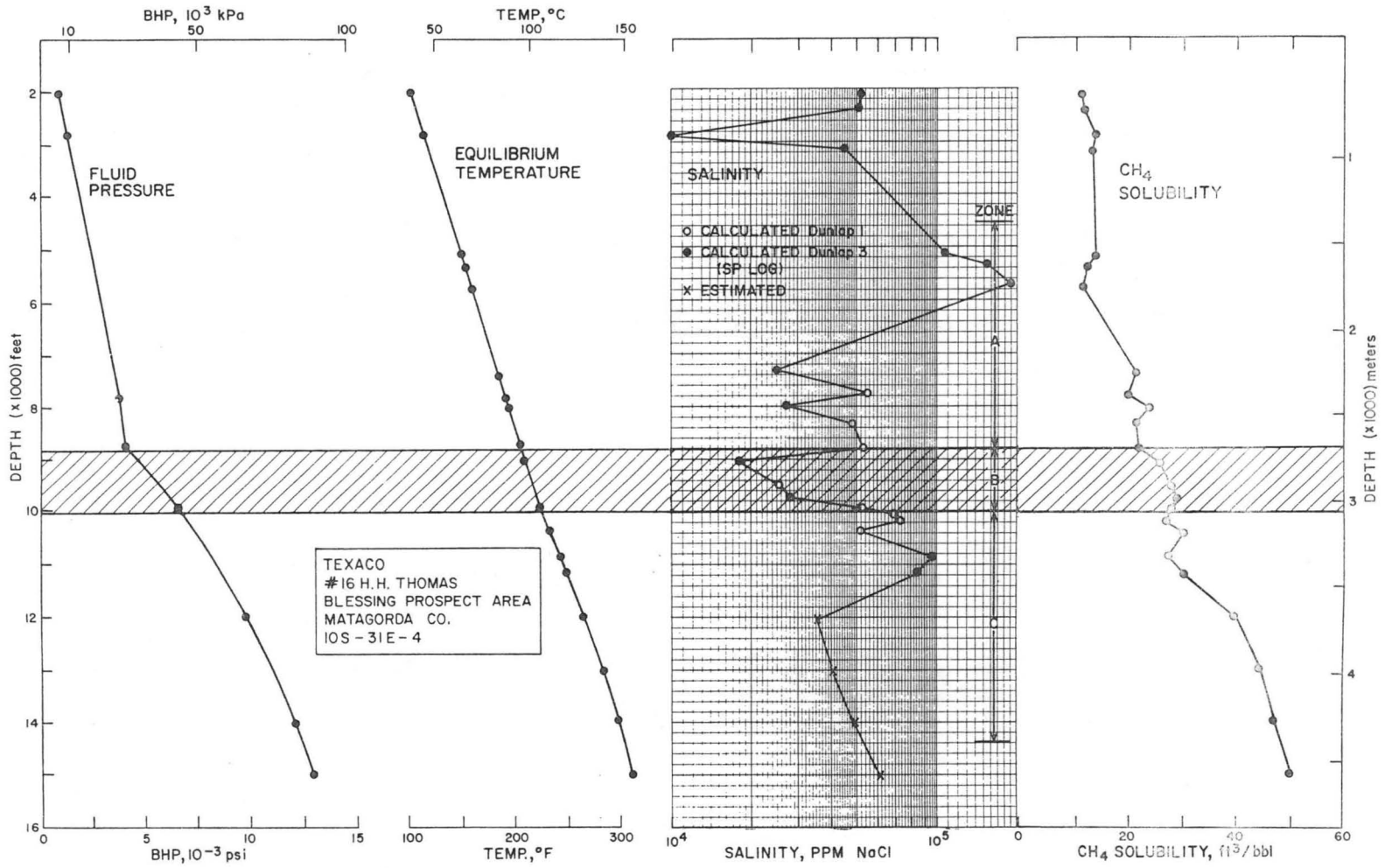

Figure 51. Formation parameters versus depth for Texaco No. 16 Thomas, Blessing Prospect Area, Matagorda County, Texas.

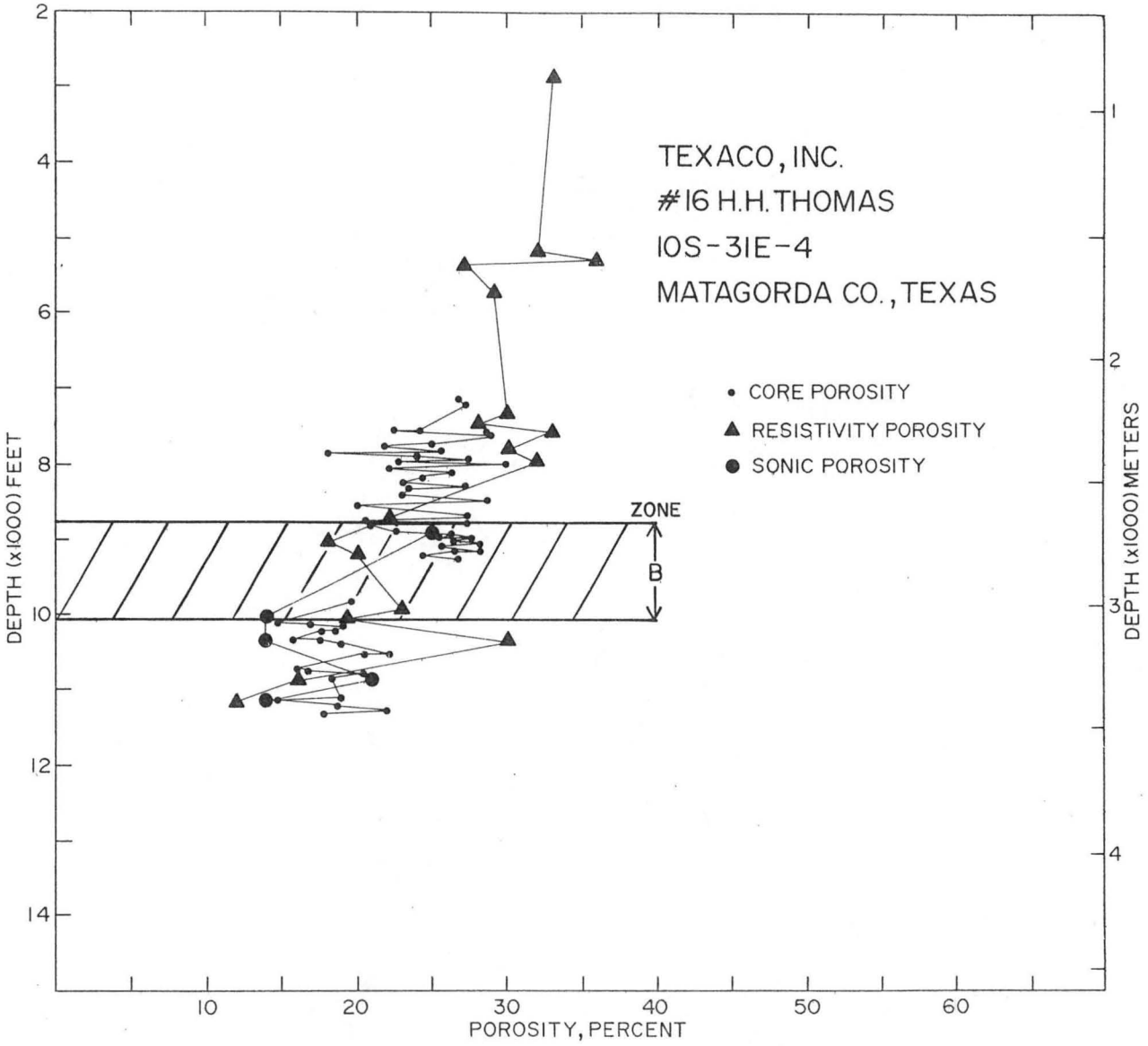

Figure 52. Comparison of porosity data from sidewall cores, resistivity log, and sonic log, Texaco No. 16 Thomas, Blessing Prospect Area, Matagorda County, Texas.

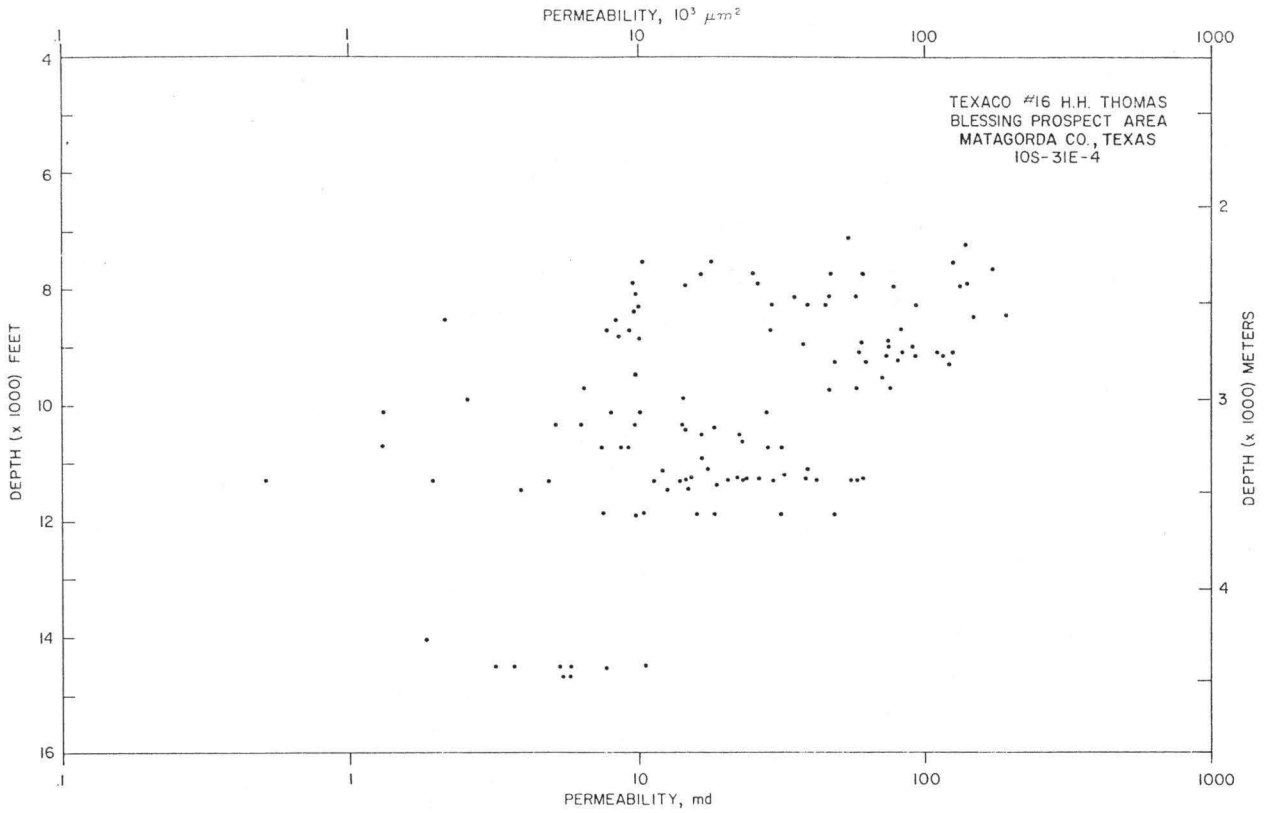

Figure 53. Sidewall-core air permeability versus depth, Texaco No. 16 Thomas, Blessing Prospect Area, Matagorda County, Texas.

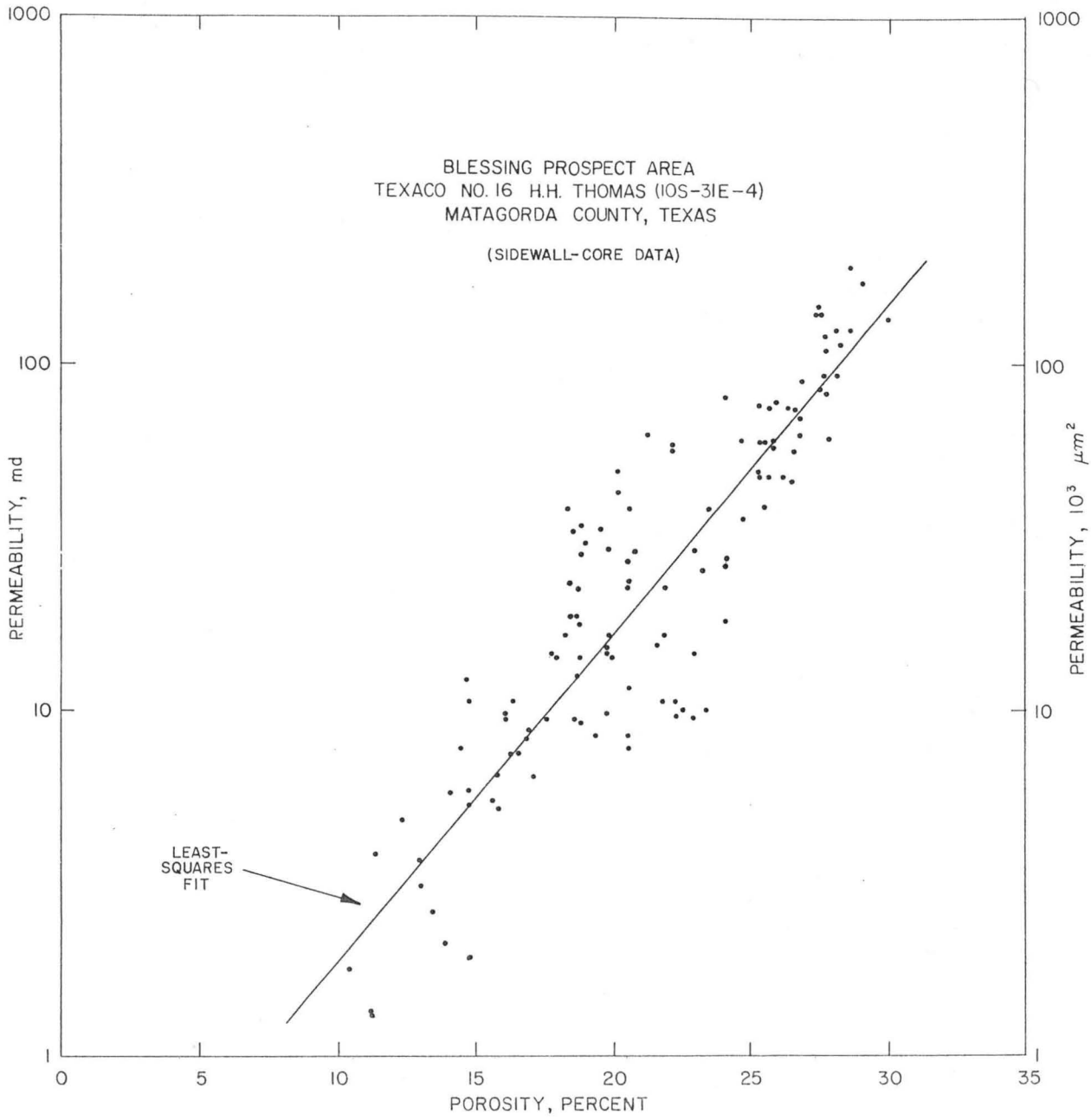

Figure 54. Sidewall-core air permeability versus porosity, Texaco No. 16 Thomas, Blessing Prospect Area, Matagorda County, Texas.

Table 2. Reservoir parameters of selected sandstones in the prospect areas.

Prospect	Depth (ft)	Sandstone thickness (ft)	Porosity* (%)	Permeability* (md)	T_E (°F)	Pressure gradient (psi/ft)	Salinity (10^{-3} ppm)	CH_4 (SCF/B)	Fault block area (mi^2)	Zone	Type Well
Blessing	10,790	100	18(SWC)	23(SWC)	241	0.76	97	23.0	25	C	Texaco No. 16 Thomas
	11,160	70	21(SWC)	26(SWC)	248	0.77	85	25.6	25	C	10S-31E-4, Matagorda Co.
Old Ocean	10,700	200	6 (calc.)	no	227	0.65	170	19.0	35	B	Abercrombie No. 16 BRLD
	11,570	140	13 (calc.)	core	238	0.66	72	29.0	35	B	8S-35E-9
	12,180	80	14 (calc.)	data	247	0.75	70	32.5	35	C	Brazoria Co.
Nueces	8,360	50	16 (calc.)	no	200	0.46	87	19.0	120	A	Mobil No. 8-A Donigan
Bay	9,450	50	16 (calc.)	core	215	0.46	31	25.0	120	A	18S-21E-9
	10,335	85	8 (calc.)	data	230	0.66	60	28.0	120	B	Nueces Co.
Corpus	7,265	85			185	0.46	126	15.5	120	A	Hamon No. 3 St. Tr. 8
Channel	7,580	60	11-20 (calc.)		189	0.46	131	15.6	120	A	18S-22E-1
	7,970	100	22.7†	331†	195	0.55	101	17.7	120	B	Nueces Co.
Sarita	8,910	45	25	100-200	200	0.46	80	19.9	17	A/B	Arkansas Fuel No. 1 Hubert
(shallow)	8,975	90	25	750	204	0.46	78	20.3	17	A/B	22S-19E-4, Kleberg Co.
Sarita	11,205	50	26†	30-60†	254	0.86	123	27.8	2	C	Humble No. B-9 East
(deep)	11,300	70	21 (calc.)		257	0.86	120	28.6	2	C	23S-19E-2
	11,590	95	19 (calc.)		263	0.87	126	28.9	2	C	Kenedy Co.
	12,365	45	15 (calc.)		280	0.88	143	29.6	2	C	
	12,560	110	14 (calc.)		285	0.85	148	29.4	2	C	
	13,310	80	14 (calc.)		303	0.87	147	32.7	2	D	
	13,690	160	14 (calc.)		310	0.87	120	38.0	2	D	
Tordilla	10,725	100	9 (calc.)	no	261	0.56	138	22.2	27	B	Humble No. 12 Kleberg
	11,410	130	10 (calc.)	core	279	0.85	146	27.8	27	C	28S-17E-2
	12,340	>120	8 (calc.)	data	294	0.77	70	39.4	27	C	Willacy Co.
Lake	11,248	65	12-14	<7.7	267	0.60	76	29.9	58	B	Superior
Creek	11,676	70	10-14	<15.0	276	0.63	88	30.6	58	B	No. 3 So. Tx. Dev. Co.
	11,800	155	11-14	<21.0	279	0.65	52	36.3	58	B	2N-36E-3
	13,588	80	12-15	1-5	313	0.78	172	29.5	58	D	Montgomery Co.

* Values from whole-core analyses unless indicated
† Data from wells in vicinity of type well
SWC = sidewall-core analysis
calc. = calculated

Old Ocean Prospect Area

The Old Ocean Prospect Area is in the eastern part of the Matagorda Fairway (fig. 30). The area is 12 mi long from east to west, 9 mi wide, and covers approximately 108 mi^2. Electric logs from 80 wells were correlated, and two cross sections were constructed for this prospect area (fig. 33). Eight correlation markers (O1 to O8) divide the section below -4,500 ft into nine study intervals. However, a lack of deep well control prevented mapping of sandstones in the B and C Zone below the O6 marker.

Most of this prospect area is within the Old Ocean oil and gas field, which has been producing since 1934. Production has been mostly from the A and shallow B Zones between the depths of 8,500 ft and 11,500 ft. Although significant amounts of sandstone occur below -11,500 ft, few wells in this area were drilled below this level.

Structure

According to Gardner (1952), the Old Ocean Field overlies a deep-seated salt dome, which gives rise to a domal structure in the prospective fault block (fig. 55). However, Frio sandstones have not been significantly uplifted or thinned by salt movement. As shown by the structure map of the Old Ocean area (fig. 55), the shallowest part of the structure is 10,000 ft below sea level at the O5 marker.

The density of faulting is lower in the Old Ocean area than it is in the Blessing area. A series of branching growth faults form the northern boundary of the area. These faults enclose several wedge-shaped blocks that trend northeast-southwest (fig. 55). The low temperature and pressure conditions, and limited areal extents of these blocks make them nonprospective for the production of methane-bearing waters. The southern boundary of the Old Ocean area is also a series of faults enclosing small, wedge-shaped blocks.

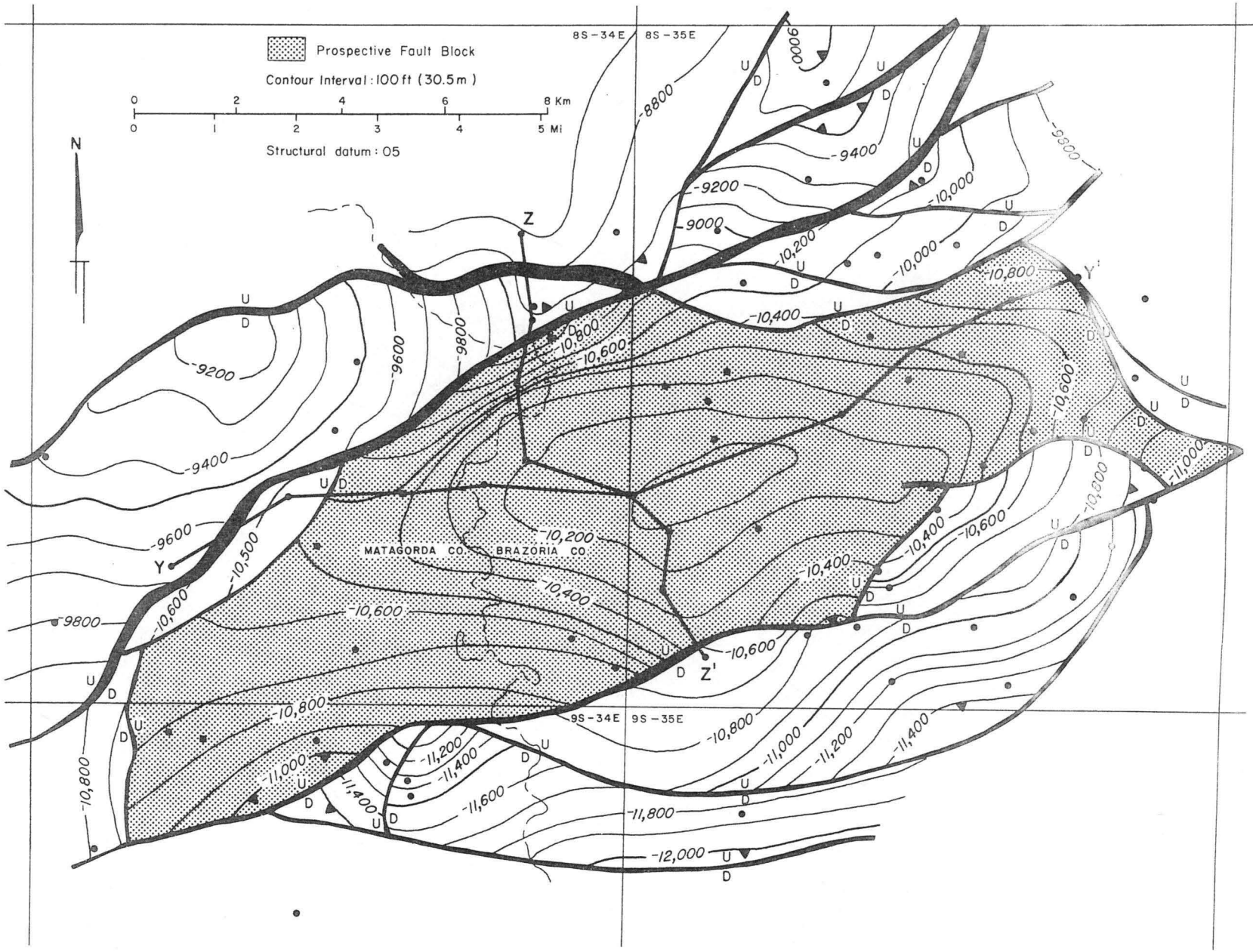

Figure 55. Structure on the 05 correlation marker, Old Ocean Prospect Area.

The prospective fault block, the largest block in the Old Ocean area, covers 35 mi^2 at the 05 horizon. The structural configuration at deeper intervals in the northern part of the block is not clear because of the lack of deep well control (see wells 7 and 26 on Z-Z', fig. 56); therefore, the intervals below the 06 correlation marker could not be mapped.

Sandstone distribution and characteristics

The 01 to 02 interval includes the Miocene Fleming sandstones. These A Zone sandstones occur between -5,000 to -7,000 ft and are continuous throughout most of the Old Ocean area. Net-sandstone values range from 500 to over 1,000 ft for the 01 to 02 interval, and individual sandstones are 20 to 150 ft thick.

The 02 to 03 interval consists of the upper half of the Anahuac Shale, which is 1,500 to 2,000 ft thick in this area (fig. 56). The 03 marker is a distinctive shale resistivity pattern in the Anahuac. It is the stratigraphic datum for the Old Ocean Prospect Area and is correlative with the B2 marker in the Blessing Prospect Area.

The top of the Frio sandstones occurs within the 03 to 04 interval at depths ranging from 8,000 to 9,000 ft. These uppermost Frio sandstones are thin, averaging less than 20 ft thick, and are separated by abundant, thick shales (fig. 56). Net sandstone for this A Zone interval is less than 200 ft in the prospective fault block (fig. 57).

The 04 to 05 interval averages 600 ft thick, but its net sandstone is no greater than 200 ft and is typically much less (fig. 58). Individual sandstones in this A Zone interval are less than 30 ft thick.

In the 05 to 06 interval, the sandstones are thicker and more numerous than in the overlying Frio intervals (fig. 56). This deep A Zone interval averages 600 to 800 ft thick but expands considerably (up to 2,000 ft) in the northern part of the prospective fault block. Individual sandstones

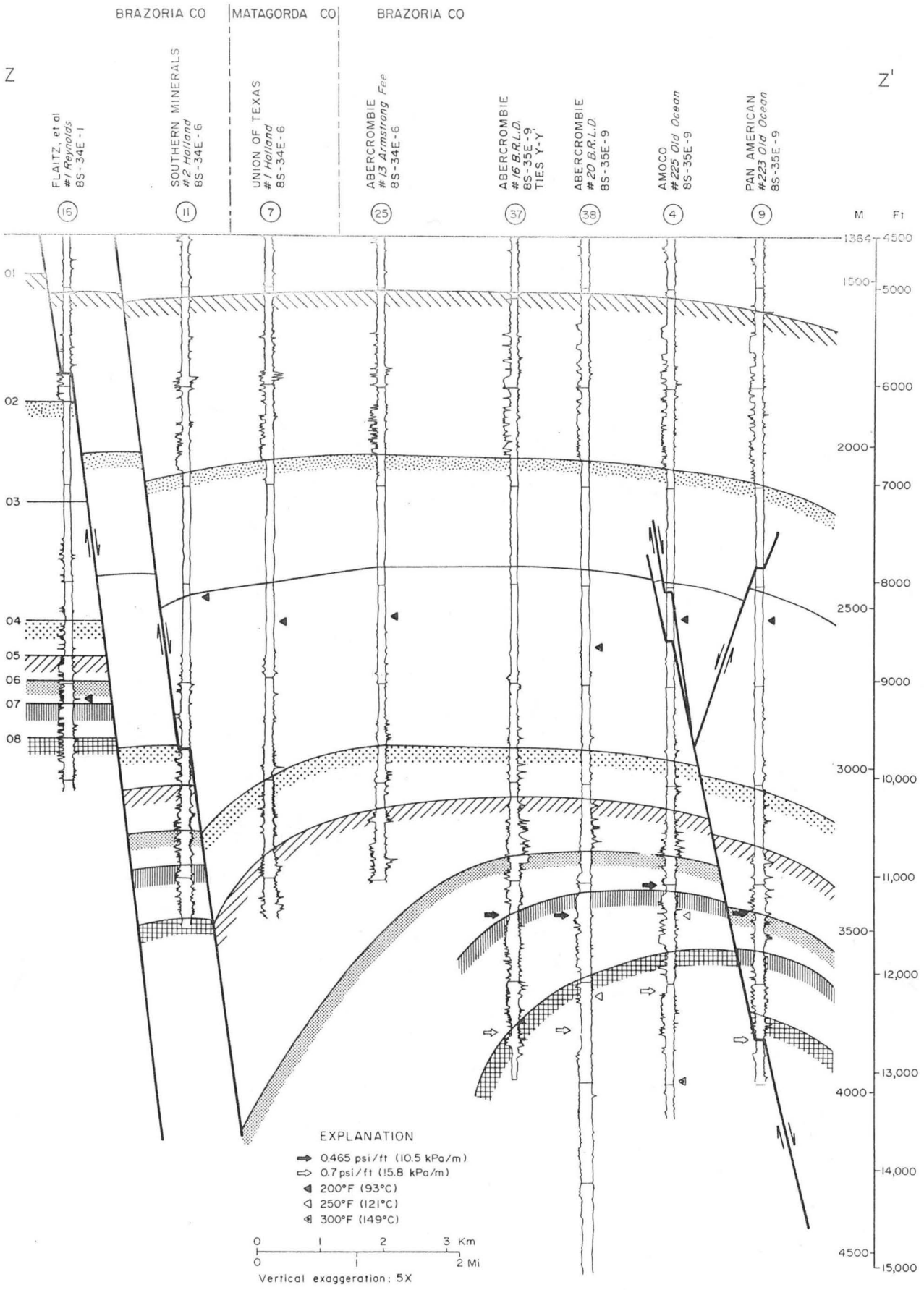

Figure 56. Structural dip section Z-Z', Old Ocean Prospect Area.

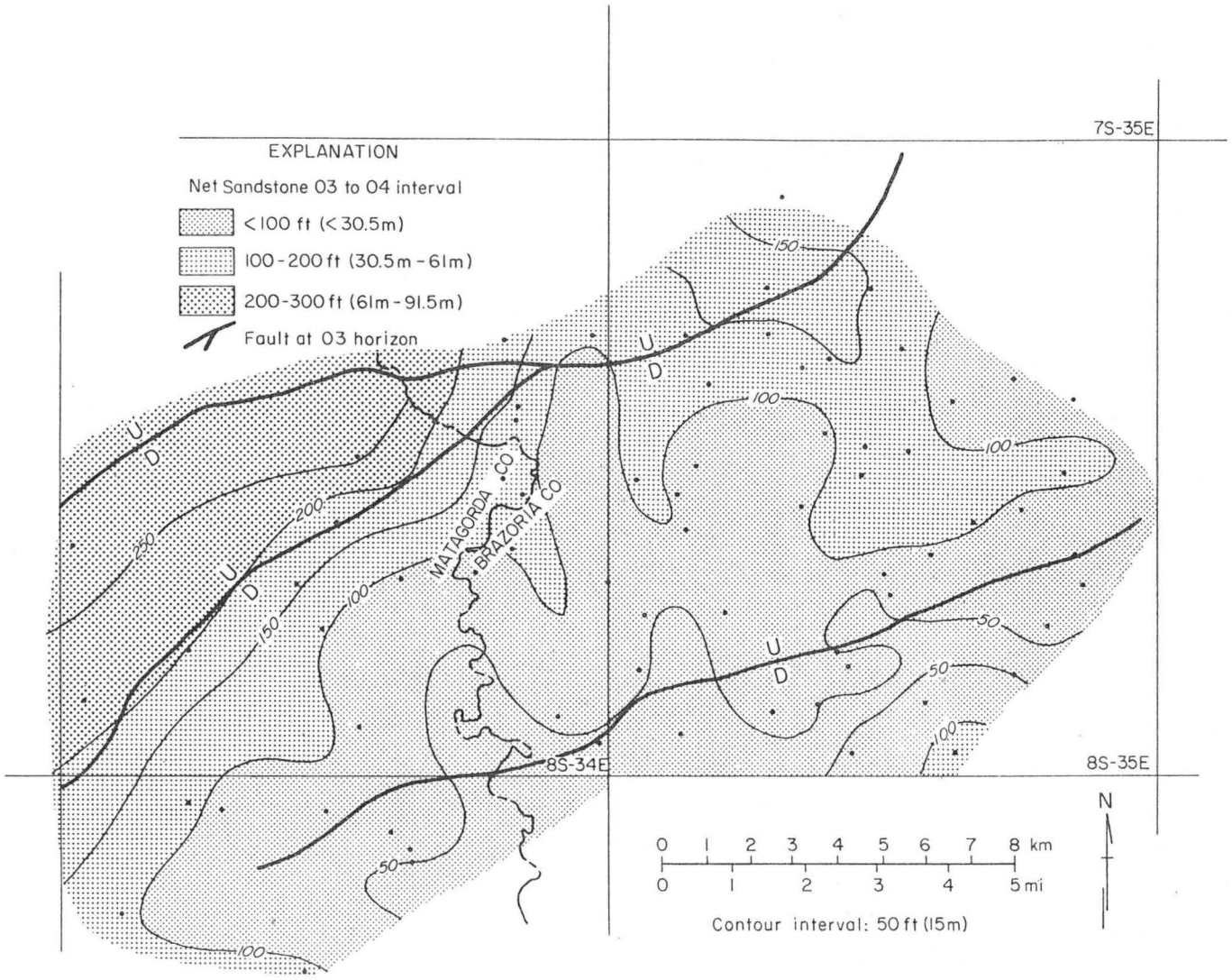

Figure 57. Net sandstone, 03 to 04 interval, Old Ocean Prospect Area.

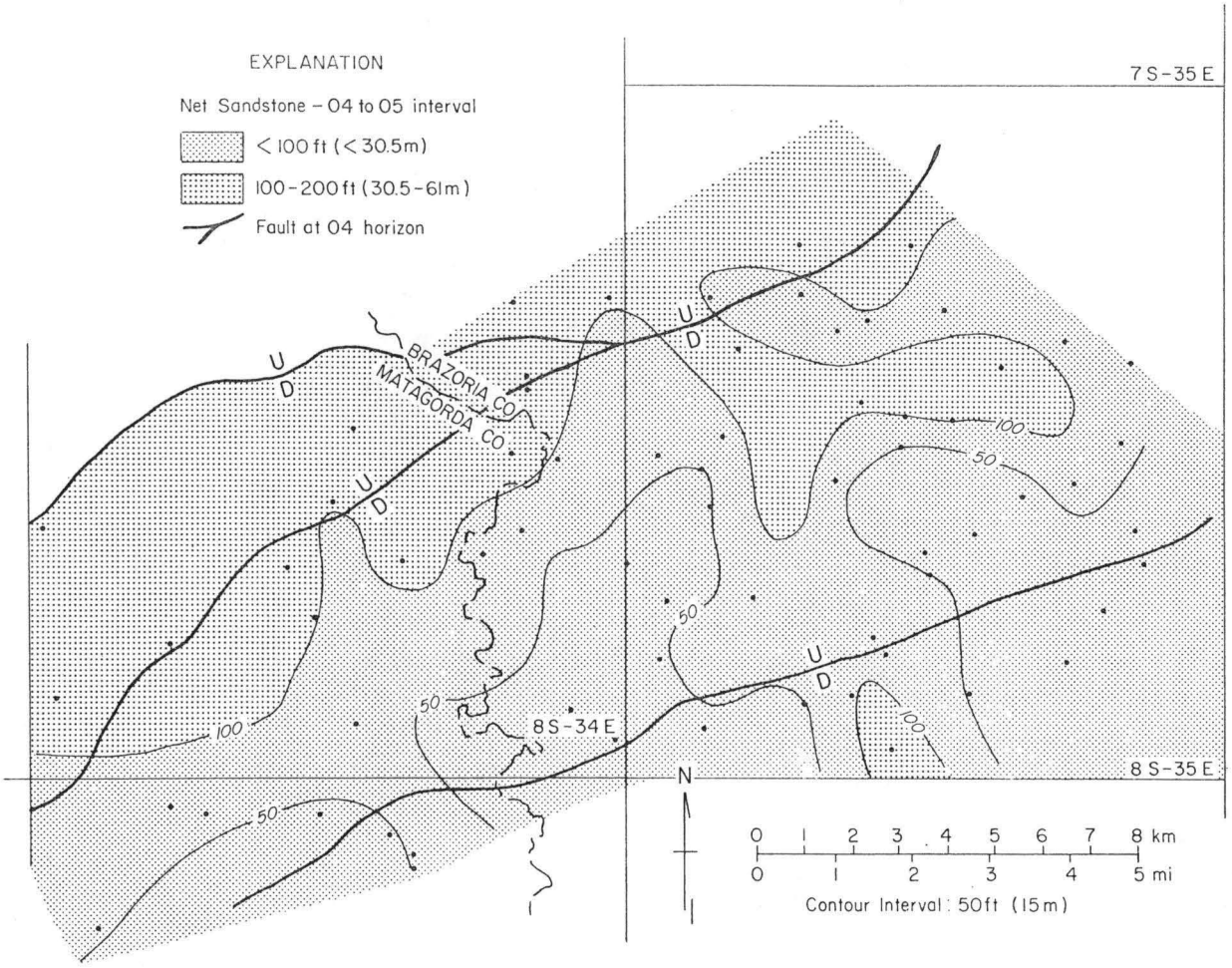

Figure 58. Net sandstone, 04 to 05 interval, Old Ocean Prospect Area.

are 20 to 100 ft thick. Net-sandstone values for this interval exceed 300 ft in some areas in the northern and western parts of the prospective fault block (fig. 59).

For the intervals below the 06 correlation marker, well data are sparse. The 06 horizon ranges in depth from 10,700 ft in the south to at least 12,700 ft in the north. In several wells in the southern part of the area along the line of section Z-Z' (fig. 60), high percentages of sandstone occur in the 06 to 08 interval in the B Zone. Sandstones in the C zone occur below the 08 marker at depths of 12,000 ft and greater. Individual sandstones are up to 100 ft thick but cannot be traced updip because these intervals plunge steeply to the north below the total depths of any wells north of the Abercrombie No. 16 B.R.L.D. well (fig. 60). Thus, net-sandstone maps for these intervals could not be made.

Formation parameters

Available data in the Old Ocean Prospect Area are too sparse to establish pressure and thermal gradients. Hence, the average depths and thicknesses of the A, B, and C Zones assumed for the prospect area were those determined from BHSIP data (fig. 13) and geothermal gradients (fig. 7) for Matagorda County and are the same as those data used for the Blessing Prospect Area that were previously discussed.

Temperatures in the A Zone are less than 250° F. B Zone temperatures along strike section Y-Y' (fig. 61) are also less than 250° F, as shown by the one well (No. 5) for which temperature data are available for the zone.

The four wells in the updip (left) part of dip section Z-Z' (figs. 55 and 62) are hydropressured and therefore do not penetrate the B Zone. The four wells that form the downdip part of section Z-Z' penetrate the B Zone at an average depth of 11,450 ft. Temperatures at the top and base of the B Zone average 250° and 279° F, respectively.

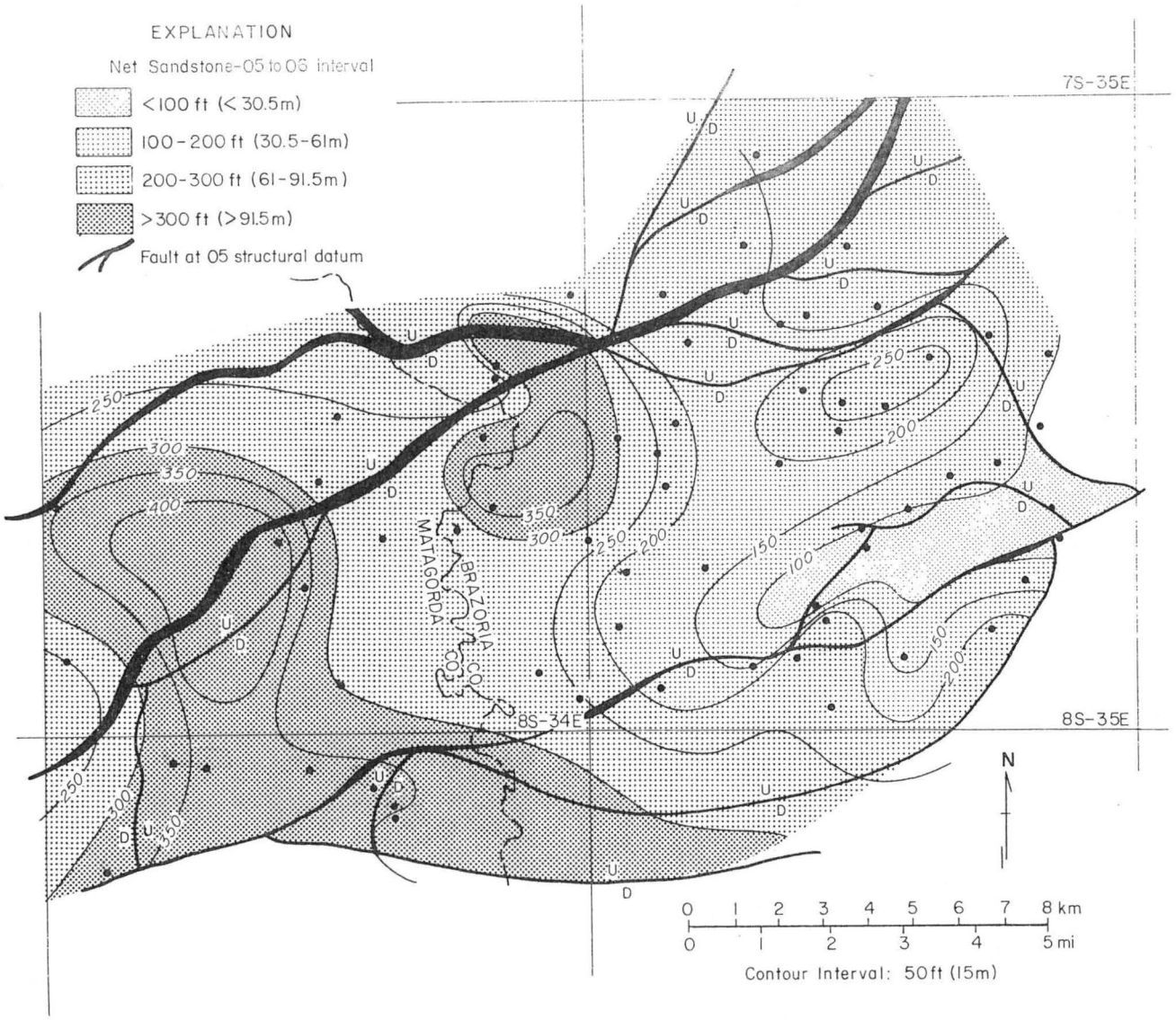

Figure 59. Net sandstone, 05 to 06 interval, Old Ocean Prospect Area.

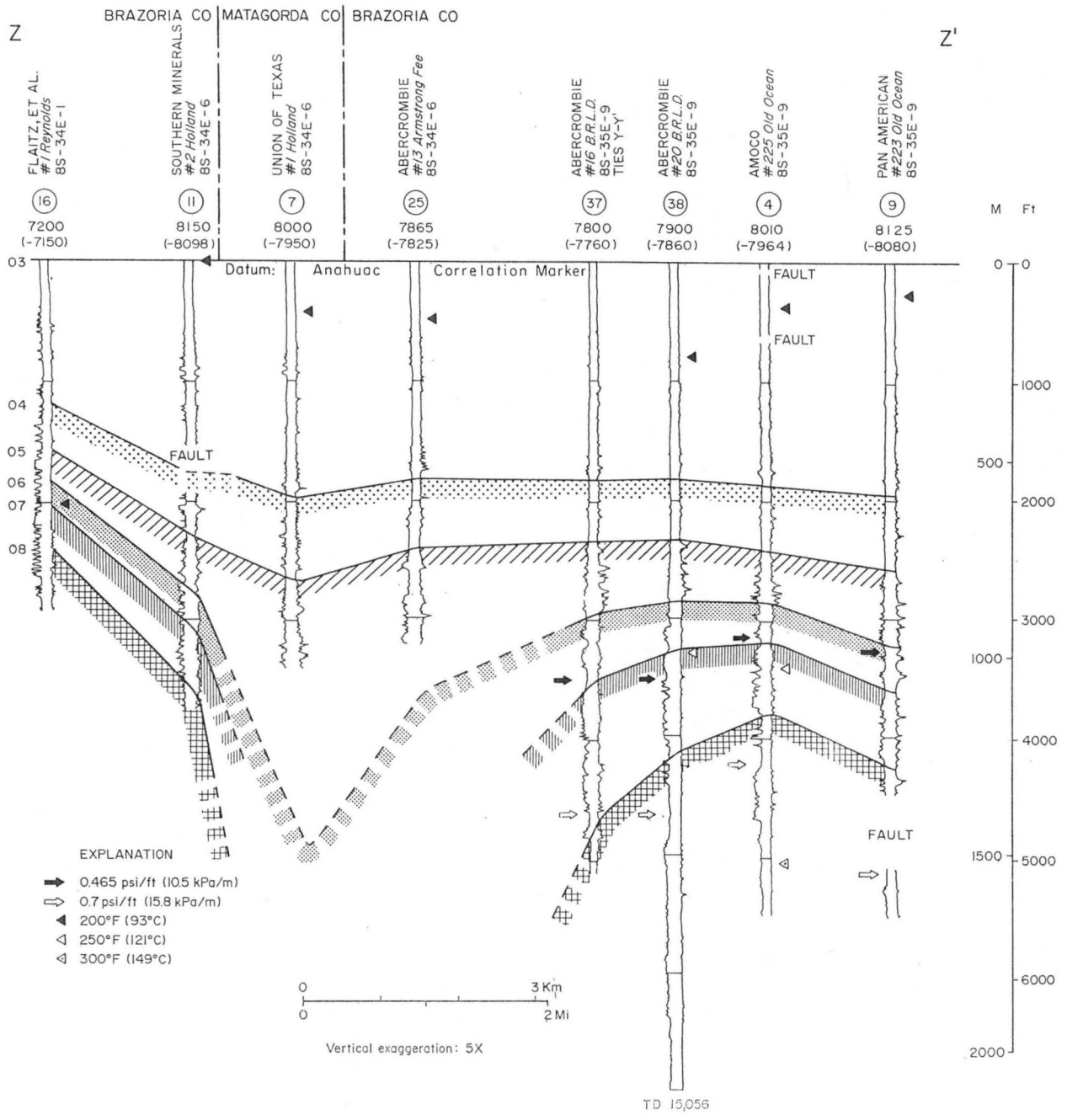

Figure 60. Stratigraphic dip section Z-Z', Old Ocean Prospect Area.

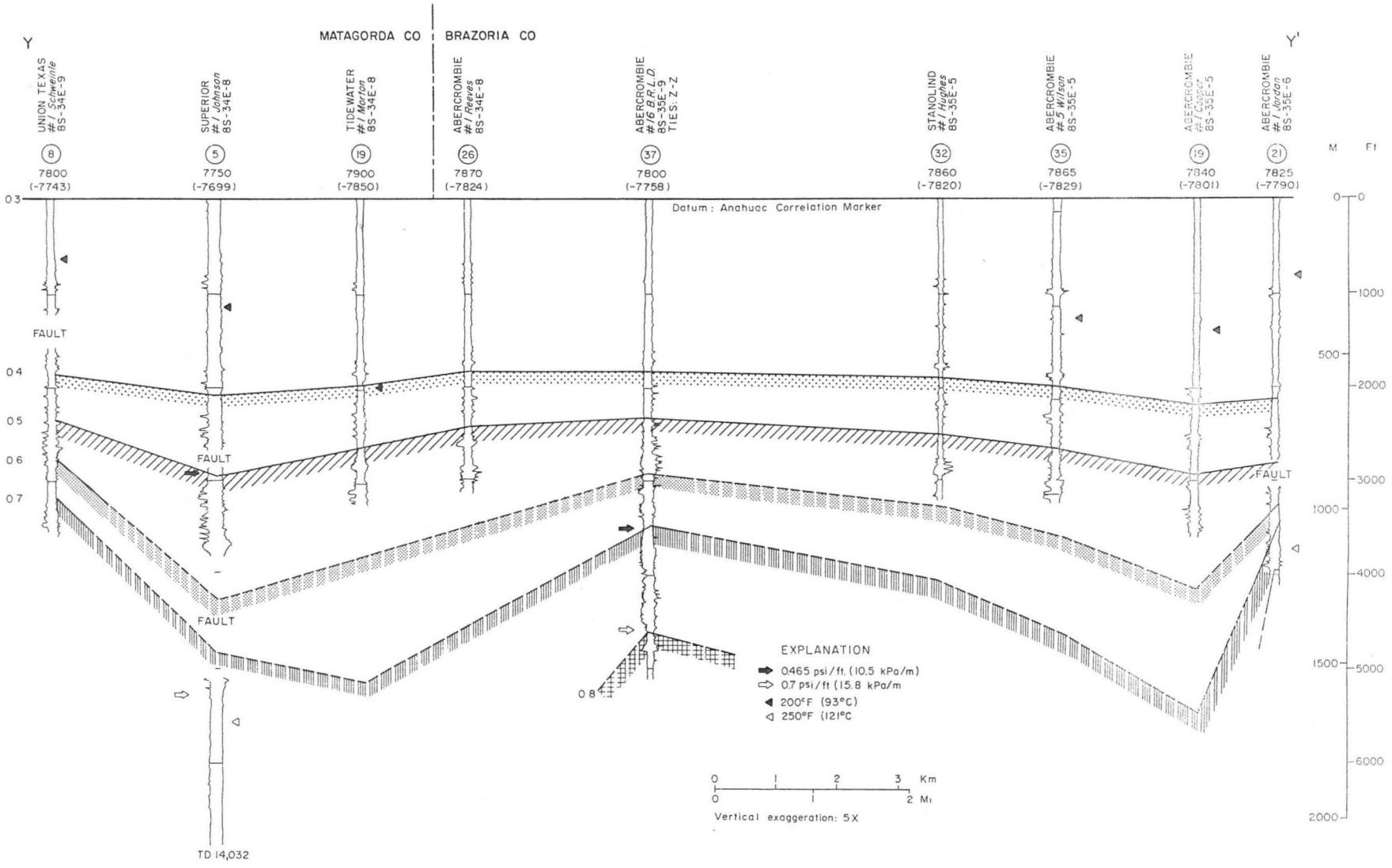

Figure 61. Stratigraphic strike section Y-Y', Old Ocean Prospect Area.

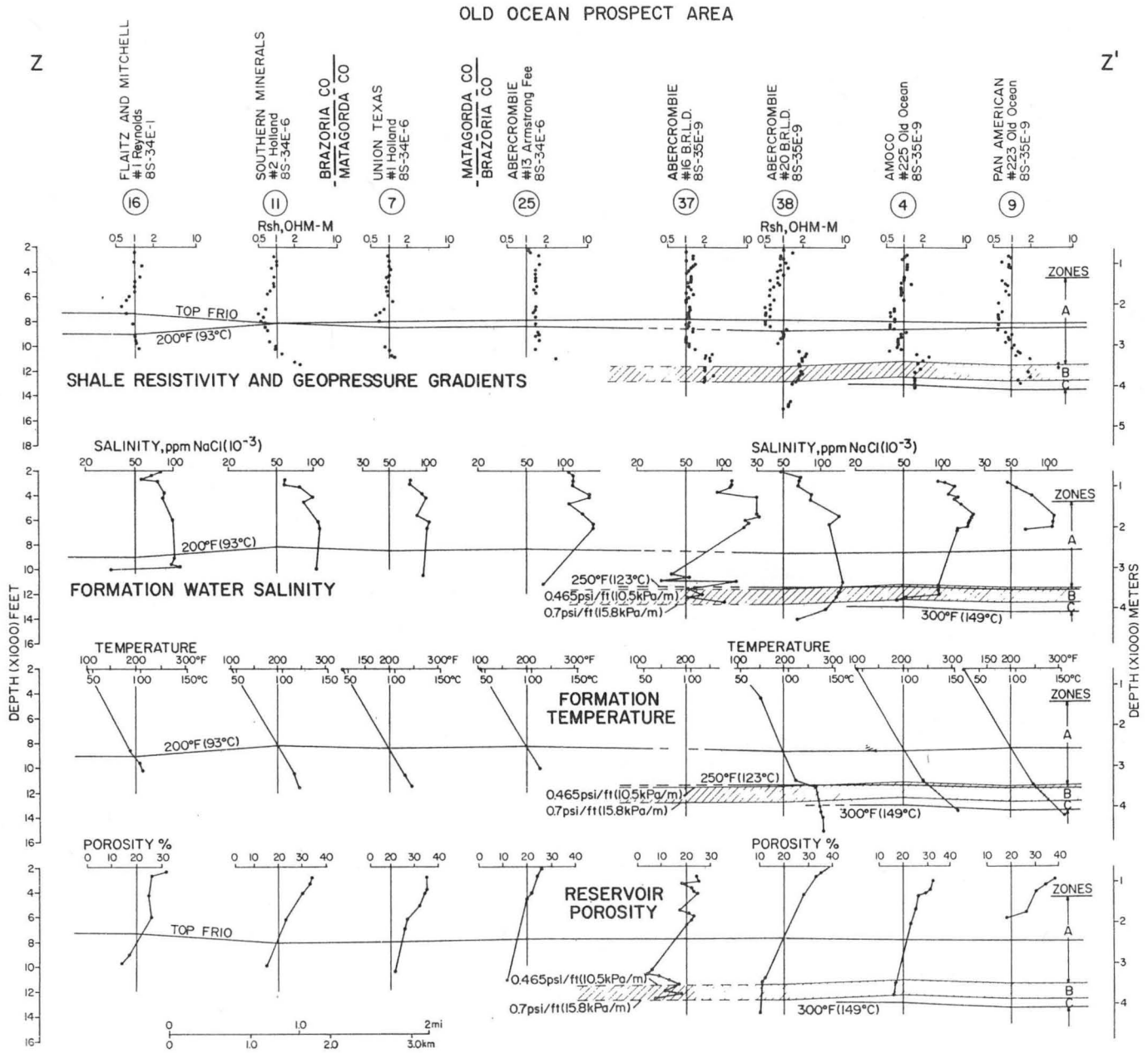

Figure 62. Parameter plots for dip section Z-Z', Old Ocean Prospect Area, Brazoria and Matagorda Counties, Texas.

A plot of salinity versus depth for 5 wells in the prospect area (fig. 63) shows that numerous sandstone units in the A and C Zones contain brine with salinities that exceed 100,000 ppm NaCl. Salinity data in the B Zone are relatively scarce but average about 46,000 ppm NaCl.

Whole-core data are not available for the area, but porosities calculated from induction and SP logs at the top and base of the B Zone average 15 and 11 percent, respectively, along Y-Y' (fig. 64) and Z-Z' (fig. 62).

Potential for testing

The Abercrombie No. 16 B.R.L.D. well (No. 37) is the type well for the Old Ocean Prospect Area (figs. 61 and 60). In the B and C Zones, about 700 ft of sandstone occur in a 1,200-ft interval below the depth of 11,300 ft in this well. Individual sandstones range from 10 to 100 ft thick and are separated by shales ranging from 5 to 30 ft thick. The minimum areal extent of these sandstones is about 15 mi^2, but they possibly extend over an area as great as 35 mi^2.

Temperatures were not listed in the induction well log header for the type well, but average values from 4 surrounding wells range from 227° to 247° F in the 06 to 08 interval, the potential reservoir section.

No core data are available in the prospect area, but porosities determined from induction and SP logs range from 6 to 14 percent in the B Zone and generally decrease with depth. Salinities derived from "curve" R_{mf} values are higher, as expected, than those from log header values of R_{mf} (fig. 65). Salinities from the "curve" method for three of the most prospective reservoir sandstones at depths of 10,500, 11,500, and 12,130 ft range from 70,000 to 170,000 ppm NaCl, and methane solubilities are estimated to range from 19 to 32 SCF/B (table 2).

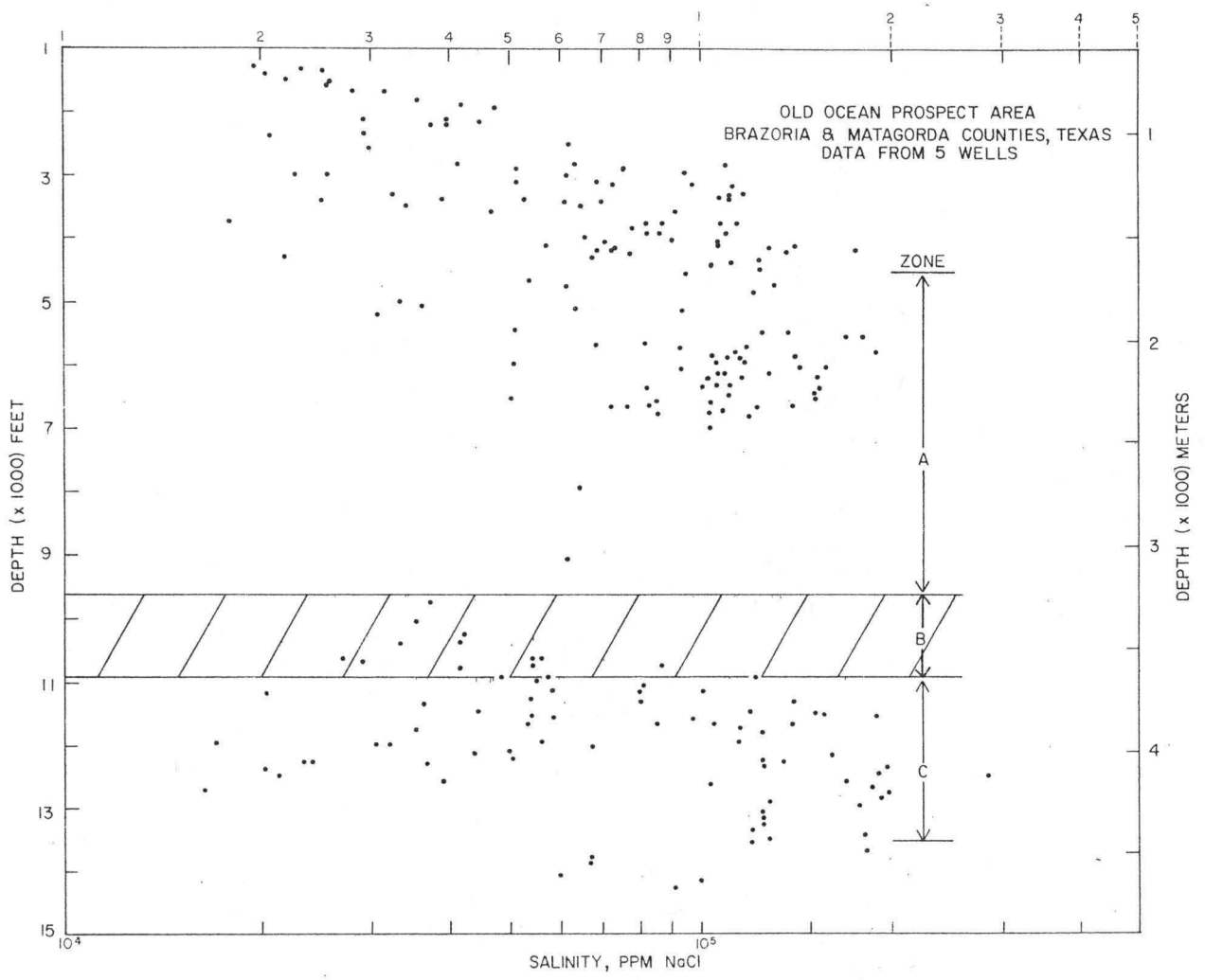

Figure 63. Salinity versus depth for five wells, Old Ocean Prospect Area, Brazoria and Matagorda Counties, Texas.

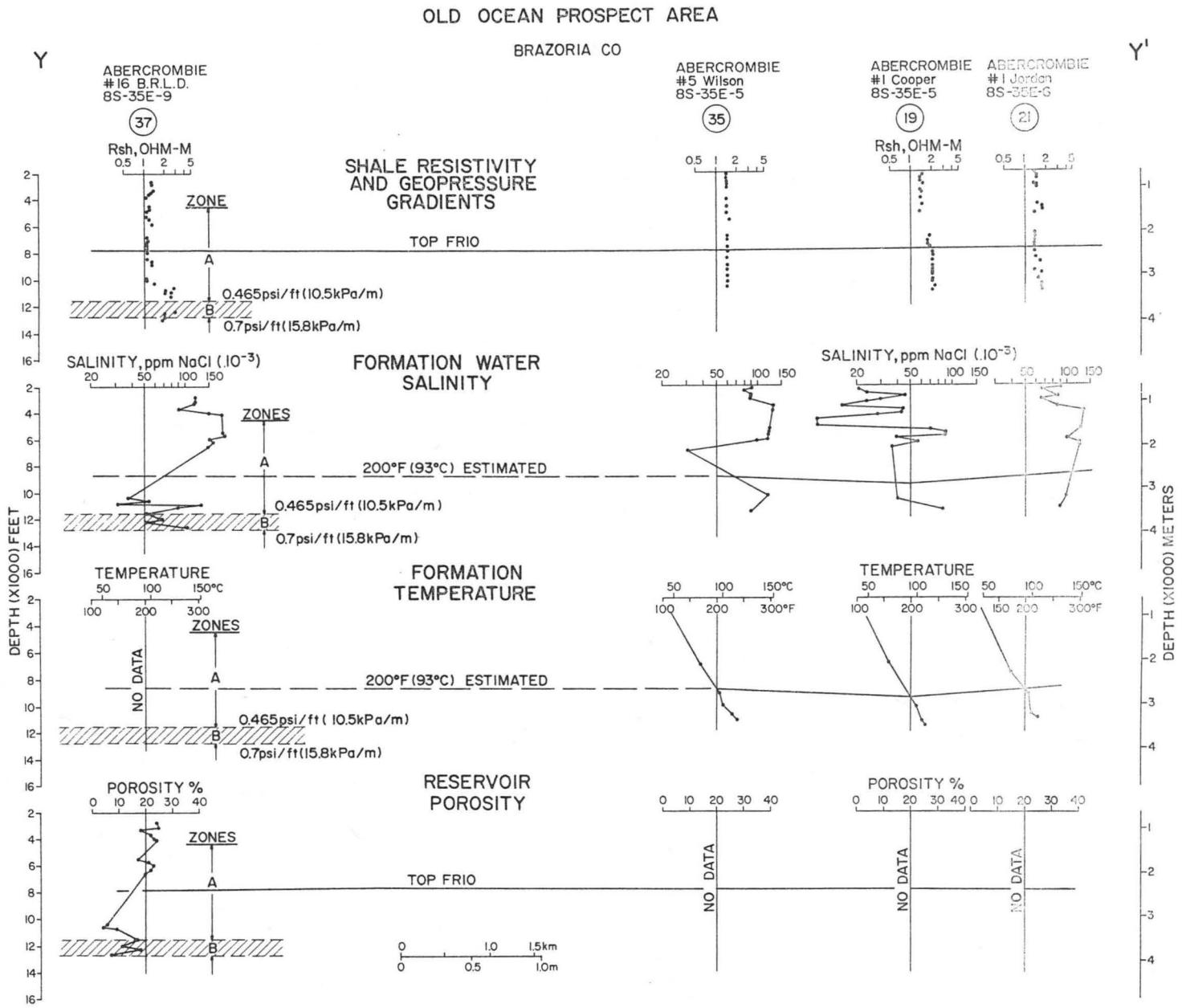

Figure 64. Parameter plots for wells on the eastern part of strike section Y-Y', Old Ocean Prospect Area, Brazoria County, Texas.

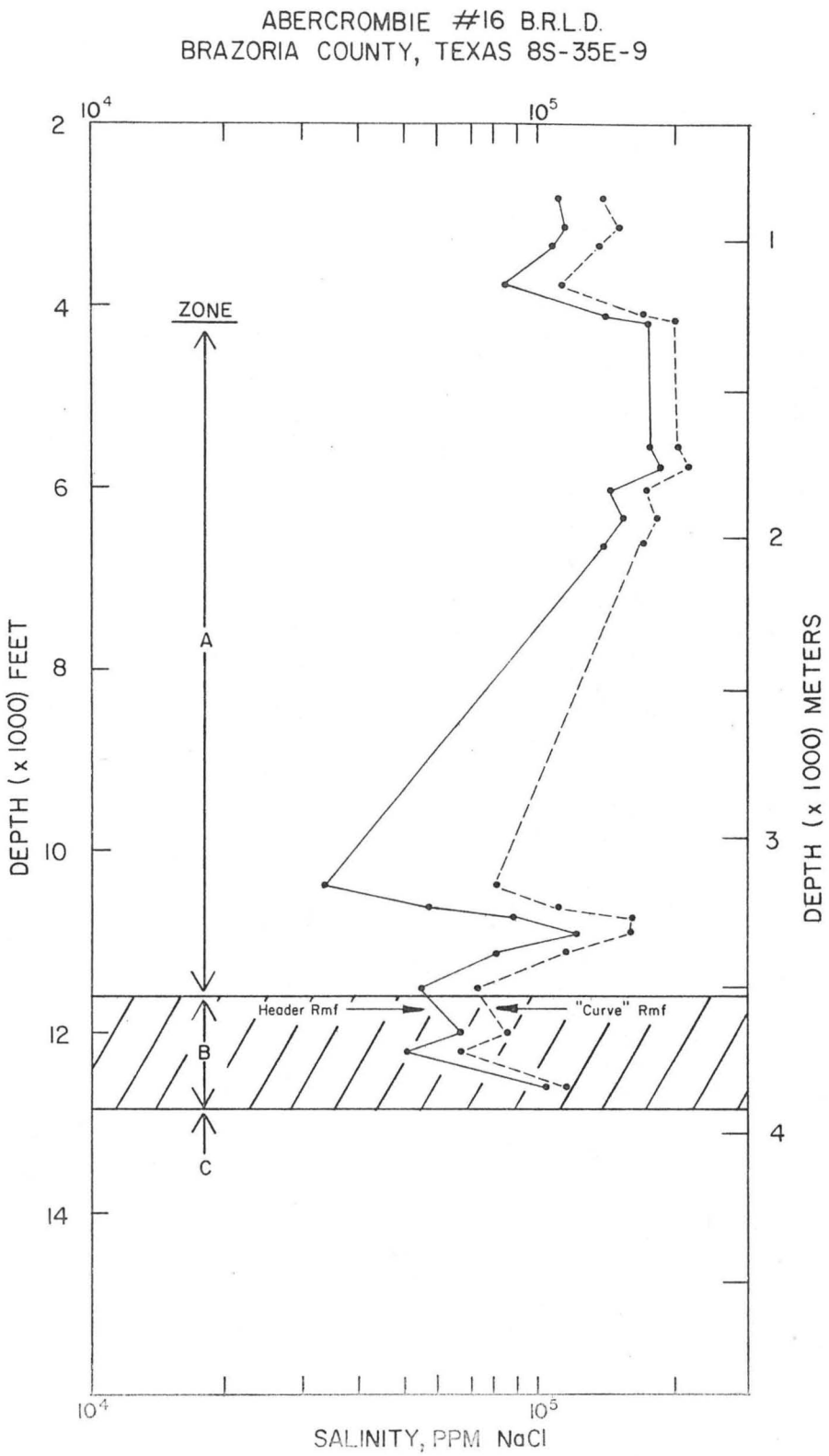

Figure 65. Comparison of salinity profiles obtained with mud filtrate resistivities from the well log header and from the "curve" method, Abercrombie No. 16 B.R.L.D., Old Ocean Prospect Area, Brazoria County, Texas.

No test site was selected within the Old Ocean Prospect Area because of the lack of reliable reservoir quality data, particularly permeability data from whole-core analyses. However, the Old Ocean Prospect is considered a potential test area that should be further evaluated if reservoir-quality data become available.

Corpus Christi Fairway

The Corpus Christi Fairway is located primarily in eastern Nueces and San Patricio Counties and extends into Aransas County along the Texas Gulf Coast (fig. 66). The fairway is approximately 30 mi wide in a northwest-southeast (dip) direction and extends 35 mi in a southwest-northeast (strike) direction, covering an area of 1,050 mi^2. In this area, reservoir sandstones of the deep hydropressured and shallow geopressured zones are primarily in the Oligocene Frio Formation. The top of the Frio Formation ranges in depth from approximately 5,000 ft in updip areas to the west to 8,000 ft in downdip areas to the east. Across the fairway from west to east, the Frio Formation thickens from about 3,000 ft to at least 8,000 ft. The top of the Frio is defined as the top of a sandstone-rich sequence overlain by the widespread, thick Anahuac Shale (Holcomb, 1964). In the fairway area, the uppermost sandstones in the Frio Formation as defined in this study occur in the Marginulina and Heterostegina zones, which some geologists do not include in the Frio (fig. 35).

Faults divide the fairway area into five major strike-aligned structural blocks (fig. 66). Major faults and smaller subsidiary faults are permeability barriers which limit the lateral extent of any prospective reservoir. The major blocks generally range from 3 to 10 mi in width and extend along strike for tens of miles. Vertical displacement along the faults is most commonly 100 to 500 ft at the top of the Frio but increases

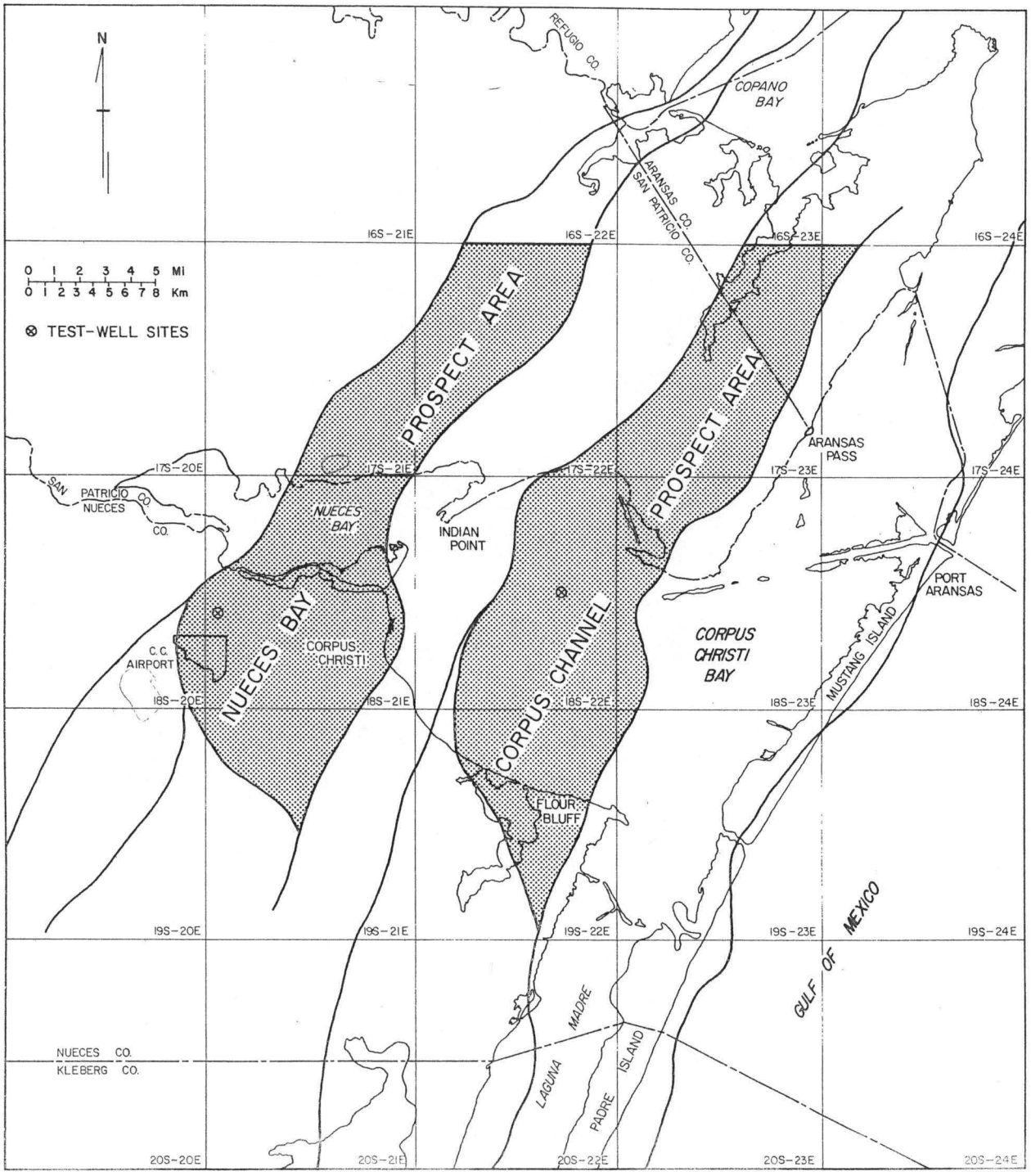

Figure 66. Corpus Christi Fairway, Nueces Bay and Corpus Channel Prospect Areas, and proposed test-well sites.

with depth to 2,000 ft or more. These faults are the major features used to subdivide the fairway into prospect areas. Of the five recognized fault blocks, three were studied in detail and parts of two are here designated as prospect areas, the Nueces Bay and Corpus Channel Prospect Areas (fig. 66).

The geology of the Corpus Christi Fairway was analyzed by detailed correlation of approximately 600 electric logs (fig. 67; appendix C), both within and between fault blocks. To cover the entire fairway, six structural dip and three stratigraphic strike sections were constructed (figs. 67 through 76). In addition, detailed stratigraphic sections were made for the reservoir intervals of interest in each prospect area. Markers CC1 to CC11 were used on both regional and local sections, and each could be recognized in at least two fault blocks. Additional markers delineating units CC-A to CC-D were used only locally in the Corpus Channel Prospect Area. Previous studies of the Frio Formation in this area have agreed on a coastal environment of deposition but disagreed as to whether this occurred in the setting of a barrier coastline (Boyd and Dyer, 1964) or delta (Martin, 1969). This study and that of Galloway and others (in press) suggest that deposition occurred on barrier bars and strandplains adjacent to major deltaic depocenters located along strike from the study area.

The correlations allow some important generalizations to be made about the fairway. (1) Within a fault block, sandstones are continuous along strike but tend to grade into shales downdip, reflecting the depositional environment of the sediments. In addition, stratigraphic units thicken updip toward the bounding fault, indicating a greater subsidence rate in that area. This structural control of thickness of deposits indicates that the faults were active during sedimentation and are therefore growth faults.

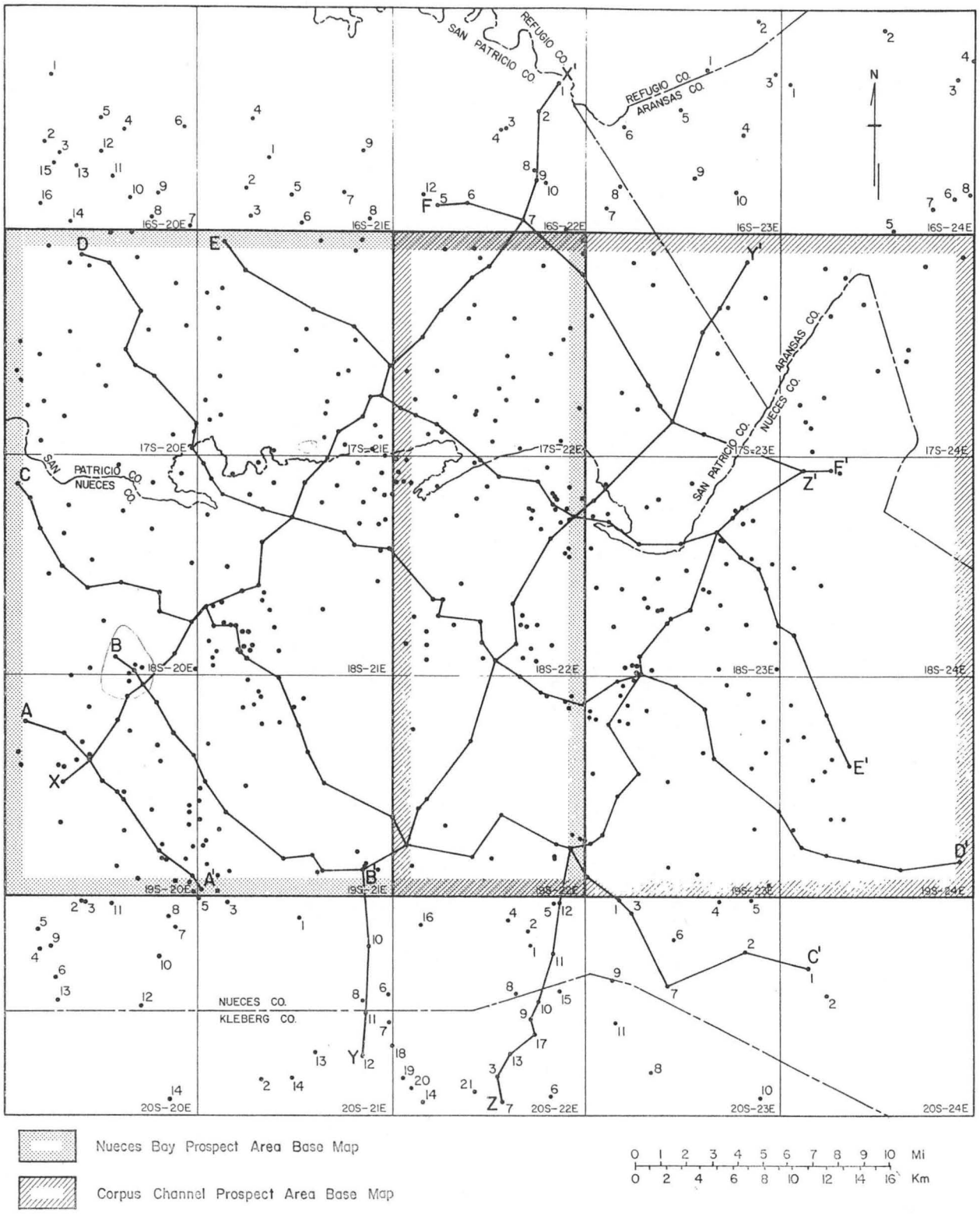

Figure 67. Well locations and lines of cross section, Corpus Christi Fairway. The two rectangles show the areas covered by detailed maps for both the Nueces Bay (fig. 77) and Corpus Channel (fig. 93) Prospect Areas.

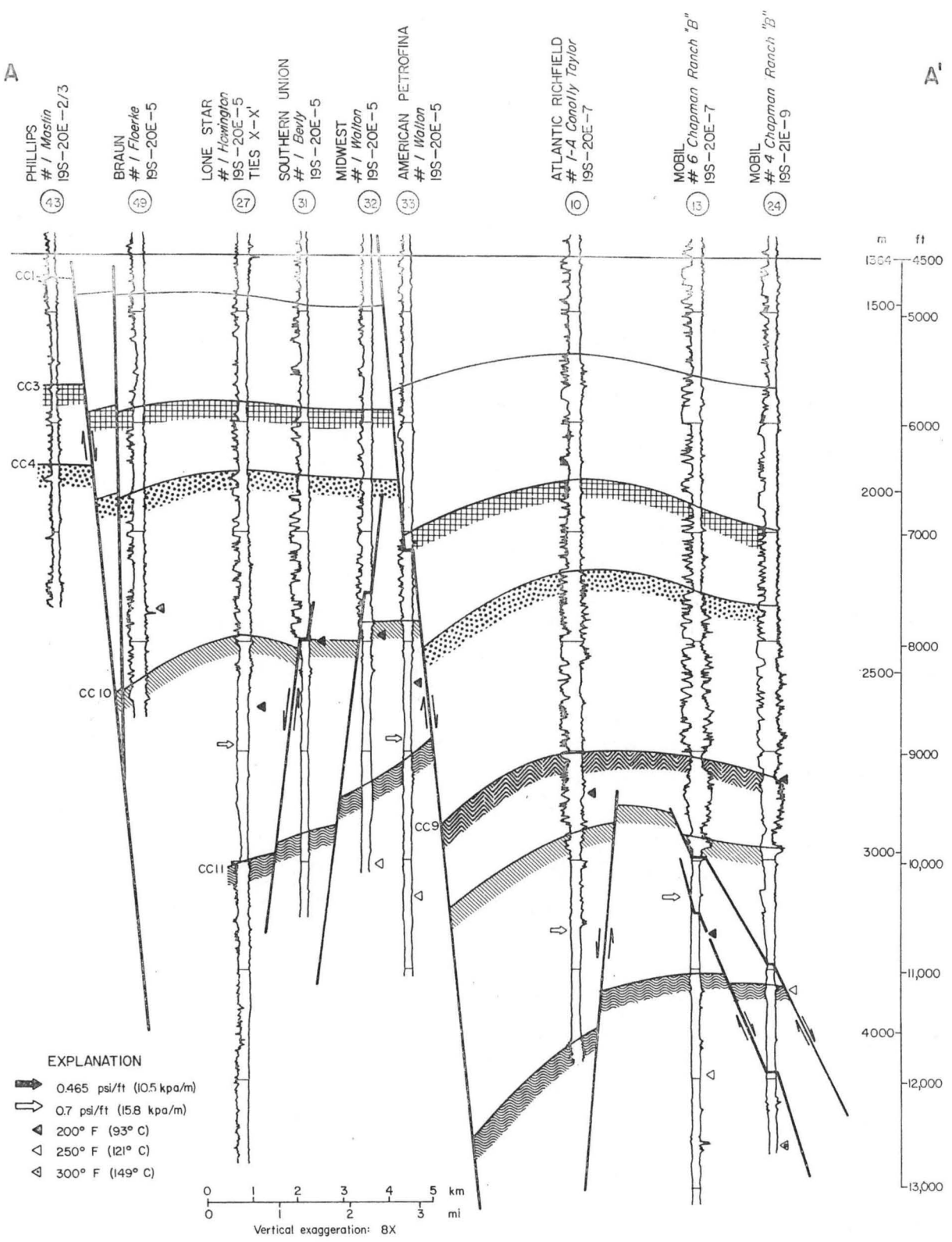

Figure 68. Structural dip section A-A' through the Corpus Christi Fairway.

Figure 69. Structural dip section B-B' through the Corpus Christi Fairway.

Please Note:

Pages 113 – 118 are oversized cross sections included in an envelope in the back pocket of the paper version.

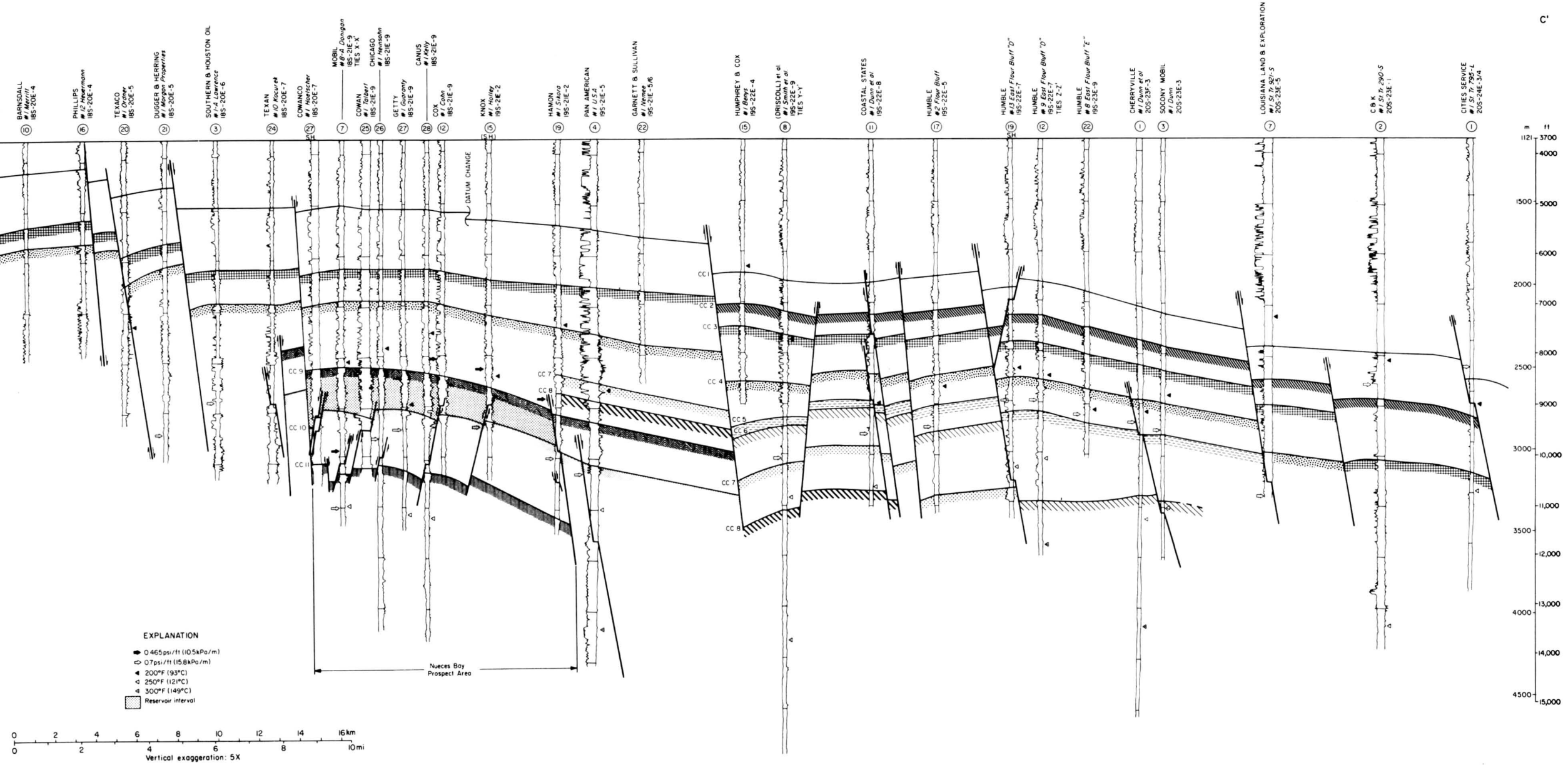

Figure 70. Structural dip section C-C' through the Corpus Christi Fairway.

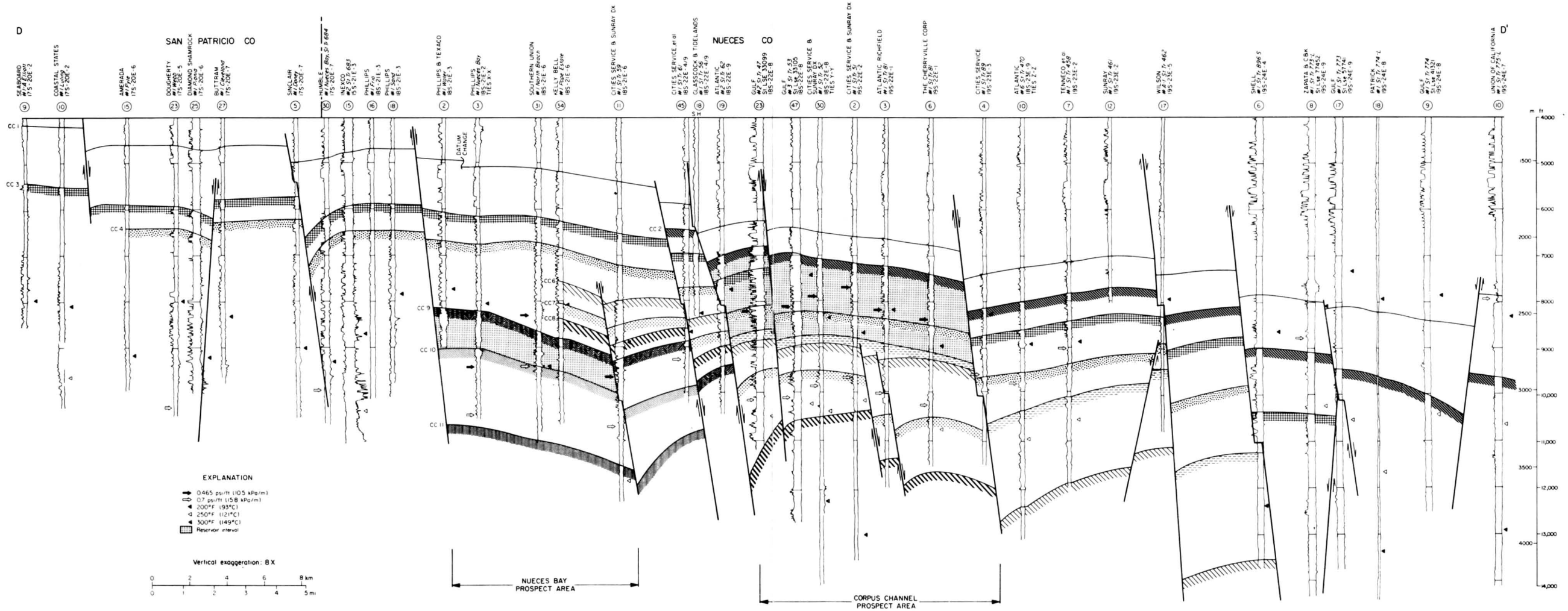

Figure 71. Structural dip section D-D' through the Corpus Christi Fairway.

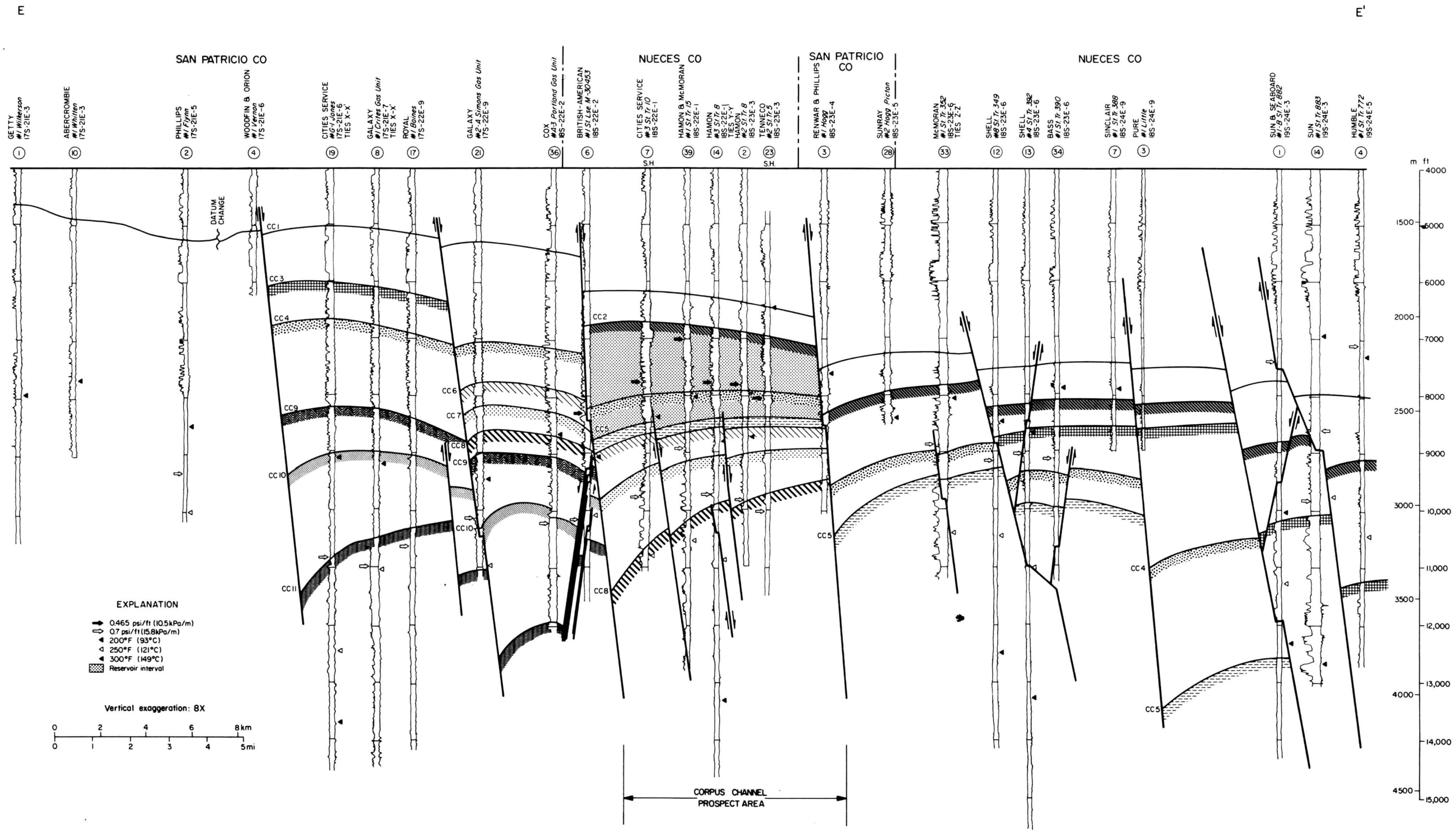

Figure 72. Structural dip section E-E' through the Corpus Christi Fairway.

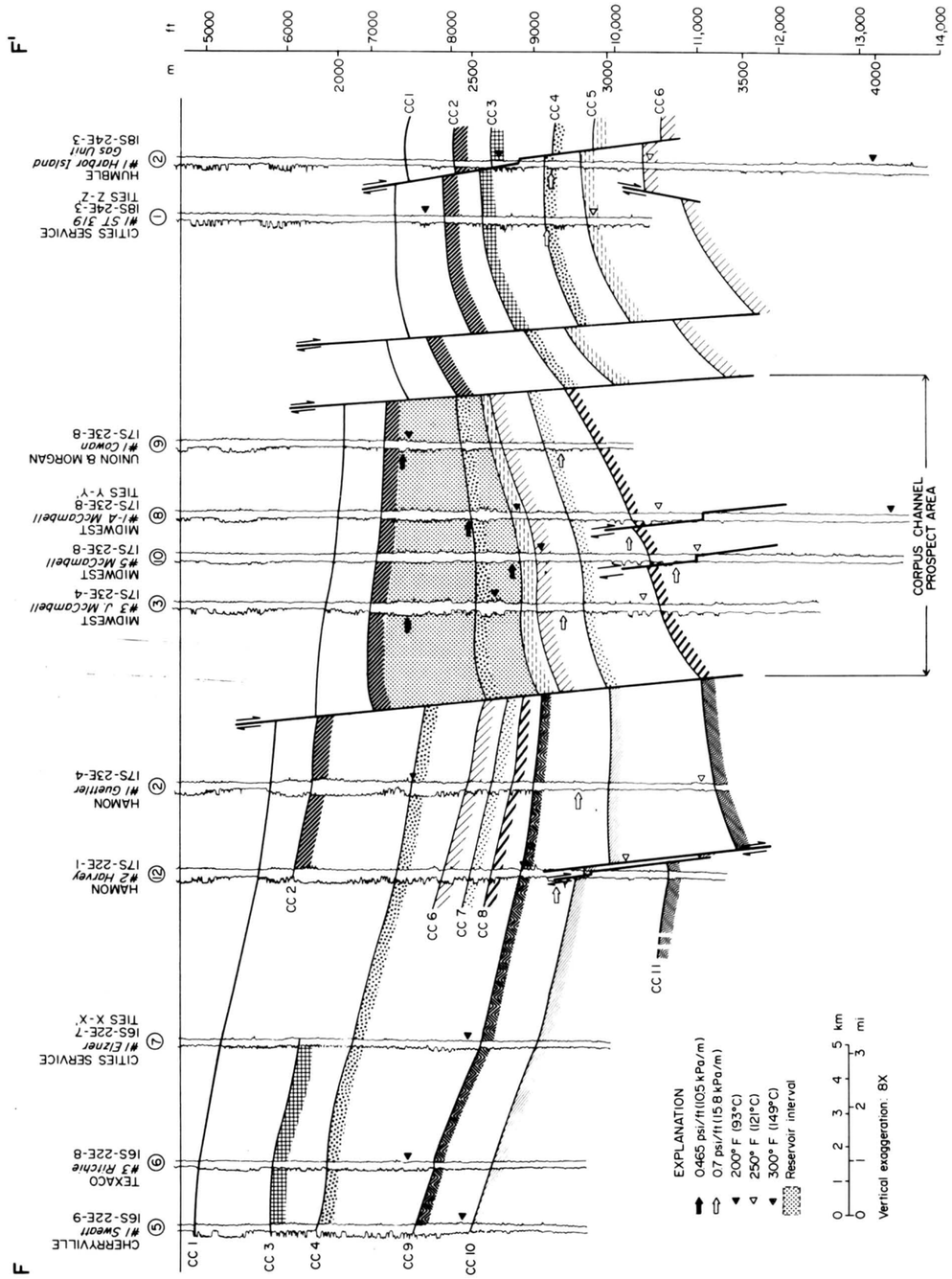

Figure 73. Structural dip section F-F' through the Corpus Christi Fairway.

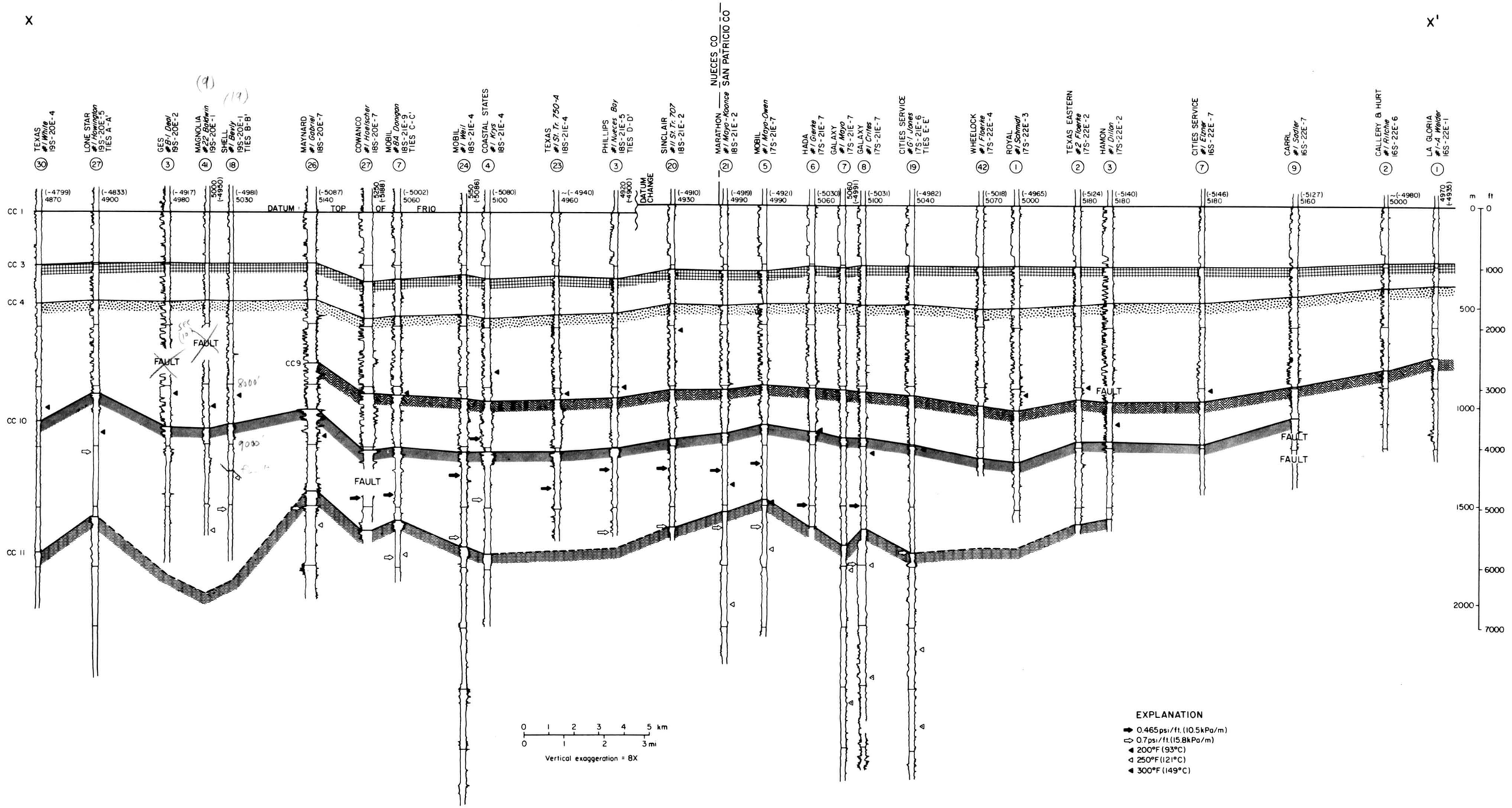

Figure 74. Stratigraphic strike section X-X' through the Corpus Christi Fairway.

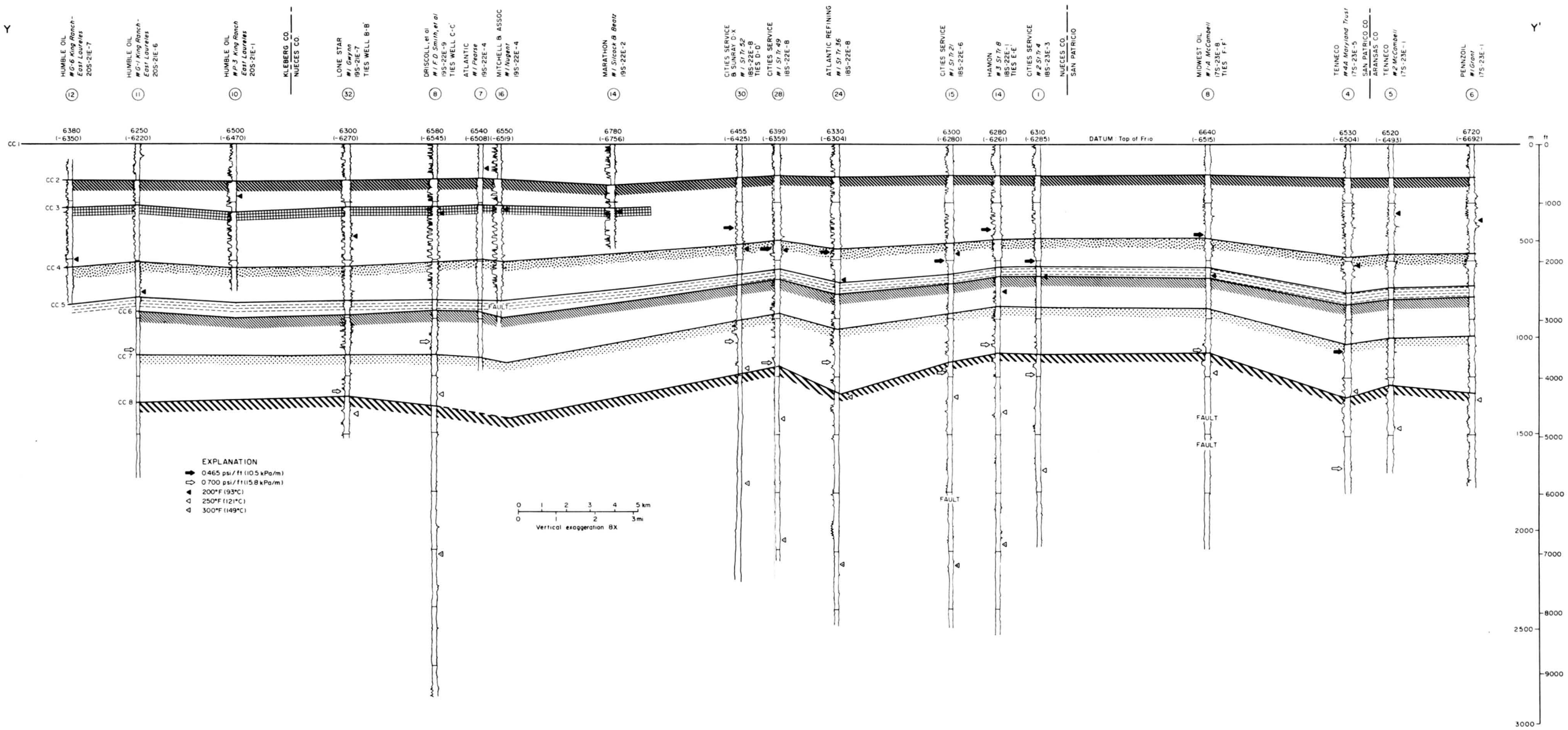

Figure 75. Stratigraphic strike section Y-Y' through the Corpus Christi Fairway.

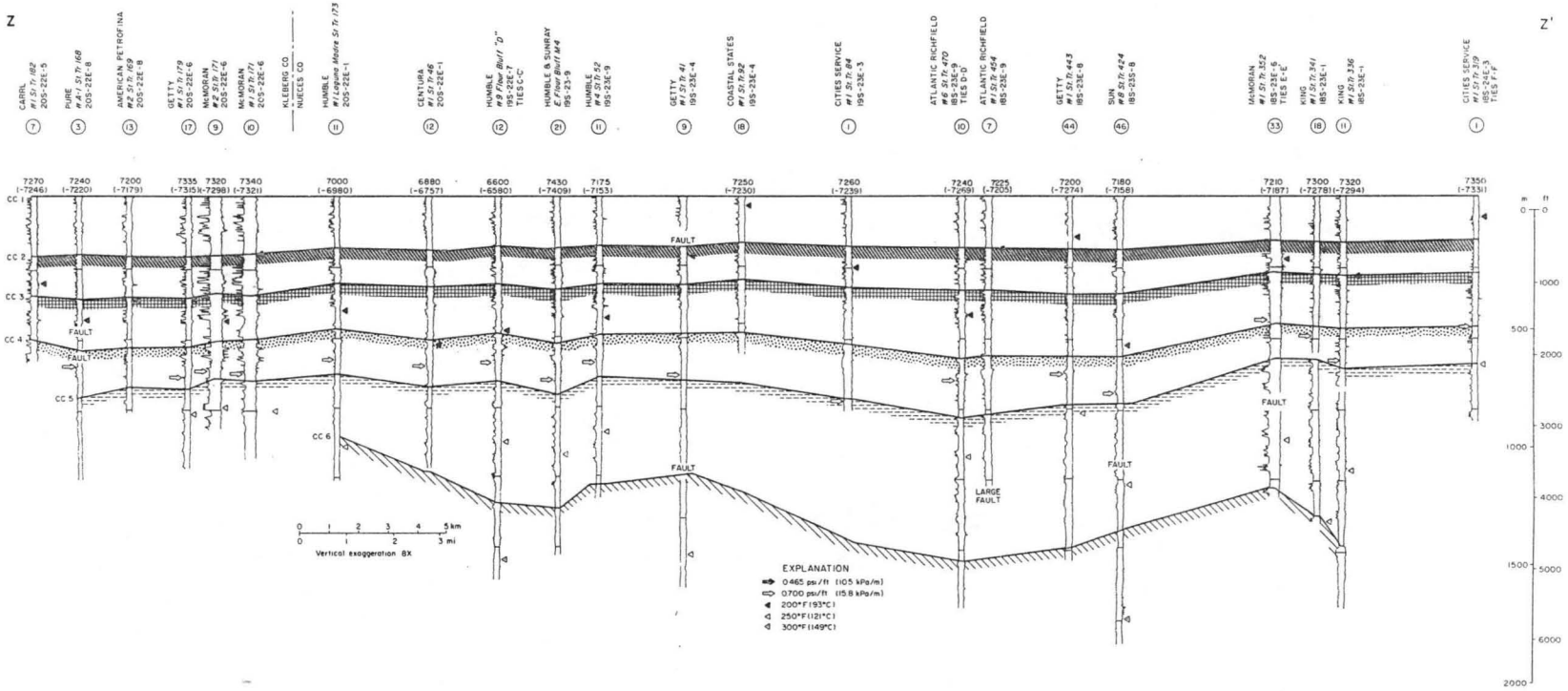

Figure 76. Stratigraphic strike section Z-Z' through the Corpus Christi Fairway.

The greater subsidence rates in the updip part of the fault block also resulted in the reversal of the regional gulfward dip and formation of a rollover anticline. With increasing depths, the degree of landward dip increases so that in some areas the deeper strata dip entirely landward and no rollover anticlines are present.

(2) Across faults bounding adjacent blocks, stratigraphic units in the deeper layers expand greatly in a gulfward direction, sometimes by a factor of 5. Sandstone units persist across faults; however, the expanded sections on the downthrown sides contain a great amount of interbedded shale that causes reservoir qualities to be poorer than on the upthrown sides. Thus, the downthrown sandstone units are not prospective for this project. The shallow layers typically show only slight thickening across faults and correspondingly do not change appreciably in lithology.

Based on the distribution of sandstone, temperature, and pressure gradients in the Corpus Christi Fairway, two fault blocks were chosen as prospect areas, the Nueces Bay Prospect in the west and the Corpus Channel Prospect in the east (fig. 66). The Nueces Bay Prospect contains up to 800 ft of sandstone, predominantly in the B Zone, while the Corpus Channel Prospect contains up to 1,500 ft of sandstone, chiefly in the A Zone. Limited whole-core porosity and permeability data suggest that sandstones in the C and D Zones are of too low a quality to be considered as reservoirs for the purpose of this study.

Nueces Bay Prospect Area

The Nueces Bay Prospect Area includes Nueces Bay and parts of the city of Corpus Christi (figs. 66 and 77). The fault-bounded block varies from 4 to 8 mi wide and was studied over a length of almost 25 mi. The prospect area covers 120 mi^2 and contains up to 800 ft of sandstone, principally

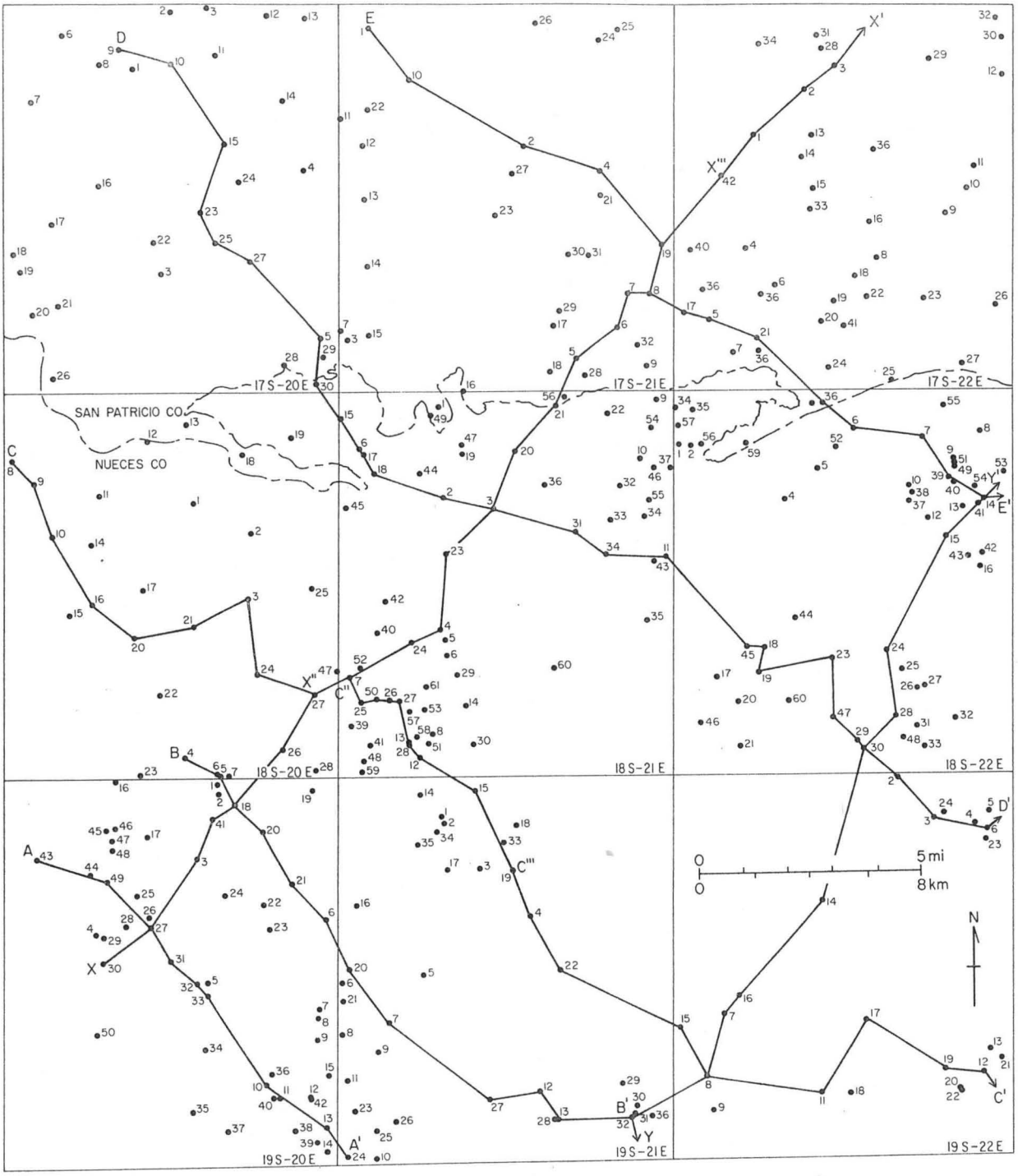

Figure 77. Well locations and lines of cross section, Nueces Bay Prospect Area. The location of the area within the Corpus Christi Fairway is shown in figure 67.

in the B Zone. Oil and gas fields in the prospect area include Saxet, Nueces Bay, and White Point.

The prospective structural block is bounded by a major growth fault to the west and a smaller growth fault to the east. The block is terminated to the south by a cross fault. The northern end of the block is defined by a decrease in the amount of massive sandstone units (fig. 74) with blocky SP patterns.

Structure

The Nueces Bay Prospect Area is outlined by growth faults on three sides; to the north, the decreasing sandstone content provides a less well defined boundary. The growth fault along the western margin of the block is a major fault across which correlation could not be achieved below the CC4 marker (fig. 70). It is likely that at depths of about 9,000 ft the throw is many hundreds of feet. The fault forming the eastern margin is minor, with the throw averaging a few hundred feet. The cross fault forming the southern boundary has a throw exceeding 1,000 ft.

The fault block reaches a maximum width of 8 mi in the south and narrows to 4 mi in the north. A map of structure on the top of the Harvey Sand (CC9 marker) shows that the overall structure is a homocline dipping toward the Gulf at a rate of 200 ft/mi (fig. 78). This trend is reversed along parts of the western margin of the block where small rollover anticlines are developed. In addition, a dip-aligned, gulfward-plunging nose occurs at the southern end of the block in association with the bounding cross fault. A dip section through this structure is shown in figure 70.

The structure at the base of the Harvey Sand, marker CC10, contrasts strongly with that at the top. Structural dip section C-C' (fig. 70) shows the many faults that occur in the shales underlying the Harvey Sand between markers CC10 and CC11, and that occasionally extend upward into the lower

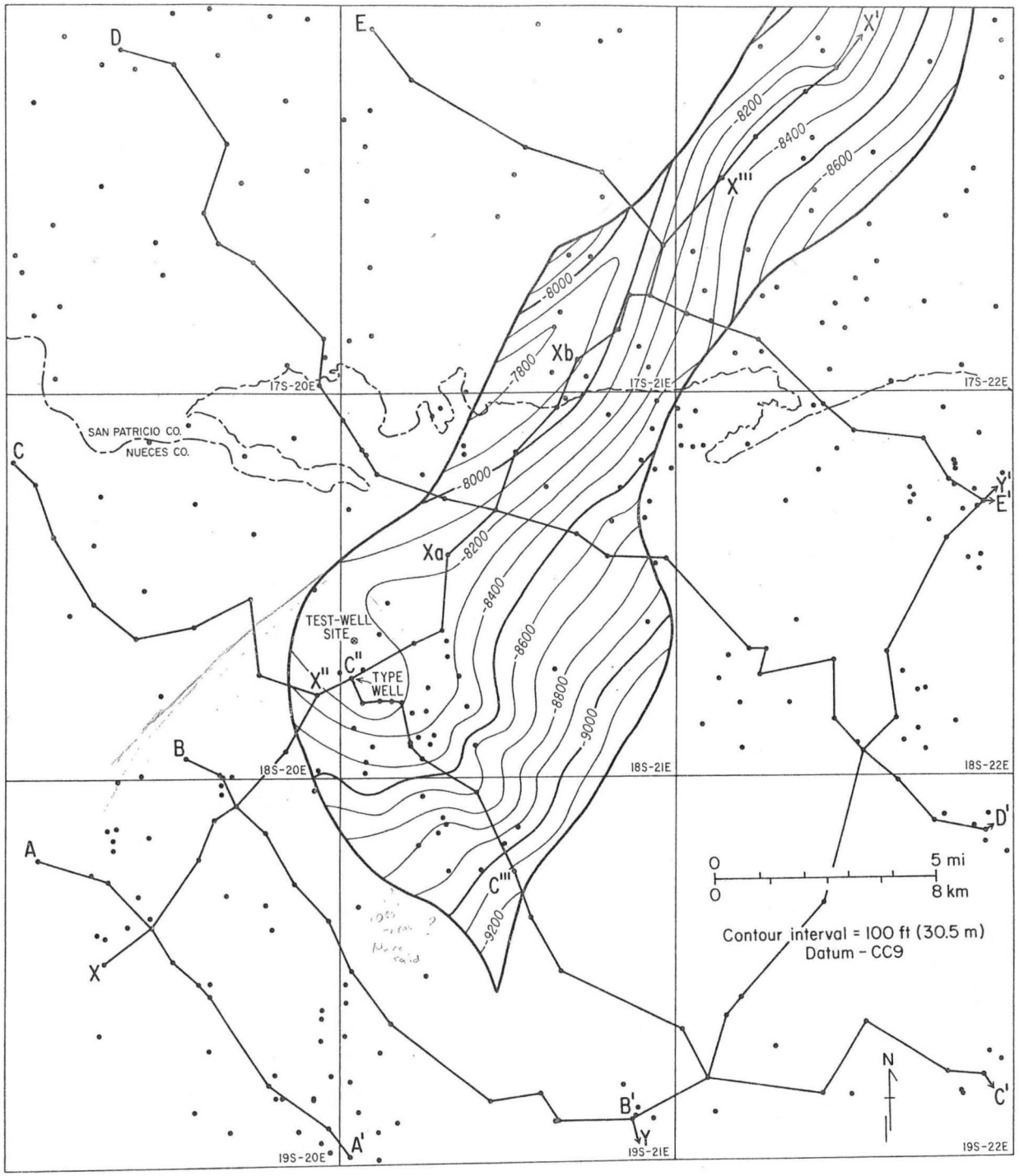

Figure 78. Structure on the top (CC9) of the reservoir interval in the Nueces Bay Prospect Area. Locations of the type well and the proposed test-well site are also shown.

part of the Harvey Sand. These faults could reduce reservoir size or continuity for the lower part of the Harvey Sand, even though the throws do not appear to exceed 200 ft. However, the upper part of the Harvey Sand is probably little affected by the faults.

Sandstone distribution and characteristics

In the Nueces Bay Prospect, sandstones are abundant from the top of the Frio (marker CC1) at depths of about 5,000 ft down to the CC10 marker at about 9,000 ft. This interval was subdivided by the markers into five sandstone-rich units. Sandstones at the top of the Frio are referred to by petroleum geologists as the Greta Sands. Below marker CC3 at about 6,300 ft are the Sinton Sands. At a depth of about 7,000 ft is a thick sandstone sequence, starting with the La Rosa Sand below marker CC4. The main reservoir interval, chosen because it is the deepest high-sandstone interval in the fault block, occurs from depths of about 8,300 ft at the Harvey Sand marker (CC9) down to about 9,200 ft just below the CC10 marker at the top of the Lehman, or Floerke, Sand. In this report, the sandstones in the CC9 to CC10 interval are referred to as the Harvey Sand.

A net-sandstone map of the Harvey Sand (fig. 79) and a detailed stratigraphic cross section (fig. 80) show that the amount of sandstone decreases downdip. Isoliths on the map trend parallel to strike with only slight deviations. The highest values of up to 800 ft occur along the western margin of the prospect area and decrease gradually to less than 100 ft at the eastern margin. In addition, the immediately underlying Lehman Sand, also considered part of the reservoir interval, contains from 100 to 200 ft of sandstone. The sandstone map also shows that sand decreases to the north in the prospect area.

The geometry of the sandstone units in the reservoir interval is shown in both dip- and strike-oriented stratigraphic sections (figs. 80 and 81).

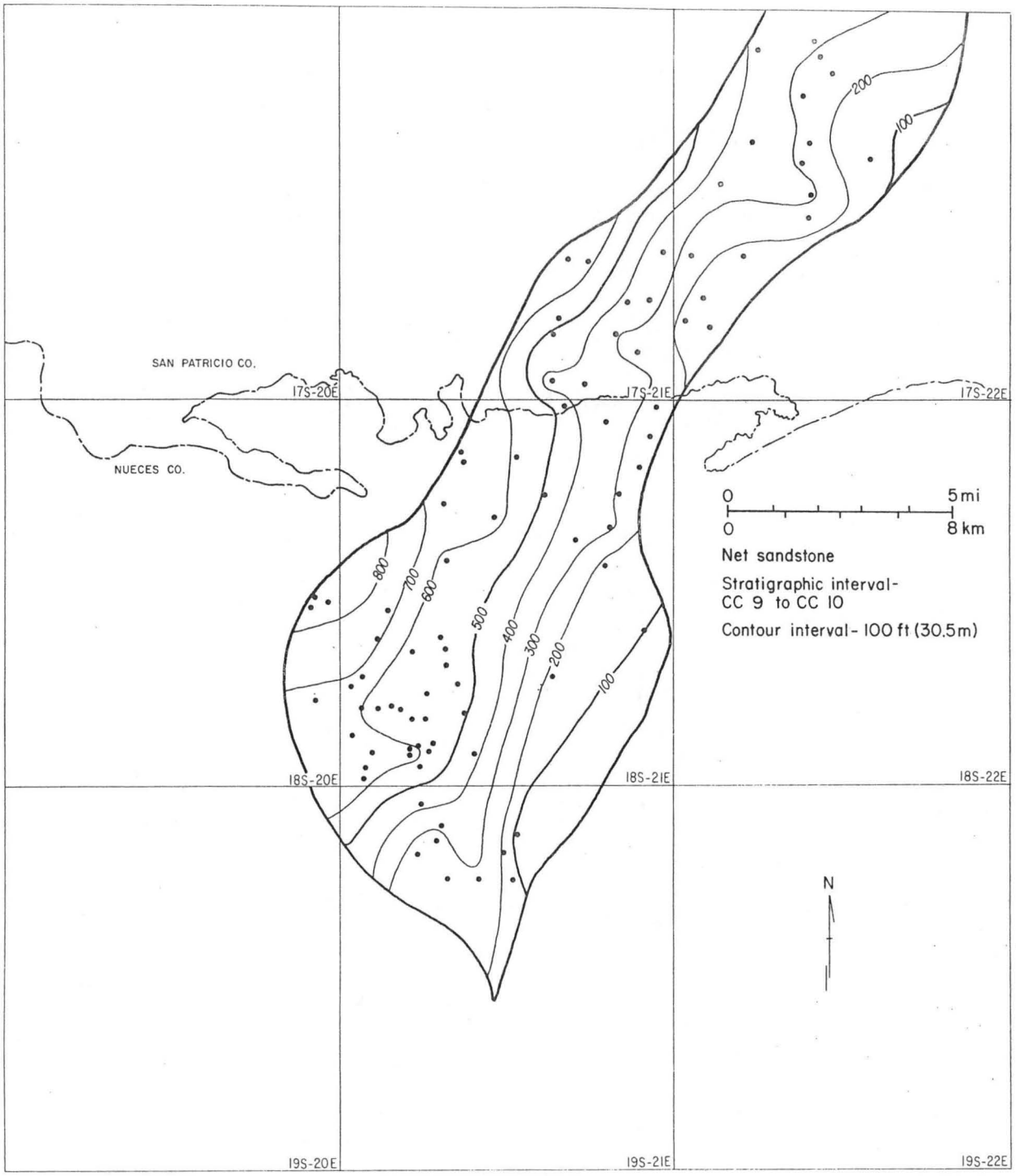

Figure 79. Net sandstone in the reservoir interval between markers CC9 and CC10, Nueces Bay Prospect Area.

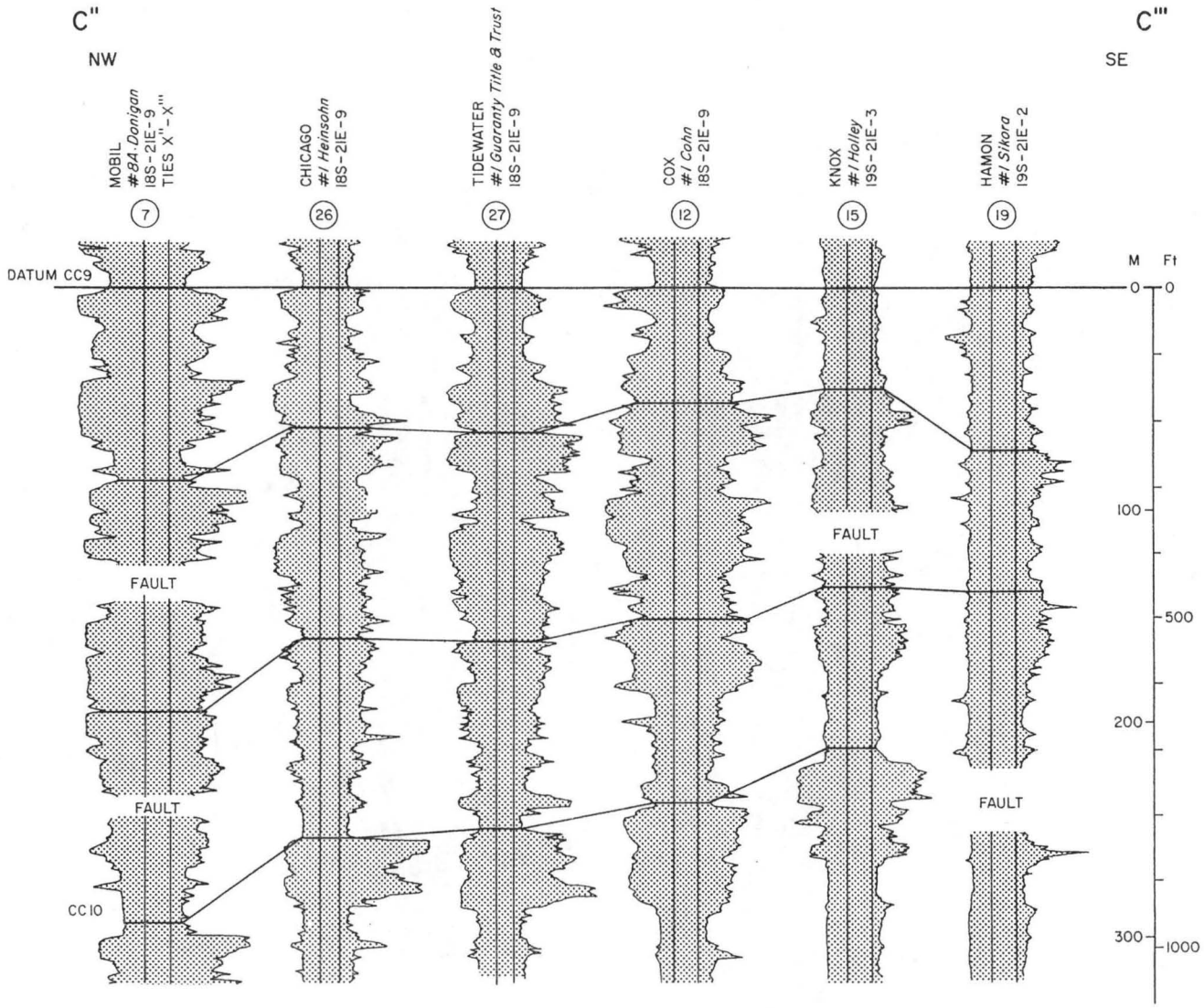

Figure 80. Stratigraphic dip section C''-C''' through the reservoir interval between markers CC9 and CC10 in the Nueces Bay Prospect Area. Note the downdip thinning and decrease in sandstone content. Line of section shown in figure 77.

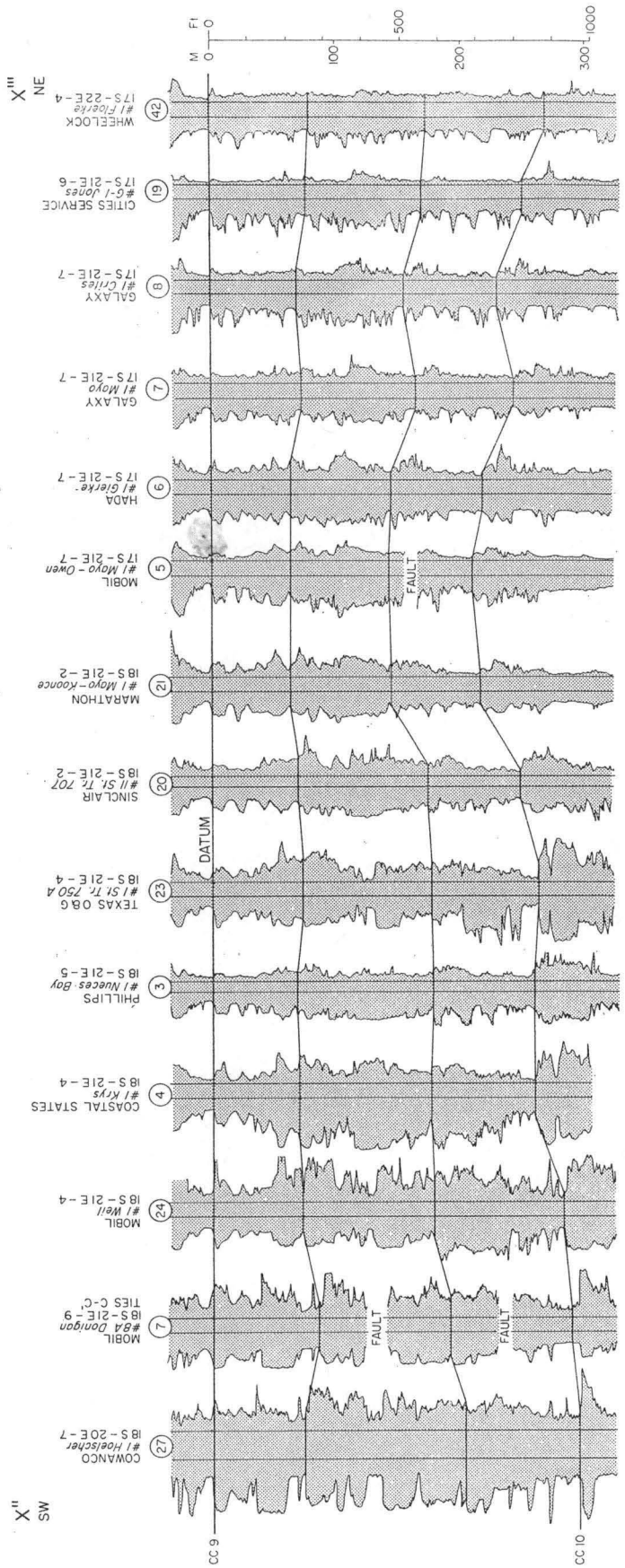

Figure 81. Stratigraphic strike section X''-X''' through the interval between markers CC9 and CC10 in the Nueces Bay Prospect Area. Note the lateral persistence of many sandstone units in a strike direction. Line of section shown in figure 77. Horizontal scale is variable.

In general, units are wide, gentle wedges because they are highly uniform and persistent along strike; downdip, they thin and grade into shale. In updip areas, the great percentage of sandstone results in paucity of shale correlation markers, and consequently, our knowledge of the geometry of the sandstones is uncertain. However, elsewhere, especially downdip, the wedge-like geometry is clearly seen, and the amount of sandstone occurring at any selected drill site should be easy to predict.

Patterns shown by the SP log include both blocky shapes, which are most abundant in updip areas, and upward-coarsening funnel shapes, which are most abundant in the central areas. Some sandstones exhibit ragged SP patterns reflecting rapid alternation of sandstone and shale; these units are probably poor reservoirs. The depositional environment is not well understood due to the lack of cores. However, considerations of the regional distribution of sand and the character of the log traces suggest that the sands originated on wave-dominated coastlines, with each shale-to-sandstone upward-coarsening sequence deposited during regression of the sea and progradation of the coastline. The vertical stacking of upward-coarsening sequences indicates numerous trangressions and regressions of the sea during deposition of the Harvey Sand. In general, 50 to 150 ft of sediment accumulated during each cycle.

Formation fluid pressures and temperatures

In the Nueces Bay Prospect Area, the B Zone is 1,100 ft thick, as determined from the plot of bottom-hole shut-in pressure versus depth (fig. 82) for 27 wells in Nueces and San Patricio Counties. In this plot, the top and base of the B Zone occur at depths of 9,500 and 10,600 ft, respectively. The base of the C Zone occurs at a depth of 13,150 ft, as determined from the plot of equilibrium temperature versus depth for 75 wells (fig. 83) in Nueces and San Patricio Counties. The top of geopressure (top

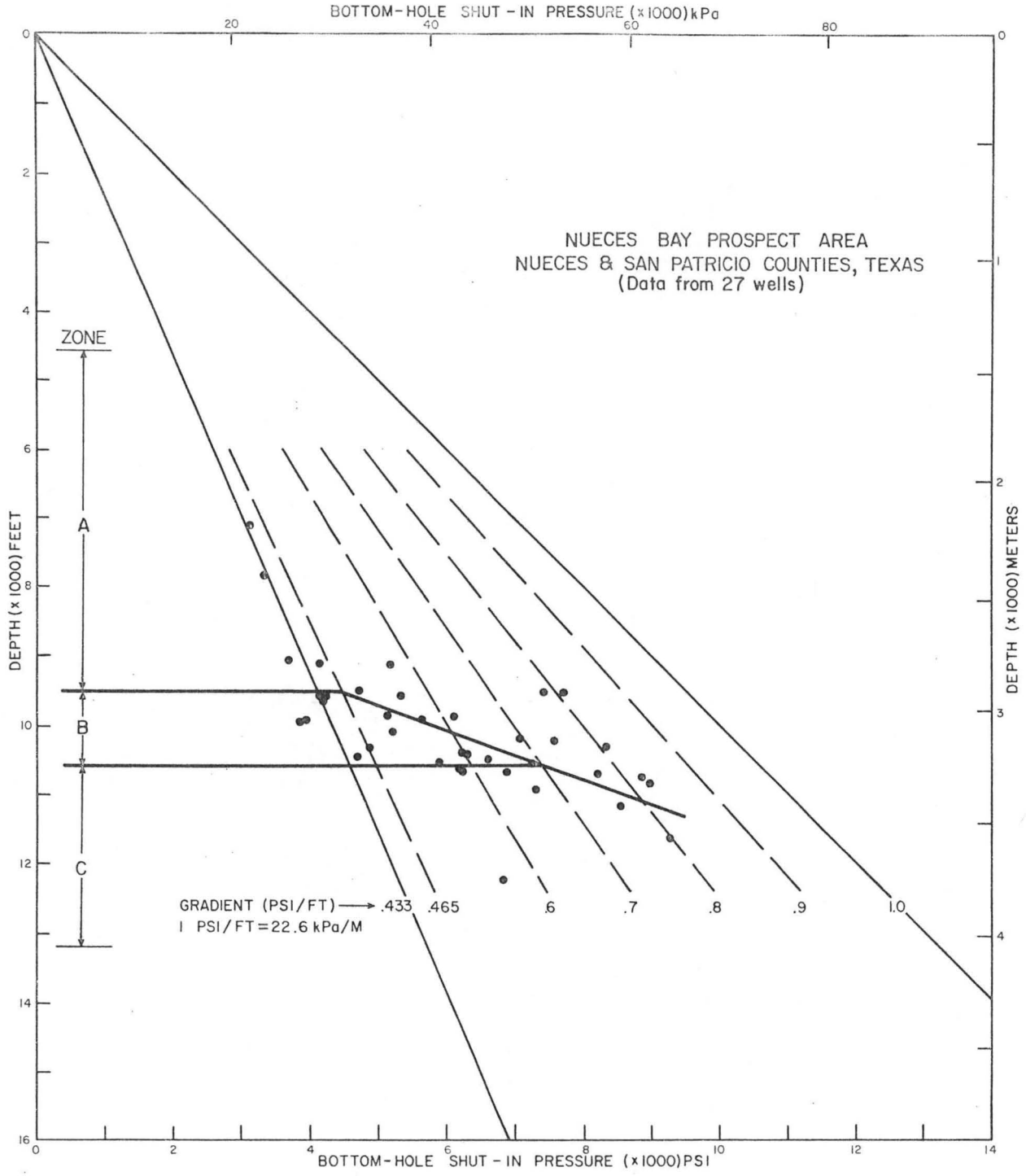

Figure 82. Bottom-hole shut-in pressure versus depth for producing wells, Nueces Bay Prospect Area, Nueces and San Patricio Counties, Texas.

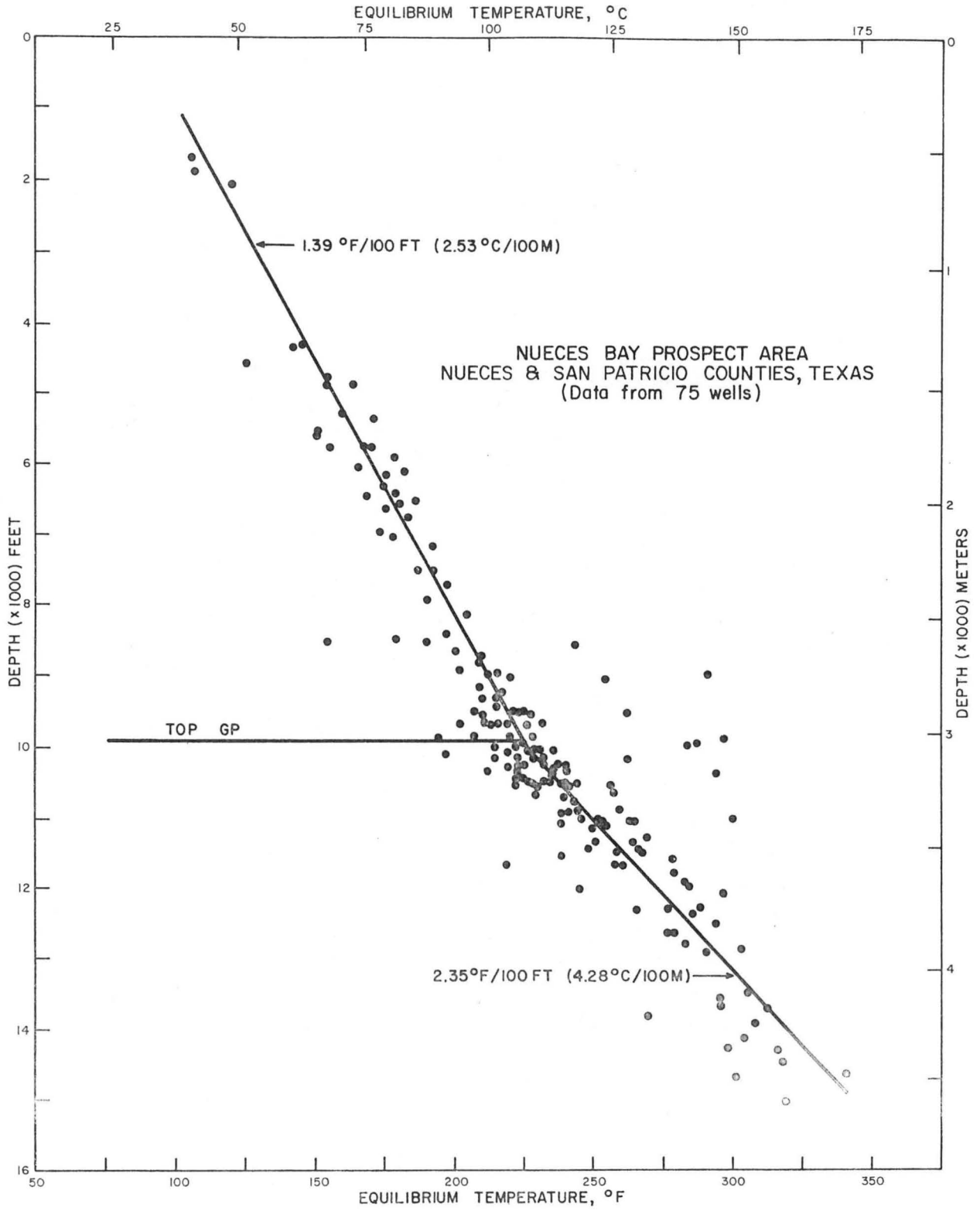

Figure 83. Plot of equilibrium temperature versus depth, showing geothermal gradients in the Nueces Bay Prospect Area, Nueces and San Patricio Counties, Texas.

of the B Zone) determined from the change in geothermal gradient occurs at a depth of 9,900 ft, 400 ft deeper than the depth determined from the BHSIP plot (fig. 82).

The geothermal gradient is 1.39° F/100 ft in the A Zone and increases to 2.35° F/100 ft in the B and C Zones. Several temperatures in the depth interval of 8,600 to 10,400 ft (fig. 83) are considerably higher than the average for the area and may indicate that the zone is a heat insulator with low thermal conductivity and higher-than-normal water content (porosity). These hot spots occur in 4 wells located in the southwest corner of Tobin Grid 18S-21E (fig. 77). One of these wells is No. 26 on dip section C"-C'''. Temperatures lower than average along the gradient line below 13,500 ft possibly indicate the beginning of a reduced geothermal gradient; this gradient line may be developing into the third part of a geothermal dogleg as depth increases below well control.

Strike section X"-X''' (fig. 77) is divided into three shorter sections (X"-Xa, Xa-Xb, and Xb-X''') for the purpose of presenting parameter plots (figs. 84, 85, and 86). The top of the B Zone is shallowest in the middle part of the prospect area, averaging 9,250 ft deep along section Xa-Xb (fig. 85). In the southwestern part of the area, the top of the B Zone averages 9,850 ft in depth along section X"-Xa (fig. 84); at the northeastern end, the zone top averages 9,825 ft in depth along section Xb-X''' (fig. 86). Perhaps as a consequence of the shallower depths, equilibrium temperatures at the top of the B Zone are lowest in the middle part of the prospect area, averaging 219° F along section Xa-Xb, compared with 227° F on X"-Xa and 220° F on Xb-X'''. Similarly, temperatures at the bottom of the B Zone are lowest in the middle section, averaging 235° F on Xa-Xb, compared with 245° F on X"-Xa and 240°F on Xb-X'''.

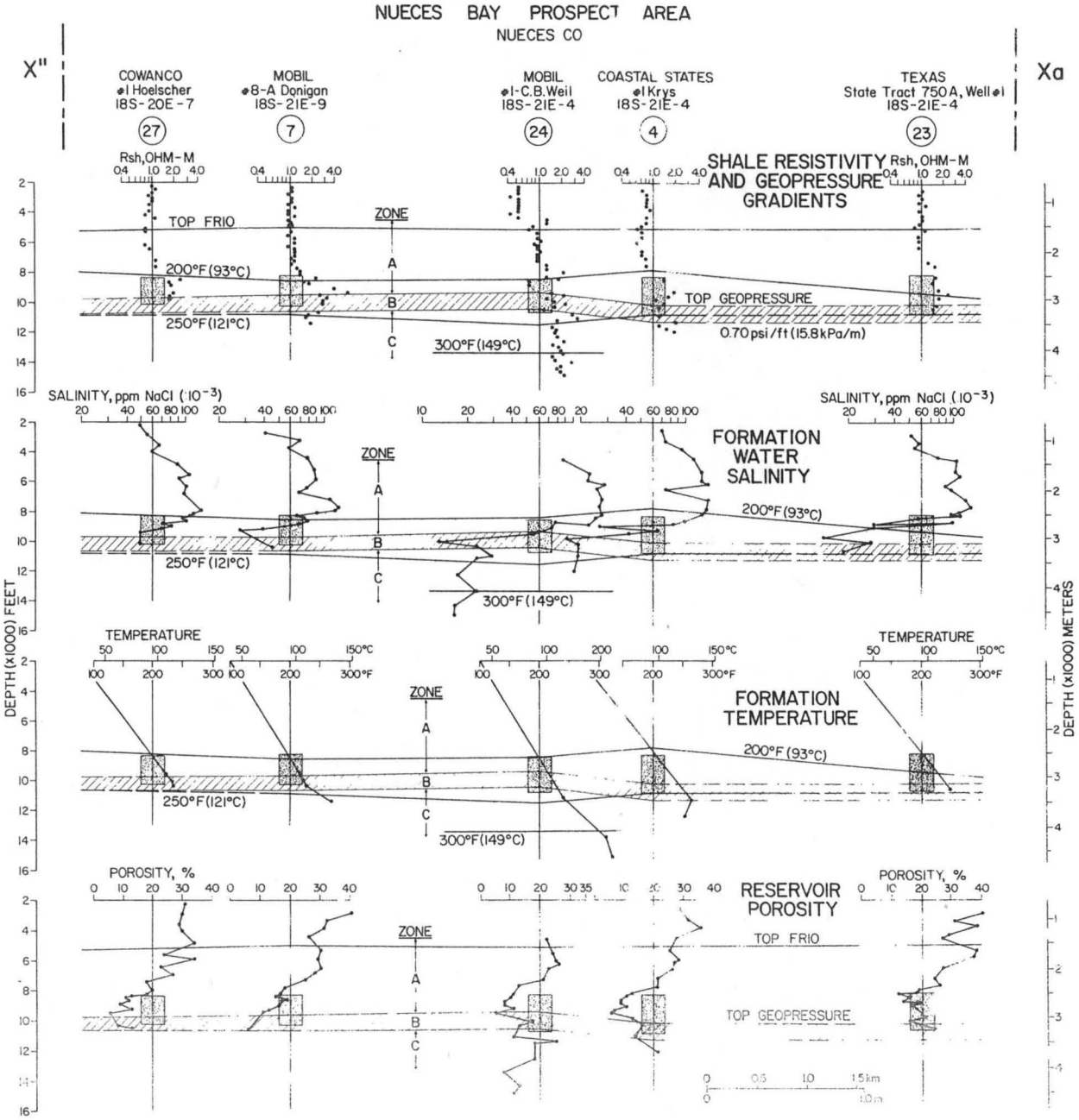

Figure 84. Parameter plots for wells along strike section X''-Xa, Nueces Bay Prospect Area, Nueces County, Texas. The reservoir interval is indicated by the stippled columns.

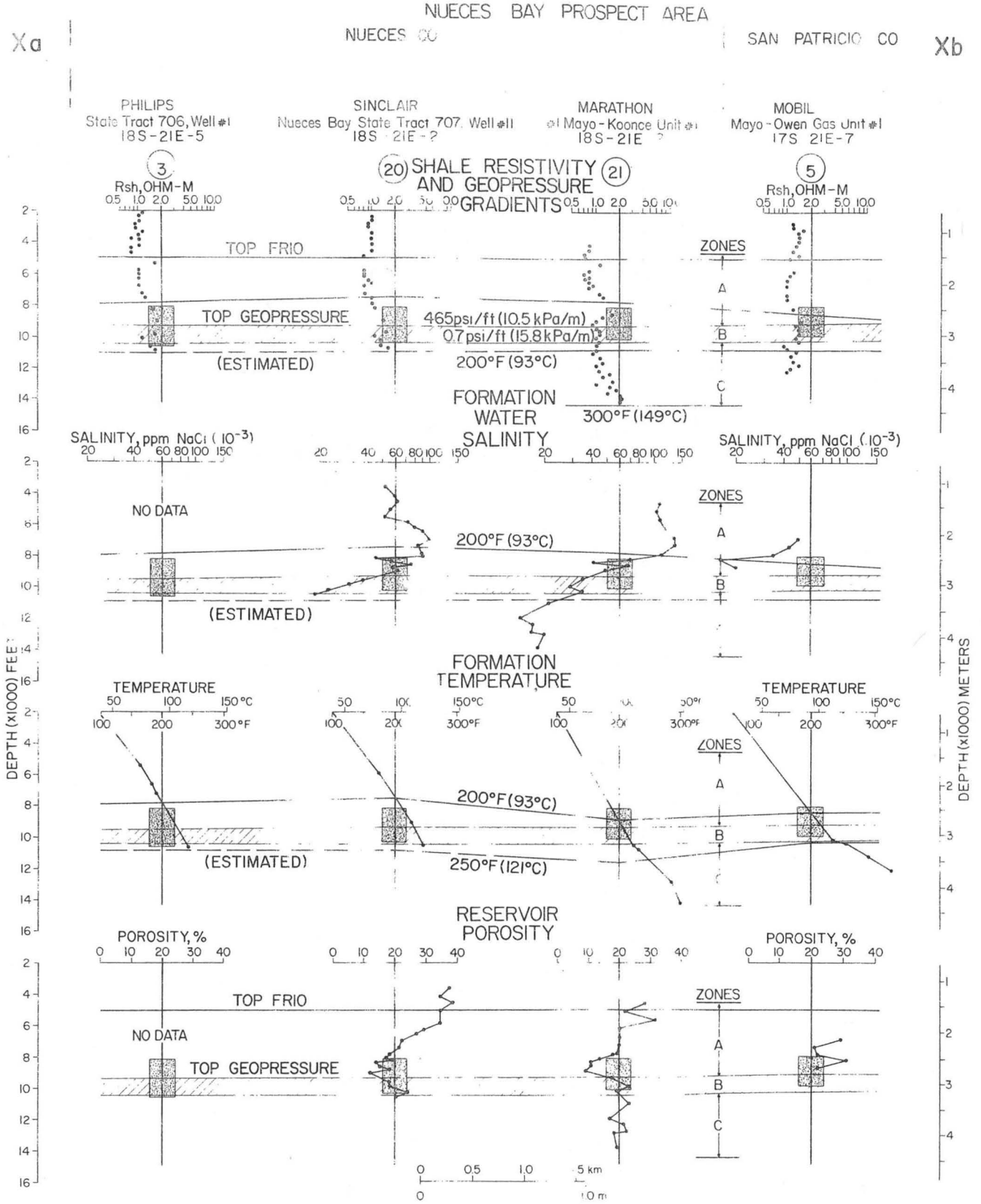

Figure 85. Parameter plots for wells along strike section Xa-Xb, Nueces Bay Prospect Area, Nueces County, Texas. The reservoir interval is indicated by the stippled columns.

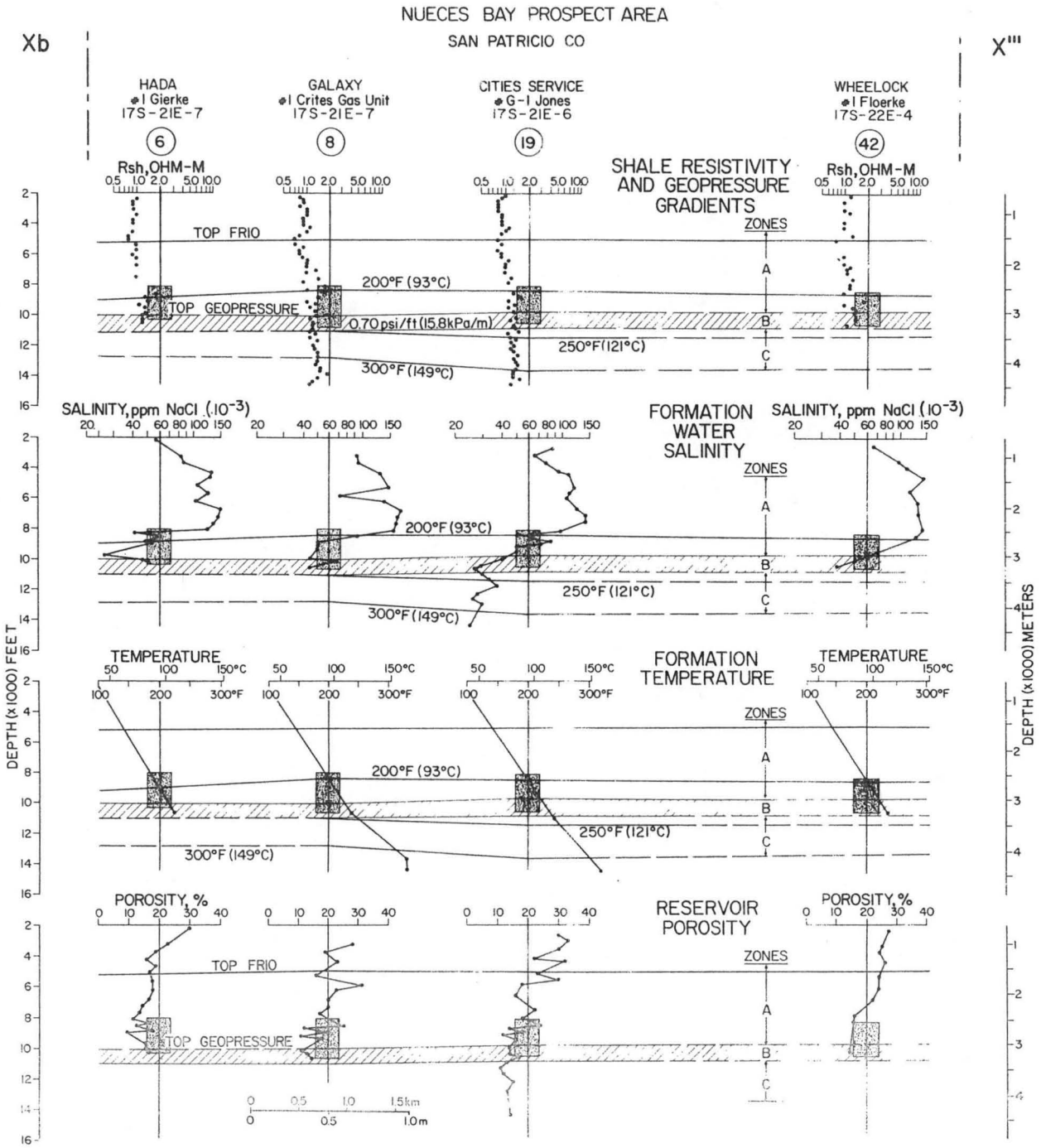

Figure 86. Parameter plots for wells along strike section Xb-X''', Nueces Bay Prospect Area, Nueces County, Texas. The reservoir interval is indicated by the stippled columns.

The top of the B Zone along dip section C-C' (fig. 87) rises downdip from a depth of 9,900 ft at well No. 7 (Tobin Grid 18S-21E-9) to 8,900 ft at well No. 19 (Tobin Grid 19S-21E-2); the average depth along the section is 9,150 ft. Equilibrium temperatures average 217° and 238° F at the top and base of Zone B, respectively.

Formation water salinity

The salinity versus depth plot for Nueces, Aransas, and San Patricio Counties (fig. 88) contains some salinity data for wells located in the Nueces Bay Prospect Area, but much of the data comes from wells located outside the prospect area. Salinity profiles for wells located on strike and dip sections across the Nueces Bay Prospect Area are shown on parameter plots for these sections (figs. 84 through 87). Salinities at the top and base of the B Zone average 37,000 and 31,000 ppm NaCl along strike section X"-Xa (fig. 84), 40,000 and 25,000 ppm NaCl along strike section Xa-Xb (fig. 85), and 51,000 and 30,000 ppm NaCl along strike section Xb-X''' (fig. 86). On dip section C"-C''' (fig. 87), salinities average 34,000 and 23,000 ppm NaCl at the top and base of the B Zone. All sections show that salinity decreases with depth within the B Zone.

Porosity and permeability

Porosities determined from induction and SP logs at the top and base of the B Zone average 11.5 and 12 percent on strike section X"-Xa (fig. 84), 16 and 20 percent on strike section Xa-Xb (fig. 85), 15 and 15 percent on strike section Xb-X''' (fig. 86), and 13 and 10 percent on dip section C"-C''' (fig. 87), respectively. A small cluster of whole-core porosity data located in the depth interval from 7,400 to 8,500 ft in the deep A Zone (fig. 89) shows a porosity range of 21 to 27.5 percent. A porosity versus permeability plot (fig. 90) for the Corpus Christi Fairway shows the common trend of permeability increasing with porosity that can be

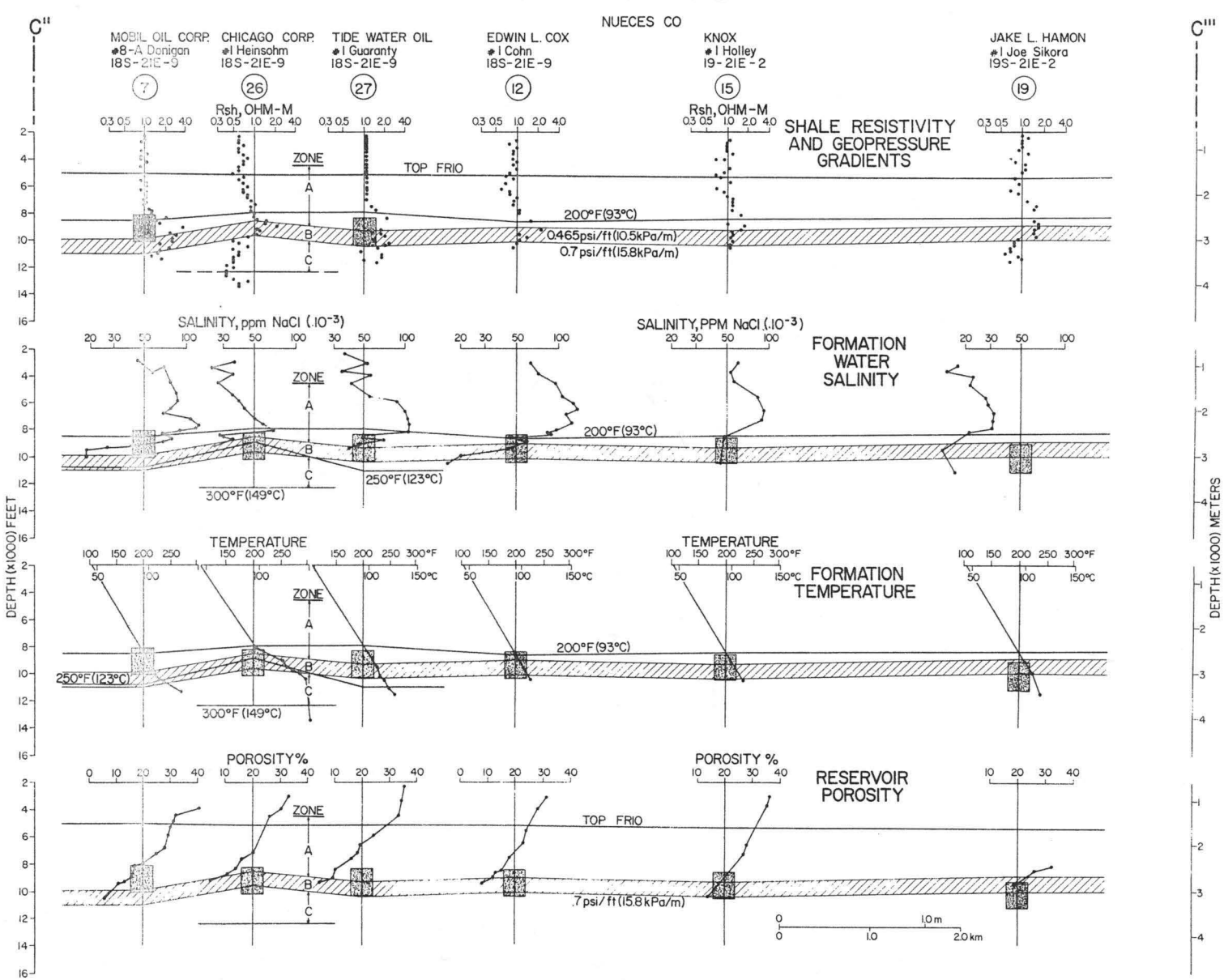

Figure 87. Parameter plots for wells along dip section C''-C''', Nueces Bay Prospect Area, Nueces County, Texas. The reservoir interval is indicated by the stippled columns.

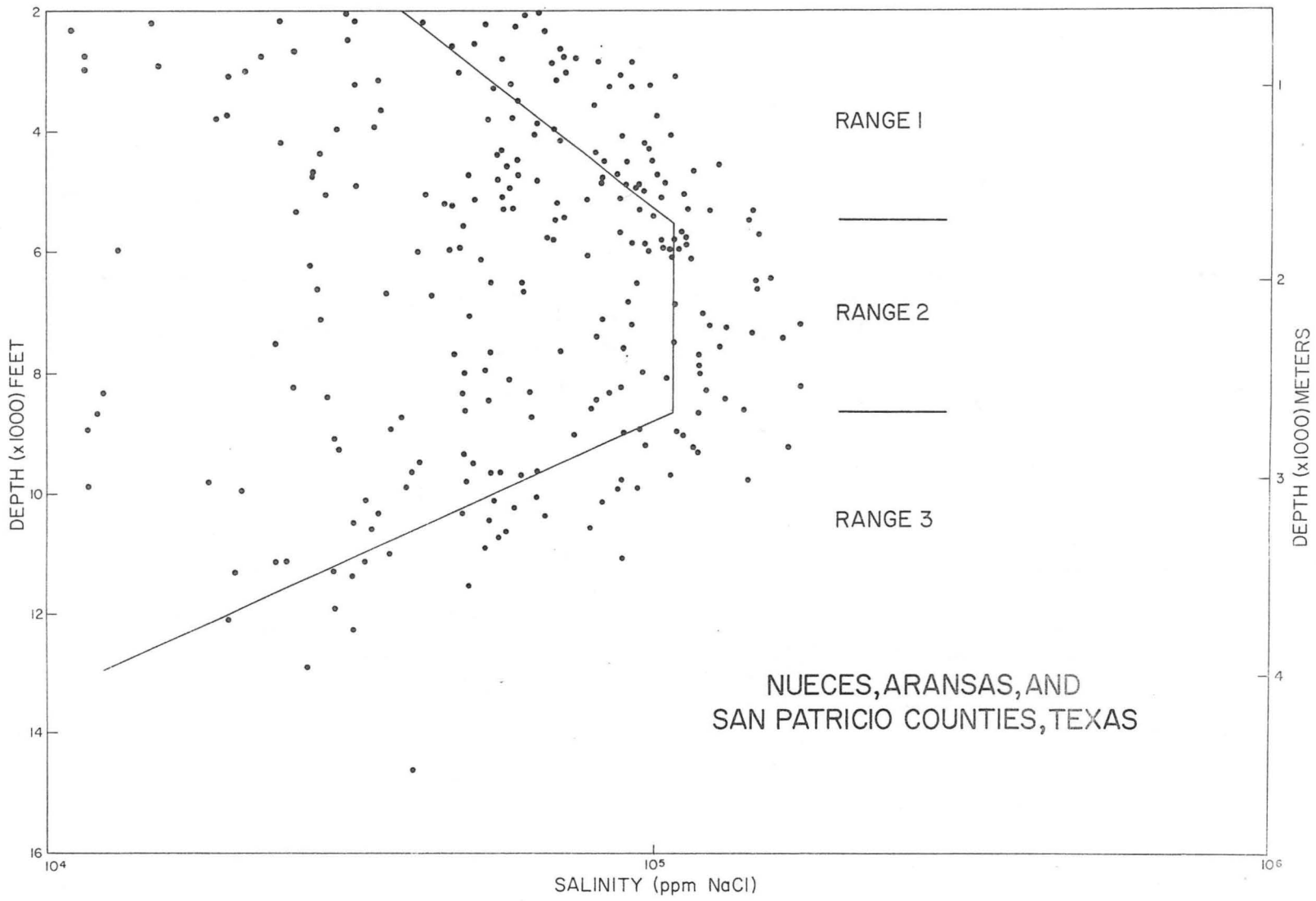

Figure 88. Salinity versus depth for sandstones in Nueces, Aransas, and San Patricio Counties, Texas.

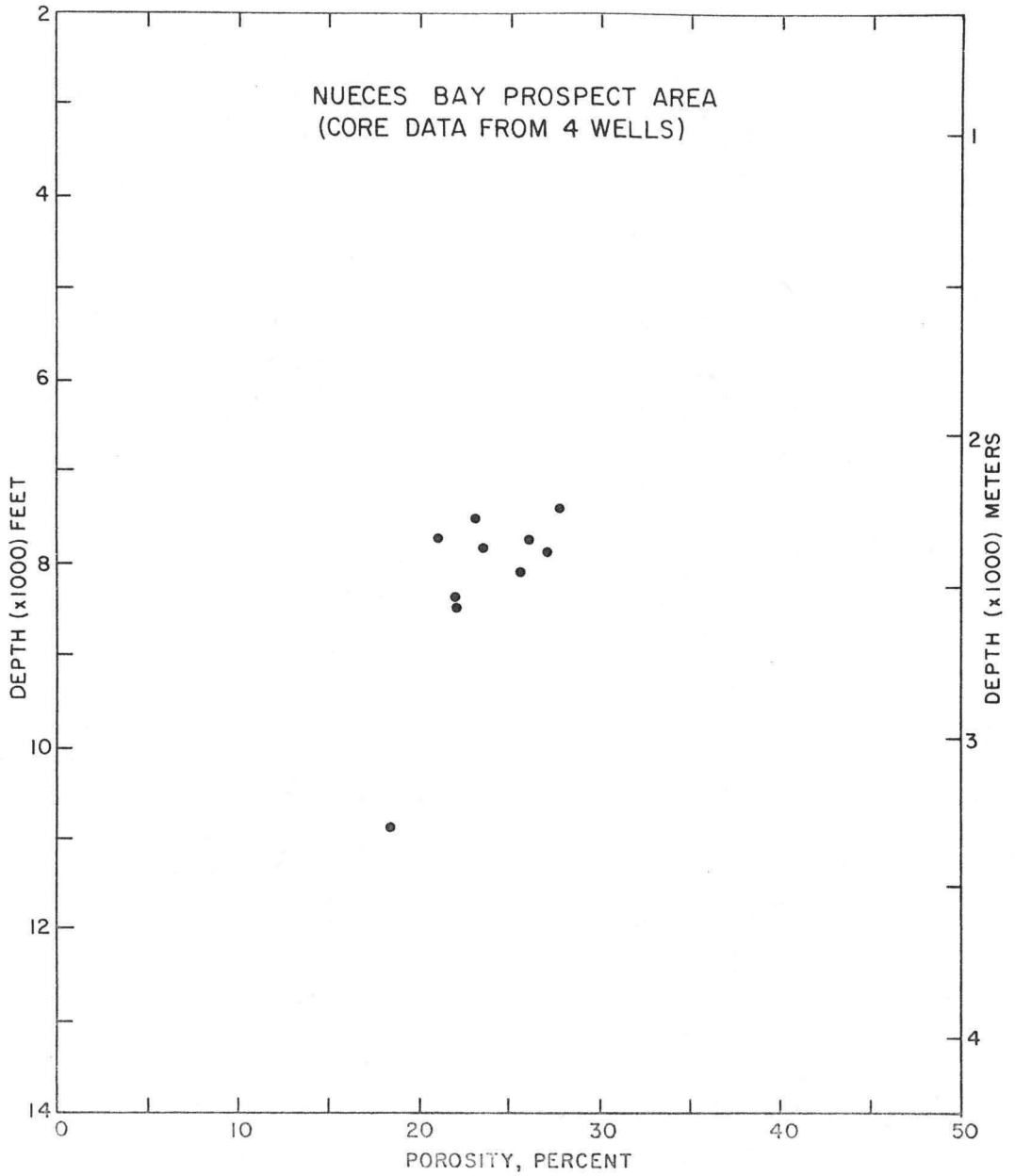

Figure 89. Whole-core porosity versus depth for four wells, Nueces Bay Prospect Area.

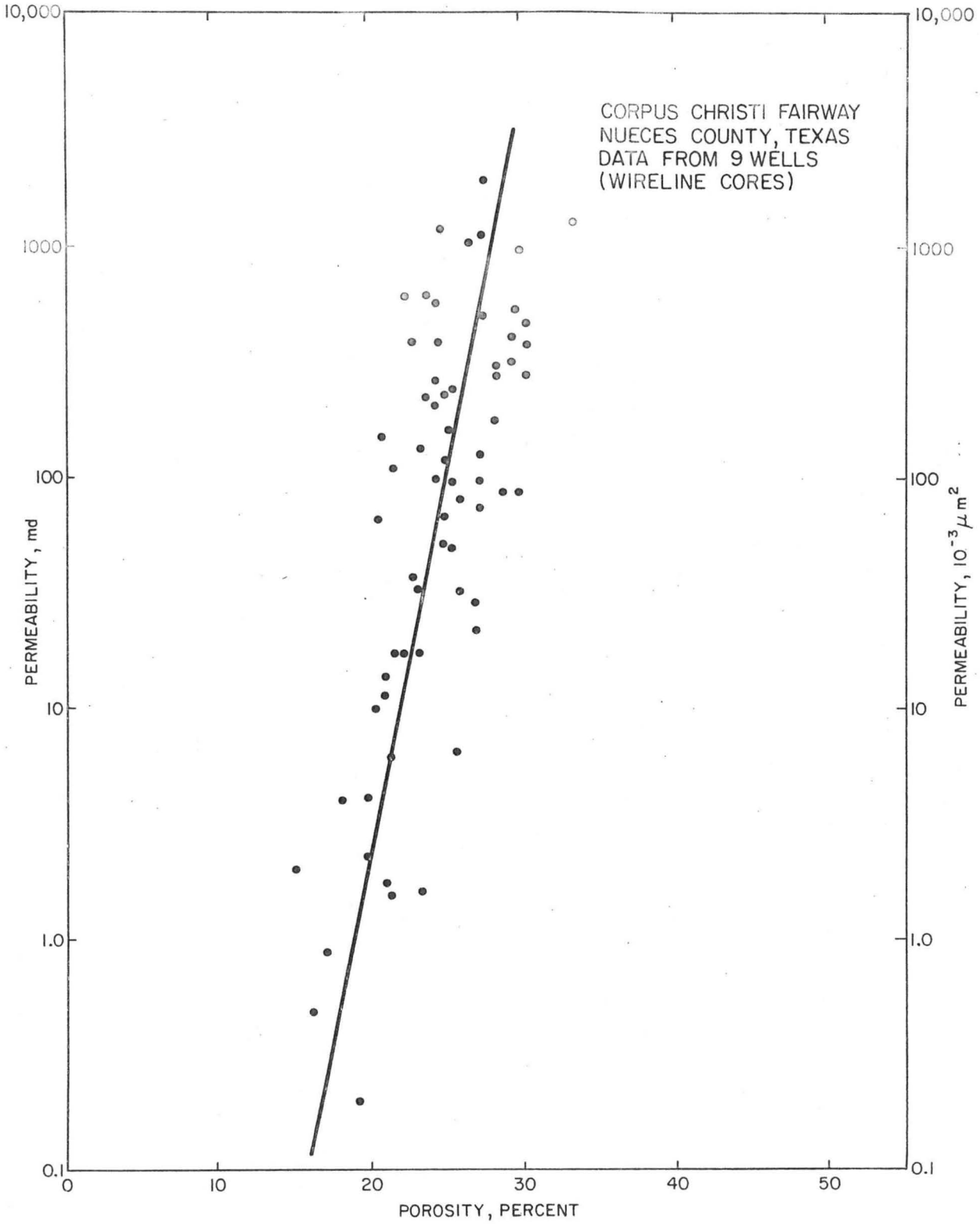

Figure 90. Air permeability versus porosity in whole cores from nine wells, Nueces County, Texas.

applied in general to the Nueces Bay Prospect Area. Likewise, the Nueces Bay Prospect is expected to show permeability generally decreasing with depth, as indicated by figure 91, which is a plot of data from the Corpus Christi area.

Nueces Bay test-well site

The proposed test-well site is located in the southwestern part of the prospect area, north of the Corpus Christi International Airport and south of Saxet Field (fig. 66). The well site is within the city limits of Corpus Christi. The site is approximately 1.2 mi from the western margin of the block and is about 0.7 mi north of the type well (Mobil No. 8-A Donigan; fig. 78).

Based on projections from nearby wells, the anticipated depth to the top of the Frio at the test site is 5,005 ft. The depth to the top of the reservoir interval is 8,175 ft; the thickness of the reservoir interval is 850 ft. The net sandstone is 740 ft. Most sandstone units range in thickness from 30 to 100 ft.

The CC9 to CC10 interval contains the prospective reservoirs of primary interest and lies within the deep A Zone. Some sandstones in the section immediately below CC10 are also considered prospective and occur within the upper part of the B Zone. Other massive sandstones above CC9 are additional prospective reservoirs for testing the deep hydropressured A Zone. Particularly of interest are sandstones in the interval from CC4 to CC9 (fig. 70), which contains from 800 to 1,000 ft of sandstone.

The test-well site is favorably located in terms of quantity of sandstone present. However, the proximity to the western growth fault suggests that some small faults may be present in the reservoir interval. It is possible that seismic data will be needed to determine the structural integrity of the reservoir horizon in this area.

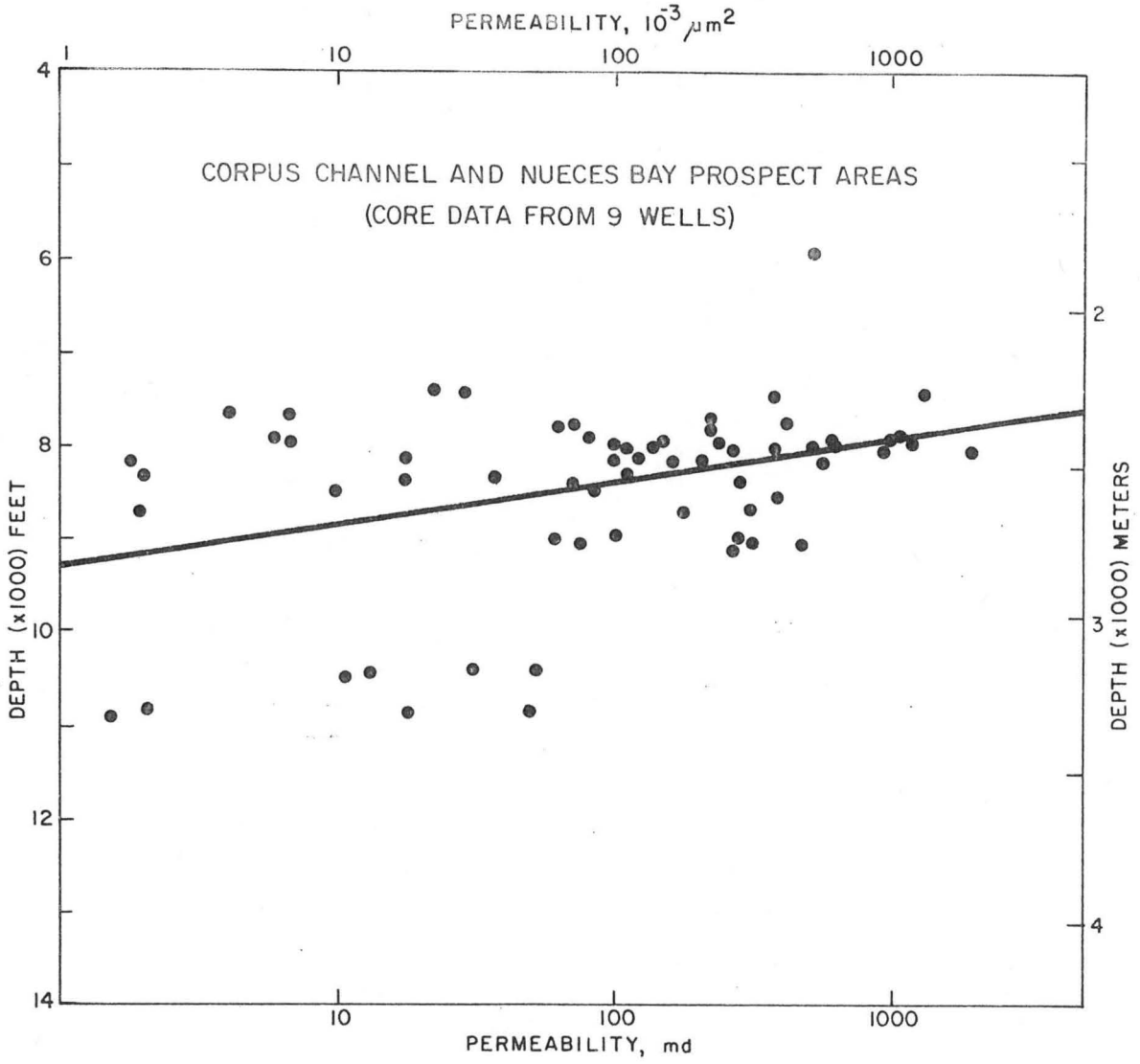

Figure 91. Whole-core porosity versus depth for nine wells in Corpus Channel and Nueces Bay Prospect Areas.

Fluid pressure, formation temperature, and salinity data plotted versus depth provide the information necessary for estimating methane solubility as a function of depth (fig. 92). Methane solubility in the A Zone in the type well, Mobil No. 8-A Donigan, varies from 12 to 26 SCF/B (from "curve" R_{mf} method) and averages about 27 SCF/B in the upper portion of the B Zone. Methane solubility in individual reservoir sandstones at depths of 8,360, 9,450, and 10,335 ft range from 19 to 28 SCF/B (table 2).

Corpus Channel Prospect Area

Much of the Corpus Channel Prospect Area is situated over Corpus Christi Bay in eastern Nueces County (figs. 66 and 93). The prospect extends south to Flour Bluff in Nueces County and north into San Patricio and Aransas Counties. The prospect area is a structural block bounded on three sides by growth faults and limited to the north by poor reservoir quality. It ranges from 4 to 7 mi in width, is 27 mi long, and has an area of 120 mi^2. The prospect contains up to 1,600 ft of sandstone primarily in the A Zone. Oil and gas fields in the prospect area include Flour Bluff, Encinal Channel, Corpus Channel, Corpus Christi Bay, and Gregory.

Markers used for correlation are both the fairway markers CC1, 2, 4, 5, 6, 7, and 8, and additional markers used only in the prospect area to subdivide the reservoir interval into units CC-A to CC-D (fig. 94).

Structure

The Corpus Channel Prospect Area is bounded by growth faults on three sides. To the west and east are major growth faults with throws of several hundred feet at the top of the Frio and more than 2,000 ft at the level of deeper horizons. The cross fault forming the southern boundary of the block has a throw of several hundred feet at the level of the prospective

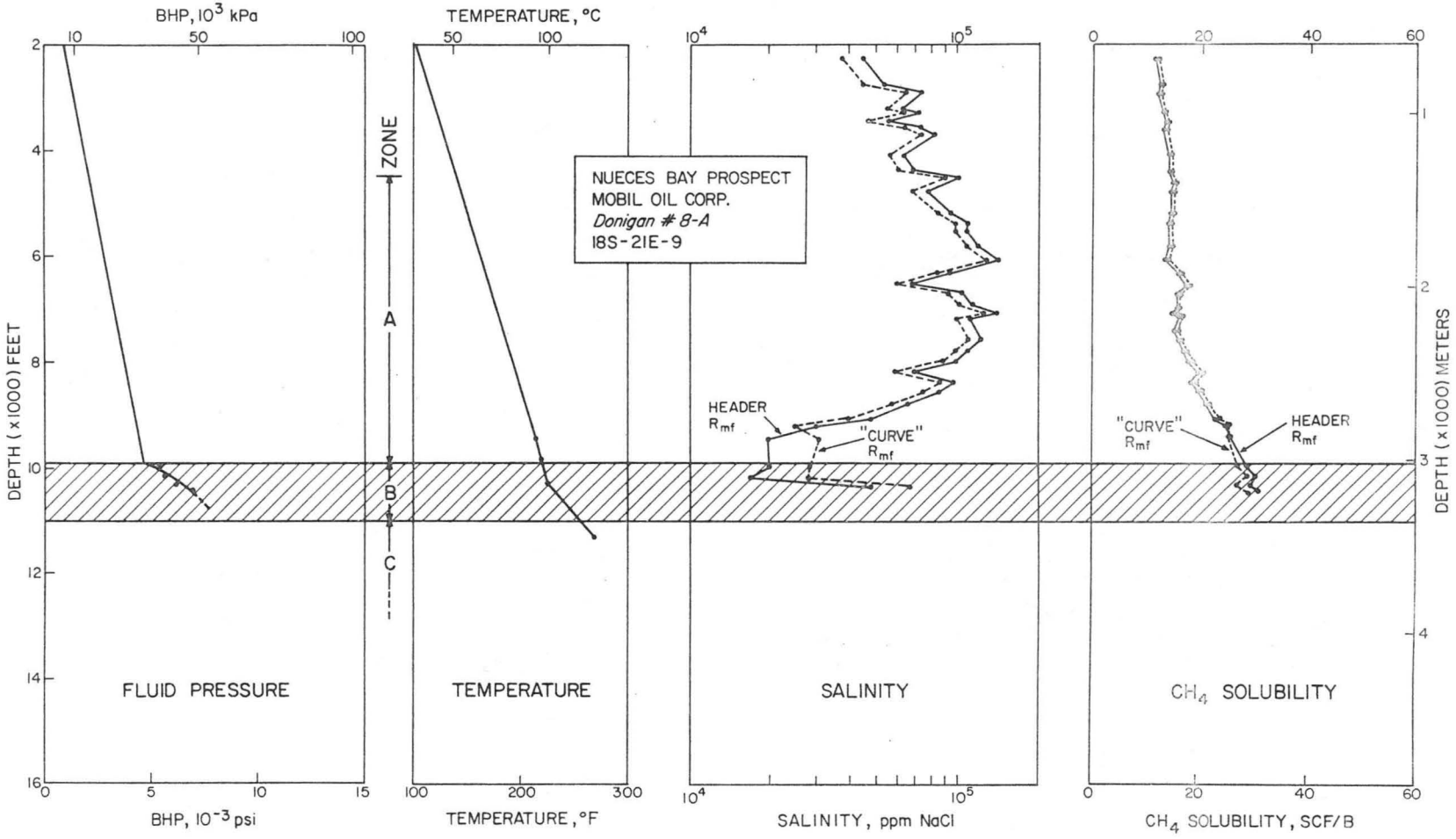

Figure 92. Parameter profiles for Mobil No. 8-A Donigan (18S-21E-9), type well for Nueces Bay Prospect Area, Nueces County, Texas.

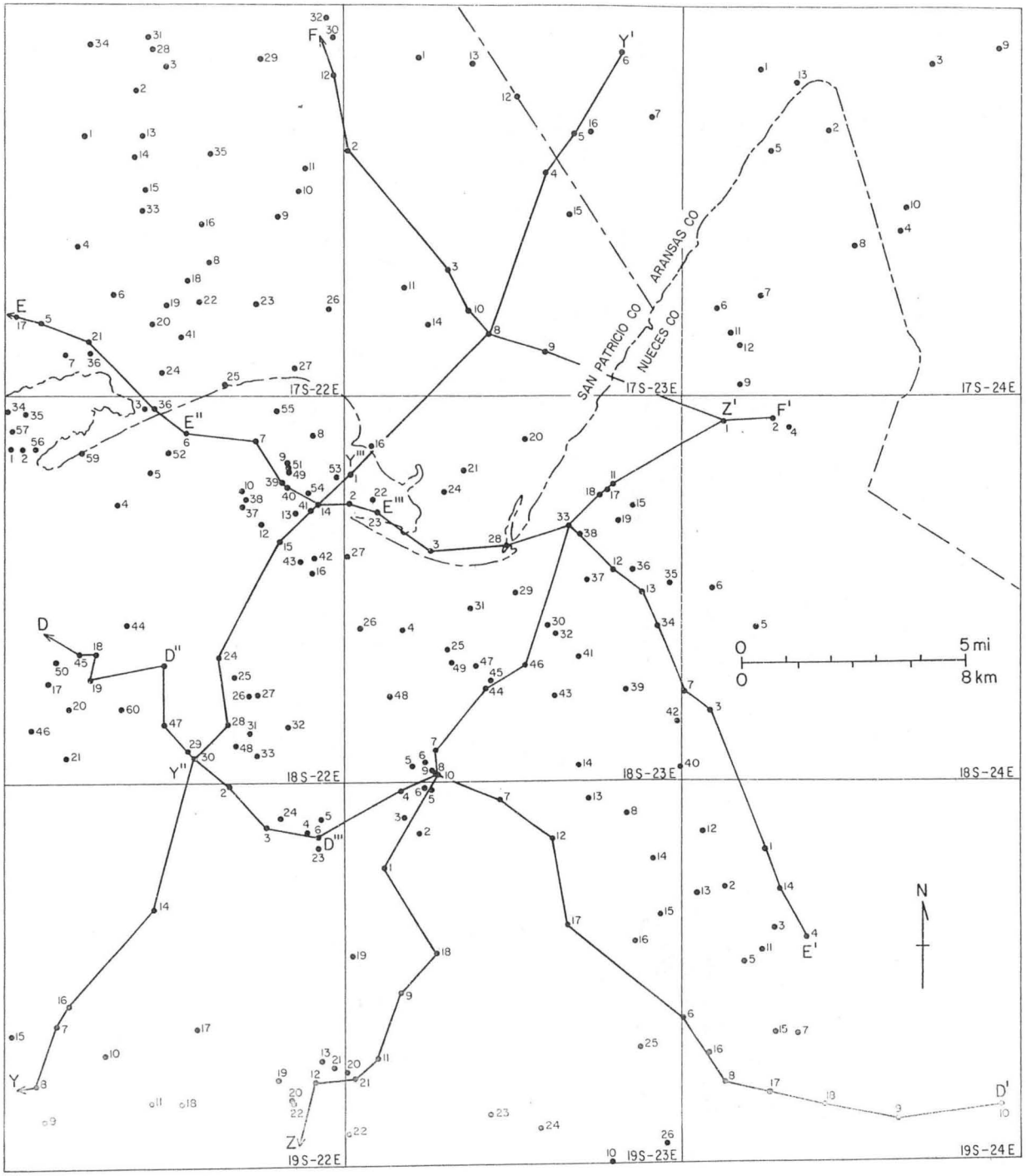

Figure 93. Well locations and lines of cross section, Corpus Channel Prospect Area. The location of the area within the Corpus Christi Fairway is shown in figure 67.

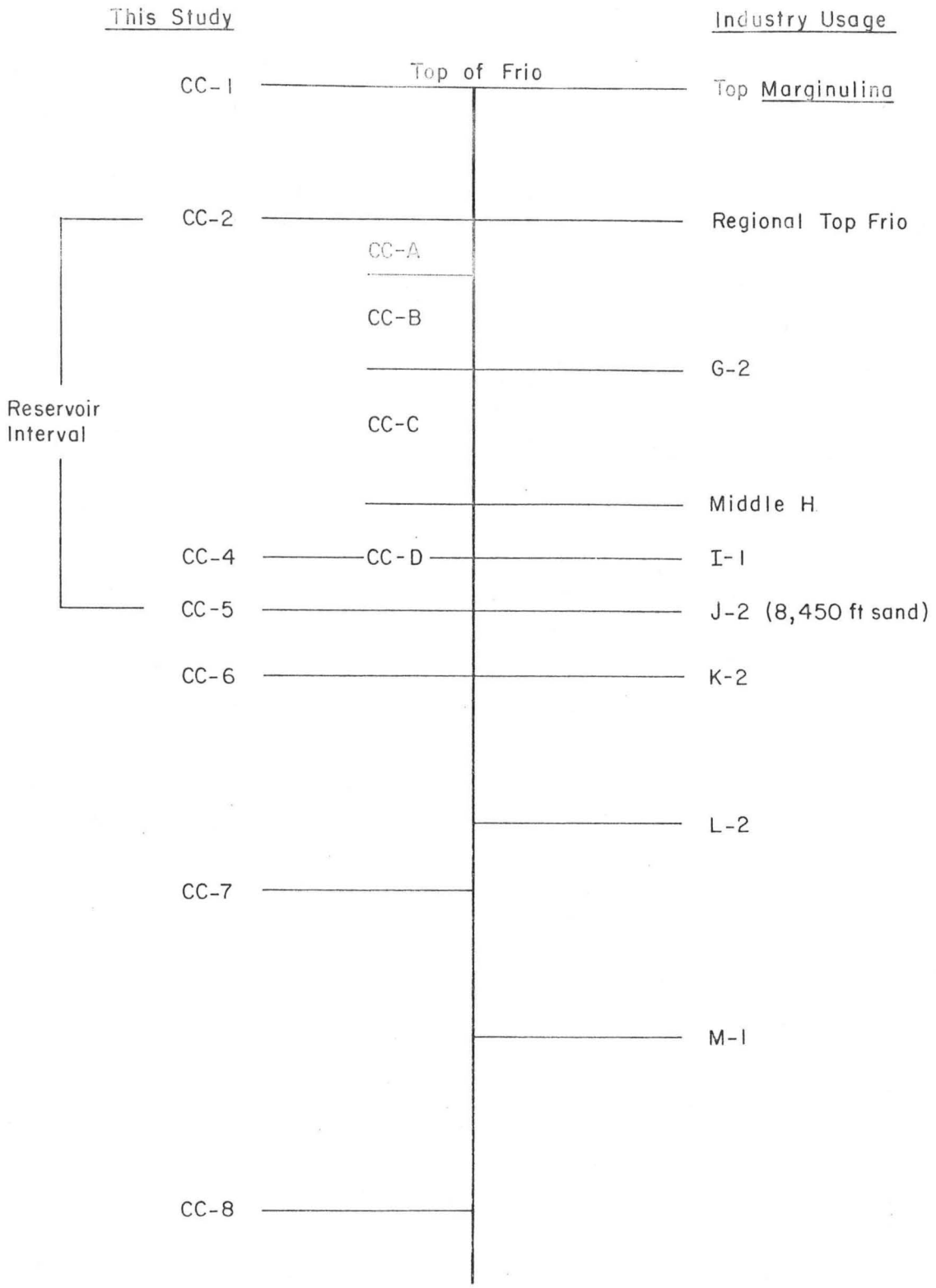

Figure 94. Correlation of stratigraphic markers used in this study with some markers and key productive sandstones named in the petroleum industry.

reservoir interval. The northern boundary of the prospect was chosen where primary reservoir sandstones begin to thin (fig. 95).

The fault block is at a maximum width of 7 mi in the south, and thins to about 4 mi in the north (fig. 96). The structure map on the top of the Frio (fig. 96) shows the structure associated with the upper part of the reservoir interval. Important features are the dome cut by a small growth fault in the southwestern part of the block, which is the area of the Encinal Channel Field, and north of this, a gentle dome, which is the area of the Corpus Channel Field. Additional positive features are located in the southeastern tip and in the northern part of the fault block.

The deeper structure map of marker CC4 (fig. 97) illustrates the structure in the lower part of the reservoir interval. The map is broadly similar to the structure map of the top of the Frio. However, comparison shows a gulfward migration of positive features that is due to greater subsidence rates in the western part of the fault block and is typical of the Tertiary Gulf Coast Basin. The concentration of wells is clearly related to the position of structural highs. Both of these maps suggest that there is little faulting within the prospect area at the level of the reservoir interval. This structure favors the lateral continuity of component reservoirs.

Sandstone distribution and characteristics

In the Corpus Channel Prospect, sandstones in the Frio Formation are abundant from the top of the Frio (CC1) at depths as shallow as 6,200 ft and extend down to the CC8 marker at depths as great as 11,000 ft. Marker CC2 was chosen as the top of the reservoir interval in this prospect. It ranges in depth from about 6,800 ft to 7,400 ft. Approximately 200 ft below CC2 is a resistivity marker used as the base of unit CC-A, the upper stratigraphic interval of the Corpus Channel Prospect (fig. 98). The

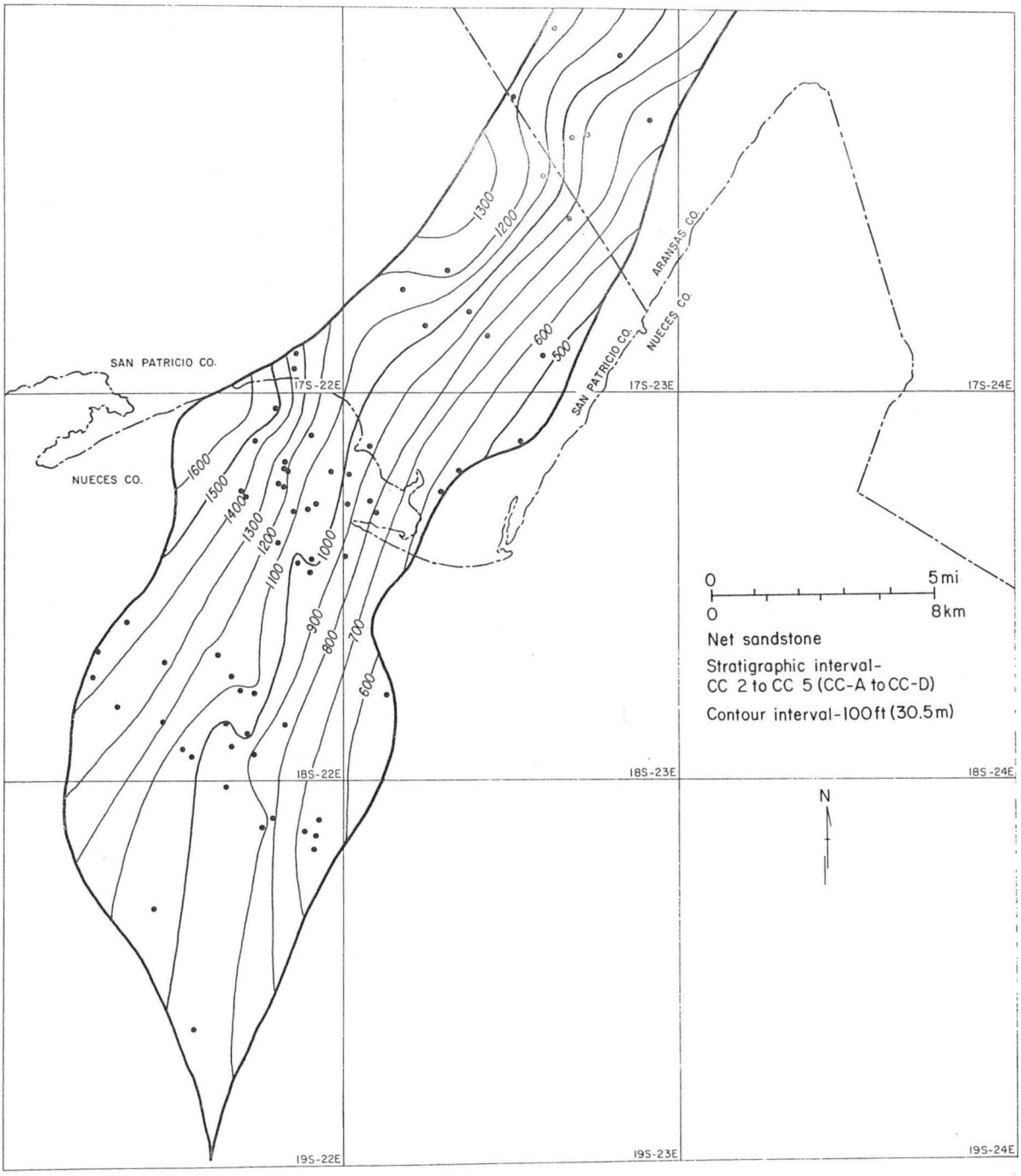

Figure 95. Net sandstone in the reservoir interval (CC2 to CC5), Corpus Channel Prospect Area.

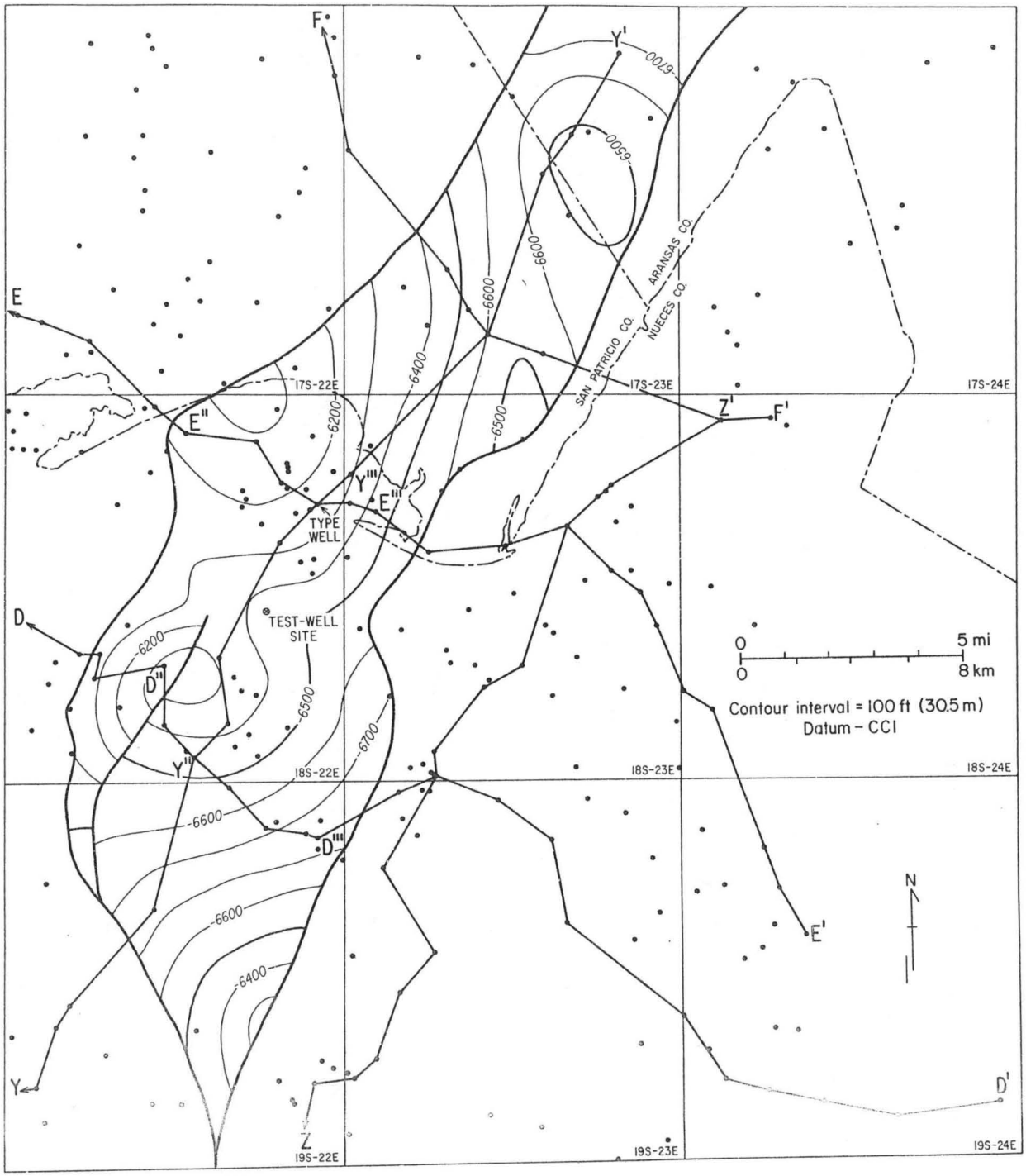

Figure 96. Structure on the top of the Frio (CC1) in the Corpus Channel Prospect Area. The top of the reservoir interval occurs from 200 to 400 ft (60 to 120 m) below this datum, depending upon location in the fault block.

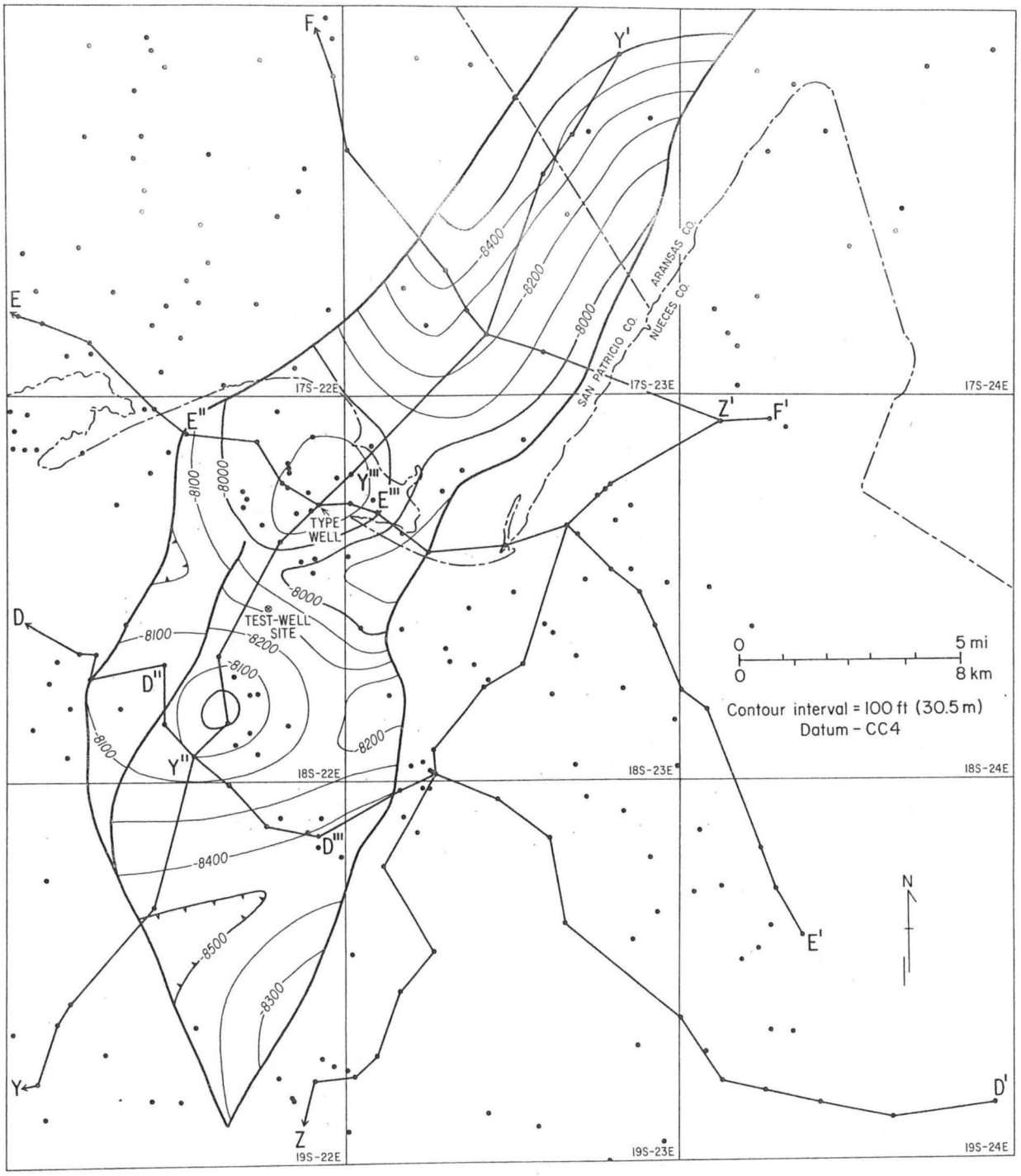

Figure 97. Structure on the CC4 marker in the Corpus Channel Prospect Area. The base of the reservoir interval occurs from about 450 to 550 ft (135 to 165 m) below the CC4 marker, depending upon location in the fault block.

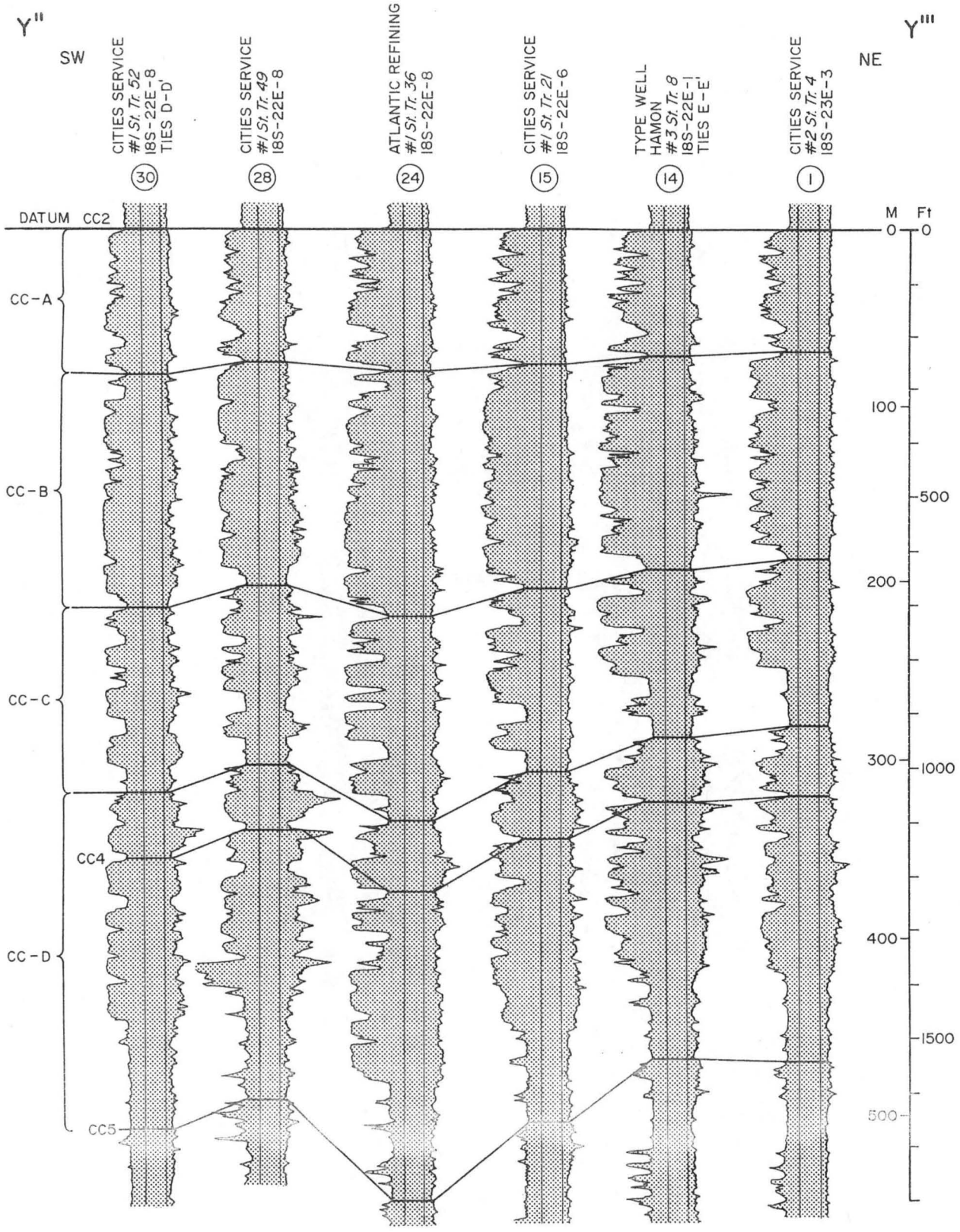

Figure 98. Stratigraphic strike section Y''-Y''' through the reservoir interval (CC2 to CC5) in the Corpus Channel Prospect Area. Note the great lateral continuity of the individual sandstone units. Line of section is shown in figure 93.

underlying unit, CC-B, is about 500 ft thick, and its base is a resistivity marker referred to as "G-2" (fig. 94) by petroleum geologists. Unit CC-C is about 300 ft thick, and its base is a resistivity marker referred to as "middle H." The lowermost unit in the prospective interval, CC-D, extends down to marker CC5, which corresponds with the 8,450-ft sand, just below the top of J-2 sand. In this prospect area, marker CC4, which corresponds to the top of I sands of the petroleum industry, is included in unit CC-D. This unit is approximately 600 ft thick.

Shale dominates the interval between markers CC5 and CC7 at depths of 8,500 to 9,500 ft, but thin sandstones (10 to 30 ft) showing both good SP response and high whole-core porosity and permeability are also present. Detailed log correlation also indicates that the sandstones form gentle wedges or extensive sheets and are therefore potentially excellent reservoirs. These sandstones have not been included in the reservoir zone for this study because they are comparatively thin. However, they occur in the B Zone and, therefore, could be included as reservoirs in a test of the main reservoir interval above. In this area, marker CC6 corresponds to the K-2 sands (fig. 94), marker CC7 occurs between the L and M series of sands, and marker CC8 occurs within the M series of sands.

Below marker CC7, at depths greater than about 9,000 ft, sandstones show a ragged SP curve that indicates a small-scale alternation of shale and sandstone and that suggests very low porosity and permeability. In addition, available core data show that these sandstones should not be regarded as potential reservoirs.

To portray the sandstone distribution in the prospect area in detail, five net-sandstone maps of the reservoir interval were constructed. A net-sandstone map for the entire interval (fig. 95) shows a pattern similar

to that observed in the Nueces Bay Prospect Area. The isoliths are generally aligned parallel to strike, with some minor departures. There is a uniform decrease in sandstone from a maximum of 1,600 ft along the west-central margin of the block to a minimum of less than 500 ft along the eastern margin. The shallowest subdivision of the reservoir interval, unit CC-A, shows a similar trend, decreasing from 400 ft in the west to less than 100 ft in the east (fig. 99). Unit CC-B shows a small elongate sandstone high of more than 450 ft adjacent to the western margin of the area, decreasing to 150 ft in the east (fig. 100). Unit CC-C contains more than 300 ft of sandstone in the west, decreasing to less than 100 ft in the east (fig. 101). The deepest unit, CC-D, decreases in net sandstone from 500 ft of sandstone in the west to less than 150 ft in the east (fig. 102).

The geometry of the component sandstone units has been determined using detailed correlations to construct both strike- and dip-aligned stratigraphic sections of the reservoir interval. The strike section (fig. 98) illustrates the lateral continuity of individual sandstone bodies. The dip sections (figs. 103 and 104) illustrate that many sandstones thin and pinch out downdip. For example, sandstones that are 50 to 100 ft thick in the west thin and disappear eastward within several miles. However, many sandstones maintain their thickness across the entire fault block. Thus, both gentle wedge- and sheet-shaped sandstone bodies are present in the prospect. As with the Nueces Bay Prospect, the net sandstone within the reservoir interval in the Corpus Channel Prospect is highly predictable.

Electric log (SP) patterns are dominantly blocky with subordinate upward-coarsening patterns and few upward-fining patterns. A ragged pattern is scarce and appears to be limited to the downdip parts of unit CC-A (fig. 103). The repetitive alternation of thick sandstones with fairly homogeneous shales suggests a marine-dominated coastline, probably

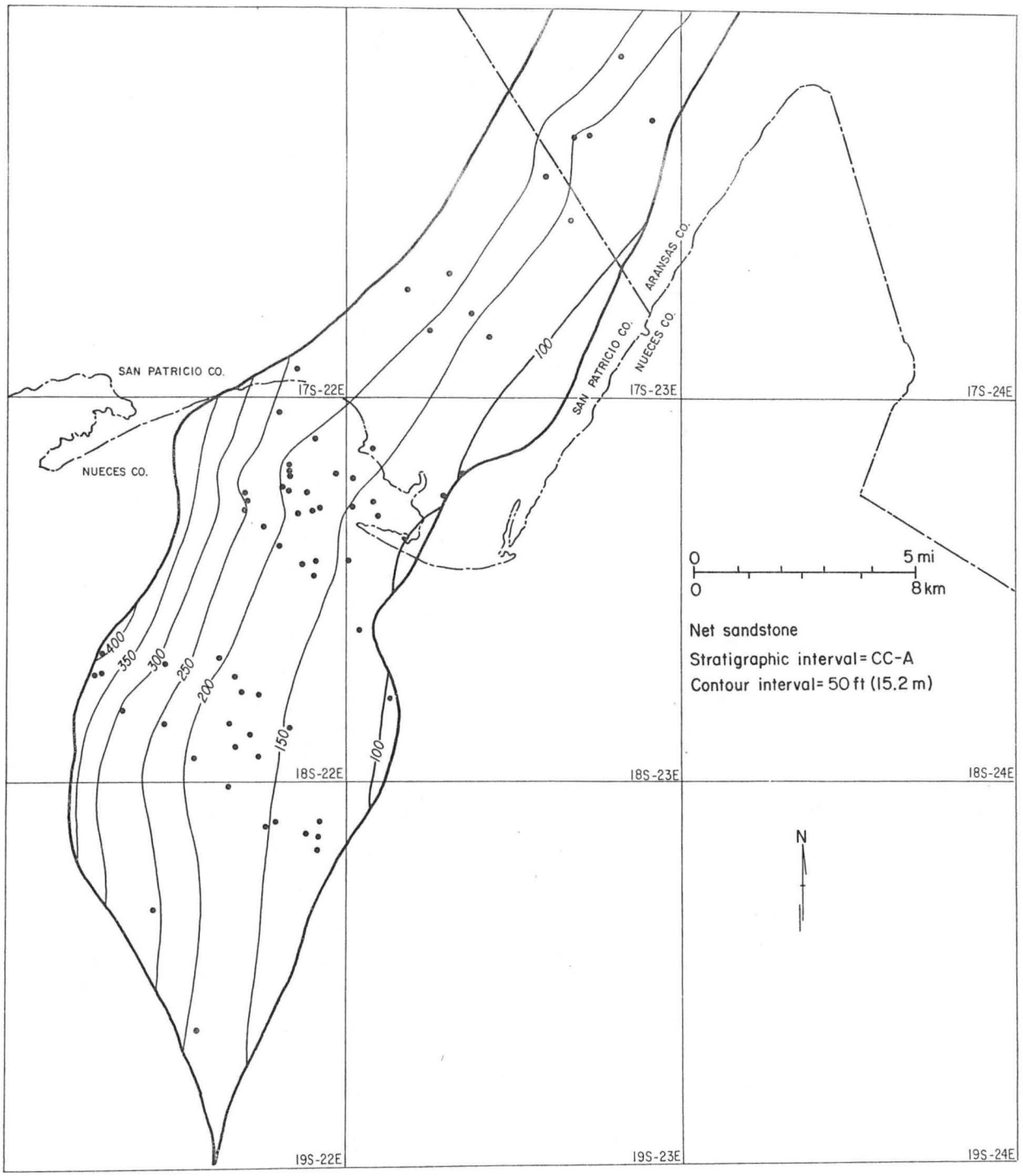

Figure 99. Net sandstone in unit CC-A, the uppermost stratigraphic unit in the Corpus Channel reservoir interval.

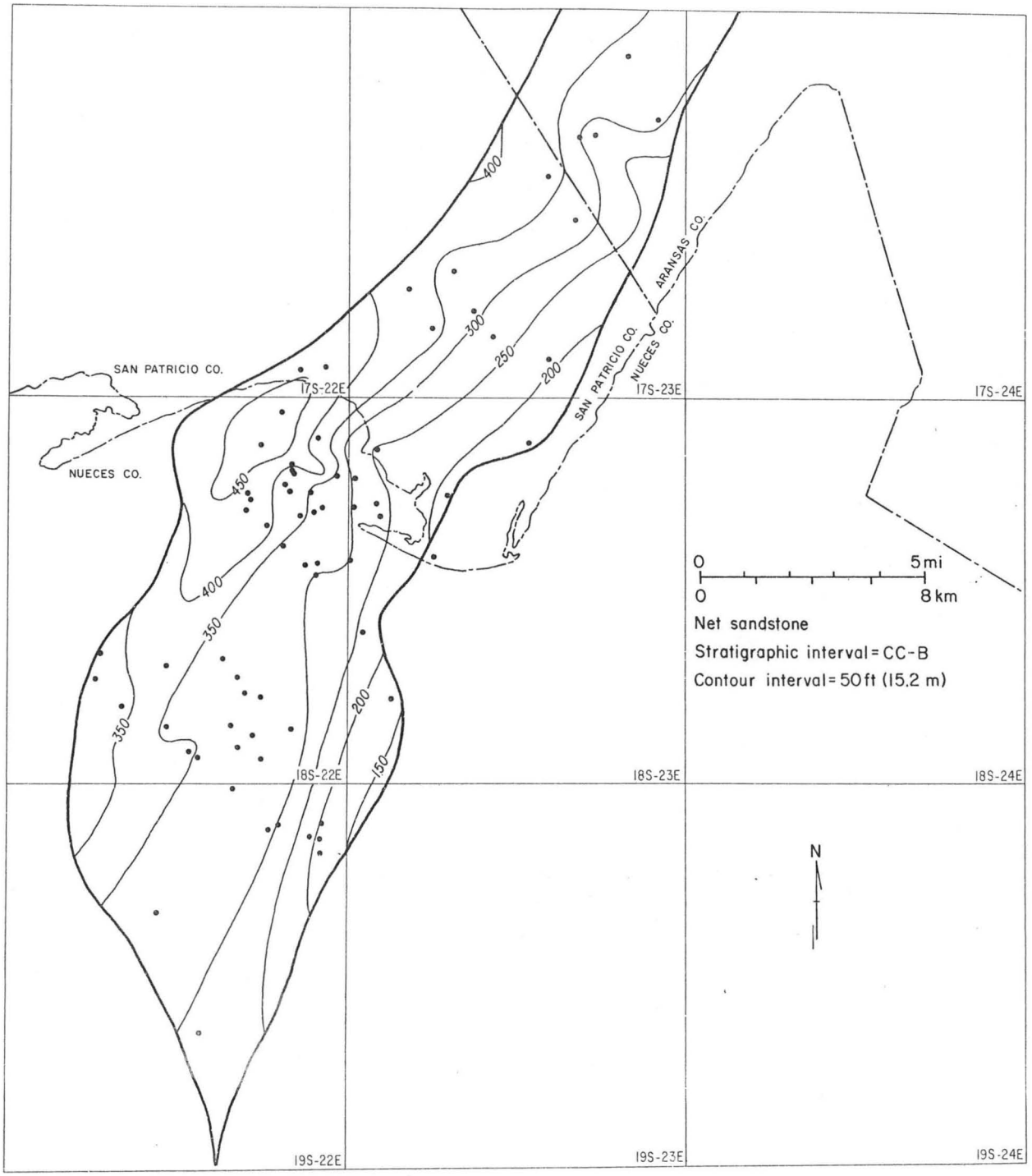

Figure 100. Net sandstone in unit CC-B, the second stratigraphic unit in the Corpus Channel reservoir interval.

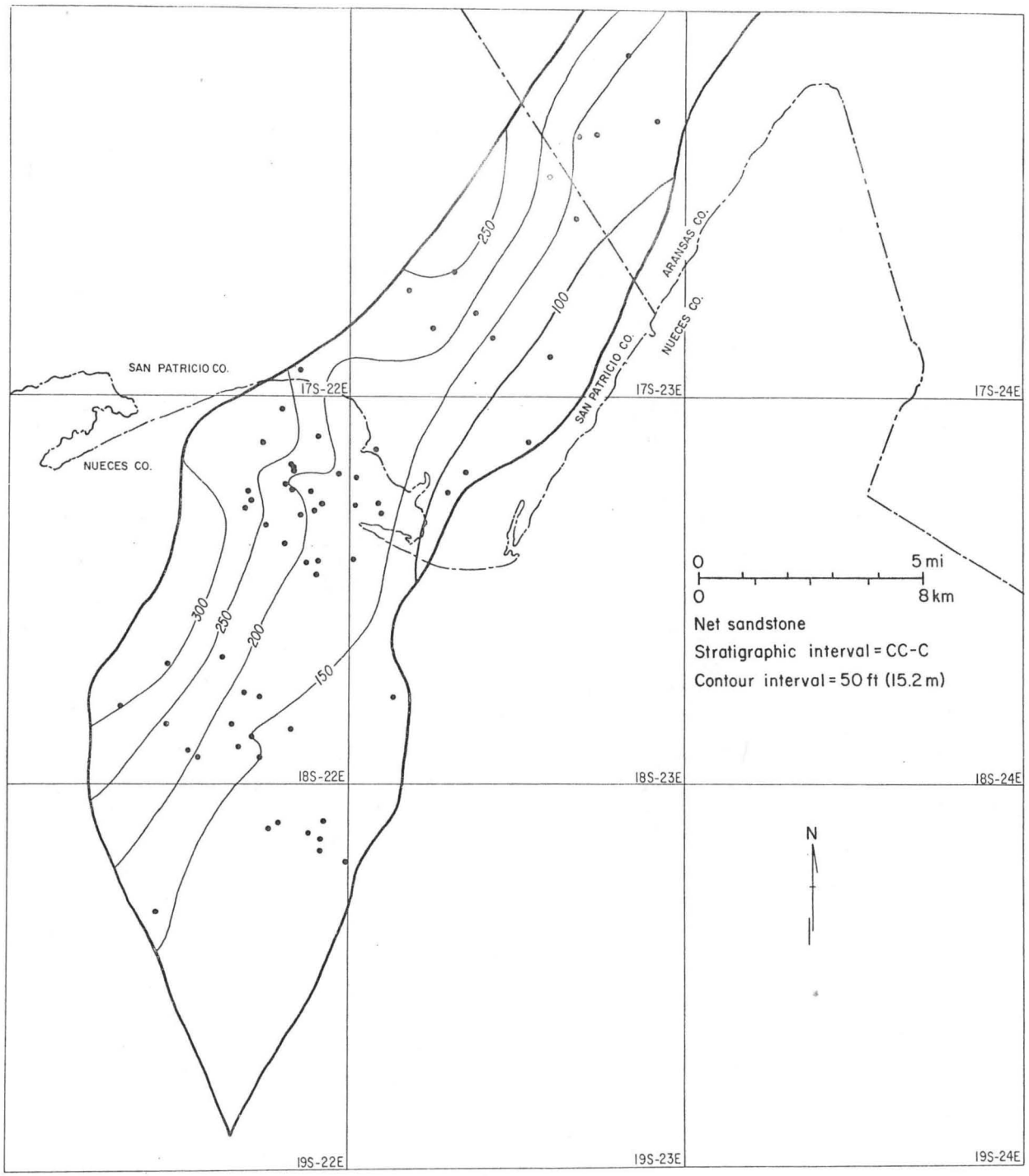

Figure 101. Net sandstone in unit CC-C, the third stratigraphic unit in the Corpus Channel reservoir interval.

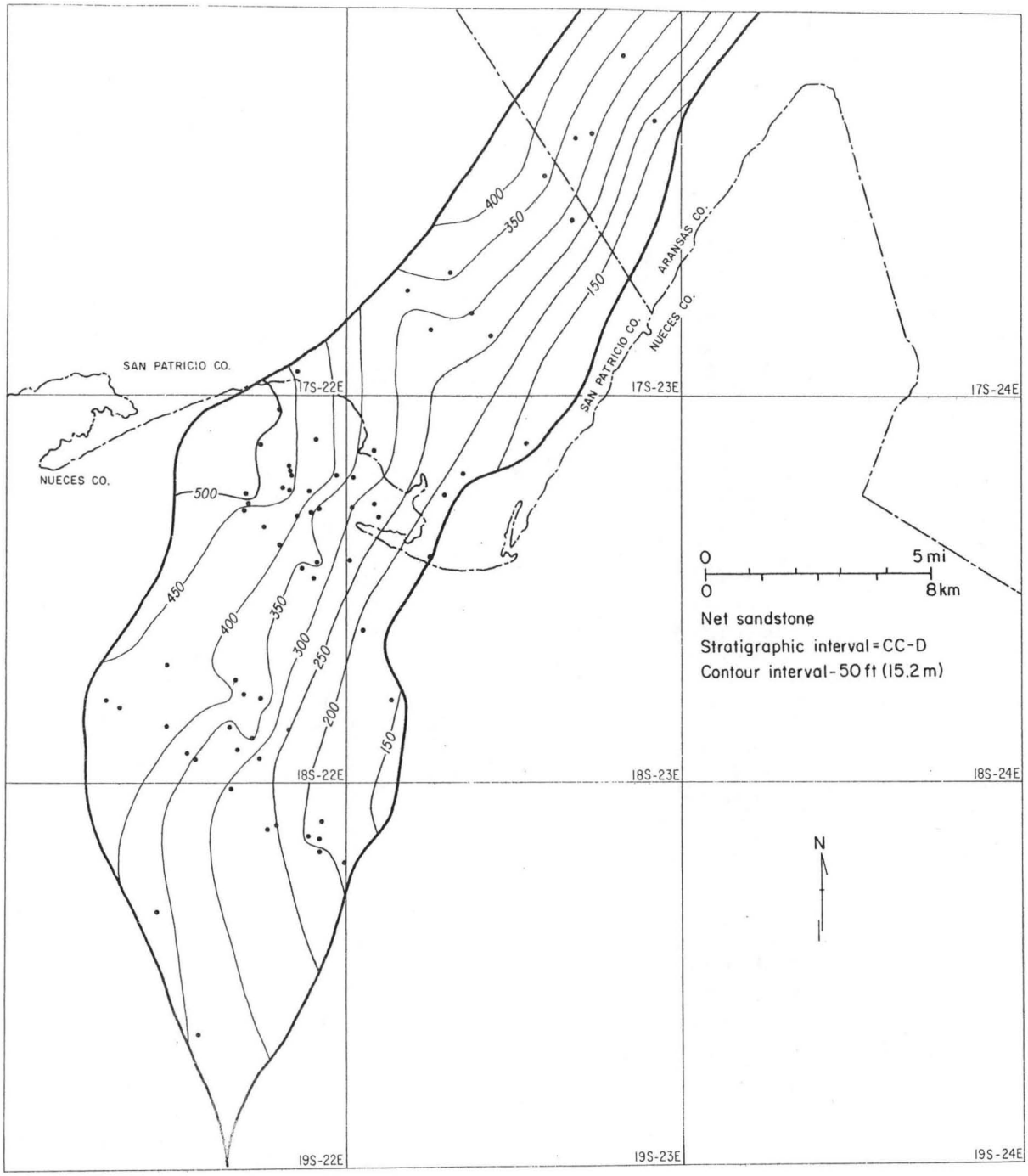

Figure 102. Net sandstone in unit CC-D, the fourth and deepest stratigraphic unit in the Corpus Channel reservoir interval.

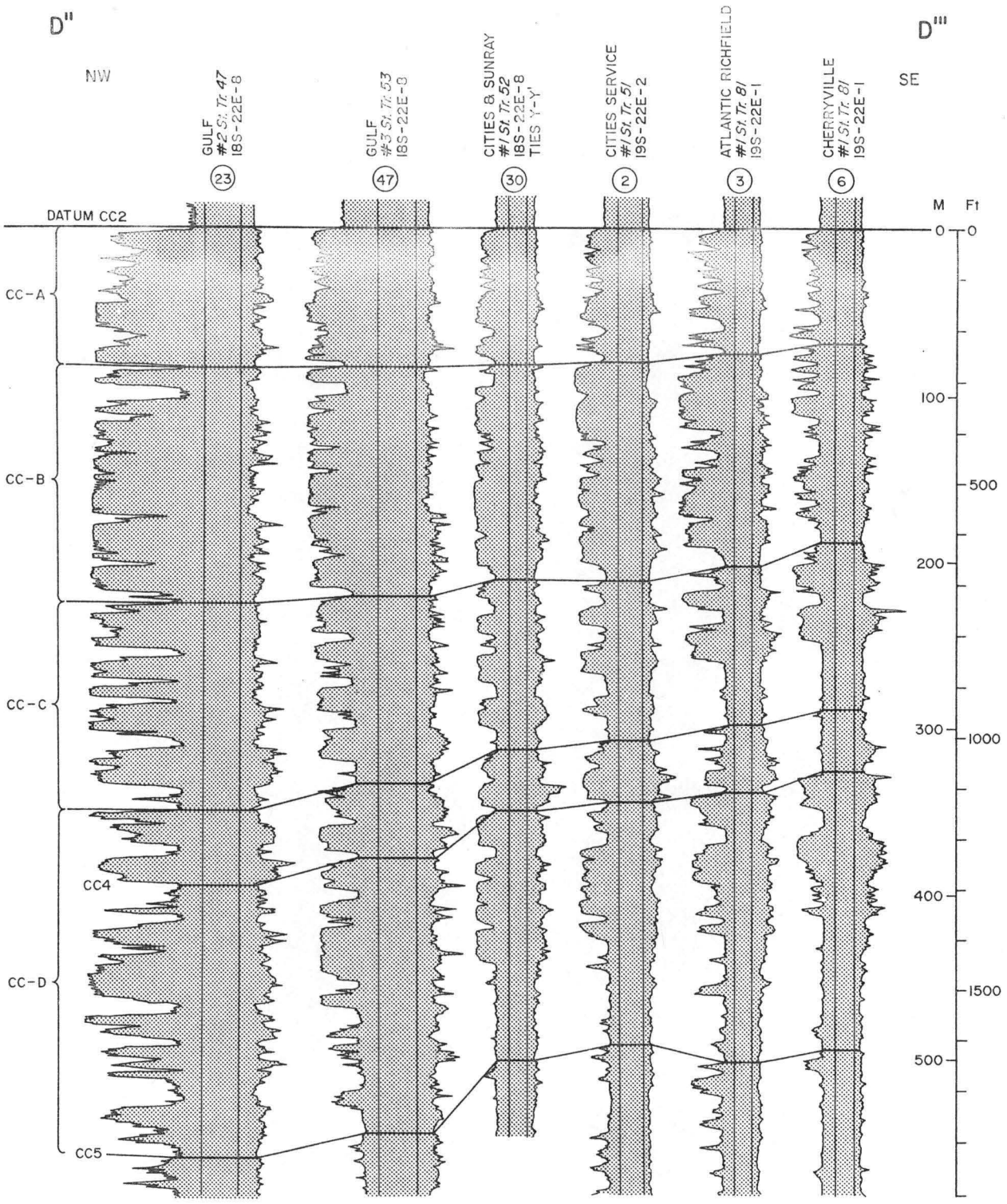

Figure 103. Stratigraphic dip section D''-D''' through the reservoir interval (CC2 to CC5) in the Corpus Channel Prospect Area. Note the downdip decrease in sandstone content and the pinching out of individual sandstone units.

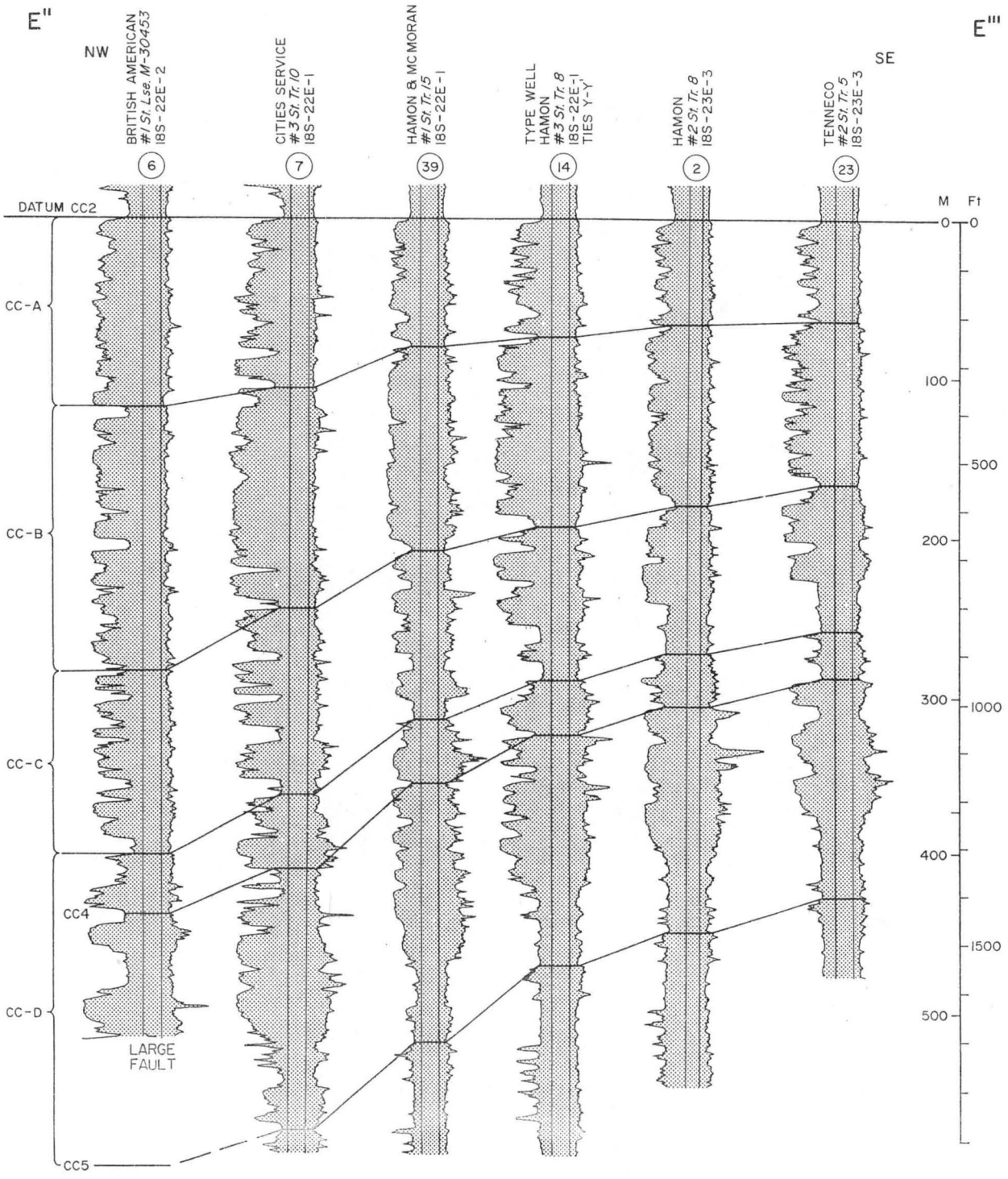

Figure 104. Stratigraphic dip section E''-E''' through the reservoir interval (CC2 to CC5) in the Corpus Channel Prospect Area. Note the downdip thinning of the entire unit, as well as the decrease in sandstone content.

associated with a wave-dominated delta. However, the lack of cores does not allow further substantiation of this interpretation. As in the Nueces Bay Prospect, each shale-to-sandstone upward-coarsening sequence probably represents a regression of the sea and a progradation of the coastline. The numerous cycles in the reservoir interval indicate that the coastline fluctuated across this area many times. Seaward progradations generally deposited 50 to 150 ft of sediment.

Formation fluid pressures and temperatures

The thickness of the B Zone in the Corpus Channel Prospect Area is 1,950 ft, as determined from the plot of bottom-hole shut-in pressure versus depth for 28 wells in Nueces and San Patricio Counties (fig. 105). The top of the B Zone that is indicated at a depth of 8,400 ft by BHSIP data is 400 ft higher in the section than the top of the B Zone that is indicated by the plot of equilibrium temperature versus depth (fig. 106). A 400-ft difference was also observed in the Nueces Bay Prospect Area discussed earlier. The geothermal gradient is 1.49° F/100 ft in the A Zone and increases to 2.2° F/100 ft in the B and C Zones.

The top of the B Zone deepens northeastward along strike section Y"-Y''' (figs. 93 and 107) from a depth of 7,900 ft at well No. 30 (18S-22E-8) to 8,450 ft at well No. 1 (18S-23E-3). The 300° F isotherm (base of the C Zone) also deepens northeastward along the section from depths of 12,800 ft to 14,000 ft. Equilibrium temperatures at the top and base of the B Zone average 198° and 234° F, respectively (fig. 107).

Along dip section E"-E''' (figs. 93 and 108), the top of the B Zone rises downdip from a depth of 8,250 ft at well No. 6 (18S-22E-2) to 7,050 ft at well No. 39 (18S-22E-1), then drops to an 8,050-ft depth at well No. 23. Formation equilibrium temperatures along the section average 193° and 229° F at the top and base of the B Zone, respectively.

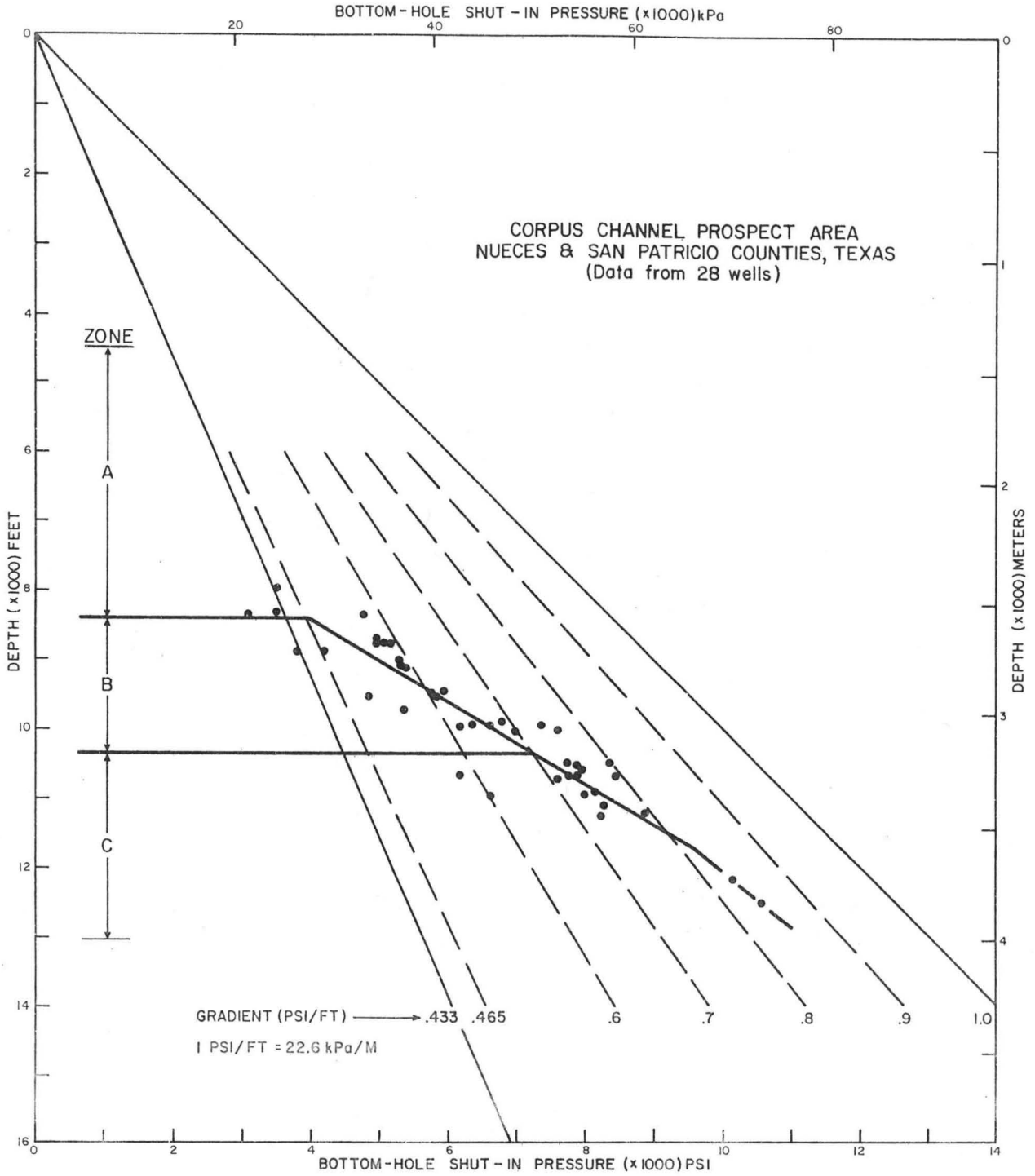

Figure 105. Bottom-hole shut-in pressures from drill-stem tests for production wells in the Corpus Channel Prospect Area, Nueces and San Patricio Counties, Texas.

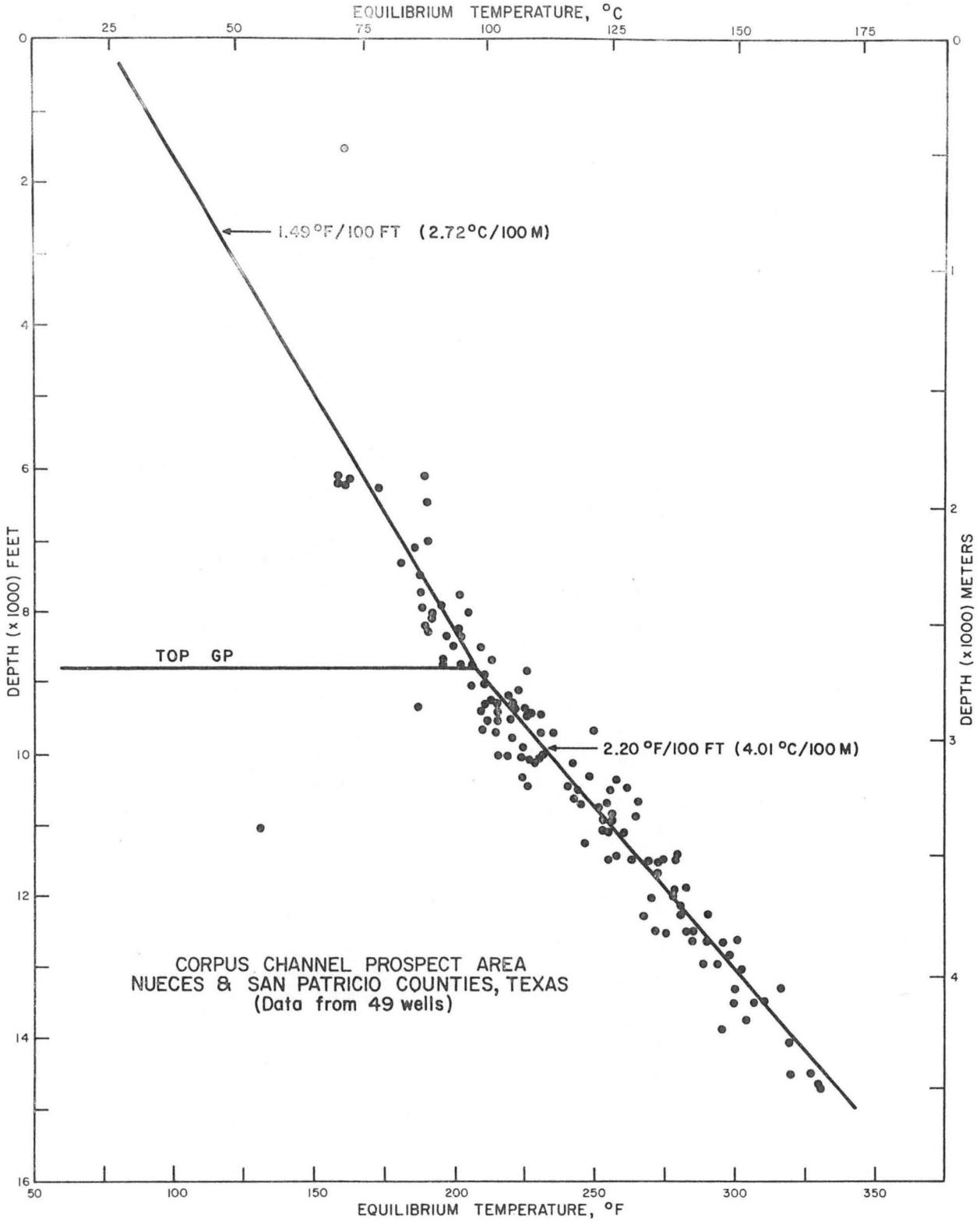

Figure 106. Geothermal gradients based on well log temperatures corrected to equilibrium values for 49 wells, Corpus Channel Prospect Area, Nueces and San Patricio Counties, Texas.

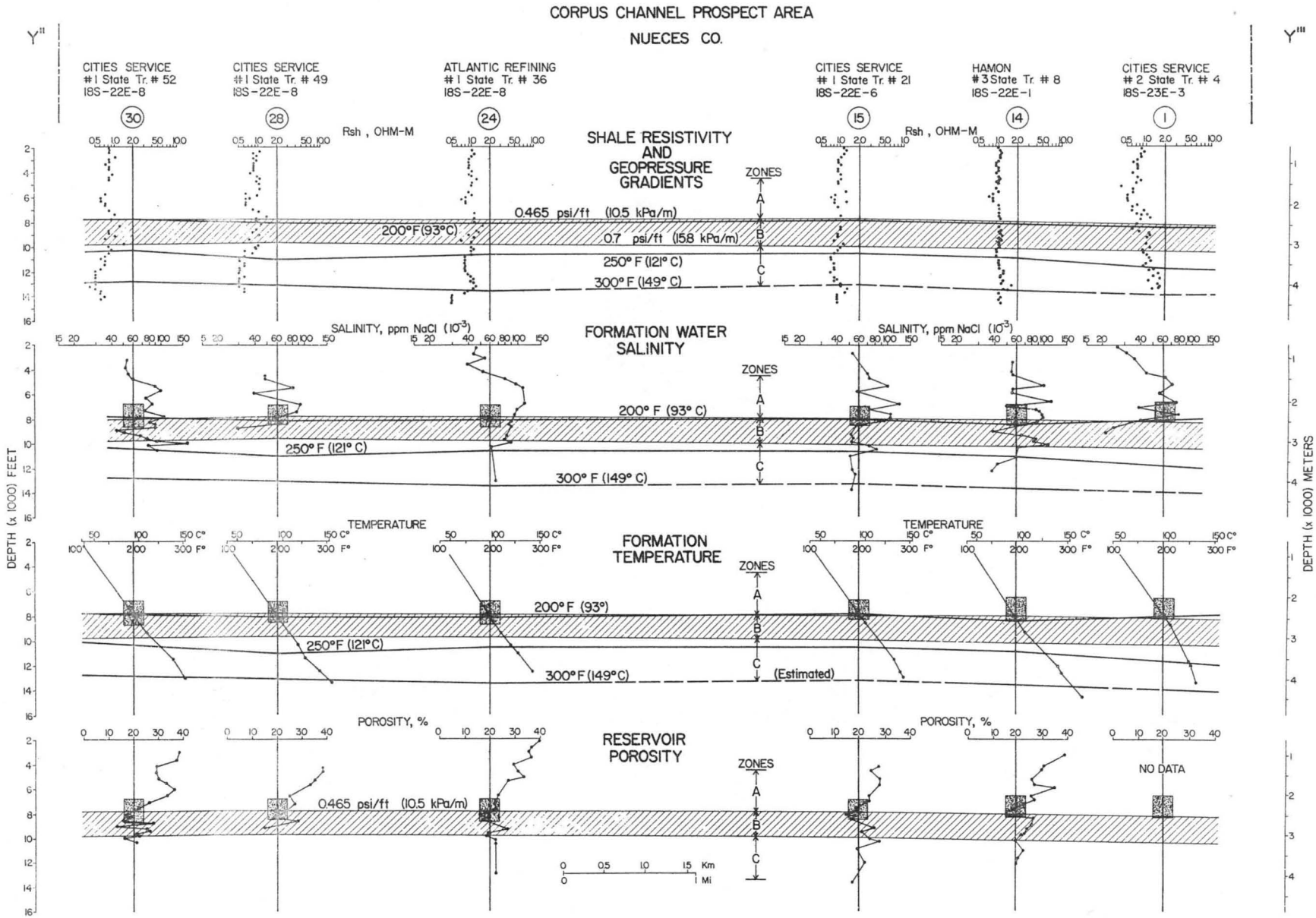

Figure 107. Parameter plots for wells along strike section Y''-Y''', Corpus Channel Prospect Area, Nueces County, Texas. The reservoir interval is indicated by the stippled columns.

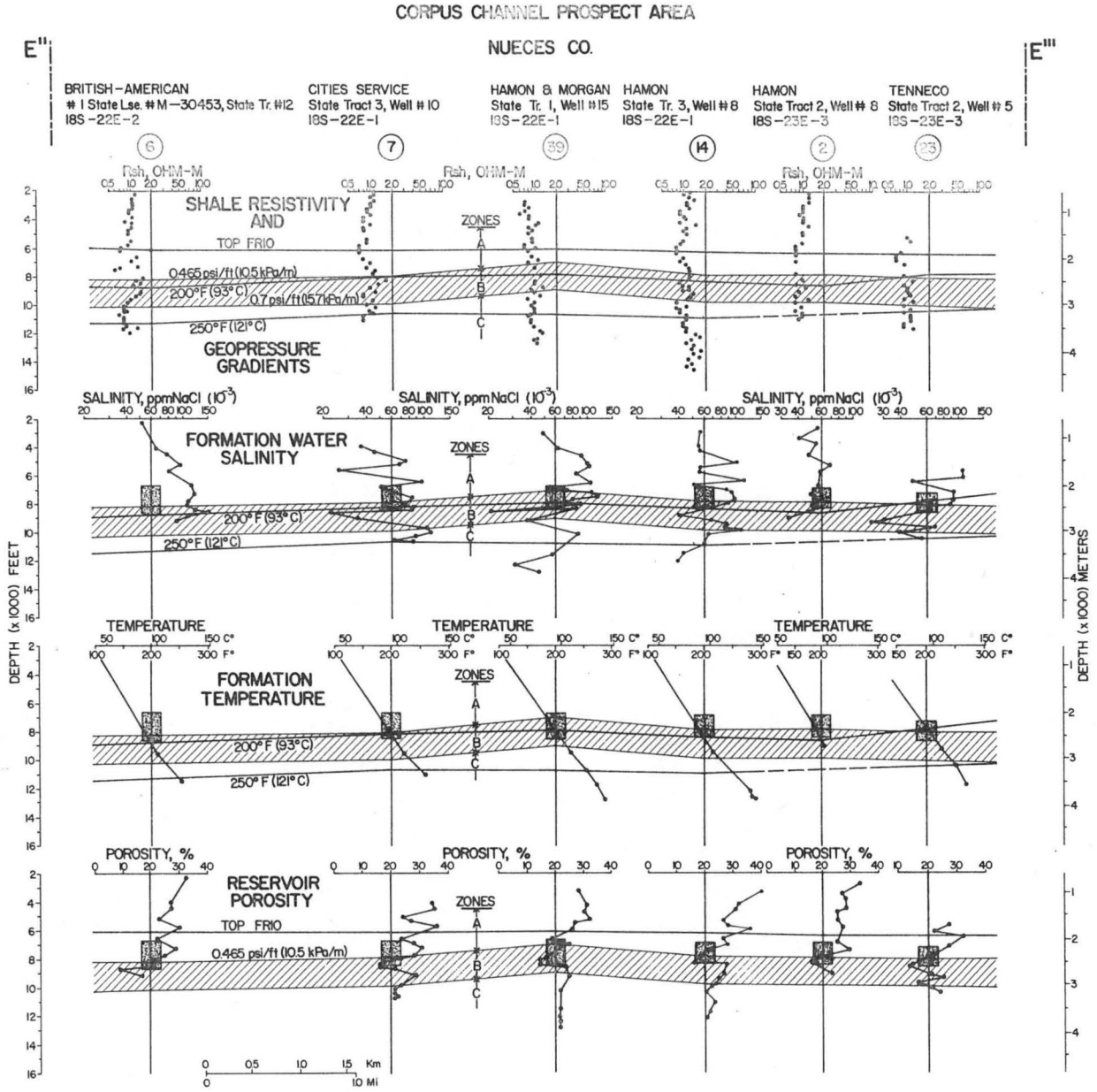

Figure 108. Parameter plots for wells along dip section E''-E''', Corpus Channel Prospect Area, Nueces County, Texas. The reservoir interval is indicated by the stippled columns.

On dip section D"-D''' (figs. 93 and 109) the top of the B Zone shows a configuration similar to that along dip section E"-E''', rising downdip from a depth of 8,350 ft at well No. 23 (18S-22E-8) to 7,650 ft at well No. 2 (19S-22E-1), then falling to a depth of 8,450 ft at well No. 6 (19S-22E-1). Formation equilibrium temperatures along the section average 203° and 241° F at the top and base of the B Zone, respectively.

Formation water salinity

Salinities from an area including Nueces, Aransas, and San Patricio Counties (fig. 88) show trends that are similar to generalized trends for the Texas Gulf Coast area (fig. 14). At the top and base of the B Zone, salinities average 79,500 and 95,000 ppm NaCl along strike section Y"-Y''' (fig. 107), 91,000 and 68,000 ppm NaCl along dip section E"-E''' (fig. 108), and 98,000 and 65,000 ppm NaCl along dip section D"-D''' (fig. 109).

Porosity and permeability

The relation between porosity and permeability is linear on a semilog plot (fig. 90) of whole-core data from nine wells located in Corpus Christi Fairway, Nueces County, Texas. Limited whole-core porosity data from the Corpus Channel Prospect Area (fig. 110) show that porosities lie between 19 and 29 percent in the depth interval from 5,900 to 10,800 ft. Porosities calculated from induction and SP logs average between 18 and 23 percent within the B Zone in the prospect area. Whole-core air permeabilities vary from less than 2 md to more than 1,000 md in the depth interval from 7,400 to 9,100 ft (fig. 91). Very limited core permeability data at depths between 10,400 and 10,900 ft indicate maximum values of about 50 md.

Corpus Channel test-well site

The proposed test-well site is located in the central part of the Corpus Channel Prospect Area in the center of Corpus Christi Bay

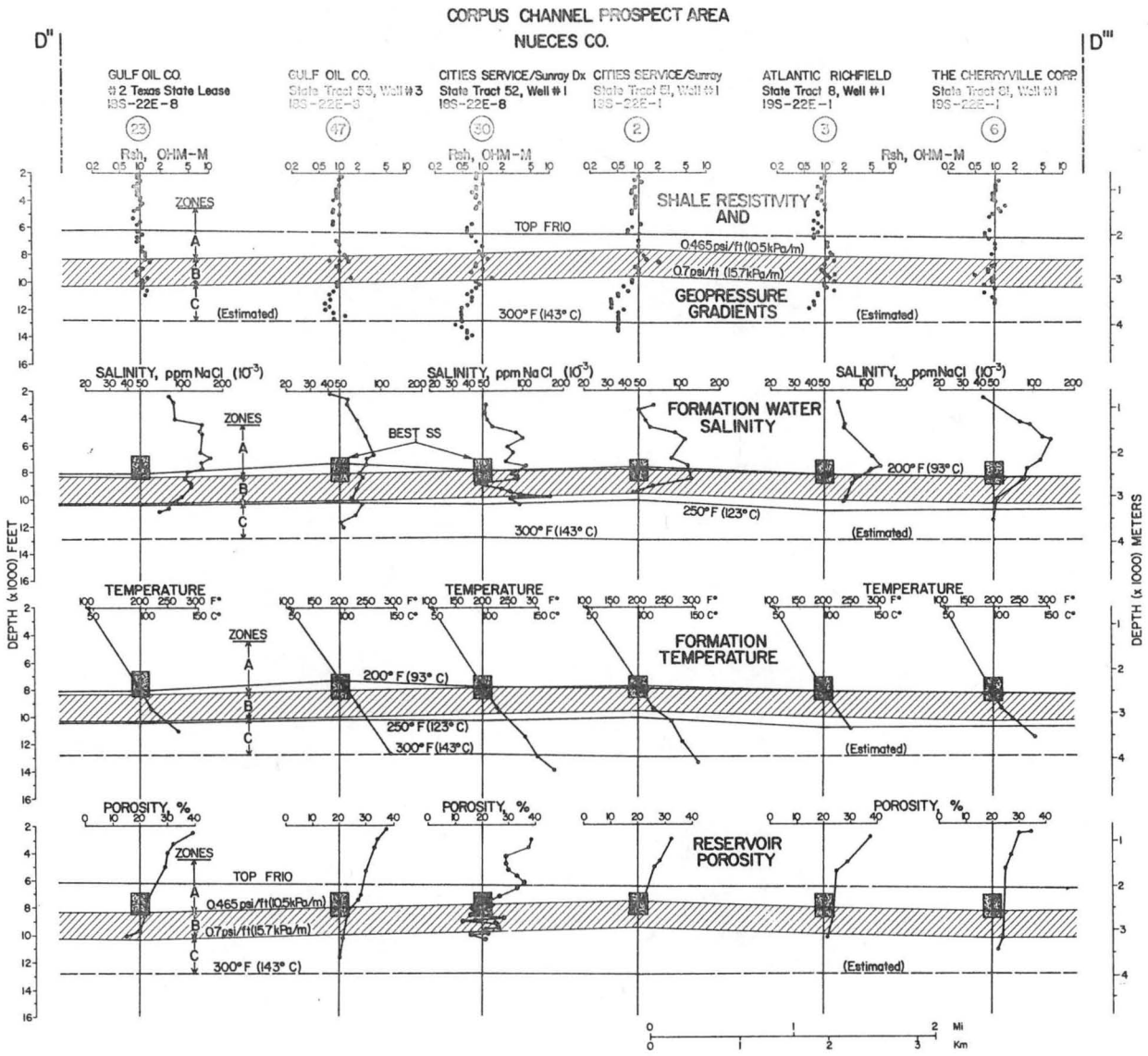

Figure 109. Parameter plots for wells along dip section D''-D''', Corpus Channel Prospect Area, Nueces County, Texas. The reservoir interval is indicated by the stippled columns.

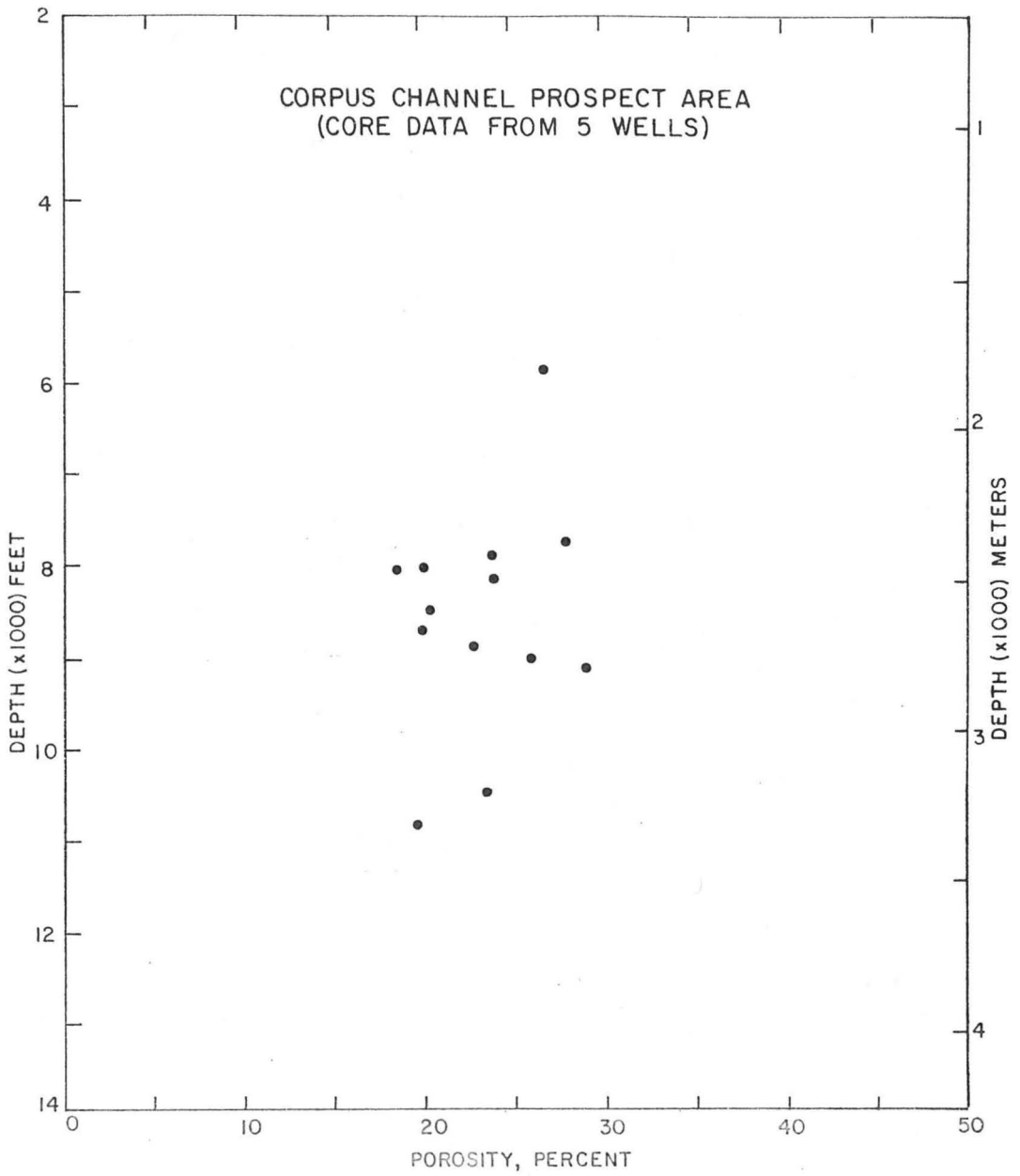

Figure 110. Whole-core porosity versus depth for five wells, Corpus Channel Prospect Area.

(figs. 66 and 96). The site is 1 mi east of a possible fault through part of the reservoir interval (figs. 96 and 97) and is 2.3 mi west of the eastern margin of the prospect. The site is 2.5 mi south of the type well, Hamon No. 3 State Tract 8.

Based on extrapolations from nearby wells, the anticipated depth to the top of the Frio at the test site is 6,425 ft; the depth to the top of the reservoir is 6,805 ft, the thickness of the reservoir interval is 1,680 ft; and the amount of sandstone present is 1,080 ft. Individual sandstone units are several tens to hundreds of feet thick. These reservoir sandstones lie in the deep A Zone and uppermost B Zone. Approximately 300 ft of sandstone occurs between markers CC1 and CC2 above the main reservoir interval, and approximately 200 ft of sandstones occur below, between markers CC5 and CC7 in the B Zone. These sandstones above and below the main interval are also potential reservoirs.

The test-well site has a thick sandstone column and is located in an area of little structural complexity at the level of the reservoir interval. This suggests that individual reservoir sandstones will have great lateral continuity.

In the type well (fig. 111), methane solubility in the A Zone varies from 14 to 18 SCF/B, generally increasing with depth. In the B Zone, methane solubility is more variable, ranging from 17 to 24 SCF/B using the "curve" method for determining R_{mf} required for salinity calculations. Methane solubility increases with depth from 21 to 47 SCF/B in the C Zone. Sandstones in the C Zone, however, are probably too thin to be prospective. In individual prospective sandstones in the depth interval from 7,265 to 7,970 ft, calculated methane solubility is between 15.5 and 17.7 SCF/B (table 2).

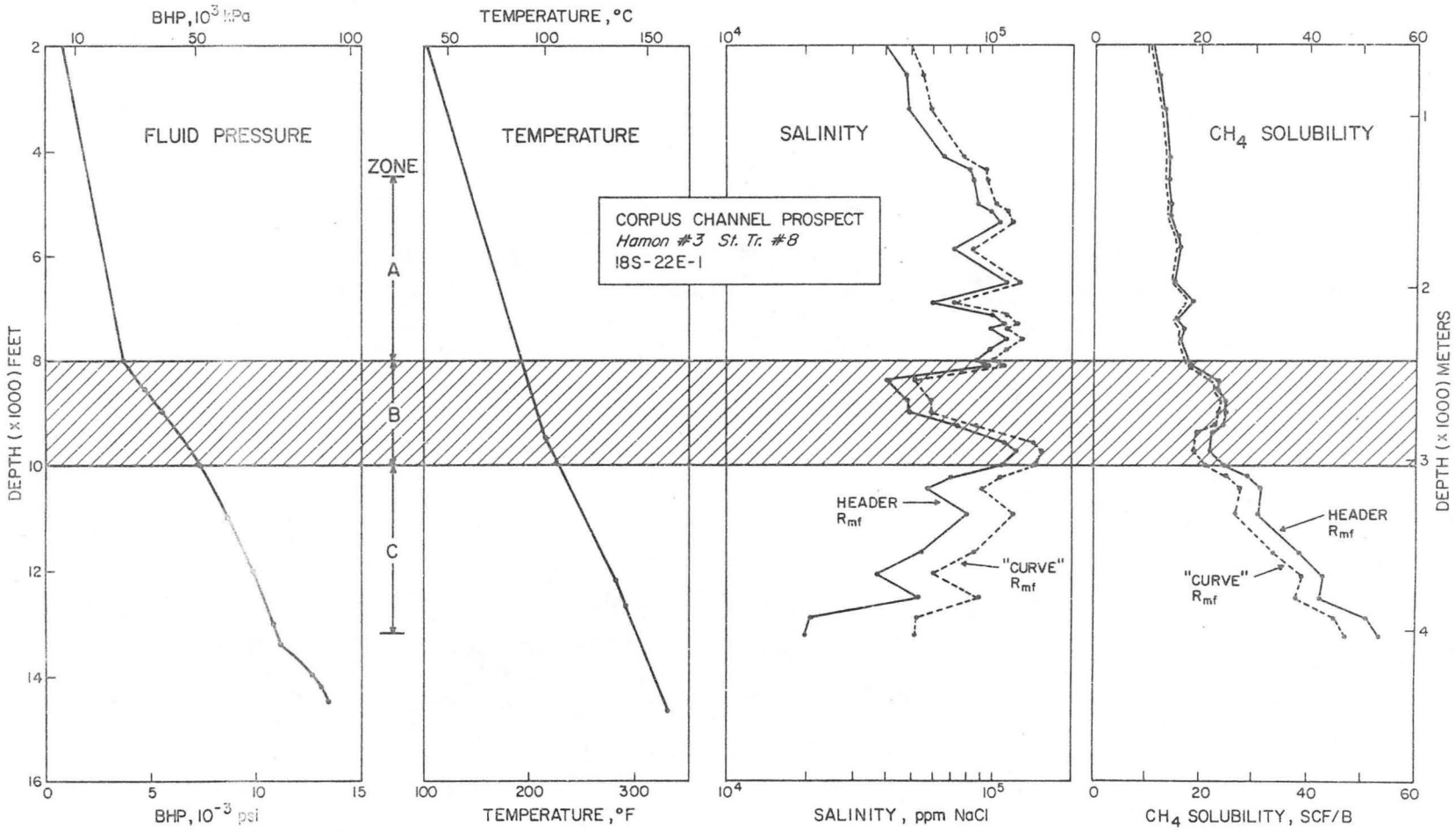

Figure 111. Parameter profiles for Hamon No. 3 State Tract 8 (18S-22E-1), type well in Corpus Channel Prospect Area, Nueces County, Texas.

Kenedy Fairway

The Kenedy Fairway is located principally in Kenedy County and extends north into Kleberg County, west into Brooks County, and southwest into Hidalgo County (fig. 29). The fairway is 54 mi long north to south and 48 mi wide east to west, covering an area of 2,027 mi^2. The Kenedy area was selected as a shallow geopressured fairway primarily on the basis of the high sandstone content of the B and C Zones of the Oligocene Frio Formation (figs. 26 and 27).

For detailed study of the Kenedy Fairway, nine structural dip sections and four stratigraphic strike sections were constructed. Structural and stratigraphic analyses were based primarily on the correlation of low resistivity shales and high SP sandstone units traceable within certain areas. Due to sparse well data in some areas and abrupt facies variations within the Kenedy Fairway, different sets of correlation markers were used for each of the two prospect areas; markers S1 to S8 were used in the Sarita area and Cn1 to Cn10 in the Candelaria area (fig. 112). The S1 marker in the Sarita area and the Cn1 marker in the Candelaria area occur at or near the top of the Heterostegina-Marginulina zone, the approximate top of the Frio as defined by Bebout and others (1975b). Thus, the two markers may be considered stratigraphic equivalents. It should be noted, however, that in the area of the Kenedy Fairway, the Heterostegina-Marginulina zone has been considered by some geologists as occurring within the Anahuac Formation.

The Kenedy Fairway is located in an extensively growth-faulted area of the Frio trend. The faults trend northeast-southwest parallel to regional strike, and vertical displacements of most down-to-the-basin faults range from tens to several hundreds of feet, with the largest faults in the

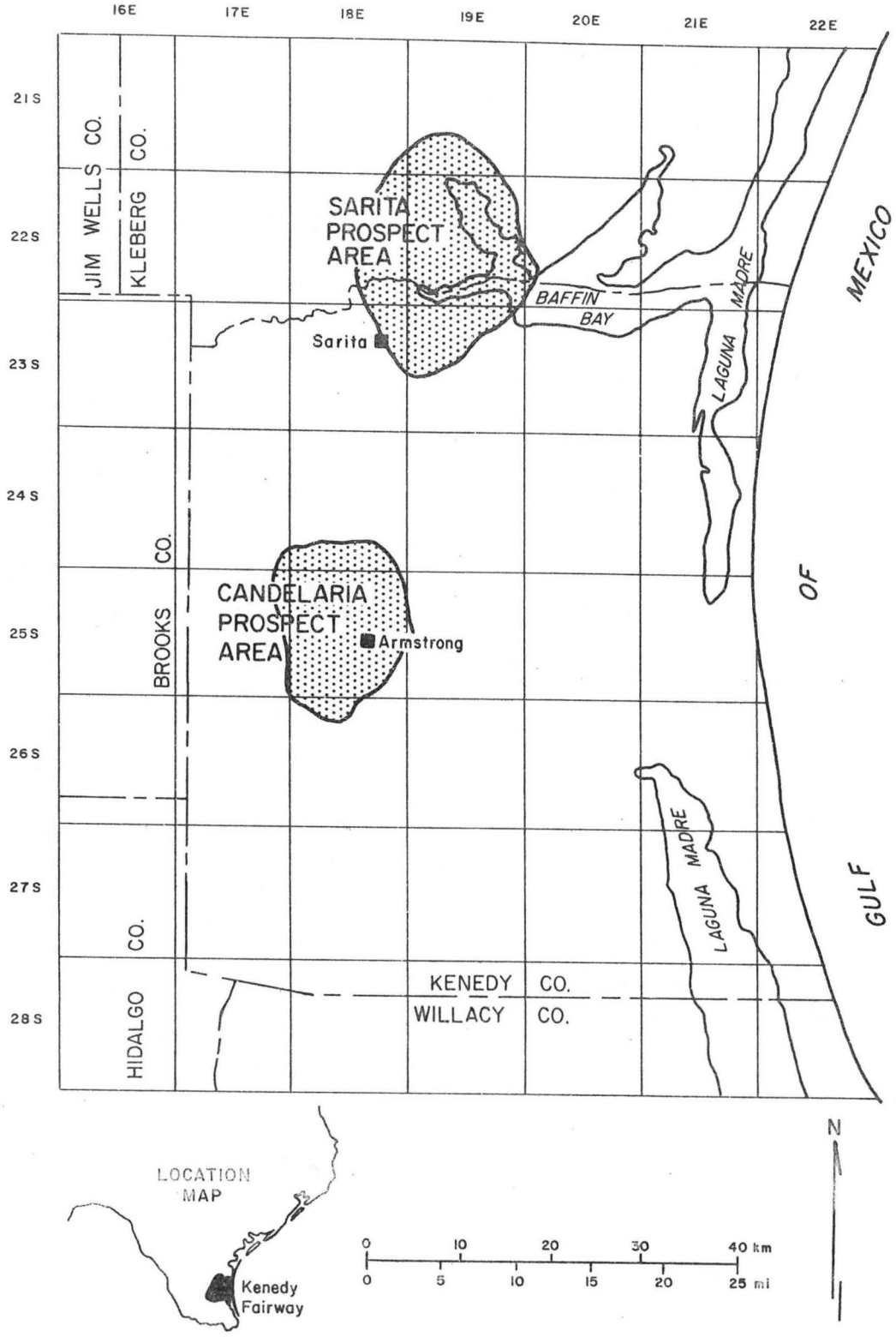

Figure 112. Location of prospect areas, Kenedy Fairway.

fairway showing displacements of thousands of feet. Numerous antithetic faults accompany many of the down-to-the-basin faults and exhibit vertical displacements of tens to hundreds of feet. Sandstone and shale sections expand downdip across the growth faults and thicken up regional dip into the faults.

Several structural blocks formed by these growth faults were selected for detailed study within the Sarita and Candelaria Prospect Areas. These areas occur along strike in the same Frio fault zone. Prospect selection was done on the basis of sandstone distribution, shown by the regional cross sections constructed for the DOE-funded methane assessment (Gregory and others, 1980) and numerous well logs. However, parts of the Kenedy Fairway were eliminated from further study because of sparse well control.

Sarita Prospect Area

The Sarita Prospect Area is located in the vicinity of Baffin Bay in the northern part of the Kenedy Fairway (fig. 112). The area covers approximately 135 mi^2 and includes several fault blocks along the Frio growth fault trend. Detailed study of the prospect area was based on electric logs from 167 wells (fig. 113; appendix C) that penetrate the shallow geopressured zone. Structural dip and stratigraphic strike cross sections constructed through the Sarita Prospect Area (figs. 114 through 118) illustrate growth and antithetic faults, and correlations of the Frio Formation within the area. Thickening of some deeper intervals (especially those below S6) on the downthrown sides of growth faults is illustrated by cross section H-H' (fig. 116). Within the Sarita area, the A-B Zone boundary occurs at depths ranging from 8,750 to 10,500 ft, and the B-C boundary occurs at depths between 9,850 and 11,800 ft.

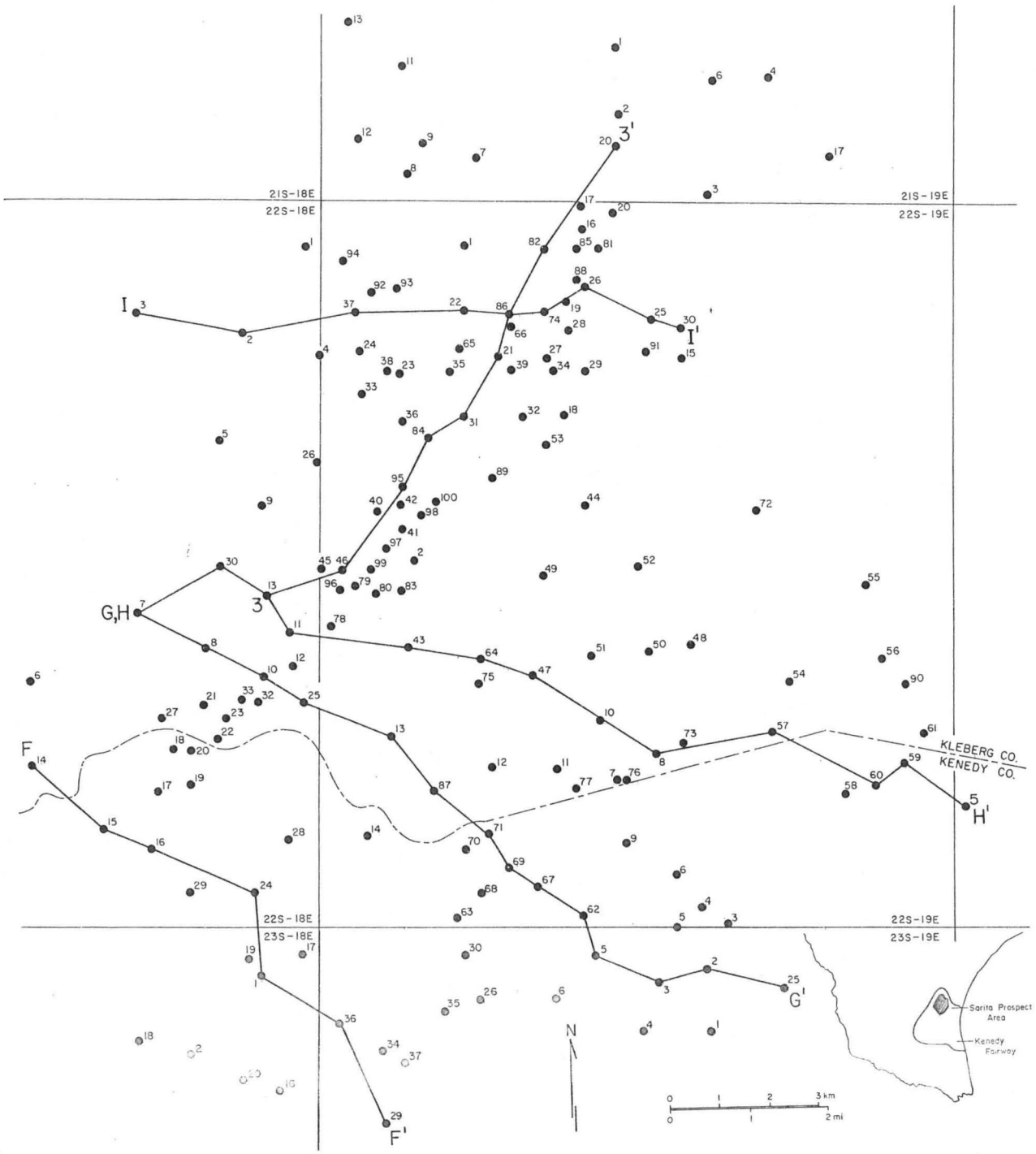

Figure 113. Location of wells and lines of cross section, Sarita Prospect Area.

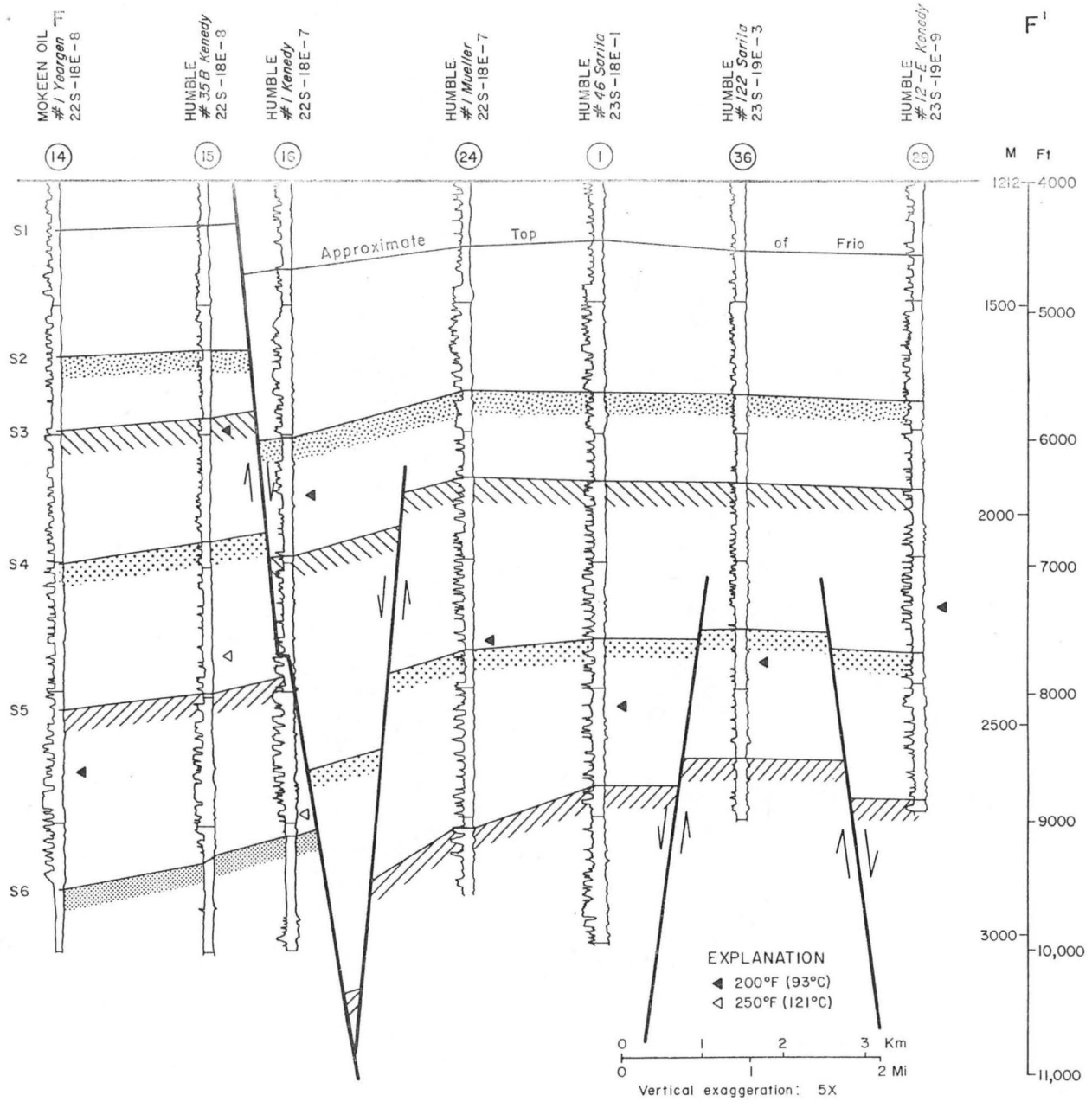

Figure 114. Structural dip section F-F', Sarita Prospect Area.

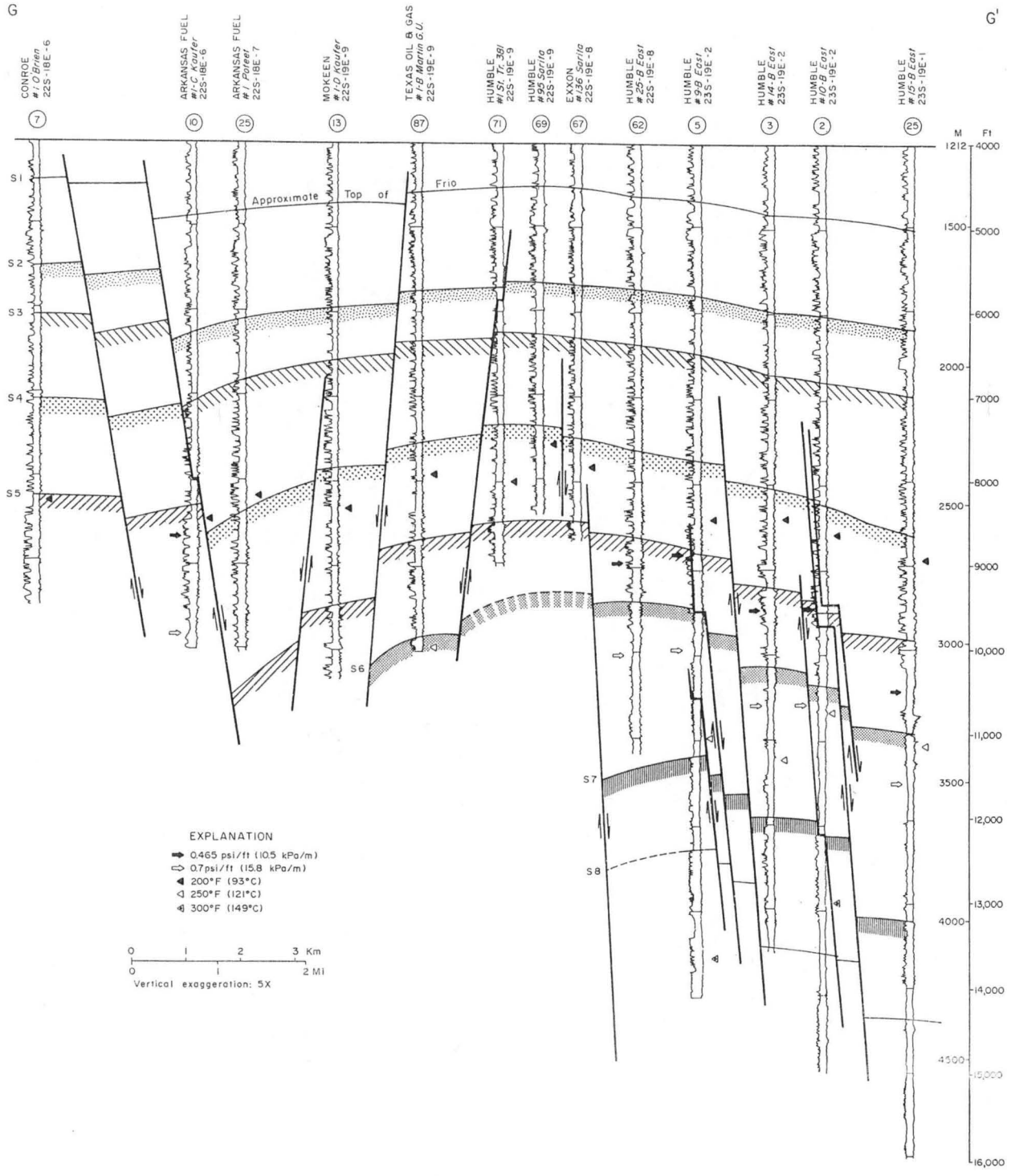

Figure 115. Structural dip section G-G', Sarita Prospect Area.

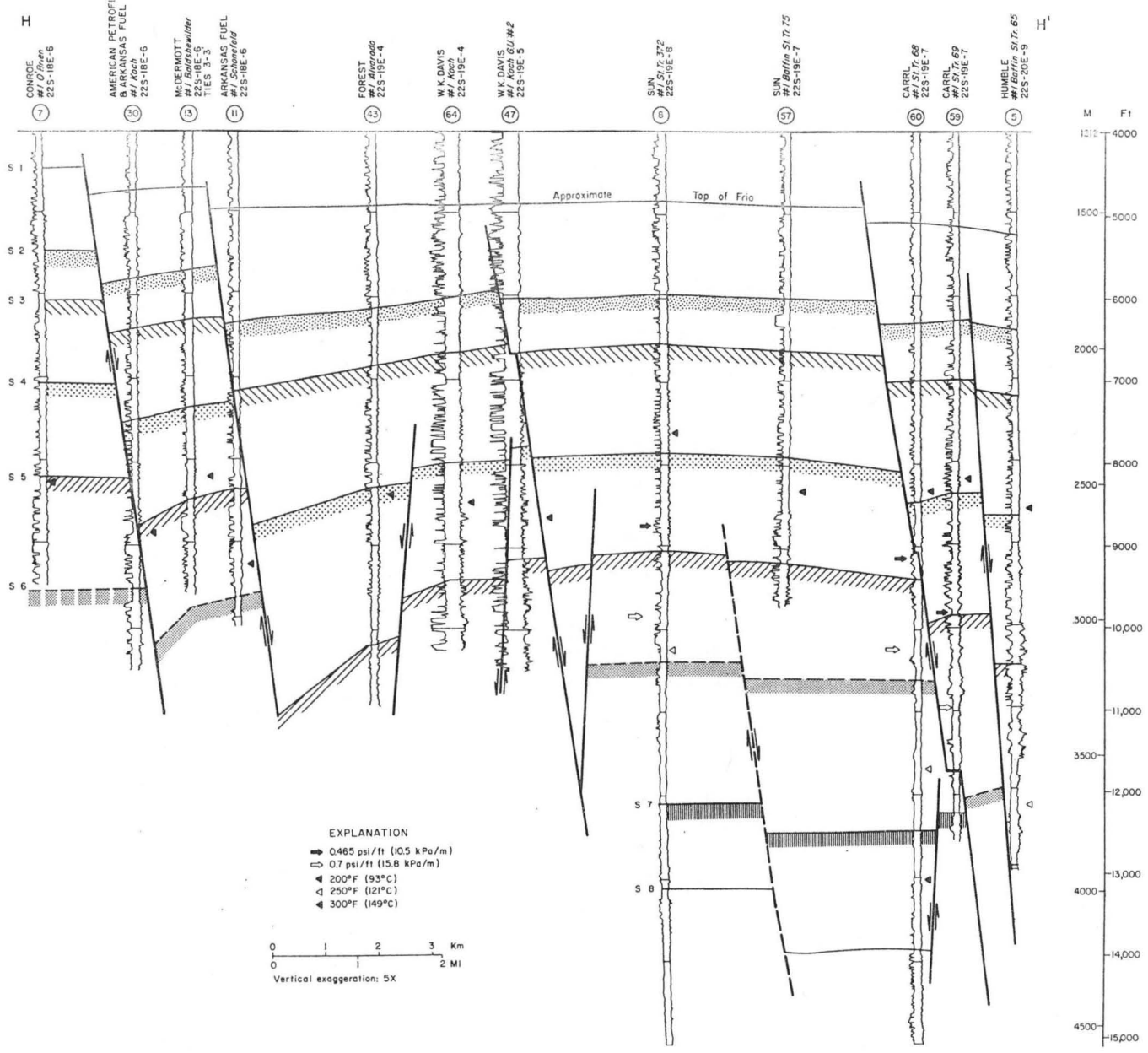

Figure 116. Structural dip section H-H', Sarita Prospect Area.

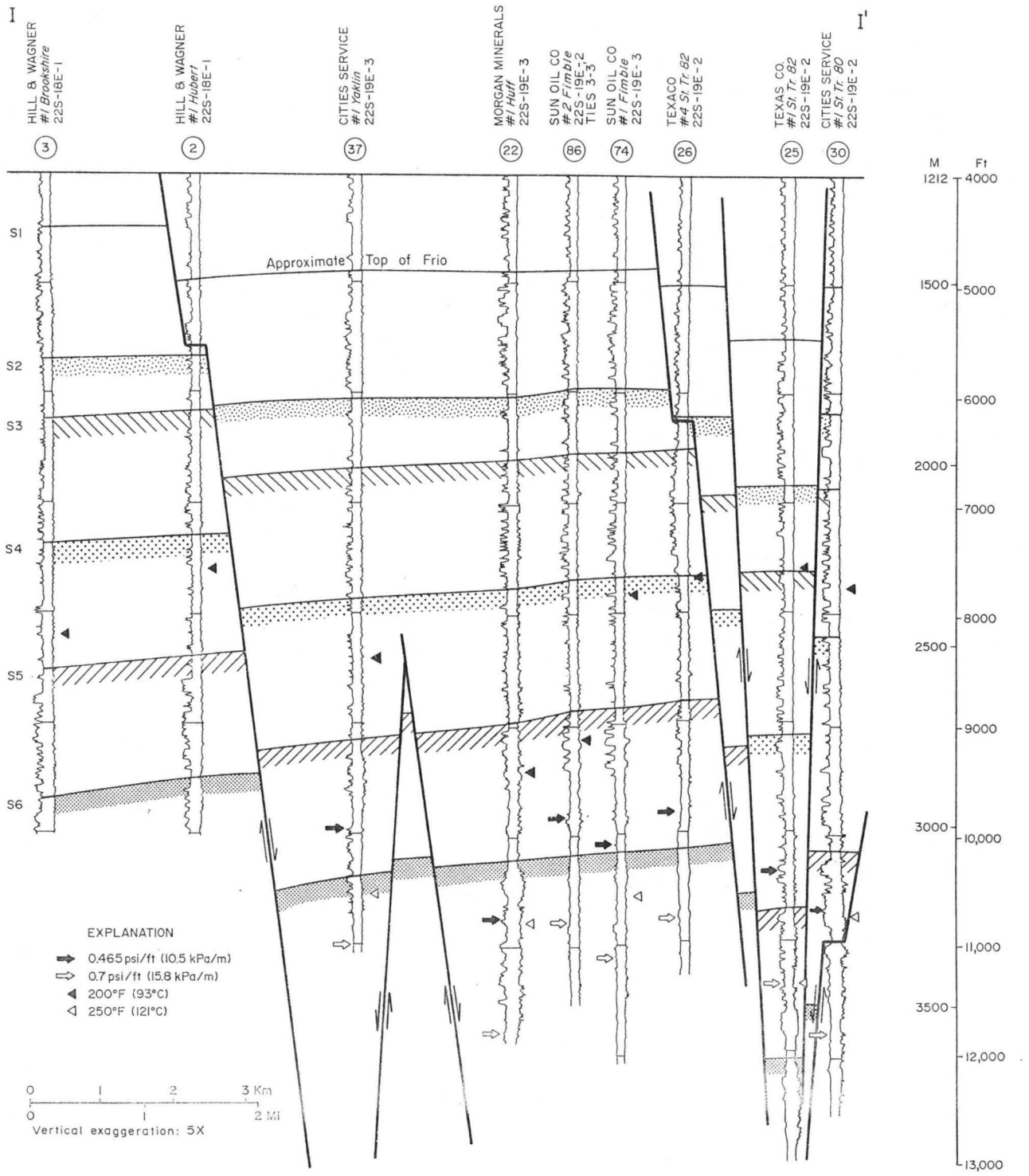

Figure 117. Structural dip section I-I', Sarita Prospect Area.

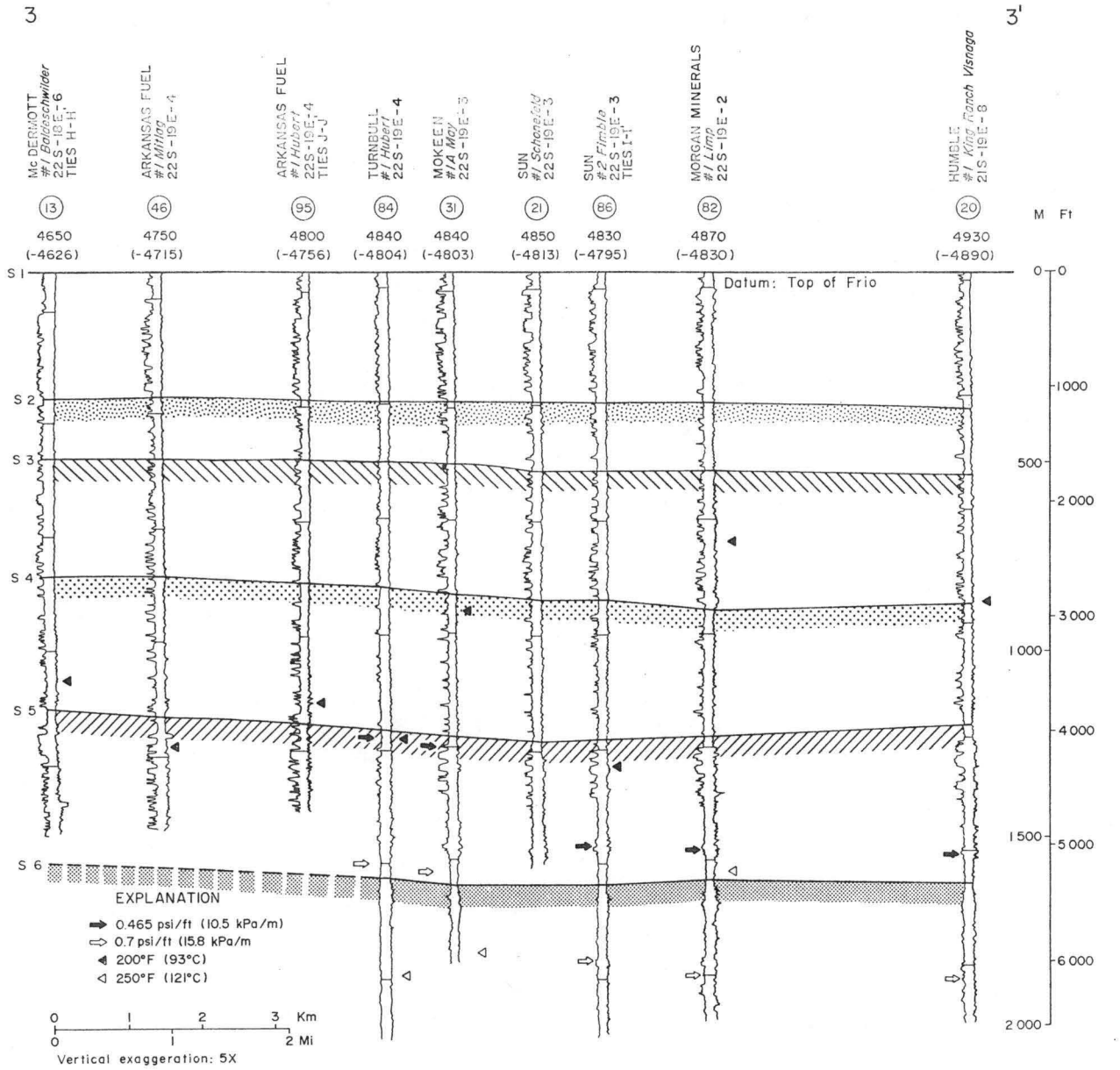

Figure 118. Stratigraphic strike section 3-3', Sarita Prospect Area.

Structure

The major structural feature of the Sarita area is a large, northeast-southwest-trending growth fault in the west-central part of the prospect area (fig. 119). Vertical displacement averages 1,500 ft at the S5 marker. The area downdip (southeast) of the fault is characterized by a number of smaller down-to-the-basin and antithetic faults with vertical displacements averaging 400 ft. These faults segment a large anticline that is part of the rollover associated with the major growth fault described above and, thus, segment the reservoir sandstones in that area (fig. 119). The fault farthest downdip was designated the eastern border of the Sarita Prospect Area.

Updip from the major fault, one antithetic and one down-to-the-basin fault have been interpreted at the S5 marker between the major fault and the westernmost fault that is the updip boundary of the prospect area. The relatively minor amount of faulting in this updip area allows reasonable continuity and lateral persistence of the prospective reservoir sandstones that occur within the B Zone (fig. 118).

Sandstone distribution and characteristics

The Frio Formation in the Sarita Prospect Area can be divided into three lithologically distinct parts: the lower part beneath the S5 marker, the middle part between the S3 and S5 markers, and the upper part from the S3 to the top of the Frio (fig. 115, well No. 3). The lower, geopressured section (S5 to lower limits of well control) is characterized by generally upward-coarsening sandstone and shale sequences several hundred feet thick, separated by equally thick shales. Galloway (in press) has interpreted the deep upward-coarsening sequences as progradational deltaic facies grading from prodelta shales into delta-front sandstones. Higher in the section,

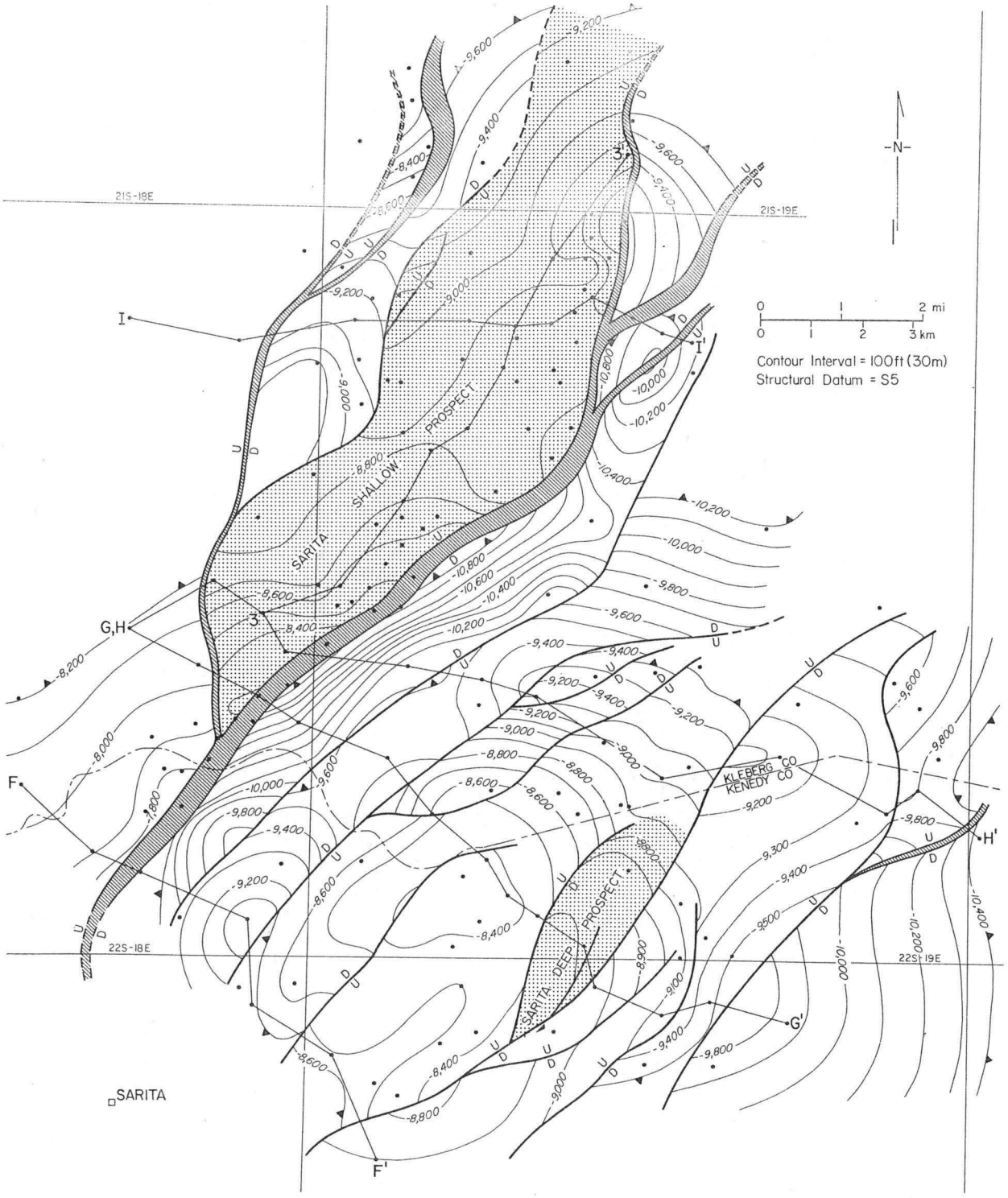

Figure 119. Structure on top of the S5 marker, Sarita Prospect Area, Kenedy Fairway.

near the S5 to S6 interval, the dominant upward-coarsening sequences are thinner, probably indicating rapid deposition in shallow water. The middle section (S3 to S5) lies within the hydropressured A Zone and consists mostly of shales and laterally discontinuous sandstones 10 to 90 ft thick showing blocky SP patterns on electric logs. Galloway (in press) has interpreted these deposits as dominantly aggradational delta-plain facies. A few sandstone units, however, show upward-coarsening cycles typical of progradational deltaic deposits. The upper part of the section (S3 to the top of the Frio) contains thick, dominantly upward-coarsening sandstones, probably delta-front sandstones, separated by relatively thin shales. These sandstone units are fairly persistent over the Sarita area. The occurrence of a section dominated by delta-front deposits overlying a section of dominantly delta-plain facies indicates an overall marine transgression from the middle to upper parts of the Frio.

The S1 marker occurs at depths ranging from 4,400 to 5,500 ft through the Sarita area and corresponds to the top of the Heterostegina-Marginulina zone, or the approximate top of the Frio (Bebout and others, 1975b). The interval S1 to S2, approximately 1,100 ft thick, averages 650 to 850 ft of net sandstone, and exhibits net-sandstone maxima of more than 800 ft on the downthrown side of the major growth fault (fig. 120). Correlation of the net-sandstone highs with the mapped structure illustrates structural control of sediment thicknesses at this interval as well as all deeper intervals. The sandstone bodies in this interval display some upward-coarsening sequences, and range from 30 to 160 ft thick, thinning slightly gulfward across the series of faults (fig. 115).

The S2 marker occurs at depths ranging from 5,500 to 6,800 ft in the Sarita area. The S2 to S3 interval, approximately 650 ft thick, contains

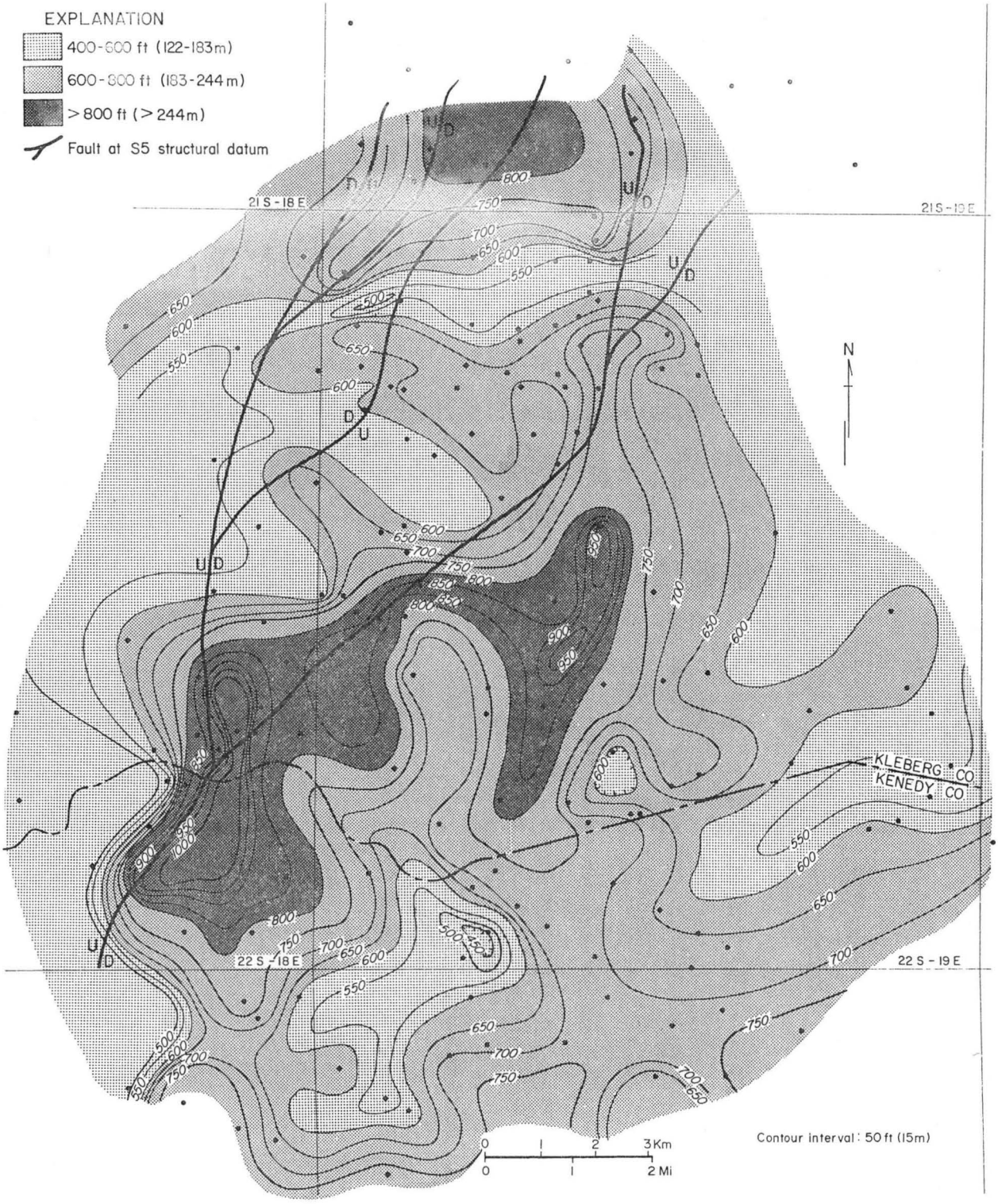

Figure 120. Net sandstone between correlation markers S1 and S2, Sarita Prospect Area.

the least amount of sandstone of any interval in the prospect area, averaging about 250 ft of sandstone, with maximum values occurring on the downthrown side of the major growth fault (fig. 121). The individual sandstone bodies range from 10 to 50 ft thick and are interbedded with shale. The section expands slightly, mostly in the shale sections, on the downthrown side of the growth faults and becomes even more shaly downdip (fig. 116).

The S3 marker occurs at depths ranging from 6,100 to 7,600 ft through the Sarita area. The S3 to S4 interval, approximately 1,200 ft thick, is characterized by relatively high net-sandstone values averaging 450 to 650 ft, with maximum sandstone content on the downthrown side of the major growth fault (fig. 122). Sandstone bodies 10 to 90 ft thick are interbedded with shale and show a 50 percent expansion of the interval across the growth fault. Gradual thickening of the section also occurs downdip (fig. 115). The sandstones show rapid facies changes and are very irregular in thickness throughout the area.

The S4 marker occurs at depths ranging from 7,100 to 9,100 ft through the Sarita area. The S4 to S5 interval, approximately 1,000 ft thick, is characterized by net-sandstone values averaging 300 to 400 ft (fig. 123). This interval is predominantly shale updip, with a few sandstones less than 50 ft thick. Across the major growth fault, the interval expands twofold although the sandstone percentage decreases. Farther down regional dip, the section thickens on the downthrown sides of other growth faults; there, however, sandstone bodies become more massive, and some approach thicknesses of 200 ft (fig. 116, well No. 5).

The S5 marker occurs at depths ranging from 8,100 to 10,700 ft through the Sarita area. The A-B Zone boundary generally occurs within the S5 to S6 interval. The interval is approximately 1,200 ft thick, and averages

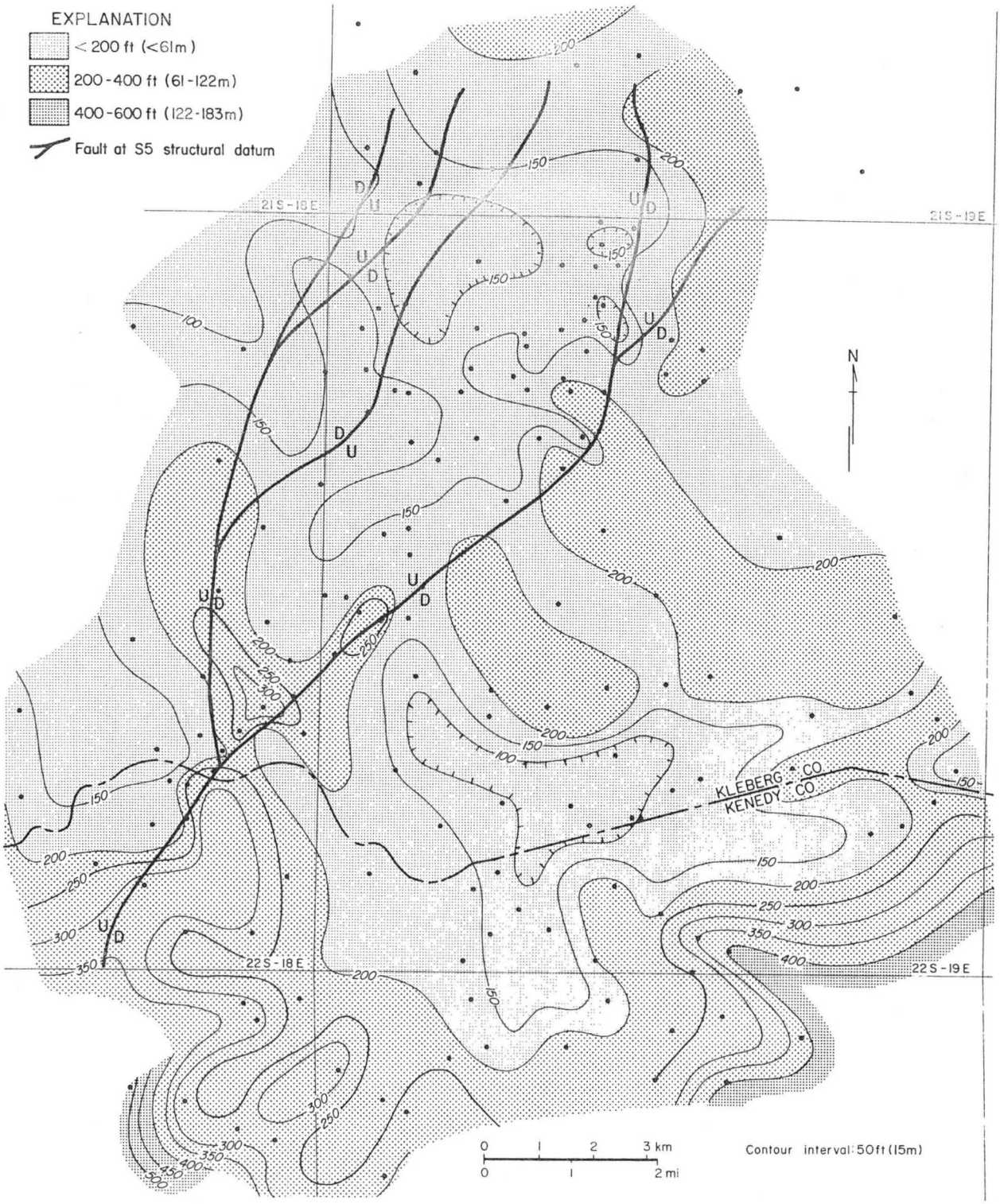

Figure 121. Net sandstone between correlation markers S2 and S3, Sarita Prospect Area.

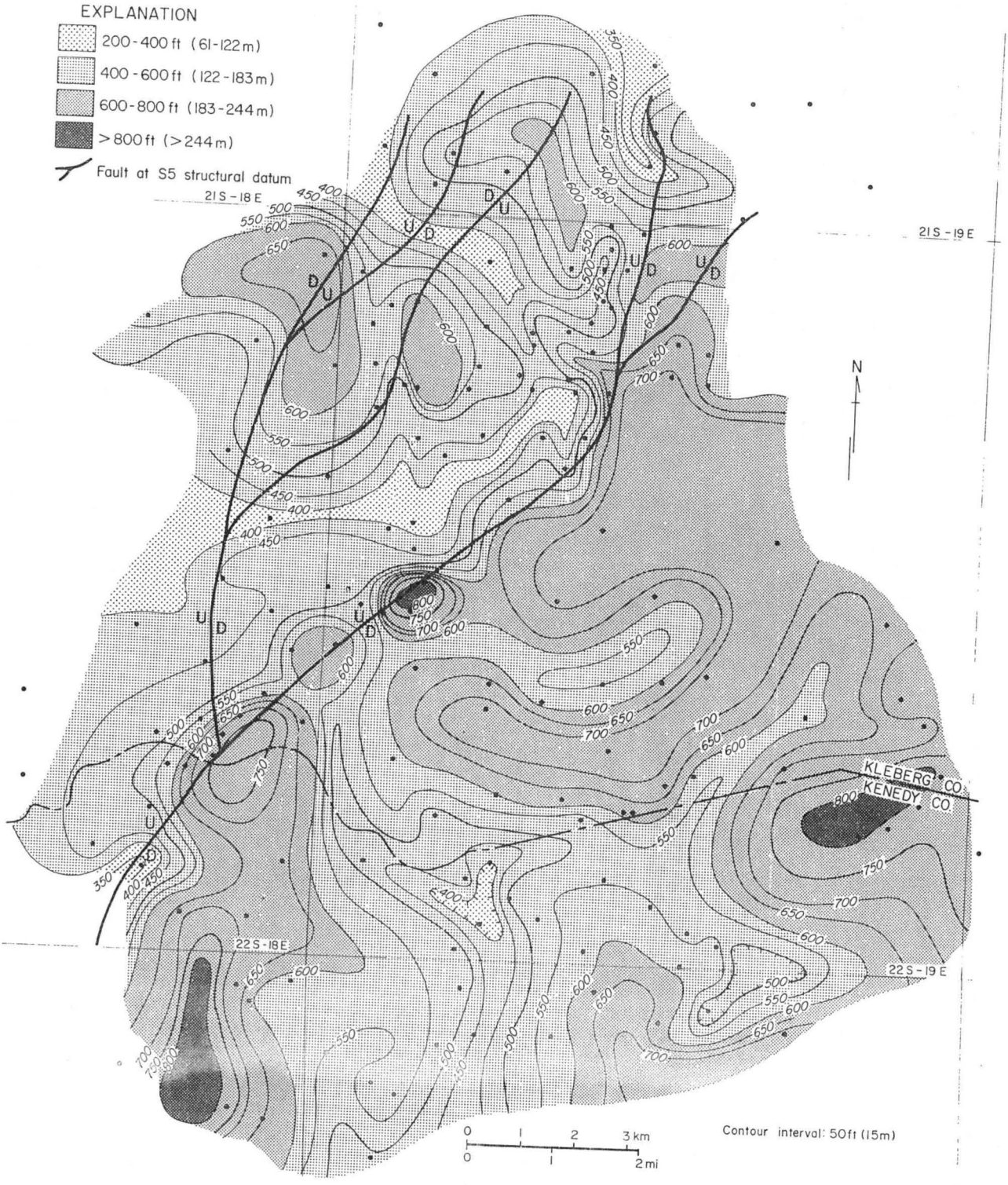

Figure 122. Net sandstone between correlation markers S3 and S4, Sarita Prospect Area.

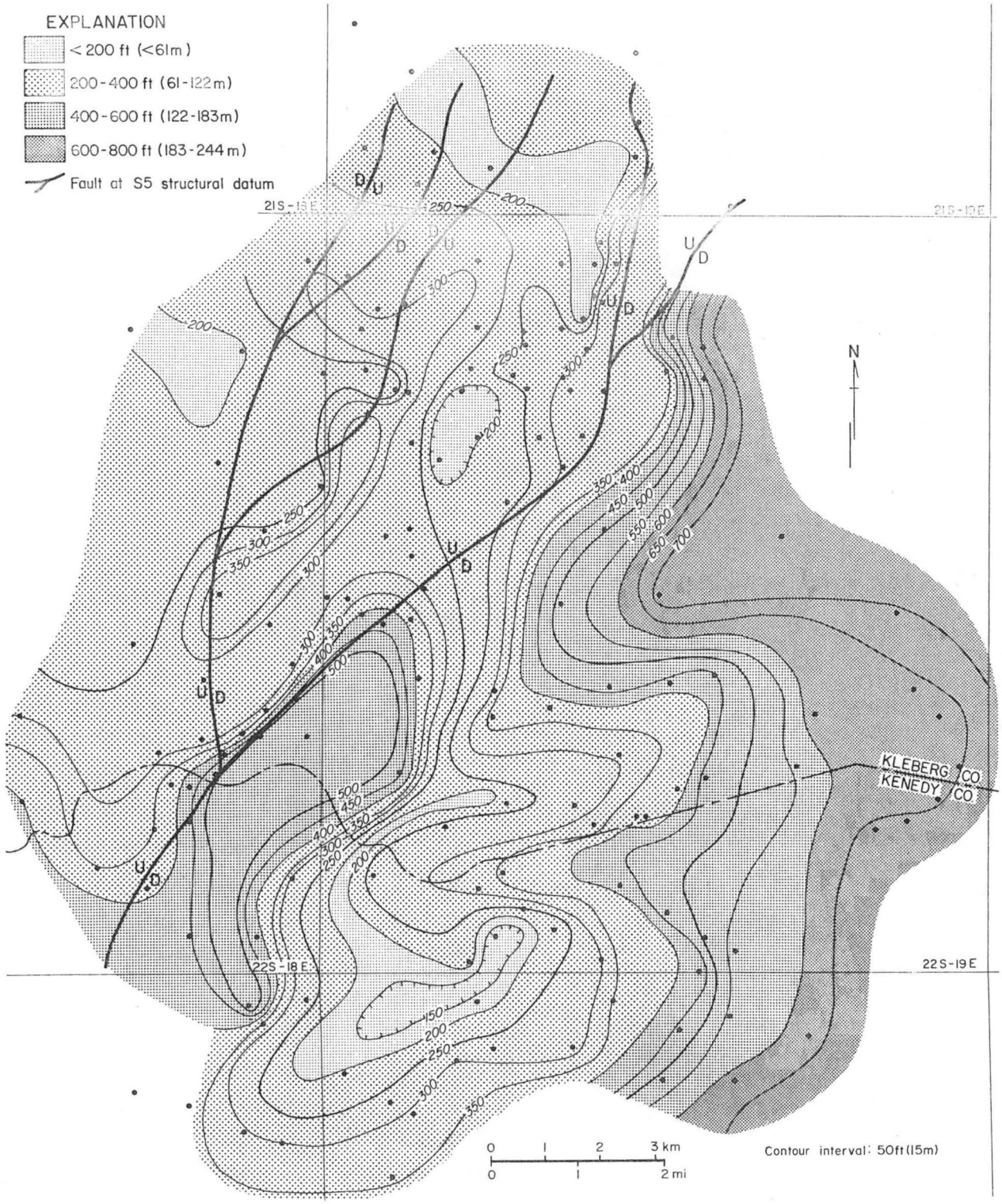

Figure 123. Net sandstone between correlation markers S4 and S5, Sarita Prospect Area.

500 ft of net sandstone in the area updip of the major growth fault (fig. 124). In the central and southwestern parts of this updip area, the interval contains massive sandstones up to 200 ft thick (figs. 114, 115, and 116). Immediately downdip of the major fault, net sandstone could not be determined because no wells penetrate the entire interval. However, because of the tremendous expansion of the section, sandstone thicknesses there should predictably be greatest. Farther gulfward, sandstone percentage begins to decrease in the interval as facies change to distal delta and only the shales expand on the downthrown sides of faults (fig. 116). In the northern part of the prospect area, a net-sandstone maximum occurs downdip of the major fault and its branches (fig. 124).

Markers S7 and S8 define intervals within the C and D Zones. However, very few wells penetrate these deeper intervals; consequently, net-sandstone maps and discussion of intervals below the S6 marker are not included in this report.

Sarita shallow prospect area and test-well site

Geology.--Extensive growth faulting has segmented the Sarita Prospect Area into numerous fault blocks. The fault block located in the northwestern (updip) part of the area has been selected as an area suitable for the location of a test-well site (fig. 125). This elongate fault block, which covers approximately 17 mi^2, is bounded on the south and east by major growth faults and on the west by a large antithetic fault. The proposed test-well site is located in the southeastern part of the block on the flank of a structural high, 4 mi northeast of the town of Sarita.

In the test block, the top of the reservoir sandstone interval (S5 to S6) ranges in depth from 8,500 to 9,000 ft; in the type well, this interval

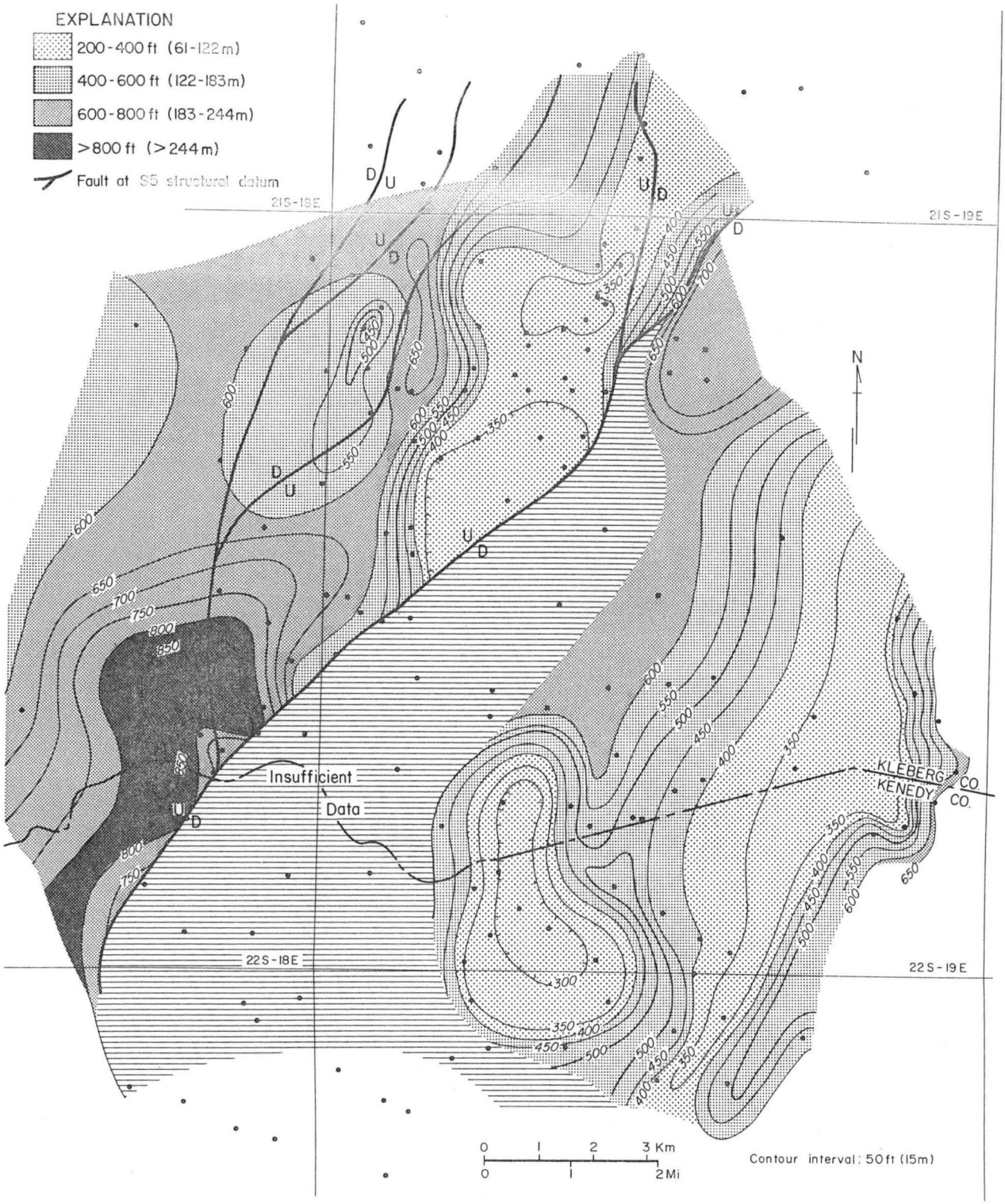

Figure 124. Net sandstone between correlation markers S5 and S6, Sarita Prospect Area.

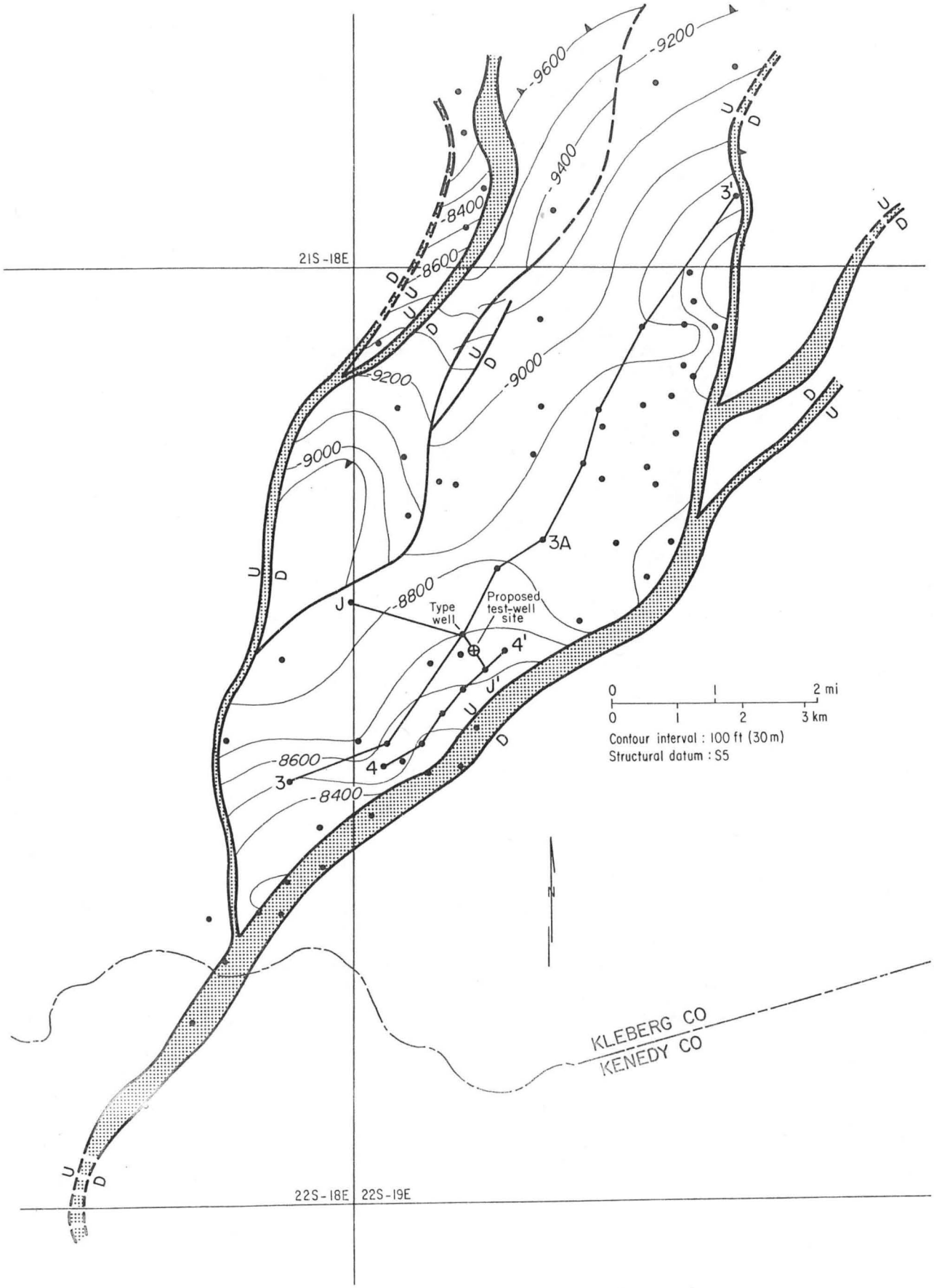

Figure 125. Structure, well control, lines of section, and location of the Sarita test-well site.

occurs at a depth of 8,705 ft. The top of the prospective reservoir sandstone interval can be expected to be at a depth of 8,650 ft in the test well. The reservoir sandstone interval (S5 to S6) has been subdivided into units A through E for the purpose of more detailed correlation in the area surrounding the test well (figs. 126 and 127). The base of the interval (S6 marker) should occur at a depth of 9,900 ft in the test well because total interval thickness in adjacent wells averages approximately 1,200 ft.

In the type well, Arkansas Fuel No. 1 Hubert, individual sandstone bodies within the S5 to S6 interval range from 10 to 100 ft thick; intervening shales are 20 to 50 ft thick (fig. 127). The upward-coarsening sandstones are interpreted as delta-front deposits. Unit A contains a sandstone body that varies in thickness from 20 to 60 ft locally. Unit B consists of a thick (90 ft) sandstone bed at the top of a upward-coarsening sequence that thins downdip (fig. 127) and along strike (fig. 126). Units C, D, and E contain thin sandstone bodies 10 to 60 ft thick, separated by 20- to 80-ft shales.

Net-sandstone thickness for the prospective S5 to S6 interval in the type well is uncertain because the well does not penetrate the entire section. However, on the basis of total interval thickness in deep wells of the prospect fault block, sandstone percentage in the type well, and documented net-sandstone trends, the net-sandstone value for the prospective reservoir section in the test well should be approximately 450 ft.

Formation fluid pressures and temperatures.--Plots of temperature and bottom-hole shut-in pressure (BHSIP) versus depth (figs. 128 and 129) show that the thickness of the B Zone in the Sarita Shallow Prospect Area is 1,050 ft. Geothermal gradients average 1.39° F/100 ft in the hydropressured zone and 2.01° F/100 ft in the geopressured zone. BHSIP data from

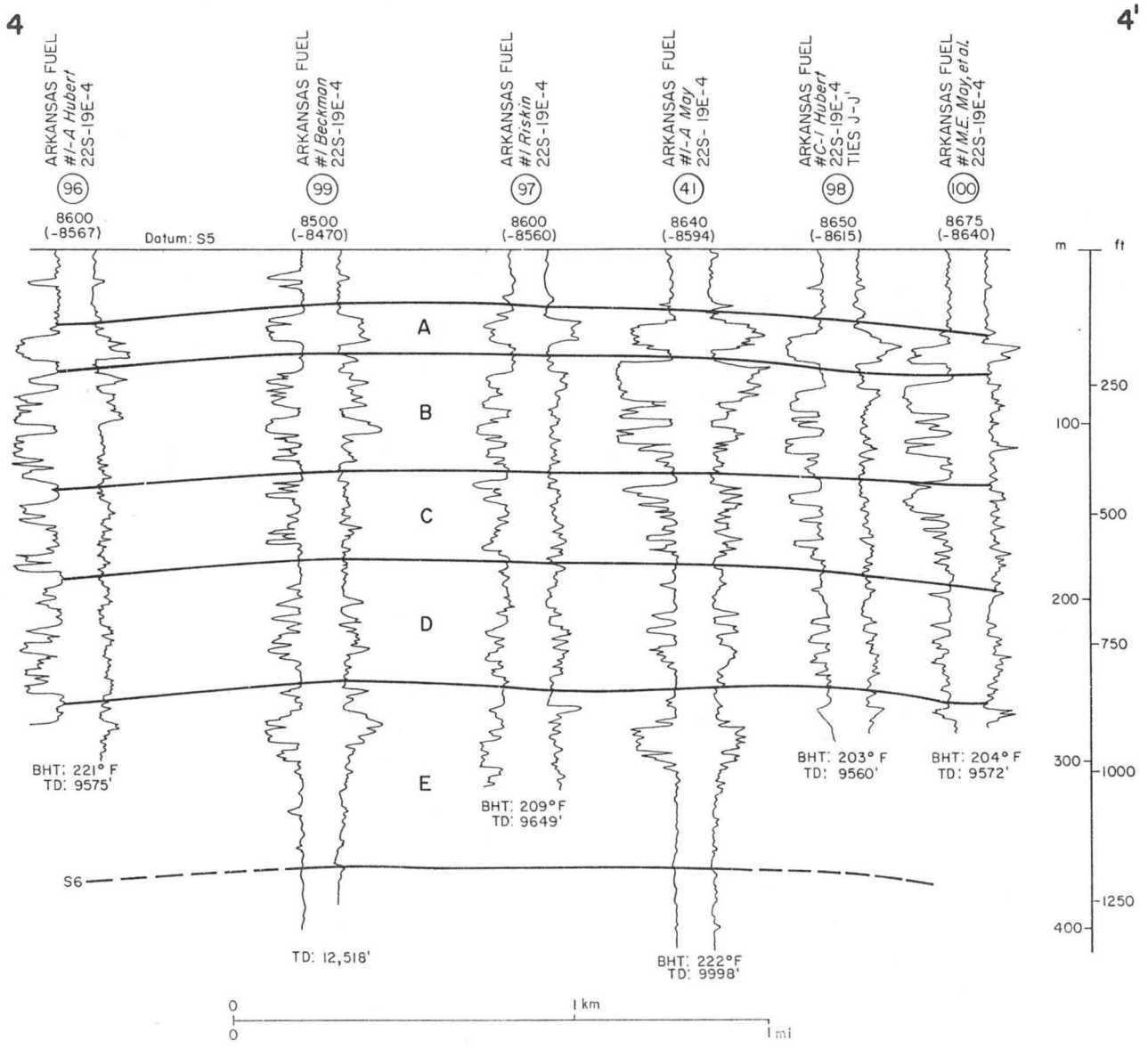

Figure 126. Stratigraphic strike section 4-4', Sarita Prospect Area.

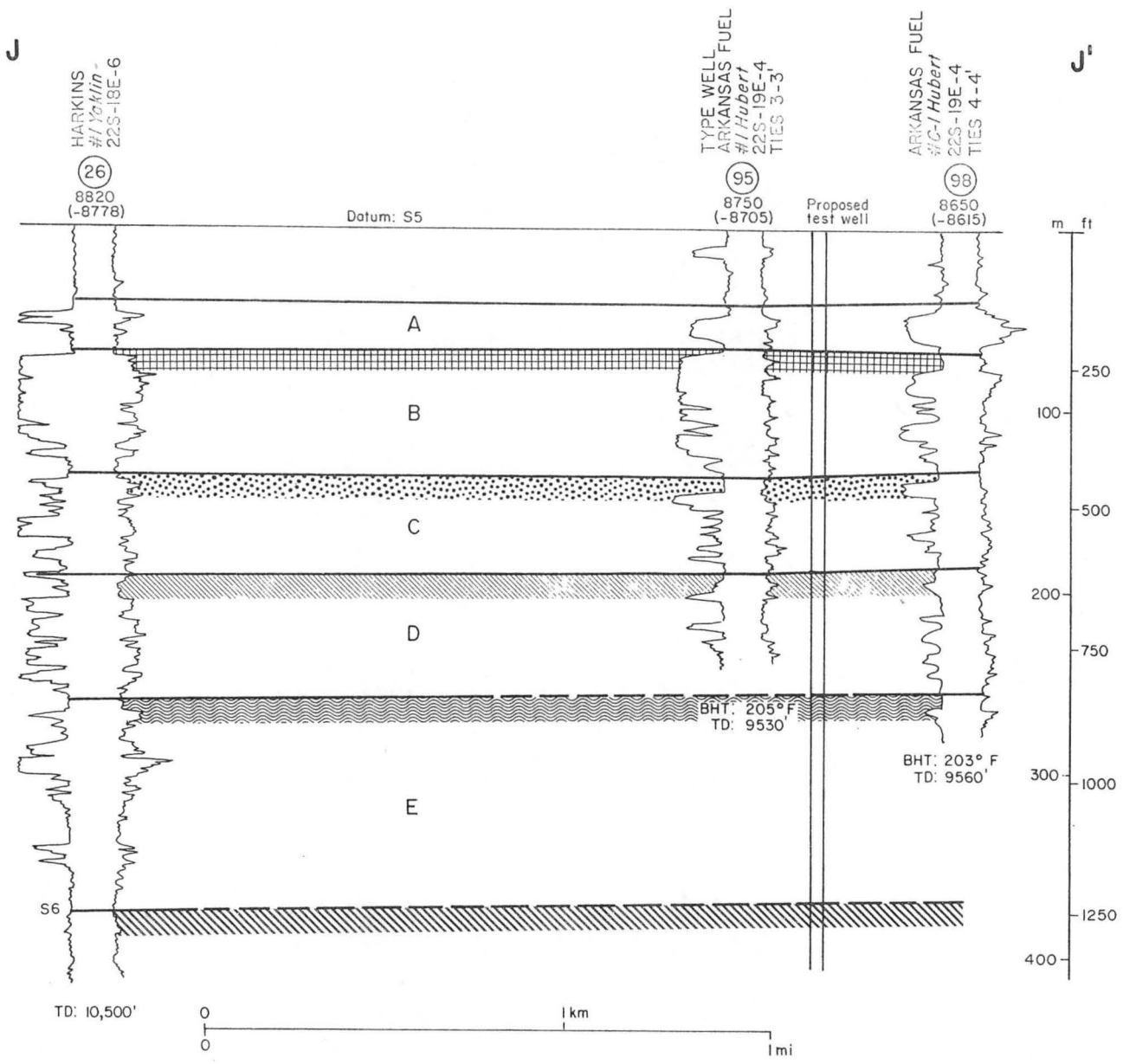

Figure 127. Stratigraphic dip section J-J' and proposed location of test well, Sarita Prospect Area.

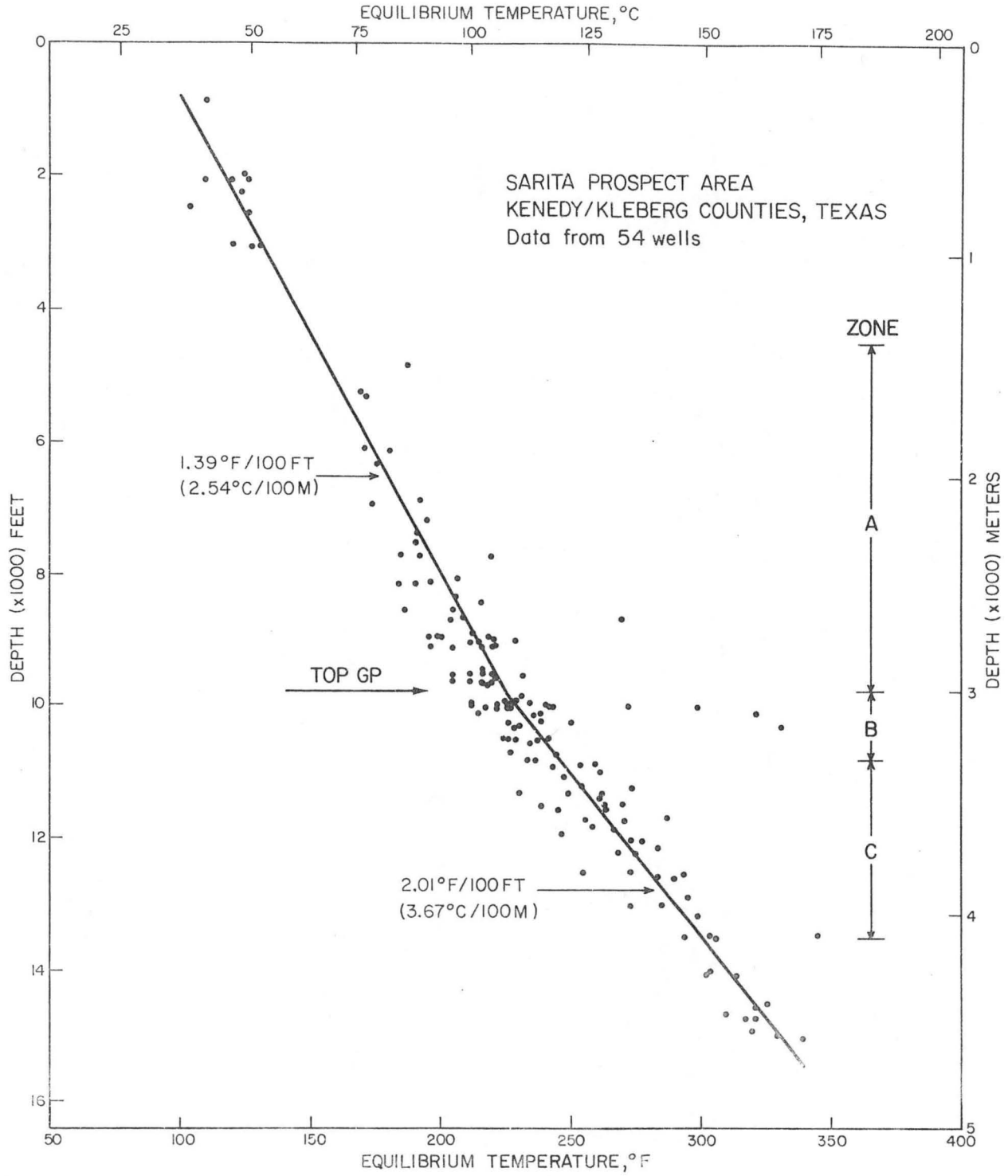

Figure 128. Geothermal gradients based on well log temperatures corrected to equilibrium values for 54 wells, Sarita Shallow Prospect Area, Kleberg and Kenedy Counties, Texas.

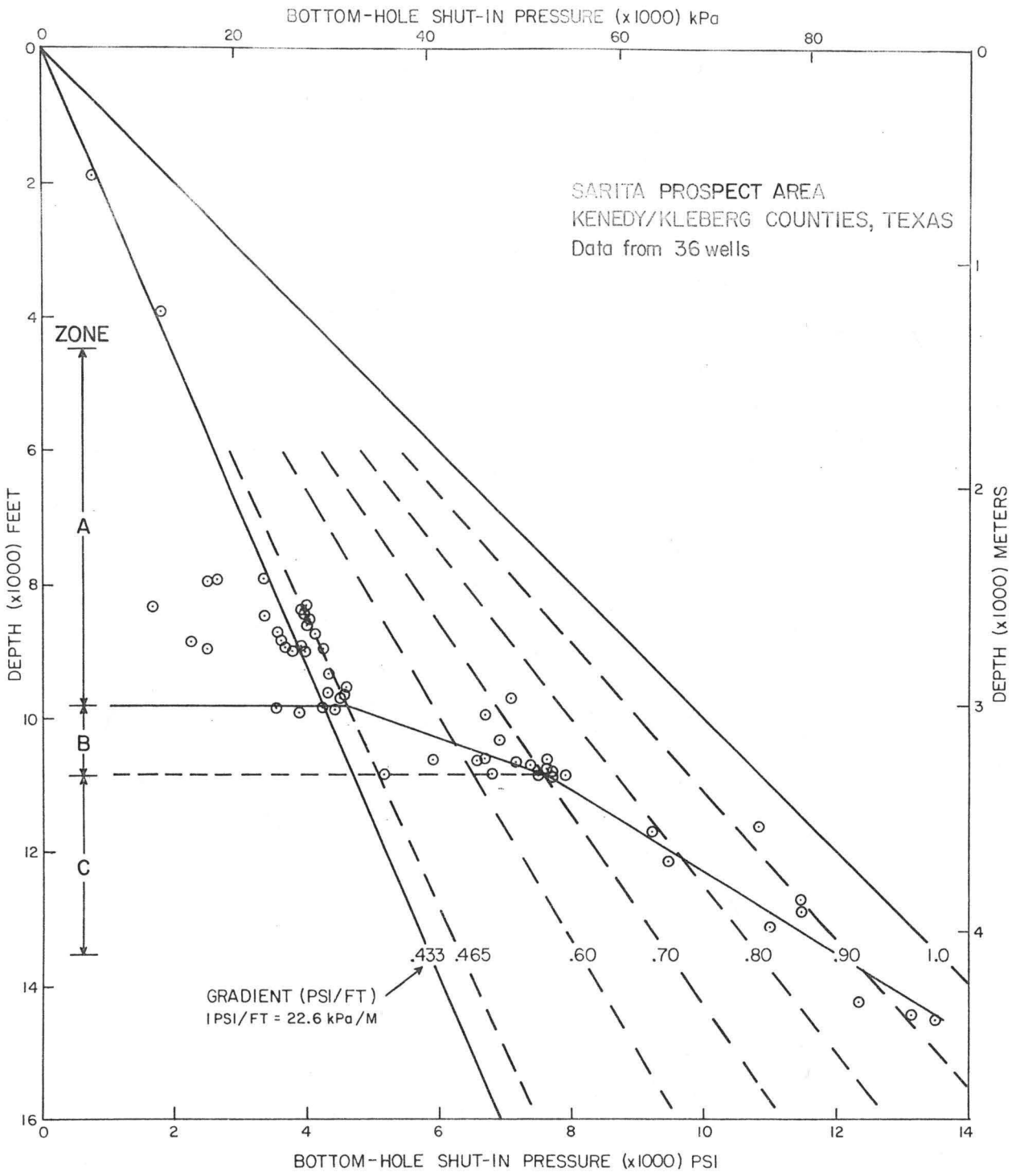

Figure 129. Bottom-hole shut-in pressures from drill-stem tests for production wells in Sarita Shallow Prospect Area, Kenedy and Kleberg Counties, Texas.

drill-stem tests show that pressure gradients in the C Zone range up to at least 0.93 psi/ft.

Parameter plots for strike sections 3-3A (fig. 130) and 3A-3' (fig. 131) show that the top of the B Zone deepens northeastward along section 3-3' (fig. 125) from depths of 8,600 to 10,150 ft; zone depth averages 9,315 ft. Average equilibrium temperatures at the top and base of the B Zone equal 203° and 221° F on section 3-3A, and 218° and 231° F on section 3A-3'. Temperatures at the top of the B Zone rise from 212° to 240° F as the zone deepens northeastward along strike. The base of the C Zone in this area is below available well control.

Parameter plots for dip section I-I' (fig. 132) also verify that the average depth of the B Zone (10,242 ft) is greatest in the northeastern part of the prospective fault block. The deepest point is at a depth of 10,650 ft in well No. 22 (22S-19E-3). The shallowest point is at a depth of 9,850 ft in well No. 86 (22S-19E-2). Temperatures at the top and base of the B Zone average 236° and 255° F, respectively.

The average top of the B Zone (depth of 8,950 ft) on dip section J-J' (fig. 133), which includes the type well and proposed test well, is shallower than average depth on sections 3-3' and I-I'. Maximum depth is 9,150 ft at well No. 26 (22S-18E-6), decreasing southeastward to 8,750 ft at well No. 98 (22S-19E-4). Temperatures at the top and base of the B Zone along J-J' average 203° and 217° F, respectively.

Well No. 95 (Arkansas Fuel No. 1 Hubert) is the type well for the Sarita Shallow Prospect Area. The top and base of the B Zone in this well occur at depths of 8,850 and 9,900 ft, and equilibrium temperatures are 200° and 215° F, respectively. Prospective sandstones at average depths of 8,910 and 8,975 ft occur mostly in the A Zone and uppermost B Zone. Temperatures in these sandstones average 202° F.

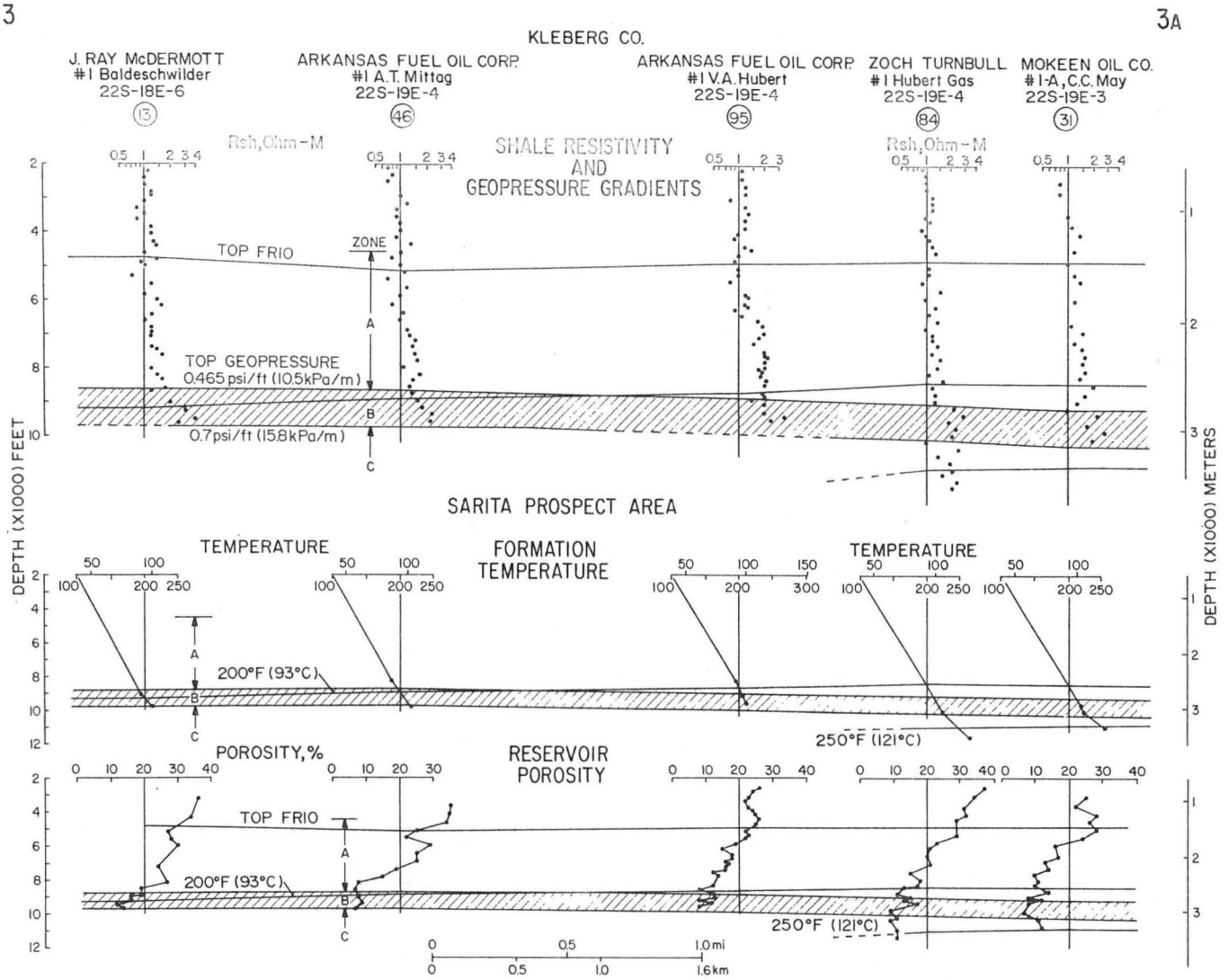

Figure 130. Parameter plots showing well profiles of shale resistivity, geopressure gradients, equilibrium temperature, and calculated reservoir porosity along strike section 3-3A, Sarita Shallow Prospect Area, Kleberg County, Texas.

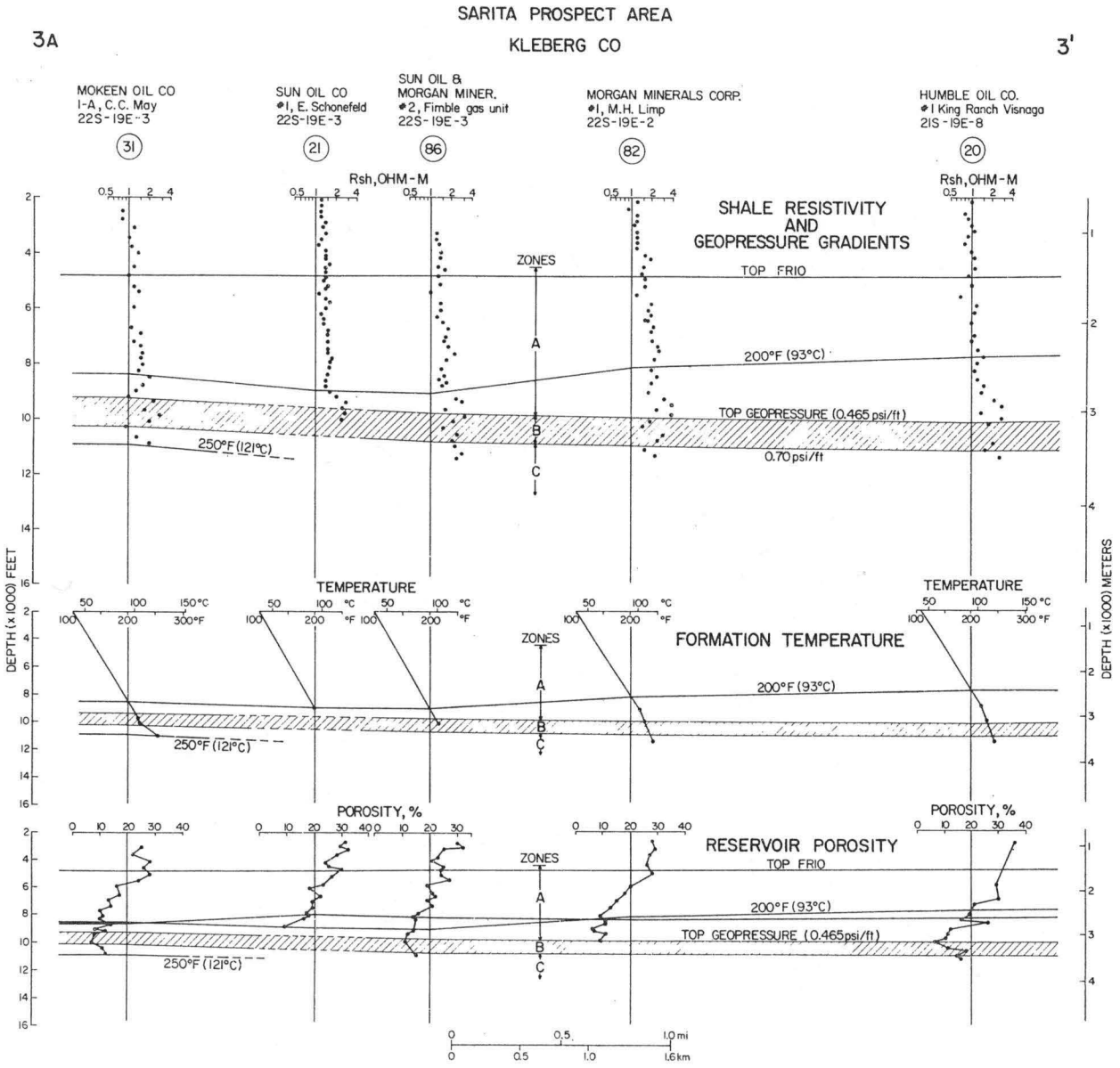

Figure 131. Parameter plots showing well profiles of shale resistivity, geopressure gradients, equilibrium temperatures, and calculated reservoir porosity along strike section 3A-3', Sarita Shallow Prospect Area, Kleberg County, Texas.

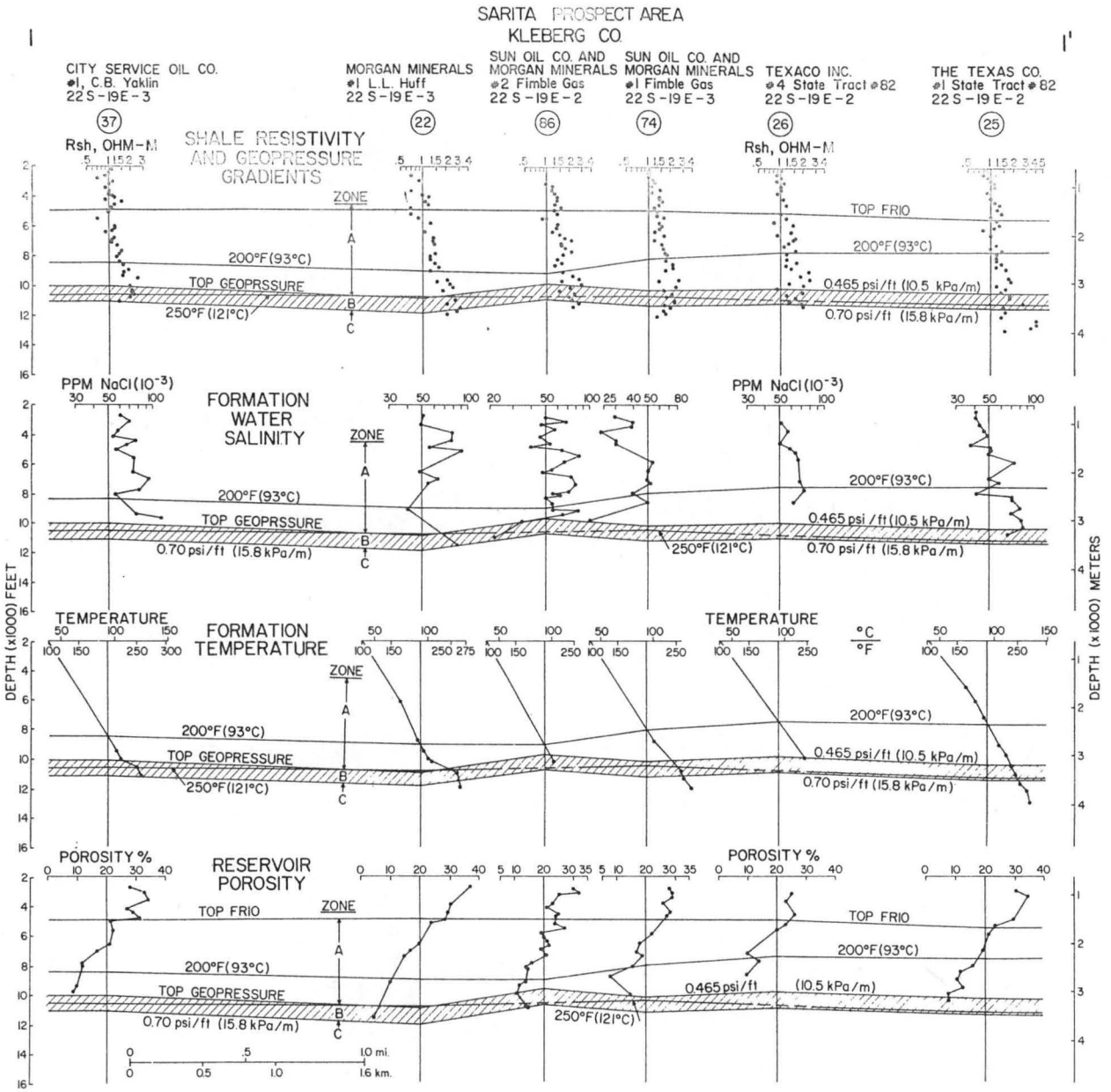

Figure 132. Parameter plots for wells along dip section I-I', Sarita Shallow Prospect Area, Kleberg County, Texas.

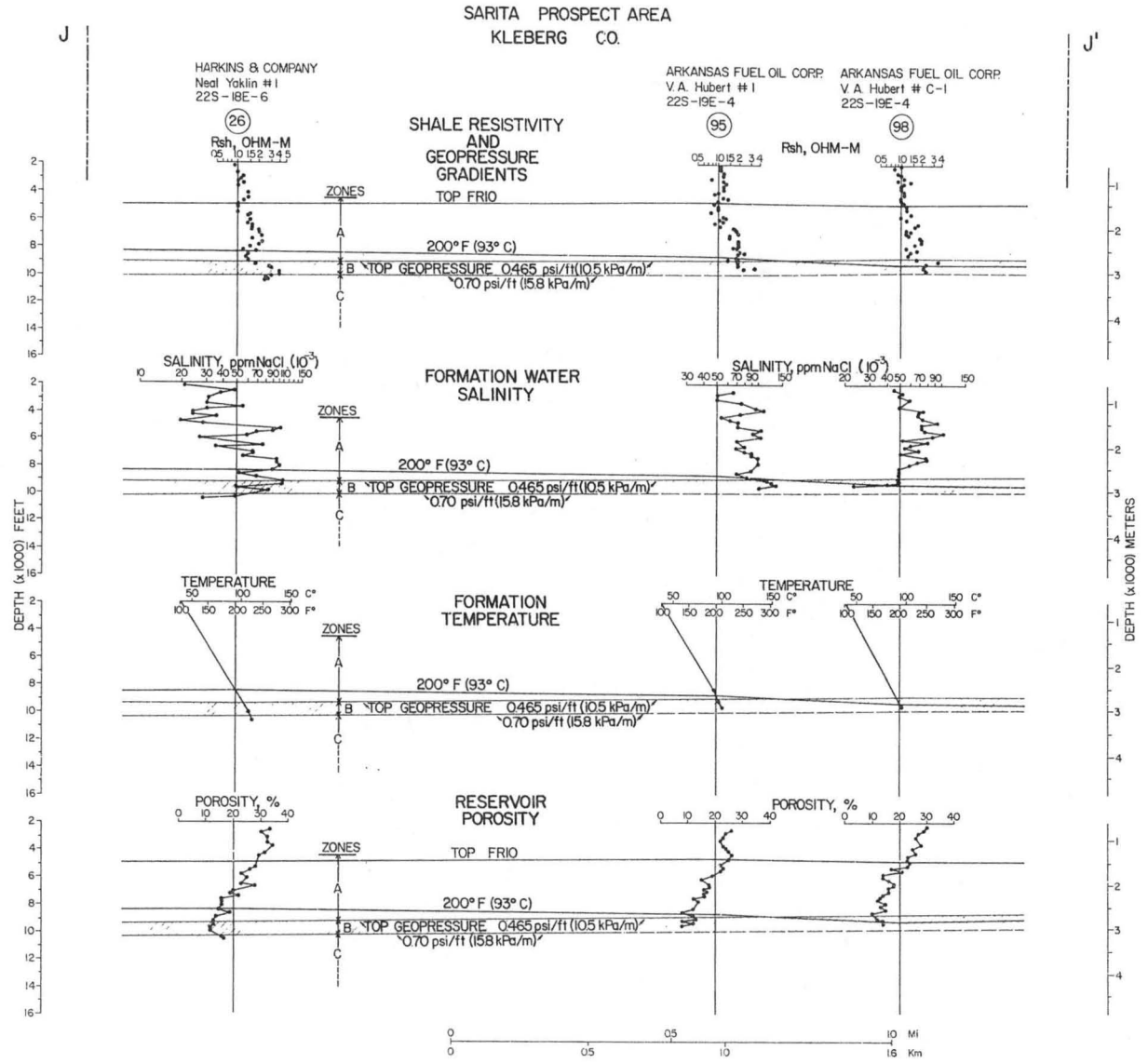

Figure 133. Parameter plots for wells along dip section J-J', Sarita Shallow Prospect Area, Kleberg County, Texas.

Formation water salinity.--Salinities determined from the SP log and R_{mf} values from the log header (fig. 134) follow general trends established for the Texas Gulf Coast area (fig. 14). Peak values of salinity, exceeding 150,000 ppm NaCl, occur in the depth interval from 8,400 to 9,050 ft. Below a depth of about 9,800 ft, salinities decrease with depth. Average salinities at the top and base of the B Zone on section 3-3A (fig. 135) are 85,000 and 61,000 ppm NaCl, respectively; thus, salinity decreases with depth through the B Zone by an average of 24,000 ppm NaCl. On section 3A-3' (fig. 136) in the northeastern part of the prospective fault block, average salinities decrease with depth through the B Zone from 54,000 ppm NaCl at the top of the zone to 28,000 ppm NaCl at the bottom. The trend of salinities at the top of the B Zone in the prospect area increases from 42,000 ppm NaCl northeastward along section 3-3A to 106,000 ppm NaCl and then decreases to about 40,000 ppm NaCl along section 3A-3'. At the base of the B Zone, salinities are more variable but generally decline northeastward along strike section 3-3' from a maximum of 100,000 ppm NaCl at well No. 46 to a minimum of 24,000 ppm NaCl at well No. 86.

Salinity profiles of wells that penetrate the B Zone on dip section I-I' (fig. 132), which crosses the northeastern end of the fault block, show average values of about 53,000 ppm NaCl within the B Zone. On dip section J-J' (fig. 133), which includes the type well and proposed test well, salinities average 89,000 ppm NaCl at the top of the B Zone and decrease sharply to a projected average salinity of 53,000 ppm NaCl at the base of the B Zone.

Salinities in the type well (No. 95 in figs. 133 and 135) are 105,000 ppm NaCl at the top of the B Zone and about 80,000 ppm NaCl projected to the base of the zone. The average salinity is 79,000 ppm NaCl in prospective sandstones at depths of 8,910 and 8,975 ft.

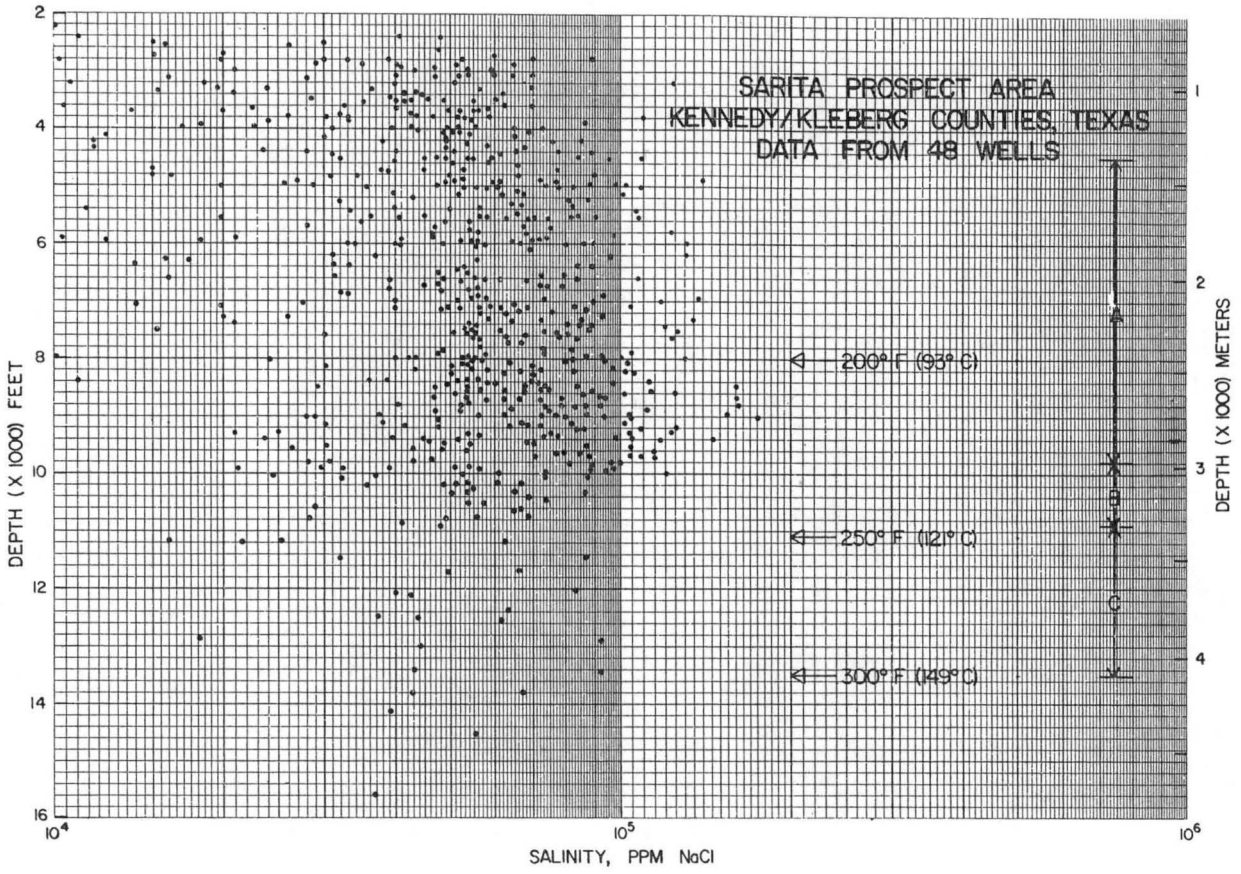

Figure 134. Salinity (computed from SP logs) versus depth for 48 wells, Sarita Shallow Prospect Area, Kenedy and Kleberg Counties, Texas.

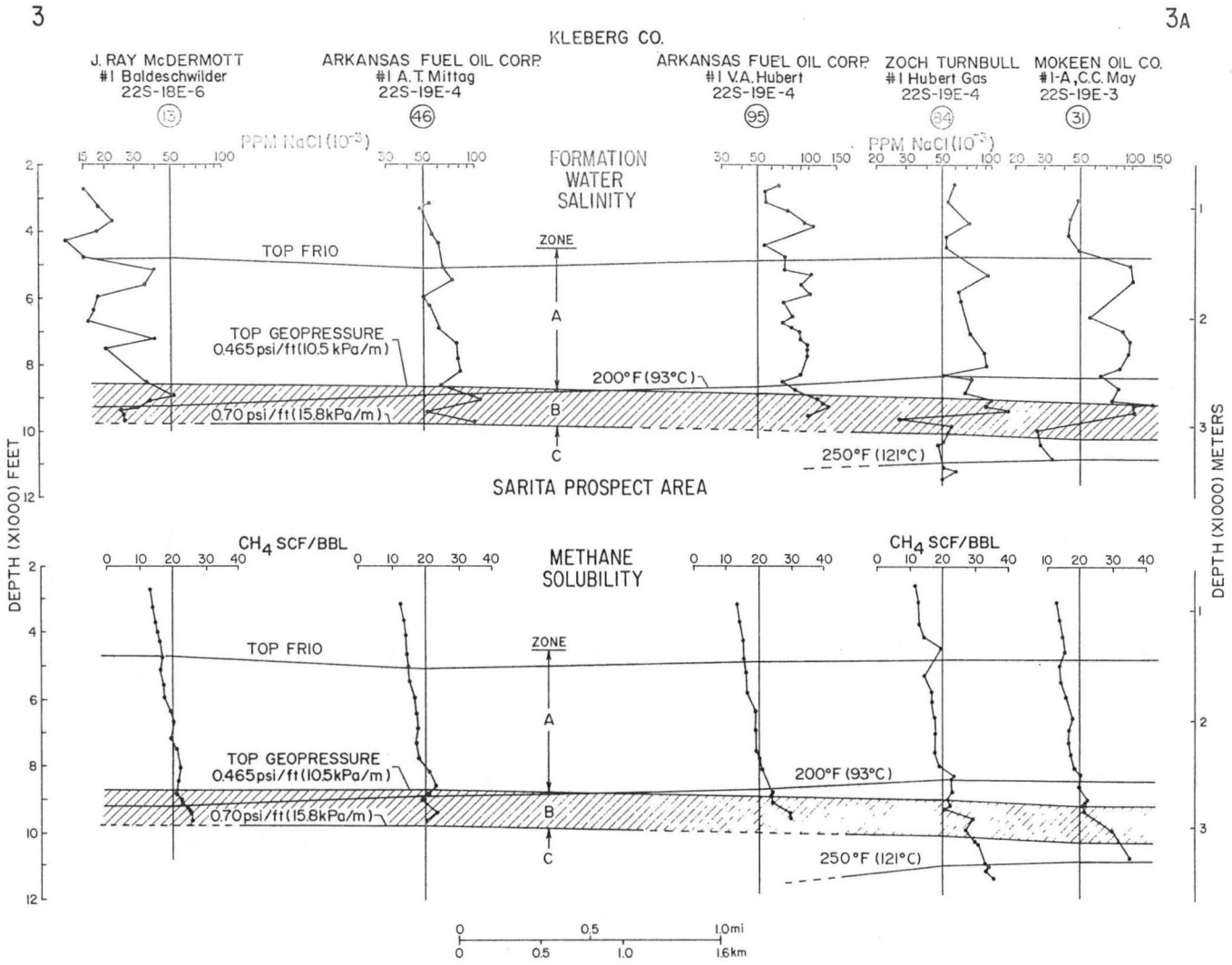

Figure 135. Parameter plots showing well profiles of formation water salinity and methane solubility (using well log header values of R_{mf}) along strike section 3-3A, Sarita Shallow Prospect Area, Kleberg County, Texas.

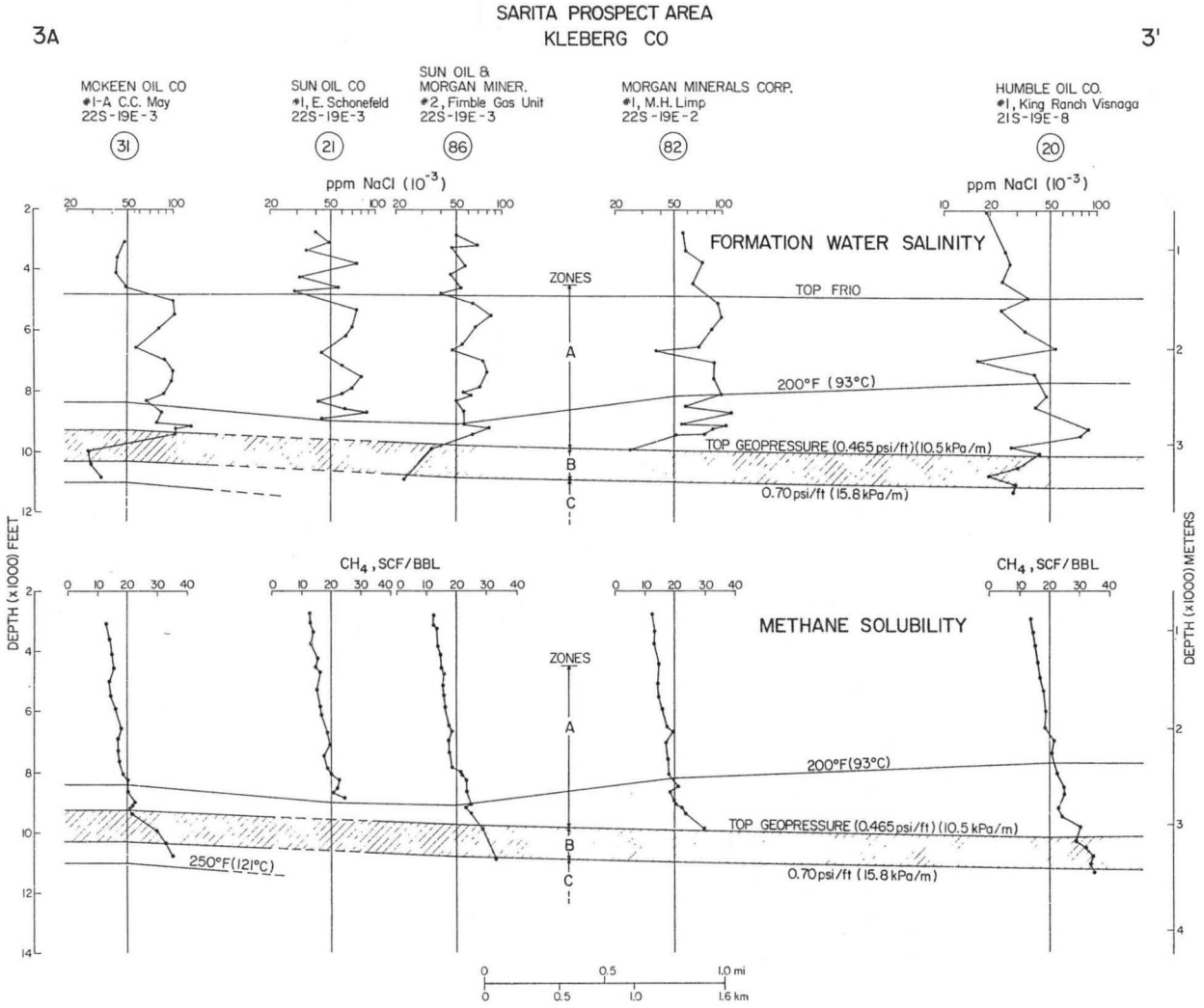

Figure 136. Parameter plots showing well profiles of formation water salinity and methane solubility (using well log header values of R_{mf}) along strike section 3A-3', Sarita Shallow Prospect Area, Kleberg County, Texas.

Porosity and permeability.--Porosities calculated from the relationship of Archie (1942) tend to be lower than those measured from whole cores. For example, in the depth interval from 8,000 to 8,500 ft (fig. 137), calculated porosities average about 13 percent compared with about 20 percent for porosities from core measurements. Porosities calculated for the B Zone and shown on parameter plots for section 3-3A and 3A-3' (figs. 130 and 131) range from 5 to 19 percent and average about 11 percent, decreasing slightly with depth. Porosities in section 3-3' are highest in well No. 13 (fig. 130) and decrease from 19 to 14 percent from the top to the base of the B Zone. Porosity profiles of wells that penetrate the B Zone on dip section I-I' (fig. 132) show average values of 10 and 7 percent at the top and base of the B Zone, respectively. On dip section J-J' (fig. 133) porosities average about 12.5 percent in the B Zone.

A plot of porosity versus horizontal air permeability measured from whole cores shows that the average permeability is about 23 md in rocks with an average porosity of 20 percent (fig. 138). A plot of whole-core air permeability versus depth in the area (fig. 139) shows a wide range of permeabilities from 3.5 to 1,000 md in the cored depth interval from 8,000 to 9,400 ft. The least-squares-regression curve indicates a gentle reduction in permeability as depth increases in the zone where core data are available. No core data are available for the type well, No. 95. However, permeabilities in a nearby well, No. 98 on section J-J' (fig. 133), ranged from 100 md to more than 200 md in the sandstone unit that is stratigraphically equivalent to the sandstone at a depth of 8,910 ft in the type well. The sandstone in well No. 98 that is stratigraphically equivalent to the sandstone at a depth of 8,975 ft in the type well has permeabilities that range from 16 to 3,570 md and average about 750 md.

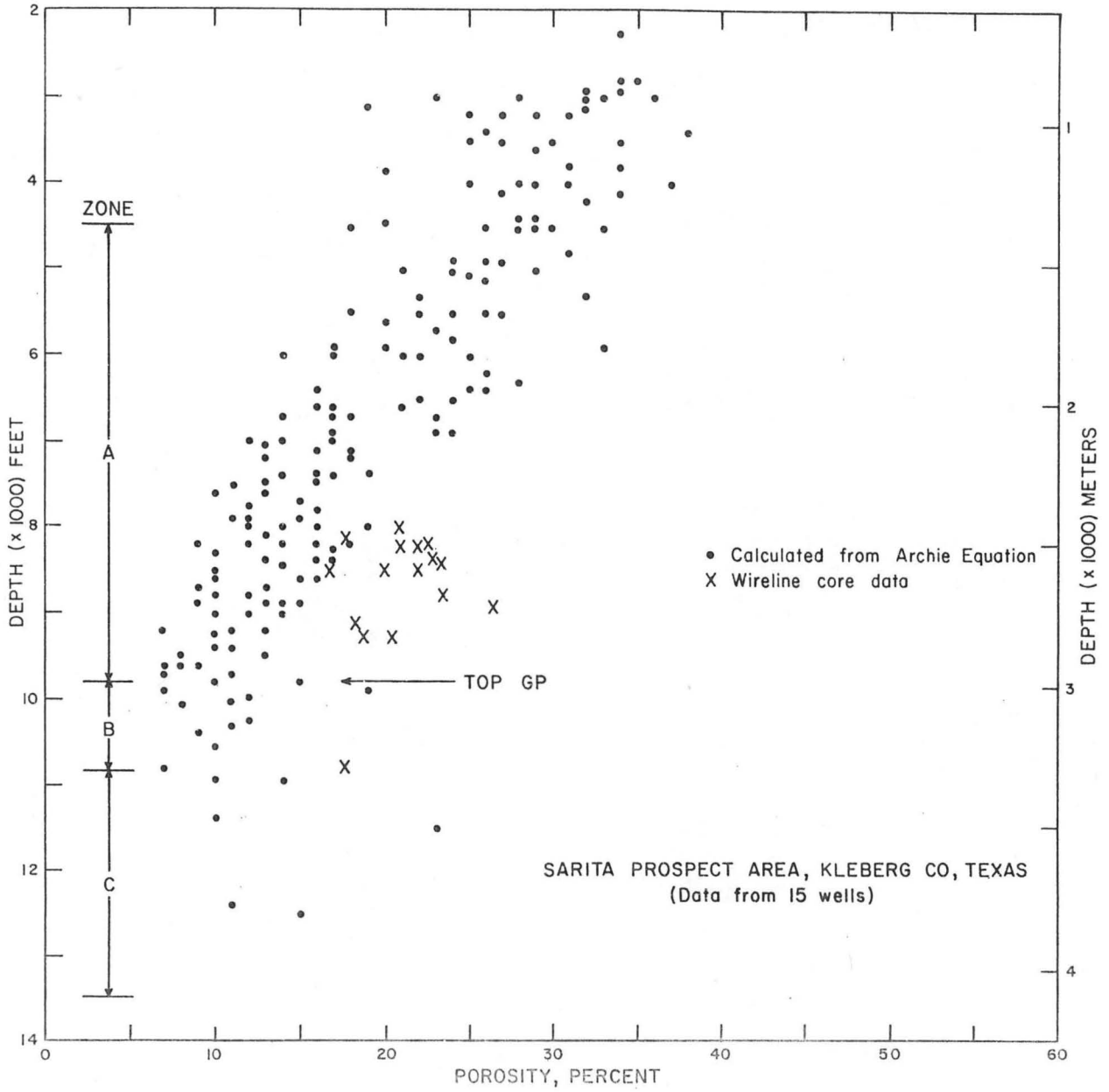

Figure 137. Porosity versus depth for 15 wells, Sarita Shallow Prospect Area, Kleberg County, Texas.

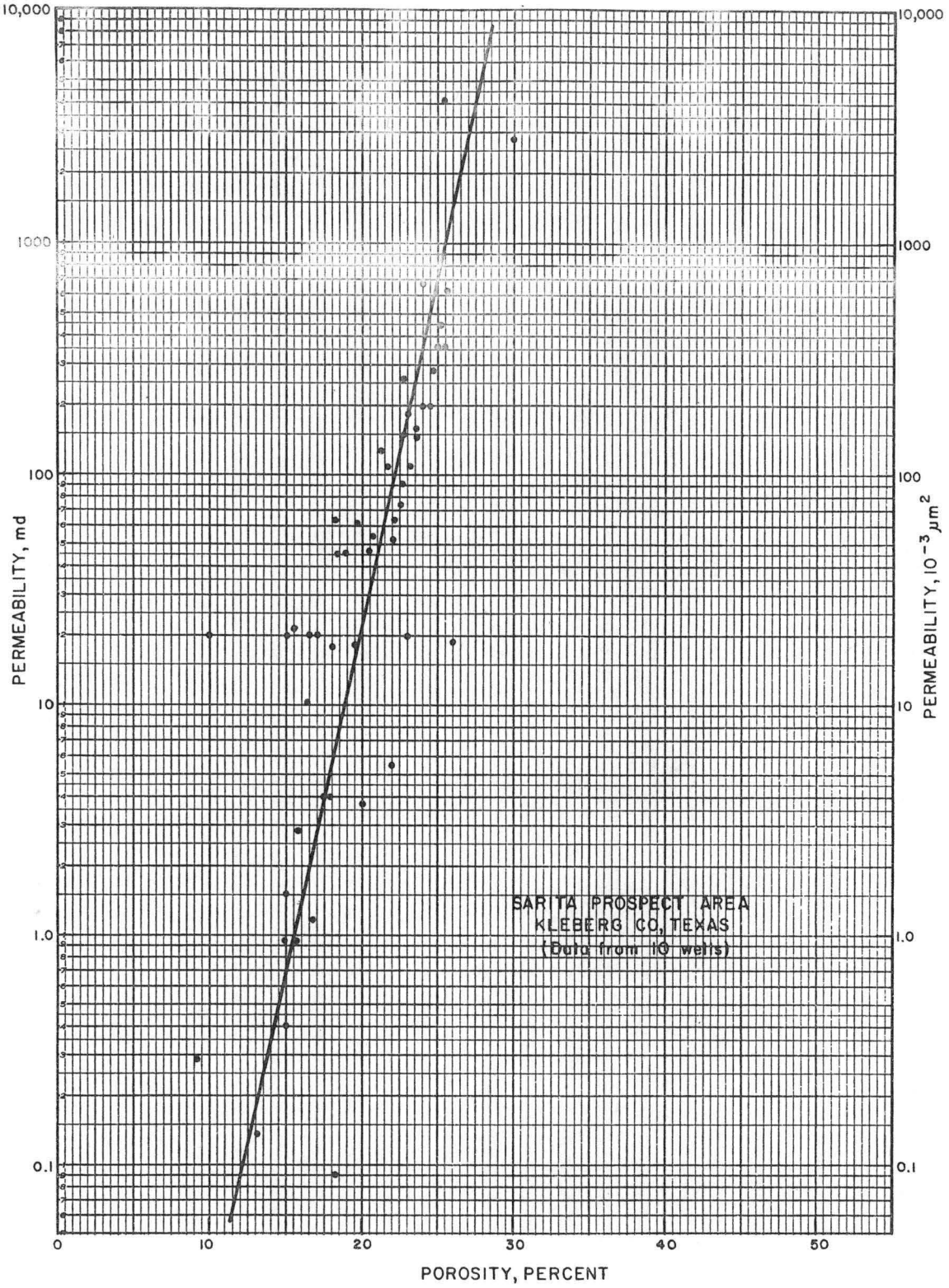

Figure 138. Porosity versus air permeability from whole-core data, Sarita Shallow Prospect Area, Kleberg County, Texas.

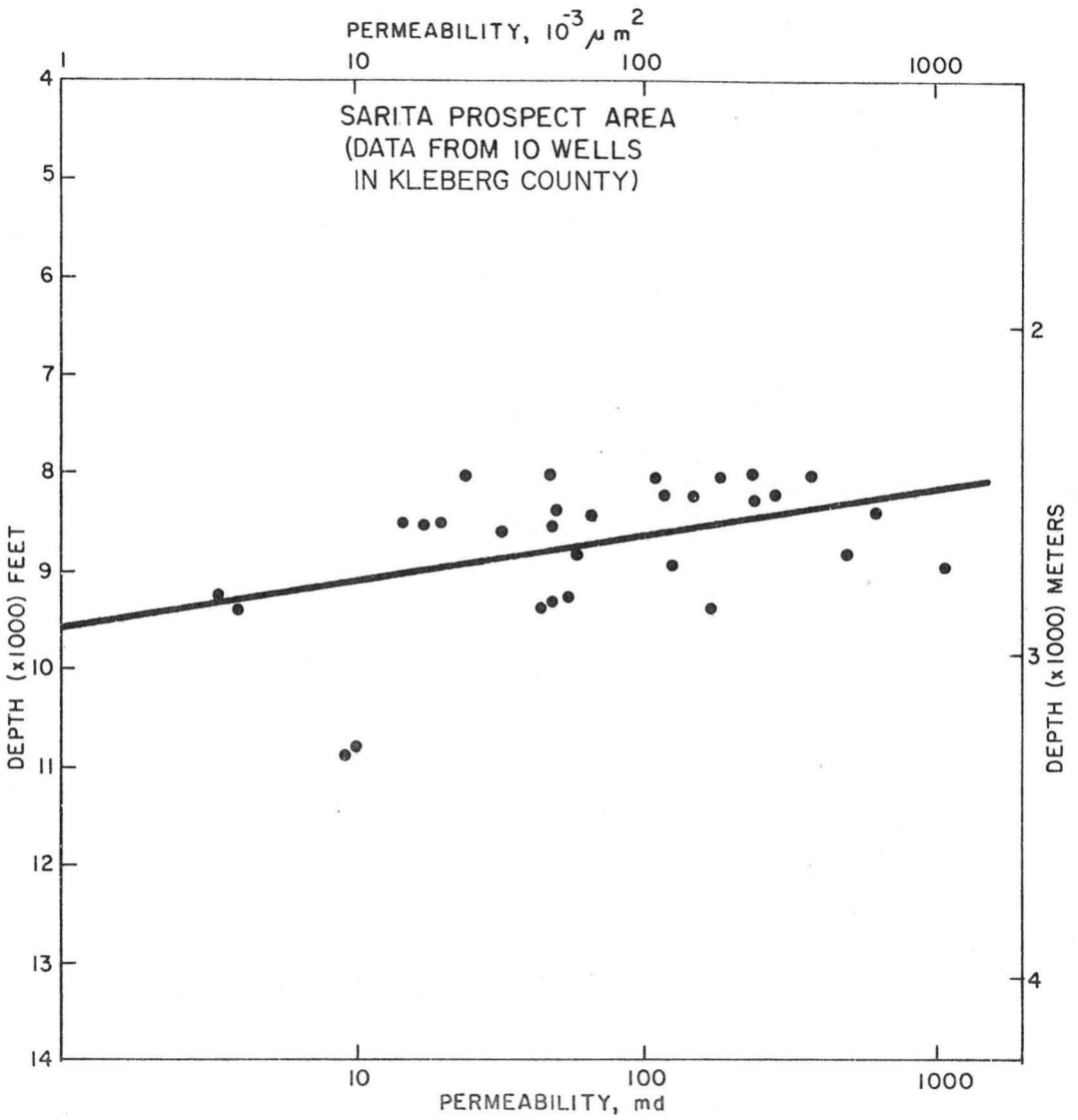

Figure 139. Whole-core air permeability versus depth, Sarita Shallow Prospect Area, Kleberg County, Texas.

Methane solubility.--Methane solubility on strike section 3-3A (fig. 135) averages 22 SCF/B at the top of the B Zone and 27 SCF/B at the base. Solubility increases northeastward along strike section 3A-3' (fig. 136), where it averages 27 and 34 SCF/B at the top and the base of the B Zone. Methane solubility averages 20 SCF/B in the prospective sandstones at depths of 8,910 and 8,975 ft in the type well.

With methane solubility increasing toward the northeastern end of the fault block, and net reservoir sandstone and porosity increasing toward the southwestern end, the test-well site was located near the central part of the fault block as a compromise between these opposing trends of favorable factors. However, the presence of known high permeability in reservoir sandstones near the proposed test site was an even greater factor in site selection.

Sarita deep prospect area

Geology.--An area favorable for testing geopressured sandstones of the C Zone is located in Kenedy County in the southeastern part of the Sarita Prospect Area (fig. 119). The 2 mi^2 test block lies within a complexly faulted zone of the lower Frio, where extensive faulting occurs at depths below 10,000 ft (fig. 115). The relatively small area of the prospective test block must be considered a minimum as faults may not form permeability barriers where sandstone lies against sandstone.

Humble No. 9-B East has been selected as the type well for the Sarita Deep Prospect (fig. 115, well No. 5). The top of the prospective reservoir interval occurs at a depth of 11,200 ft and extends through the well to its total depth of 14,000 ft. Within this section most sandstone units range in thickness from 30 to 175 ft.

Formation parameters.--The average thickness of the A, B, and C Zones is assumed to be the same (1,050 ft) for the Sarita Deep Prospect Area as

for the Sarita Shallow Prospect Area (fig. 129). The average depth to the top of the B Zone along section G-G' is 9,150 ft (fig. 140). Well No. 67 on the updip end of the section does not penetrate the B Zone. Temperatures at the top and base of the B Zone average 208° and 227° F; salinities average 96,000 and 55,000 ppm NaCl; porosities derived from induction and SP logs average 11 and 12 percent; and methane solubility averages 20 and 29 SCF/B, respectively.

In some of the prospective reservoir sandstones at depths from 11,200 to 13,690 ft (table 2) in the type well (Humble No. 9-B East) on section G-G' (fig. 140), temperatures range from 254° to 310° F; pressure gradients equal or exceed 0.85 psi/ft, salinities equal or exceed 120,000 ppm NaCl; and methane solubilities are estimated to be between 28 and 38 SCF/B. Porosities determined from induction and SP logs vary from 14 to 23 percent. No core data are available for the type well, but whole cores from stratigraphically equivalent sandstones in the upper part of the reservoir interval in a nearby well (Humble No. 18-B East) have average porosities of 26 percent and average permeabilities of 37 md.

Because of the lack of sufficient reservoir quality data, structural complexity, and sparse well control in the prospective fault block, a test-well site has not been selected. Seismic and additional reservoir data are needed to further evaluate this potential test area.

Candelaria Prospect Area

The Candelaria Prospect Area is in the central part of the Kenedy Fairway near the town of Armstrong (fig. 112). The Candelaria area is coincident with the Armstrong Fairway, an area studied previously by Bebout and others (1978b) for its potential production of geopressured-geothermal energy resources. The Candelaria Prospect Area measures approximately

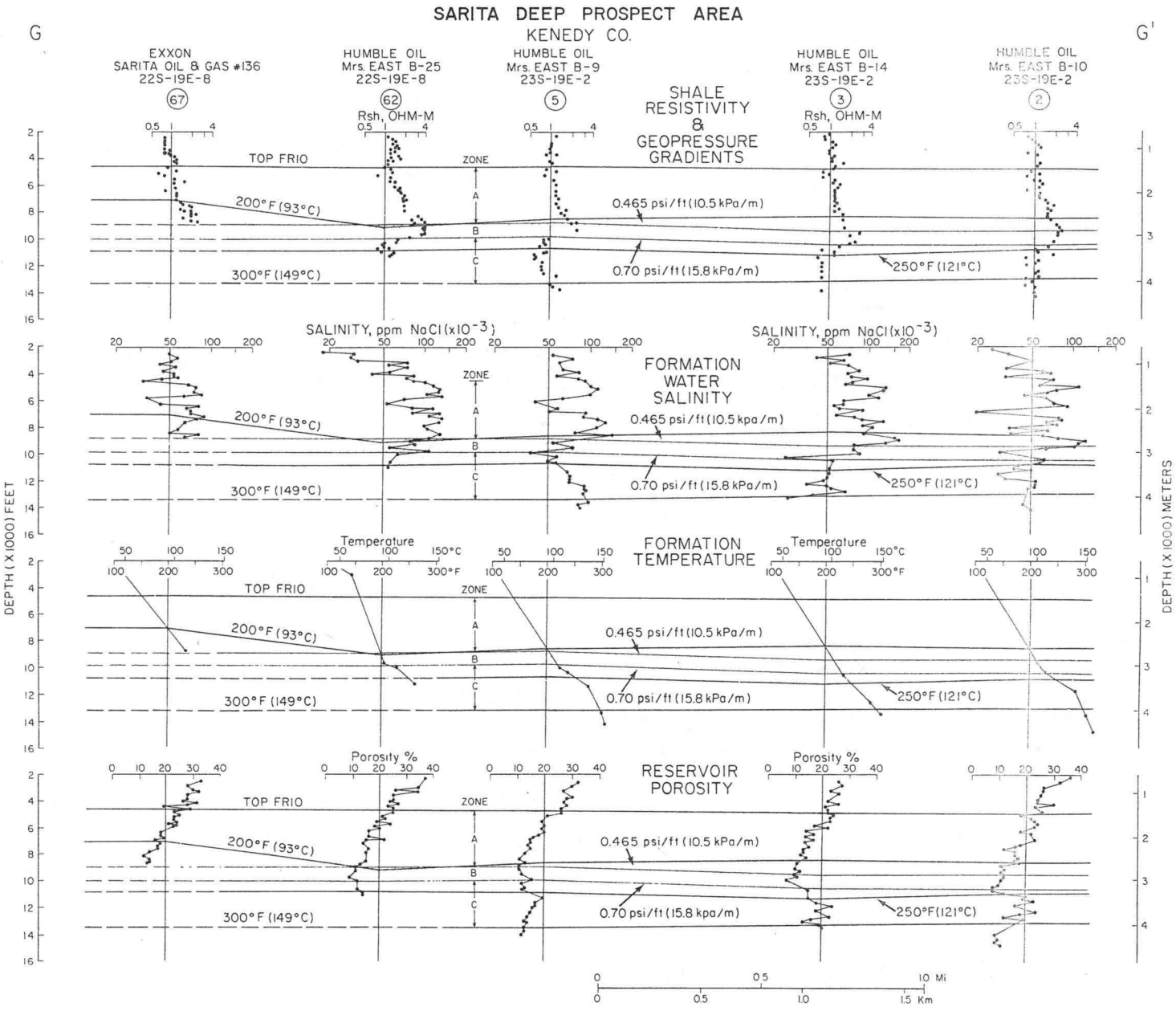

Figure 140. Parameter plots for part of dip section G-G', Sarita Deep Prospect Area, Kenedy County, Texas.

86 mi^2 and lies within a complexly faulted zone of the Frio trend, which extends along strike to the northeast and includes the fault zone in which the previously discussed Sarita Prospect Area occurs. Sixty electric logs from wells in the Candelaria area (fig. 141; appendix C) were used to analyze sandstones and shales within the hydropressured and geopressured zones. Figures 142 through 147 depict a series of structural and stratigraphic cross sections constructed through the Candelaria area to illustrate local faulting and correlations of the Frio Formation within the area. Detailed correlations of markers Cn1 to Cn10 subdivide the formation into several units.

Structure

The major structural feature of the Candelaria area is a northeast-southwest trending growth fault located in the west-central part of the area. Vertical displacement at this fault averages 350 ft at the Cn6 horizon (fig. 148). Downdip are a few down-to-the-basin faults with smaller displacements (100 to 300 ft), which segment the overall anticline in the area; the fault farthest downdip was chosen as the eastern boundary of the prospect area.

Sandstone distribution and characteristics

The Frio Formation in the Candelaria area exhibits two lithologically distinct parts: a lower part below the Cn5 marker and an upper part from Cn5 to the top of the Frio. The lower section is lithologically very similar and is the approximate stratigraphic equivalent of the lower Frio of the Sarita area. The upper Frio section in the Candelaria area consists mainly of thin (generally 10 to 50 ft), laterally discontinuous sandstones separated by shales. This interval is lithologically similar to the middle part of the Frio in the Sarita area (delta-plain facies) but is not overlain by the dominantly delta-front sandstones that occur in the upper Frio

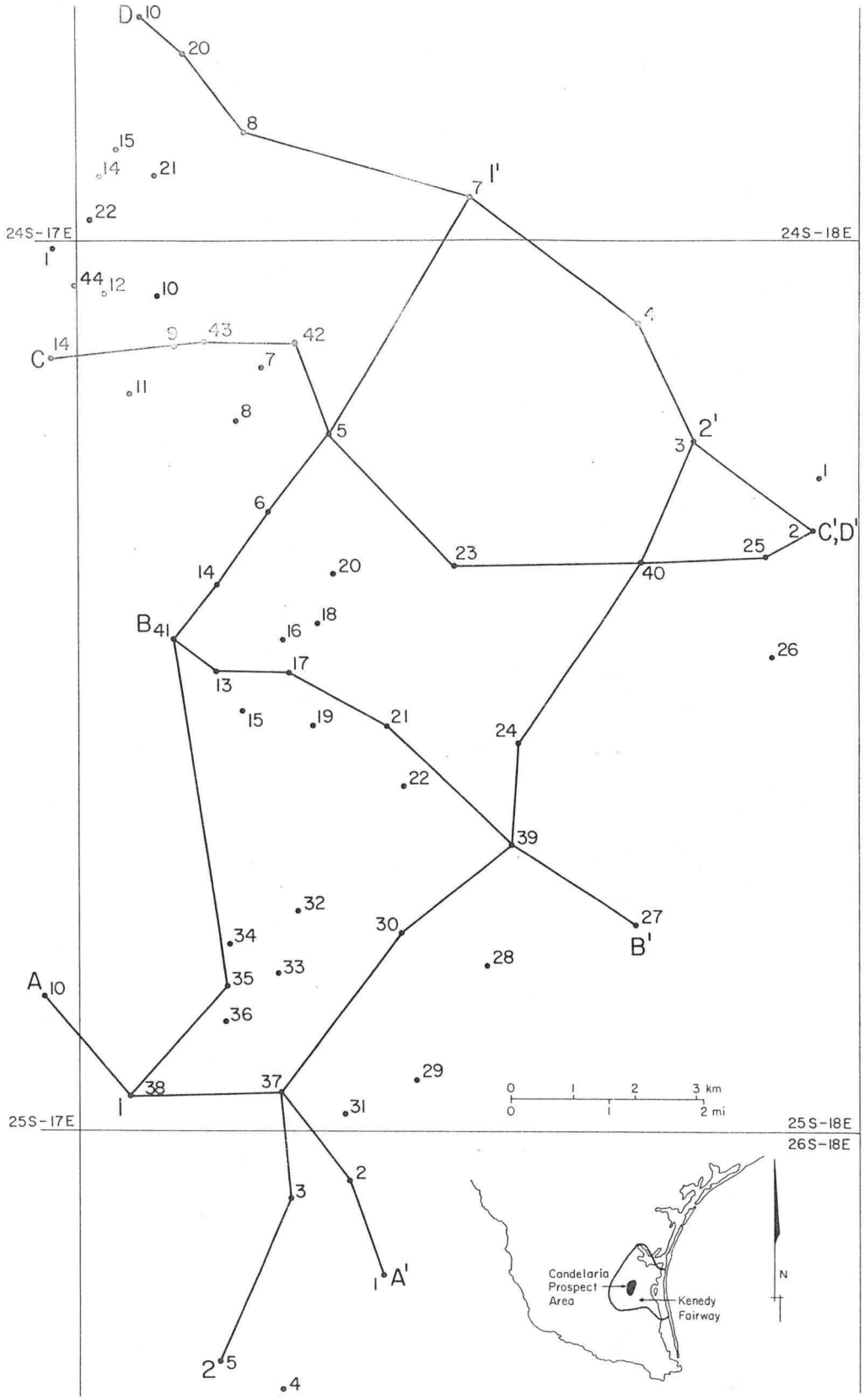

Figure 141. Location of wells and lines of cross section, Candelaria Prospect Area.

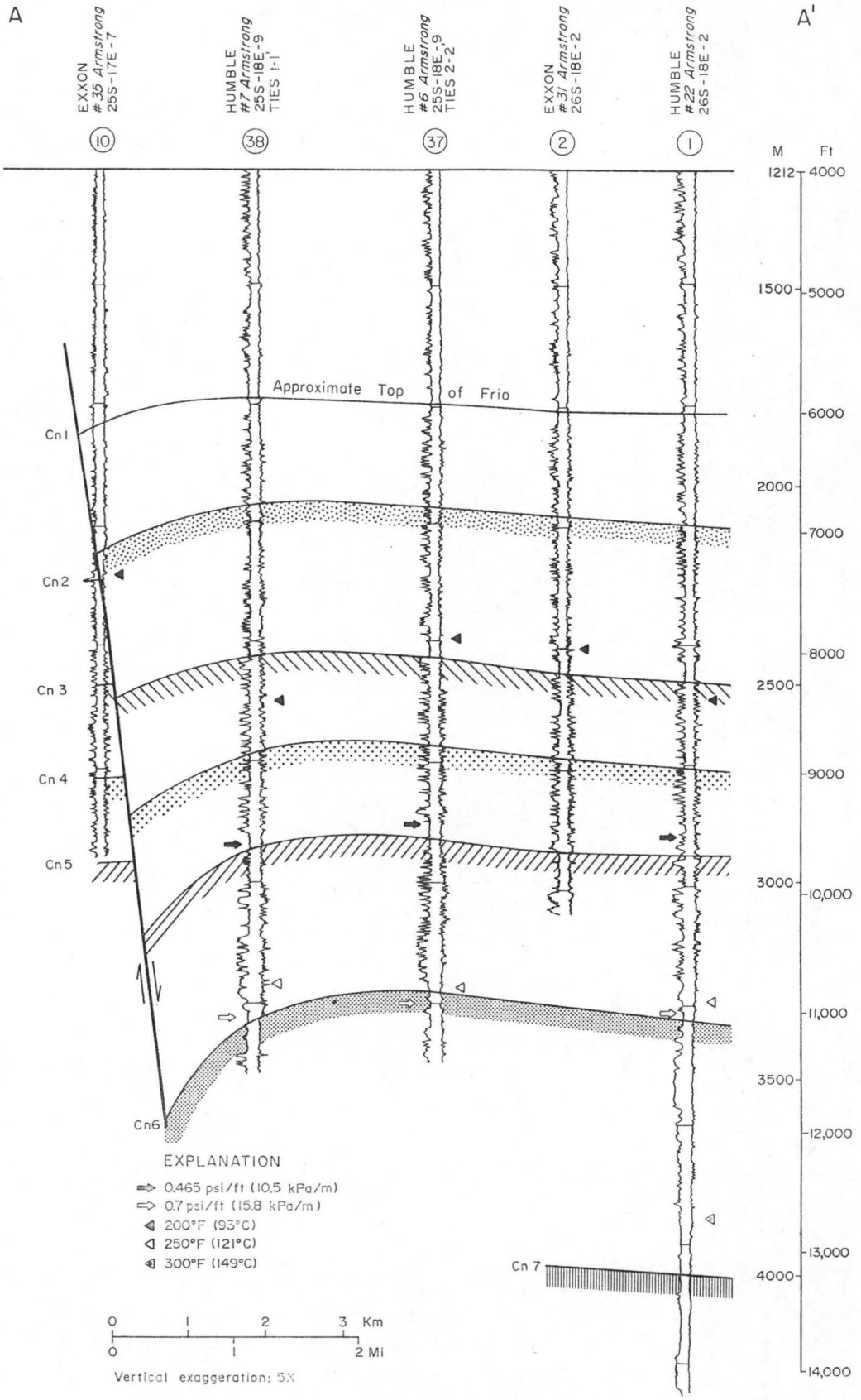

Figure 142. Structural dip section A-A', Candelaria Prospect Area.

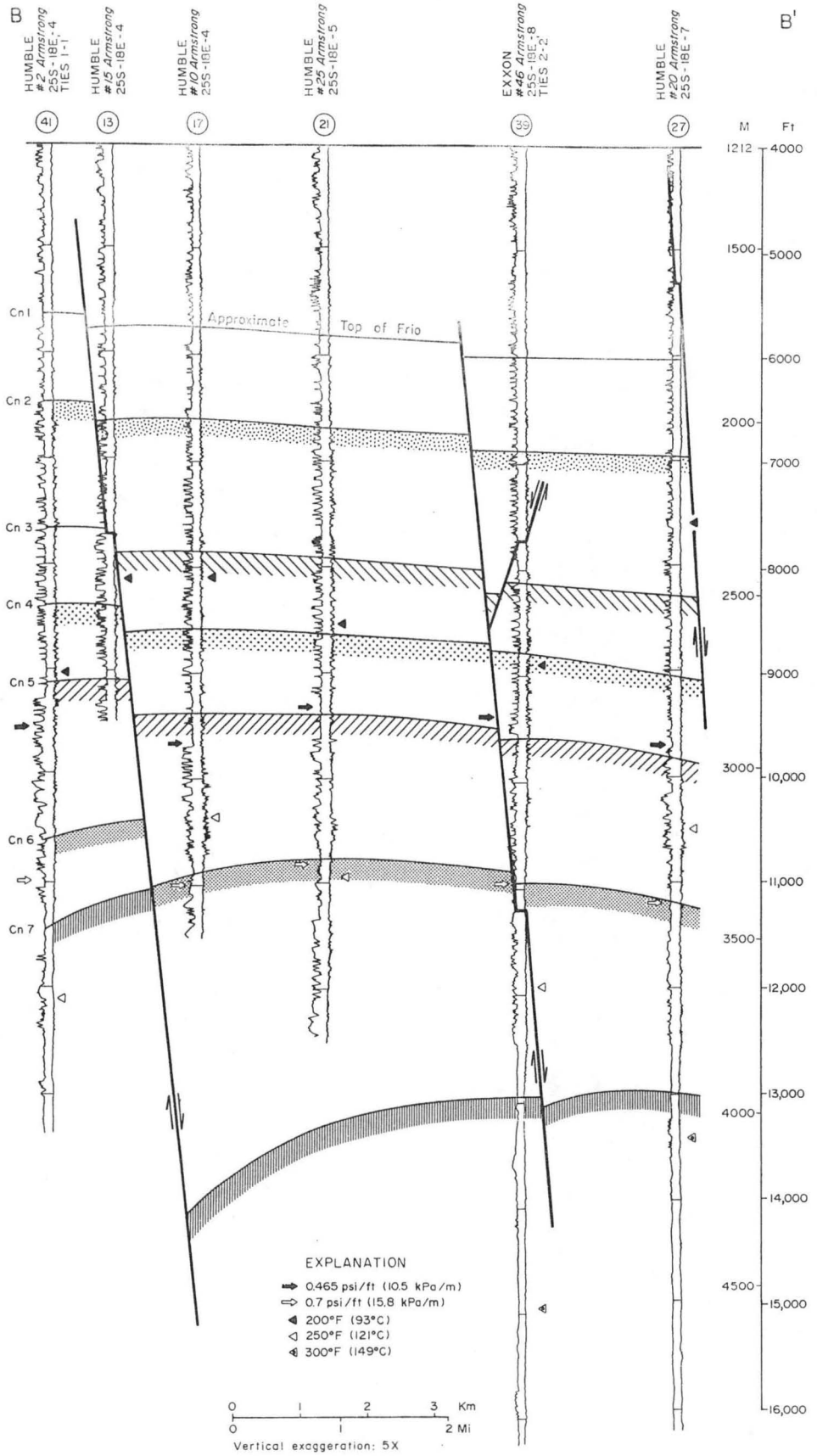

Figure 143. Structural dip section B-B', Candelaria Prospect Area.

Figure 144. Structural dip section C-C', Candelaria Prospect Area.

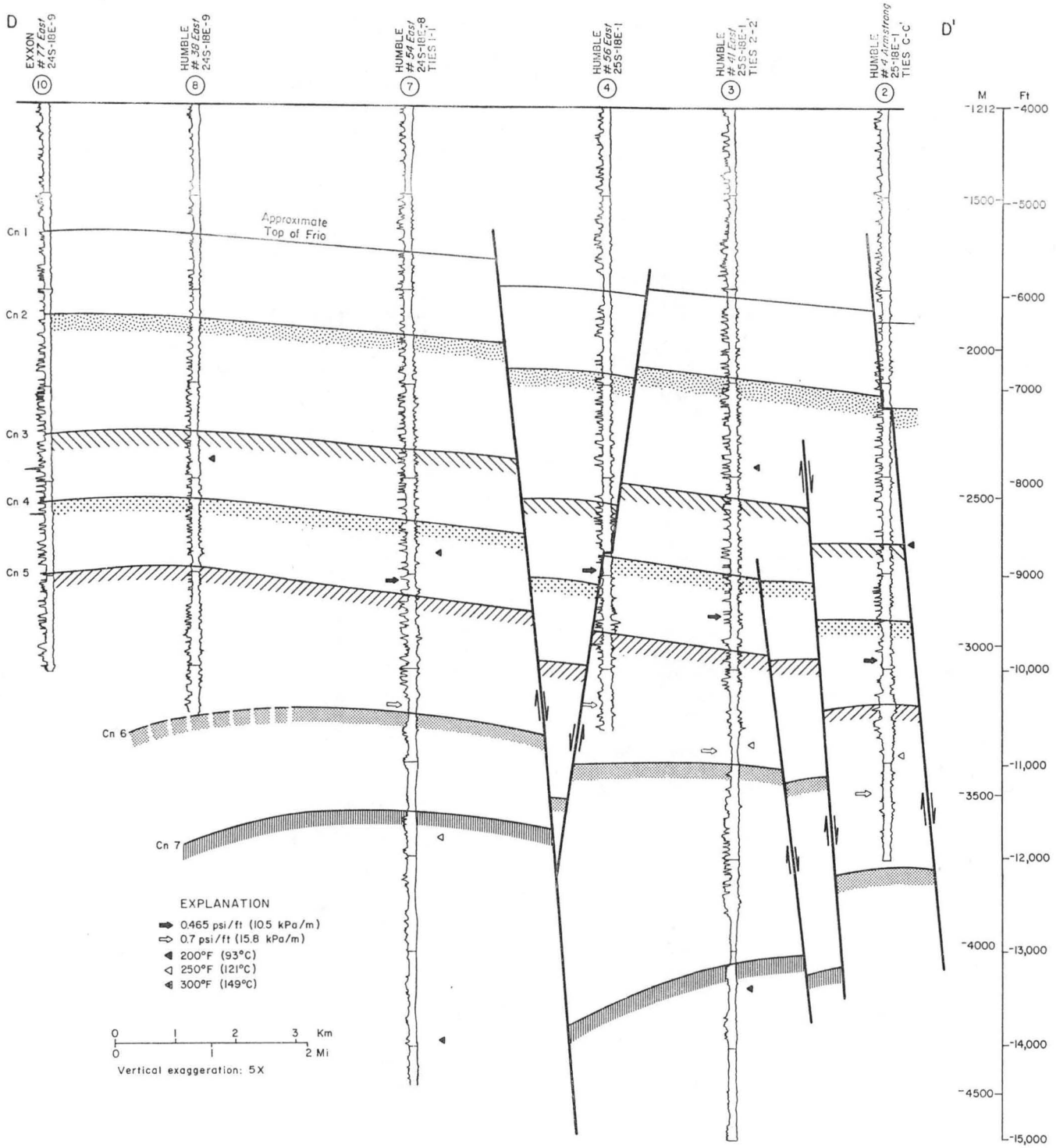

Figure 145. Structural dip section D-D', Candelaria Prospect Area.

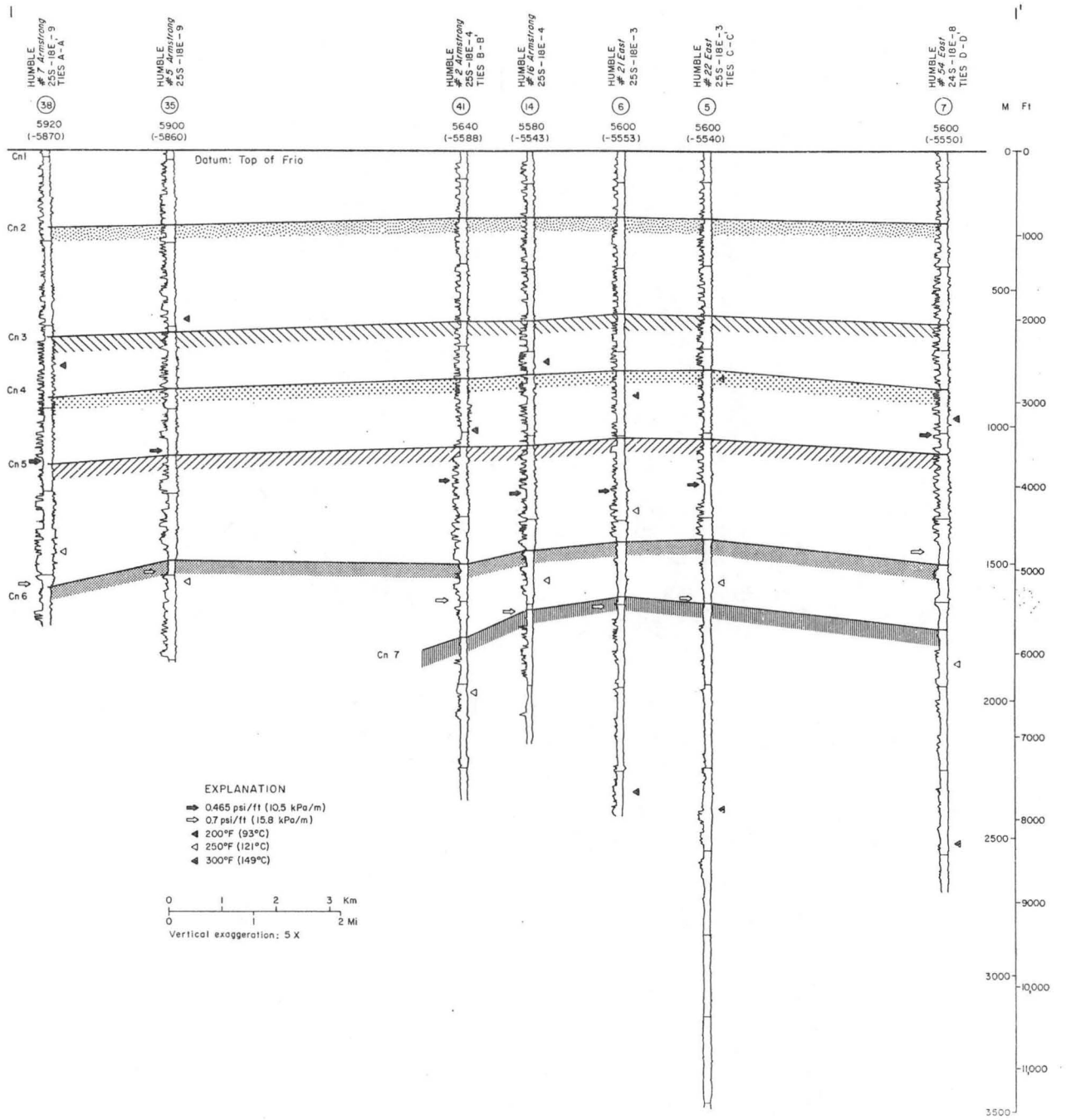

Figure 146. Stratigraphic strike section 1-1', Candelaria Prospect Area.

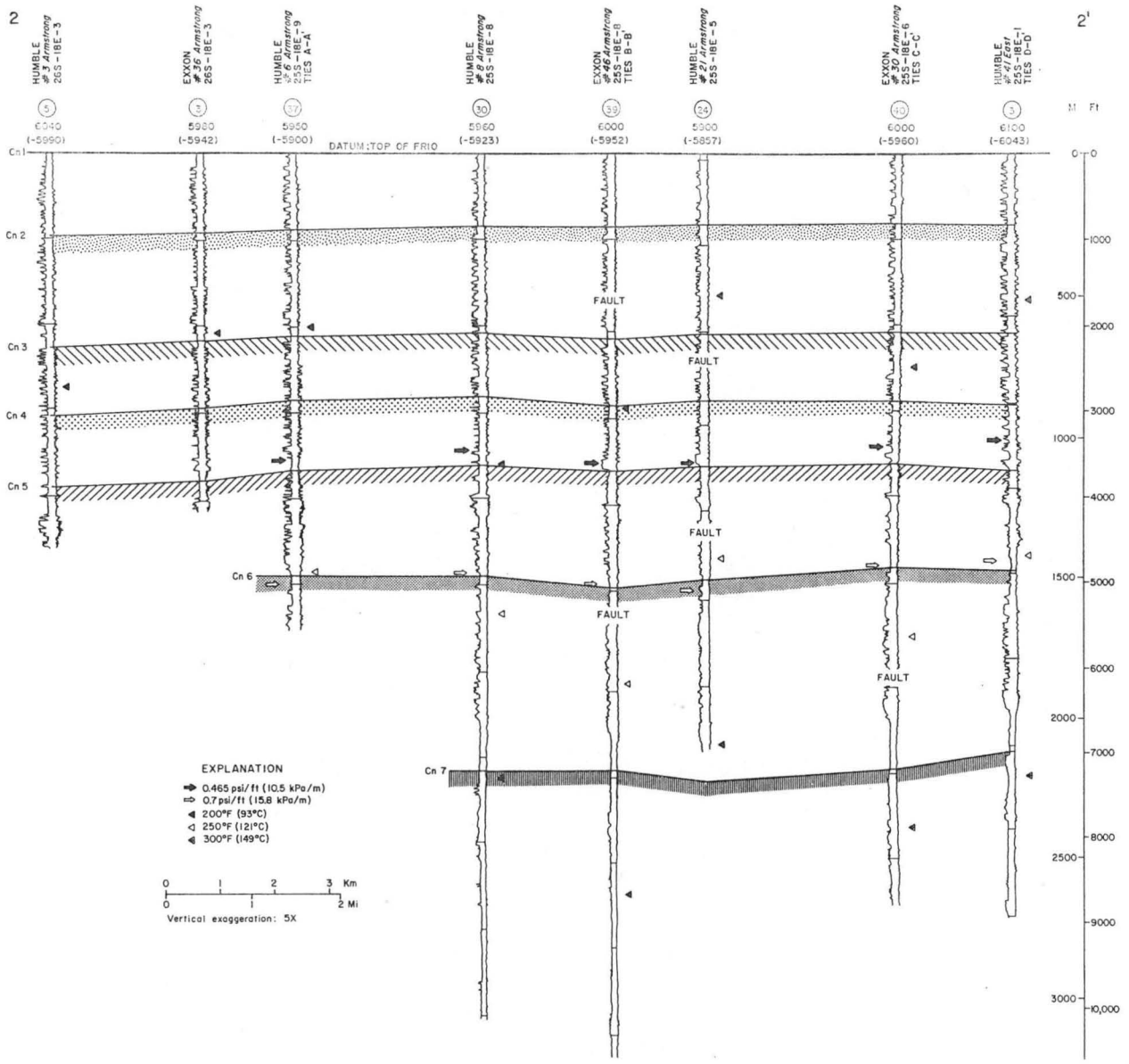

Figure 147. Stratigraphic strike section 2-2', Candelaria Prospect Area.

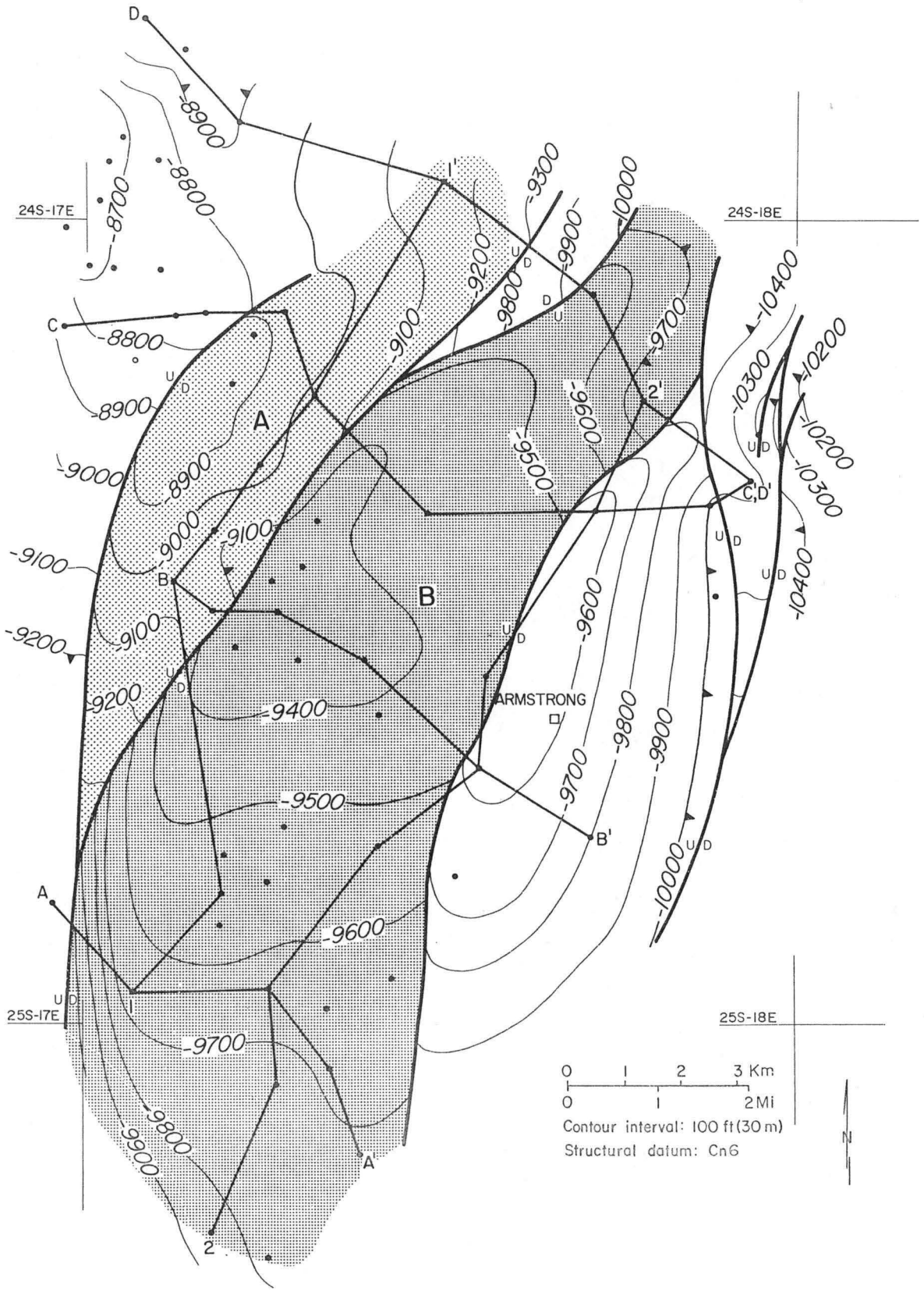

Figure 148. Structure on top of the Cn6 marker, Candelaria Prospect Area, Kenedy Fairway. Fault blocks of primary interest are labeled A and B.

in the Sarita area. Instead, delta-plain facies and a few progradational deltaic deposits predominate through the entire upper section. This may indicate that during the transgression from middle to upper Frio, the Candelaria area was updip of and lateral to a major center of deposition located near the Sarita area.

The Cn1 marker occurs at depths ranging from 5,400 to 6,300 ft within the Candelaria area (figs. 142 to 145). The Cn1 to Cn2 interval, approximately 900 ft thick, averages 300 ft of net sandstone through the area with dip-aligned highs (greater than 500 ft) in the southern part of the area (fig. 149). Thin sandstones (10 to 50 ft) separated by shales characterize this interval; because of rapid facies changes, individual sandstone bodies are not laterally persistent.

The Cn2 marker occurs at depths ranging from 6,300 to 7,200 ft. The Cn2 to Cn3 interval, approximately 1,300 ft thick, averages 500 ft of net sandstone with high values located in the center part of the area on the downthrown side of the major growth fault (fig. 150). The interval has sandstone characteristics similar to the Cn1 to Cn2 interval, but contains more sandstone, and some of the bodies are almost 100 ft thick. Individual sandstones are difficult to correlate areawide because of rapid facies changes.

The Cn3 marker occurs at depths ranging from 7,500 to 8,700 ft throughout the area. The Cn3 to Cn4 interval, approximately 800 ft thick, averages 350 ft of net sandstone, with the maxima (greater than 400 ft) occurring on the downthrown side of the local growth faults (fig. 151). The Cn3 to Cn4 interval is characterized by numerous sandstones 10 to 50 ft thick, separated by shales. As in the overlying intervals, the individual sandstones do not correlate well laterally, but the interval as a unit can be traced throughout the prospect area.

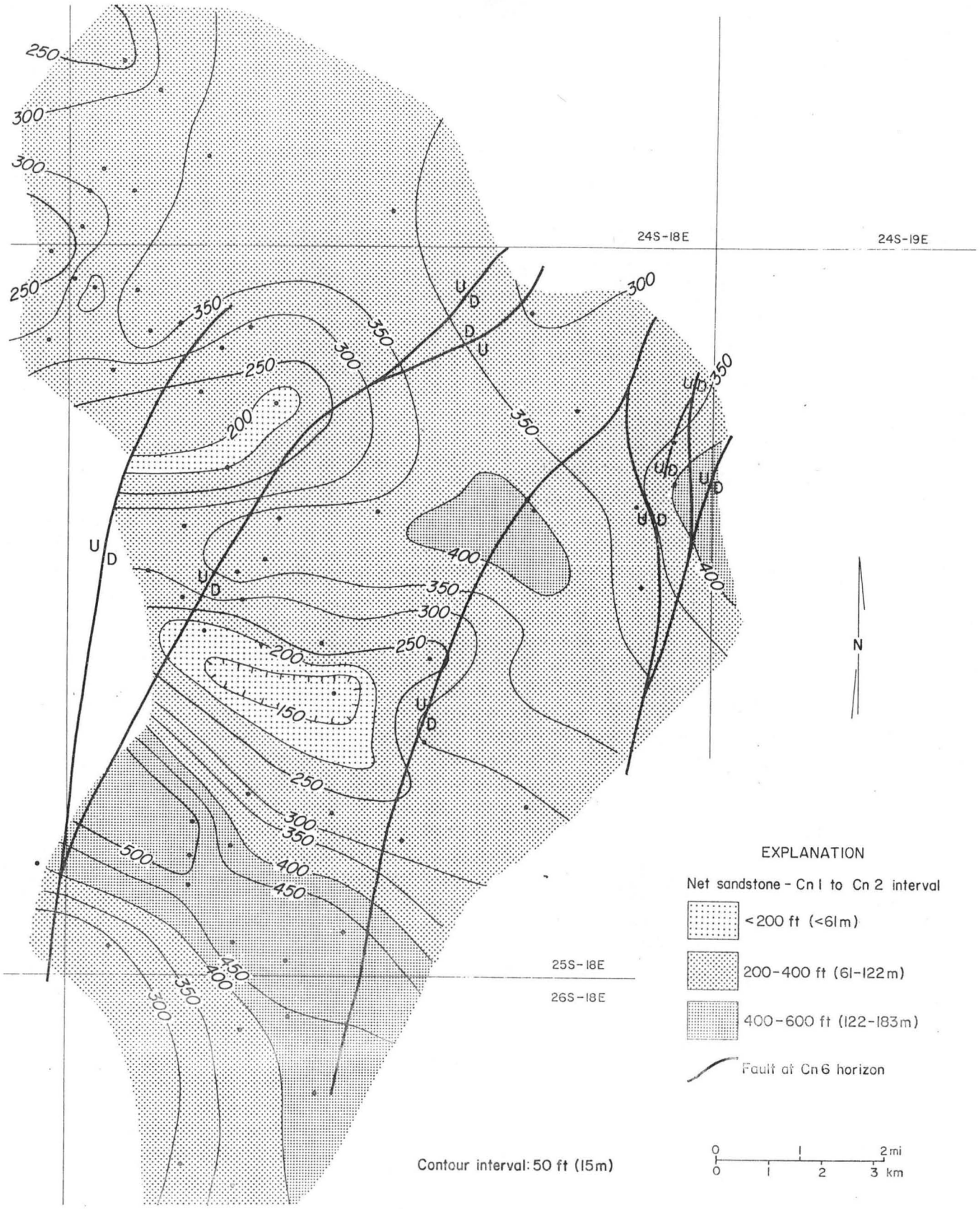

Figure 149. Net sandstone between correlation markers Cn1 and Cn2, Candelaria Prospect Area.

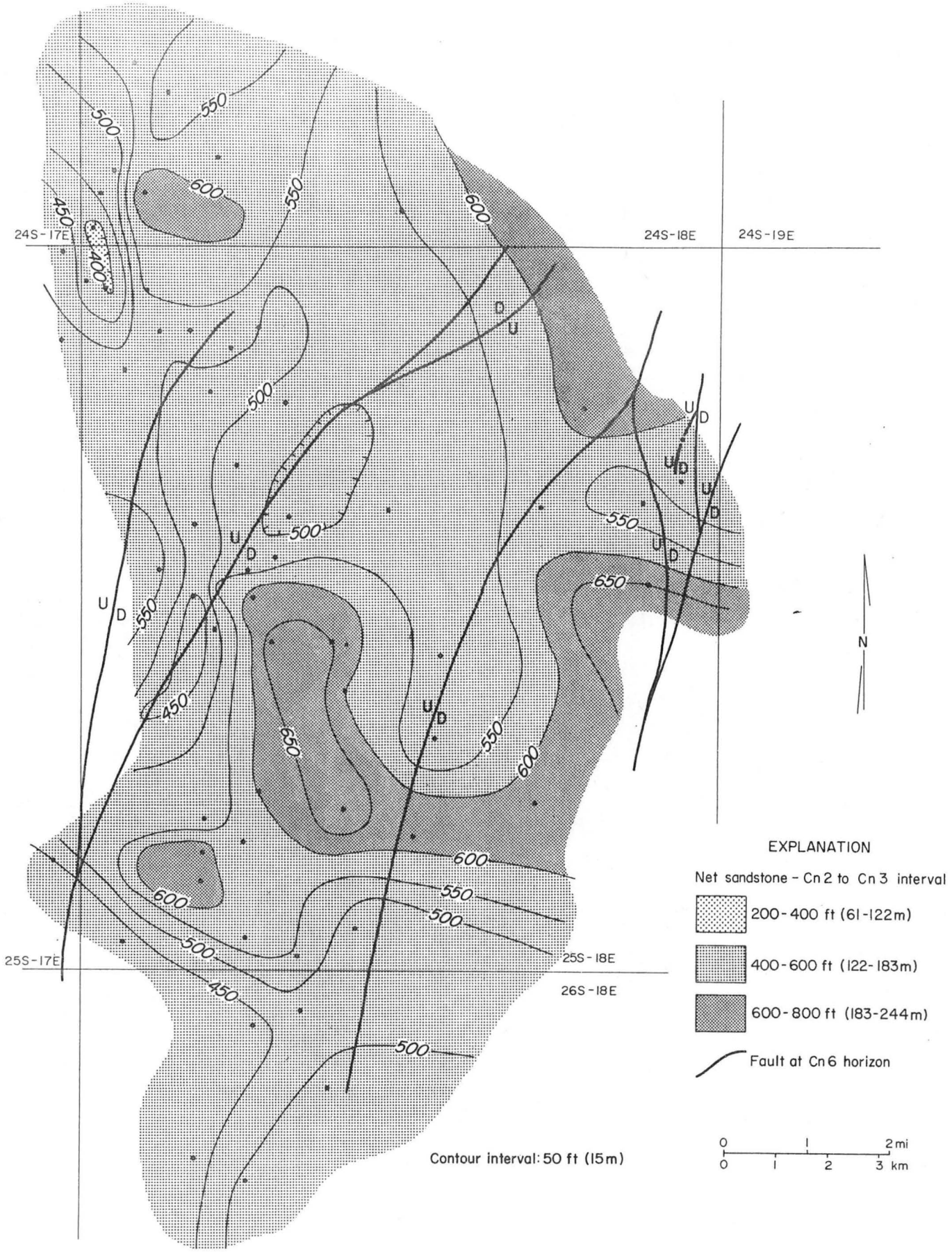

Figure 150. Net sandstone between correlation markers Cn2 and Cn3, Candelaria Prospect Area.

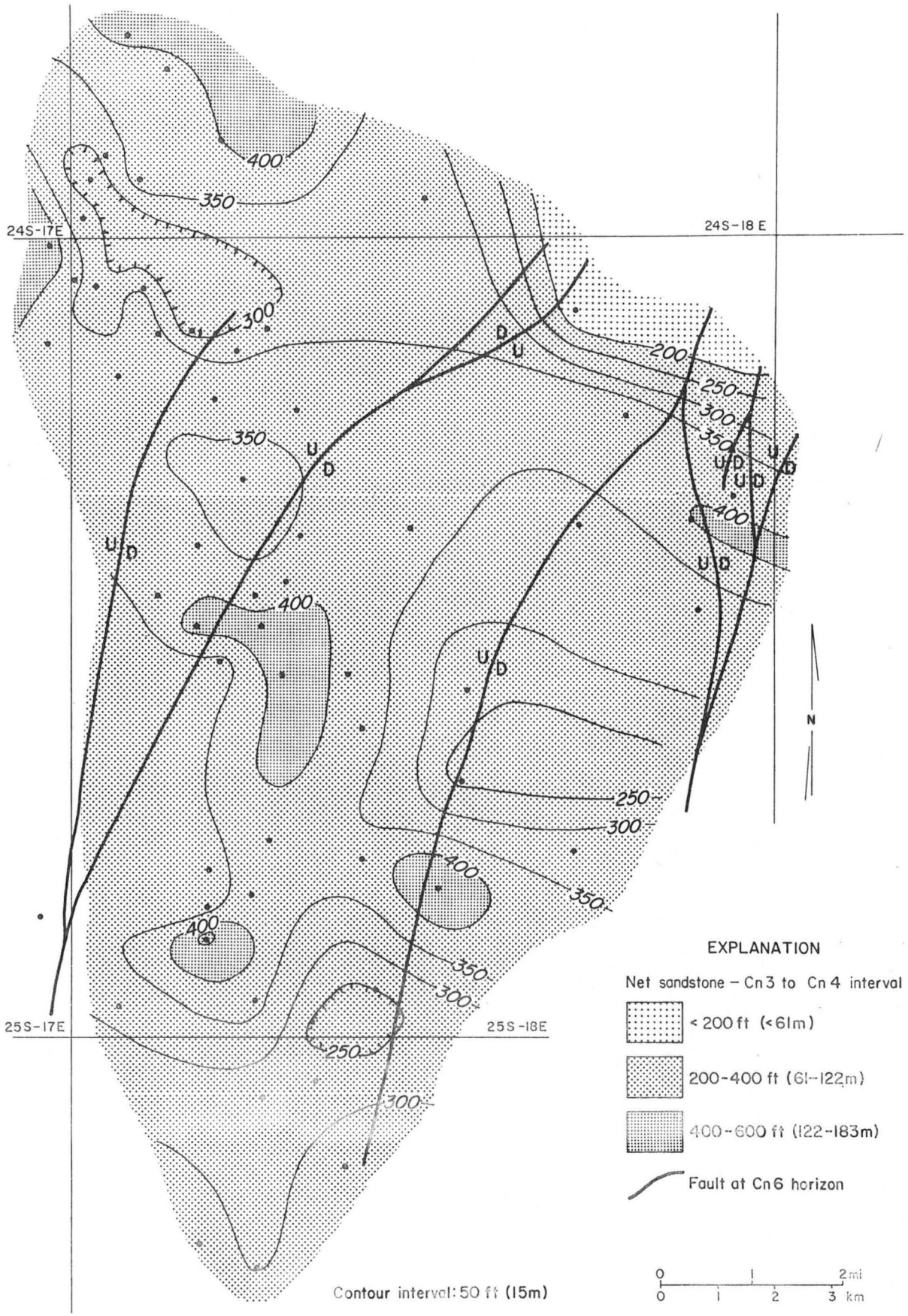

Figure 151. Net sandstone between correlation markers Cn3 and Cn4, Candelaria Prospect Area.

The Cn4 marker occurs at depths ranging from 8,250 to 9,400 ft. The Cn4 to Cn5 interval, approximately 700 ft thick, averages 250 ft of net sandstone distributed fairly uniformly across the area (fig. 152). The vertical character of this interval is similar to the intervals above, with two exceptions. First, interval Cn4 to Cn5 is slightly shalier than intervals Cn3 to Cn4 and Cn2 to Cn3. Second, in the downdip part of the prospect area is an anomalously large sandstone unit (100 ft thick) that has a blocky SP pattern; this unit is traceable only a short distance along strike (fig. 147).

The Cn5 marker occurs at depths ranging from 9,000 to 10,350 ft in the Candelaria area. The Cn5 to Cn6 interval, approximately 1,300 ft thick, averages 600 ft of net sandstone. This interval, which generally falls within the B Zone, displays the widest variation of net-sandstone values, exceeding 800 ft updip and diminishing to less than 400 ft in certain areas downdip (fig. 153). This is the shallowest interval in the series to exhibit characteristics common to growth-faulted areas--expansion of the total section on the downthrown side of the fault and counter-regional dip ("rollover") against the bounding fault (fig. 142). Updip, interval Cn5 to Cn6 contains thick (50 to 150 ft) upward-coarsening sequences that persist within the small fault block traversed by section 1-1' (fig. 146). Downdip to the east, these units become shalier, especially in the northern part of the area (fig. 147).

Markers Cn7 through Cn9 bound intervals within the C Zone. Most sandstones below marker Cn10 occur within the D Zone. Few wells penetrate these deep intervals, and, consequently, net-sandstone maps and further discussion of intervals below the Cn6 marker are not included in this report.

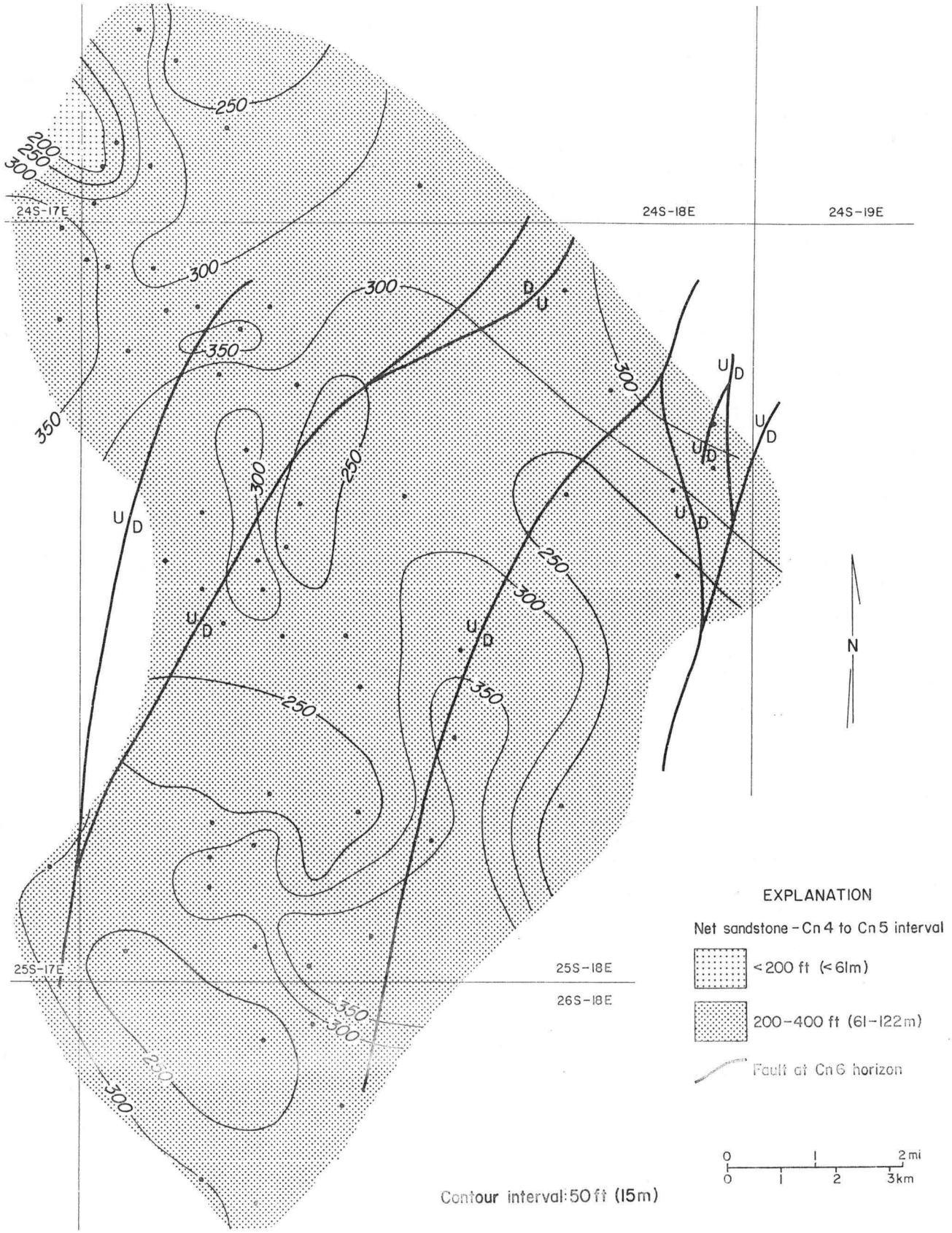

Figure 152. Net sandstone between correlation markers Cn4 and Cn5, Candelaria Prospect Area.

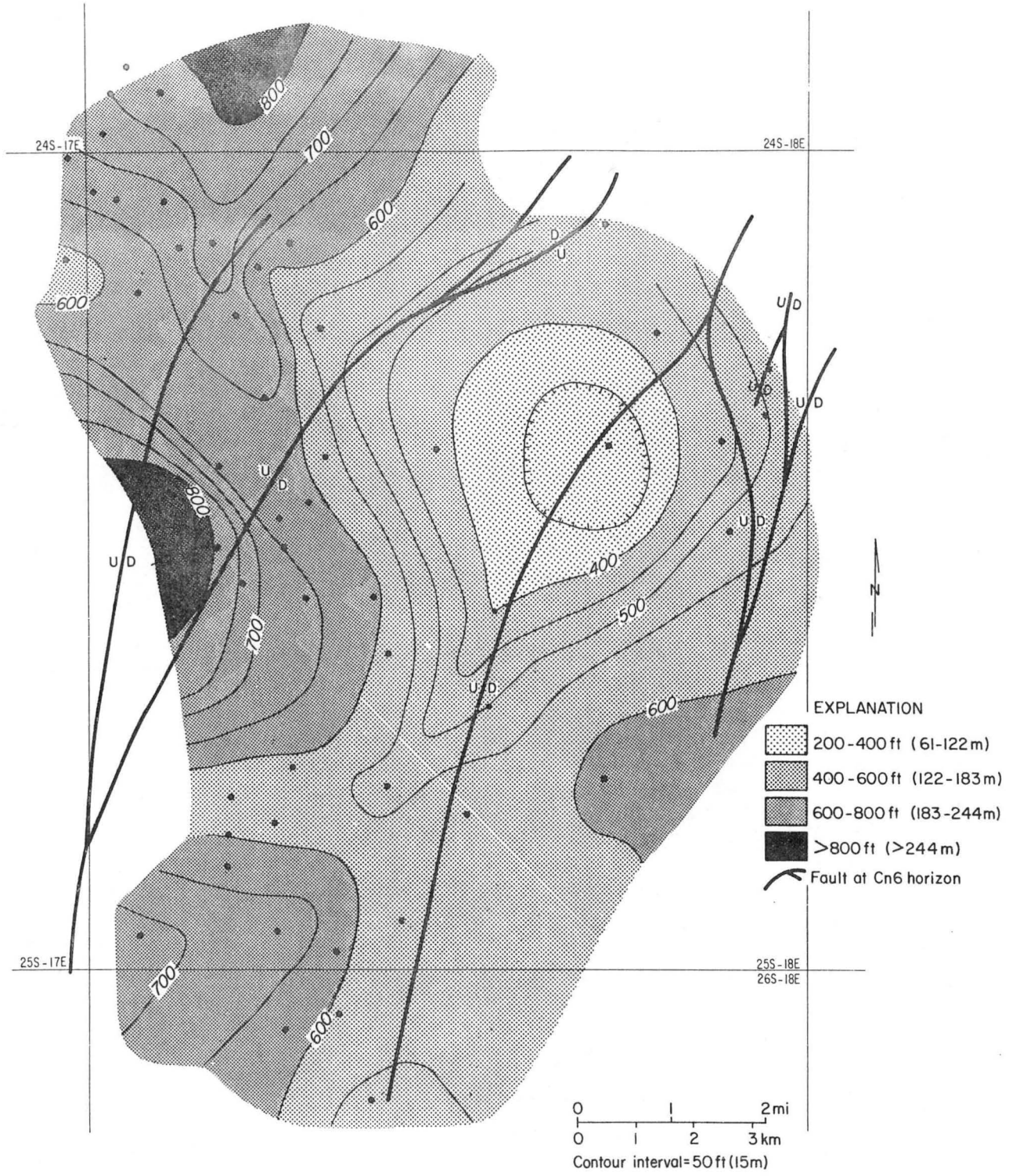

Figure 153. Net sandstone between correlation markers Cn5 and Cn6, Candelaria Prospect Area.

Formation parameters

Thickness of the B Zone in the Candelaria Prospect Area is 1,450 ft, as determined from bottom-hole shut-in pressures in production wells in Kenedy County (fig. 154). There were not enough BHSIP data from within the prospect area to determine pressure gradients; therefore, it was necessary to use data from wells in other parts of Kenedy County. The depth to the top of the B Zone determined from BHSIP versus depth (fig. 154) is 9,050 ft. However, a plot of equilibrium temperature versus depth (fig. 155) indicated the top of geopressure is at a depth of 9,800 ft. Where differences exist between these two methods for locating the top of the B Zone, the method using BHSIP data is preferred. The base of the B Zone occurs at a depth of 10,500 ft, and the base of the C Zone is at a depth of 13,500 ft.

The geothermal gradient in the Candelaria area is 1.38° F/100 ft in the hydropressured zone and increases to 2.02° F/100 ft in the geopressured zone. Below a depth of 14,750 ft the geothermal gradient declines to 1.36° F/100 ft, which approximates the gradient in the hydropressured zone. The dogleg geothermal gradient indicates that zones with relatively high thermal conductivities exist above and below the geopressured zone (a heat insulator).

Most salinities are less than 100,000 ppm NaCl in the prospect area (fig. 156). A general trend of salinity decreasing with depth is observed in the B Zone.

Potential for testing

The Candelaria area is segmented into several small fault blocks which were considered for the location of a test-well site. Two of these fault blocks are of particular interest: the largest fault block (B), located in the center of the prospect area, and the block (A) immediately updip of it (fig. 148). A specific test-well site was not selected for either of these

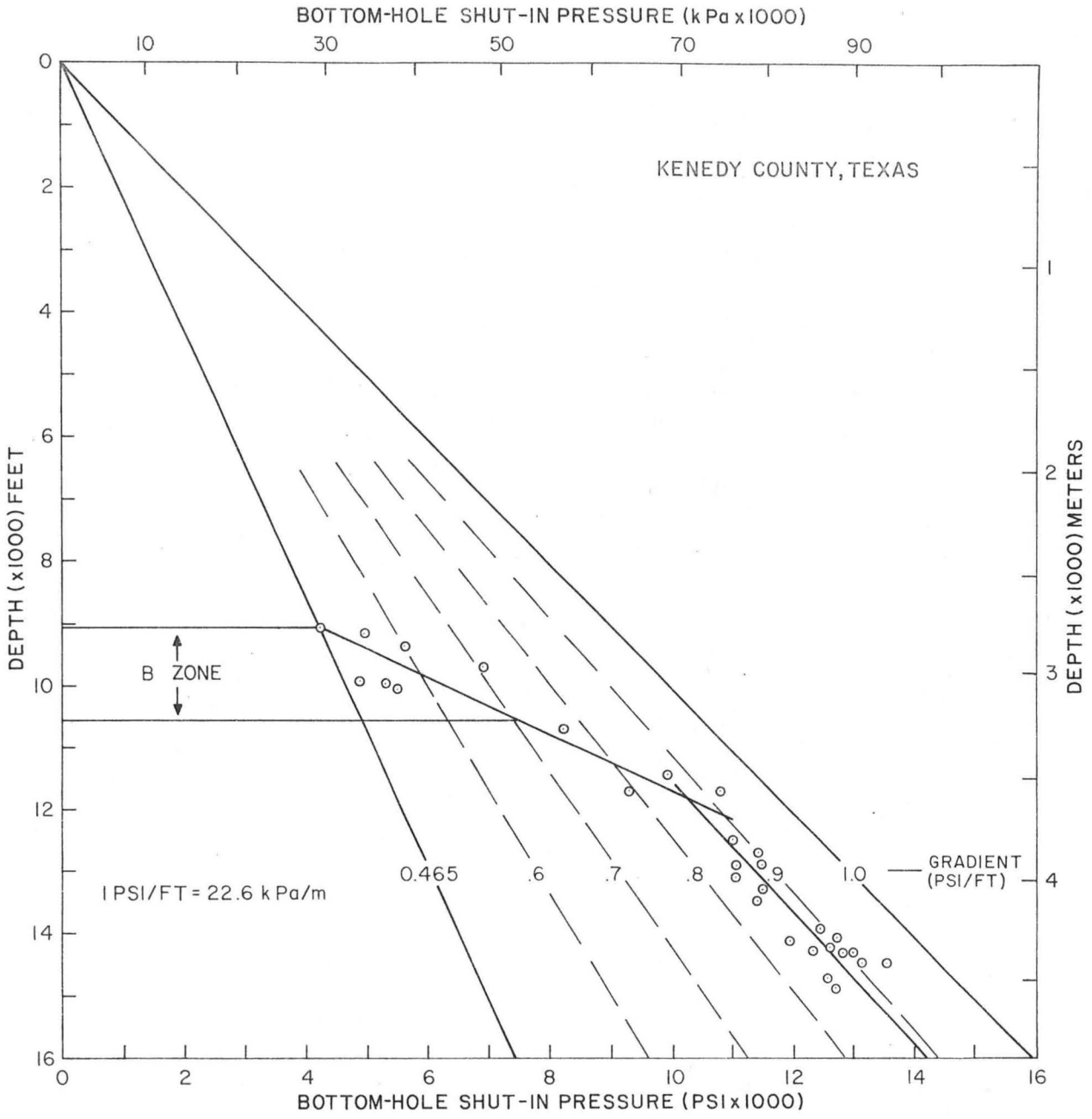

Figure 154. Bottom-hole shut-in pressures from drill-stem tests for production wells in Kenedy County, Texas.

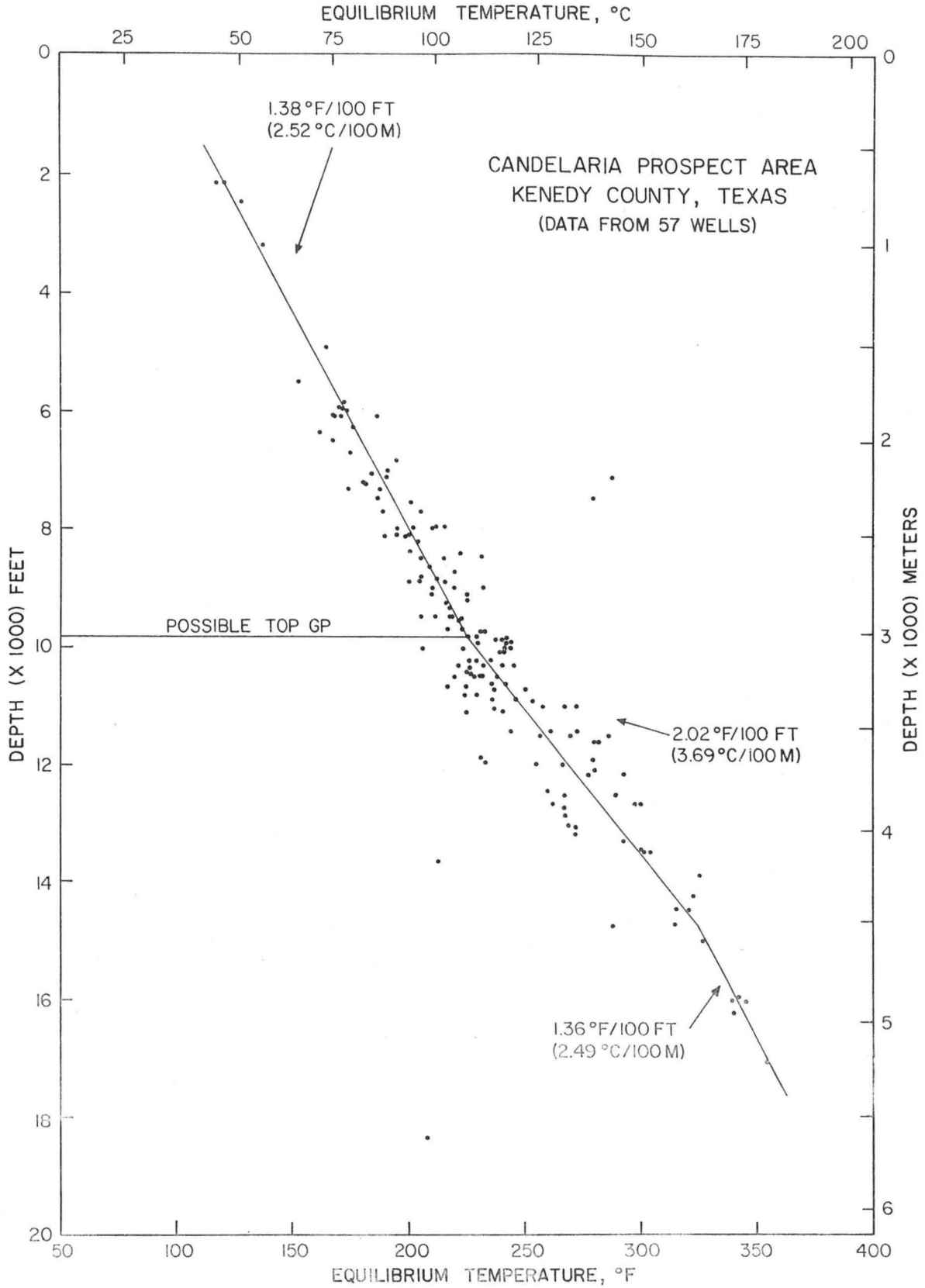

Figure 155. Plot of equilibrium temperature versus depth, showing geothermal gradients in the Candelaria Prospect Area, Kenedy County, Texas.

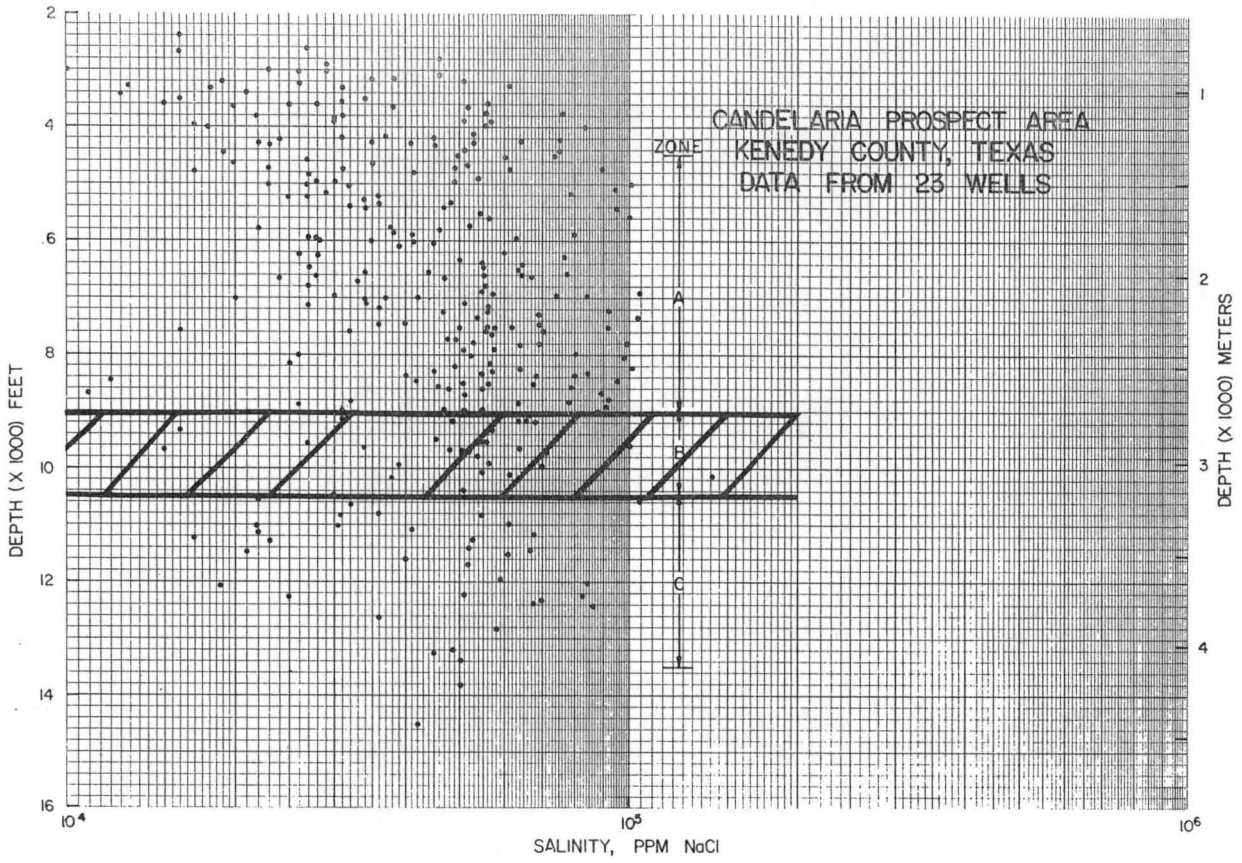

Figure 156. Salinity versus depth for 23 wells, Candelaria Prospect Area, Kenedy County, Texas.

areas because whole-core porosity and permeability data were unavailable. However, these areas should remain potential candidates for a test-site location, and, therefore, a general description of each fault block has been included.

Fault block A.--Fault block A covers approximately 15 mi^2. The fault defining the western (updip) side of the block has a vertical displacement of 50 ft at the Cn6 marker, and the fault on the downdip side has a displacement of 350 ft at the same marker. These two faults converge toward the south, forming a southern closure to the fault block. The northern extent of the faults is unknown because of an area of very sparse well control. Seismic data would be needed for structural analysis.

Within the fault block, the top of the B Zone occurs at a relatively constant depth, ranging from 9,000 to 9,750 ft. Prospective reservoir sandstones of the B Zone are those of the Cn5 to Cn6 interval, the top of which occurs at depths ranging from 8,900 to 9,100 ft. The base of the prospective interval occurs at depths ranging from 10,200 to 10,700 ft. The prospective sandstone beds range from 10 to 200 ft thick. In well No. 41, section 1-1' (fig. 146), the sandstone bodies are thickest and yield the maximum net-sandstone value. The total interval thins slightly from 1,400 to 1,150 ft along strike to the northeast. The individual sandstone beds are fairly continuous through most of the fault block, although facies changes alter the SP character and bed thicknesses laterally (fig. 146). The few net-sandstone data (few wells penetrate the entire interval) indicate highest values are in the south-central part of the block where they exceed 800 ft. To the northeast, the values decrease to a minimum of 500 ft (fig. 153).

Fault block B.--Fault block B is in the central part of the Candelaria Prospect Area (fig. 148), extending over an area of 37 mi^2. The fault

block is within the Candelaria oil and gas field, and coincides with the area selected as a potential geothermal prospect by Bebout and others (1978b). The fault defining the western (updip) side of the block has approximately 350 ft of vertical displacement at the base of the prospective reservoir section (Cn6); the fault on the eastern (downdip) side has an approximate displacement of 100 ft at the same marker.

Within the fault block, the top of the B Zone occurs at depths ranging from 8,950 to 9,700 ft. Net-sandstone values are lower overall in fault block B than in block A, with maximum values of about 700 ft nearest the updip fault. Along strike to the northeast, values decrease to 400 ft as the sandstone units thin (fig. 147). Within fault block B, the sandstones of interest are most commonly beds 10 to 100 ft thick. Thickest sandstones occur in the southern end of the mapped part of the fault block near well Nos. 5 and 37 on section 2-2' (fig. 147). Thinning occurs along strike to the northeast and downdip (well No. 3, fig. 145), where the entire section becomes more shaly.

Cameron Fairway and Tordilla Prospect Area

The Cameron Fairway is the southernmost shallow geopressured fairway along the Frio trend (fig. 29). The fairway covers 2,720 mi^2 primarily in Cameron and Willacy Counties, and extends into parts of Hidalgo and Kenedy Counties. Cameron was designated a fairway and possible location of a prospect area because of the great amounts of Frio sandstone present in the B and C Zones (figs. 26 and 27). The Frio Formation in the Cameron Fairway is similar in lithology to the Frio in Kenedy Fairway, consisting primarily of deltaic or delta-related sandstones and shales. Also, the overlying Anahuac Formation in both Cameron and Kenedy Fairways contains

much more sandstone than the Anahuac in the Corpus Christi and Matagorda Fairways.

Regional cross sections constructed for the DOE methane assessment (Gregory and others, 1980), preliminary fairway cross sections, and 276 well logs (fig. 157; appendix C) were used to identify the fault blocks within the Cameron Fairway most prospective for shallow geopressured test sites. Much of the fairway was eliminated from further study because few wells were deep enough to penetrate the zones of interest. Only one prospect, Tordilla (initially named La Sal Vieja), was selected for detailed study.

The Tordilla Prospect occupies a north-south trending fault block at the boundary between Willacy and Kenedy Counties in the northern part of the Cameron Fairway (fig. 157). This prospect area, which covers at least 27 mi^2, lies along the same Frio fault trend as do the Candelaria and Sarita Prospects of the Kenedy Fairway to the north. One structural dip section (A-A'; fig. 158) and one stratigraphic strike section (B-B'; fig. 159) were constructed across the Tordilla and adjacent fault blocks (fig. 160).

Seven markers, To1 through To7 (fig. 159), were correlated in the prospect area. The To1 marker is at or near the Heterostegina-Marginulina zone and, for this report, is considered the approximate top of the Frio Formation. The boundary between the A and B Zones most commonly occurs above the To3 marker. The B-C boundary generally occurs between the To4 and To6 markers. Sandstones of primary interest in this study occur below the To5 marker in the B and C Zones. The B-C boundary (0.7 psi/ft) and the A-B boundary (0.465 psi/ft) are anomalously deep in the Humble No. 5 Kleberg (figs. 158 and 159). It is very likely that the shale resistivity plot underestimated pressure gradients for the well.

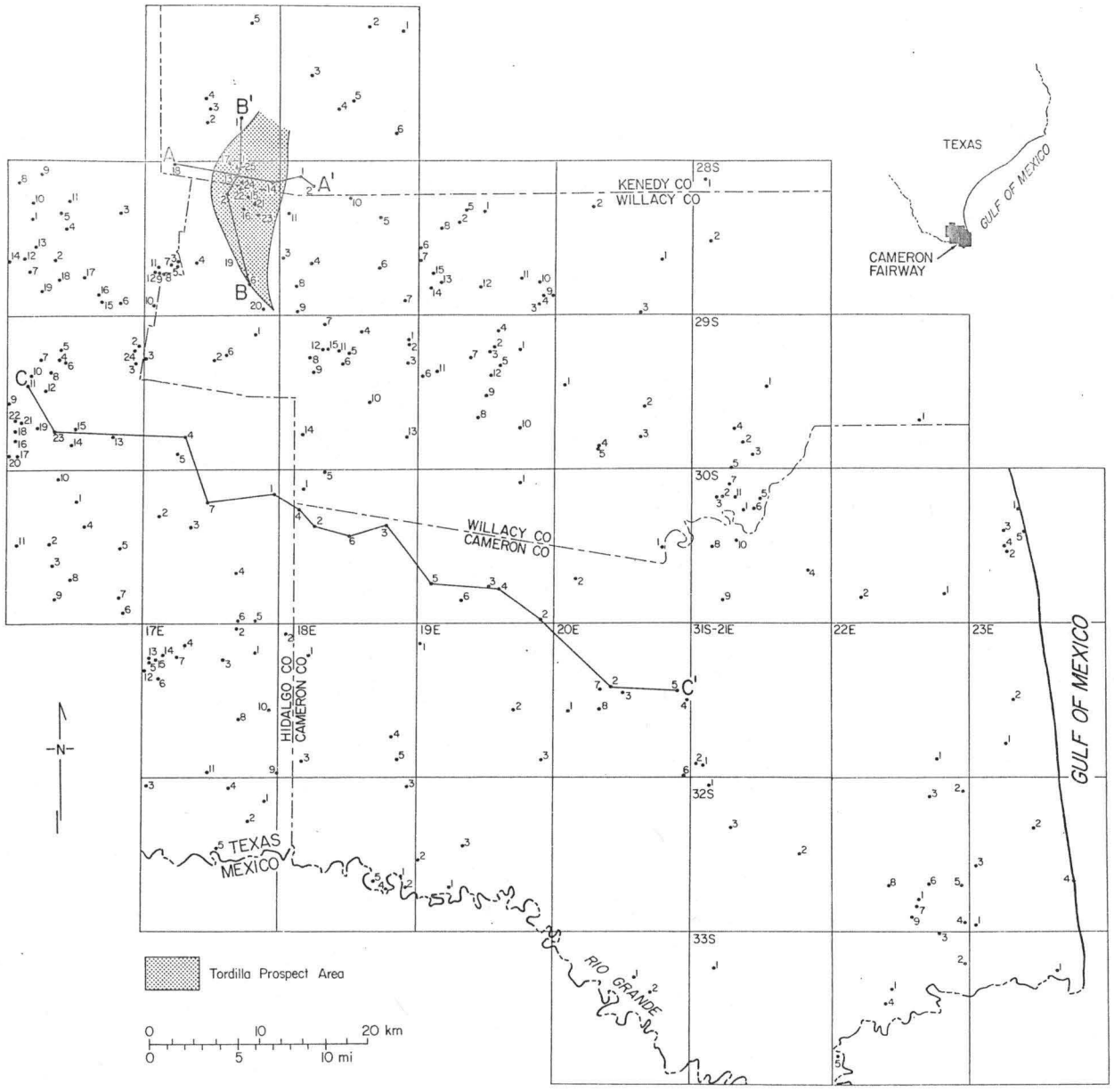

Figure 157. Well locations and lines of cross section, Cameron Fairway.

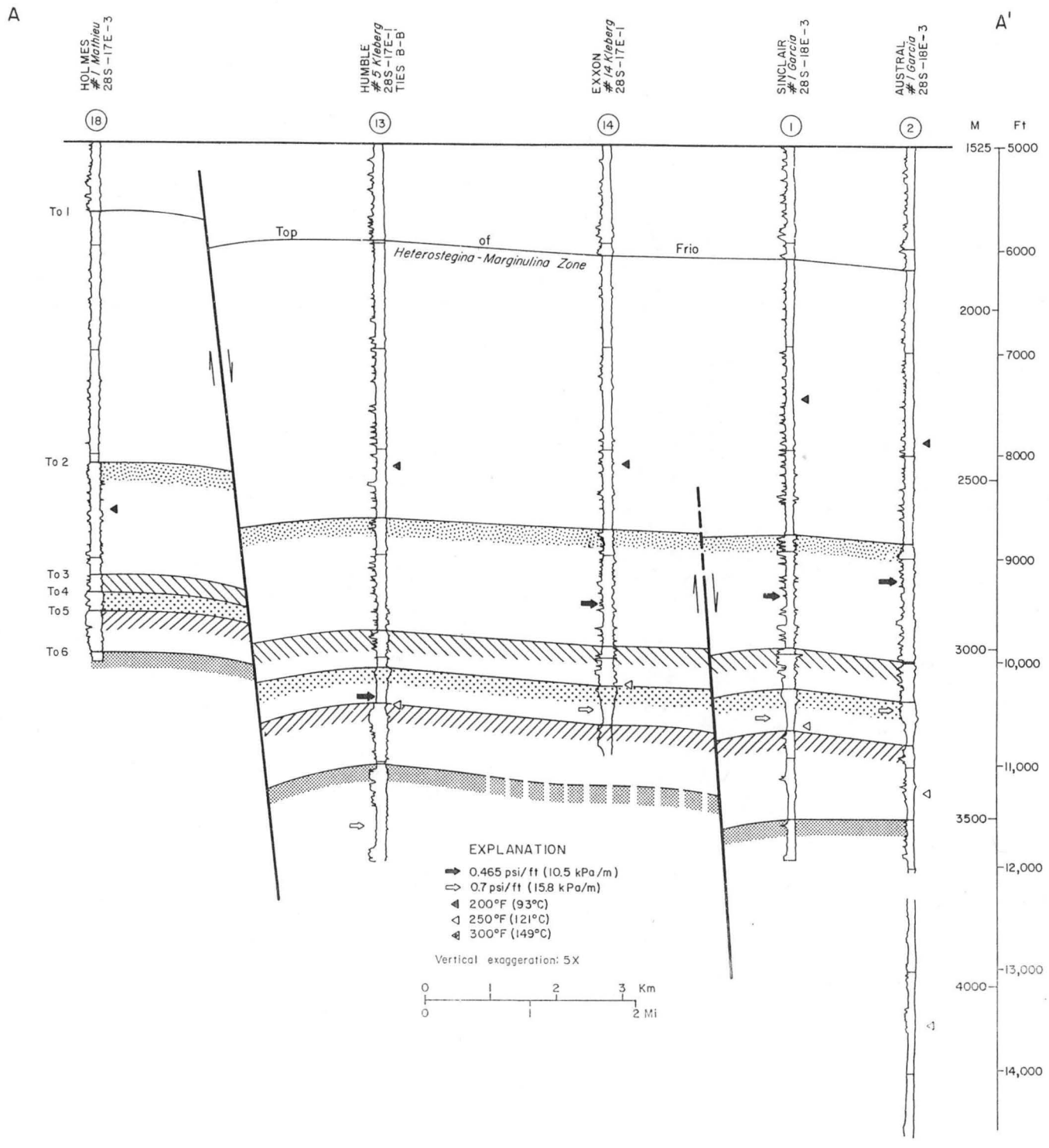

Figure 158. Structural dip section A-A', Tordilla Prospect Area.

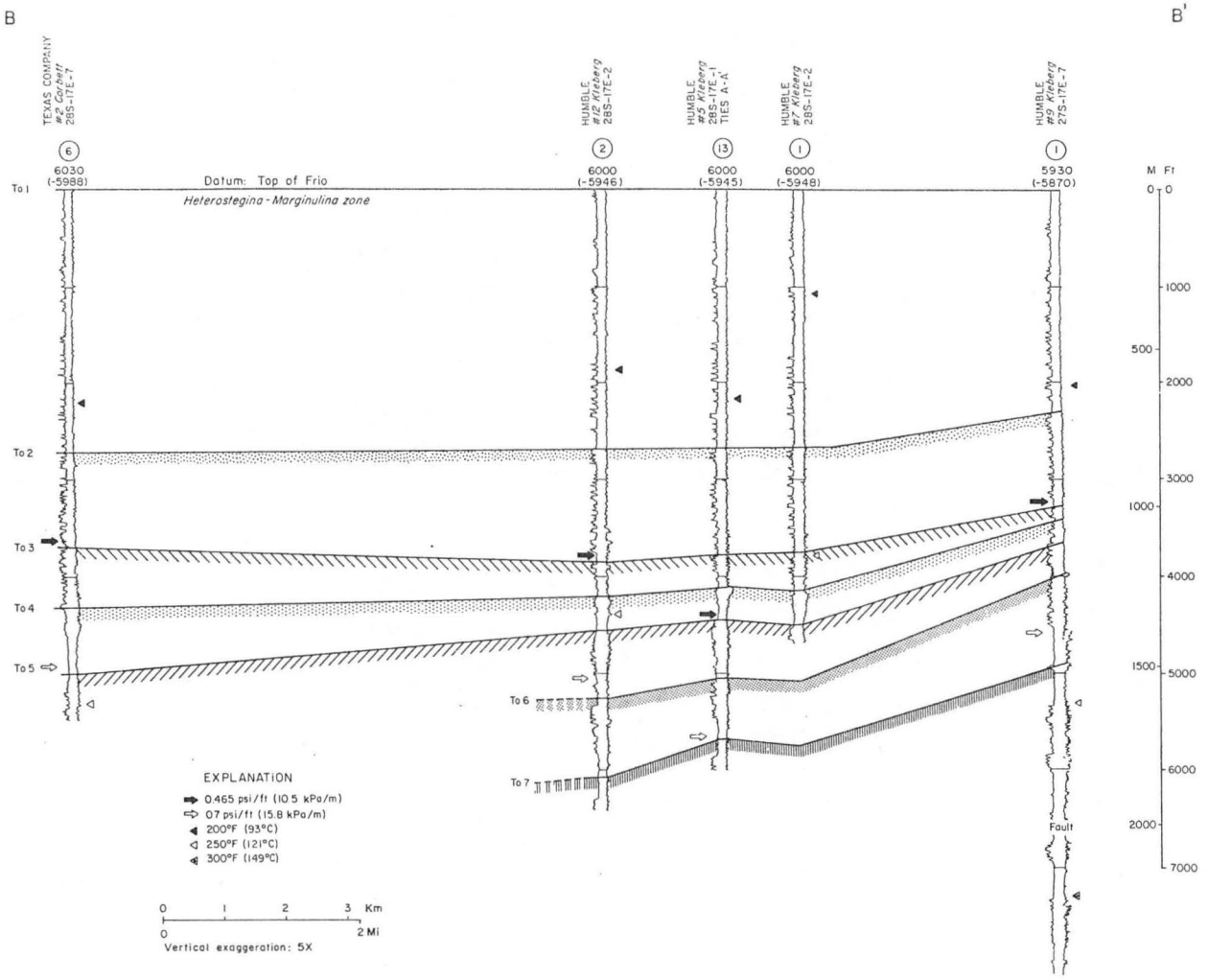

Figure 159. Stratigraphic strike section B-B', Tordilla Prospect Area.

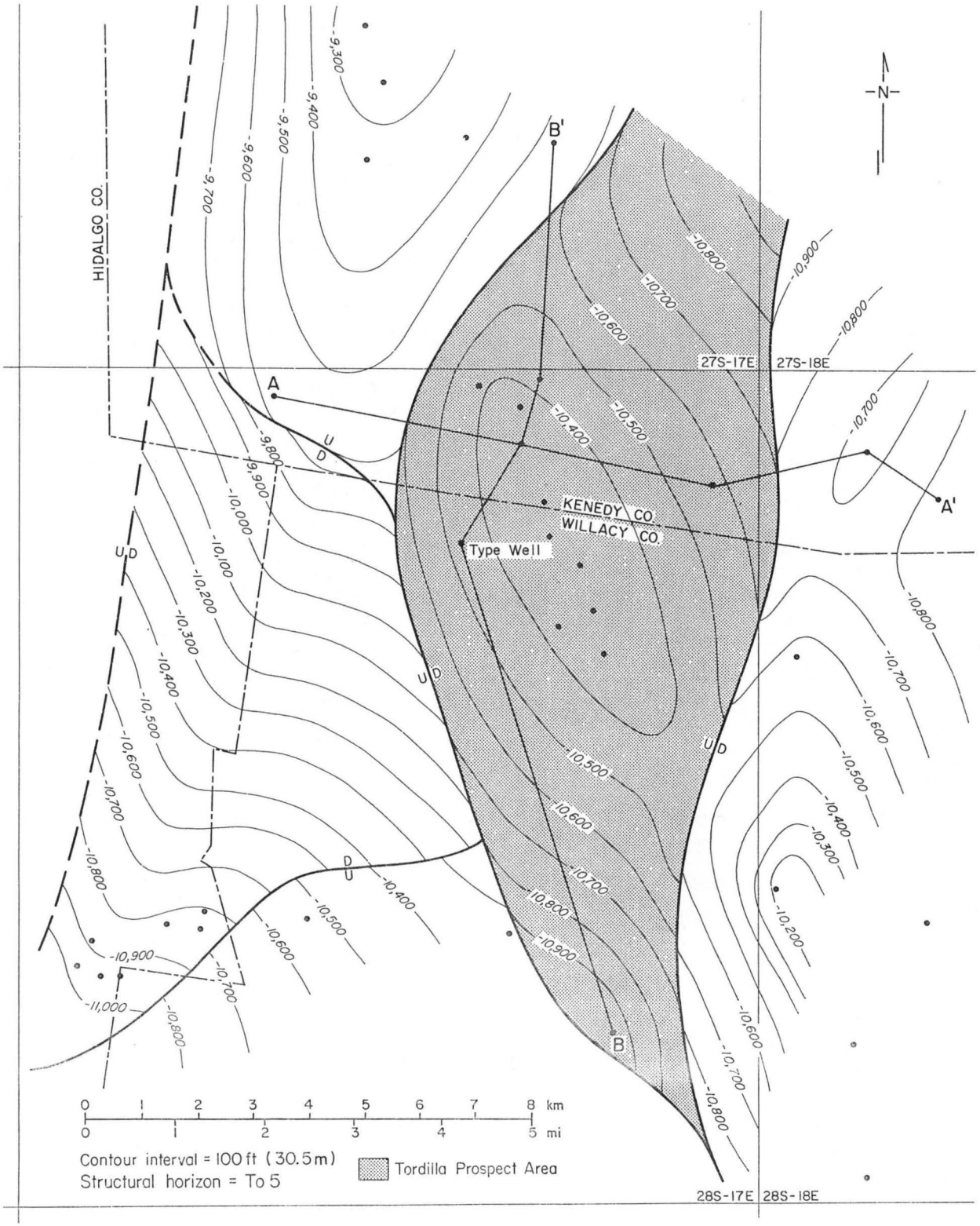

Figure 160. Structure on the To5 marker, Tordilla Prospect Area.

Structure

The Tordilla Prospect is bounded on the east and west by two growth faults that converge toward the south and form the southern boundary of the fault block. To the north, sparse well control prohibits sufficient structural analysis to define a boundary of the prospect area. Even if the structural block is continuous far to the north, however, individual reservoir sandstones probably would not extend north of the shaded area shown in figure 160.

Vertical displacement of the western bounding fault at the To5 marker along dip section A-A' (figs. 158 and 160) is estimated to be approximately 1,000 ft, with displacement probably decreasing to the south. The fault bounding the east side of the prospect area has a vertical displacement of about 100 ft at the To5 marker along section A-A', which is much smaller than that of the western fault. However, dip reversal and expansion of the section below To5 from well No. 2 to well No. 1 along section A-A' (fig. 158) indicate that the displacement of this eastern fault increases with depth.

The dominant structural feature within the prospective fault block is a large anticline, probably a rollover anticline associated with the western bounding fault (fig. 160). Most of the well data used to evaluate the prospect are from the Tordilla oil and gas field that was developed on this anticline in the central part of the fault block. All Frio hydrocarbon production in the Tordilla Field is from sandstones between the To1 and To4 correlation markers (figs. 158 and 159).

Sandstone Distribution and Characteristics

In the Tordilla Prospect the upper Frio interval between To1 and To4 (figs. 158, 159, and 161) is characterized by aggradational deposits that

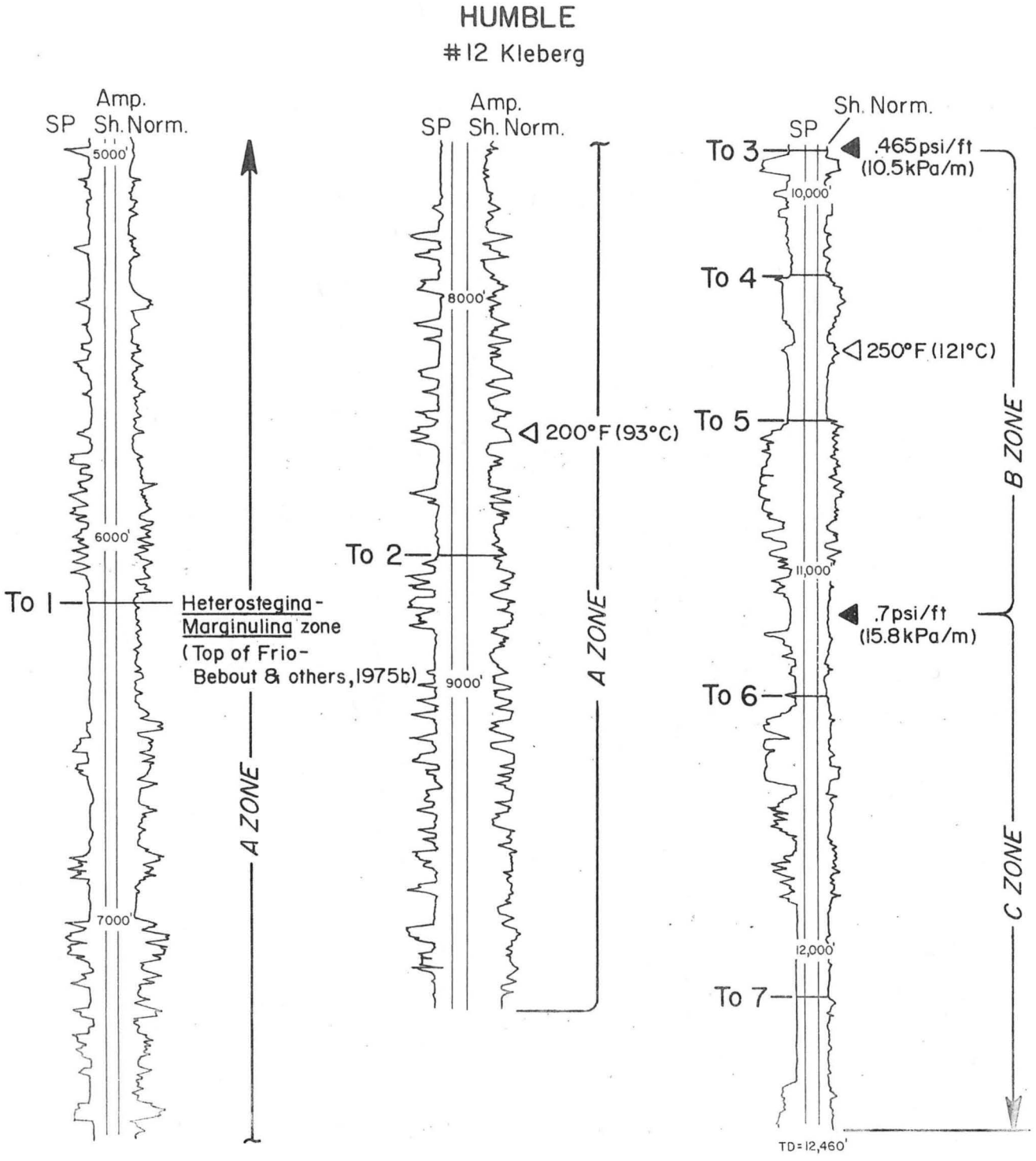

Figure 161. Type log, Humble No. 12 Kleberg, Tordilla Prospect Area.

accumulated in delta-plain environments. This lithology is very similar to that of the upper part of the Frio Formation in the Kenedy Fairway; Cameron and Kenedy delta deposits are parts of a major Frio deltaic regime in South Texas. The numerous sandstones within the To1 to To4 interval are thin, generally ranging from 10 to 40 ft thick, and are not laterally continuous. These sandstones, which occur in the A Zone and upper part of the B Zone, have low potential as reservoirs that could produce large quantities of water.

The Frio below the To4 marker, in contrast with that above, is dominated by several upward-coarsening progradational cycles, probably deltaic sequences of thick prodelta shales grading upward into delta-front and channel-mouth-bar sandstones (figs. 158, 159, and 161). These upward-coarsening sequences, which occur in the C and deep B Zones, can be traced across the Tordilla Prospect Area and into adjacent fault blocks. The massive sandstones in the deltaic cycles are up to 130 ft thick and are considered the primary reservoirs of interest in the Tordilla Prospect Area.

Formation Parameters

In the Tordilla Prospect Area, the B Zone has a thickness of 1,250 ft as determined from a plot of BHSIP data versus depth for production wells (fig. 162). The top of the B Zone, determined from BHSIP data to be at a depth of 9,000 ft, is the same as the top indicated by the change in geothermal gradient (fig. 163). The base of the B Zone occurs at an average depth of 10,250 ft; the base of the C Zone is projected to be 12,400 ft deep. The geothermal gradient is 1.56° F/100 ft in the hydropressured zone and increases to 2.67° F/100 ft in the geopressured zone (fig. 163).

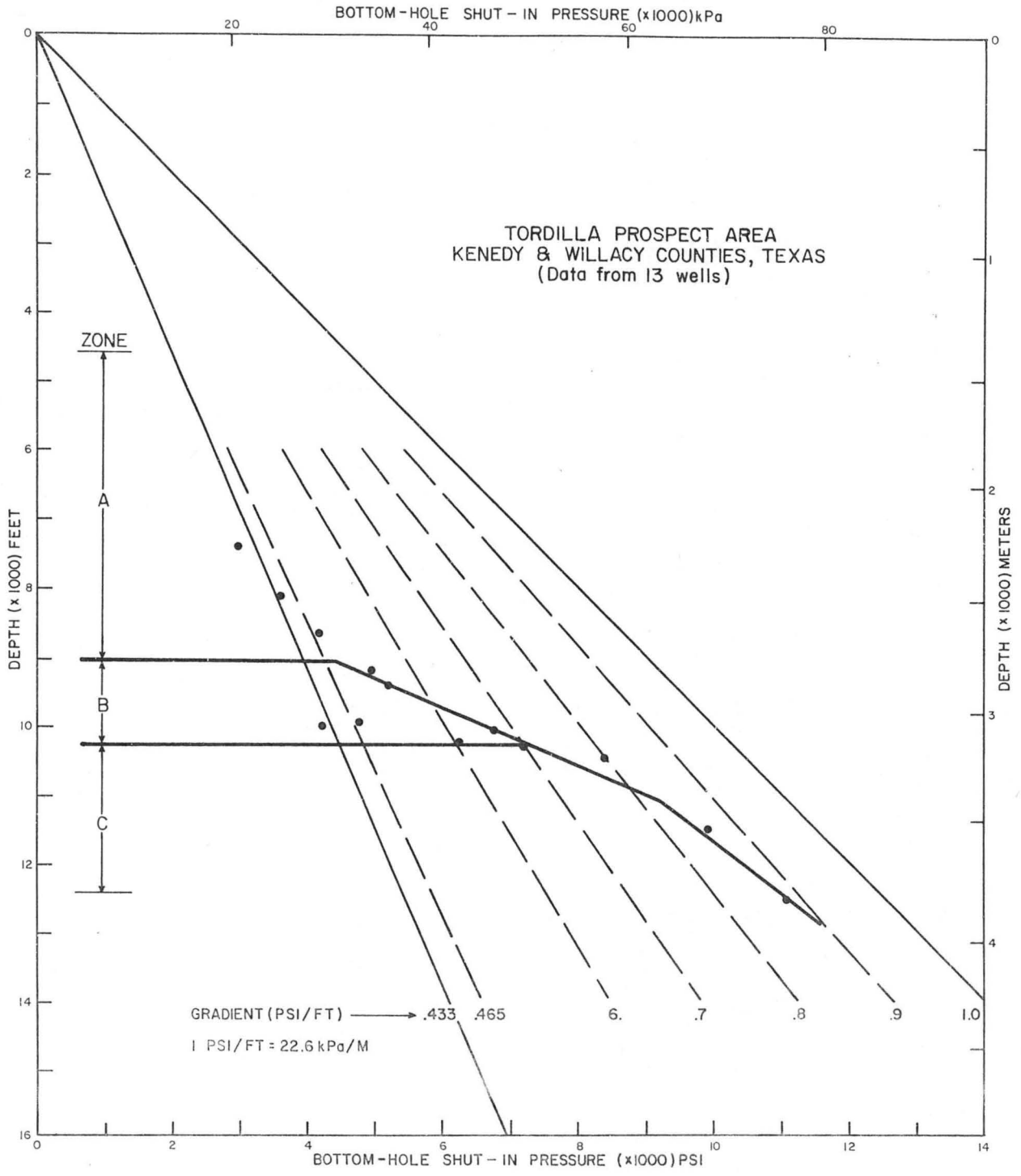

Figure 162. Bottom-hole shut-in pressure versus depth for production wells in the Tordilla Prospect Area, Kenedy and Willacy Counties, Texas.

Potential for Testing

Within the Tordilla Prospect Area, massive sandstones up to 130 ft thick occur within the C Zone and the lower part of the B Zone. These sandstones have good lateral continuity and are judged to have good potential for testing entrained methane resources of the shallow geopressured zone. Fluid temperatures are between 250° and 300° F, and pressure gradients range from 0.56 to 0.85 psi/ft. Calculated salinities range between 70,000 and 146,000 ppm NaCl. Calculated methane solubilities (uncorrected) range from 22 SCF/B in the B Zone reservoirs to 39 SCF/B in the C Zone reservoirs (table 2). However, data were not available to evaluate trends in reservoir quality, and, therefore, a site was not selected within the prospect area. The Tordilla area shall be considered a potential candidate for testing but should be further evaluated if reservoir quality data become available.

Montgomery Fairway and Lake Creek Prospect Area

The Montgomery Fairway is the only shallow geopressured fairway outlined within the sandstone trend of the Wilcox Group (fig. 29). The fairway, approximately 2,300 mi^2 in area, covers most of Montgomery County and extends into parts of Waller, Washington, Grimes, Walker, San Jacinto, Polk, Liberty, and Harris Counties. Montgomery was designated a fairway because of the net sandstone maximum, mostly lower Wilcox, in the B Zone (fig. 26). Middle and upper Wilcox sandstones are also concentrated in this fairway, occurring in the deep hydropressured A zone (fig. 25). In parts of the Montgomery Fairway, sandstones of the Yegua Formation (fig. 1) occur within the A Zone and may be prospective for tests of the deep hydropressured zone. Little or no C Zone exists in the Montgomery Fairway

because temperatures of 300° F generally occur very near the shallowest depths at which 0.7 psi/ft pressure gradients occur.

Two areas, Lake Creek and Copeland Creek (fig. 164), were designated prospective on the basis of fairway cross sections (figs. 165, 166, and 167) and 359 well logs (appendix C). The Copeland Creek area in San Jacinto County was judged to have too few deep wells for detailed study of the intervals of interest and, therefore, received no further attention.

The Lake Creek Prospect Area, which covers at least 58 mi^2, occupies a fault block trending northeast-southwest in the southwestern part of Montgomery County (fig. 168). Structural dip section E-E' (fig. 169) and stratigraphic strike section F-F' (fig. 170) were constructed across the Lake Creek and adjacent fault blocks.

Markers M1 through M6 were correlated in the Lake Creek Prospect Area, as well as through the rest of the Montgomery Fairway (figs. 166, 167, 169, and 170). Marker M1 is the top of the Wilcox, M2 marks the top of the middle Wilcox, and M5 is defined as the top of the lower Wilcox. These correlation markers are equivalent to those used by Bebout and others (1979). Within the Lake Creek Prospect Area and immediately adjacent fault blocks, the lower Wilcox section below M6 was correlated in detail with markers "a" through "f" (figs. 169 and 170). Most of this lower Wilcox section occurs in the B Zone in the prospect area.

Structure

The Lake Creek Prospect is bounded on the northwest and southeast by two down-to-the-basin growth faults, and on the northeast by a cross fault (fig. 168). To the southwest, sparse well control prohibits sufficient structural analysis to precisely define a boundary of the prospect area. The prospective fault block is illustrated on section E-E' (fig. 169) as

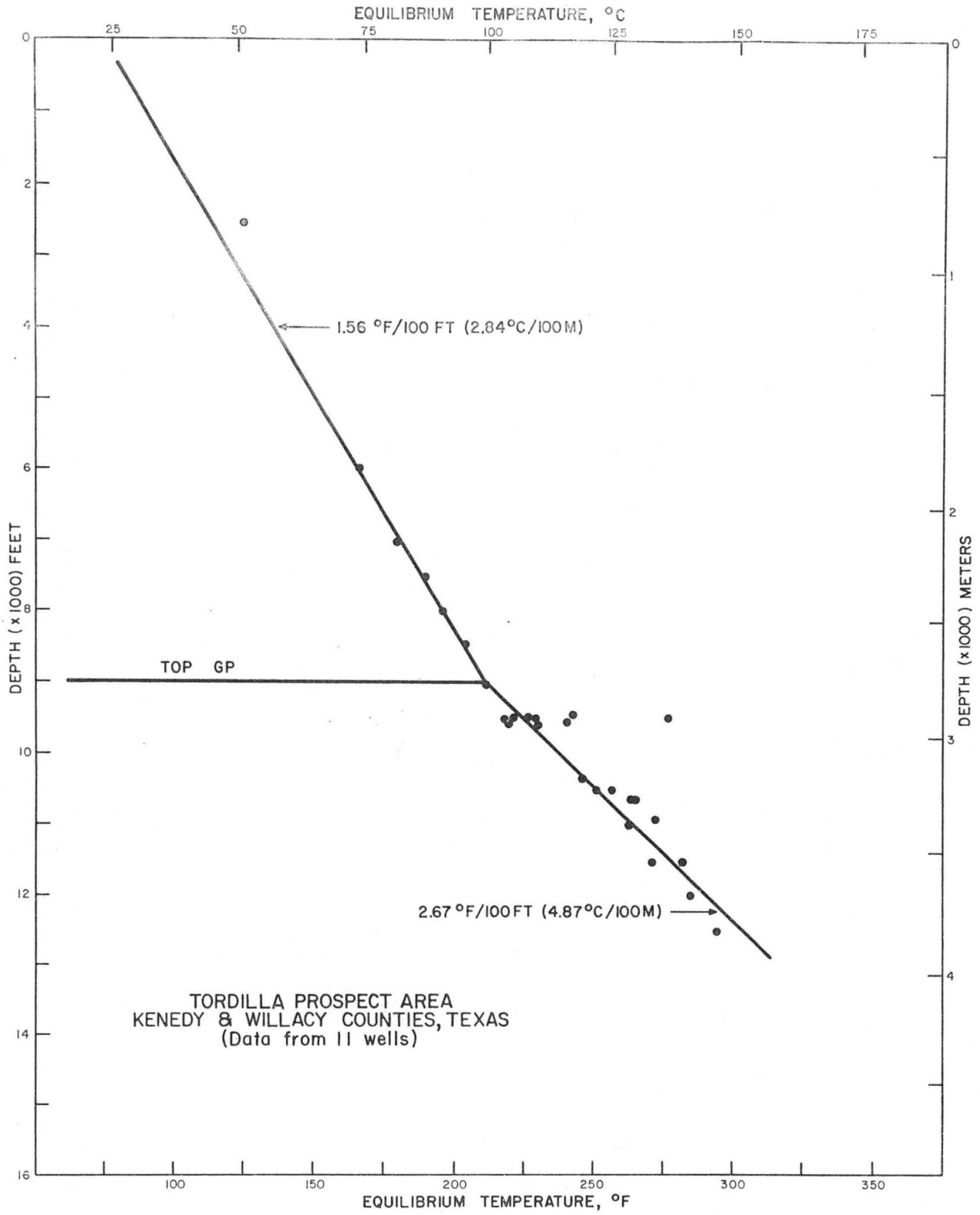

Figure 163. Plot of equilibrium temperature versus depth, showing geothermal gradients in the Tordilla Prospect Area, Kenedy and Willacy Counties, Texas.

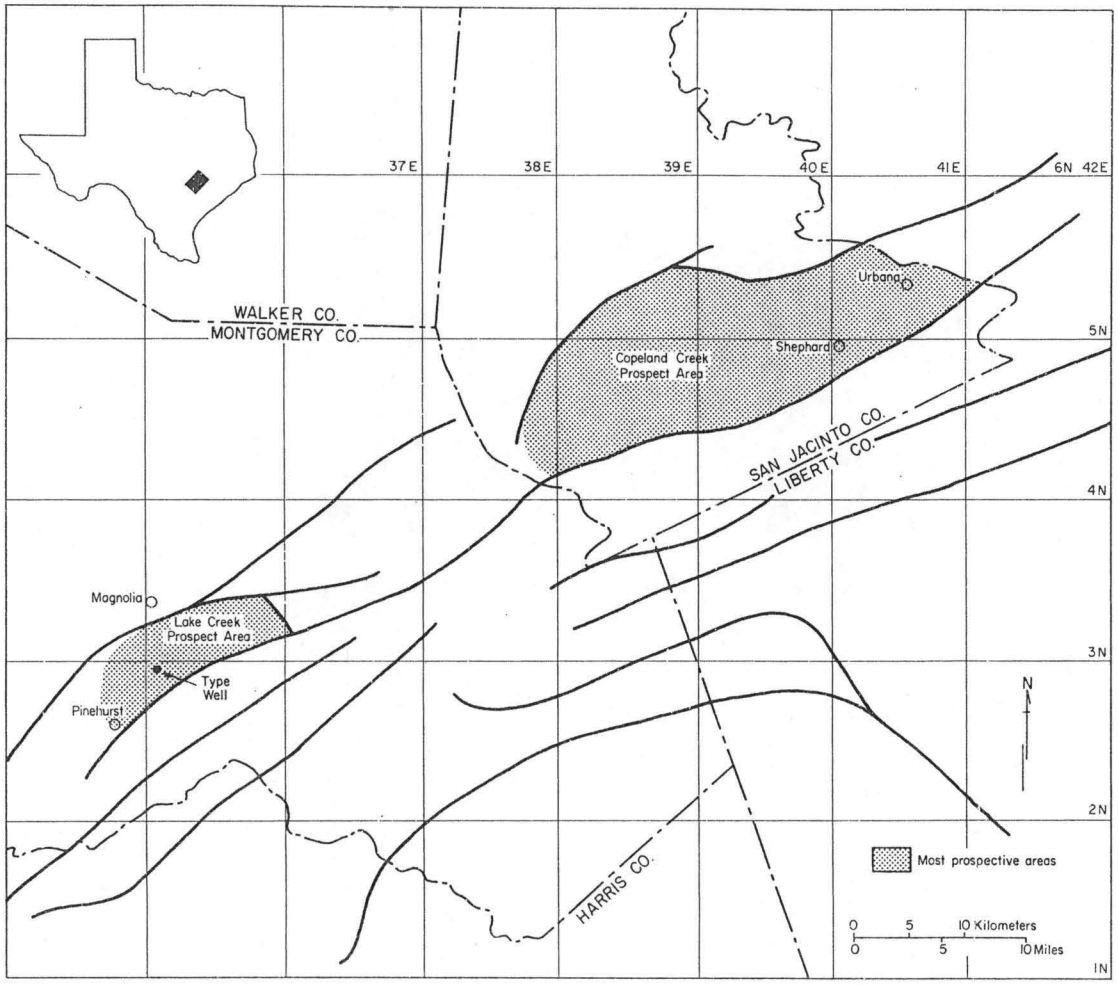

Figure 164. Lake Creek and Copeland Creek Prospect Areas, Montgomery Fairway.

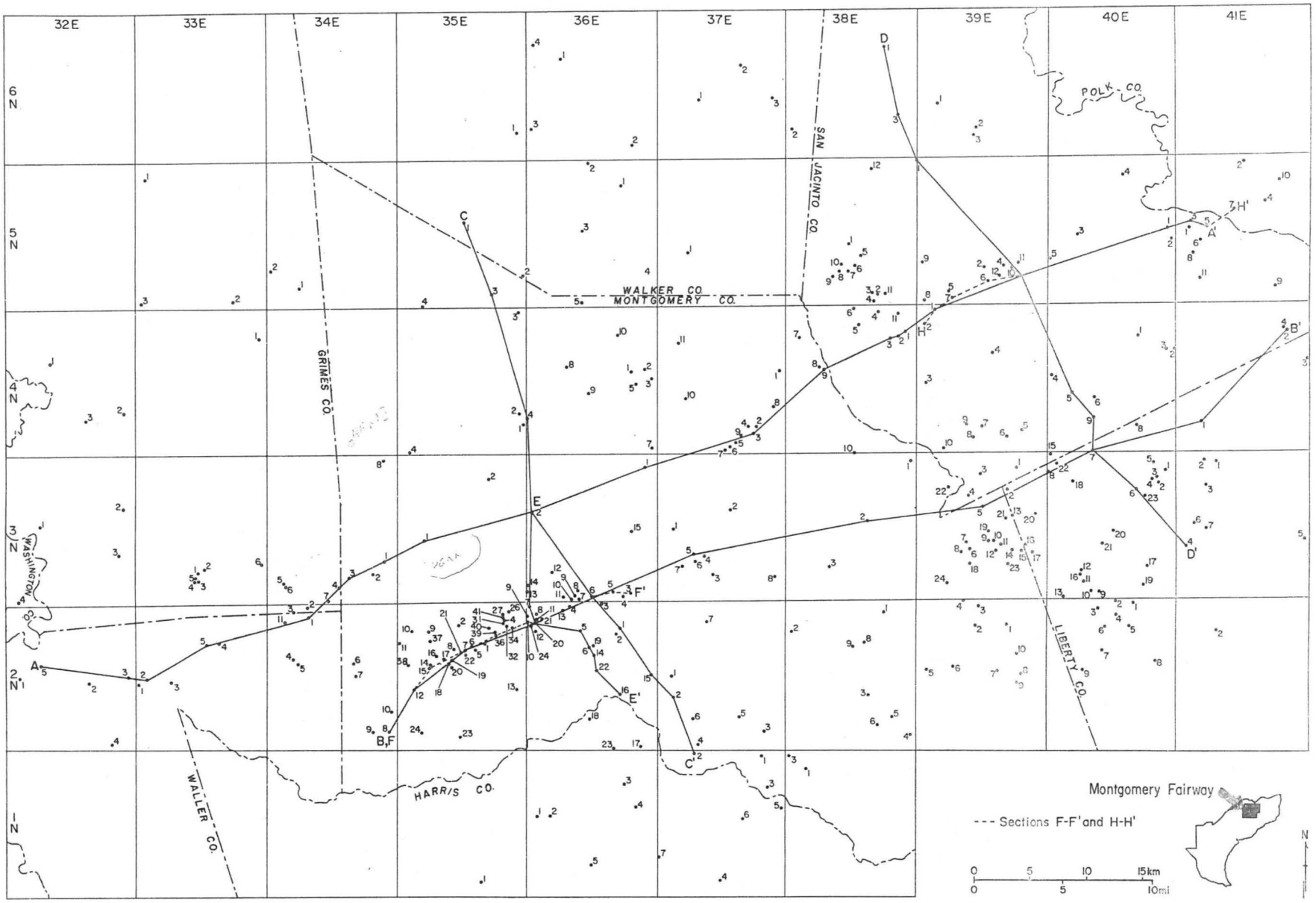

Figure 165. Well locations and lines of cross section, Montgomery Fairway.

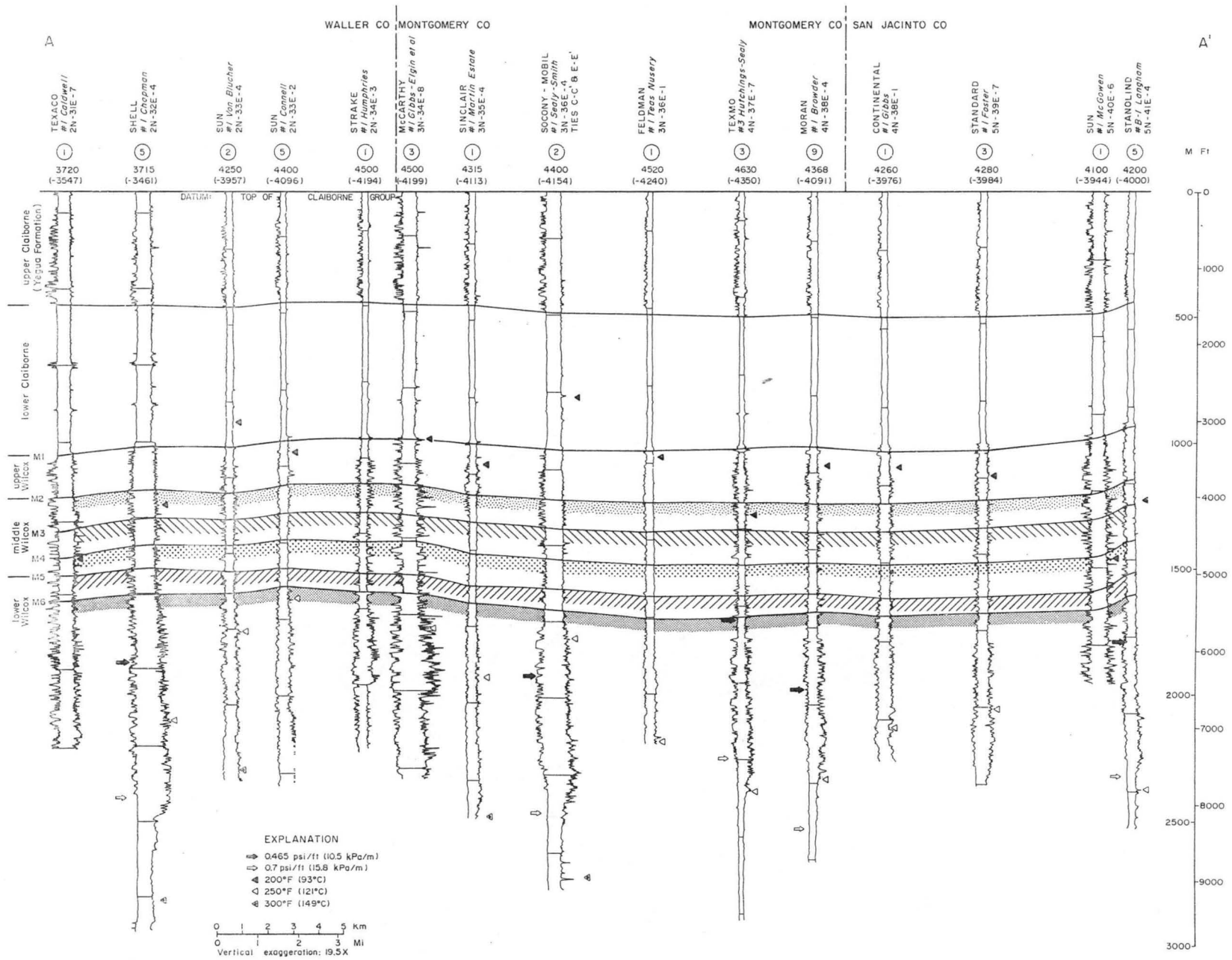

Figure 166. Stratigraphic strike section A-A', Montgomery Fairway.

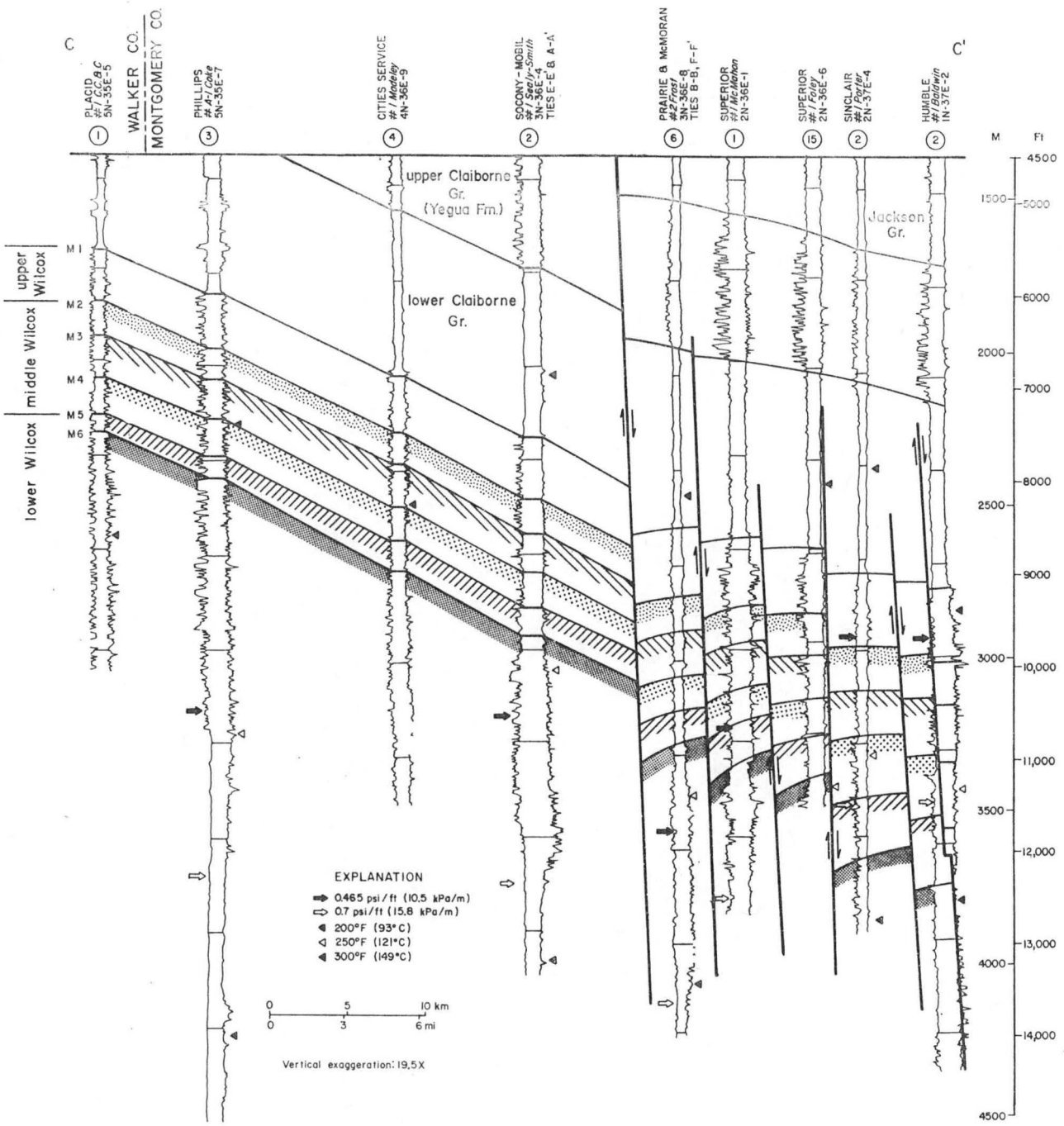

Figure 167. Structural dip section C-C', Montgomery Fairway.

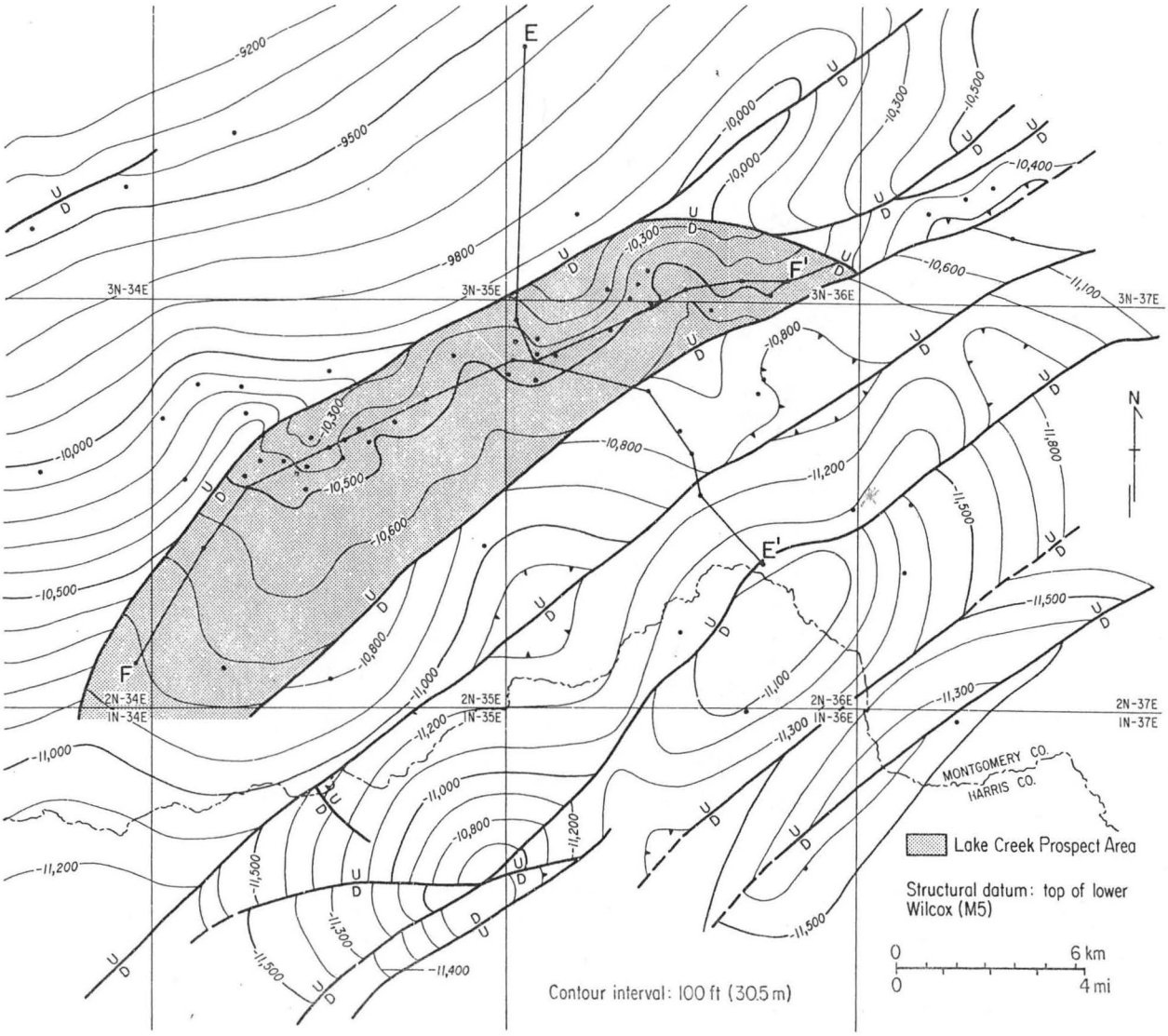

Figure 168. Structure on top of the lower Wilcox (M5), Lake Creek Prospect and adjacent areas.

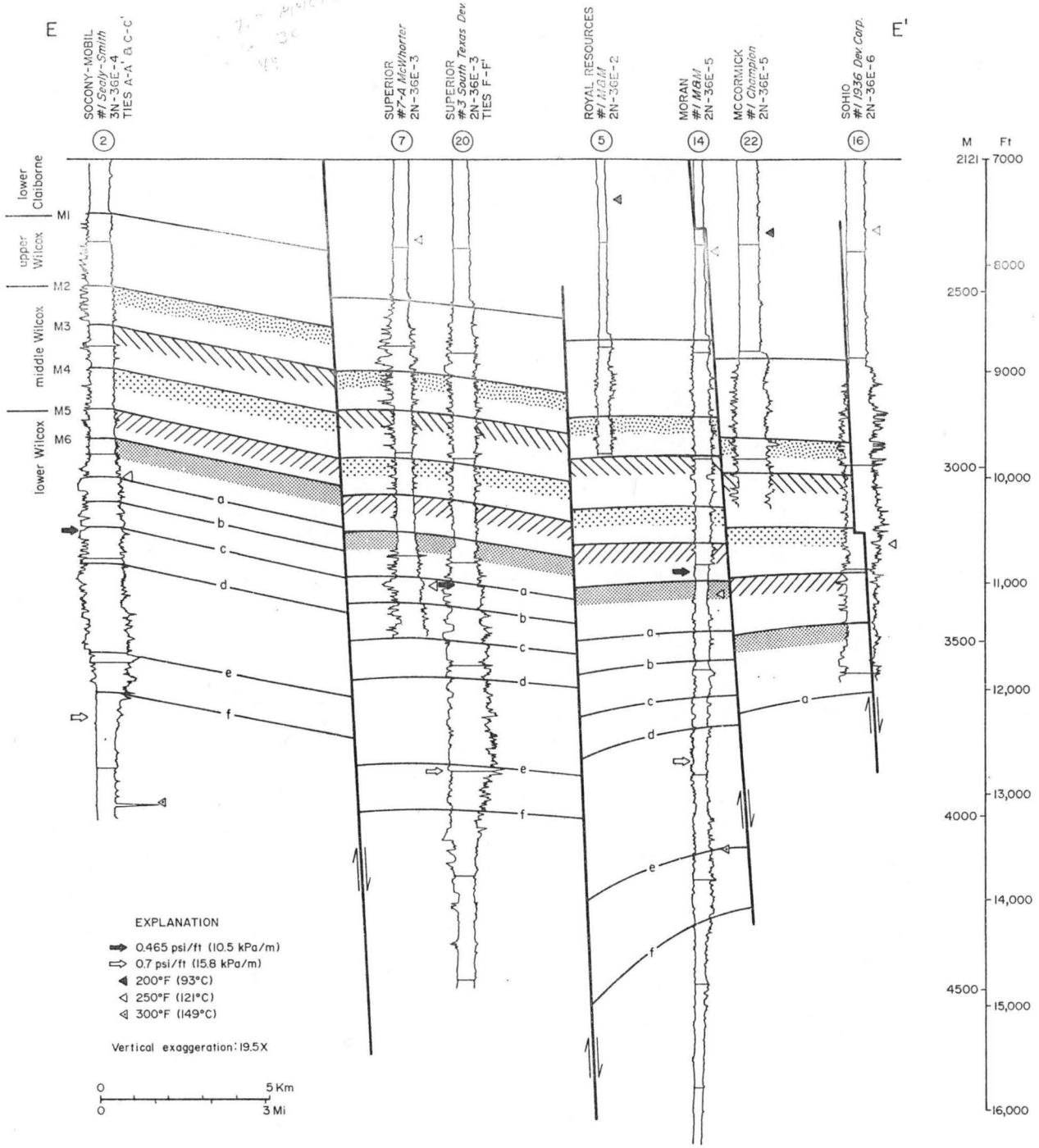

Figure 169. Structural dip section E-E', Lake Creek Prospect Area.

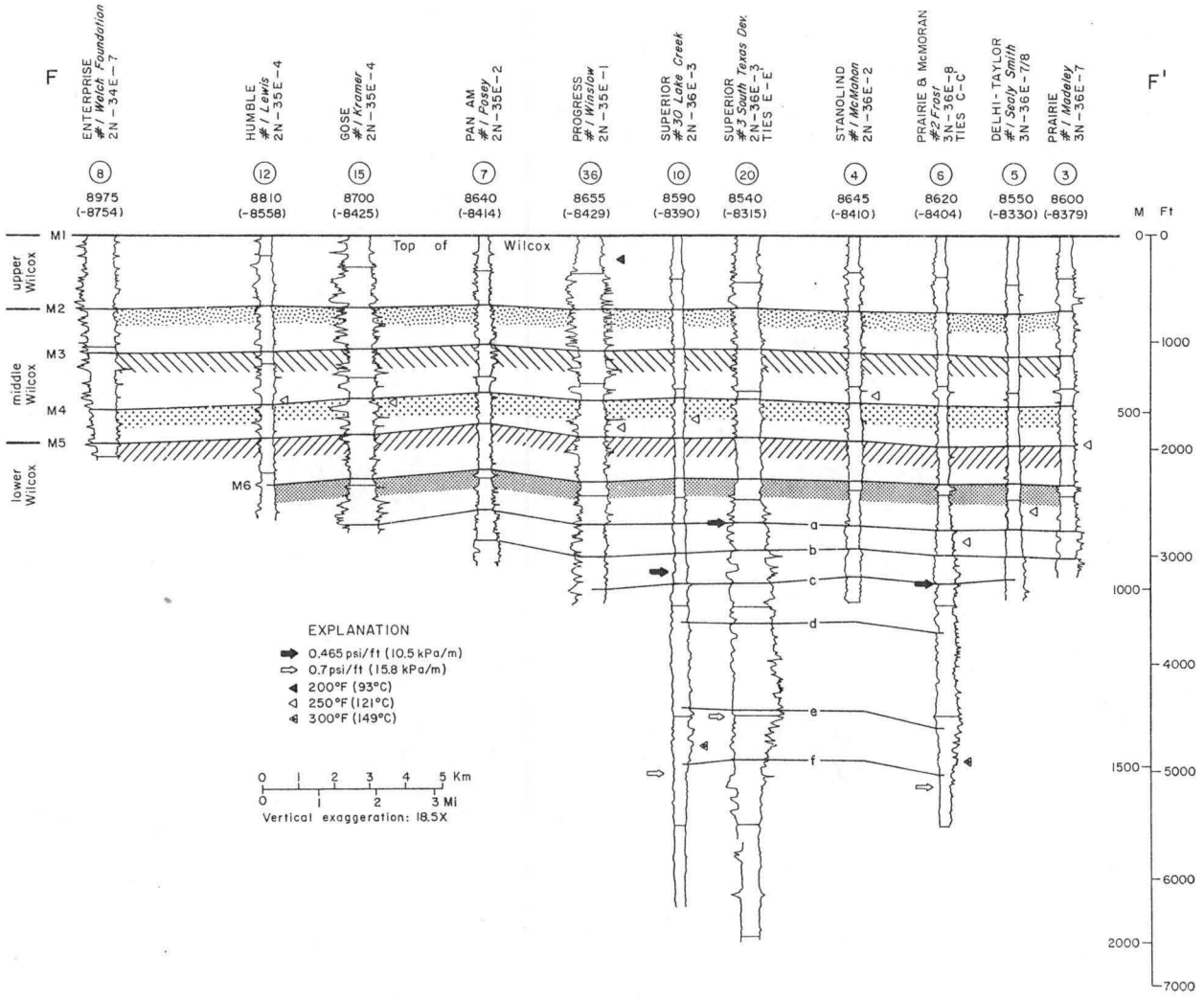

Figure 170. Stratigraphic strike section F-F', Lake Creek Prospect Area.

the block in which the Superior No. 7-A McWhorter and the Superior No. 3 South Texas wells are located. On cross section E-E', vertical displacement of the northwest-bounding fault is between 300 and 400 ft at the top of the lower Wilcox (M5), but varies along the fault as shown by the structure contours on the map (fig. 168). The fault bounding the southeastern side of the prospect has a vertical displacement of 100 to 200 ft at the M5 marker along E-E', but this displacement also varies along the fault. Expansion of section on the downthrown sides of the faults due to sedimentation contemporaneous with faulting is not nearly as pronounced in the Wilcox in this locality as it is in the Wilcox farther downdip and in some of the Frio prospect areas described in this study.

Within the fault block, the structural highs at the M5 horizon are along the northwest-bounding fault and the diverging cross fault at the northeastern end of the fault block. Although not indicated on the structure map of the M5 marker (fig. 168), a dip reversal likely occurs immediately adjacent to the fault. Most of the well data studied within the Lake Creek fault block are from the Pinehurst, Lake Creek, and Lake Creek North gas fields developed on the structural highs.

Sandstone Distribution and Characteristics

The most prospective Wilcox sandstones are the massive sandstones of the lower Wilcox (below M5) primarily in the B Zone. Many of these sandstones have thicknesses between 70 and 100 ft; a few are as thick as 150 ft (figs. 169 and 170). The thick sandstones are generally continuous over much of the prospect area. The lower Wilcox sandstones in the Lake Creek area are mostly delta-front sandstones of the high-constructive Rockdale Delta System described by Fisher and McGowen (1967). The deepest sandstones of this lower Wilcox section are within the C Zone; the total C Zone

is very thin, however, because temperatures of 300° F (C-D boundary) occur very near the shallowest depths at which pressure gradients of 0.7 psi/ft (B-C boundary) occur.

The lower part of the middle Wilcox (M2 to M5) is dominated by marine shales deposited during a major marine transgression (fig. 169). The upper part of the middle Wilcox in the Lake Creek Area is characterized by relatively thin sandstones (10 to 30 ft thick), some of which occur in small upward-coarsening sequences. The upward-coarsening sequences were the first minor regressive units deposited at the beginning of a major progradational episode that extended through deposition of the upper Wilcox. These middle Wilcox sandstones, all of which occur in the A Zone, are generally too thin to be considered prospective.

Although not as massive as lower Wilcox sandstones, some of the upper Wilcox (M1 to M2) sandstones are relatively thick (up to 100 ft). Fisher (1969) described these sandstones as mostly coastal barrier and strandplain deposits associated with wave-dominated deltaic systems. Because the deltaic sands were spread by waves and currents along strike, many of the resulting sandstone units are fairly continuous laterally. Some of these upper Wilcox sandstones are considered potential A Zone test reservoirs.

Formation Parameters

The B Zone is 1,800 ft thick as determined from plots of temperature versus depth (fig. 171) and bottom-hole shut-in pressure (BHSIP) versus depth (fig. 172). However, wells with BHSIP data from drill-stem tests in the geopressured zones are sparse in this area, and the B Zone thickness based on BHSIP data is not reliable. Parameter plots for strike section F-F' (fig. 173) show that the top of the B Zone occurs at an average depth of 10,700 ft.

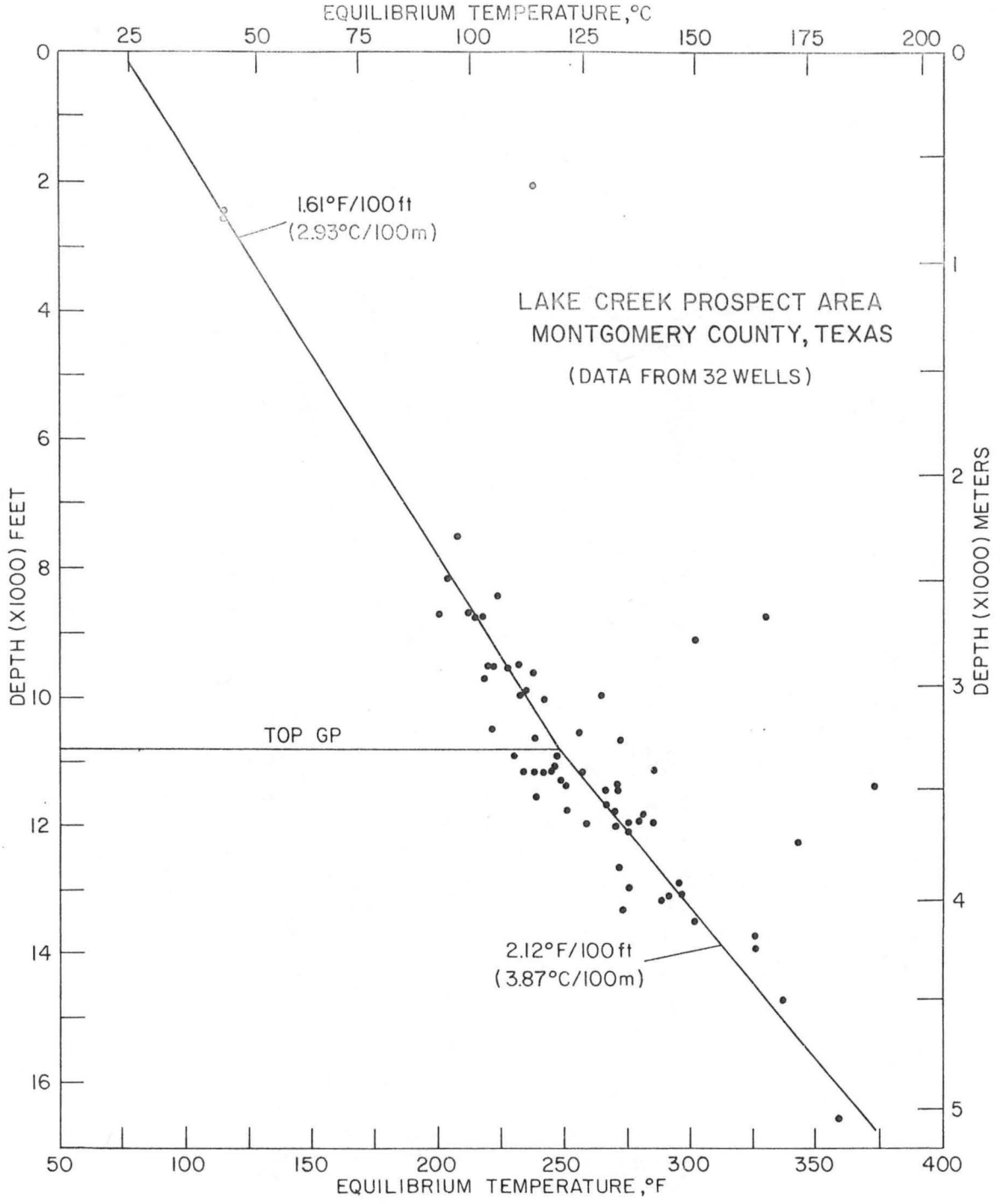

Figure 171. Geothermal gradients based on well log temperatures corrected to equilibrium values for 32 wells, Lake Creek Prospect Area, Montgomery County, Texas.

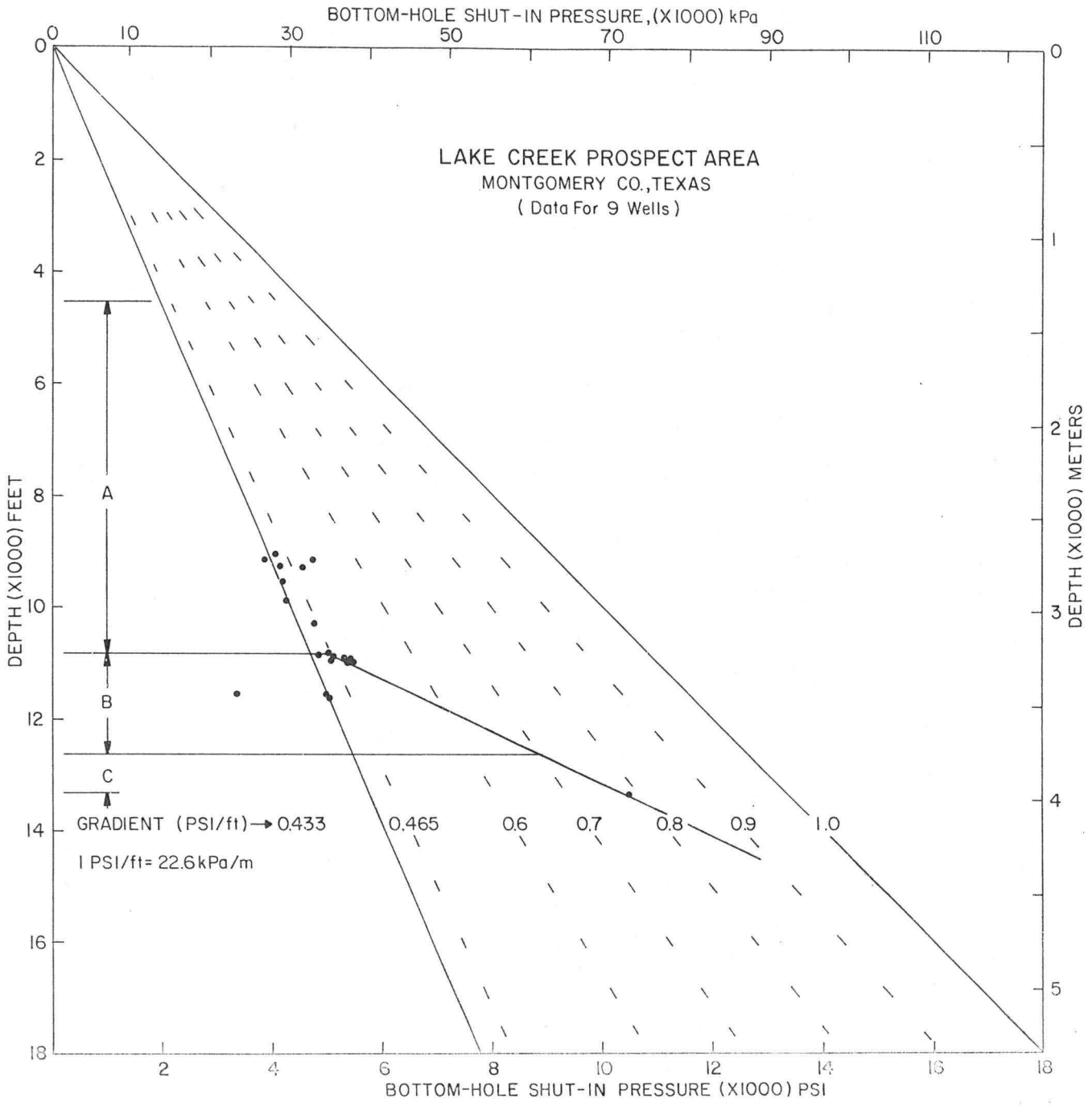

Figure 172. Bottom-hole shut-in pressures from drill-stem tests for production wells in Lake Creek Prospect Area, Montgomery County, Texas.

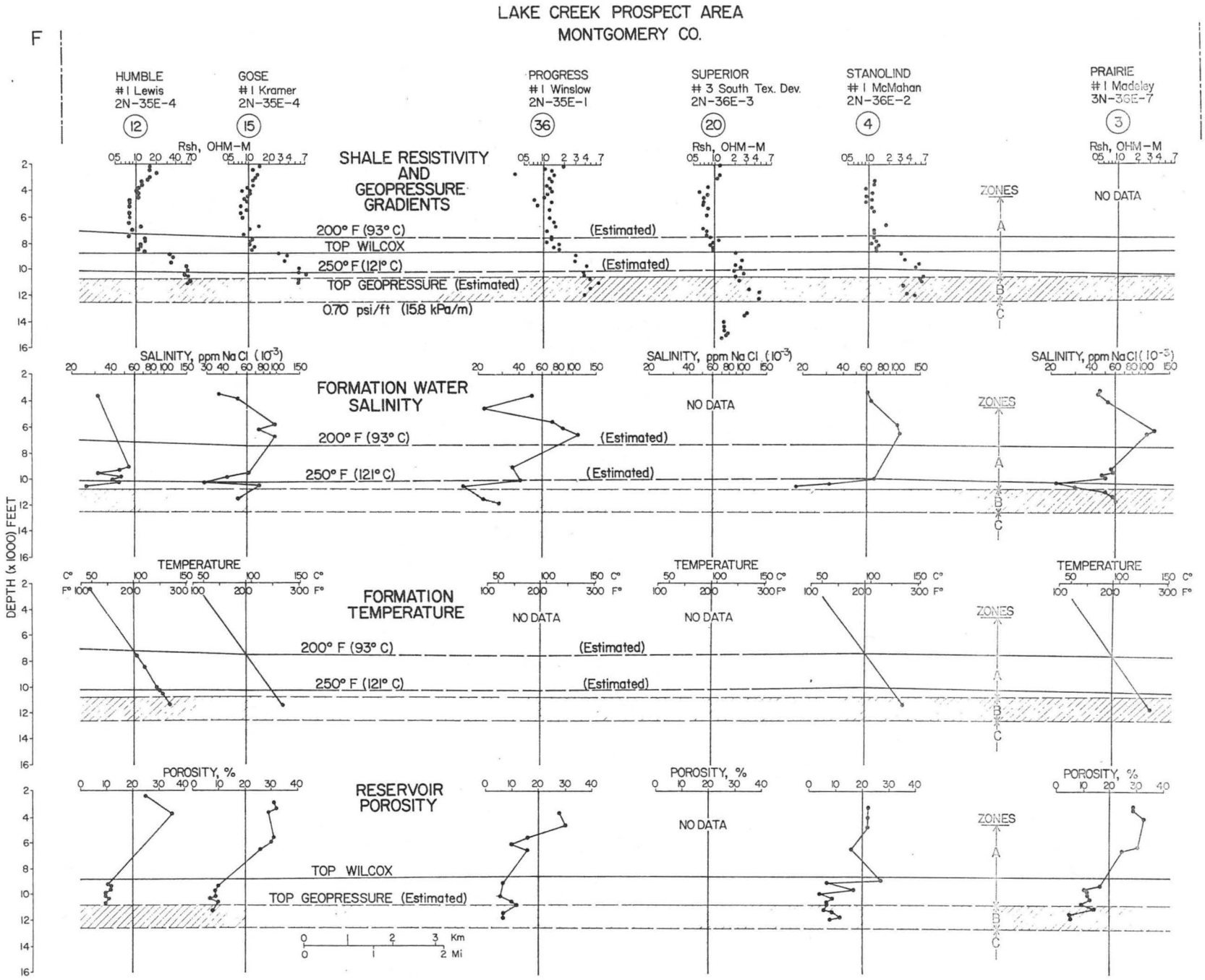

Figure 173. Parameter plots for wells along strike section F-F', Lake Creek Prospect Area, Montgomery County, Texas.

Average geothermal gradients are 1.61° F/100 ft in the hydropressured zone and 2.12° F/100 ft in the geopressured zone. Average equilibrium temperatures at the top and the base of the B Zone in strike section F-F' (fig. 173) are 260° and 296° F, respectively, and thus, the average change in temperature across the zone is 36° F.

A composite plot of salinity versus depth for 20 wells in the Lake Creek Prospect Area (fig. 174) shows that most salinity values are less than 100,000 ppm NaCl. However, there is a wide range of salinities in the shallow geopressured and deep hydropressured zones, with peak values approaching 200,000 ppm NaCl and minimum values of about 12,000 ppm NaCl. Average salinity at the top of the B Zone is 32,000 ppm NaCl in section F-F' (fig. 173).

Porosities determined from induction and SP logs on strike section F-F' are less than 15 percent in the B Zone. Whole-core data for well No. 20 on section F-F' generally show low permeabilities (less than 1 md) in the cored intervals at depths from 11,015 to 14,915 ft. Many of the sandstone cores were described in the core analysis report as having zero values of permeability. A few thin sandstone units had permeabilities that ranged from 2 to 27 md. The highest average permeability of 27 md is that of an 8-ft thick sandstone in the B Zone in the depth interval from 11,019 to 11,027 ft. Porosities in the same interval average 17 percent.

Potential for Testing

The Lake Creek Prospect Area contains numerous thick (70 to 150 ft) lower Wilcox sandstone units mostly in the B Zone. These sandstones are continuous over much of the prospective fault block of 58 mi^2. Calculated methane solubilities (uncorrected) range from 29 to 36 SCF/B. These factors would make the Lake Creek Prospect attractive as a shallow

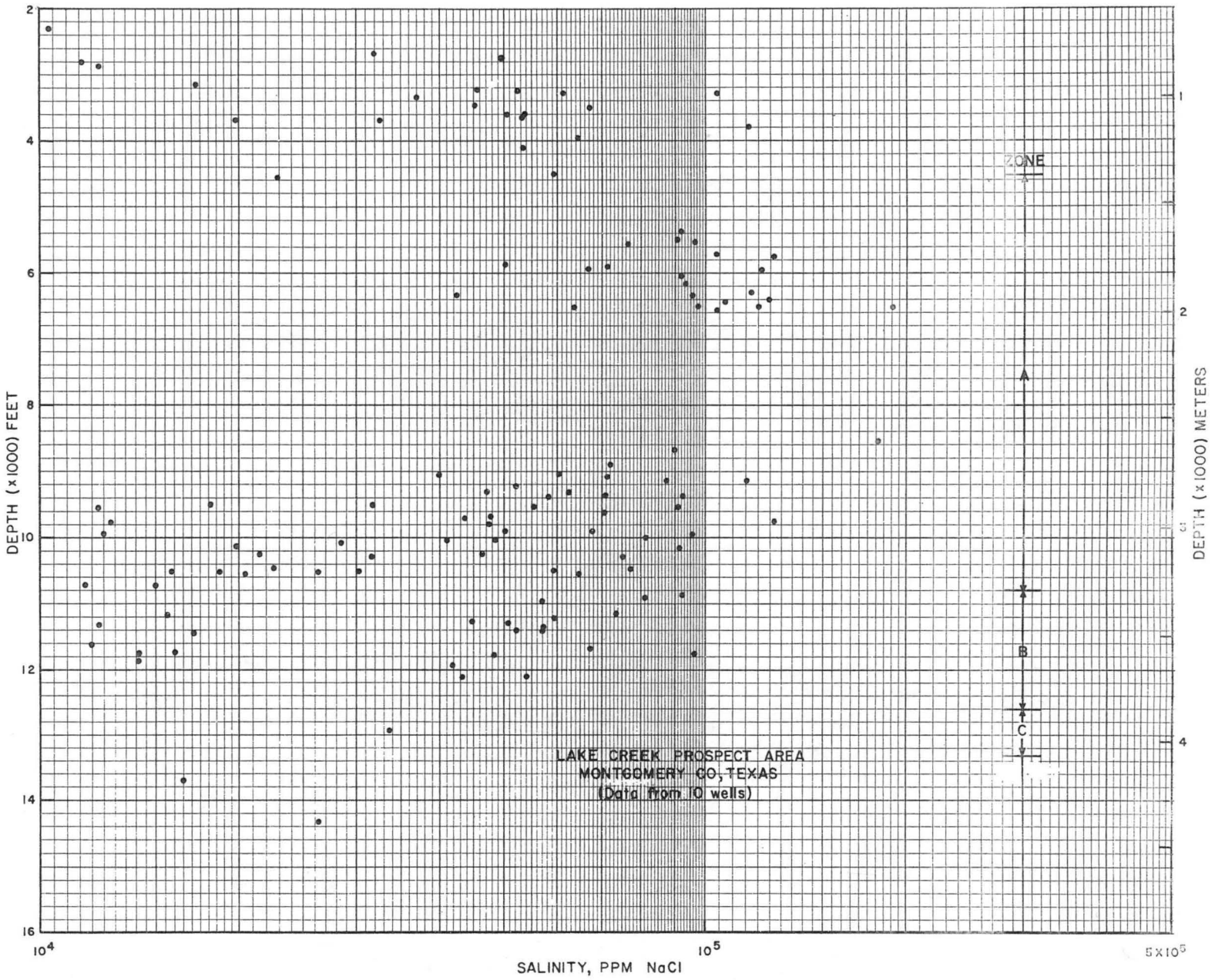

Figure 174. Salinity (computed from SP logs) versus depth for 10 wells, Lake Creek Prospect Area, Montgomery County, Texas.

geopressured test area, but core analyses show that porosities and permeabilities of the lower Wilcox sandstones are consistently low. With almost all permeabilities less than 1 md and porosities less than 15 percent, the lower Wilcox sandstones of the Lake Creek Prospect are not recommended for testing.

CONCLUSIONS AND RECOMMENDATIONS

This study has shown that the Frio Formation has the greatest potential of all the Texas Gulf Coast Tertiary sandstone formations for testing entrained methane resources of the shallow geopressured zones. Sandstones of the Wilcox Group, initially considered to have good potential for shallow geopressured prospects, have consistently low permeabilities in the B Zone (fluid pressure gradients greater than 0.465 psi/ft but less than 0.7 psi/ft) in the area of high net sandstone (fairway) outlined in this study. Permeabilities are also low in sandstones of the C Zone (pressure gradients greater than 0.7 psi/ft and fluid temperatures less than 300° F), which is very thin or absent over much of the Wilcox trend.

Five shallow geopressured fairways were outlined within the sandstone trends of the Texas Gulf Coast region. Within these fairways a total of 8 prospect areas were studied in detail to determine their favorability for location of test sites. One site is recommended for testing: the C Zone in the Blessing Prospect Area in the Matagorda (Frio) Fairway (refer to table 2 for a list of reservoir parameters in the prospect areas). Sites for wells that could test both the shallowest geopressured zone (B Zone) and the deep hydropressured zone (A Zone) were located in three Frio prospect areas: the Nueces Bay and Corpus Channel Prospect Areas in the Corpus Christi Fairway, and the Sarita Prospect Area (shallow) in the Kenedy

Fairway. In addition, other Frio prospect areas have potential for testing geopressured resources, but no sites were selected within them during this study because of the lack of reservoir quality data needed to fully evaluate the prospects. These prospects are (1) the Old Ocean Prospect in the Matagorda Fairway, in which primarily the B Zone could be tested; (2) deeper intervals (C Zone) in the Sarita Prospect in the Kenedy Fairway; (3) the Candelaria Prospect (B and C Zones) in the Kenedy Fairway; and (4) the Tordilla Prospect (B and C Zones) in the Cameron Fairway. The Lake Creek Prospect (Wilcox) in the Montgomery Fairway was rejected as a test location because of low permeability in shallow geopressured sandstones.

The approach used to select prospect areas and test sites in this study began with a regional survey and mapping of net sandstone in the Texas Gulf Coast region. Areas in which prospects were chosen were limited to the fairways that were outlined solely on the basis of total sandstone in the zones of interest. This method of narrowing the study area is necessary when investigating a large region, and obviously the areas of highest net sandstone have the greatest potential of providing test reservoirs. However, good test reservoirs may also occur in areas with lower total sandstone outside the fairways outlined. Therefore, the prospects selected in this study should not be considered the only areas favorable for testing entrained methane resources of the shallow geopressured and deep hydropressured zones in the Texas Gulf Coast region. If additional prospect areas are needed for testing, it is recommended that individual sandstone reservoirs in areas with low and medium values of net sandstone as shown on the regional maps be investigated; although total sandstone may be low, one or a few individual sandstones may be thick enough for long-term testing, providing other conditions are also satisfactory.

ACKNOWLEDGMENTS

We thank the Gas Research Institute for providing the funds and opportunity for this project (under Contract Number 5011-321-0125) and the GRI Project Advisors for their guidance. We also thank Don G. Bebout and Robert G. Loucks for conducting the initial stages of the study, and Adrienne D. Allie and James L. Lockley for their work in the early part of prospect evaluation. The following people provided valuable assistance during the project: Izielen Abgon, Nancy Bolz, Barbara E. Castens, Michael J. Darr, Donald W. Downey, Victor J. Gavenda, Bryant W. Hainey, Susan L. Hallam, Jong H. Han, Jonathan C. Herwig, Mary W. Jackson, Evans U. Jegbefume, Akanni Lawal, Victor Lombeida, Steven D. Mann, Robert K. Manning, W. Dallam Masterson, Katie J. McDonough, David M. Okoye, Gary A. Poole, William K. Rack, Francis M. Rago, Richard A. Schatzinger, Lynette S. Schillo, Nat Smith, Douglas H. Wilson, Kingston Yong, and Jackson Yoong.

A number of companies provided valuable data, and we especially thank Cities Service Company, Exxon Company, U.S.A., Monsanto Company, Tenneco Oil Company, and Texaco, Inc., for their support. In addition, we thank Landon Curry for sharing some of his extensive knowledge of the geology in the Corpus Christi area.

Mary A. Bauer, Steven J. Seni, and Noel Tyler reviewed the report and provided valuable suggestions. The manuscript was prepared by word processing under the supervision of Lucille C. Harrell and edited under the direction of Susann Doenges. Illustrations, design, and paste-up were prepared under the direction of James W. Macon, Chief Cartographer.

REFERENCES

Archie, G. E., 1942, The electrical resistivity log as an aid in determining some reservoir characteristics: American Institute of Mining, Metallurgical, and Petroleum Engineers Transactions, v. 146, p. 54-62.

Bateman, R. M., and Konen, C. E., 1977, The log analyst and the programmable pocket calculator: The Log Analyst, v. 18, no. 5, p. 3-21.

Bates, R. L., and Jackson, J. A., eds., 1980, Glossary of geology: Falls Church, Virginia, American Geological Institute, 749 p.

Bebout, D. G., 1977, Geopressured geothermal fairway evaluation and test-well site location, Frio Formation, Texas Gulf Coast, in Proceedings, Third U.S. Gulf Coast Geopressured-Geothermal Energy Conference: The University of Texas at Austin, Center for Energy Studies, v. 1, p. GI-225 - GI-313.

Bebout, D. G., Agagu, O. K., and Dorfman, M. H., 1975a, Geothermal resources, Frio Formation, Middle Texas Gulf Coast: The University of Texas at Austin, Bureau of Economic Geology Geological Circular 75-8, 43 p.

Bebout, D. G., Dorfman, M. H., and Agagu, O. K., 1975b, Geothermal resources--Frio Formation, South Texas: The University of Texas at Austin, Bureau of Economic Geology Geological Circular 75-1, 36 p.

Bebout, D. G., Gavenda, V. J., and Gregory, A. R., 1978a, Geothermal resources, Wilcox Group, Texas Gulf Coast: The University of Texas at Austin, Bureau of Economic Geology, report to the U.S. Department of Energy, Division of Geothermal Energy, Contract No. AT-E(40-1)-4891 (EY-76-S-05-4891), 82 p.

Bebout, D. G., Loucks, R. G., Bosch, S. C., and Dorfman, M. H., 1976, Geothermal resources--Frio Formation, Upper Texas Gulf Coast: The

University of Texas at Austin, Bureau of Economic Geology Geological Circular 76-3, 47 p.

Bebout, D. G., Loucks, R. G., and Gregory, A. R., 1978b, Frio sandstone reservoirs in the deep subsurface along the Texas Gulf Coast--their potential for the production of geopressured geothermal energy: The University of Texas at Austin, Bureau of Economic Geology Report of Investigations No. 91, 92 p.

Bebout, D. G., Weise, B. R., Gregory, A. R., and Edwards, M. B., 1979, Wilcox sandstone reservoirs in the deep subsurface along the Texas Gulf Coast, their potential for production of geopressured geothermal energy: The University of Texas at Austin, Bureau of Economic Geology, report to the U.S. Department of Energy, Division of Geothermal Energy, Contract No. DE-AS05-76ET28461, 219 p.

Blount, C. W., Price, L. C., Wenger, L. M., and Tarullo, M., 1979, Methane solubility in aqueous NaCl solutions at elevated temperatures and pressures: Idaho State University and U.S. Geological Survey, progress report to U.S. Department of Energy, Contract No. ET-78-S-07-1716, 38 p.

Boyd, D. R., and Dyer, B. F., 1964, Frio barrier bar system of South Texas: Gulf Coast Association of Geological Societies Transactions, v. 14, p. 309-322.

Brown, W. M., 1976, One hundred thousand quads of natural gas?: New York, Hudson Institute, Research Memorandum No. 31, 32 p.

Bruce, C. H., 1973, Pressured shale and related sediment deformation--mechanism for development of regional contemporaneous faults: American Association of Petroleum Geologists Bulletin, v. 57, no. 5, p. 878-886.

Burst, J. F., 1969, Diagenesis of Gulf Coast clayey sediments and its possible relation to petroleum migration: American Association of Petroleum Geologists Bulletin, v. 53, no. 1, p. 73-93.

Dorfman, M. H., 1977, Natural gas from geopressured zones in the U.S. Gulf Coast Basin: Gas supply review, v. 5, no. 6, p. 1-3.

Dunlap, H. F., and Dorfman, M. H., in press, Problems and partial solutions in using the SP log to predict water salinity in deep hot wells, in Proceedings, Fifth Geopressured-Geothermal Energy Conference: Baton Rouge, Louisiana, October 13-15, 1981.

Fertl, W. H., and Timko, D. J., 1970, Association of salinity variations and geopressures in soft and hard rock: Eleventh Annual Logging Symposium, Society of Professional Well Log Analysts, p. 1-23.

Fisher, W. L., 1969, Facies characterization of Gulf Coast Basin delta systems, with some Holocene analogues: Gulf Coast Association of Geological Societies Transactions, v. 19, p. 239-261.

Fisher, W. L., and McGowen, J. H., 1967, Depositional systems in the Wilcox Group of Texas and their relationship to occurrence of oil and gas: Gulf Coast Association of Geological Societies Transactions, v. 17, p. 105-125.

Fowler, W. A., 1970, Pressures, hydrocarbon accumulation, and salinities, Chocolate Bayou Field, Brazoria County, Texas: Journal of Petroleum Technology, v. 22, p. 411-423.

Freed, R. L., 1980, Shale mineralogy of the No. 1 Pleasant Bayou Geothermal Test Well, a progress report, in Dorfman, M. H., and Fisher, W. L., eds., Proceedings, Fourth U.S. Gulf Coast Geopressured-Geothermal Energy Conference: The University of Texas at Austin, Center for Energy Studies, v. 1, p. 153-165.

Galloway, W. E., Hobday, D. K., and Magara, K., in press, Frio Formation of the Texas Gulf Coast Basin--depositional systems, structural framework, and hydrocarbon origin, migration, distribution, and exploration potential: The University of Texas at Austin, Bureau of Economic Geology Report of Investigations.

Gardner, F. J., 1952, The oil and gas fields of the Texas Upper Gulf Coast: Austin, Texas Railroad Commission, p. 66-68.

Gregory, A. R., and Backus, M. M., 1980, Geopressured formation parameters, geothermal well, Brazoria County, Texas, in Dorfman, M. H., and Fisher, W. L., eds., Proceedings, Fourth U.S. Gulf Coast Geopressured-Geothermal Energy Conference: The University of Texas at Austin, Center for Energy Studies, v. 1, p. 235-311.

Gregory, A. R., Dodge, M. M., Posey, J. S., and Morton, R. A., 1980 [1981], Volume and accessibility of entrained (solution) methane in deep geopressured reservoirs--Tertiary formations of the Texas Gulf Coast: The University of Texas at Austin, Bureau of Economic Geology, report to the U.S. Department of Energy, Division of Geothermal Energy, Contract No. DE-AC08-78ET01580, 390 p.

Haas, J. L., Jr., 1978, An empirical equation with tables of smoothed solubilities of methane in water and aqueous sodium chloride solutions up to 25 weight percent, 360° C, and 138 MPa: U.S. Geological Survey Open-file Report No. 78-1004, 41 p.

Hardin, G. C., Jr., 1961, Subsurface geology, in Geology of Houston and vicinity, Texas: Houston Geological Society, Academic and Library Committee, p. 21-26.

Hedberg, W. H., 1967, Pore-water chlorinities of subsurface shales: The University of Wisconsin, Ph.D. dissertation.

Holcomb, C. W., 1964, Frio Formation of southern Texas: Gulf Coast Association of Geological Societies Transactions, v. 14, p. 23-33.

Hottmann, C. E., and Johnson, R. K., 1965, Estimation of formation pressures from log-derived shale properties: Journal of Petroleum Technology, v. 17, p. 717-723.

Houston Geological Society, 1959, Frio Study Group report--The Frio Formation of the Upper Gulf Coast of Texas: Houston, 17 p.

Hunt, J. M., 1979, Petroleum geochemistry and geology: San Francisco, California, W. H. Freeman, 617 p.

Kehle, R. O., 1971, Geothermal survey of North America, 1971 annual progress report: American Association of Petroleum Geologists, Research Committee, 31 p.

Kharaka, Y. K., Lico, M. S., Wright, V. A., and Carothers, W. W., 1980, Geochemistry of formation waters from Pleasant Bayou No. 2 well and adjacent areas in coastal Texas, in Dorfman, M. H., and Fisher, W. L., eds., Proceedings, Fourth U.S. Gulf Coast Geopressured-Geothermal Energy Conference: The University of Texas at Austin, Center for Energy Studies, v. 1, p. 168-199.

Lewis, C. R., and Rose, S. C., 1970, A theory relating high temperatures and overpressures: Journal of Petroleum Technology, v. 22, p. 11-16.

Magara, K., 1968, Compaction and migration of fluids in Miocene mudstone, Nakaoka Plain, Japan: American Association of Petroleum Geologists Bulletin, v. 52, no. 12, p. 2466-2501.

Martin, G. B., 1969, Depositional history: key to Frio exploration: Gulf Coast Association of Geological Societies Transactions, v. 19, p. 489-501.

Overton, H. L., 1958, A correlation of electrical properties of drilling fluids with solids content: American Institute of Mining, Metallurgical, and Petroleum Engineers Transactions, v. 213, p. 333-336.

Overton, H. L., and Timko, D. J., 1969, The salinity principle, a tectonic stress indicator in marine sands: The Log Analyst, v. 10, no. 6, p. 34-43.

Price, L. C., Blount, C. W., McGowen, D., and Wenger, L., in press, Methane solubility in brines with application to the geopressured resource: Proceedings, Fifth Geopressured-Geothermal Energy Conference, Louisiana State University, Baton Rouge, Louisiana, October 13-15, 1981.

Ransom, R. C., ed., 1975, Glossary of terms and expressions used in well logging: Society of Professional Well Log Analysts, 74 p.

Runnells, D. D., 1969, Diagenesis, chemical sediments, and the mixing of natural waters: Journal of Sedimentary Petrology, v. 39, no. 3, p. 1188-1201.

Schlumberger, 1974, Log interpretation, v. 2--Applications: New York, Schlumberger Limited, 116 p.

Schlumberger, 1978, Log interpretation charts: New York, Schlumberger Limited, 83 p.

Von Engelhardt, W., and Gaida, K. H., 1964, Concentration changes of pore solutions during compaction of clay sediments: Journal of Sedimentary Petrology, v. 33, no. 4, p. 919-930.

Wyllie, M. R. J., Gregory, A. R., and Gardner, L. W., 1956, Elastic wave velocities in heterogeneous and porous media: Geophysics, v. 21, no. 1, p. 41-70.

GLOSSARY

The glossary below defines terms as they are used in this report. The American Geological Institute Glossary of Geology (2nd edition), edited by Robert L. Bates and Julia A. Jackson (1980), was consulted for aid in defining some of the terms. For definitions more extensive than those given below, the reader is referred to the Glossary of Geology and to the Glossary of Terms and Expressions Used in Well Logging, edited by R. C. Ransom (1975) and published by the Society of Professional Well Log Analysts.

Aggradation. Upbuilding of the land surface by deposition of sediments.

Air permeability. The ease with which air flows through a small sample (core) of rock under measurement conditions that satisfy Darcy's law.

Antithetic fault. Minor fault whose dip is opposite that of the major fault with which it is associated.

A Zone. An arbitrary designation for the subsurface interval between a depth of 4,500 ft and the shallowest occurrence of geopressure (fluid pressure gradients greater than 0.465 psi/ft); the deep hydropressured zone.

Blocky sandstone pattern. Box-shaped spontaneous potential (SP) log pattern produced by a layer of sandstone that has a low shale content and sharp contacts with overlying and underlying shale.

Bottom-hole shut-in pressure. Refers to the pressure measured in a perforated interval of the borehole by a drill stem test when the flow of fluids from the reservoir is shut in.

B Zone. An arbitrary designation for the shallow geopressured zone in which formation fluid pressure gradients are between 0.465 psi/ft and 0.70 psi/ft.

Correlation. Determination of the equivalence of stratigraphic units across an area. In subsurface studies, correlation is based largely on detailed examination of electric logs.

Correlation marker. A distinctive pattern on the SP and/or resistivity logs that can be traced over a large area and is interpreted to represent a widely occurring sandstone or shale layer or some other lithologic unit.

Corridor. A linear belt roughly parallel to the Texas Gulf coastline in which sandstones of the Tertiary occur with specified pressure and/or temperature conditions. Geopressured corridors are recognized for the Wilcox Group, and Vicksburg and Frio Formations.

Counter-regional dip. The inclination of strata in a direction opposite the basinward direction. Counter-regional dip commonly occurs along growth faults as a feature of rollover anticlines.

Cross fault. A fault whose orientation in plan view (trend) is at a large angle to the dominant regional structure.

C Zone. An arbitrary designation for the shallow geopressured zone in which formation fluid pressure gradients are greater than 0.70 psi/ft and fluid temperatures are less than 300°F.

Cuttings. Rock particles cut from formations by the drill bit and carried to the surface by circulation of drilling mud.

Delta. The land and submarine area and the associated body of sediment formed where a river enters the sea. Deltas vary greatly in type depending on the sediment load of the river, the climate, the tides and waves in the sea, and other factors.

Delta front. The shallow submerged part of the delta where sedimentation is most active. The delta front separates the delta plain landward from the prodelta basinward.

Delta plain. The flat landward part of a delta, transected by distributary channels and typically covered by extensive shallow bays or marshes.

Depocenter. The area of maximum sediment accumulation of a given stratigraphic interval in a depositional basin.

Depositional system. Three-dimensional assemblages of genetically related environments of deposition. For example, a deltaic system may include delta plain, delta front, and prodelta environments, each of which comprises characteristic sedimentary processes and deposits.

Diagenesis. The chemical and physical changes that take place in a sediment after its burial and prior to metamorphism at high temperatures and pressures. Diagenesis of sandstones usually reduces porosity and permeability by physical compaction of the sand grains and precipitation of cement minerals around the grains and in the pore spaces, although some diagenetic processes increase porosity and/or permeability by dissolution of material.

Dip. The angle that a structural surface (for example, fault plane) or stratigraphic surface (for example, bedding plane) makes with the horizontal. The dip direction is at a right angle to the strike direction.

Downdip. The direction in which a given stratigraphic unit increases in depth. Along the Texas Gulf Coast, the regional downdip direction is generally to the east or southeast.

Down-to-the-basin fault. A fault that dips toward the basin (toward the Gulf of Mexico in the Texas Gulf Coast region).

Drill-stem test (DST). A procedure for testing a formation through drill pipe to determine the fluid content of a reservoir and its ability to produce fluids. Hydrostatic, flowing, and shut-in pressures are recorded versus time.

D Zone. An arbitrary designation for the deep geopressured zone in which fluid temperatures are at least 300°F and fluid pressure gradients are at least 0.70 psi/ft.

Electric log. Any of several well logs showing measurements of various electric properties of formations, such as spontaneous potential, resistivity, and conductivity, recorded in a borehole.

Entrained methane. Methane (CH_4) gas, dissolved in formation water or existing as dispersed free gas within the formation.

Equilibrium temperature. The temperature that has been measured in the borehole and corrected to approximate the temperature of the formation before disturbance by drilling.

Facies (rock). A distinctive rock type characteristic of a certain environment of deposition.

Fairway. Area of maximum net sandstone, occurring within a sandstone trend, or corridor, of one of the Tertiary formations of the Texas Gulf Coast. See corridor.

Fault block. A block of the earth that is bounded either completely or partly by faults and behaves as a single unit during movement along the faults.

Formation fluid. The fluid (or fluids) that exist within the pore spaces of reservoir rocks.

Geopressured zone. The subsurface interval in which fluid pressures show gradients greater than the hydrostatic pressure gradient of 0.465 psi/ft. Geopressure is generally attributed to confinement of fluids, which then supports part of the rock overburden.

Geothermal dogleg. An analogy used to describe the resemblance between a dog's leg and the changes in slope exhibited by geothermal gradients.

Geothermal gradient. The change in subsurface temperature per unit of depth, for example, °F/100 ft or °C/100 m.

Growth fault. A fault that forms contemporaneously with deposition, so that the vertical displacement of the fault increases with depth and the stratigraphic units on the downthrown side are thicker than the equivalent units on the upthrown side.

High-constructive delta. A delta that builds relatively rapidly seaward because the amount of sediment supplied by the river is greater than that which can be reworked laterally by marine processes (waves and tides).

Homocline. A rock unit characterized by uniform dip, such as within a fault block.

Horizon. The surface of a stratigraphic unit, such as a sandstone or shale bed, that is used as a stratigraphic or structural datum for maps or cross sections.

Hydropressured zone. The subsurface interval in which fluid pressures are hydrostatic (pressure due to the weight of the overlying water). The fluid pressure gradient is 0.465 psi/ft in the Gulf Coast area, varying slightly with the density of the water. The hydropressured zone extends from the water table down to the geopressured zone.

Index fossil. A fossil that can be used to date the strata in which it is found.

Induction log. The electric well log which uses electromagnetic induction principles for measuring and recording the resistivity or conductivity of formations in uncased boreholes.

Isolith. A line of equal thickness of a particular lithology, such as sandstone, either drawn on a map or imagined within the rocks themselves.

Isopiestic gradient lines. Lines connecting equal pressure gradients between wells on cross sections.

Least-squares-regression curve. A curve drawn to fit a set of plotted points so that the sum of the squares of the distances of the points from the curve is a minimum.

Lignosulfonate. A class of material added to drilling fluids which (1) acts as an emulsifier by creating a heterogeneous mixture of two fluids and (2) helps control borehole caving by swelling or hydrous disintegration of shales.

Lithology. The physical character of a rock.

Log header (or log heading). The form attached to the top of a well log which supplies vital information regarding the well, the survey, and well-bore conditions.

Marker bed. A bed of laterally uniform lithology that can be used as a correlation marker. See correlation marker.

Massive sandstone. A thick, homogeneous body of sandstone.

Methane solubility. The amount of methane (CH_4), measured in standard cubic feet at atmospheric pressure and at a temperature of 60°F, which can be dissolved in formation water. Methane solubility increases as temperature and pressure increase, and decreases as salinity increases.

Mud filtrate. The effluent liquid of drilling mud which penetrates porous and permeable rock, leaving a mud cake on the drilling surface of the rock.

Mud weight. The density of mud circulated in a borehole to aid drilling, remove cuttings, and control formation pressure. Normally, units are recorded in pounds per gallon (lb/gal).

NaCl (in ppm). Sodium chloride solution (brine) with units expressed as parts per million (ppm) by weight (wt/wt).

Net sandstone. Total thickness of sandstone present within a given stratigraphic unit.

Parameter plot. A series of selected formation parameters plotted as a function of depth for wells along dip and strike cross sections in an area of interest.

Permeability. The ability of fluid to flow through a porous rock. The most common unit of measurement is the millidarcy (md).

Porosity. The percentage of the bulk volume of a rock that is occupied by interstices (pore spaces).

Prodelta. The submerged part of a delta that lies basinward of the delta front. Sediments deposited in the prodelta environment are primarily muds.

Progradation. The building outward of the coastline into the sea, such as that associated with deltas.

Prospect area. An area most commonly encompassing one or a few adjacent, closely related fault blocks, with a high potential for yielding a site for a well that will successfully test and/or produce desired fluids (methane-bearing water in this study) from a specified subsurface zone.

Pseudo-velocity. Term applied to acoustic velocity determined by an empirical relation between formation resistivity and acoustic velocity established from well log data for a given area.

Quad. A unit of measurement of the volume of natural gas equal to 10^{12} standard cubic feet (SCF) or a trillion cubic feet (TCF).

Regression. A withdrawal of the sea from land areas. Regression can be caused either by an actual fall in sea level or a building outward (progradation) of the land into the sea, such as in a delta.

Reservoir continuity. A measure of the lateral extent of an uninterrupted reservoir, throughout which reservoir fluids are in communication.

Reservoir interval. The gross stratigraphic interval that includes the reservoir(s) of interest. The interval generally contains non-reservoir rock such as shale and shaly sandstone and is therefore thicker than the sandstone reservoirs.

Reservoir quality. The porosity and permeability of a reservoir rock, which determine the quantity of fluids such as hydrocarbons or water that can be produced from the reservoir.

Resistivity (electrical). Resistance to an electric current as measured by an electric logging tool in an uncased borehole and recorded on the resistivity (induction) log.

Rollover anticline. An anticline formed along the downthrown side of a growth fault, due to a reversal of the regional gulfward dip.

Salinity. The quantity of dissolved salts in water, measured by weight in parts per million (ppm).

Sandstone. A sedimentary rock composed primarily of grains coarser than silt (0.063 mm) and finer than gravel (2 mm). Sandstone is the major reservoir rock in the Gulf Coast Tertiary basin.

Sandstone continuity. A measure of the lateral extent of a sandstone body to its limits defined by lithologic changes or faulting. Sandstone continuity is not synonymous with reservoir continuity because part or all of the sandstone body might have undergone diagenetic changes that reduced porosity and permeability below that necessary for a viable reservoir.

Shale. A sedimentary rock composed primarily of clay particles (finer than 0.002 mm) with some silt particles (0.002 to 0.063 mm in diameter).

Shale resistivity. Refers to the electric resistivity of shale measured by an induction (resistivity) log.

Sidewall core. A formation sample obtained from a borehole with a tool from which a hollow cylindrical bullet is fired into the formation and retrieved by wires attached to the bullet.

Sonic log. An acoustic velocity log; a well logging record of acoustic travel time (usually refers to compressional wave) over a unit distance. Most commonly, measurement is in microseconds per foot (μsec/ft).

SP log. The electric well log that records the spontaneous potential produced by current flow generated by electrochemical and electrokinetic potentials in a borehole. See also spontaneous potential.

Spontaneous potential (SP). The natural potential of different rock layers to conduct electric currents in an uncased borehole. Spontaneous potential is recorded as the SP curve on electric logs and can be used to distinguish shale from sandstone, correlate stratigraphic intervals, and help determine certain formation parameters such as salinity.

Strandplain. A prograding coastline, built seaward by sediment transported and deposited by waves and currents. Compared to most other depositional environments, strandplains are laterally very extensive.

Strata. Layers of sedimentary rock.

Stratigraphic cross section. A cross section in a vertical plane of a particular stratigraphic interval, showing changes in thickness and facies in both the horizontal and vertical dimensions. Stratigraphic cross sections have a certain stratigraphic horizon or correlation marker, rather than sea level, as a datum.

Strike. The direction or trend of the line of intersection of a geologic surface (such as a structural plane [for example, a fault] or stratigraphic plane [for example, a bedding surface]) with the horizontal. The strike direction is at a right angle to the dip direction.

Structural cross section. A cross section through a subsurface interval showing the interpreted structural configuration of the sedimentary layers. Structural cross sections have sea level or some constant depth below sea level as a datum.

Structure map. A map showing the depth below sea level of a particular stratigraphic horizon or marker. Structure-contour lines, which indicate points of equal depth, and faults drawn on the map illustrate the structural configuration at the horizon mapped.

Subsidence. Lowering of the land surface or any subsurface horizon. Subsidence is most commonly caused by compaction of sediments or fault movement.

Subsidiary fault. A fault having a relatively small throw and limited length, compared to the major faults that control structural trends in an area.

Test well. An exploratory well drilled to determine the economic and technical feasibility of producing fluids from a specific reservoir(s).

Thermal conductivity. The coefficient which multiplies the temperature gradient to give the rate of heat transfer by conduction.

Throw. The vertical distance a given stratigraphic marker is displaced where it has been cut by a fault.

Tie well. A well located on at least two cross sections at the point of intersection of those sections. A tie well can be used to relate information from the different cross section lines.

Top of geopressure. The shallowest depth at which the fluid pressure gradient exceeds 0.465 psi/ft (in the Texas Gulf Coast area).

Transgression. The spread of the sea over land areas, caused either by an actual rise in sea level or by subsidence of the land.

Transit time. The time required for an acoustic (sonic) pulse to travel a specified distance through some material. For acoustic logs, transit time is measured in microseconds per foot (μsec/ft).

Type well. A well selected within a prospect area to show conditions representative of the reservoirs(s) for which testing is desired. Formation conditions observed in the type well are projected as those expected in any test well proposed to be drilled nearby.

Updip. The direction in which a given stratigraphic unit becomes shallower. Along the Texas Gulf Coast the regional updip direction is generally to the west or northwest.

Upward-coarsening sequence. Vertical succession of sedimentary rocks from shale at the base, grading upward to sandstone at the top. Thus, the average grain size and the SP deflection on the electric log increases toward the top of the sequence.

Upward-fining-sequence. Vertical succession of sedimentary rocks from sandstone at the base, grading upward to shale at the top. Thus, the average grain size and the SP deflection on the electric log decreases toward the top of the sequence.

Wave-dominated. Refers to a coastline that is more significantly affected by wave processes than by other processes such as those associated with rivers and tides.

Whole core. A cylindrical sample of a subsurface formation (commonly 4 inches in diameter) analyzed for porosity, permeability, and other physical properties.

APPENDIX A: METRIC CONVERSION FACTORS

Customary unit		Conversion factor		Preferred metric unit
bbl (42 gals)	x	0.158983	=	m^3
Btu/hr · ft^2 · °F/ft	x	1.730735	=	W/m · K
SCF (std ft^3)	x	0.02831685	=	m^3
°F		(°F - 32)/1.8	=	°C
°C	+	273.1500	=	K
°F/100 ft	x	18.22689	=	mK/m
ft	x	0.3048	=	m
ft/sec	x	0.0003048	=	m/ms
gal	x	0.003785412	=	m^3
g/cm^3	x	1000	=	kg/m^3
md	x	0.0009869233	=	μm^2
psi	x	6.894757	=	kPa
psi/ft	x	22.62059	=	kPa/m
lb/gal	x	119.8264	=	kg/m^3
SCF/bbl (std ft^3/bbl)	x	0.1801175	=	std m^3/m^3
sq mi (mi^2)	x	2.589988	=	km^2

APPENDIX B: EXPLANATION OF SYMBOLS

A	=	cross sectional area of substance, measured perpendicular to flow of heat, ft^2
bbl (or B)	=	barrel, 42-gallon capacity
BHT	=	bottom-hole temperature, °F
BHP	=	bottom-hole pressure, psi
BHSIP	=	bottom-hole shut-in pressure, psi
°C	=	degrees Celsius (Centigrade)
CH_4	=	methane solubility, SCF/B
C_p	=	compaction correction factor
D	=	depth, feet
DST	=	drill-stem test
F	=	formation factor
°F	=	degrees Fahrenheit
FPG	=	formation pressure gradient, psi/ft
GP	=	geopressure
K	=	kelvin
K_h	=	coefficient of thermal conductivity, Btu/hr · ft^2 · °F/ft
m	=	cementation factor
md	=	millidarcy
NaCl	=	sodium chloride
P	=	pressure, psi
ϕ	=	porosity, percent or fraction
ppm	=	parts per million, weight/weight
psi	=	pounds per square inch
Q	=	heat flow rate, Btu/hr
R_{mf}	=	mud filtrate resistivity, ohm-meter

R_o	=	resistivity of rock that is fully saturated with water, ohm-meter
R_{sh}	=	shale resistivity, ohm-meter
R_t	=	true resistivity of rock, ohm-meter
R_w	=	formation water resistivity, ohm-meter
SCF/B	=	standard cubic feet per barrel, ft^3
SP	=	spontaneous potential
T	=	temperature, kelvin
T_E	=	equilibrium temperature, °F
T_L	=	temperature measured in borehole and recorded on well log header, °F
ΔT	=	temperature change across a substance, °F
ΔT_f	=	transit time of fluid contained in pore spaces of rock, μsec/ft
ΔT_m	=	transit time of solid matrix material of rock, μsec/ft
ΔT_{log}	=	transit time from acoustic log, μsec/ft
Y	=	NaCl concentration, weight percent
Z	=	thickness of substance, ft

APPENDIX C: WELL NAMES AND LOCATIONS

Matagorda Fairway

Tobin Grid	Well number	Well name
6S-32E-7	1	Texkan #1 Rowe
6S-32E-7	2	Sinclair #1 Hawes
6S-32E-7	3	Superior #1 Hawes
6S-33E-7	1	Texas Gulf Sulphur #2 Taylor
6S-33E-3	2	Davidor & Davidor #1 Moore
6S-33E-8	3	Cerro de Pasco #1 Gary
6S-33E-2	4	Texas #1 Moore
6S-33E-7	5	Texas Gulf Sulphur #1 Bassett
6S-34E-8	1	Rowan #1 Krause
6S-34E-3	2	Oil & Gas #1 Byrne
6S-34E-7	3	Taylor #1 Becker
6S-34E-9	4	Houston Oil & Minerals #1 Moore
7S-32E-8	1	Humble #70 Cockburn
7S-32E-7	2	Mitchell #1 Cockburn
7S-32E-8	3	Texaco #C-129 Pierce
7S-32E-2	4	Texas Republic #1 Hawes
7S-32E-9	5	Texaco #C-143 Pierce
7S-32E-1	6	Humble #1 Rogers
7S-33E-2	1	Mac & Mayo #1 Gary
7S-33E-8	2	Frazier & Ferguson #1 Pierce
7S-33E-8	3	Goldking #1 Pierce
7S-34E-4	1	Hunt Trust Estate #1 Pratt
7S-34E-7	2	Southwest Gas #1 McDonald
7S-34E-8	3	Humble #2 McFarland
7S-34E-4	4	Mid-Century #A-1 Howard
7S-34E-2	5	Texas Gulf Sulphur #1 Pratt
7S-34E-5	6	Exxon #36 Pledger
7S-34E-7	7	Skelly #1 Vieman
7S-35E-7	1	McCarthy #1 Giesecke
7S-35E-4	2	Stanolind #1 Robertson
7S-35E-8	3	Texas #1 Sweeney-McFarland
7S-35E-8	4	Gulf #1 Clark
7S-35E-1	5	Kirby & McFarland #1 Groce
8S-31E-1	1	Keck #1 Leissner
8S-31E-4	2	Moore & Ahern #1 Johnson
8S-31E-7	3	Texas #1 Hurlbut
8S-31E-7	4	Robinson #1 Anderson
8S-31E-7	5	Texas #1 Hiltpold
8S-32E-2	1	Brazos & Halbouty #2 Blue Creek Ranch
8S-32E-7	2	Bradco #1 Burkhart
8S-32E-5	3	Sun #C-1 Braman
8S-32E-5	4	Halbouty #1 Crouch
8S-32E-1	5	Woodward #1 Pierce Ranch
8S-32E-3	6	Coastal States #A-1 Roberts
8S-32E-8	7	Bright & Schiff #1 Camp
8S-32E-6	8	Sun #1 Olcese
8S-33E-2	1	Josey #2 Pierce
8S-33E-5	2	Skelly #14-B Cobb
8S-33E-6	3	Sun #27-C Braman
8S-33E-7	4	BBM #1 Miekow
8S-33E-8	5	Cerro de Pasco #1 Lewis
8S-33E-2	6	Josey #1 Pierce
8S-33E-4	7	Skelly #B-30 Cobb
8S-33E-9	8	Cyprus #1 Rugley
8S-33E-1	9	Phillips #1 Matagorda
8S-33E-1	10	Samedan #1 Pierce
8S-33E-1	11	Union California #2 Armour
8S-33E-2	12	Flaitz & Mitchell #1 Runnells Ranch
8S-33E-9	13	Cyprus #1 Miller
8S-34E-1	1	Superior #A-1 MacDonald
8S-34E-1	2	Lone Star #1 Frede
8S-34E-5	3	Ancon, et al. #1 Tew
8S-34E-5	4	Halbouty-Reserve, et al. #1 Bouldin-Picton, et al.
8S-34E-8	5	Superior #1 Johnson
8S-34E-9	6	Lario & Felmont #1 Corbett

Tobin Grid	Well number	Well name
8S-34E-6	7	Union Texas #1 Holland
8S-34E-9	8	Union Texas #1 Schweinle
8S-34E-3	9	Ada #1 Stovall
8S-34E-2	10	Skelly #1 Stern
8S-34E-6	11	Southern Minerals #2 Holland
8S-34E-2	12	Davis #3 Duran
8S-34E-4	13	Sun #1 Ewing
8S-34E-6	14	Southern Minerals #1 Holland
8S-34E-3	15	Stanolind #1 Hawes-Vineyard
8S-34E-1	16	Flaitz, et al. #1 Reynolds
8S-34E-7	17	Mobil #1 Finley
8S-34E-2	18	Superior #1 Carlson
8S-34E-8	19	Tidewater #1 Morton
8S-34E-3	20	Halbouty #1-A Pierce
8S-34E-1	21	Colorado #1 Boone
8S-34E-7	22	Tidewater #1 Mueller
8S-34E-8	23	Frankel #1 Johnson
8S-34E-8	24	Phillips #2 Ocean
8S-34E-6	25	Abercrombie #13 Armstrong
8S-34E-7	26	Abercrombie #1 Reeves
8S-35E-5	1	Halbouty #1 Ellis
8S-35E-8	2	Pan American #A-1 B.R.L.D.
8S-35E-8	3	Davis #1 Miller
8S-35E-9	4	Amoco #225 Old Ocean
8S-35E-7	5	Sunray Mid-Continent #1 McDonald
8S-35E-8	6	Humble #1 Hast, et al.
8S-35E-9	7	Pan American #A-2 B.R.L.D.
8S-35E-8	8	Amoco #226 Old Ocean
8S-35E-9	9	Pan American #223 Old Ocean
8S-35E-1	10	Abercrombie #1 Stern
8S-35E-1	11	Josey #1 Womack
8S-35E-1	12	Dow Chemical, et al. #1 Christian
8S-35E-2	13	Petkas, et al. #1 Carlson
8S-35E-2	14	Kerr-McGee #1 Klopf
8S-35E-3	15	McCarthy #1 B.R.L.D.
8S-35E-3	16	Texas Gas #1 Brewster, et al.
8S-35E-3	17	Smith & Kilroy #1 Damon, et al.
8S-35E-3	18	Smith & Kilroy #1 Lone Star Saltwater
8S-35E-5	19	Abercrombie #1 Cooper
8S-35E-6	20	Abercrombie #B-1 Maxwell
8S-35E-6	21	Abercrombie #1 Jordan
8S-35E-6	22	Stanolind #222 Old Ocean
8S-35E-7	23	Abercrombie #1-D McDonald
8S-35E-7	24	Abercrombie & Magnolia #1-C McDonald
8S-35E-7	25	Union California #1 Davis
8S-35E-8	26	Pan American #A-1 Roberts
8S-35E-8	27	Humble #1 Brockman
8S-35E-6	28	Abercrombie #1 Eldridge-Gilbert
8S-35E-4	29	Union California #1 Sears
8S-35E-6	30	Magnolia & Abercrombie #1 Allhands
8S-35E-4	31	Sun & Abercrombie #4 Campbell
8S-35E-5	32	Stanolind #1 Hughes
8S-35E-4	33	Harrison & Abercrombie #1 Larsen-Edling
8S-35E-5	34	Texas #1 Herrick
8S-35E-5	35	Abercrombie #5 Wilson
8S-35E-8	36	Abercrombie #1 Walker
8S-35E-9	37	Abercrombie & Magnolia #16 B.R.L.D.
8S-35E-9	38	Abercrombie #20 B.R.L.D.
8S-35E-5	39	Abercrombie #1 Texas-McDonald
8S-35E-5	40	Stanolind #1 Love, et al.
8S-35E-9	41	Abercrombie & Magnolia #19 B.R.L.D.
8S-35E-5	42	Abercrombie & Magnolia #1 Smith
8S-35E-4	43	Harrison & Abercrombie #1 Fisher-Larsen
8S-35E-6	44	Magnolia & Abercrombie #1 Gamble
8S-35E-4	45	Abercrombie #2 Waddy
8S-35E-5	46	Stanolind #1 McDonald
8S-35E-5	47	McDermott #1 Texas Gulf Sulphur

Tobin Grid	Well number	Well name
8S-36E-4	1	Pan American #1 Hobbs
8S-36E-2	2	Humble #1 Ward-Byers
8S-36E-4	3	Abercrombie #1 Maxwell
8S-36E-1	4	Davis #1 Howard
8S-36E-1	5	Humble #1 South Angleton Gas Unit 4
8S-36E-1	6	Mobil #1 Williams, et al.
8S-36E-1	7	Mobil #1 Brock
8S-36E-1	8	Mobil #1 R.S.F. Tract 1
8S-36E-6	9	Humble #2 R.S.F. Tract 5
8S-36E-2	10	Austral #1 Bintliff
8S-36E-7	11	Monsanto #1 Austin
8S-36E-3	12	McCarthy #1 Marmion
8S-36E-3	13	Superior #1 Marmion
8S-36E-3	14	Dorchester #1 Crowell
8S-36E-8	15	Rutherford #4-A Hinkle
8S-36E-8	16	Rutherford #2-A Hinkle
9S-31E-8	1	Coastal States #2 Cornelius
9S-31E-9	2	Fullerton #1 Heffelfinger
9S-31E-4	3	Josey-Coffee #1 Reifslager
9S-31E-7	4	Sun #1 Junek
9S-31E-1	5	Union #1 Graddy
9S-31E-5	6	Gardner #1 Trull
9S-31E-5	7	Brewster-Bartle #1 Rugeley
9S-31E-7	8	Stanolind #1 Lezak
9S-31E-8	9	Energy Enterprises, et al. #2 Heffelfinger
9S-31E-6	10	Placid #1 Le Tulle
9S-31E-7	11	Evans #1 Stasta
9S-31E-6	12	Coastal States #1 Ferguson
9S-31E-5	13	Falcon Seaboard #1 Cornelius
9S-31E-2	14	Atlantic #A-1 Kountze
9S-31E-6	15	Barron Kidd #1 Krenek
9S-31E-8	16	McDermott #1 Brown
9S-31E-7	17	Huber #1 Kopecky
9S-31E-7	18	Monsanto, et al. #1 Fay
9S-31E-7	19	Monsanto #2 Fay
9S-31E-7	20	Monsanto #1 Newmont
9S-31E-7	21	Monsanto #1 Saha
9S-31E-8	22	Magnolia #1 Pierce
9S-31E-8	23	Magnolia #1 Live Oak
9S-31E-8	24	Coastal States #1 Heffelfinger
9S-31E-7	25	Davis #1 Hickl
9S-31E-7	26	Harrison #1 Rugeley
9S-31E-7	27	La Gorce #1 Madsen
9S-31E-9	28	Renwar #1 Thomason
9S-32E-1	1	Cosden #1 Cornelius Unit 2
9S-32E-5	2	Occidental #1 Dawdy, et al.
9S-32E-9	3	Monsanto #1 Mehrens
9S-32E-2	4	Monsanto #1 Cornelius Cattle Company
9S-32E-7	5	Continental #1 Fondren, et al.
9S-32E-4	6	Sohio #1 Insall
9S-32E-3	7	So Relle #1 Le Tulle
9S-32E-6	8	Huber #1 Dawdy
9S-32E-6	9	Huber, et al. #2 Wolf
9S-32E-6	10	North Central, et al. #1 Huebner
9S-32E-1	11	Sun #D-1 Braman
9S-32E-9	12	Superior #2 Dawdy
9S-32E-8	13	Halbouty #1 Stoddard
9S-32E-9	14	Superior #1 Dawdy
9S-32E-9	15	Superior #1 Poole
9S-32E-7	16	Bradco #2 Dawdy
9S-32E-1	17	Hamman, et al. #1 Doman
9S-32E-2	18	Coastal States #1 Holman
9S-32E-3	19	Huber, et al. #1 Le Tulle
9S-32E-5	20	Rowan #1 Robertson
9S-32E-7	21	Superior #1-B Dawdy

Tobin Grid	Well number	Well name
9S-32E-1	22	Fidelity, et al. #2 Doman
9S-32E-4	23	Rowan #1 Le Tulle
9S-32E-8	24	Lario & Felmont #1 Lewis
9S-32E-6	25	Stanolind #4 Huebner
9S-32E-6	26	Gill # 2 Cornelius
9S-32E-6	27	Huber #B-1 Wolf
9S-32E-3	28	Texas Gulf Sulphur, et al. #1 Cornelius
9S-32E-2	29	Rowan, et al. #1 Mason
9S-32E-8	30	Patrick #1 Lewis, et al.
9S-32E-9	31	Monsanto #2 Mehrens
9S-32E-9	32	Monsanto #1 Munger
9S-32E-9	33	Johnson #1 Doman, et al.
9S-32E-8	34	Humble #B-1 Lewis
9S-32E-9	35	Monsanto #1 Moers
9S-32E-4	36	Williams #1 Fisher, et al.
9S-33E-1	1	Skelly # 1 Long
9S-33E-4	2	Humble #1 Huebner
9S-33E-5	3	Hamman-Callery #1 Huebner
9S-33E-5	4	Hamman #2 Richter
9S-33E-6	5	Monsanto #1 Lee
9S-33E-7	6	Prairie #1 Cornelius
9S-33E-7	7	Gulf #1 Gilmore
9S-33E-2	8	Pan American #1 Sherrill
9S-33E-7	9	Gulf #1 Gilmore Gas Unit 2
9S-33E-2	10	Atlantic #1 Glover
9S-33E-1	11	Mellon #1 Reese
9S-33E-2	12	Skelly #1 Gest
9S-33E-4	13	Stanolind #1 Huebner
9S-33E-5	14	Brewster & Bartle #1 Huebner
9S-33E-6	15	Harrison #31 Steinmayer
9S-33E-6	16	Humble #B-1 Huebner
9S-33E-9	17	Texas #1 Buckner
9S-33E-7	18	Magnolia #8 Cornelius
9S-33E-5	19	Michael #1 Richers
9S-33E-9	20	Michael #1 Simon
9S-33E-4	21	Texas Gulf Sulphur, et al. #1 Huebner
9S-33E-3	22	Stanolind #4 Thompson
9S-33E-6	23	Union Texas #2 Kilbride
9S-33E-8	24	Magnolia #1 Savage
9S-33E-9	25	Stanolind #1 Buckner
9S-34E-2	1	Hoard #1 FCNBHT
9S-34E-2	2	Mosbacher #1 Livengood
9S-34E-2	3	Occidental #1 FCNBHT, et al.
9S-34E-3	4	Plymouth #1 Lawson
9S-34E-5	5	Hunt #1 Burkhart
9S-34E-5	6	Davis #1 Johnson
9S-34E-6	7	British-American #1 Guess
9S-34E-6	8	Pan American #1 Allen
9S-34E-6	9	Occidental #1 Fay
9S-34E-7	10	Stanolind, et al. #1 Sanborn
9S-34E-8	11	Gulf #1 Rugeley
9S-34E-9	12	Gulf #1 Baker
9S-34E-2	13	Humble #1 FCNBHT
9S-34E-9	14	Mobil #15 Cornelius
9S-34E-9	15	Gulf #1 Ferguson
9S-34E-7	16	Magnolia #2 Hawkins
9S-34E-7	17	Stanolind, et al. #1 Fall
9S-34E-6	18	Coastal States #1 Fay
9S-34E-8	19	Standard of Texas #1 Lewis, et al.
9S-34E-2	20	Midwest #1 Hanson
9S-34E-3	21	Prince #1 Lawson
9S-34E-4	22	Quintana #1 Sirmon
9S-34E-7	23	McCormick #1 Slone
9S-34E-4	24	Arkansas, et al. #1 Ferguson
9S-34E-3	25	Arkansas #1 Matthews

Tobin Grid	Well number	Well name
9S-35E-1	1	Pan American #1 Mellon
9S-35E-3	2	Texas #1 Smith
9S-35E-5	3	Continental #1 Caldwell
9S-35E-5	4	Gulf #B-2 Vineyard
9S-35E-8	5	Gulf #B-1 Vineyard
9S-35E-5	6	Buttes #1 Vineyard
9S-35E-8	7	Cockrell, et al. #1 Neal
9S-35E-6	8	Napeco #1 Vineyard
9S-36E-1	1	Mobil #3 State Tract 7
9S-36E-2	2	Dow #1 Bell
9S-36E-2	3	Dow #1 McCarthy
9S-36E-6	4	Continental #2 Perry
9S-36E-5	5	North American Royalties #1 Hampil
10S-30E-5	1	Tenneco #1-C Gresham
10S-30E-5	2	Gardner-Trunkline #1 Gresham
10S-30E-6	3	C & K #1 Potthast
10S-30E-6	4	C & K #2 Potthast
10S-30E-6	5	Union #1 Potthast
10S-30E-6	6	Tenneco #A-1 Gresham
10S-30E-6	7	Tenneco #A-2 Trull
10S-30E-6	8	Tenneco #A-3 Trull
10S-30E-6	9	Tenneco #4 Trull
10S-30E-7	10	Southern Minerals #1 Slone
10S-30E-7	11	Texkan #1-C Slone
10S-30E-8	12	Cockrell #1 Neuszer
10S-30E-8	13	Tenneco #1 Davis
10S-30E-8	14	Tenneco #1 Davis Gas Unit 2
10S-30E-8	15	Texkan #1 Neuszer
10S-30E-1	16	Cherry & Lower #1 Kolaja
10S-30E-1	17	Oil & Gas #1 Trull & Pybus
10S-30E-1	18	Oil & Gas #2 Trull & Pybus
10S-30E-5	19	Houston #4 Lovett
10S-30E-5	20	Superior #1 Trull
10S-30E-9	21	Cockrell #1 Marek
10S-30E-9	22	Cockrell #1 Moody
10S-30E-9	23	Superior #D-1 Moody
10S-30E-7	24	Texkan #1 Slone
10S-30E-7	25	Christie, et al. #1 Slone
10S-30E-9	26	Pel Tex #2 Moody
10S-30E-1	27	Texaco #1 Nedbalek
10S-30E-6	28	Wainoco #1 Potthast
10S-30E-1	29	Texaco #1 Pennzoil
10S-30E-1	30	Texaco #1 Rhodes
10S-30E-1	31	Amoco #1 Lipscomb
10S-30E-1	32	Texas #1 Williams
10S-30E-1	33	Pan American #1 Pennzoil
10S-30E-7	34	Mobil #1 Michalik
10S-30E-7	35	Mobil #1 G. Harrison
10S-30E-7	36	Mobil #1 L. Harrison
10S-30E-7	37	Magnolia & Sinclair #1 Matl
10S-30E-5	38	Pel Tex #1 Trull
10S-30E-5	39	Tenneco #B-1 Gresham
10S-30E-6	40	Tenneco #D-1 Gresham
10S-30E-5	41	Callery #1 Trull
10S-31E-2	1	Coastal States #1 Marathon
10S-31E-2	2	Brown #1 Grant
10S-31E-5	3	Mosbacher, et al. #1 Vigus
10S-31E-5	4	Ada #1 Fletcher
10S-31E-9	5	Gardner-Lowe #1 H.N.G.
10S-31E-9	6	Travis-Tidewater #1 Backen
10S-31E-7	7	Mobil #2 Kubela
10S-31E-6	8	Humble #1 South El Maton
10S-31E-1	9	Humble #1 Williams
10S-31E-2	10	Argo #1 Murphy
10S-31E-1	11	Sun #1 Heffelfinger
10S-31E-5	12	Halbouty #1 McDonald
10S-31E-5	13	Getty #2 Sullivan
10S-31E-6	14	Belco #1 Johnson

Tobin Grid	Well number	Well name
10S-31E-7	15	Sinclair #1 Nelson
10S-31E-7	16	Magnolia #1 Scarborough
10S-31E-8	17	Kilroy, et al. #1 Hogg-State
10S-31E-2	18	Rutherford #1 Trull
10S-31E-3	19	Coastal States #1 Pennzoil
10S-31E-2	20	Coastal States #1 Wylie
10S-31E-1	21	Sun #1 Beal
10S-31E-6	22	Sinclair #1 McKissick
10S-31E-6	23	Coastal States & Superior #1 Laughlin
10S-31E-5	24	Brown #1 Eberstein
10S-31E-5	25	Halbouty #1 McDonald Unit 2
10S-31E-1	26	Smith & Judd #1 Alderman
10S-31E-5	27	Superior #1 Nelsen
10S-31E-1	28	Texkan #1 McKissick
10S-31E-6	29	Amerada #1 Laughlin
10S-31E-2	30	Brown #1 Dawdy
10S-31E-1	31	Texkan #1 Cunningham
10S-31E-1	32	Mesa, et al. #1 Peterson
10S-31E-1	33	Texkan #1 Peterson
10S-31E-1	34	Apache #1 Murphy
10S-31E-3	35	Superior #1 Fant
10S-31E-3	36	Texaco #1 Culver
10S-31E-3	37	Superior #1 Burke-Herman
10S-31E-3	38	North Central #1 Schwenn
10S-31E-9	39	Magnolia, et al. #1 Trull
10S-31E-4	40	Texaco #16 Thomas
10S-31E-5	41	Halbouty #1 McDonald Gas Unit 3
10S-31E-4	42	Superior #1 Heffelfinger
10S-31E-4	43	Skelly #1 Jackson
10S-31E-9	44	Stanolind #2 Burkhart
10S-31E-4	45	Mitchell #1 Cunningham
10S-31E-3	46	North Central #1 Swain
10S-31E-3	47	Throop #1 Heffelfinger
10S-31E-4	48	Union Texas #2 Martin
10S-31E-2	49	McCarter #1 Heffelfinger
10S-31E-2	50	Apache #1 Harter
10S-31E-1	51	Cyprus #1 Hahn
10S-31E-2	52	Oil & Gas #1 Svetlik
10S-31E-2	53	Smith, et al. #1 Dunn
10S-32E-1	1	Stanolind #1 Buckner
10S-32E-1	2	British-American #1 Buckner
10S-32E-2	3	Humble #5 Lewis
10S-32E-6	4	Phillips #1 Pierce
10S-32E-6	5	Amoco #1 Penny
10S-32E-7	6	Brazos #1 Lawson
10S-32E-9	7	Halbouty #1 Kubela
10S-32E-7	8	Magnolia #1 Rugeley
10S-32E-2	9	Humble #1 Pierce
10S-32E-5	10	Royal Resources #1-A Pierce
10S-32E-5	11	Royal Resources #2-A Pierce
10S-32E-5	12	Kinsey #1 Pierce
10S-32E-4	13	Royal Resources #1 Steele
10S-32E-3	14	Union Texas #1 Trousdale
10S-32E-2	15	Sinclair #1 Lewis
10S-32E-6	16	Tenneco #2 Petrucha
10S-32E-7	17	Sun #1 Rugeley
10S-32E-8	18	Sun #1 Robbins
10S-32E-3	19	Monsanto #1 Buckeye
10S-32E-2	20	Halbouty #1 Pierce
10S-32E-3	21	Monsanto #1 Doman
10S-32E-3	22	Union California #1 Stoddard
10S-32E-3	23	Phillips #3 Stoddard
10S-32E-3	24	Abercrombie #1 Pierce
10S-32E-2	25	Humble #C-1 Lewis
10S-32E-2	26	Mejlaender, et al. #1 Lewis
10S-32E-1	27	Tidewater, et al. #1 Simon
10S-32E-3	28	Humble #9 Lewis
10S-32E-3	29	Ada #1 McDonald & Lewis
10S-32E-3	30	Humble #2 Pierce

Matagorda Fairway

Tobin Grid	Well number	Well name
10S-33E-1	1	Magnolia #1 Cornelius
10S-33E-2	2	Halbouty #1 Simons
10S-33E-3	3	Superior #1 Fondren
10S-33E-4	4	Pan American #1 Petrucha
10S-33E-4	5	Amoco #2 Butter
10S-33E-4	6	Amoco #2 Petrucha
10S-33E-1	7	Texas #1 Lewis
10S-33E-4	8	Mobil #1 Petrucha
10S-33E-4	9	Amoco #1 Culver
10S-33E-2	10	Tennessee #1 Doss
10S-33E-1	11	Magnolia #6 Cornelius
10S-33E-2	12	Texas #1 Burke
10S-33E-3	13	Van Dyke, et al. #1 Savage
10S-34E-3	1	Gulf #2 Hawkins
10S-34E-8	2	Magnolia, et al. #1 Le Tulle
10S-34E-8	3	Falcon Seaboard #1 Le Tulle
10S-34E-9	4	Falcon Seaboard #A-3 Baer Ranch
10S-34E-9	5	Falcon Seaboard #A-4 Baer Ranch
10S-34E-1	6	Skelly #1 Hawkins
10S-34E-9	7	Falcon Seaboard #A-1 Baer Ranch
10S-34E-1	8	Gulf #1 Hawkins
10S-34E-3	9	Brazos #1 G.A.L.I.
10S-35E-1	1	Gulf #A-1 Sanborn
10S-35E-5	2	Gulf #1 Phillips
10S-35E-5	3	Gulf #1 Baer
10S-35E-3	4	Socony-Mobil #3 Hawkins
11S-30E-1	1	McCulloch #1 Palacios
11S-31E-6	1	Brazos-Dow #1 Holsworth
11S-31E-2	2	Tidewater #1 Nelsen
11S-31E-6	3	Brazos #2 Savage
11S-31E-2	4	Tidewater #2 Nelsen
11S-31E-3	5	Sun #1 Bayshore
11S-31E-3	6	Magnolia #1 Palacios
11S-32E-6	1	Superior #1 Robbins
11S-32E-5	2	Cockburn #1 Vanwormer
11S-32E-2	3	Slick #1 Johnson
11S-33E-2	1	American Petrofina #1 Braman
11S-34E-3	1	Falcon Seaboard #2-A Baer Ranch
11S-34E-3	2	Ethyl-Subsurface #1 Baer Ranch
11S-34E-3	3	Falcon Seaboard #A-5 Baer Ranch
11S-34E-3	4	North Central #1 State Tract 105
11S-34E-3	5	Ethyl-Subsurface #2 Baer Ranch
11S-34E-2	6	Ethyl-Subsurface #1 Le Tulle

Corpus Christi Fairway

Tobin Grid	Well number	Well name
16S-20E-3	1	Midland #1 Hunt
16S-20E-4	2	North America #1 Powers
16S-20E-4	3	Chiles et al. #1 Kolb
16S-20E-5	4	Hamon #1 Heath
16S-20E-5	5	Delhi-Taylor #1 Hughes
16S-20E-6	6	Plymouth #A-9 Welder
16S-20E-7	7	Transcontinental #2 Ewing
16S-20E-7	8	Kirkwood #1 Brown
16S-20E-7	9	Texas Gulf #3 Hollan
16S-20E-8	10	Tidewater #3 San Antonio Loan & Trust
16S-20E-8	11	Morgan #1 Johnson
16S-20E-5	12	Delhi-Taylor #1 Hayes
16S-20E-8	13	Hamill #1 Diedrich, et al.
16S-20E-8	14	Haring, et al. #1 Lane
16S-20E-9	15	Southern Minerals #1 Miller
16S-20E-9	16	Golden Trend #1 Matula
16S-21E-8/9	1	Sun #1-A Broughton
16S-21E-9	2	Lone Star #1 Bonorden
16S-21E-9	3	Smith #1 Cage
16S-21E-4	4	Superior #5-1 Welder
16S-21E-8	5	Shoreline #1 Dycus
16S-21E-8	6	Atlantic #1 Fite
16S-21E-7	7	Magnolia #1 McGregor
16S-21E-7	8	Austral #1 Green
16S-21E-6	9	Humble #1 Baldwin
16S-22E-1	1	La Gloria #A-1 Unit
16S22-E-6	2	Collery #1 Richie
16S-22E-5	3	Harkins #1 H&F Properties
16S-22E-5	4	McCulloch & I.D.S. #1 Boehm, et al.
16S-22E-9	5	Cherryville #1 Sweatt
16S-22E-8	6	Texas #1 Ritchie
16S-22E-7	7	Cities Service #1 Elzner
16S-22E-7	8	Hunt #1 A222
16S-22E-7	9	Carrl (General Crude) #1 Sadler
16S-22E-7	10	Mobil #1 Bren
16S-22E-1	11	Pan American #1 Welder
16S-22E-9	12	Fargason #1 Patrick
16S-22E-7	13	Herd #1 Wendland
16S-23E-2	1	Cities Service #1 St. Tr. 86
16S-23E-1	2	Alcoa #1 St. Tr. 100
16S-23E-1	3	Sun #1-B Copano St. Tr. 59
16S-23E-6	4	Midwest #1 St. Tr. 122
16S-23E-5	5	Cities Service #1 St. Tr. 117
16S-23E-4	6	Graham et al. #1 Easley
16S-23E-9	7	American Petrofina #1 Ray, et al.
16S-23E-9	8	Sun #1 Gabriel
16S-23E-8	9	Carrl & Southern Minerals #1 Bankers Mortgage
16S-23E-7	10	Hamon #1 Bankers Mortgage
16S-24E-3	1	Amoco #1 St. Tr. 46
16S-24E-2	2	Phillips #1 Pano
16S-24E-1	3	Getty #1 St. Tr. 119
16S-24E-1	4	Getty #1 St. Tr. 94
16S-24E-8	5	Amerada #1 St. Tr. 191
16S-24E-7	6	Humble #1 St. Tr. 166
16S-24E-7	7	Humble #1 St. Tr. 174
16S-24E-7	8	Humble #1 St. Tr. 165
17S-20E-2	1	Spartan #1 Whatley
17S-20E-2	2	Rush #1 San Antonio Loan & Trust
17S-20E-8	3	Southern Minerals #1 Griffith
17S-20E-6	4	Spartan #1 Granberry
17S-20E-7	5	Sinclair #1 Dorey
17S-20E-3	6	Clark, et al. #1 Comer et al.
17S-20E-3	7	Commercial #1 Lane
17S-20E-2	8	Hamon #1 Hardwick
17S-20E-2	9	Seaboard #1-A Elliott

Tobin Grid	Well number	Well name
17S-20E-2	10	Coastal States #1 Luling
17S-20E-1	11	Seaboard #1 Roos, et al.
17S-20E-1	12	Seaboard #1 Barrier
17S-20E-1	13	Transcontinental #1 Taft-Morrow
17S-20E-1	14	Southern Minerals #1 Gillespie
17S-20E-6	15	Amerada #1 Pyle
17S-20E-5	16	Renwar #1 Peeks
17S-20E-4	17	Seaboard #1 Smith
17S-20E-4	18	Union of California #1 Parker
17S-20E-9	19	Union of California #A-1 Spessard
17S-20E-9	20	Clinton #1 McGregor
17S-20E-9	21	Texaco #1 Terry
17S-20E-5	22	Teal #1 Griffith
17S-20E-5	23	Dougherty #1 Webb
17S-20E-6	24	Dorchester #1 Fleetwood
17S-20E-6	25	Diamond Shamrock #1 Pianta
17S-20E-9	26	Skelly #1 Ramsey
17S-20E-6	27	Buttram #1 Cleveland
17S-20E-7	28	Hamon #B-1 Odem
17S-20E-7	29	Sinclair #1 St. Tr. 52976
17S-20E-7	30	Humble #1 Nueces Bay St. Tr. 684
17S-20E-2	31	Kirkwood #1 Miller
17S-21E-3	1	Getty #1 Wilkerson
17S-21E-5	2	Phillips #1 Flynn
17S-21E-9	3	Sinclair #1 McLaughlin Gas Unit
17S-21E-6	4	Woodfin & Orion #1 Vernor
17S-21E-7	5	Mobil #1 Mayo-Owen Gas Unit
17S-21E-7	6	Jada&ImperialAmericanManagement#1Gericke
17S-21E-7	7	Galaxy #1 Mayo Moore Gas Unit
17S-21E-7	8	Galaxy #1 Crites Gas Unit
17S-21E-7	9	Houston Natural Gas #1 Watson
17S-21E-3	10	Abercrombie #1 Whitten
17S-21E-3	11	Coastal States #1 Hart
17S-21E-4	12	Turnbull, et al. #1 Ewing
17S-21E-4	13	Goldston #1 Willis
17S-21E-4	14	Henshaw Bros. & Mitchell #1 Ragsdale
17S-21E-9	15	Glasscock & Phillips #1 Ragsdale
17S-21E-8	16	Stanolind #1 Taft Syndicate
17S-21E-8	17	Marathon #1 Brooks Gas Unit
17S-21E-8	18	Marathon #2 Kellogg Gas Unit
17S-21E-6	19	Cities Service #G-1 Jones
17S-21E-7	20	Houston Natural Gas & Tidewater #1 Campbell, et al. Unit
17S-21E-6	21	Aztec #1 Texoil-Moore
17S-21E-3	22	Tomco #1 Guaranty National Bank & Trust
17S-21E-5	23	Hunt #1 Mayo
17S-21E-1	24	Hiawatha #1 Green
17S-21E-1	25	Canus #1 Green
17S-21E-2	26	Maguire & May #1 McCann
17S-21E-5	27	Phillips #1 Tillery
17S-21E-7	28	Mobil #2 Jones, et al.
17S-21E-7	29	Marathon #1 Flinn Gas Unit
17S-21E-6	30	Hamon #1 Phillips
17S-21E-6	31	Cities Service #1-A Hutto
17S-21E-7	32	Marine Gathering #1 Grimshaw
17S-21E-9	33	Sinclair #1 Hunter
17S-22E-4	1	Royal #1 Schmidt
17S-22E-2	2	Texas Eastern #2 Floerke et al.
17S-22E-2	3	Hamon #1 Dillon
17S-22E-4	4	Lawbar #1 Hunt-Dugat
17S-22E-9	5	Houston Natural Gas #1 Hoskinson
17S-22E-9	6	Republic Natural Gas & Forest #1 Floerke
17S-22E-9	7	Conroe et al. #1 Hunt
17S-22E-5	8	Hewitt #1 Abrey
17S-22E-6	9	Union Texas Natural Gas #1 Jones
17S-22E-6	10	Tidewater #1-"A" McKamey Unit
17S-22E-6	11	Tidewater #1 Priday
17S-22E-1	12	Hamon #2 Harvey

Tobin Grid	Well number	Well name
17S-22E-2	13	Arkansas Fuel & Tidewater #2 McKamey
17S-22E-5	14	Arkansas Fuel #1 McKamey
17S-22E-5	15	Arkansas Fuel, et al. #1-A McKamey
17S-22E-5	16	Quintana #1 Hunt, et al.
17S-22E-9	17	Royal #1 Baines
17S-22E-8	18	Canus #1 Garrett
17S-22E-8	19	Texas Crude & Halbouty #2 Garrett
17S-22E-8	20	Texas Crude #3 Garrett
17S-22E-9	21	Galaxy #A-2 Simons Gas Unit
17S-22E-8	22	Goldston #1 Garrett
17S-22E-7	23	Lone Star #1 Hester
17S-22E-8	24	Royal #1 Green
17S-22E-8	25	Texaco #1 Green
17S-22E-7	26	American Petrofina #1 Green
17S-22E-7	27	Hamon et al. #1 Reynolds Aluminum
17S-22E-2	28	Plymouth #1 Patrick
17S-22E-1	29	Coastal States #1 Merriman
17S-22E-1	30	Texas #1-A Ray "B"
17S-22E-2	31	Harkins & Hurt #1 Patrick
17S-22E-1	32	Mobil #3 Ray & Harvey
17S-22E-5	33	Lawbar #2 McKamey
17S-22E-3	34	Harkins #1 Brannon
17S-22E-5	35	Wainoco #1 Taylor
17S-22E-9	36	Galaxy #1 Wilson Unit
17S-22E-9	37	Republic & Forest #1 Lang
17S-22E-9	38	Republic & Forest #1 Flourke
17S-22E-9	39	Royal #1 Moore
17S-22E-4	40	Taggart-Weaver & Sharp #1 Kennedy
17S-22E-8	41	American #1 Garrett
17S-22E-4	42	Wheelock #1 Floerke
17S-23E-3	1	Pan American #1 Bankers Mortgage
17S-23E-4	2	Hamon & Sinclair #1 Guettler
17S-23E-9	3	Midwest #3 McCampbell
17S-23E-5	4	Tenneco #4 Maryland Trust "A"
17S-23E-1	5	Tenneco #2 McCampbell, et al.
17S-23E-1	6	Pennzoil United #1 Grant
17S-23E-1	7	Bass #1 Atlantic-Posterfield
17S-23E-8	8	Midwest #1-A McCampbell
17S-23E-8	9	Union Oil of California & Morgan #1 Coward Unit
17S-23E-8	10	Midwest #5 McCampbell
17S-23E-9	11	Mokeen (Stanolind) #1 McCampbell
17S-23E-2	12	Conroe, et al. #1 Chandler
17S-23E-2	13	Conroe, et al. #2 Bankers Mortgage
17S-23E-9	14	Conroe, et al. #A-1 Wheeler
17S-23E-5	15	Getty #1 Dycus-McCampbell Gas Unit
17S-23E-1	16	Flournoy #1 McCampbell
17S-24E-3	1	Halbouty #1 Hepworth, et al.
17S-24E-2	2	Midwest #1 St. Tr. 218
17S-24E-1	3	Amerada #1 St. Tr. "G", Aransas Bay 198
17S-24E-5	4	Cities Service #B-1 St. Tr. 260
17S-24E-4	5	Humble #1 East Aransas Pass Gas Unit 1
17S-24E-9	6	Shell #1 St. Tr. 277
17S-24E-9	7	Getty #1 St. Tr. 275
17S-24E-5	8	Wessely #1 St. Tr. 258
17S-24E-1	9	Cherryville & Flournoy #1 St. Tr. 201
17S-24E-5	10	Cities Service #1 St. Tr. 242
17S-24E-9	11	Mobil #1 Redfish Bay Gas Unit "B"
17S-24E-9	12	Mobil #1 St. Tr. 284, St. Lease #53063
17S-24E-2	13	Skelly #1 Schnitz
18S-20E-2	1	Tenneco #C-4 Kennedy
18S-20E-6	2	Houston Oil #16 McGregor
18S-20E-6	3	Southern Minerals & Houston Oil #1-A Lawrence
18S-20E-8	4	Morgan Minerals #A-4 Cody
18S-20E-7	5	Morgan Minerals #5 Gallagher
18S-20E-7	6	Morgan Minerals #2 Gallagher
18S-20E-7	7	Republic, et al. #B-2 Bevly

Tobin Grid	Well number	Well name
18S-20E-3	8	Guest & Wolfson #1 Bickham
18S-20E-3	9	Carrl & Hamon #1 Hearn
18S-20E-4	10	Barnsdall #1 Merritt
18S-20E-3	11	Rutherford, et al. #1 Stewart
18S-20E-2	12	Gulf #1 McGregor
18S-20E-2	13	Flournory #1 McGregor
18S-20E-4	14	Hanover #1 Head
18S-20E-4	15	Phillips #1 Heuermann
18S-20E-4	16	Phillips #2 Heuermann
18S-20E-5	17	Tenneco #1 Morgan
18S-20E-1	18	Phillips #1 "Turk"
18S-20E-1	19	Humble #1 Nueces Bay St. Tr. 745
18S-20E-5	20	Texaco #1 Ordner
18S-20E-5	21	Dugger & Herring #1 Morgan Properties
18S-20E-8	22	Texaco #1 Weil
18S-20E-8	23	Union Sulphur #1 Hill
18S-20E-7	24	Texon #10 Kocurek
18S-20E-6	25	Southern Minerals #1-A Cole-Ocker-Till Gas Unit
18S-20E-7	26	Maynard, et al. #1 Gabriel
18S-20E-7	27	Cowanco #1 Hoelscher
18S-20E-7	28	Superior #1 Kelly
18S-20E-7	29	USU #1 Morgan
18S-20E-7	30	Chicago #1 Morgan
18S-20E-7	31	Renwar #1 Scoggins
18S-21E-3	1	Republic #60 Rachal
18S-21E-3	2	Phillips & Texaco #1 Water
18S-21E-2	3	Phillips #1 St. Tr. 706
18S-21E-4	4	Coastal States & Dansfield #1 Krys
18S-21E-4	5	Dansfield #1 Hatch
18S-21E-4	6	Coastal States #1 Butt
18S-21E-9	7	Mobil #8-A Donigan
18S-21E-9	8	Dansfield #1 Baldwin Farms Unit D
18S-21E-1	9	Arkansas Fuel #2 St. Tr. 751
18S-21E-1	10	Sun #1 Nueces St. Tr. 786
18S-21E-6	11	Cities Service & Sunray DX #1 St. Tr. 59
18S-21E-9	12	Cox #1 Cohn
18S-21E-9	13	Carrl, et al. #1 Kelly
18S-21E-8	14	Bell & Dansfield #1 Baldwin Farms
18S-21E-3	15	Inexco #2 St. Tr. 683
18S-21E-3	16	Phillips #1 Frio
18S-21E-3	17	Mobil #1 St. Tr. 686
18S-21E-3	18	Phillips #1 Sand
18S-21E-2	19	Sinclair #1 St. Tr. 692
18S-21E-2	20	Sinclair #11 St. Tr. 707
18S-21E-2	21	Marathon #1 Mayo-Koonce Unit 1
18S-21E-1	22	Mobil #1 St. Tr. FGH Unit 1
18S-21E-4	23	Texas #1 St. Tr. 750-A
18S-21E-4	24	Mobil #1 Weil
18S-21E-9	25	Cowanco #1 Talbert
18S-21E-9	26	Chicago #1 Heinsohn
18S-21E-9	27	Getty #1 Guaranty Title & Trust
18S-21E-9	28	Canus #1 Kelly
18S-21E-8	29	Dansfield #1 Locke
18S-21E-8	30	Coastal States #1 City of Corpus Christi
18S-21E-6	31	Southern Union #1 North Beach
18S-21E-1	32	Shenandoah #1 St. Tr. 749
18S-21E-1	33	Shenandoah #1 Pope
18S-21E-6	34	Bell #1 Pope
18S-21E-6	35	Forest #1-A St. Tr. 59-A
18S-21E-2	36	Shenandoah #1 St. Tr. 708
18S-21E-1	37	Forest & Cities #1 St. Tr. 788
18S-21E-9	38	McFarlane #1 Guaranty Title & Trust
18S-21E-1	39	Southwestern #1 Guaranty Title & Trust
18S-21E-4	40	Chicago #1 Weil
18S-21E-9	41	Southland Royalty #1 Kelly
18S-21E-4	42	Burch, et al. #1 Dunn-Meaney
18S-21E-6	43	Bell #1 St. Tr. 59

Tobin Grid	Well number	Well name
18S-21E-4	44	Phillips #1 Plymouth
18S-21E-3	45	Phillips #A-3 West
18S-21E-1	46	Forest #3 St. Tr. 788
18S-21E-9	47	Dillard and Waltermire D-1 Donigan
18S-21E-9	48	Amoco #1 Kelly
18S-21E-3	49	Republic #56 Rachal
18S-21E-9	50	Canus #1 Wilson
18S-21E-9	51	Haas Brothers #1 Cox, et al., Unit 1
18S-21E-9	52	Champlin #C-1 Weil Brothers
18S-21E-9	53	Dansfield #1-C Flato
18S-21E-1	54	Forest #11 St. Tr. 786
18S-21E-1	55	Forest #2 St. Tr. 788
18S-21E-1	56	Atlantic Richfield #2 St. Tr. ABC Unit
18S-21E-9	57	Tidewater #2 Guaranty Title & Trust
18S-21E-9	58	Hanson and Metal Service #1 Baldwin Farms
18S-21E-9	59	Carrl #1 Kelly
18S-21E-8	60	Bell #2 Texas Mexican Railroad "A"
18S-21E-9	61	Bell and Dansfield #1 Allen
18S-21E-4	62	Cities Service & Sunray DX #1 St. Tr. 60
18S-22E-3	1	Republic & Forest #3 St. Tr. 786
18S-22E-3	2	Forest & Mobil #7 St. Tr. 786
18S-22E-2	3	Bell #1 Portland Gas Unit "D"
18S-22E-3	4	Cities Service #1 St. Tr. 40
18S-22E-2	5	Cities Service #1 St. Tr. 26
18S-22E-2	6	British-American #1 St. Lease #M-30453
18S-22E-1	7	Cities Service #3 St. Tr. 10
18S-22E-1	8	Cities Service #5 St. Tr. 9
18S-22E-1	9	Cities Service #2 St. Tr. 10
18S-22E-1	10	Cities Service #3 St. Tr. 14
18S-22E-1	12	Cities Service #1 St. Tr. 22
18S-22E-1	13	Cities Service & Sunray DX #3 St. Tr. 15
18S-22E-1	14	Jake Hamon #3 St. Tr. 8
18S-22E-6	15	Cities Service #1 St. Tr. 21
18S-22E-6	16	Austral #1 St. Tr. 20
18S-22E-9	17	Cities Service #1-B St. Tr. 72
18S-22E-4	18	Glasscock & Tidelands #1 St. Tr. 56
18S-22E-9	19	Atlantic #2 St. Tr. 62
18S-22E-9	20	Cities Service & Sunray DX #B-1 St. Tr. 71
18S-22E-9	21	Southland #1 St. Tr. 70
18S-22E-8	23	Gulf #2 St. Tr. 47, Lease #33099
18S-22E-8	24	Atlantic Refining #1 St. Tr. 36
18S-22E-8	25	Gulf #3 Texas St. Tr. 35, Lease #36611
18S-22E-8	26	Gulf #4 St. Tr. 48, Lease #33100
18S-22E-7	27	Atlantic Richfield #1 St. Tr. 34
18S-22E-8	28	Cities Service & Sunray DX #1 St. Tr. 49
18S-22E-8	29	Cities Service & Sunray DX #1 St. Tr. 64
18S-22E-8	30	Cities Service & Sunray DX #1 St. Tr. 52
18S-22E-7	31	Cities Service #4 St. Tr. 49
18S-22E-7	32	Atlantic Richfield #1 St. Tr. 33
18S-22E-7	33	Atlantic Richfield #1 St. Tr. 50
18S-22E-3	34	Mobil #1 St. Tr. 751
18S-22E-3	35	Arkansas Fuel #1 State Nueces Bay 751
18S-22E-2	36	Cox #A3 Portland Gas Unit
18S-22E-1	37	Atlantic #1 St. Tr. 23
18S-22E-1	38	Arkansas Fuel #1 St. Tr. 14
18S-22E-1	39	Hamon & McMoran #1 St. Tr. 15
18S-22E-1	40	Arkansas Fuel #1 St. Tr. 15
18S-22E-1	41	Cities Service & Sunray DX #2 St. Tr. 16
18S-22E-6	42	Arkansas #1 St. Tr. 16
18S-22E-6	43	Sun #1 Corpus Christi St. Tr. 21
18S-22E-5	44	Cities Service & Sunray DX #1 St. Tr. 45
18S-22E-4	45	Cities Service, et al. #1 St. Tr. 61
18S-22E-9	46	Cities Service #1 St. Tr. 74
18S-22E-8	47	Gulf #3 St. Tr. 53, Lease #33105
18S-22E-7	48	Cities Service #3 St. Tr. 52
18S-22E-1	49	Cities Service #4 St. Tr. 9
18S-22E-9	50	Cities Service #2 St. Tr. 61
18S-22E-1	51	Arkansas & Sunray #1 St. Tr. 10

Tobin Grid	Well number	Well name
18S-22E-2	52	Tenneco #2 St. Tr. 25
18S-22E-1	53	Texaco #1 St. Tr. 9
18S-22E-1	54	Hamon & McMoran #1 St. Tr. 9
18S-22E-1	55	Sinclair #1 St. Tr. 11
18S-22E-3	56	Forest #1 St. Tr. 786
18S-22E-3	57	Forest & Mobil #8 St. Tr. 786
18S-22E-3	59	Smith & Carr #1 Medical Prof. Building
18S-22E-8	60	Atlantic #1 St. Tr. 63
18S-22E-1	61	Arkansas Fuel, et al. #1 St. Tr. 2
18S-22E-8	62	Cities Service #2 St. Tr. 49
18S-23E-3	1	Cities Service #2 St. Tr. 4
18S-23E-3	2	Hamon #2 St. Tr. 8
18S-23E-4	3	Renwar & Phillips #1 Hogg
18S-23E-4	4	Sunray DX #1 St. Tr. 448
18S-23E-9	5	Atlantic Richfield #2 St. Tr. 471
18S-23E-9	6	Atlantic Richfield & Tidewater #1 St. Tr. 471
18S-23E-9	7	Atlantic Richfield #1 St. Tr. 454
18S-23E-9	8	Atlantic Richfield & Tidewater #1 St. Tr. 470
18S-23E-9	9	Atlantic Richfield & Tidewater #3 St. 45-47 Unit Tr. 470
18S-23E-9	10	Atlantic Richfield #6 St. Tr. 470
18S-23E-1	11	King Resources #1 St. Tr. 336
18S-23E-6	12	Shell #8 St. Tr. 349
18S-23E-6	13	Shell #4 St. Tr. 392
18S-23E-7	14	Atlantic Richfield #9 St. Tr. 429
18S-23E-1	15	La Gloria St. #334-1
18S-23E-3	16	Morgan #1-A Welder, et al.
18S-23E-1	17	Atlantic #2 St. Tr. 341
18S-23E-1	18	King Resources #1, St. Tr. 341
18S-23E-1	19	McMoran #2 St. Tr. 343
18S-23E-2	20	Renwar #1 Brown-Knight
18S-23E-2	21	Renwar #6 Hogg
18S-23E-3	22	Cities Service #1 St. Tr. 334
18S-23E-3	23	Tenneco #2 St. Tr. 5
18S-23E-3	24	Renway #4 Hogg
18S-23E-4	25	Getty #1 St. Tr. 446
18S-23E-4	26	Royal #1 St. Tr. 19
18S-23E-4	27	Cities Service #1 St. Tr. 17
18S-23E-5	28	Sunray #2 Hogg Picton
18S-23E-5	29	Atlantic #2 St. Tr. 415
18S-23E-5	30	Atlantic #3 St. Tr. 396
18S-23E-5	31	Pan American #1 St. Tr. 421
18S-23E-5	32	Atlantic #2 St. Tr. 413
18S-23E-6	33	McMoran #1 St. Tr. 352
18S-23E-6	34	Bass #1 St. Tr. 390
18S-23E-6	35	Shell #1 St. Tr. 346
18S-23E-6	36	Shell #1 St. Tr. 345
18S-23E-6	37	Shell #6 St. Tr. 349
18S-23E-6	38	McMoran #2 St. Tr. 351
18S-23E-7	39	Sinclair #1 St. Tr. 401
18S-23E-7	40	Arkansas Fuel et al. #1-C Wilson
18S-23E-7	41	Atlantic #1 St. Tr. 411
18S-23E-7	42	Sinclair #1 St. Tr. 404
18S-23E-8	43	Atlantic #1 St. Tr. 426
18S-23E-8	44	Getty #1 St. Tr. 443
18S-23E-8	45	Sun Gas #7 St. Tr. 424
18S-23E-8	46	Sun #8 St. Tr. 424
18S-23E-8	47	Sun #10 St. Tr. 423
18S-23E-9	48	Stanolind #1 St. Tr. 451
18S-23E-9	49	Getty #1 St. Tr. 445
18S-23E-9	50	Getty #1 St. Tr. 444
18S-23E-9	51	Cities Service #4 St. Tr. 456
18S-23E-6	52	McMoran #1 St. Tr. 351
18S-24E-3	1	Cities Service #1 St. Tr. 319
18S-24E-3	2	Humble #1 Harbor Island Gas Unit
18S-24E-9	3	Pure #1 Little
18S-24E-3	4	Conroe, et al. #1 St. Tr. 313
18S-24E-4	5	Panhandle #1 Grant et al.

Corpus Christi Fairway

Tobin Grid	Well number	Well name
18S-24E-4	6	Blanco #1 St. Tr. 485
18S-24E-9	7	Sinclair #1 St. Tr. 388
19S-20E-1	1	Republic #3 Gallagher
19S-20E-1	2	Republic #4 Gallagher
19S-20E-2	3	G.E.S. #1-B Deal
19S-20E-4	4	Hamon #1 Hoepfner
19S-20E-5	5	Newman Bros. et al. #1 Walton
19S-20E-6	6	Cherryville #1 Geistman Unit
19S-20E-6	7	Atlantic Richfield, et al. #1 London Gas Unit
19S-20E-6	8	Atlantic Richfield #1 London "B" Gas Unit
19S-20E-7	9	Atlantic Richfield #1 Callaway Gas Unit
19S-20E-7	10	Atlantic Richfield #A-1 Connolly Taylor Gas Unit
19S-20E-7	11	Mobil #5 Lehman
19S-20E-7	12	Socony Mobil #1 Lehman
19S-20E-7	13	Mobil #6 Chapman Ranch "B"
19S-20E-7	14	Socony Mobil #1 Chapman Ranch "B"
19S-20E-7	15	Socony Mobil, et al. #1 Lehman Gas Unit
19S-20E-2	16	Hoover #1 Baker
19S-20E-2	17	Thomas et al. #1 Hellman
19S-20E-1	18	Shell #1 Bevly
19S-20E-1	19	Huffington #1 Caldwell
19S-20E-1	20	Midwest #1 Head
19S-20E-1	21	Coastal States #1 Cuddihy Airport
19S-20E-1	22	Topp, et al. #1 Ratcliff, et al.
19S-20E-6	23	Inexco #1 Bevly
19S-20E-1	24	Phillips #1 Morgan "B"
19S-20E-2	25	Brown #2 Shields Gas Unit
19S-20E-5	26	Arkansas Fuel #1 Clark
19S-20E-5	27	Lone Star #1 Harrington
19S-20E-5	28	Lone Star #1 Smith "A"
19S-20E-4	29	Stanolind #1 Ocker
19S-20E-4	30	Texaco #1 White
19S-20E-5	31	Southern Union #1 Bevly
19S-20E-5	32	Midwest #1 Walton
19S-20E-5	33	American Petrofina & Walton #1 Walton
19S-20E-8	34	Richardson #1 Walton
19S-20E-8	35	Morgan & Geiser #40-1 Chapman Ranch
19S-20E-7	36	Atlantic & Skelly #1 Horne
19S-20E-7	37	Morgan & Geiser #40-2 Chapman Ranch
19S-20E-7	38	Texaco #31 Chapman
19S-20E-7	39	Texaco #30 Chapman
19S-20E-7	40	Atlantic #1 Taylor-Conolly
19S-20E-1	41	Magnolia #22 Baldwin
19S-20E-7	42	Mobil #2 Leman
19S-20E-3	43	Phillips #1 Mastin
19S-20E-3	44	Shield & Chapman #1 Hoting
19S-20E-2	45	Kinksmith & Ward #1 Merritt
19S-20E-2	46	Gilly #1 Merritt
19S-20E-2	47	May #2 Merritt Unit
19S-20E-2	48	May et al. #1 Merrit Unit
19S-20E-2	49	Brawn #1 Flornke
19S-20E-9	50	Anderman #1 Ocker
19S-21E-3	1	Hamon #1 Peterson Properties
19S-21E-3	2	Nor Am #1 Peterson Properties
19S-21E-2	3	Sinclair #1 Corpus Christi ISD
19S-21E-5	4	Pan American #1 U.S.A.
19S-21E-4	5	Coastal States #1 Kraft
19S-21E-4	6	Sunray DX #3 Manley
19S-21E-4	7	Getty #1 Bevly
19S-21E-4	8	Socony Mobil, et al. #1 Russell
19S-21E-9	9	Mobil #1 Johnson
19S-21E-9	10	Mobil & Mitchell #1 Crook Gas Unit
19S-21E-9	11	Mobil #3 Lehman Gas Unit
19S-21E-8	12	Centennial #1 Smith
19S-21E-8	13	Cherryville #1 Cech
19S-21E-3	14	Harkins #1 Woodman & Evans
19S-21E-2	15	Knox #1 Holley

Tobin Grid	Well number	Well name
19S-21E-3	16	Sinclair-Prairie #1 Folda
19S-21E-3	17	Sinclair #1 City of Corpus Christi Gas Unit 1
19S-21E-2	18	Hamon #1 Pulliam
19S-21E-2	19	Hamon #1 Sikora
19S-21E-4	20	Morgan #1 Cooke
19S-21E-4	21	Sunray DX #4 Manley
19S-21E-5	22	Garnett & Sullivan #1 Nemee
19S-21E-9	23	Mobil #B-8 Chapman Ranch
19S-21E-9	24	Mobil #B-4 Chapman Ranch
19S-21E-9	25	Morgan & Geiser #B-1 Crook
19S-21E-9	26	Clinton #1-V Sines
19S-21E-8	27	Jocelyn-Varn #1 Garrett, et al.
19S-21E-8	28	Renwar #1 Cech
19S-21E-7	29	Heard & BDK #1 Guaranty National Bank & Trust
19S-21E-7	30	Aztec (Davis) #1 Gwynn et al.
19S-21E-7	31	Engelke, et al. #1 Gwynn
19S-21E-7	32	Lone Star #1 Gwynn
19S-21E-2	33	Hamon #1 Pernitas Partners
19S-21E-3	34	Nor Am #1 Vision Unit
19S-21E-3	35	Brown & Wheeler #1 Folda
19S-21E-7	36	Hamon, et al. #1-A Katz
19S-21E-9	37	Mobil, et al. #2 Lehman Gas Unit
19S-22E-3	1	Bennett #1 Polnisch
19S-22E-1	2	Cities Service & Sunray DX #1 St. Tr. 51
19S-22E-1	3	Atlantic-Richfield (Cities Service) #1 St. Tr. 81
19S-22E-1	4	Southern Petroleum & Southland Royalty #1 St. Tr. 81
19S-22E-1	5	Kilroy, et al. #1 St. Tr. 83
19S-22E-1	6	Cherryville #1 St. Tr. 81
19S-22E-4	7	Atlantic Refining #1 A.T. Pearse
19S-22E-9	8	Lone Star (Driscoll, et al.) #1 Smith, et al.
19S-22E-9	9	Marion #1 Peterson
19S-22E-9	10	Arnold & Morgan #1 Koemel
19S-22E-8	11	Coastal States #1 Dunn, et al.
19S-22E-7	12	Humble #D-9 East Flour Bluff - State
19S-22E-7	13	Humble #4 East Flour Bluff - State "F"
19S-22E-2	14	Marathon #1 Silcock & Baetz
19S-22E-4	15	Humphrey & Cox #1 Benys
19S-22E-4	16	Mitchell, et al. #1 Nugent
19S-22E-5	17	Humble #2 Flour Bluff Gas Unit #1
19S-22E-8	18	Humble #1 Duncan
19S-22E-7	19	Humble #13 East Flour Bluff "D"
19S-22E-7	20	Humble #8 East Flour Bluff "E"
19S-22E-7	21	Humble #F-3 East Flour Bluff
19S-22E-1	23	Cities Service #2 St. Tr. 96
19S-22E-1	24	Anadarko #1 St. Tr. 81
19S-23E-3	1	Cities Service #1 St. Tr. 84
19S-23E-3	2	Cities Service #1 St. Tr. 88
19S-23E-3	3	Cities Service #4 St. Tr. 88
19S-23E-3	4	Cities Service #1 St. Tr. 89
19S-23E-3	5	Atlantic-Richfield #4 St. 45-47, Unit Tract 470
19S-23E-3	6	Atlantic-Richfield & Tidewater #5 St. Tr. 420
19S-23E-2	7	Tenneco, et al. #1 St. Tr. 458
19S-23E-1	8	Atlantic-Richfield, et al. #1 Mustang Island Deep Unit
19S-23E-4	9	Getty #1 St. Tr. 41
19S-23E-9	10	Humble #1 Laguna Madre St. Tr. 52
19S-23E-7	11	Arkansas Fuel #1 St. Tr. 905-S
19S-23E-2	12	Sunray #2 St. Tr. 461
19S-23E-1	13	Atlantic #1 State - Corpus Christi Bay 436
19S-23E-1	14	Atlantic, et al. #1 Wilson, St. Tr. 595
19S-23E-6	15	Southland Royalty #1 St. Tr. 886
19S-23E-6	16	Cherryville #1 St. Tr. 886
19S-23E-6	17	Wilson, et al. #A-1 St. Tr. 462
19S-23E-4	18	Coastal States #1 St. Tr. 92

Corpus Christi Fairway

Tobin Grid	Well number	Well name
19S-23E-4	19	McMoran #1 St. Tr. 37
19S-23E-9	20	Humble #5 East Flour Bluff - State "M"
19S-23E-9	21	Humble & Sunray DX #"M"-4 East Flour Bluff - State
19S-23E-9	22	Humble #2 East Flour Bluff - State "FF"
19S-23E-8	23	McMoran #1 Wilson
19S-23E-8	24	McMoran #1 St. Tr. 906-S
19S-23E-7	25	Shell #1 St. Tr. 899-S
19S-23E-7	26	Cities Service #1 St. Tr. 773
19S-23E-3	27	Cities Service #2 St. Tr. 88
19S-23E-3	28	McMoran #2 St. Tr. 97
19S-23E-3	29	McMoran #1-A St. Tr. 84
19S-23E-3	30	Cities Service #1 St. Tr. 87
19S-23E-3	31	Cherryville #1 St. Tr. 84
19S-23E-3	32	Union Oil (Los Nietos) #1 St. Tr. 87
19S-23E-6	33	Wilson #A-2 St. Tr. 462
19S-23E-3	34	McMoran Exploration #1 St. Tr. 97
19S-24E-3	1	Sun & Seaboard #1-B St. Tr. 882
19S-24E-3	2	Shell #1 St. Tr. 884
19S-24E-4	3	Gulf #1 St. Tr. 889, Lease #41338
19S-24E-5	4	Humble #1 Gulf of Mexico St. Tr. 772
19S-24E-4	5	Shell #1 St. Tr. 891-S
19S-24E-4	6	Shell #1 St. Tr. 896-S
19S-24E-5	7	Gulf, et al. #B-1 Block 772
19S-24E-9	8	Zapata & C&K #1 St. Tr. 773-L, Lease #57742
19S-24E-8	9	Gulf #1 St. Tr. 774, Lease #41321
19S-24E-7	10	Union of California #1 St. Tr. 775-L
19S-24E-4	11	Gulf, et al. #A-3 St. Tr. 889
19S-24E-3	12	Arkansas Fuel #1 St. Tr. 880-S
19S-24E-3	13	Shell #1 St. Tr. 885-S
19S-24E-3	14	Sun #1 St. Tr. 883
19S-24E-4	15	Gulf Energy & Minerals #1 St. Tr. 898-S
19S-24E-9	16	Zapata & C&K #3 St. Tr. 773-L, Lease #57742
19S-24E-9	17	Gulf #1 St. Tr. 773, Lease #57741
19S-24E-8	18	Patrick #1 St. Tr. 774-L
20S-20E-9	1	Humble #33 King Ranch-Chiltipin
20S-20E-2	2	Morgan & Southern Minerals #43-1 Chapman
20S-20E-2	3	Morgan & Southern Minerals #43-2 Chapman
20S-20E-3	4	Texaco #55 Luby
20S-20E-3	5	Texaco #65 Luby
20S-20E-4	6	Sun #19 McCain
20E-20E-1	7	Chicago #1-73 Chapman Ranch
20S-20E-1	8	Morgan & Geiser #1-73 Chapman Ranch
20S-20E-3	9	Texaco #30 K. L. Shaffer NCT-1
20S-20E-1	10	Morgan & Geiser #1 Chapman "B"
20S-20E-6	11	Morgan #1 Chapman Heirs-Cowles-Chapman
20S-20E-6	12	Morgan, et al. #117-1 "B" Chapman Heirs
20S-20E-4	13	Exxon #60 King Ranch Chiltipin
20S-20E-7	14	Humble #3 King Ranch-Lobo
20S-20E-4	15	Seaboard #52 Luby
20S-21E-2	1	Marion & Double U #1 Chapman
20S-21E-8	2	Humble #G-21 King Ranch-East Laureles
20S-21E-3	3	Morgan, et al. #C-1 Chapman
20S-21E-3	5	Mobil #B-9 Chapman Ranch
20S-21E-6	6	Exxon #G-38 King Ranch
20S-21E-6	7	Exxon #G-35 King Ranch-East Laureles
20S-21E-6	8	Humble #G-14 King Ranch-East Laureles
20S-21E-5	9	Morgan, et al. #2 Chapman Heirs "C"
20S-21E-1	10	Humble #3 King Ranch-East Laureles "P"
20S-21E-6	11	Humble #G-1 King Ranch-East Laureles
20S-21E-7	12	Humble #G-6 King Ranch-East Laureles
20S-21E-8	13	Humble #G-3 King Ranch-East Laureles
20S-21E-8	14	Humble #G-9 King Ranch-East Laureles
20S-22E-1	1	Humble #1 Laguna Madre St. Tr. 150
20S-22E-1	2	Humble #1 Pita Island Field Gas Unit 1
20S-22E-8	3	Pure #A-1 Laguna Madre State 168
20S-22E-2	4	Hill #1 Richardson, et al.
20S-22E-1	5	Humble #3 "DD" East Flour Bluff State

Tobin Grid	Well number	Well name
20S-22E-7	6	Sun #6 Dunn-McCampbell "B"
20S-22E-8	7	Carrl #1 St. Tr. 182
20S-22E-5	8	Lone Star #1 St. Tr. 148
20S-22E-6	9	McMoran #2 St. Tr. 171
20S-22E-6	10	McMoran #1 St. Tr. 171
20S-22E-1	11	Humble #1 Laguna Madre St. Tr. 173
20S-22E-1	12	Centura #1 St. Tr. 46
20S-22E-8	13	American Petrofina #2 St. Tr. 169
20S-22E-9	14	Exxon #B-10 King Ranch-East Laureles
20S-22E-6	15	Coquina #1 St. Tr. 177
20S-22E-3	16	Humble #B-3 King Ranch-Laureles
20S-22E-6	17	Getty #1 St. Tr. 179
20S-22E-9	18	Humble #G-4 King Ranch-East Laureles
20S-22E-9	19	Exxon #B-11 King Ranch-East Laureles
20S-22E-9	20	Exxon #B-12 King Ranch-East Laureles
20S-22E-8	21	Carrl #1 St. Tr. 167
20S-23E-3	1	Cherryville #1 Dunn, et al.
20S-23E-1	2	C&K #1 St. Tr. 920-S
20S-23E-3	3	Socony Mobil #1 Dunn
20S-23E-1	4	Arkansas Fuel #1 St. Tr. 910-S
20S-23E-1	5	Arkansas Fuel #1 St. Tr. 911-S
20S-23E-2	6	Coastal States, et al. #1 St. Tr. 915-S
20S-23E-5	7	Louisiana Land & Exploration #1 St. Tr. 921-S
20S-23E-8	8	Standard of Texas #1, State Gulf #932-58
20S-23E-4	9	Samedan #2 Jones
20S-23E-9	10	Gulf #1 St. Tr. 818-L, Lease #57591
20S-23E-4	11	McMoran #2 St. Tr. 924-S
20S-24E-3	1	Cities Service #1 St. Tr. 795-L
20S-24E-4	2	Inexco #1 St. Tr. 797-L

Tobin Grid	Well number	Well name
21S-19E-8	1	Humble #4 King Ranch Visnaga
21S-19E-8	2	Humble #3 King Ranch Visnaga
21S-19E-8	3	Exxon #11 King Ranch Visnaga
21S-19E-7	4	Humble #8 King Ranch Visnaga
21S-19E-8	6	Humble #10 King Ranch Visnaga
21S-19E-9	7	Mokeen #1-A HAM
21S-19E-9	8	Mokeen #1 HAM Fee
21S-19E-9	9	Mokeen #1 May
21S-19E-9	11	Mokeen #1 Nossel
21S-19E-1	12	Humble #1 Heep Field GU
21S-19E-9	13	Viking #1 Muil
21S-19E-7	17	Humble #13 King Ranch - Madero
21S-19E-8	20	Humble #1 King Ranch Visnaga
22S-18E-1	1	Assoc. Oil & Gas #1 Keepers
22S-18E-1	2	Hill, et al. #1 Hubert
22S-18E-1	3	Hill, et al. (Wagner, Hay & Texas Crude) #1 Brookshire
22S-18E-1	4	Morgan Minerals #1 Hubert
22S-18E-1	5	Mokeen #1-A Hubert
22S-18E-5	6	Hill #1 Hayse
22S-18E-6	7	Conroe #1 O'Brien
22S-18E-6	8	Cities Service #1-B May, et al.
22S-18E-6	9	Heep, et al. #1 Hubert
22S-18E-6	10	Arkansas Fuel #1-C Kaufer
22S-18E-6	11	Arkansas Fuel #1 Schonefeld
22S-18E-6	12	Cities Service #1 Poteet
22S-18E-6	13	McDermott #1 Baldeschwiler
22S-18E-8	14	Mokeen, et al. #1 Yeargan
22S-18E-8	15	Humble #35-B Kenedy
22S-18E-7	16	Humble #1 Kenedy
22S-18E-7	17	Humble #32-B Kenedy
22S-18E-7	18	Humble #34-B Kenedy
22S-18E-7	19	Humble #33-B Kenedy
22S-18E-7	20	Humble #31-B Kenedy
22S-18E-7	21	Arkansas Fuel #1 Womack
22S-18E-7	22	Arkansas Fuel #2-B Kaufer
22S-18E-7	23	Arkansas Fuel #1-B Kaufer
22S-18E-7	24	Humble #1 Mueller
22S-18E-7	25	Arkansas Fuel #1 Poteet
22S-18E-6	26	Harkins, et al. #1 Yaklin
22S-18E-7	27	Cities Service #1-B Koch GU
22S-18E-7	28	Humble #70 Sarita
22S-18E-7	29	Humble #20 Sarita
22S-18E-6	30	Conroe, et al. #1 Koch
22S-18E-7	32	Arkansas Fuel #1 Stubhart
22S-18E-7	33	Arkansas Fuel #1 Kaufer
22S-19E-3	1	Morgan #1 Hiethaus, et al.
22S-19E-4	2	Arkansas Fuel #1 Bryant
22S-19E-8	3	Humble #24-B East
22S-19E-8	4	Humble #23-B East
22S-19E-8	5	Humble #18-B East
22S-19E-8	6	Humble #21-B East
22S-19E-8	7	Sun #1 St. Tr. 376
22S-19E-8	8	Sun #1 St. Tr. 372
22S-19E-8	9	Humble #1-F East
22S-19E-8	10	Superior #1 Koch
22S-19E-8	11	Texas Oil & Gas #1 Turcotte
22S-19E-9	12	Southern Minerals #1 Fimble
22S-19E-9	13	Mokeen #1-D Kaufer
22S-19E-9	14	Exxon #140 Sarita
22S-19E-2	15	Texas #1 St. Tr. 79
22S-19E-2	16	Pan American #2 St. Tr. 84
22S-19E-2	17	Pan American #3 St. Tr. 84
22S-19E-2	18	Sun #1 Hubert
22S-19E-2	19	Sun #3 Fimble
22S-19E-2	20	Pan American #1 St. Tr. 81

Tobin Grid	Well number	Well name
22S-19E-3	21	Sun #1 Schonefeld
22S-19E-3	22	Morgan #1 Huff
22S-19E-3	23	McCormick, et al. #1 King Ranch
22S-19E-3	24	Cities Service #1 Schonefeld
22S-19E-2	25	Texas #1 St. Tr. 82
22S-19E-2	26	Texaco #4 St. Tr. 82
22S-19E-2	27	Mokeen #1 Goetsch
22S-19E-2	28	Mokeen #2 Goetsch
22S-19E-2	29	Mokeen #1 Prailes
22S-19E-2	30	Cities Service #1 St. Tr. 80
22S-19E-3	31	Mokeen #1-A May
22S-19E-3	32	Mokeen #1 Yeary
22S-19E-3	33	McCormick, et al. #1 Schonefeld
22S-19E-3	34	Mokeen #2 Yaklin
22S-19E-3	35	Tenneco #1 Hubert
22S-19E-3	36	Arkansas Fuel #1 Baker, et al.
22S-19E-3	37	Cities Service #1 Yaklin
22S-19E-3	38	Arkansas Fuel #1 Schonefeld
22S-19E-3	39	Sun #2 May
22S-19E-4	40	Arkansas Fuel #1 Orr
22S-19E-4	41	Arkansas Fuel #1 May
22S-19E-4	42	Arkansas Fuel #1 Langham
22S-19E-4	43	Forest #1 Alvarado
22S-19E-5	44	Arkansas Fuel #1 Ferrell
22S-19E-4	45	Cities Service (Arkansas Fuel) #1-B Mittag, et al.
22S-19E-4	46	Arkansas Fuel #1 Mittag
22S-19E-5	47	Davis, et al. #1 T. Koch Gas Unit #2
22S-19E-5	48	Cosden #1 Hubert
22S-19E-5	49	Gulf #1 Dietz
22S-19E-5	50	Cosden #2 Hubert
22S-19E-5	51	Arkansas Fuel #1 Runnells
22S-19E-5	52	Katz #1 Dietz
22S-19E-2	53	Mokeen #1 Whitley
22S-19E-6	54	Coastal States #1 St. Tr. 74
22S-19E-6	55	Carrl #1 St. Tr. 71
22S-19E-6	56	Continental #1 St. Tr. 70
22S-19E-7	57	Sun #1 St. Tr. 75
22S-19E-7	58	Humble #19-B East
22S-19E-7	59	Carrl #1 St. Tr. 69
22S-19E-7	60	Carrl, et al. #1 St. Tr. 68
22S-19E-7	61	Carrl #1 Coastal States, et al.
22S-19E-8	62	Humble #25-B East
22S-19E-9	63	Humble #69 Sarita
22S-19E-4	64	Davis, et al. #1 J. Koch Unit
22S-19E-3	65	Sun #3 May
22S-19E-3	66	Sun #2 Schonefeld
22S-19E-8	67	Exxon #136 Sarita
22S-19E-9	68	Exxon #137 Sarita
22S-19E-9	69	Humble #95 Sarita
22S-19E-9	70	Humble #81 Sarita
22S-19E-9	71	Humble #1 St. Tr. 381
22S-19E-6	72	Whiffen #1 St. Tr. 72
22S-19E-8	73	Mokeen #1 Neubaurer
22S-19E-3	74	Sun #1 Fimble
22S-19E-9	75	Davis and Chiles #1 Koch Unit
22S-19E-9	76	Sun #1 Baffin St. Tr. 373
22S-19E-8	77	Sinclair #1 St. Tr. 377
22S-19E-4	78	Arkansas Fuel #1 Huff
22S-19E-4	79	Heep & Modesett #1 Childs
22S-19E-4	80	Heep & Modesett #2 Childs
22S-19E-2	81	Pan American #2 St. Tr. 81
22S-19E-2	82	Morgan Minerals #1 Limp
22S-19E-4	83	Heep, et al. #1 Hubert
22S-19E-3	84	Turnbull & Cox #1 Hubert
22S-19E-2	85	Pan American #1 St. Tr. 84
22S-19E-3	86	Sun #2 Fimble
22S-19E-9	87	Texas Oil & Gas #1-B Martin G. U. (#2 Collins)

Kenedy Fairway

Tobin Grid	Well number	Well name
22S-19E-2	88	Texaco #3 St. Tr. 82
22S-19E-4	89	Cities Service #1-C May
22S-19E-6	90	Carrl, et al. #1 St. Tr. 70
22S-19E-2	91	Texas #1 St. Tr. 83
22S-19E-3	92	Tana #1 Hubert
22S-19E-3	93	Cities Service #1-B Huff
22S-19E-3	94	Mokeen #1 Hubert
22S-19E-4	95	Arkansas Fuel #1 Hubert
22S-19E-4	96	Arkansas Fuel #A-1 Hubert
22S-19E-4	97	Arkansas Fuel #1 Riskin-McGee
22S-19E-4	98	Arkansas Fuel #C-1 Hubert
22S-19E-4	99	Arkansas Fuel #1 Beckman
22S-19E-4	100	Arkansas Fuel #1 May, et al.
22S-20E-9	5	Humble #1 St. Tr. 65
23S-18E-1	1	Humble #46 Sarita
23S-18E-1	2	Humble #2-B Kenedy
23S-18E-1	16	Exxon #19-E Kenedy
23S-18E-1	17	Exxon #138 Sarita
23S-18E-1	18	Humble #1 Beyer
23S-18E-1	19	Humble #128 Sarita
23S-18E-1	20	Humble #1-B Kenedy
23S-19E-2	1	Humble #17-B East
23S-19E-2	2	Humble #10-B East
23S-19E-2	3	Humble #14-B East
23S-19E-2	4	Humble #13-B East
23S-19E-2	5	Humble #9-B East
23S-19E-2	6	Humble #8-B East
23S-19E-1	25	Humble #15-B East
23S-19E-3	26	Exxon #35 Sarita
23S-19E-3	29	Humble #12-E Kenedy
23S-19E-3	30	Humble #5-B East
23S-19E-3	34	Humble #97 Sarita
23S-19E-3	35	Humble #98 Sarita
23S-19E-3	36	Humble #122 Sarita
23S-19E-3	37	Humble #7-E Kenedy
24S-18E-9	7	Humble #54 East
24S-18E-9	8	Humble #38 East
24S-18E-9	10	Exxon #77 East
24S-18E-9	14	Humble #32 East
24S-18E-9	15	Humble #39 East
24S-18E-9	20	Exxon #85 East
24S-18E-9	21	Humble #43 East
24S-18E-9	22	Humble #34 East
25S-17E-1	1	Exxon #58 East
25S-17E-7	10	Exxon #35 Armstrong
25S-17E-1	14	Exxon #87 East
25S-18E-1	1	Humble #1-E East
25S-18E-1	2	Humble #4 Armstrong
25S-18E-1	3	Exxon #41 East
25S-18E-1	4	Humble #56 East
25S-18E-3	5	Humble #22 East
25S-18E-3	6	Humble #21 East
25S-18E-3	7	Exxon #83 East
25S-18E-3	8	Humble #17 East
25S-18E-3	9	Exxon #71 East
25S-18E-3	10	Humble #36 East
25S-18E-3	11	Humble #2 East
25S-18E-3	12	Exxon #61 East
25S-18E-4	13	Humble #15 Armstrong
25S-18E-4	14	Humble #16 Armstrong
25S-18E-4	15	Exxon #29 Armstrong
25S-18E-4	16	Humble #23 Armstrong
25S-18E-4	17	Humble #10 Armstrong
25S-18E-4	18	Humble #12 Armstrong
25S-18E-4	19	Humble #11 Armstrong

Tobin Grid	Well number	Well name
25S-18E-4	20	Humble #14 Armstrong
25S-18E-5	21	Humble #25 Armstrong
25S-18E-5	22	Exxon #32 Armstrong
25S-18E-5	23	Exxon #44 Armstrong
25S-18E-5	24	Humble #21 Armstrong
25S-18E-6	25	Humble #9 Armstrong
25S-18E-6	26	Humble #17 Armstrong
25S-18E-7	27	Humble #20 Armstrong
25S-18E-8	28	Exxon #34 Armstrong
25S-18E-8	29	Exxon #29 Armstrong
25S-18E-8	30	Humble #8 Armstrong
25S-18E-8	31	Exxon #38 Armstrong
25S-18E-9	32	Humble #18 Armstrong
25S-18E-9	33	Exxon #37 Armstrong
25S-18E-9	34	Exxon #40 Armstrong
25S-18E-9	35	Humble #5 Armstrong
25S-18E-9	36	Exxon #33 Armstrong
25S-18E-9	37	Humble #6 Armstrong
25S-18E-9	38	Humble #7 Armstrong
25S-18E-8	39	Exxon #46 Armstrong
25S-18E-6	40	Exxon #30 Armstrong
25S-18E-4	41	Humble #2 Armstrong
25S-18E-3	42	Exxon #92 East
25S-18E-3	43	Exxon #75 East
25S-18E-3	44	Humble #1 East
26S-18E-2	1	Humble #22 Armstrong
26S-18E-2	2	Exxon #31 Armstrong
26S-18E-3	3	Exxon #36 Armstrong
26S-18E-3	4	Humble #27 Armstrong
26S-18E-3	5	Humble #3 Armstrong

Tobin Grid	Well number	Well name
27S-17E-7	1	Humble #9 Kleberg-Stillman
27S-17E-8	2	Exxon #28 Kleberg-Stillman
27S-17E-8	3	Humble #4 Kleberg-Stillman
27S-17E-4	4	Humble #16 Kleberg-Stillman
27S-17E-8	5	Exxon #42 Stillman
27S-18E-1	1	Humble #10 Saltillo
27S-18E-2	2	Humble #1 King Ranch - Loma Prieta Area
27S-18E-4	3	Humble #2 King Ranch - Loma Prieta Area
27S-18E-5	4	Standard of Texas #1 Garcia
27S-18E-5	5	Humble #1 Garcia, et al.
27S-18E-7	6	Abercrombie #1 Garcia
28S-16E-4	1	Shell #1 Villareal
28S-16E-5	2	Humble #3 Del Ray Cattle
28S-16E-6	3	Humble #1 Garcia
28S-16E-5	4	Mobil #4-3 Garza
28S-16E-5	5	Magnolia #1 Garza
28S-16E-7	6	Humble #1 Corrales
28S-16E-9	7	Humble #13 Shepperd
28S-16E-3	8	Argo & Coates #1 Guerra
28S-16E-3	9	Shell #1 Guerra
28S-16E-3	10	Sun #1 Guerra
28S-16E-2	11	Magnolia #2-1 Garza
28S-16E-4	12	Humble #10 Shepperd
28S-16E-4	13	Humble #11 Shepperd
28S-16E-4	14	Humble #14 Shepperd
28S-16E-7	15	Forrest #2 Schaleben
28S-16E-7	16	Forrest #1 Schaleben
28S-16E-8	17	Humble #4 Del Ray Cattle
28S-16E-8	18	Humble #1 Del Ray Cattle
28S-16E-9	19	Humble #9 Shepperd
28S-17E-1	1	Humble #7 Kleberg-Stillman
28S-17E-2	2	Humble #12 Kleberg-Stillman
28S-17E-4	3	Hanson #1 Dobbins
28S-17E-5	4	Hanson #1 Corbett
28S-17E-9	5	Hanson #1 Fryer-Corbett
28S-17E-7	6	Texas #2 Corbett
28S-17E-4	7	Southwestern #3 First National Bank
28S-17E-9	8	Forrest #1-1 Rudman
28S-17E-9	9	Smith #1 McAllen
28S-17E-9	10	Slick & Rudman #1 McAllen
28S-17E-9	11	Smith #1 First National Bank
28S-17E-9	12	Louisiana Land #1 McAllen
28S-17E-1	13	Humble #5 Kleberg-Stillman
28S-17E-1	14	Humble #14 Kleberg-Stillman
28S-17E-1	15	Humble #8 Kleberg-Stillman
28S-17E-1	16	Humble #18 Kleberg-Stillman
28S-17E-2	17	Exxon #24 Stillman
28S-17E-3	18	Holmes #1 Mathieu
28S-17E-7	19	Superior #1 Banker
28S-17E-7	20	Magnolia & Abercrombie #1 Yturria Cattle
28S-17E-1	21	Exxon #37 Stillman
28S-17E-1	22	Exxon #36 Stillman
28S-17E-6	23	Exxon #40 Kleberg-Stillman
28S-17E-1	24	Exxon #41 Stillman-Pasture
28S-17E-1	25	Exxon #39 Stillman-Pasture
28S-18E-3	1	Sinclair #1 Garcia
28S-18E-3	2	Austral #1 Garcia
28S-18E-4	3	De Lange-Neathery #1 Yturria Cattle
28S-18E-4	4	Tidewater, et al. #1 Bakke
28S-18E-6	5	Humble #2 Garcia
28S-18E-7	6	Humble #1 "B" Garcia
28S-18E-7	7	Coastal States #1 Conley

Cameron Fairway

Tobin Grid	Well number	Well name
28S-18E-9	8	Newman #1 Yturria Cattle
28S-18E-9	9	Monsanto #1 Myers
28S-18E-2	10	Continental #2 Garcia
28S-18E-4	11	Heep #1 Garcia-Dougherty
28S-19E-2	1	Texas #8 Yturria Cattle
28S-19E-4	2	Texaco #10A Yturria Cattle
28S-19E-7	3	Humble #1 Deming
28S-19E-7	4	Humble #1 Murphy
28S-19E-2	5	Texaco #A-13 Yturria Cattle
28S-19E-4	6	Texas #9 Yturria Cattle
28S-19E-4	7	Texas #7 Yturria Cattle
28S-19E-4	8	Texas #6 Yturria Cattle
28S-19E-7	9	Humble #2 Murphy
28S-19E-7	10	Hunt #1 Hearne
28S-19E-7	11	Samedan #1 Bomba
28S-19E-8	12	Burns #1 Freeman
28S-19E-9	13	Texas #2 Southern Fruit
28S-19E-9	14	Texas #1 Southern Fruit
28S-19E-9	15	Geodynamics #1 Morrow
28S-20E-6	1	Humble #1 Sauz Ranch-Tenerias
28S-20E-3	2	Humble #1 Sauz Ranch-Jardin
28S-20E-8	3	Humble #5 Sauz Ranch
28S-21E-3	1	Humble #1 King Ranch-Parral
28S-21E-4	2	Humble #2 Sauz Ranch-Tenerias
29S-15E-9	20	Mobil #9 Santa Cruz Farms
29S-16E-1	2	Magnolia #1 Hidalgo-Willacy Oil
29S-16E-1	3	Hargrave #1 Rio Farms
29S-16E-2	4	Humble #3 Shepperd Estate
29S-16E-2	5	Humble #6 Shepperd Estate
29S-16E-2	6	Humble #1 La Coma Gas
29S-16E-3	7	Humble #12 Shepperd Estate
29S-16E-4	8	Calvert & Manley #1 Hidalgo-Willacy Oil
29S-16E-4	9	Hidalgo-Willacy Oil #1 Lacona Land & Cattle
29S-16E-4	10	Gulf #3 Lee
29S-16E-4	11	Gulf #2 Lee
29S-16E-4	12	Gulf #1 "A" Lee
29S-16E-7	13	Sun #3 Heard-Davenport
29S-16E-8	14	Pan American #1 Juan
29S-16E-8	15	California Time #1 Schultz Heirs
29S-16E-9	16	Western Natural #1 Roberts
29S-16E-9	17	Magnolia #1 Santa Cruz-Hendrix
29S-16E-9	18	Western Natural #1 Evans
29S-16E-9	19	Atlantic Richfield #2 Smith Gas
29S-16E-9	20	Mobil #9 Santa Cruz Farms
29S-16E-9	21	Gulf Oil #1 Taylor
29S-16E-9	22	Gulf #1 Turner
29S-16E-8	23	Western Natural Gas #5 Cardenas
29S-16E-1	24	Energy Resources "B" 2 Rio Farms
29S-17E-1	1	Pan American #1 Yturria
29S-17E-2	2	Pan American #1 Rio Farms
29S-17E-3	3	Magnolia #1 Pollock
29S-17E-9	4	McCulloch #1 Harding
29S-17E-9	5	Mobil #1 Patrick
29S-17E-2	6	Inexco #1 Hidalgo-Willacy
29S-18E-1	1	Hunt #1 Wertz
29S-18E-1	2	Sinclair-Prairie #1 Wertz
29S-18E-1	3	Lone Star #1 Wertz
29S-18E-2	4	Pan American #1 Riggan
29S-18E-2	5	Pan American #1 Coleman
29S-18E-2	6	Pan American #1 Morrow
29S-18E-3	7	Mobil-Magnolia #1 Garrett
29S-18E-3	8	Mitchell #1 Joseph

Tobin Grid	Well number	Well name
29S-18E-4	9	Standard of Kansas #1 Mann
29S-18E-5	10	Union #1 Gillet
29S-18E-2	11	Amoco #1-3 Oberg
29S-18E-3	12	Mitchell #1 Cox
29S-18E-7	13	Stanolind #1 Boden
29S-18E-9	14	Mid West #1 Dayton
29S-18E-2	15	Mitchell #2 Cox
29S-19E-1	1	Sun #1 Scott
29S-19E-2	2	Shell #1 Gerdts
29S-19E-2	3	Quintana #1 Ladd
29S-19E-2	4	Hamon #1 Iness
29S-19E-2	5	Shell #1 McCullough
29S-19E-4	6	H.P.S. Prod., et al., #1 Martin
29S-19E-2	7	Shoreline #1 Walker
29S-19E-5	8	Bering #1 Santa Rosa
29S-19E-5	9	Sun #1 Santa Rosa
29S-19E-7	10	Magnolia #1 Seliger
29S-19E-4	11	Geochemical Surveys #1 Cole
29S-19E-5	12	Harkins & MacDonald #1 Hildebrandt
29S-20E-4	1	Gulf #1 Stone
29S-20E-5	2	Humble #1-1 Willimar Field
29S-20E-8	3	Pan American #5 Bell
29S-20E-9	4	Bridwell #6 Bridwell
29S-20E-9	5	Bridwell #7 Bridwell
29S-21E-5	1	Humble #3 Sauz Ranch-Nopal
29S-21E-8	2	Humble #2 Sauz Ranch-Nopal
29S-21E-8	3	Humble #6 Sauz Ranch-Nopal
29S-21E-9	4	Humble #1 Sauz Ranch-Nopal
29S-21E-9	5	Humble #5 Sauz Ranch-Nopal
29S-22E-8	1	Pan American #1 S. T. 569
30S-16E-2	1	Pan American #25 La Blanca
30S-16E-4	2	Union #2 Wysong
30S-16E-5	3	Union #1 Garcia
30S-16E-5	4	La Gloria #2 Harding
30S-16E-6	5	La Gloria #2-2 La Blanca
30S-16E-7	6	Houston #1 Bach
30S-16E-7	7	Harkins, Mayfair #1 Yahlsing
30S-16E-8	8	Coastal States #1 Kuhn
30S-16E-8	9	Union Prod. #1 Ostrum
30S-16E-2	10	Magnolia #1 Santa Cruz Farms
30S-16E-4	11	Hamon #1 Ashley
30S-17E-1	1	Continental #1 Johnson
30S-17E-3	2	General Crude #1 Stegle
30S-17E-5	3	Cities Service, et al. #1 Rio Farms
30S-17E-7	4	Voss Properties #1-A Wade
30S-17E-7	5	Tex-Star #1 Lacy
30S-17E-7	6	Tex-Star #5 Painter
30S-17E-2	7	Standard #1 Rio Farms
30S-18E-3	1	Carrl #1 Nance
30S-18E-4	2	Texaco #1 Johnson
30S-18E-6	3	Humble #1 Austin
30S-18E-3	4	Magnolia #1 Giesc
30S-18E-3	5	Mound #1 Oaks
30S-18E-5	6	Union #1 Bell
30S-19E-1	1	Mound #1 Dudensing
30S-19E-7	2	Amerada #1 Huff
30S-19E-8	3	Gulf Coast Leaseholds #1 Schussler
30S-19E-8	4	Skelly #1 Schussler
30S-19E-9	5	Gulf #1 McDaniel
30S-19E-9	6	Houston #1 Bouldin
30S-20E-6	1	Phillips #1 Livingston
30S-20E-9	2	Union #1 Hardin
30S-21E-2	1	Kirkwood #2-"B2" Armendiaz
30S-21E-3	2	Kirkwood #1 Armendiaz
30S-21E-3	3	Arriba #1 Armendiaz

Tobin Grid	Well number	Well name
30S-21E-6	4	Shell #1 Continental
30S-21E-2	5	Magnolia #4 Armendiaz
30S-21E-2	6	Magnolia #3 Armendiaz
30S-21E-3	7	Magnolia #1 Armendiaz
30S-21E-4	8	Wilson #1 Gardens Development
30S-21E-9	9	Standard of Texas #1 Parks
30S-21E-4	10	Maguire #1 Gibbons-Parks
30S-21E-3	11	Pan American #1 De Armendiaz
30S-22E-7	1	Humble #1 Laguna Madre S. T. 657
30S-22E-9	2	Shell #1 Buttes
30S-23E-2	1	Magnolia #1 Kerlin
30S-23E-4	2	Sundance #1 Jones
30S-23E-4	3	Gulf #1 Kerlin
30S-23E-4	4	Sundance #1 Kerlin
30S-23E-5	5	Gulf #2-A Kerlin
31S-17E-1	1	Moody #2 O'Quinn
31S-17E-1	2	American Petrofina #3 Graham
31S-17E-2	3	Tidewater #1 Hoblitzelle
31S-17E-3	4	Huber #1 "A" Miller
31S-17E-3	5	Northern Pump. #2 Harris
31S-17E-4	6	Bettis & Shepperd #1 Olivares
31S-17E-3	7	Forrest #1 Myers
31S-17E-6	8	May #1 Neuhaus
31S-17E-7	9	Shell #1 Drawe
31S-17E-6	10	MacDonald #1 Pettus Estate
31S-17E-8	11	Bettis & Shepperd #1 Baingo
31S-17E-3	12	Northern Pump. #4 Henry
31S-17E-3	13	Northern Pump. #3 Harris
31S-17E-3	14	Forrest #1 Pettis
31S-17E-3	15	Forrest #1 Waters
31S-18E-3	1	Hydrocarbon #1 Bevers
31S-18E-3	2	Lacy #2 Fee
31S-18E-9	3	Forrest #1 Kempner
31S-18E-7	4	Hunt #1 Messmer
31S-18E-7	5	Sinclair-Prairie #1 Mid-Continent Life
31S-19E-3	1	Arkansas & Mosbacher #1 Rohman
31S-19E-6	2	Goldrus & Echols #1-A Parker
31S-19E-7	3	Superior #1 San Benito
31S-20E-4	1	Voss Drilling #1 Duncan
31S-20E-5	2	Chevron #1 Rodriguez
31S-20E-5	3	Wilson Exploration #12-1 Bowie Unit
31S-20E-6	4	Phillips #1 Roloff
31S-20E-6	5	Aluminum Co. of America #1 Old Colony Trust Estat
31S-20E-7	6	Aluminum Co. of America #1 Laakso-Lockwood
31S-20E-5	7	Shell #1 Hulsey
31S-20E-5	8	Wilson Exploration #1 "A" Day
31S-21E-9	1	Danciger #1 Weikel
31S-21E-9	2	Sundance #1 Weikel
31S-22E-7	1	Texaco #1 S. T. 726
31S-23E-9	1	Southland Royalty #1 S. T. 717
31S-23E-4	2	Street #1 Laguna Madre S. T. 692
32S-17E-1	1	La Gloria #1 S. Mercedes
32S-17E-1	2	Bettis-Shepperd #1 Schwarz
32S-17E-3	3	La Gloria #1-5 So. Weslaco
32S-17E-2	4	Quintana #1 McDaniel
32S-17E-5	5	Mason #1 Ranco
32S-18E-6	1	Sun #1 Cameron County Water District
32S-18E-7	2	Sun #A-1 Cameron County Water District
32S-18E-1	3	Standard #1 Moot-Hart
32S-18E-7	4	Sun #1 Anderson
32S-18E-7	5	McCarthy #1 Anderson
32S-19E-9	1	Pan American #1 Wentz

Cameron Fairway

Tobin Grid	Well number	Well name
32S-19E-4	2	Sun #1 Tanamachi
32S-19E-5	3	Sun #1 Paule
32S-21E-3	1	Holmes #1 Sweeney
32S-21E-6	2	Dow Chemical #1 Continental Oil
32S-21E-3	3	Pan American #1 Greer
32S-22E-8	1	Samedan #1 Yturria
32S-22E-1	2	Gulf #2 Laguna Madre S. T. 729
32S-22E-1	3	Gulf #1 S. T. 740
32S-22E-7	4	Pure #4 Newberry
32S-22E-7	5	Vieja #1 Garcia
32S-22E-7	6	Gulf #1 Yturria
32S-22E-8	7	Skelly #1 Newberry
32S-22E-8	8	Getty #1-B Newberry
32S-22E-8	9	Skelly #2 Newberry
32S-23E-9	1	Union #1 Esperson
32S-23E-2	2	Anadarko #1 S. T. 749
32S-23E-4	3	Southern Union #2 Garcia
32S-23E-7	4	Magnolia #1 All American Cables & Radio
33S-20E-2	1	Humble #6-1 Cameron County Water Control
33S-20E-6	2	Texas #1 Davis
33S-21E-3	1	Standard of Texas #1 Cameron Park Dev.
33S-22E-5	1	Texas Gulf #1 Lerma
33S-22E-1	2	Fundamental #1 Newberry
33S-22E-1	3	Texas Gulf #1 Esperson Estate
33S-22E-5	4	Texas Gulf #1 Vista Del Mar Irrigation
33S-22E-9	5	Texas Gulf #1 Mentz
33S-23E-2	1	Glasscock #1 Esperson

Tobin Grid	Well number	Well name
1N-35E-8	1	Texaco #1 Mergele
1N-36E-4	1	Humble #10 Milo
1N-36E-4	2	Humble #1 Tomball Unit 11
1N-36E-1	3	K & H #1 Hildebrandt
1N-36E-6	4	Texaco #1 Hallson
1N-36E-8	5	Slick #1 Jackson
1N-37E-1	1	Humble #1 Bender
1N-37E-2	2	Humble #1 Baldwin
1N-37E-1	3	Star #1 Packinpough
1N-37E-6	5	Davis #1 Couch Unit
1N-37E-5	6	Wolcott #1 Panzarella
1N-37E-9	7	Sorelle & Sorelle #1 Smith
1N-38E-3	1	Mobil #1 Bender
1N-38E-3	3	Texaco #1 Bender
2N-32E-4	1	Pan American #1 O'Connor
2N-32E-5	2	Continental #1 Thomas & Scardino
2N-32E-6	3	Harrison #1 Gaines
2N-32E-7	4	Sinclair #1 McDade
2N-32E-4	5	Shell #1 Chapman
2N-33E-4	1	Brazos #1 Sledge
2N-33E-4	2	Sun #1 Von Blucher
2N-33E-4	3	Mana #1 Smith
2N-33E-2	4	Brazos #1 Connell
2N-33E-2	5	Sun #1 Connell
2N-34E-3	1	Strake #1 Humphries
2N-34E-3	2	Speed #1 Sauerbrunn
2N-34E-3	3	Texaco #1 Humphries
2N-34E-4	4	Associated #1-A Rice University
2N-34E-4	5	Texaco #1 Rice Institute
2N-34E-6	6	Superior #1 Brown
2N-34E-6	7	McCarthy #1 Tucker
2N-34E-7	8	Enterprises Resources #1 Welch Foundation
2N-34E-7	9	Ashland #1 Welch Foundation
2N-34E-7	10	Johnson #1 Frost, et al.
2N-34E-5	11	Panuco #1 Brown
2N-35E-1	1	Pan American #1 Winslow
2N-35E-2	2	Superior #1 Mostyn
2N-35E-1	4	Superior #B-1 McWhorter
2N-35E-2	5	Gray Wolfe #4 Pan American
2N-35E-2	6	Gray Wolfe #3 Pan American
2N-35E-2	7	Pan American #1 Posey
2N-35E-2	8	La Gloria #2 Grogan Cochran
2N-35E-3	9	Hawkins #1 Streety
2N-35E-3	10	Christie-Mitchell #1 Streety
2N-35E-3	11	Standard #1 Dean
2N-35E-4	12	Humble #1 Lewis
2N-35E-6	13	Mellon Energy #1 Gibbs Bros.
2N-35E-4	14	Superior #1 Kramer
2N-35E-4	15	Gose #1 Kramer
2N-35E-4	16	Mitchell #1 Hagan
2N-35E-5	17	Superior #A-3 Dean
2N-35E-5	18	Superior #A-1 Dean
2N-35E-5	19	Gray Wolfe #6 Pinehurst
2N-35E-5	20	Superior #A-2 Dean
2N-35E-5	21	Gray Wolfe #1 Pinehurst
2N-35E-5	22	Gray Wolfe #4 Pinehurst
2N-35E-8	23	Commercial #1 Pills & Leyle
2N-35E-9	24	Pan American #1 Welch Foundation
2N-35E-1	26	Superior #A-5 McWhorter
2N-35E-1	27	Superior #2-C McWhorter
2N-35E-1	31	Superior #1-C McWhorter
2N-35E-1	32	Superior #1-D McWhorter

Tobin Grid	Well number	Well name
2N-35E-1	34	Superior #4-A McWhorter
2N-35E-1	36	Progress #1 Winslow
2N-35E-3	37	Hedge #1 Streety
2N-35E-4	38	Falcon-Seaboard #1 Heflin
2N-35E-1	39	Superior #3-C McWhorter
2N-35E-1	40	Superior #5-C McWhorter
2N-35E-1	41	Stanolind #1-B McWhorter
2N-36E-1	1	Superior #1 McMahan
2N-36E-1	2	Texaco #1 Winslow
2N-36E-2	3	Prairie #1 M&M Minerals
2N-36E-2	4	Stanolind #1 McMahan
2N-36E-2	5	Royal Resources #1 M&M Minerals
2N-36E-2	6	Magnolia #1 Chase National Bank
2N-36E-3	7	Superior #A-7 McWhorter
2N-36E-3	8	Stanolind #A-1 South Texas Development
2N-36E-3	9	Superior #1 Brown
2N-36E-3	10	Superior #30 Lake Creek Unit
2N-36E-3	11	Superior #1 South Texas Development
2N-36E-3	12	Superior #1 M&M Minerals
2N-36E-3	13	Del Mar #1 South Texas Development
2N-36E-5	14	Moran #1 M&M Minerals
2N-36E-6	15	Superior #1 Foley
2N-36E-6	16	Sohio #1 1936 Development Corp.
2N-36E-7	17	Shell #1 Peden
2N-36E-8	18	Shell #1 Holderreith
2N-36E-2	19	Vaquero #B-1 M&M Minerals
2N-36E-3	20	Superior #3 South Texas Development
2N-36E-3	21	Superior #2 South Texas Development
2N-36E-7	23	Enserch #1 Boone
2N-36E-3	24	Superior #27 Lake Creek
2N-37E-4	1	Sinclair #1 Grogan
2N-37E-4	2	Sinclair #1 Porter
2N-37E-7	3	Gordon #1 Bender
2N-37E-9	4	Shenandoah #1 Evans
2N-37E-8	5	Byrd #1 Walton
2N-37E-9	6	McDaniel #1 Baldwin
2N-37E-2	7	Hunt #1 Doyle
2N-38E-1	1	Atlantic #1 South Texas Development
2N-38E-3	2	Sun #27 Keystone Mills
2N-38E-5	3	Standard #1 Anderson Unit
2N-38E-7	4	Winwell #1 Schwing
2N-38E-7	5	Lacal #1 Schwing
2N-38E-7	6	Humble #1 Wickizer
2N-38E-2	8	Humble #1 Hines
2N-38E-2	9	Goodale #1 Maynard
2N-39E-1	1	Samedan #1 Coleman
2N-39E-2	2	McHenry #2 Neff
2N-39E-2	3	Humble #B-1 Texas
2N-39E-2	4	Kurth Trustee #4 Southland Paper
2N-39E-4	5	Humble #1 Owalline
2N-39E-4	6	Sinclair #1 Foster Lumber
2N-39E-5	7	Humble #1 Patton
2N-39E-6	8	Union #1 Foster Lumber
2N-39E-6	9	Atlantic #1 Foster Lumber
2N-39E-6	10	McCormick #1 Krohn
2N-40E-2	1	Humble #B-1 Quinn
2N-40E-2	2	Sun #2 Quinn
2N-40E-2	3	Sundance #1 Quinn
2N-40E-2	4	Sun #1 Quinn
2N-40E-2	5	Gulf #1-C Quinn
2N-40E-2	6	Allday #1 Quinn
2N-40E-5	7	Sun #1 Friendswood Development
2N-40E-6	8	Fuller #1 Foster Lumber
2N-40E-4	9	General Crude #1 McClain
2N-41E-3	2	Acorn #1 Berry
3N-32E-4	1	Olsen #1 Harris
3N-32E-6	2	Sessions #1 Barry
3N-32E-7	3	Placid #1 Harris
3N-32E-9	4	Sinclair #1 Henry

Montgomery Fairway

Tobin Grid	Well number	Well name
3N-33E-8	1	Gulf #2 Gardner
3N-33E-8	2	Millican #1 Gardner
3N-33E-8	3	Gulf #1 Gardner
3N-33E-8	4	Atlantic #1 Sanders
3N-33E-8	5	Millican #1 Barnes
3N-33E-7	6	Millican #2 Harris
3N-34E-7	1	Colorado #1 Rice University
3N-34E-7	2	Callery #1 Thompson Brothers
3N-34E-8	3	McCarthy #1 Gibbs-Elgin
3N-34E-8	4	Standard of Texas #1 Sanders
3N-34E-9	5	Lone Star #1 Goforth
3N-34E-9	6	Goforth #1 Goforth
3N-34E-8	7	Houston #1 Schoenfeldt
3N-34E-1	8	Petroleum Management #1 Shanks
3N-35E-4	1	Sinclair #1 Martin
3N-35E-4	2	Lester #1 White
3N-36E-1	1	Feldman #1 Teas Nursery
3N-36E-4	2	Socony-Mobil #1 Sealy-Smith
3N-36E-7	3	Prairie #1 Madeley
3N-36E-7	4	Delhi-Taylor #2 Sealy-Smith
3N-36E-7	5	Delhi-Taylor #1 Sealy-Smith
3N-36E-8	6	Prairie & McMoran #2 Frost
3N-36E-8	7	Prairie #1 Frost
3N-36E-8	8	Superior #3 Frost
3N-36E-8	9	Superior #1 Frost
3N-36E-8	10	Mecom #1 Bertrand
3N-36E-9	11	Stanolind #1 William
3N-36E-9	12	Sinclair #1 Grogan
3N-36E-9	13	Mitchell #1 Asche
3N-36E-9	14	Mitchell #1 Sealy & Smith
3N-36E-6	15	General Crude #1 Sealy-Smith
3N-37E-4	1	Moran #1 Cartwright
3N-37E-5	2	Hagen #1 Harris & Freeman
3N-37E-8	3	Skelly #1 Tipton
3N-37E-8	4	Humble #2 Grand Lakes
3N-37E-9	5	Humble #1 Grand Lake Gas Unit 1
3N-37E-9	6	Humble #1 Grand Lake
3N-37E-9	7	Humble #1 BSA
3N-37E-7	8	Humble #45 Madeley
3N-38E-1	1	Sands #1 San Jacinto Trust
3N-38E-5	2	Texaco #1 Griffin
3N-38E-8	3	Karsten #1 Knapp
3N-39E-1	1	Atlantic #1 White
3N-39E-1	2	Trice #1 Foster Lumber
3N-39E-2	3	Cauble Enterprises #1 Combe Heirs
3N-39E-1	4	Gulf #1-A Foster Lumber
3N-39E-5	5	Rowan #1 Dunham
3N-39E-5	6	Atlantic #1-A Foster Lumber
3N-39E-5	7	Halbouty #1 Foster-Gulf
3N-39E-8	8	Pure #1 Foster Lumber Unit
3N-39E-5	9	Halbouty #1-B Foster Lumber
3N-39E-5	10	Halbouty #2 Foster Lumber
3N-39E-5	11	Halbouty #1-A Foster Lumber
3N-39E-5	12	Halbouty & Union #E-1 Foster
3N-39E-6	13	Amerada #1 Foster Lumber
3N-39E-6	14	Halbouty #1 Godejohn Unit
3N-39E-6	15	Amerada #1 Godejohn
3N-39E-6	16	Halbouty #1 Burkett Unit
3N-39E-7	17	Halbouty #1 Leggett
3N-39E-8	18	Halbouty #1 Southland Paper
3N-39E-5	19	Sohio #1 Kingwood
3N-39E-6	20	Sanchez-O'Brien #1-A Friendswood
3N-39E-6	21	Sanchez-O'Brien #1 Friendswood
3N-39E-3	22	Abercrombie #1 Aylor

Tobin Grid	Well number	Well name
3N-39E-7	23	Halbouty #1 Todd
3N-39E-9	24	Head, et al. #1 Southland Paper
3N-40E-1	1	Sun #1 Quinn
3N-40E-1	2	Karsten #5-A Quinn
3N-40E-1	3	Houston Mineral #1 Ott Gas Unit
3N-40E-1	4	Pan American #1 Howard
3N-40E-1	5	Ohio #1 Quinn
3N-40E-1	6	Pan American #A-1 Kirby Lumber
3N-40E-3	8	Mitchell #1 Cherry
3N-40E-8	9	Superior #1 Bosworth
3N-40E-8	10	Hunt #1 Grogan
3N-40E-9	11	Superior #1 T. J. Hightower
3N-40E-9	12	Superior #1 C. P. Hightower
3N-40E-9	13	Humble #1 McDonald
3N-40E-3	15	Karsten #1 White
3N-40E-9	16	Starr #1 Duke
3N-40E-7	17	Gulf #35 Kirby Lumber "C"
3N-40E-3	18	Oil & Gas Property Management #1 Bryan
3N-40E-7	19	Rowan #1 Kirby Lumber
3N-40E-5	20	Shell #1 Grogan
3N-40E-5	21	Dyco #1 McDonald Trust
3N-40E-3	22	Oil & Gas Property Management #1 Quickle
3N-40E-1	23	Gulf #1-C Kirby Lumber
3N-41E-3	1	Humble #1 Smith
3N-41E-3	2	Cherryville #1 Jackson
3N-41E-3	3	Brazos #1 Ballard
3N-41E-4	4	Porter #1 Champion
3N-41E-6	5	General Crude #1 Hill
3N-41E-4	6	Wilson #1 Glenn
3N-41E-4	7	Mosbacher #1 Jett
4N-32E-5	1	Magnolia #1 Brigance
4N-32E-7	2	Placid #1 Davis
4N-32E-8	3	Placid #1 Foster
4N-33E-1	1	Victory #1 Bevans
4N-35E-7	1	Capitol #1 Alliance Trust
4N-35E-7	2	Strake #1 Peel
4N-35E-1	3	Placid #4 Central Coal & Coke
4N-35E-9	4	Texaco #1 Sealy-Smith
4N-36E-6	1	Superior #1 Elam
4N-36E-6	2	Superior #1 Sykes
4N-36E-6	3	Moran #1 Sykes
4N-36E-9	4	Cities Service #1 Madeley
4N-36E-6	5	Sunset International #1 Shawver
4N-36E-7	7	Burke #1 Ferguson
4N-36E-4	8	Garvey #1 Foster
4N-36E-5	9	Strake #1 Jones
4N-36E-1	10	Hanslip #1 Crawford
4N-37E-6	1	Oil Reserves #1 Foster
4N-37E-7	2	Moran #3-A Hutchings-Sealy
4N-37E-7	3	Texmo #3 Hutchings-Sealy
4N-37E-7	4	Moran #2-A Hutchings-Sealy
4N-37E-8	5	Texmo #1 Hutchings-Sealy
4N-37E-8	6	Texmo #1 Conroe Gas Unit
4N-37E-8	7	Donkin & Smith #1 Farrell
4N-37E-7	8	Glen Rose #1 Champion Paper
4N-37E-7	9	Moran #1-B Hutchings-Sealy
4N-37E-4	10	Womack #1 Willis Townsite
4N-37E-3	11	Moran #1 Hooper
4N-38E-1	1	Continental #1 Gibbs Bros.
4N-38E-1	2	Continental #2 Gibbs Bros.
4N-38E-1	3	Huber #1 Gibbs
4N-38E-1	4	Texas City #1 Foster
4N-38E-2	5	Cities Service #1 Frazier & Campbell
4N-38E-2	6	Dominion #1 Campbell
4N-38E-3	7	Conoco #1 Frazier
4N-38E-4	8	Donkin & Smith #1 Browder

Tobin Grid	Well number	Well name
4N-38E-4	9	Moran #1 Browder
4N-38E-8	10	Hunt Trust #1 Adriance
4N-38E-1	11	Sun #1 Gibbs Bros.
4N-39E-3	1	Prairie & Convest #1 Gibbs
4N-39E-3	2	Impact #1 Mays
4N-39E-4	3	Continental #1 Mays
4N-39E-5	4	Amerada #1-A Foster Lumber
4N-39E-7	5	Amerada #1 Central Coal & Coke
4N-39E-7	6	Russell & Moran #1 Central Coal & Coke
4N-39E-8	7	Shell #11 Central Coal & Coke
4N-39E-8	8	Superior #1 Foster Lumber
4N-39E-8	9	Manning #1 Central Coal & Coke
4N-39E-9	10	Fain #1 Baldwin
4N-40E-1	1	Stanolind #1 Roberts
4N-40E-1	2	Magnolia #2 Dixon-Falvey
4N-40E-1	3	San Jacinto #1 Ogletree
4N-40E-4	4	Vincent #1 Foster Minerals
4N-40E-4	5	Magnolia #1 Hinchcliff-Sims
4N-40E-5	6	Fuller #1 Foster Lumber
4N-40E-8	7	Davis #1 Sims
4N-40E-7	8	Johnson-Walker #1 Kirby Lumber
4N-40E-8	9	Magnolia #1 Brewer
4N-41E-9	1	Oil Reserves #1 Jefferson
4N-41E-1	2	Continental & Speed #1 Frost Lumber
4N-41E-6	3	Pan American #1 Kilburn Moore
4N-41E-1	4	Stanolind #1 Falvey
5N-33E-3	1	Texaco #1 Harris
5N-33E-7	2	Ahern #1 Bennett
5N-33E-9	3	Ranger #1 Bradley
5N-34E-9	1	Placid #1 Thomas
5N-34E-9	2	Standard of Texas #1 Brown
5N-35E-5	1	Placid #1 Central Coal & Coke
5N-35E-7	2	Lone Star #G-8 Central Coal & Coke
5N-35E-7	3	Phillips #1-A Coke
5N-35E-9	4	Placid #2 Central Coal & Coke
5N-36E-1	1	Womack #1 Foster
5N-36E-2	2	Moran #1 Foster
5N-36E-5	3	Moran #G-3 Central Coal & Coke
5N-36E-7	4	Russell #1 Malak
5N-36E-8	5	Pure #1 Central Coal & Coke
5N-37E-4	1	Clark #1 Beardsley
5N-38E-5	1	Cities Service #B-1 Browder
5N-38E-7	2	Texas City Refinery #1 Elmore
5N-38E-7	3	Dominion #2 Elmore, et al.
5N-38E-7	4	Dominion #1 Elmore
5N-38E-8	5	Houston #1 Lewis
5N-38E-8	6	Cities Service #1 Ellisor
5N-38E-8	7	Triton #1 Roche-Ellisor
5N-38E-8	8	Barnes #1 Johnson
5N-38E-8	9	Cities Service #1 Melvin Unit
5N-38E-8	10	Cities Service #1 Browder
5N-38E-7	11	Burke #1 Elmore
5N-38E-2	12	Glen Rose #1-A Central Coal & Coke
5N-39E-3	1	Glen Rose #1 Cary Heirs
5N-39E-8	2	Butcher-Arthur #1 Jones
5N-39E-7	3	Standard #1 Foster Lumber
5N-39E-7	4	Shell #1 Coline
5N-39E-9	5	Mac #1 Payne
5N-39E-8	6	Reserve #2 Richards
5N-39E-9	7	Reserve #1 Polk
5N-39E-9	8	Impact #1 Gibbs Bros.
5N-39E-9	9	McCarthy #1 Dabney
5N-39E-7	10	Commercial #10-D Foster
5N-39E-7	11	Oil Lease Operator #3-A Foster Lumber
5N-39E-8	12	Reserve #1 Richards
5N-40E-6	1	Sun #1 McGowen
5N-40E-6	2	Viking #1 Langham

Montgomery Fairway

Tobin Grid	Well number	Well name
5N-40E-4	3	Texaco #1 Foster Lumber
5N-40E-2	4	Davis #1 Hale, et al. Unit
5N-40E-9	5	Reserve #4 Foster Lumber
5N-41E-4	1	Amoco #A-3 Langham
5N-41E-2	2	Woodley #1 Edmonds
5N-41E-4	3	Pan American #2-B Langham
5N-41E-1	4	Phillips #1 Barnes
5N-41E-4	5	Stanolind #1-B Langham
5N-41E-4	6	Stanolind #1-C Langham
5N-41E-5	7	Sinclair #1 Jones
5N-41E-9	8	Amoco #1 Langham
5N-41E-7	9	Sparta, et al. #1 Humble & Moore
5N-41E-1	10	Dominion #1 Southland Paper
5N-41E-9	11	Tiger #1 Ward
5N-41E-2	12	Wadsworth #1 Crum
5N-41E-5	14	Amoco #1 Allen
6N-35E-7	1	Marr #1 Ward
6N-36E-4	1	Moran #1 Oliphant
6N-36E-7	2	Tissue #1 Pickering
6N-36E-9	3	Moran #1 Smithers
6N-36E-3	4	Moran #1 Gibbs
6N-37E-4	1	Marr #3 Gibbs
6N-37E-5	2	Marr #1 Gibbs
6N-37E-6	3	Marr #2 Gibbs
6N-38E-1	1	Stanolind #1-B Carey Land
6N-38E-9	2	Placid #2 Gibbs Bros.
6N-38E-7	3	North Central #2 Casey Heirs
6N-39E-4	1	Stanolind #2 Carey Land
6N-39E-8	2	Humble #1 Foster Lumber
6N-39E-8	3	Hunt #1 Foster